Yuliy D. Gamburg · Giovanni Zangari

Theory and Practice of Metal Electrodeposition

Springer

Theory and Practice of Metal Electrodeposition

Yuliy D. Gamburg • Giovanni Zangari

Theory and Practice of Metal Electrodeposition

Springer

Dr. Yuliy D. Gamburg
Russian Academy of Sciences
A.N. Frumkin Institute of Physical
Chemistry and Electrochemistry
Moscow
Russia
gamb@list.ru

Dr. Giovanni Zangari
University of Virginia
Department of Materials Science
and Engineering
Charlottesville VA
USA
gz3e@virginia.edu

ISBN 978-1-4419-9668-8 e-ISBN 978-1-4419-9669-5
DOI 10.1007/978-1-4419-9669-5
Springer New York Dordrecht Heidelberg London

Library of Congress Control Number: 2011930260

Printed on acid-free paper

Springer is part of Springer Science+Business Media (www.springer.com)

Preface

The book reflects in a concise form the modern state of both theoretical and applied aspects of metal electrodeposition. The theoretical part concerns the electrochemistry of metals and includes a discussion of electrochemical thermodynamics and kinetics, the structure at the metal/electrolyte interface, nucleation, growth and morphology of metals and alloys, and current distribution. The applied part contains general information on the applications of metallic coatings, their selection, electrochemical basics and technology of deposition of selected metals and alloys, including individual peculiarities, properties and structure of coatings, testing and characterization. The book includes, where possible at an elementary level, a quantitative discussion of phenomena of relevance, providing formulas for the calculation of important quantities. Additionally, it contains information on surface leveling, hydrogenation, inclusion of impurities, physical properties of deposits, that is rarely available in textbooks on electrodeposition. The section on electrodeposition technology includes the most important processes and chemistries; information on any definite material system is provided using a unified scheme, namely: properties of the coating, advantages and disadvantages, solution chemistries and methods of preparation, peculiarities, anodes, and additives.

The essential concepts in theoretical electrochemistry necessary for the investigation of metal deposition processes is provided here, including data that are commonly absent in specialized academic courses. These topics are important for the reader aiming to achieve a thorough understanding of the latest scientific publications in this field. Information on different aspects of the process of electrolytic crystallization is gathered here from a large body of publications and is considered from a unified point of view.

The book is suitable for professional electrochemists, advanced undergraduate and postgraduate students and also for electrodeposition specialists with a physical, technical or chemical education. It can also be useful for engineers and specialists engaged in research on new electrodeposition technologies related to metallic layers, crystals and other metallic objects.

One of the authors (Yu. Gamburg) is hugely grateful to his colleagues from the Laboratory of the surface layers structure (A. N. Frumkin Institute, Russian Academy of Sciences) and particularly indebted to Maria R. Ehrenburg who translated the chapters 10 and 11 written originally in Russian.

Contents

1 Introduction to Electrodeposition: Basic Terms and Fundamental Concepts 1
1.1 Electrodeposition of Metals 1
1.2 Examples of Electrocrystallization 2
1.3 Electrode Processes. Faraday's Law 2
1.4 Current Density 3
1.5 Electrodes and Electrode Potential 5
1.6 Equilibrium Potential and Overpotential 7
1.7 Mixed Potential 9
1.8 Potential–Current Curves (Voltammograms) 10
1.9 Current Efficiency 12
1.10 The Various Steps Occurring in Electrode Processes. Fast and Slow Steps 13
1.11 Electrolytes Used for Electrodeposition 15
1.12 The Influence of Deposition Parameters on Electrodeposition Processes 17
1.13 Electric Conductivity of Solutions 18
1.14 Composition, Structure and Properties of Deposits 20
1.15 Current and Metal Distribution 23
1.16 Anodic Processes 24
References 25

2 The Structure of the Metal-Solution Interface 27
2.1 Introduction: Spatial Separation of Electric Charge 27
2.2 Compact Part of the Double Layer: Helmholtz Layer 30
2.3 Diffuse Layer: Gouy-Chapman Layer 31
2.4 Adsorption at Electrodes 36
2.4.1 Model Adsorption Isotherms 37
2.5 Specific Adsorption 43
2.6 Adsorption of Uncharged Organic Species 45
2.7 Double Layer on Polycrystalline Solid Surfaces 46

2.8 Some Calculations of Double Layer Parameters 48
References 51

3 Electrochemical Thermodynamics and Electrochemical Kinetics 53
3.1 Electrochemical Potential 53
3.2 Equilibrium at Electrolyte-Solid Interfaces 54
3.3 Electrode Potential. Nernst Equation 55
3.4 Measurements of Electrode Potential 56
3.5 Theory of Charge Transfer 57
3.6 Exchange Current Density. Overpotential. Polarization Curves 62
3.7 Multistep Electrochemical Processes 66
3.8 Chemical Steps 68
3.9 Ion Discharge Kinetics in Presence of Surface-Active Agents 70
3.10 Peculiarities of the Discharge of Complexes 73
References 75

4 Influence of Diffusion on the Rate of Electrochemical Process 77
4.1 Ion Transport and Current 77
4.2 Diffusion 80
4.3 Limiting Current 82
4.4 Diffusion Overpotential 84
4.5 Mixed Kinetics 85
4.6 The Influence of the Electric Field on the Limiting Current 87
4.7 Role of Diffusion in the Discharge of Complex Species 90
4.8 Diffusion Layer on the Rotating Disc Electrode 91
References 96

5 Thermodynamics and Kinetics of Nucleation 97
5.1 Introduction 97
5.2 Homogeneous Nucleation 98
5.3 Heterogeneous Nucleation 100
5.3.1 Three-Dimensional Nucleation 100
5.3.2 Two-Dimensional Nucleation 102
5.4 Nucleation Mechanisms 103
5.5 The Peculiarities Of Electrocrystallization 104
5.6 The Partition Function For the Nuclei Size Distribution 105
5.7 The Steady State Nucleation Kinetics 106
5.7.1 Fokker–Planck Equation 106
5.7.2 The Non-Equilibrium Flux 107
5.7.3 An Estimate of the Steady State Flux 108
5.7.4 Peculiarities of the Steady State Flux Result 109
5.8 Non-Steady State Nucleation 110
5.9 Experimental Methods 112
5.10 Kinetics of Mass Crystallization 113

5.11 The Growth of an Individual Hemispheric Oluster Under Mixed Control 115
5.12 The Nucleation and Growth With Overlap 118
References 122

6 Morphology of the Growing Metal Surface 123
6.1 Steps and Kinks 123
6.2 Adatoms and Adions 125
6.3 Normal Growth and Layer-by-Layer Growth 126
6.4 The Rate of Normal Growth 127
6.5 Rate of Step Propagation During Layer-by-Layer Growth 128
6.6 Nucleation Rate Distribution Between Growth Steps 130
6.7 Influence of Adsorption on the Rate of Crystallization 132
6.8 Ohmic Drop Near a Growing Step 133
6.9 Grain Size of Deposits as a Function of Overpotential 134
6.10 Morphological Features of Compact Electrodeposits 136
6.10.1 The Morphological Types of the Deposit Surface 136
6.10.2 Pyramids and Spirals 137
6.10.3 Layered or Lamellar Morphology, and Other Morphological Types 138
6.10.4 On the Nature of Macrosteps 139
6.11 Crystalline, Irregular Roughness 140
References 141

7 Potential Distribution in the Electrolyte and Current Distribution on the Electrode Surface 143
7.1 Statement of the Problem 143
7.2 Primary, Secondary and Limiting Field Distributions. Polarization Fields 144
7.3 Basic Principles of Calculation of Electric Fields in the Electrochemical Cells 149
7.4 Typical Examples of Primary and Secondary Current Distribution ... 151
7.4.1 The Strip-Shaped Cathode; Primary Current Distribution (PCD) 151
7.4.2 The Disc Electrode; PCD 152
7.4.3 Gap Cells and Angular Cells with Linear Cathodes; PCD 153
7.4.4 The Cylindrical Cathode 154
7.4.5 The Sinusoidal Profile; PCD 154
7.4.6 Arbitrary Case; PCD 155
7.4.7 Arbitrary Case; Secondary Current Distribution (SCD) 156
7.4.8 The General Case 158
7.5 Throwing Power of Electrolytes and Polarizability of Electrodes. Standard Definition of Throwing Power 158
7.6 Throwing Power and Cathodic Polarization. Methods for Improvement of Current Distribution 161

7.7 Current Distribution on Microstructured and Nanostructured Electrodes: Through-Mask Electrodeposition 163
7.7.1 Current Distribution at the Workpiece Scale 165
7.7.2 Current Distribution at the Pattern Scale 165
7.7.3 Current Distribution at the Feature Scale 166
References 167

8 Current Distribution at Rough Electrodes 169
8.1 Introduction 169
8.2 Coefficient of Current Distribution and the Basic Problem of Microdistribution 171
8.3 Geometric Leveling 172
8.4 Microprofile Evolution as Result of a Non-Uniform Primary Current Distribution 173
8.5 Roughness Evolution Under Secondary and Tertiary Current Microdistribution 177
8.6 True Leveling 180
8.7 Stability of the Growth Front During Electrocrystallization 183
8.8 Bright Deposits 186
References 187

9 Non-steady State Electrodeposition Processes and Electrochemical Methods 189
9.1 Non-steady State Diffusion 189
9.2 On–Off Switching of the Current or Overpotential 191
9.3 Superposition of a Sinusoidal Current 193
9.4 Steady State and Pulsating Diffusion Layers 196
9.5 Rectangular Pulses 197
9.6 Role of the Pause and of the Anodic Period 199
9.7 Current Distribution, Current Efficiency and Inclusions of Impurities During Non-steady State Processes 199
9.8 Linear Current or Potential Scans; the Optimum Sweep Rate for the Acquisition of Polarization Curves 201
References 204

10 Electrodeposition of Alloys 205
10.1 Introduction 205
10.2 Applications of Electrodeposited Alloys 205
10.3 Partial Polarization Curves for Alloy Components 206
10.3.1 Construction of Partial Curves 206
10.3.2 Depolarization and Overpolarization 207
10.4 Conditions for Alloy Formation 208
10.5 Structure Types of Electrodeposited Alloys 211
10.6 Phase Diagrams of Alloys 214

10.7 Alloys of the Mechanical Mixture Type 216
10.8 Alloys of the Solid Solution Type 217
10.8.1 Underpotential Metal Deposition and Cathodic Metal Intercalation into a Foreign Substrate 217
10.8.2 Formation of Solid Solutions 219
10.9 Intermetallic Compounds and Amorphous Alloys 220
10.10 Equilibrium and Steady-State Potentials of Alloys 221
10.11 Accounting for the Energy of Alloy Formation in Calculations of Potentials of Alloy Deposition 223
10.12 Nucleation and Growth of Metal Clusters on a Foreign Substrate upon Electrodeposition of an Alloy of the Mechanical Mixture Type 225
10.13 Effect of Various Factors on Alloy Composition 226
10.14 Electrodeposition of Multilayer and Surface Alloys 228
10.14.1 Multilayer Alloys 228
10.14.2 Surface Alloys 231
References 232

11 Codeposition of Impurities 233
11.1 Sources of Impurities in Electrodeposits 233
11.2 Theoretical Analysis of the Codeposition Kinetics 234
11.2.1 Adsorption Equilibrium 235
11.2.2 Capture of Adsorbed Species 236
11.2.3 Mass Transport of Impurities to the Cathode 239
11.2.4 Derivation of the Main Equation 239
11.2.5 Limiting and Intermediate Cases 241
11.2.6 Adsorption Control of Codeposition 241
11.2.7 Diffusion Control of Incorporation 242
11.2.8 The Case of Mixed Control 242
11.3 Dependence of the Concentration of Impurities on Electrodeposition Conditions 243
11.3.1 Dependence on the Current Density 243
11.3.2 Dependence on the Impurity Concentration in Solution 244
11.3.3 Dependence on Temperature 244
11.4 Factors Complicating the Codeposition Kinetics 245
11.5 Chemical State of Codeposited Impurities 246
11.6 The Incorporation of Inhibitors Into the Deposit and Inhibition of the Electrodeposition Process 247
11.7 Hydrogenation of Deposits 248
11.8 Mechanisms of Substrate Hydrogenation 249
11.9 Hydrogen Permeability of Membranes 251
11.10 Conclusion 252
References 252

12 Technologies for the Electrodeposition of Metals and Alloys: Materials and Electrolyte Selection, Substrate Preparation 253
12.1 Materials Selection 253
12.1.1 Decorative Properties: Au, Ag, Rh, Pt, Ni, Cr, Ni–Sn 253
12.1.2 Enhancing Solderability and Welding: Sn Alloys, Ni, Cu, Au, Pd 254
12.1.3 Antifriction Properties: Pb or Sn Alloys, In, Au 254
12.1.4 Corrosion Protection: Zn, Sn, Cd, Ni, Zn–Ni, Pd, Ag, Ag–Pd, Au 255
12.1.5 Electrical Contacts and Conductivity: Cu, Ag and Its Alloys, Au and Its Alloys, Pd, Ni, Sn, Sn–Pb 255
12.1.6 Hardness and Wear-Resistance: Cr, Ni, Ni–W, Ni–B, Rh, Sn Alloys 256
12.1.7 Miscellaneous Properties 256
12.2 Deposit Thickness 257
12.3 Selection of the Electrolyte 258
12.4 Chemical and Electrochemical Degreasing 259
12.5 Pickling 260
12.6 Additional Treatments 262
References 263

13 Technologies for the Electrodeposition of Metals and Alloys: Electrolytes and Processes 265
13.1 Deposition of Copper and Its Alloys 265
13.1.1 Properties and Fields of Application of Copper Deposits 265
13.1.2 Solutions for Copper Deposition 266
13.1.3 Copper Plating for Semiconductor Interconnects 268
13.1.4 Solutions Make Up and Purification 269
13.1.5 Mechanism and Kinetics of Deposition 270
13.1.6 Peculiarities, Anodes, and Additives. Removing Deposits of Poor Quality 270
13.1.7 Brass, Bronze and Copper–Nickel Alloys Plating 271
13.2 Silver and Its Alloys with Sb, Cu and Pd 273
13.2.1 Properties and Applications of Silver Deposits 273
13.2.2 Solutions for Silver Deposition 274
13.2.3 Solutions Make Up and Purification 275
13.2.4 The Mechanism of Silver Deposition 276
13.2.5 Peculiarities; Anodes; Additives 277
13.2.6 The Silver Alloys with Antimony, Copper or Palladium 278
13.3 Electrodeposition of Gold and Its Alloys 278
13.3.1 Properties and Applications for Gold Coatings 278
13.3.2 Solution Chemistries, Compositions and Operating Conditions 279
13.3.3 Solutions Make Up 281
13.3.4 Peculiarities; Anodes; Impurities; Correction 282
13.3.5 Electrolytes for Gold Alloys Deposition 283

13.4 Electrodeposition of Zinc and Its Alloys 284
13.4.1 Properties and Applications 284
13.4.2 Electrolyte Formulations and Operating Conditions 285
13.4.3 Electrolyte Preparation 286
13.4.4 The Peculiarities; Anodes; Removal of Zinc Coatings 288
13.4.5 Electrolyte Corrections 288
13.4.6 The Additives for Zinc Deposition 289
13.4.7 Zinc Alloys Plating 289
13.5 Electrodeposition of Nickel and Its Alloys 290
13.5.1 Properties, Applications and Peculiarities 290
13.5.2 Electrolyte Formulations 292
13.5.3 Solutions Make Up and Purification 293
13.5.4 Anodes 294
13.5.5 Correction and Elimination of Harmful Impurities 295
13.5.6 Electrodeposition of Nickel Alloys 295
13.6 Chromium Electrodeposition 296
13.6.1 Properties and Applications 296
13.6.2 Bath Compositions 298
13.6.3 Preparation of the Electrolytes 299
13.6.4 Peculiarities 299
13.6.5 Anodes 300
13.6.6 Electrolyte Correction 301
13.6.7 Trivalent Electrolytes 301
13.7 Iron and Its Alloys 301
13.7.1 Electrodeposition of Soft Magnetic Materials 302
13.8 Low-Melting Metals: Bi, Cd, In, Pb, Sb, Sn. The Alloy Sn–Pb 304
13.8.1 Bismuth 304
13.8.2 Cadmium 304
13.8.3 Indium 305
13.8.4 Lead 305
13.8.5 Antimony 307
13.8.6 Tin 307
13.8.7 Tin–Lead, Tin–Bismuth, and Tin–Zinc Alloys 309
13.9 Platinum Metals: Pd, Pt, Rh 310
13.9.1 Palladium 310
13.9.2 Platinum 311
13.9.3 Rhodium 313
13.10 Troubleshooting Electroplating Operations: Some Possible Reasons for Poor Deposit Quality 314
References 316

14 Structure and Microstructure of Electrodeposited Metals and Alloys 317
14.1 Formation of the Polycrystalline Metal 317
14.2 Grain Boundaries 318

14.3 Stacking Faults and Twin Boundaries 322
14.4 Dislocations and Disclinations 325
14.5 Point Defects 326
14.6 Post-Electrolysis Structure Relaxation 327
14.7 Techniques for Structural Investigations 330
References 333

15 Physical Properties of Electrodeposited Metals and Alloys. Quality Control and Testing Methods 335
15.1 Introduction 335
15.2 Specific Electrical Resistance 336
15.3 Measurements of the Specific Electrical Resistance 339
15.4 Thermoelectric Force and Contact Resistance 341
15.5 Magnetic Properties 345
15.6 Ductility 346
15.7 Tensile Strength 348
15.8 Methods of Measurements of Strength and Ductility 350
15.9 Microhardness 352
15.10 Internal Stresses (IS) 355
15.11 Methods of IS Measurement 358
15.12 Adhesion of the Deposit to a Substrate 360
15.13 Methods to Provide Strong Adhesion 360
15.14 Methods of Adhesion Measurement 362
15.15 Porosity 365
15.16 Corrosion Resistance 367
15.17 Solderability 368
15.18 Control of the deposit thickness 368
15.19 The Peculiarities of the Properties of the Electrodeposited Alloys 371
References 373

Index 375

List of Symbols

A	atomic weight
A	different constants
A	the more electropositive metal
a	thermodynamic activity
a	first Tafel coefficient
a	attraction constant in Frumkin equation
B	the more electronegative metal
B	adsorption constant
b	second Tafel coefficient
C	electric capacitance (per unit area)
C, c	concentration
CE	current (cathodic) efficiency
D	grain size
D	diffusion coefficient
d	density
d	distance
E	Young's modulus
E	potential
E^0	standard potential
E_{eq}	equilibrium potential
e	electron
e	electronic charge
F	Faraday constant
f	F/RT
f	frequency
f	different functions
G	Gibbs energy
g	gravity factor
$\boldsymbol{g}$	number of atoms in the cluster
h	height, thickness
H	hardness
H	root-mean-square roughness

I	electric current
i	current density
i_0	exchange current density
i_d	diffusion current density
i_{lim}	limiting current density
IS	internal stress
J	flux
K, k	different constants
K	electrochemical equivalent of the metal
K_m	mass transfer coefficient
k_r	roughness coefficient
k_B	Bolzmann constant
L	ligand
l	length, distance
M	metal
M	molar mass
M^{z+}	ion of metal
m	mass
N	number of species
N_A	Avogadro number
n	net amount of transferred electrons
P	leveling power of the electrolyte
Q	net charge passed through the circuit
q	electric charge
q_m	electric charge at the metal surface
R	molar gas constant
R	Ohmic resistance
R_c	contact resistance
R	radius
r	distance along the radius
ω	angular rotation rate
RDE	rotating disc electrode
S	area
SAS	surface active substance
T	absolute temperature
TP	throwing power
t	time
U	voltage (between cathode and anode)
V	volume
v	volume per one species
V_m	molar volume of the metal
W	Wagner number
w	velocity (of a flux)
x	distance
y	distance

z	electric charge of the species in electron units
Z	number of clusters
α	transfer coefficient
β	polarizability $\partial\eta/\partial i$
γ	interface energy
Γ	adsorption
Γ_{∞}	limiting adsorption
δ	thickness of the reaction layer
δ_{N}	Nernst diffusion layer
$\delta_{\mathrm{пр}}$	Prandtl layer
ε	relative permittivity
ε	roughness amplitude
η	overpotential
η_c	cathodic overpotential
η_a	anodic overpotential
θ	coverage
κ	conductivity
l	distance of propagation
λ_D	Debye length
μ	chemical potential
μ	electrochemical potential
ν_i	stoichiometric coefficients
ν	viscosity (kinematic)
ρ	volume charge density
ρ	resistivity
σ	surface tension (specific surface energy)
σ	stress
σ_{B}	breaking stress
τ	duration of the process
Φ	electric potential
Φ	form factor
φ	Galvani potential
ω	angular rotation rate (RDE)
ω	frequency
ω	fraction (mass, molar)

Chapter 1
Introduction to Electrodeposition: Basic Terms and Fundamental Concepts

1.1 Electrodeposition of Metals

Electrodeposition refers to a film growth process which consists in the formation of a metallic coating onto a base material occurring through the electrochemical reduction of metal ions from an electrolyte. The corresponding technology is often known as *electroplating*. Besides the production of metallic coatings, electrochemical metal reduction is also used for the extraction of metals starting from their ores (*electrometallurgy*) or for the reproduction of molds to form objects directly in their final shape (*electroforming*). In most cases, the metallic deposit thus obtained is crystalline; this process can therefore be called also electrocrystallization; this term was introduced by the Russian chemist V. Kistiakovski in the early twentieth century.

The electrolyte is an ionic conductor, where chemical species containing the metal of interest are dissolved into a suitable solvent or brought to the liquid state to form a molten salt. The solvent is most often water, but recently various organic compounds and other ionic liquids are being used for selected electroplating processes. This book will be concerned exclusively with electrodeposition from aqueous solutions.

The electrodeposition process consists essentially in the immersion of the object to be coated in a vessel containing the electrolyte and a counter electrode, followed by the connection of the two electrodes to an external power supply to make current flow possible. The object to be coated is connected to the negative terminal of the power supply, in such a way that the metal ions are reduced to metal atoms, which eventually form the deposit on the surface.

This chapter introduces the terms and concepts utilized in the description of the electrochemical process for metal reduction. Additionally, it includes an introductory discussion of the various concepts that will be rigorously developed in successive chapters of the book.

Y. D. Gamburg, G. Zangari, *Theory and Practice of Metal Electrodeposition,*
DOI 10.1007/978-1-4419-9669-5_1, © Springer Science+Business Media, LLC 2011

1.2 Examples of Electrocrystallization

The process of formation of a metallic coating may occur through various mechanisms and can proceed through a variety of precursors. Some representative examples of electrodeposition include the following:

1. Electrodeposition of a zinc coating onto a low carbon steel sheet for corrosion protection; this process may occur for example through the following reaction:

$$Na_2ZnO_2 + H_2O + 2e \rightarrow Zn_{met} + 2Na^+ + 4OH^- \quad (1.1)$$

The Zn-containing salt is dissolved in water to form an aqueous solution and the electrons for the reaction are provided by the external power supply.

2. Copper powder production through copper electrodeposition from dilute acidified solutions of copper sulfate:

$$CuSO_4 + 2e \rightarrow Cu_{met} + {SO_4}^{2-} \quad (1.2)$$

Also in this case, the Cu salt is first dissolved in an aqueous solution.

3. Electroforming of nickel by means of electrodeposition of nickel metal from a neutral solution based on nickel sulfamate

$$Ni(NH_2SO_3)_2 + 2e \rightarrow Ni_{met} + 2{NH_2SO_3}^- \quad (1.3)$$

4. Formation of metallic lead at the anode of a lead acid battery during charging:

$$PbSO_4 + H^+ + 2e \rightarrow Pb^0 + {HSO_4}^- \quad (1.4)$$

All electrodeposition processes have in common the transfer of one or more electrons through the electrode/solution interface, resulting in the formation of a metallic phase Me_{met}.

Metal deposition processes are and have been utilized for practical purposes in a wide variety of technical fields, ranging from metallurgy and heavy engineering industries to (more recently) microelectronics and nanotechnology. Examples of these applications include the following: gold and gold alloy deposition for electrical contacts in electronic circuits, Cu deposition for microelectronic interconnects, Ni–Fe alloys for magnetic recording heads, or the production of high purity metals. Currently, the most intensively developing branches of electrodeposition are associated with information and energy technologies, as well as microelectronics, sensors and microsystems in general. The list of materials and structures that are being produced in commercial processes or at the development stage is also very long and will be discussed in successive chapters. Suffice here to say that the length scales of commercially synthesized materials covers many orders of magnitude, going from the hundreds of meter of tin-coated strips to the 20–100 nm width of copper interconnects.

1.3 Electrode Processes. Faraday's Law

A general reaction for the process of metal formation is the following:

$$\left(M_xL_y\right)^z + nxe \rightarrow xM^0 + yL \quad (1.5)$$

L is a molecule, an ion, or radical (e.g. H_2O or CN^-) tightly bound to the metal ion M and thus forming a *complex* species $(M_xL_y)^z$ which takes part in the charge transfer process. This intermediate compound is usually named the *electroactive species*.

In Eq. (1.5) n is the net amount of electrons transferred in the overall process per deposited metal atom; this is always a positive quantity. z is the electric charge of the electroactive species in electron units; z can be both negative or positive, and may also be zero. For instance, the charge of the $[Ag(CN)_3]^{2-}$ ion is equal to -2. The electric charges of M and L are not shown in Eq. (1.5) but in the following they may sometimes explicitly indicated.

The simplest case of metal ion discharge is that of the simple (hydrated) metal ion, where $n=z$. The reaction in this case is written:

$$M^{z+} \cdot xH_2O + ze \rightarrow M^0 + xH_2O. \tag{1.6}$$

where the dot indicates an electrostatic interaction. In general however $n \neq z$, and n should not be confused with z.

Equation (1.5) shows that n electrons, i.e. a charge of ne, need to be transferred for the deposition of one atom of the metal. Consequently, the formation of one mole of the metal requires $N_A ne = nF$ coulombs of electricity (N_A is the Avogadro number $N_A = 6.022 \times 10^{23}$ mol^{-1}; $F = N_A e$ is the Faraday constant $F = 96485$ C mol^{-1}). This relationship is referred to as Faraday's Law:

$$m = QA/nF \tag{1.7}$$

where m is the deposited metal mass (grams), Q the net charge passed through the circuit (coulombs), and A the atomic weight of the metal. At constant current $Q = I\tau$, otherwise $Q = \int I d\tau$ (I is the current, τ is the duration of electrolysis).

This equation is extremely important and widely used in practice to calculate the amount of metal deposited during electrolysis, to determine the duration of electrolysis necessary to achieve a predetermined thickness, the time of charge/discharge of a battery, etc.

The electrochemical process (1.5) occurs at the interface between metal and solution; in this respect the structure and properties of this interface, as shown in successive chapters, will greatly influence the process. Faraday's Law however does not reflect said dependence, as it only relates m to Q.

1.4 Current Density

When applied to coatings, Eq. (1.7) is often used in a different form, as the dependence of deposit thickness h upon the duration of electrolysis τ and the applied current I. Taking into account that $h = m/Sd$ (S is the surface area, d is the density) and $Q = I\tau$, we obtain after rearranging

$$h = (I/S)\, A\tau/dnF, \tag{1.8}$$

or

$$h = (V_m/nF)\, (I/S)\, \tau. \tag{1.9}$$

In the last equation $V_m = A/d$ is the molar volume of the metal. This equation highlights the importance of the *current density* (*CD*) $i = I/S$.

Current density, usually expressed in amperes per square meter A m^{-2}, governs the rate of the deposition process, usually measured in mol/cm^2 s, or in microns per hour. The current density is the most practical measure for the rate of any electrochemical process since its value is readily determined from an ammeter reading and the knowledge of the electrode area *S*.

The factor $\mathbf{K}_v = V_m/nF$ is the volume *electrochemical equivalent* of the metal; it can be expressed, for instance, in cm^3/C. Sometimes it is more convenient to use the mass equivalent $\mathbf{K}_m = \mathbf{K}_v d$, which can be expressed in g/Ah. For electrodeposited coatings the one-dimensional equivalent of $\mathbf{K}_v$, i.e. $\mathbf{K}_l$ (μm/(Ah/dm^2)) is particularly convenient, since it immediately gives the thickness of a deposit in microns:

$$h = \boldsymbol{K}_l i \tau \tag{1.10}$$

if *i* is expressed in A/dm^2, and τ in hours.

The electrochemical equivalents of some metals $\mathbf{K}_v$, $\mathbf{K}_m$ and $\mathbf{K}_l$ are listed in Table 1.1. For alloy deposition one can use the equivalent calculated for alloys $K_{m(alloy)}$ which is given by

$$\mathbf{K}_{m(alloy)} = 1/\left(\omega_1/\mathbf{K}_1 + \omega_2/\mathbf{K}_2 + \omega_3/\mathbf{K}_3 + \ldots + \omega_n/\mathbf{K}_n\right). \tag{1.11}$$

In this equation ω_i and $\mathbf{K}_i$ are respectively the mass fractions and mass equivalents of the elements in the alloy. To obtain the electrochemical equivalent for the alloy in linear form it is necessary to know the alloy density. This can be found experimentally or it can be estimated approximately, for example for a two-component alloy, by

$$d_{(alloy)} \approx d_1 d_2/\left(d_1\omega_1 + d_2\omega_2\right). \tag{1.12}$$

In order to rigorously define current density it is necessary to precisely determine the *surface area S*. In fact, real surfaces are ideally smooth only in the case of liquid metals (for example mercury or an amalgam) or in monocrystalline smooth electrodes. Only in this case the geometric surface area S_g coincides with the real one S_t. In real surfaces, any roughness results in an increased true surface as compared with S_g. The ratio $k_r = S_t/S_g$ is defined as the *roughness coefficient*. For polished or high quality electrodeposited surfaces k approximates 2–3. If $k_r > 1$ a "real current density" i_r. $i_r = i_{app}/k_r$ should be used, where i_{app} is the apparent CD, calculated for the geometrical area.

Current density is usually assumed to be uniform across the surface. However, any real surface has heterogeneous properties, and electrochemical processes at solid electrodes start first at high energy sites, called active centers or growth sites. As a consequence the current density is initially highly non-uniform and its distribution tends to change during film growth; in particular, both changes in k_r changes as well as distribution and overall area of active sites should be considered.

Table 1.1 Electrochemical equivalents of some metals

Metal	K_v, cm^3/A-h	K_m, g/A-h	K_l, μm/(A-h/dm^2)
Ag	0.3837	4.025	38.37
Au(I)	0.380	7.35	38.0
Au(III)	0.127	2.45	12.7
Bi	0.1590	1.560	15.9
Cd	0.2424	2.097	24.24
Co	0.1243	1.099	12.43
Cr	0.0449	0.323	4.49
Cu(I)	0.2652	2.371	26.52
Cu(II)	0.1326	1.186	13.26
Fe(II)	0.1324	1.042	13.24
Fe(III)	0.0883	0.695	8.83
In	0.1956	1.428	19.56
Mn	0.1374	1.025	13.74
Mo	0.0670	0.597	6.70
Ni	0.1229	1.095	12.29
Pb	0.3409	3.866	34.09
Pd	0.1651	1.985	16.51
Pt	0.1696	3.640	16.96
Re	0.0472	0.993	4.72
Rh	0.1032	1.280	10.32
Ru	0.1017	1.257	10.17
Sb	0.1359	0.909	13.59
Sn	0.3033	2.214	30.33
W	0.0587	1.143	5.87
Zn	0.1711	1.220	17.11

1.5 Electrodes and Electrode Potential

The term "*electrode*" has various connotations in electrochemistry. First, the electrode is the region at which the electrochemical process of interest is occurring; depending on the current direction or the nature of the reaction, it can be the cathode (where a reduction occurs) or the anode (where oxidation occurs); in some cases an electrode can comprise both cathodic and anodic areas. Second, the electrode in a purely electrochemical sense is the half-cell element as a whole, i.e. the combination of the solid electrode and the electrolyte region in contact with the electrode, where a predetermined reaction is occurring. In some cases the reaction forms a new phase and the term "electrode" refers to a particular sequence of phases together with their interfaces. An example of electrode is the reference electrode where the equilibrium between Ag and AgCl takes place; this electrode is schematically indicated by the series of phases Ag|AgCl|KCl present at the interface.

Electrode potential is another physical variable, along with current density, controlling the electrode process. The potential φ of the electrode is the potential drop between the solution and the bulk of the metal, otherwise called the Galvani poten-

Table 1.2 Potentials of the reference electrodes

Electrode	Symbol	Potential at 298 K, mV	Temperature coef., mV/K
1 *M* calomel	$Pt\|Hg\|Hg_2Cl_2\|1\ M\ KCl$	+283	−0.24
Satur. calomel	$Pt\|Hg\|Hg_2Cl_2\|satur.\ KCl$	+244	−0.65
Silver chloride	Ag|AgCl|HCl	+222	−0.65
Mercury sulfate	$Pt\|Hg\|Hg_2SO_4\|a(SO_4^{2-})=1$	+615	−0.82
Cadmium oxide	$Cd\|CdO,\ a(OH^-)=1$	+13	

tial difference. This quantity cannot be measured experimentally since the solution potential cannot be defined operationally without introducing an additional metal/electrolyte interface, and therefore cannot be used as a reference point. For this reason in actual practice it is conventional to measure the electrode potential with reference to some other electrode having a constant, reproducible and stable potential. Various *reference electrodes* of this kind exist; the Standard Hydrogen Electrode (SHE) uses the equilibrium between H^+ and hydrogen gas to generate this potential, and is most often used as a standard. Its potential at any temperature is defined equal to zero. Electrode potential expressed relative to SHE is symbolized by the letter E.

SHE is too inconvenient to be practical; in the laboratory practice therefore one can use other reference electrodes (calomel or silver/silver chloride electrode), using other reactions to generate the potential; their potentials at different temperatures are listed in Table 1.2.

The concepts connected with electrode potentials (the problem of absolute potential drop, the rigorous definition of Volta and Galvani potentials, etc.) are of great importance in electrochemistry but are beyond the scope of the present book; pertinent information is available elsewhere [1].

Current density and electrode potential of any given electrode reaction at steady state are related to each other through a one-to-one correspondence; however, actual conditions at an electrode where a growth process is occurring are rarely stationary. For this reason a *potentiostatic process* (at $E=\text{const}$) occurs with the current density changing over time; similarly, a *galvanostatic process* ($i=\text{const}$) is usually accompanied by variations in E. Possible reasons for these changes include the following: (a) the surface state (roughness, morphology) evolves with time, and (b) composition of the solution adjacent to the electrode (concentration of chemical species, pH) can change during the process. In the initial stages of electrolysis these changes can be significant.

Along with stationary processes, dynamically changing conditions at the electrode are rather common, particularly for the investigation of electrode phenomena; most utilized are potentiodynamic procedures. These processes are usually carried out at predetermined linear sweep rate of the potential, e.g., $E=E_0+a\tau$, where a may range from 10^{-4} to 10^6 V/s, typically 10 mV/s. At very slow sweep rate, the electrochemical process under study is quasi-stationary and it is often indistinguishable from a stationary one. At very fast sweep rates the concentrations of species near the electrode cannot follow the potential change due to the limited reaction rates and

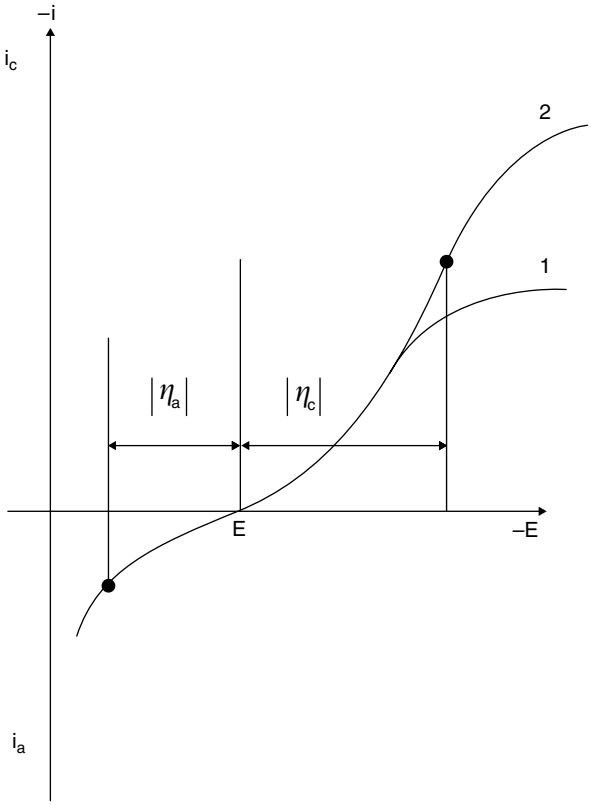

Fig. 1.1 Current–potential characteristics for a metal deposition process without agitation (*1*) and with electrolyte stirring (*2*). At high overvoltages (more negative potentials) the region of limiting current density i_{lim} is approached; i_{lim} increases by stirring. The equilibrium potential is E; cathodic η_c and anodic η_a overpotentials are also shown

the quantities of interest are often time-dependent. In general, various scan rates are necessary for the different methods used in electrode studies.

Modern studies in this field are made with experimental instruments especially built for electrochemical investigations, among which electronic potentiostats/galvanostats have a significant role and considerable capabilities. Detailed descriptions of these instruments can be found elsewhere [2]. The typical dependence of current density upon E for an electrodeposition process is shown in Fig. 1.1. This curve corresponds to copper deposition from an acidic sulfate solution. The details of the curve are discussed in the following section.

1.6 Equilibrium Potential and Overpotential

The electrode potential at which the current density i is zero assumes particular importance. If this potential corresponds to the thermodynamic equilibrium of a well defined electrode process this potential value is defined as the *equilibrium potential* of this process E_{eq}. This potential is directly determined by the thermody-

namic activity of the electroactive species in solution and is described by the Nernst equation, which in the simplest case of an equilibrium between a metal ion and a metallic electrode takes the form

$$E_{eq} = E_0 + (RT/nF)\ ln\,(a_M z+) = E_0 + (1/nf)\ ln\,(a_M z+). \tag{1.13}$$

In this equation $f=F/RT=11604/T$ (V^{-1}); $R=8.3145$ J/mol K (gas constant), and T is the absolute temperature. E_0 is called the standard potential for this process, observed under standard conditions (unit activity for all the species involved, T=298 K, and atmospheric pressure).

It is important to realize that the thermodynamic equilibrium corresponds to the condition where the observed *overall* rate for the process of interest is zero; however, this equilibrium is achieved by the balance of two partial reactions occurring in opposite directions. This very important idea was firstly stated by Ershler and Shlygin [3] where the term "*exchange current density*" i_0 was introduced to quantify the rate of these two partial processes at equilibrium. In other words, the equilibrium is a dynamic process that can occur slow or fast, depending on the characteristics of the process involved. Typically, the exchange current will be large when the energy barrier for the transformation of interest is low.

A more general form of the Nernst equation can be written for a generic electrochemical reaction:

$$\Sigma v_{ox} A_{ox} + ne \leftrightarrow \Sigma v_{red} A_{red} \tag{1.14}$$

where the v_i denote stoichiometric coefficients; the corresponding Nernst equation can be written as

$$E_{eq} = E_0 + (RT/nF)\, ln\left(\Pi {a_{\mathrm{OX}}}^{\nu(\mathrm{OX})} / \Pi {a_{\mathrm{red}}}^{\nu(\mathrm{red})}\right). \tag{1.15}$$

Very often in practice, especially for diluted solutions, the thermodynamic activities a_i are substituted by the molar concentrations c_i. It should be recalled that the activity of a pure solid phase is equal to unity; this is the reason for the absence of the corresponding term in Eq. (1.13).

In order to deposit a metal at a finite rate it is necessary to shift the electrode potential in the cathodic (negative) direction from its equilibrium value. It follows that a negative potential shift speeds up reduction processes whereas a positive shift accelerates anodic reactions (oxidation). The value of this shift is called the *overpotential* (*overvoltage*) of this process and is usually indicated by the greek letter η:

$$\eta = E - E_{eq} \tag{1.16}$$

Defined in such a manner the overpotential has a well defined sign; according to another convention however the overpotential is defined as $\eta = \left|E - E_{eq}\right|$ and is always positive, and its actual effect is determined by whether it is cathodic (η_c) or anodic (η_a).

In practical metal deposition processes the overpotential may range from few mV to more than 2 V. Its value determines the rate of the process and to a large extent the structure and properties of the deposit. Upon application of relatively high η fine grained and dense coatings are obtained. The extent of adsorption at the electrode of surface-active components from the solution, which strongly influences the deposition process and the structure of the deposit, is also determined by the electrode potential during deposition, i.e. by the overpotential.

In the following chapters we will repeatedly direct our attention to the influence of overpotential and adsorption processes on the microstructure and morphology of the deposits. Here we only underline the interesting possibility of classifying the metals according to the value of η corresponding to ordinary current densities (10–100 mA/cm^2). The first group of metals includes those having high overpotential (of the order of hundreds of millivolts): Fe, Co, Ni, Cr, Mn, Pt. The second comprises the metals with intermediate η (Cu, Bi, Zn). The overpotentials characteristic for the third group (typically low-melting elements: Pb, Sb, Ag, Sn, Cd, Tl) are low (up to tens of millivolts). This classification is closely related to the exchange current densities measured for the reduction/oxidation of these elements: high values of i_0 correspond to low overpotential and vice-versa. Metals deposited at high overpotentials are usually much more fine-grained as compared to those of the second and third groups. It should however be noted that this classification is valid only when the metal ions in solution are not bound to form complexes; in this latter case in fact it is possible to sharply increase the value of η at a given current density and correspondingly change the characteristic film morphology.

At positive (anodic) overpotential the reverse process of anodic dissolution occurs. If the process of metal deposition is performed using a soluble anode from the same metal as the counter electrode then the voltage U between cathode and anode is equal to the sum $|\eta_c|+|\eta_a|$ plus the ohmic drop in the solution:

$$U = |\eta_c| + |\eta_a| + IR \tag{1.17}$$

Finally, it should be noted that it is not always necessary to apply a potential negative to the redox potential of the metal under study in order to achieve metal deposition; a metal can be deposited at potentials more positive than the equilibrium one, due to strong interactions with the substrate material. This phenomenon is referred to as *underpotential deposition* (upd, [4]). This phenomenon, very interesting both for electrodeposition and for electrocatalysis will be considered later.

1.7 Mixed Potential

The equilibrium potential is achieved only when the influence of other electrochemical processes occurring in parallel with the reaction of interest can be neglected. If this condition is not satisfied the zero current condition corresponding to a situation of macroscopic equilibrium is achieved at a different potential, often named the steady-state, rest or mixed potential E_r. For instance, if several direct and

reverse electrode processes occur simultaneously, then in the absence of external power sources the potential assumes spontaneously the value at which the net current is zero. Under this condition, no single process is in equilibrium, and each one proceeds at a non-zero rate. Corrosion processes often occur under these conditions. The actual value of the mixed potential depends on the relevant reactions and on electrode surface conditions, for example roughness, the presence of adsorbed species and/or films produced by corrosion processes, etc.

1.8 Potential–Current Curves (Voltammograms)

The potential–current density (*E–i*) relationships for generic electrochemical reactions are also called voltammograms, *polarization curves*, or current–potential characteristics, and are of fundamental importance in electroplating. The theory of the functional dependence of *i* vs. *E* is presented in Chap. 3. These curves (see for example Fig. 1.1) can be derived experimentally or theoretically and show clearly the key features of various electrochemical processes. As a consequence, they are extensively used in general electrochemistry and particularly in investigations of metal deposition.

Potential–current density characteristics for two different processes occurring simultaneously at an electrode are shown in Fig. 1.2. Two electrochemical processes can occur in the electrodeposition of a pure metal from aqueous solutions when the applied cathodic potential is sufficient to induce the reaction of hydrogen evolution. Equilibrium potentials of the two processes are shown in the figure along with values of current densities ("*partial current densities*" and overall current den-

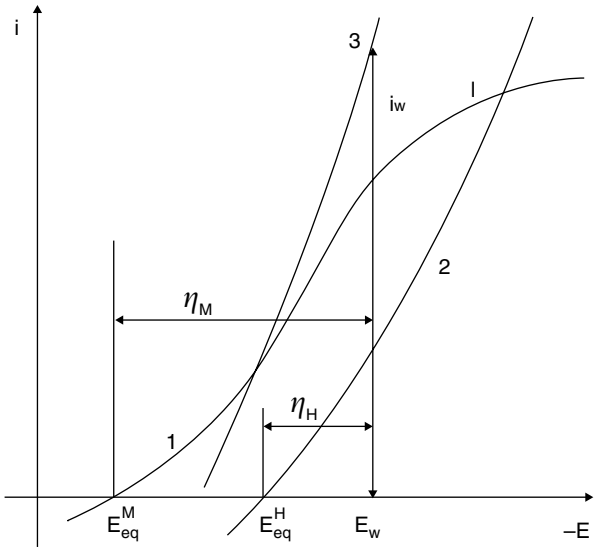

Fig. 1.2 Current–potential characteristics for simultaneous metal deposition (*1*) and hydrogen evolution (*2*). *1* and *2* are the partial current curves, and *3* represents the experimentally measured total current. Cathodic overpotentials η_1 and η_2 for both processes are shown along with equilibrium potentials and the working potential E_W

sity) and overpotentials. We emphasize that hydrogen evolution is very important in electroplating as atomic hydrogen can be incorporated in the deposit and/or into the substrate and impact their properties. Only a small fraction of the hydrogen evolved is incorporated in the metal, while the most part evolves in gaseous form.

An experimental *E–i* relationship is obtained by successively imposing various values of the electrode potentials and measuring the corresponding values of current density; after a rapid switch of potential from one value to another a certain time (about 10–100 s) is needed to stabilize the current. In an alternative experimental set-up it is also possible to impose a set of current values and measure the corresponding potentials; the first method is called potentiostatic, the second galvanostatic. The two curves can be different, especially when processes of inhibition at the electrode surface occur, causing the appearance of maxima in the *i* vs. E curve. In addition, potentiodynamic and galvanodynamic measurements (including cyclic ones), where the potential or current change continuously with time, can be performed and are often used. The shape of dynamic *E–i* curves depends on the sweep rate; some electrochemical methods are based on this dependence.

The derivative of the potential with respect to current density $dE/di = d\eta/di$ (i.e. the slope of the *E–i* curve) is designated *polarizability*. This quantity is relevant in the analysis of the uniformity of current distribution throughout the electrode surface. As a rule, the higher the polarizability, the more uniform the current distribution is; as a consequence the thickness of the metal deposited becomes more uniform. The electrode for which $d\eta/di \to \infty$ is identified as an *ideally polarizable* electrode. This idealized electrode is important in the theory of current distribution. The electrode having $d\eta/di \to 0$ on the other hand is called non-polarizable. The values of polarizabilities for several plating processes are given in Table 1.3.

The overpotential of any process depends strongly on the deposition conditions: solution composition and pH, temperature, electrolyte stirring, etc. Two methods can be used to compare *i–E* characteristics obtained under different conditions. For example, consider curves 1 and 2 in Fig. 1.1, obtained experimentally for the same reaction with and without solution agitation. It can be said that at the same potential the current density CD for curve 2 is higher than for curve 1; it can also be said however that at the same CD the deposition potential in curve 2 is decreased; both

Table 1.3 Polarizabilities of several electrolytes (averaged values)

Metal	Type of the electrolyte	Polarizability, Ohm cm^2
Ag	Cyanide	20–24
Cd	Stannate	12–14
Cd	Sulfate	1.3–1.5
Cu	Sulfate	2.2–2.5
Cu	Cyanide	11–16
Cu	Pyrophosphate	10–15
Fe	Sulfate	1.7–2.0
Ni	Sulfate	4.0–4.5
Zn	Sulfate	1.5–1.8
Zn	Zincate	8–10

statements are equivalent. The decrease in CD (η increase) is described as an *inhibition* of the process, while the decrease of η (CD raise) is called *depolarization*.

1.9 Current Efficiency

In most practical processes the overall current (charge) is consumed in part for side processes occurring in parallel with metal deposition. In this case it is important to determine the relationship between the current densities of the two or more parallel processes occurring simultaneously at some predetermined potential.

Side reactions can be of various nature. As already noted, hydrogen evolution may occur as the result of water electrolysis:

$$2H_3O^+ + 2e = H_2 + 2H_2O \tag{1.18}$$

Besides, deposition (co-deposition) of another metal can take place:

$$M_2{}^{z+} + ze \rightarrow M_2{}^0 \tag{1.19}$$

Furthermore, partial reduction of metal ions is possible, for example:

$$Fe^{3+} + e \rightarrow Fe^{2+}, \tag{1.20}$$

and finally, the reduction of surface oxide layers can occur, such as

$$M_xO_y + 2yH_3O^+ + 2ye \rightarrow xM + 3yH_2O \tag{1.21}$$

along with some other reactions, some of which can be purely chemical in origin.

If the second process is the deposition of another metal, evaluation of the current density for the two processes is closely related with the composition of the depositing alloy, considering that the ratio of the molar concentrations of the two metals in the alloy is proportional to the corresponding current densities. When other side reactions proceed, the ratio between the partial current of the process of interest i_p and the overall current is called "*current efficiency*" CE:

$$CE = i_p/\Sigma_j i_j = Q_p/\Sigma_j Q_j. \tag{1.22}$$

The current efficiency is often expressed in percent.

Practical determination of CE in electroplating processes is performed by both pre- and post-electrolysis weighing of the sample on an analytical balance in parallel with precise determination of the charge passed (by means of an electronic current integrator or by using an ammeter and a stop-watch). The current efficiency is equal to the ratio of the actual deposit mass Δm to its theoretical value calculated from Faraday's Law:

$$CE = \Delta m/(QA/nF). \tag{1.23}$$

Table 1.4 Cathodic efficiencies in some electrolytes

Metal	Type of the electrolyte	Average cathodic efficiency
Ag	Cyanide	0.98
Au	Citrate	0.60
Au	Phosphate	0.95
Cd	Cyanide	0.90
Cd	Sulf.-ammonia	0.90
Co	Sulfate	0.88
Cr	Chromate	0.18
Cu	Sulfate	1.00
Cu	Cyanide	0.75
Cu	Pyrohosphate	0.99
Fe	Chloride	0.90
Fe	Sulfate	0.92
Fe	Fluoroboric	0.95
Ni	Sulfate	0.96
Ni	Sulfamate	0.98
Pb	Fluoroboric	0.99
Pd	Amino-chloride	0.80
Re	Sulf.-ammonia	0.25
Rh	Sulfate	0.70
Sb	Citrate	0.94
Sn	Stannate	0.80
Sn	Pyrophosphate	0.90
Sn	Sulfate	0.95
Zn	Cyanide	0.80
Zn	Sulfate	0.97

When the CE value for a specific process is already known, one can input this value into the formula of Faraday's Law, to determine the actual deposit thickness

$$h = \mathrm{CE} \cdot K_l i \tau. \tag{1.24}$$

The values of CE can differ widely for different metal deposition processes of metal. CE depends on the metal, the solution type, temperature, current density, pH and so on. Commercial processes usually have relatively high CE; the tentative and averaged values for some processes are listed in Table 1.4.

The dependence of CE upon current density for several processes is depicted in Fig. 1.3; it can be noticed that CE may either rise or fall with current density.

1.10 The Various Steps Occurring in Electrode Processes. Fast and Slow Steps

The overall process of electrochemical metal deposition is complex and can be divided into sequential steps. Together with one (or more) charge transfer process(es), other steps such as chemical reactions, mass transfer and crystallization occur.

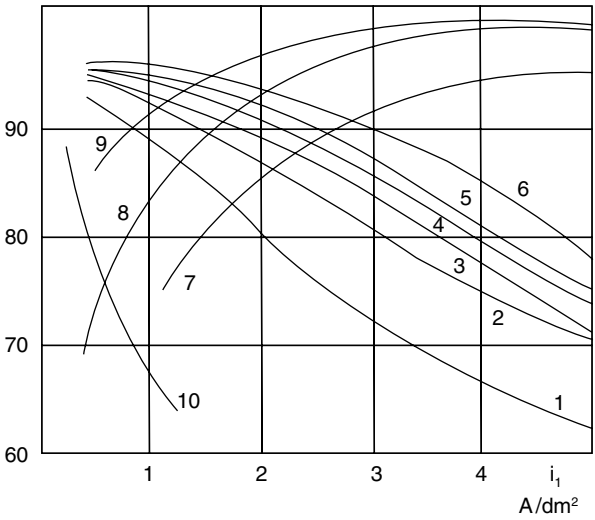

Fig. 1.3 The dependence of cathodic current efficiencies on current density for various metal deposition processes. *1* copper (cyanide solution), *2* cadmium (cyanide), *3* copper (pyrophosphate), *4* tin (stannate), *5* antimony (citrate), *6* zinc (cyanide), *7* iron (sulfate), *8* nickel (sulfate), *9* zinc (sulfate), *10* gold (citrate)

Chemical steps occurring near the electrode may involve ion dehydration or ligand dissociation.

Consumption of electroactive species at the electrode is balanced by mass transfer, which occurs by diffusion, convection and electric migration from the bulk of solution. Mass transfer of reducible species to the electrode is therefore the first step of the overall deposition process. Near the electrode the electroactive species may be dissociated from the ligand and/or dehydrated; in parallel, charge transfer occurs and the (partially) reduced metal atoms adsorbs at the growing surface. Finally, adsorbed ions or metal atoms (adions or adatoms) diffuse across the surface to active growth sites, where they are incorporated into the crystal lattice of the deposit, resulting in its growth. These steps are schematically shown in Fig. 1.4.

A generic multi-step process can be schematically represented as a chain of elementary reactions, as follows:

$$\mathrm{A} \overset{1}{\rightarrow} \mathrm{B} \overset{2}{\rightarrow} \mathrm{C} \overset{3}{\leftrightarrow} \mathrm{D} \overset{4}{\rightarrow} \mathrm{M} \tag{1.25}$$

where A represents the initial state of the electrochemical system (the ion is located in the bulk of the solution, the electrons in the crystal lattice), and M is its final state, namely the metal atom in the crystal lattice. B etc. are intermediate states of

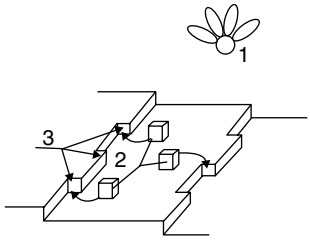

Fig. 1.4 The fundamental steps of electrodeposition at an electrode surface. *1* hydrated ions in the solution, *2* ions (atoms) at the surface while they diffuse to the surface steps, *3* kinks at the step (growth sites)

the system. At the steady state the rates of all steps 1–4 are the same and correspond to the measured current density.

Some of the steps 1–4 (for instance step 3) can be at equilibrium, that is the rates of the forward and reverse steps $C \leftrightarrow D$ are much larger than the rate of the overall process. Steps of this kind are called reversible, and may also be designated as "*fast steps*" to highlight the difference with the other steps.

Each step can simultaneously occur forward or backward; the observed rate is the difference between these rates. For an electrochemical process, the exchange current density from Sect. 1.6 has the same characteristics of the equilibrium rate of reversible electrochemical steps. At steady state the net rate for all steps are equal; however it is not so for the partial rates of the forward and reverse processes.

The partial rates (forward and reverse) of the fast steps are nearly the same and they both are much faster than the overall rate. By contrast, the rate of a slow step in the forward direction is close to the rate of the overall process; its rate in the reverse direction is much lower, and often can be neglected. The slowest steps are often said to be rate-determining or limiting. Sometimes there are two or more rate-determining steps in the overall process.

The measured value of overpotential is closely related to the rates of the various steps. In most cases the overall overpotential can be divided up into several parts, each determined by and corresponding to a given step:

$$\eta = \eta_1 + \eta_2 + \eta_3 + \ldots \tag{1.26}$$

The limiting step does not necessarily give the largest contribution to η. In experimental studies of electrochemical processes such portioning of the overpotential is helpful but it is not universally correct and requires strictly specified methods [5]. At high overvoltages the value of η is predominantly due to diffusion processes, while at low overvoltages it is for the most part due to charge transfer.

The step-wise nature of electrochemical processes is often reflected in the shape of current vs. potential plots. For example, if diffusion is the limiting step the curve shows an asymptotic part, designated as the "*limiting current*" (Fig. 1.1).

1.11 Electrolytes Used for Electrodeposition

In principle, metal deposition is possible from simple solutions of some salt or other soluble compound containing the metal in the form of cation, anion or complex (electrically charged or uncharged). For instance, deposition of copper from acidic solutions occurs through hydrated cations Cu^{2+} (and—at a much lower concentration—Cu^{+}); silver in commonly employed solutions is present as a complex $Ag(CN)_x$ where x is from 1 to 3. Nickel in acetic acid solutions forms $Ni(CH_3COO)^{+}$ ions.

One component solutions are however rarely used in practice since they do not provide high quality deposits. Electrolytes used in practice do contain some additional compounds, each playing a specific role.

To increase the electrical conductivity of the solution, inorganic acids or alkali are added; more conductive electrolytes permit to decrease voltage (and therefore

save energy) and to increase the uniformity of deposit thickness. Substances taking no part in electrode processes are called "*supporting electrolytes*". Moreover, acids and alkali are also used for adjusting pH; the standard recipes of plating solution compositions indicate optimum pH values. Acidity has to be stable and constant throughout the entire bath (the cell volume) including the region near the electrode; this is achieved by addition of buffering agents (e.g. boric acid in nickel deposition).

Buffering is especially necessary when hydrogen evolution occurs because the latter leads to higher pH near the electrode as a consequence of H^+ consumption, resulting eventually in metal hydroxide precipitation. The value of acidity near the electrode can differ from that of the bulk by several pH units.

Along with these most important components, so-called 'additives' are also widely used in practice. An example of this sort of substances are surfactants added to the solution to decrease the surface energy of the electrode and facilitate the detachment of hydrogen bubbles from the surface. Adhesion of hydrogen bubbles to the electrode leads to undesirable 'pitting', that is the occurrence of macroscopic point defects (pits or pores) at the plated surface.

Other surface-active agents are widely used in metal deposition. These are often very specific for each process; some substances, very useful for the deposition of one metal may be useless or harmful for other processes. Without these substances the deposition process is possible but their presence enhances the properties of deposit and thickness uniformity. Additives can be classified as: 'brighteners' (allowing the production of bright deposits without post-deposition polishing), or 'levellers' (filling pre-existing scratches or pits and smoothening the surface). Additionally, some additives contribute to decrease internal stresses in the deposit, activate anode dissolution, increase current efficiency, suppress dendrite formation, etc. The additives usually inhibit the deposition (η increases), as it is shown in Fig. 1.5.

The concentration of additives in the plating solutions is usually between 10^{-4} and 10^{-2} moles per liter, but some of them can influence the deposition process at much lower concentrations. The mechanism of their action is based predominantly

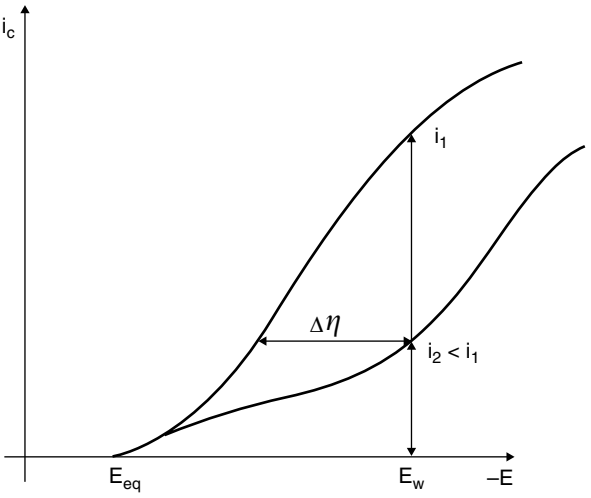

Fig. 1.5 A generic current–potential characteristics: *1* without inhibition, *2* with inhibition. i_2/i_1 is the inhibition extent, $\Delta\eta$ is the additional overpotential at i = const

on adsorption at the electrode surface, resulting in much higher surface concentration as compared to the solution bulk. Additive concentration decreases in the course of plating as a result of incorporation by the growing deposit or following decomposition at the cathode. Therefore periodic correction of each additive concentration is necessary.

1.12 The Influence of Deposition Parameters on Electrodeposition Processes

In addition to current density and electrode potential, other parameters and process conditions such as solution temperature, pH, concentration of reacting species, substrate and parasitic processes such as hydrogen evolution, may influence the electrodeposition process.

Temperature T is one of the most important. The operation temperature is ordinarily in the range from 15 to 70°C. In some cases (e.g. the autocatalytic deposition of Ni–P alloy) T may be as high as 99°C. Elevated temperatures provide some advantages: solubility and electric conductivity improve, and the tendency for anodic passivation decreases. High T on the other hand tends to accelerate solution evaporation and corrosion processes, limiting the practical temperatures achievable. Additionally, an increase in T stifles additive adsorption, decreasing their efficacy; as a consequence, deposits become more coarse-grained.

A low solution temperature requires a drop in current density (and in growth rate) in order for deposition not to occur under diffusion limiting conditions. Lower temperatures slow down diffusion kinetics, often resulting in stressed deposits, prone to embrittlement. In different instances the role of temperature may vary, since each process has its own optimum operating temperature. With regard to temperature control, in most cases a deviation of ±3°C from the optimum one is acceptable; however, some processes, in particularly at the laboratory scale, require rigourous temperature control.

Temperature has also an influence on rate processes; typically, a temperature increase by 1°C results in a 10% increase in the rate of electrochemical processes, and in an enhancement in the rate of mass transfer by 2%.

The material and the surface finish of the *substrate* influence the deposition process, particularly in the initial plating stages. This is due to the fact that the nucleation rate on the substrate differs from that on the freshly plated deposit. In some cases, particularly when the substrate is free of oxides and with a crystal structure similar to that of the deposit, the substrate influence may propagate up to a thickness of about 10 μm. A smooth, mechanically polished substrate has a minimal influence on film growth, whereas chemical etching enhances such influence.

The nature of the substrate also determines the type of surface treatment (solutions for cleaning, degreasing, chemical or electrochemical etching) necessary to remove surface films and/or contaminants and insure good adhesion. This important aspect may sometimes be overlooked, but it is essential to enable the formation of a continuous, high quality coating with good adhesion.

The deposition process and deposit properties depend also on the *concentration of reacting (electroactive) ions*. Depositing from dilute solutions at a given potential results in more fine-grained coatings and lower deposition rate. Cations and anions present in the solution which do not participate in electrode reactions can nevertheless influence the electrodeposition process through their adsorption to the substrate, the change in ionic strength and of the solution conductivity.

In most cases *stirring* of the solution is desirable since it enhances ion transport to the substrate and decreases the thickness of the diffusion layer. Stirring is performed by mechanical (magnetic) stirrers or by compressed air. Ultrasound stirring is very effective. Stirring by itself does not change the characteristics of the resulting deposit but shifts the optimum CD to higher values.

Solution pH also plays an important role because of its influence on CE, hydrogen evolution and hydroxides precipitation. pH dictates bulk electrochemical equilibria and the relative concentration of the various compounds formed by the electroactive species.

Hydrogen evolution may occur in parallel to metal deposition, particularly during the deposition of transition metals; this results in the formation of hydrogen bubbles and in stirring of the solution near the electrode. The rate i of the hydrogen reaction is described by the Tafel equation

$$E = a + b \ln i, \tag{1.27}$$

where *ln* stands for the natural logarithm, and the coefficients a and b (characteristic of the reaction and the substrate) are tabulated and can be found elsewhere [5]. The coefficients b ("*Tafel slopes*") are close to 0.12 V per decade for most metals, whereas a values may differ widely. Using Eq. (1.27) the rate of hydrogen evolution on different substrates can also be calculated if the potential is known.

During the initial stage of deposition (seconds to minutes) hydrogen may evolve at the substrate. If the hydrogen evolution reaction has low overpotential (or low Tafel coefficient a) on the substrate then hydrogen is produced predominantly, current efficiency of metal deposition is low and only after production of a thin deposit the current efficiency of metal electrodeposition increases. This happens e.g. for zinc deposition on steel. At said initial stage hydrogen concentration can reach saturation on a thin electrode layer and then can diffuse into the substrate resulting in its embrittlement and other unwanted side effects [6]. The hydrogenation of the substrate may continue later while hydrogen evolves in the pores of the thin deposit or by diffusion through the coating.

1.13 Electric Conductivity of Solutions

The electric conductivity is one of the most important properties of electrolytes. Conductivity depends on concentration and mobility of the component ions. The conductivity of very dilute solutions can be written as

$$\kappa = \kappa_1 + \kappa_2 + \ldots + \kappa_n, \tag{1.28}$$

where κ_n are the conductivities of the ionic components at their concentrations in the mixed solution. This rule is however unsuitable for commercial solutions, due to interactions of the ionic components with one another or with water molecules; in this case, the conductivity of the solution is not equal to the sum of the conductivities due to the single ionic species. It is therefore simpler in practice to measure the real conductivity of a given solution instead of calculating it. Conductivity measurements are important for deposition processes since κ determines both the deposition voltage and the uniformity of metal distribution.

The numerical values of conductivity of different commercial plating baths are of the same order of magnitude; at room temperature an acidic copper solution has conductivity κ (in $\mathrm{Ohm^{-1}\ m^{-1}}$) of about 15–25 whereas for nickel solutions it averages 3–7, for chromium solutions 40–60, for acidic zinc and cadmium solutions 5–10, for cyanide copper, zinc and cadmium solutions 6–16. Each particular solution has a specific composition, so these data are averaged; in any specific case precise measurements are needed. If the conductivity is known at a given temperature, its value at another temperature is readily calculated considering that a temperature rise of 1°C increases κ of approximately 2%. This strong dependence is one of the reasons for requiring careful temperature control.

Conductivity changes may also occur due to the presence in the solution of small nonconductive particles or gas bubbles; in such a case one can calculate the effective conductivity value as approximately

$$\kappa = \kappa_0(1 - \varepsilon)^{1.5}, \tag{1.29}$$

κ_0 being the conductivity of the pure solution, and ε the volume fraction of the nonconductive phase.

The measurements of conductivity are performed in specific cells made of chemically resistant glass and provided with electrodes of platinized platinum (Fig. 1.6) with alternate current techniques at a relatively high frequency. The cell conductance (in $\mathrm{Ohm^{-1}}$) is first measured for a solution having a well-known specific conductivity (usually a KCl solution), then the solution is exchanged with the one of interest and the measurement is repeated. The ratio of cell conductances in the two cases is equal to that of the corresponding conductivities.

Knowing the solution conductivity it is possible to calculate the ohmic resistance R of the electrodic system in the electrolyte of interest. For two parallel flat electrodes, each with an area S and at a distance l:

$$R = l/\kappa S, \tag{1.30}$$

Fig. 1.6 An electrochemical cell for conductivity measurements. *1*, *2* platinum electrodes

for two coaxial electrodes with radii r_1 and r_2 and height h

$$R = (2\pi h\kappa)^{-1} ln\,(r_2/r_1), \tag{1.31}$$

for n spherical electrodes with radii r and overall surface area $S = 4\pi r^2 n$, if they are at a distance a from a larger counter electrode ($a \gg r$):

$$R = r/\kappa S. \tag{1.32}$$

In the common case when various objects with an overall surface S are located at an average distance l from the counter electrode

$$R = kl/\kappa S \tag{1.33}$$

with k being about 1–2.

Once the value of R is known, one can calculate the voltage U of the cell at the current I using Eq. (1.17):

$$U = IR + \eta_c + \eta_a.$$

1.14 Composition, Structure and Properties of Deposits

Metal deposition processes occurring in parallel with the process of interest result in the incorporation of impurities in the deposit; when the addition of other metals occurs purposely, an alloy deposit is formed. Growth of the deposit may also result in the incorporation of any component present in the near-electrode region of the solution; these processes mat be beneficial or harmful to the deposit properties and should be monitored. Present-day physical methods for example allow the determination of most chemical elements in the deposit without resorting to sophisticated chemical analysis.

If some component is codeposited electrochemically (i.e. as a result of charge transfer) its concentration in the deposit is determined by the Faraday's Law and is proportional to its partial current density. On the other hand, the incorporation rate of adsorbed species which occurs by motion of the growth front is proportional to their coverage and depends on the residence time of said species on the surface. This incorporation mechanism is characteristic for molecules of most additives and auxiliary compounds present in the electrolyte. Hydrogenation of the deposit is also a codeposition process, characterized by its own trends.

The structure of the deposit is characterized first of all by its grain size and shape. The size of crystallographic grains is determined by X-ray diffraction studies, while the grains observed by electron or optical microscopy may be composed of assemblies of grains that cannot be resolved by microscopy methods. Other defects, such as point defects, twins and stacking faults can be characterized by transmission electron microscopy. Crystallographic orientation of deposits can be determined by use of X-ray diffraction methods.

In addition to said characteristics, metallographic studies are used to reveal morphological features such as columnar or layered crystal growth and/or distinctive type of deposits consisting in non-oriented randomly packed small grains. Surface morphology can be examined also by scanning electron microscopy, enabling the observation of various features such as pyramidal, step-wise or spheroid types of surface shapes which can sometimes be related to the interior structure of the deposit.

When studying the substrate influence on deposit structure it is common to specify whether epitaxial growth is exhibited and the maximum deposit thickness to which it may propagate. Above this thickness the deposit structure becomes usually determined completely by the deposition conditions and not by the substrate.

The characterization of alloy deposits involves in addition a determination of their phase composition. In the case of alloys it is necessary to determine (by X-rays analysis) whether the deposit is a solid solution, or a mechanical mixture of crystals of the components, or an intermetallic compound. These data are then compared with thermodynamic phase diagram of the alloy with the same chemical composition [7]. As a rule, phase composition of electrodeposited alloys may differ from that of the equilibrium state (for instance, of the annealed metallurgical alloy). The formation of supersaturated solid solution for example is often observed.

Of special interest is the structure of deposits with bright surface; the literature on this subject is quite extensive [8]. In most cases, bright deposits are observed when the grain size is much smaller than the wavelength of visible light, but there are exceptions to this rule. Once more, X-rays methods and microscopy at high magnification are very useful in this respect to relate surface morphology, grain size and orientation to the degree of brightness.

One further problem that can be tackled with structural studies is the degree of porosity of deposits and its dependence on substrate, deposit thickness and deposition conditions.

Finally, we briefly survey the topic of the physical properties of electrodeposited metals.

Metal purity and structure depend on a number of factors, which also affect the physical characteristics of the deposits. This concerns both mechanical (strength, ductility, hardness, adhesion to substrate) and electrical (conductivity, contact resistance) properties, and in the case of iron group metals also their magnetic properties (magnetization, coercive force). An example is the dependence of the specific electrical resistance on current density and temperature (Fig. 1.7).

Variations of deposit properties are partly due to changes in microstructure; in particular, to the influence of grain boundaries. The segregation of impurities at these boundaries and their structure, e.g. dislocations density or disorientation angle, are of particular importance. The relative volume of boundaries increases strongly in fine-grained metal.

High internal stress is one of the peculiarities of electrodeposited metals and alloys [9]. Internal stresses may be distinguished in macroscopic and microscopic. Macrostresses are similar to thermal stresses arising in bimetallic plates as a consequence of changes in temperature, but have a more varied nature. Just to illustrate

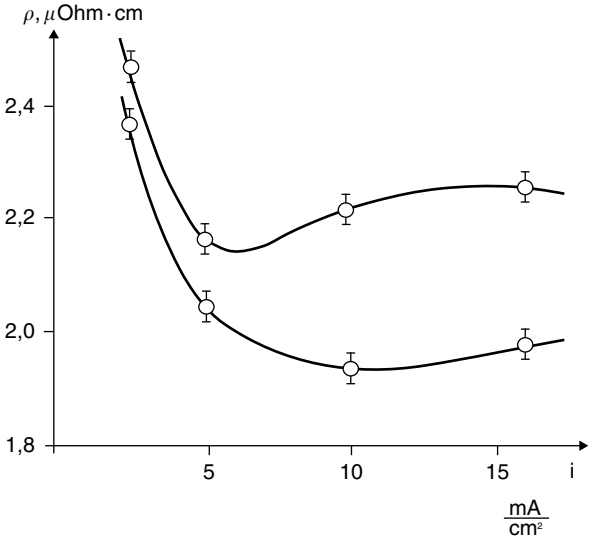

Fig. 1.7 Resistivity of copper deposits obtained from a pyrophosphate solution vs. applied current density. Temperature: 20°C and (the lower curve) 50°C

the character of these stresses, consider stretching a rubber film and sticking it in this state to a solid substrate; tensile stresses will be present in the rubber foil, and compressive ones in the surface layer of the substrate. Electrodeposited films may exhibit either tensile (positive) or compressive (negative) stresses. The numerical value of macrostresses may be as much as several hundred MPa.

Microstresses are caused by distortions of the crystal lattice at the atomic level and in general cannot be characterized with any sign, since different regions of a lattice can be either compressed or expanded. They are usually treated as microstrains and are measured by the ratio of the dimensional change of the lattice constant with respect to the original value.

Electrodeposits having high tensile macrostresses (chromium, nickel) can crack resulting in a net of cracks on their surface (Fig. 1.8).

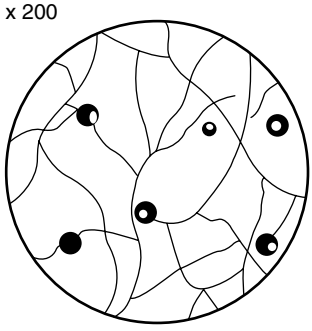

Fig. 1.8 Scheme of nickel deposits cracking. The lines show the cracks, the rounds are the pits generated by hydrogen bubbles

Additional physical properties may also be important when the deposits are obtained for different functional purposes; examples of such properties are the friction coefficient, wear resistance, and corrosion resistance.

1.15 Current and Metal Distribution

Current distribution throughout the electrode is one of the most important features of electrochemical processes. Since in the case of electrodeposition the metal growth rate is proportional to the current density, this problem is connected with the deposit thickness uniformity. For example, regions at the cathode that are farther spaced from the anode usually have a lower CD; correspondingly, thinner deposit are obtained for an equivalent deposition time.

Current distribution is classified in microscopic and macroscopic, and is designated respectively as microdistribution and macrodistribution. The former indicates the distribution of current at the scale of surface roughness, surface defects such as scratches or areas with micrometer scale (Fig. 1.9). Microdistribution is relevant when dealing with very small features or with the overgrowth of small imperfections. The term macrodistribution on the other hand refers to the current distribution at the overall electrode (or at the whole plated surface, Fig. 1.10).

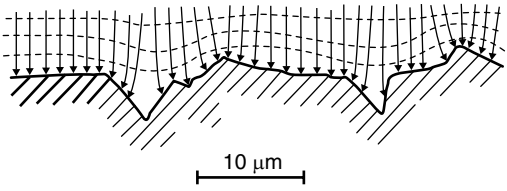

Fig. 1.9 Cross-sectional view of a rough surface and the corresponding current distribution in the adjacent solution

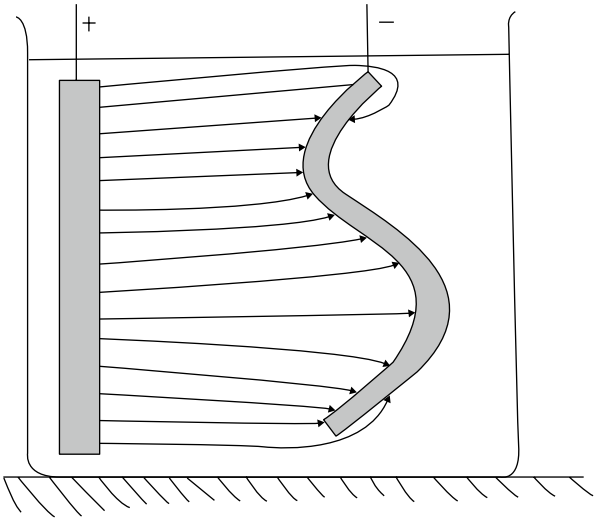

Fig. 1.10 Current distribution throughout the overall electrode

Current distribution may differ from metal distribution when the current efficiency is non-uniform across the electrode surface.

The problems of current and metal distribution are intimately related with the concepts of throwing power and leveling action of the electrolytes, which will be discussed in detail in Chap. 8. There the terms “primary”, “secondary” and “tertiary” distributions will be defined and the link of metal distribution to the polarizability and solution conductivity will be discussed.

The development of various techniques to improve metal distribution (for example by the use of screens, auxiliary cathodes and anodes, etc.) is of great importance in practical electrodeposition processes; this issue is also considered in Chap. 8.

Macro- and microdistribution may widely differ. For example, the macroscopic current distribution may be uniform within a given electrode area, while the presence of microridges and microvalleys in the same area may generate an inhomogeneous distribution of CD over the same area. If, as usual, CD is higher at a ridge, the metal coating will grow faster than the remainder of the surface, and thus the film roughness would increase.

1.16 Anodic Processes

For electric current to flow through the electrochemical cell the overall electrical circuit should be closed; therefore, an additional electrode (the anode) is also immersed in the solution and connected with the positive pole of the power supply.

Both soluble and insoluble anodes are used in electrodeposition. For example, the electrodeposition of copper, nickel zinc, silver and many other metals is performed usually with soluble anodes, whereas chromium, gold, palladium, etc. require insoluble anodes.

Soluble anodes play an additional role beyond completion of the electrical circuit: they are the sources of the metal ions which are being consumed (deposited) at the cathode. For this to occur, when electrodepositing for instance nickel, nickel anodes should be used.

Soluble anodes work under an active regime of dissolution. Metallic ions transfer immediately to the solution, although not always in the electroactive form active in the cathodic reaction. Anodic dissolution takes place at potentials more positive (anodic) than the equilibrium one. Sometimes dissolution is hindered by the formation of salt layers at high dissolution rates, or as a result of very high viscosity near the anode; anodic current efficiency in active dissolution remains however close to 100%.

Anodic passivity occurs in some cases at high anodic potentials. This phenomenon consists in the formation of a poorly conductive layer on the surface; this causes an increase in local current density at several surface sites, resulting in the attainment of a critical potential of passivity. Under these conditions a thin inert film is formed on the surface, resulting in a sharp decrease in current density. This phenomenon is undesirable in electrodeposition. In some cases chloride or fluoride

ions are used to maintain the anodes in the active state; most often however it is sufficient to design the anode to ensure a sufficiently low anodic CD.

At the surface of insoluble anodes oxygen evolves or other oxidation processes may take place. Periodic corrections of electrolyte composition are therefore needed when employing insoluble anodes.

References

1. Overbeek J.Z.G., Colloid Science, v. 1, Kruyt, ed., Elsevier,1952, pp. 115 – 193
2. Bard A.J., Faulkner L.R., Electrochemical methods, Fundamentals and Applications. John Wiley & Sons, 2001
3. Dolin P., Ershler B., Frumkin A., Acta Physicochimica URSS, 13, 779 (1940)
4. J.O'M.Bockris, A.K.N.Reddy and M.Gamboa-Aldeco, "Modern Electrochemistry", 2nd edition, Volume 2A, Kluwer Academic/Plenum Publishers, 2000
5. Vetter K.J. Elektrochemische Kinetik. Springer – Verlag, 1961, s. 177
6. Jewett, R.P. (1973). Hydrogen Environment Embrittlement of Metals. NASA CR-2163.
7. Hansen M., Anderko K. Constitution of binary Alloys. McGraw-Hill, 1958
8. Hoar T.P., Trans. Inst. Metal Finishing, 1953, v. 29, p. 302
9. Armyanov S., Sotirova G., Surface Technology, 1982, v. 17, p. 321, 1983, v. 20, p. 175

Chapter 2
The Structure of the Metal-Solution Interface

2.1 Introduction: Spatial Separation of Electric Charge

The electrodeposition of metals or alloys occurs within a spatial region of finite thickness at the interface (or, more precisely, an interphase) between the growing material and the solution. The structure of this region, in particular the distribution of ions, solvent molecules and other uncharged species, and the resulting distribution of electric charges and potential, has an important bearing on the interface energy of the system, the nature and rate of charge transfer processes, and on the processes of nucleation and growth of metallic crystals. In general, charge separation occurs at this interface as a result of the different nature of the mobile charges in the two regions considered: electrons in the solid and ions in the electrolytic solution. The electronic charge distribution in the electrode extends into the solution farther than the charges generated by the ionic cores, and this excess of charges must be balanced by an opposite charge in the electrolyte. In the simplest approximation this separation of charges can be thought of as a parallel arrangement of opposite charges; for this reason, this region is also called *double layer*.

Many comprehensive and thorough discussions of the double layer are available in the literature [1]; our objective in this chapter is limited to a discussion of how and why the double layer influences the deposition process and how quantitative calculations of the properties of interest can be performed using experimental data. Practitioners in the area of electrodeposition often underestimate the role of double layer and surface phenomena in the electrode processes; here we try to highlight this role.

The presence of a metal/electrolyte interface not only results in charge separation, but also makes it possible for the exchange of charged particles between the two phases to occur: electrons and metallic ions may enter the solution, while ions transfer to the metal surface and may adsorb there. As a result of these processes an interfacial region is generated, which includes both charged and uncharged (dipolar or multipolar) species. The name electrical double layer (for brevity Double Layer, DL) underlines that the positively and negatively charged layers become spatially separated. More precisely, regions are formed having predominantly positive or negative charges.

Y. D. Gamburg, G. Zangari, *Theory and Practice of Metal Electrodeposition,*
DOI 10.1007/978-1-4419-9669-5_2, © Springer Science+Business Media, LLC 2011

Upon immersion of an electrode in an electrolyte, the DL forms by rearrangements of surface charges. An important characteristic of the DL is the potential drop $\Delta\varphi$ between the solid and electrolyte phases. Experimentally the presence of a DL is manifested as an electrical capacitance at the interface. In other words, the rearrangement of charges can be modeled as an electrical capacitor made up of oppositely charged conductors placed at the metallic and electrolyte sides, respectively, which generate a potential drop. The capacitance of the DL is usually of the order of $C_{DL} \approx 0.1\mathrm{Fm}^{-2}$. Since maximum values of $\Delta\varphi$ are about 1 V, this corresponds to a charge density of about 0.1 C/m^2 or 10 μC/cm^2.

It is necessary to distinguish between the real interface structure and the various models developed to simplify quantitative calculations of the DL properties. Usually the real system is modeled by replacing the discrete charge distribution with a continuous medium, and the dipole layer of the solvent with a continuous dielectric.

In order to describe current flow through the electrochemical cell, the complicated system of atoms, electrons, ions and molecules is replaced by a set of capacitors and resistors connected in a predetermined order (*equivalent circuit*), Fig. 2.1, which reproduces the electrical response of the real system. In this equivalent circuit, each element has its real equivalent; refinement and improvement of the model circuit can be achieved by comparison of the theoretical and experimental electrical responses at different frequencies. The overall impedance (i.e. complex resistance) of the system is measured in a wide range of frequencies (from 10^{-2} to 10^6 Hz), and the analysis of the data set permits to extract substantial amount of information on C_{DL} and other electrochemical quantities [2].

The value of capacitance C_{DL} is of immediate practical importance when imposing currents or voltages at the interface. For example, a step-like variation of the voltage applied at an electrode results in an exponential transient of the resulting current, which achieves a new steady state value only after a time of the order of the time constant $\tau = \mathrm{R}\cdot C_{\mathrm{DL}}$, where R is the equivalent resistance of the interface. In other processes of interest, an Alternating Current (AC) $I(t) = I^0 cos\,(2\pi ft)$ may be superimposed to a constant current during metal deposition. At high frequencies this superimposed current does not influence the electrode processes. The reason is that DL charging by the superimposed AC current occurs over a finite time, of the order of:

$$\tau = (RT/nF) \cdot C_{DL}/I^0 \tag{2.1}$$

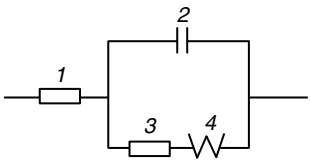

Fig. 2.1 Equivalent circuit of the electrode. The double layer capacitance (*2*), charge transfer resistance (*3*) and diffusion impedance (*4*) along with the Ohmic electrolyte resistance (*1*) are taken into account

where $RT/nF = 25.7/n$ mV at 25°C. The quantity τ must be less than $1/f$, otherwise the alternate current will be damped due to DL charging and discharging. It follows that the condition

$$f < (nF/RT) \cdot I^0/C_{DL} \tag{2.2}$$

determines the upper frequency limit that can be utilized to study double layer processes.

A change in the potential drop across the DL by using an external power source results in a change of the charge density at both the liquid and solid surfaces; under certain conditions the charge may even change sign, from negative to positive or vice versa. The electrode potential φ_M^0 at which this change in the sign of surface charge occurs is termed *Potential of Zero Charge* (PZC); its value depends on the chemical identity of the electrode and on the chemistry of the solution. This situation corresponds to the absence of free charges on the surface. Among other contributions, the difference between the actual electrode potential and the PZC determines the nature of the species adsorbing at the surface: at more negative potentials positively charged species are adsorbed, and vice versa. It is essential in practical electrodeposition processes to predict which species adsorb at various electrode potentials since these substances may influence the process. Values of PZC for some metals are given in the Table 2.1.

From the experimental viewpoint, the DL may be characterized by measuring its capacitance as a function of electrode voltage. Various models of the DL have been

Table 2.1 Zero charge potentials

Metal	Solution	ZCP, Volts
Ag	0.0025 *M* Na_2SO_4	−0.67
Au	Calculated value	+0.20
Bi	0.002 *M* KF	−0.39
Cd	0.001 *M* NaF	−0.75
Co	Calculated value	−0.40
Cr	Calculated value	−0.45
Cu	0.01 *M* NaF	+0.09
Fe	Calculated value	−0.35
Ga	0.01 *M* $HClO_4$	−0.69
Hg	0.01 *M* NaF	−0.193
In	0.003 *M* NaF	−0.65
Ni	Calculated value	−0.25
Pb	0.001 *M* NaF	−0.56
Pd	0.05 *M* Na_2SO_4 + 0.001 *M* H_2SO_4	+0.26 (full charge)
Pd	0.05 *M* Na_2SO_4 + 0.001 *M* H_2SO_4	+0.10 (free charge)
Pt	0.03 *M* HF + 0.12 *M* KF	+0.235 (full charge)
Pt	0.03 *M* HF + 0.12 *M* KF	+0.185 (free charge)
Sb	0.002 *M* $KClO_4$	−0.15
Sn	0.00125 *M* Na_2SO_4	−0.43
Zn	Calculated value	−0.60

developed to describe the observed experimental behavior; they are discussed in the following. These models are able to describe and predict also other DL characteristics, such as volume and surface charge density, potential distribution and interface energy. Capacitance data in particular enable the determination of the extent of adsorption of ions and organic substances (Sect. 2.4).

2.2 Compact Part of the Double Layer: Helmholtz Layer

An electric charge q_m at the metal surface in contact with the solution is induced by the excess or deficiency of electrons in the surface layer. This charge must be compensated by an equal and opposite charge $q_2 = -q_m$ at the solution side; q_2 is provided by ions present in the solution layer adjacent to metal surface.

The simplest model of DL consists of two charges q_m and q_2 distributed on two parallel planes, separated by a dielectric layer of solvent molecules (dipoles); in this model the charges are assumed to be point-like and spaced by a distance x_o, determined by the size of the solvation sheath generated by the solvent dipoles between the ionic layer and the metal surface; this region is of the order of 0.3 nm.

This model is referred to as compact DL or Helmholtz layer. It describes rigorously the DL structure at the interface of concentrated solutions and normal metals. It is similar to the familiar electric capacitor with one of the "plates" being liquid. The development of this concept is due to Helmholtz and Kohlrausch.

The capacitance per unit area of said capacitor is

$$C_1 = \varepsilon_0 \varepsilon_1 / d \tag{2.3}$$

where d is the distance between the charged planes; if the origin is placed at the metallic surface, then $d = x_o$; ε_0 is the permittivity of free space.

In Eq. (2.3) ε_1 is the relative permittivity in the region between the two charged layers; this space is filled by dipole molecules of the solvent but, due to the limited mobility of these dipoles, its permittivity is much less than that of the free solvent and assumed to be constant in $0 < x < d$.

The electric potential within the DL varies linearly since no volume charge is present. At each point x

$$\varphi(x) = \varphi_0 + q\,(x_0 - x)\,/\varepsilon_0 \varepsilon_1 \tag{2.4}$$

where φ_0 is the potential at the plane where the ionic charges are located.

The outlined model is a strong simplification of the real structure and severely limited in its predictive capabilities. In order to improve on this model it is important to list such limitations, as follows.

1. The actual electron density in the metal near the interface cannot change sharply but does so gradually. As a result, the charged metal layer has a finite thickness of about 0.1 nm, and the charge distribution depends on the nature of the metal; semimetals and semiconductors for example are characterized by a much wider

distribution of the electronic charge. Moreover, the electron density decreases exponentially in the solution region adjacent to the metal surface, causing a non-linear drop of potential in the DL.

The penetration depth of the electric field into the metal (the Thomas–Fermi length l_{TF}) is given by

$$l_{TF} \approx \left(\varepsilon_0 E_F / e^2 n_e\right)^{1/2} \tag{2.5}$$

where E_F is the Fermi energy of the metal, and n_e its electronic density. Typical values are 5 eV and 10^{29} m^{-3}, respectively, giving for $l_{TF} \approx 0.05$ nm. In the case of semiconductors l_{TF} can be 2–4 orders of magnitude higher. It is apparent from this result that the metallic plate of the capacitor is not localized at the interface but has a finite thickness; this will affect the actual value of the capacitance.

2. The value of the relative dielectric constant ε_1 depends on the properties of metal and solvent and on the electric field in the DL, and is in fact a function of both metal and solution. Also, the thickness d in Eq. (2.3) is obviously not identical to x_o; whereas x_o is the minimum distance of the ions centers from the metallic surface, d corresponds to the thickness of the layer having said specific value of ε_1 [3, 4].

   Interestingly, the overall C_1 does not depend on solution concentration [5] (up to concentrations of about 0.1 M) but only on q: a change in q implies a change in ε_1/d.

3. Finally, the Helmholtz model assumes that the ions in the solution are frozen in a predetermined configuration; this is true only at the absolute zero temperature. At any other temperature, thermal motion should be considered; this is discussed in the next section.

2.3 Diffuse Layer: Gouy-Chapman Layer

At any finite temperature, the thermal motion of the ions results in a shift of the center of charges from the fixed plane considered above, thus delocalizing the charge distribution. Part of the ions move from the surface into the bulk of solution, generating a volume charge distribution, or a *diffuse layer.*

The diffuse layer consists of ions of both signs, with one sign being present in some excess, which gradually reduces with increasing distance from the electrode (Fig. 2.2). It is common to represent the ionic atmosphere as a continuum characterized by a charge density ρ function of position, its integral value (the overall charge) being q_2. The permittivity of this medium is equal to the bulk value of the solvent. This region conventionally starts at a distance x_o from the electrode; closer to the electrode charged particles are absent.

The interface between the compact and diffuse layers is called *Outer Helmholtz Plane* (OHP). This plane can be thought of as the location where the point-like

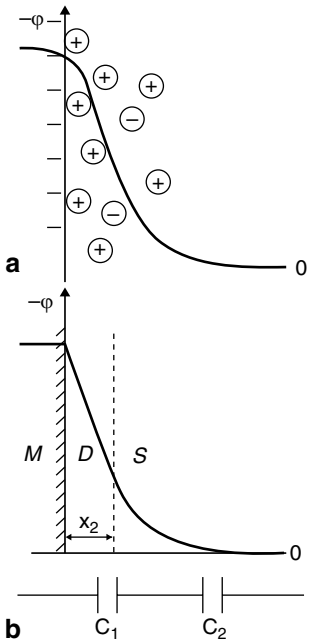

Fig. 2.2 Distribution of the electrical charge and potential in the case of diluted solution. **a** compact and diffuse layers: *M* – metal, *D* – dielectric, *S* – solution; **b** the electric model of the double layer with compact and diffuse parts

charges adsorbed on the electrode at zero temperature are concentrated; while some models assume that a certain charge is located at this plane also at finite temperature, other models consider that the surface charge is zero at the plane itself, and that the OHP represents the boundary between the double layer, where no charge is present, and the diffuse layer, with a finite volume charge density q_v. In this latter depiction, for $x<x_o q_v=0$ while for $x\geq x_o |q_v|>0$, gradually decreasing in the direction of the solution bulk. Due to the sharp change in the medium properties at the OHP, this model requires a discontinuous jump in permittivity. This discontinuity in permittivity is unrealistic; as a consequence, while the model often describes adequately the potential and charge distributions in the DL, such description cannot be completely rigorous.

The overall capacitance C_{DL} (or, for simplicity, C) of the system consisting of the compact and diffuse layers is determined by the series capacitances of the two layers, C_1 and C_2 as [6]:

$$C^{-1} = C_1^{-1} + C_2^{-1}, \text{ or } C = C_1 C_2 / (C_1 + C_2) \tag{2.6}$$

From the electrostatic standpoint this picture is analogous to placing in the plane x_o a conductive non-charged plate. This introduces no changes to the charge and potential distribution and is needed only to develop a model with two capacitors. Actually these two capacitors model the dense layer and the diffuse layer, respectively (Fig. 2.2). The charge of the latter is distributed across a finite thickness.

The capacitance C_2 can be determined by calculating the potential distribution in the diffuse layer. This was first accomplished independently by Gouy and Chapman, approximately 100 years ago; the calculation is based on the assumption that the position of the ions is determined by a Poisson–Boltzmann distribution and has an important standing in electrochemistry; this is why we include here the corresponding derivation.

Assuming point-like ionic charges, the volume charge density can be written as an algebraic sum of all the ionic charges:

$$\rho = \Sigma c_i z_i F = F \Sigma c_i^0 z_i \exp(-z_1 f \varphi) \tag{2.7}$$

When c_i is expressed in moles per liter, ρ is in Coulombs/liter. The local concentration of ions i is assumed to depend on the local potential as $c_i(\varphi) = c_i^0 \exp(-z_1 f \varphi)$; this corresponds to assuming that i) only electrostatic forces are important, and ii) the electrostatic field is not influenced by the ion under consideration.

The volume charge density ρ is related to the potential φ by the Poisson equation $d_2\varphi/dx^2 = -\rho/\varepsilon_0\varepsilon$; together with Eq. (2.7) this gives

$$d^2\varphi/dx^2 = -(F/\varepsilon_0\varepsilon)\, \Sigma c_i^0 z_i \exp(-z_1 f \varphi)\,. \tag{2.8}$$

Here, f=F/RT.

We consider here a one-dimensional configuration, where the field changes only normal to the surface. Contrary to Eq. (2.3), ε is now the bulk dielectric permittivity of the solution. Equation (2.8) has the form $\varphi'' = f(\varphi)$; it can be integrated using a standard method, by multiplying both sides with $2\varphi' dx = 2d\varphi$, therefore obtaining exact differentials.

As a result of the integration two quantities are obtained. The first is the potential φ as a function of distance from the OHP; for a symmetrical z, z-charged electrolyte (that is, an electrolyte obtained by dissolution of a $A^{z+}B^{z-}$ salt), $\varphi(x)$ is given for x>x_o by the Stern formula [7]:

$$\varphi = 4z^{-1} f^{-1} \arctan\{\tan(z f \varphi_o/4) \cdot \exp[(x_o - x)/\lambda_D\} \tag{2.9}$$

φ_o is the potential at the OHP, $\lambda_D = |z|^{-1} F^{-1} (RT\varepsilon\varepsilon_0/2c)^{\frac{1}{2}}$ has the dimensions of a length and is termed *Debye length*. When q_m=0 this is the length at which the potential falls by e≈2.7 times (for x>$2x_o$ Eq. (2.9) corresponds practically to an exponential decrease as shown in Fig. 2.3).

For nonsymmetrical electrolytes the solutions of Eq. (2.8) can also be derived by the method of the auxiliary functions of φ [8].

The second result of the integration is a relationship between φ_o and q_2:

$$(q_2)^2 = 2RT\varepsilon\varepsilon_0 \Sigma c_i^0 \left[\exp(-z_1 f \varphi_o) - 1\right] \tag{2.10}$$

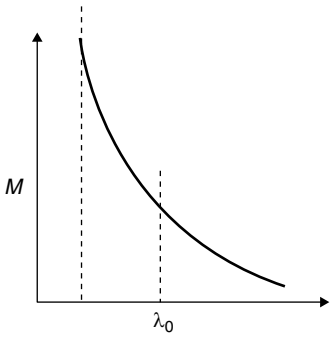

Fig. 2.3 Potential decay in the diffuse layer. λ_0 – Debye length, *M* – metal, *D* – compact layer (dielectric), *S* – solution

or for a *z,z*-electrolyte

$$q_2 = q_D \sinh (zf\varphi_o/2) \tag{2.11}$$

where $q_D = (8RTc\varepsilon\varepsilon_0)^{1/2} = 2\varepsilon\varepsilon_0/(\lambda_0 |z| f)$; this quantity has the dimensions of a charge per square meter and can be called *Debye charge*. In other reference books a different notation is often used: $A = {}^1/_2 q_D$.

The overall charge consists in the sum of cationic charges

$$q_2^{(+)} = q_D \left[\exp (-zf\varphi_o/2) - 1\right] \tag{2.12}$$

and of anionic charges

$$q_2^{(-)} = q_D \left[\exp (-zf\varphi_o/2) - 1\right]. \tag{2.13}$$

Furthermore, φ_o can also be expressed in terms of q:

$$\varphi_o = 2z^{-1} f^{-1} \operatorname{arcsin} h\, (q_2/q_D)\,. \tag{2.14}$$

This very important expression has two limiting cases: when $q_2 \ll q_D$

$$\varphi_o = 2q_2/|z| f q_D = q_2 \lambda_D/\varepsilon\varepsilon_0 \tag{2.15}$$

and when $q_2 \gg q_D$

$$|\varphi_o| = \text{const} + (2/zf)\, ln\, |q_2| - (1/zf)\, lnc \tag{2.16}$$

Equation (2.16) permits to find the capacitance of the diffuse layer as $C_2 = dq_2/d\varphi_o$:

$$C_2 = {}^1/_2 |z| f q_2 cosh\, ({}^1/_2 zf\varphi_o) = (\varepsilon\varepsilon_0/\lambda_D)\, cosh\, ({}^1/_2 zf\varphi_o) \tag{2.17}$$

or, as a function of charge:

$$C_2 = {}^1/_2 |z| f (q_2 + q_D)^{1/2} \tag{2.18}$$

We can see from Eq. (2.15) that $\varphi_o = 0$ when $q_2 = 0$. Under these conditions also $q_m = 0$, i.e. the metal surface is at its zero charge potential. At $q_m = 0$, C_2 goes through its minimum:

$$C_2 = {}^1\!/_2 |z| f q_D = |z| F (2\varepsilon\varepsilon_0 c/RT)^{1/2} = \varepsilon\varepsilon_0/\lambda_D \tag{2.19}$$

This minimum becomes deeper the more diluted is the solution.

The above formulae give the capacitance of the diffuse layer; the total C_{DL} may be measured experimentally, and then the capacitance of the dense layer is obtained as

$$C_1^{-1} = C^{-1} - C_2^{-1}, \tag{2.20}$$

If C_1 does not depend on potential then C_{DL} has its minimum at the same potential as C_2, i.e. at the PZC. In reality, in symmetric electrolytes as $c \to 0$ the minimum in C_{DL} is obtained at the PZC [6]. In most cases the minimum is somewhat shifted from the PZC (Fig. 2.4). Curves of this sort are obtained with low melting metal electrodes such as Hg, Pb, Cd, Bi, Ga etc.

Considering the diffuse layer as a conventional capacitor with $C = C_2$ and permittivity ε it is possible to determine its equivalent thickness λ; i.e., by placing the overall charge at this distance from the OHP we obtain a capacitor with the same capacitance. When $q_2 = 0$ this thickness is equal to

$$\lambda = \varepsilon\varepsilon_0/C_2 = |z|^{-1} F^{-1} (RT\varepsilon\varepsilon_0/2c)^{1/2} \tag{2.21}$$

This coincides with the Debye length λ_D. At $q_2 \neq 0$

$$\lambda = \lambda_D / ch\,(|z| f\varphi) \tag{2.22}$$

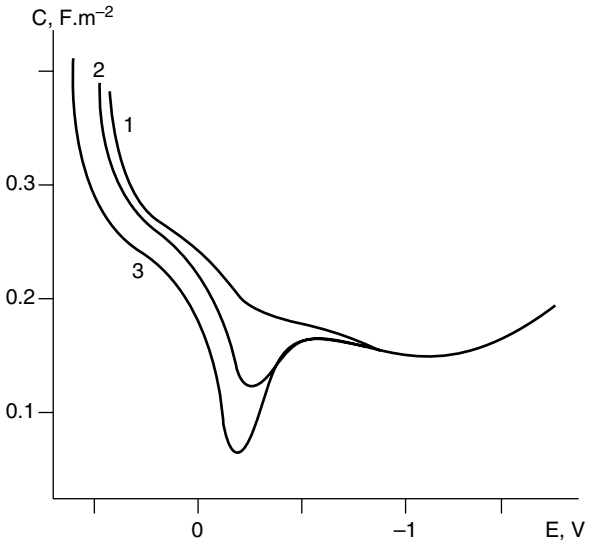

Fig. 2.4 Differential DL capacity at mercury in NaF solutions: *1* 0.1 M, *2* 0.001 M. The minima are close to PZC

As the concentration and/or q increase, λ_D diminishes. In concentrated solutions $\lambda_D \to 0$ and the overall volume charge concentrates near the OHP; in this case the model of two capacitors in series simplifies to that of a compact layer. In this limiting case the charge of the "liquid plate" is attributed to the OHP.

2.4 Adsorption at Electrodes

Before proceeding further, it is necessary to discuss the process of adsorption of electrolyte species at the electrode. Several types of adsorption phenomena and the corresponding interactions should be considered, namely: (a) the adsorption of surface-active substances, (b) the adsorption of ions (including specific adsorption), (c) the adsorption of electroactive species: reagents, products and intermediates, and (d) the formation of adsorbed ionic or molecular layers.

The thermodynamic analysis of adsorption is based on the *Gibbs adsorption equation*; this description is most general and is independent of any model of the interface. At the boundary between two phases 1 and 2, the thermodynamic properties of these two phases change gradually across the boundary. Assume that this transition occurs within a narrow region 3 between 1 and 2 (Fig. 2.5), which is bounded by the planes I and II; the thickness of this region is of molecular dimensions. In this region the concentrations of the various species differ from those in the regions 1 and 2. For each species i we define the "surface excess" Γ_i as the excess of the surface concentration (number of moles n_i per unit area A) of component i in the region 3 relative to 1 or 2. The planes I and II are named the Gibbs planes, and $\Gamma_i = n_i/A$ is referred to as "adsorption" (moles per unit surface). In the case of adsorption at a metal electrode from solution only one Gibbs plane is necessary since the second one coincides with the metal surface.

Under conditions of constant temperature and pressure (conditions characteristics of electrochemical systems) the Gibbs adsorption equation has the form

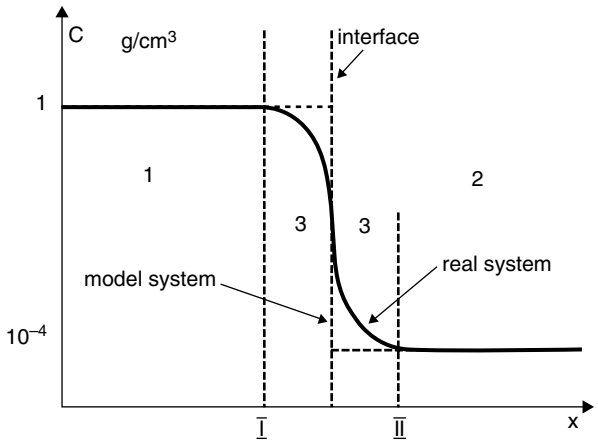

Fig. 2.5 Intermediate region (3) between the phases 1 and 2

$$d\gamma = -\Sigma_i \Gamma_i d\mu_i, \tag{2.23}$$

In particular, for a two-component system

$$d\gamma = -\Gamma_1 d\mu_1 - \Gamma_2 d\mu_2. \tag{2.24}$$

Another important equation is the Gibbs–Duhem equation for the chemical potential:

$$x_1 d\mu_1 + x_2 d\mu_2 = 0 \tag{2.25}$$

In these equations γ is the solid/electrolyte interface energy, and x_i is the molar fraction of the component i in the solution. The Gibbs Eq. (2.23) may be considered as the surface analogue of Eq. (2.25).

If we consider Eq. (2.23) for the case of a solute (sol) and the solvent (water) it is possible to write

$$\mathrm{d}\gamma = -\Gamma_{sol}\mathrm{d}\mu_{sol} - \Gamma_w \mathrm{d}\mu_w \tag{2.23'}$$

and, assuming that Γ_w is zero, this simplifies further to

$$\mathrm{d}\gamma = -\Gamma_{sol}\mathrm{d}\mu_{sol} \tag{2.23''}$$

This equation relates the adsorption of a solute species to the change in interface energy of the electrode; the driving force for adsorption is therefore a decrease in interface energy.

The extent of adsorption of the various species in general depends on the concentration of the species in solution and on the interactions between these species. A different set of assumptions will therefore result in different forms for the adsorption isotherms, describing the dependence of adsorption of a certain species on the above variables.

2.4.1 Model Adsorption Isotherms

2.4.1.1 The Langmuir Isotherm

The simplest and most commonly used adsorption equation, suitable for the description of both gas adsorption and adsorption from solutions is the *Langmuir isotherm*

$$Bc = \theta / (1 - \theta), \tag{2.26}$$

which relates the electrode coverage $\theta = \Gamma/\Gamma_\infty$ by a certain species to the concentration of that species in solution, c. Γ_∞ is the limiting adsorption when $c \to \infty$, and B is a constant. This equation can also be written as:

$$Bc = \Gamma / (\Gamma_\infty - \Gamma). \tag{2.27}$$

In many cases the limiting adsorption Γ_∞ is equal to the number of active electrode sites per unit surface n_s/N_A, but this correspondence may not always be cor-

rect; a large molecule for example may occupy several active centers, and then $\Gamma_\infty \neq n_s/N_A$. The adsorption constant B depends on temperature, and in the case of electrochemical systems also on the electrode potential.

The kinetic derivation of the Langmuir isotherm equation is well known; the constant B is derived as the ratio of the rate constants for adsorption and desorption. Both rates are equal at equilibrium, therefore:

$$K_{ads} c\,(1-\theta) = K_{des}\theta$$

and:

$$K_{ads} c / K_{des} = \theta/(1-\theta)\,, \tag{2.28}$$

or

$$B = K_{ads}/K_{des}. \tag{2.29}$$

The Langmuir equation however can also be derived without resorting to any kinetic considerations, only on the basis of thermodynamic and statistical methods. In this way, it can be found that the value of B depends on the adsorption energy ΔG_{ads}:

$$B = B_o \exp(-\Delta G_{ads}/RT); \tag{2.30}$$

this expression separates explicitly the temperature dependence from the dependence on the electrode potential (as will be seen later, ΔG_{ads} depends on potential).

Obviously, in the Langmuir isotherm the value of B does not depend on the coverage θ. This isotherm is usually considered valid only for localized adsorption, i.e. when the species are adsorbed at fixed sites; in the case of adsorption from solution however this feature has limited significance because adsorption is actually a replacement process: the solute substitutes for the molecules of the solvent at the surface. At low concentrations this isotherm becomes the linear Henry isotherm, whereas at sufficiently high concentrations of the adsorbed substance $\theta \to 1$.

The adsorption isotherm corresponds to a two-dimensional equation of state for the interface energy: $\Delta\gamma = f(T, \theta)$, that generalizes the usual three-dimensional equation of state $P = f(T,V)$. The quantity $\Delta\gamma$ is the change in interface energy upon adsorption. This two-dimensional equation of state can be derived using the Gibbs adsorption isotherm for one component. By approximating the thermodynamic activity with the concentration:

$$d\gamma = -\Gamma d\mu = -RT \cdot \Gamma d\ln c. \tag{2.31}$$

Combining this equation with the Langmuir equation leads to

$$d\gamma = -RT\Gamma\theta d\ln(\theta/(1-\theta)) \tag{2.32}$$

(B = const, and then $d\ln B = 0$).

After integration, and taking $\gamma_o = \gamma\ (\theta = 0)$

$$\gamma - \gamma_o = \Delta\gamma = -RT\Gamma_\infty \ln(1-\theta)\,, \tag{2.33}$$

This result is obtained through a change of variables: $\theta/(1-\theta)=z$, or $\theta=z/(1+z)$, from which

$$d\gamma = -RT\Gamma_\infty z/(1+z)\cdot dz/z = -RT\Gamma_\infty dz/(1+z),$$

and then

$$\int d\gamma = -RT\Gamma_\infty \int dz/(1+z), \text{ or} \tag{2.34}$$

$$\gamma = \gamma_o + RT\Gamma_\infty \ln(1+z) = \gamma_o - RT\Gamma_\infty \ln(1-\theta). \tag{2.35}$$

This two-dimensional equation of state for the Langmuir isotherm describes the ideal two-dimensional adsorbed layer, whose behavior corresponds to that of the ideal gas.

2.4.1.2 The Frumkin Isotherm

In the three-dimensional case a deviation from the ideal gas law is usually taken into account by the Van der Waals equation of state, in which two coefficients *a* and *b* are included. For N particles in the system this equation has the form:

$$\left(p + aN^2/V^2\right)(V - bN) = Nk_BT. \tag{2.36}$$

The coefficient *a* takes into account interparticle interactions. A statistical analysis shows that *a* can be expressed as

$$a = 2\pi \int |u| r^2 dr, \tag{2.37}$$

where $u(r_{ik})$ is the interaction energy between particle pairs, and the integration is carried out for all the pairs in the system. Then the total variation of potential energy (as compared with that of the ideal gas) is proportional to $N(N-1)$, which at high N can be approximated by N^2.

The same procedure can be generalized to take into account pair-wise interactions in the two-dimensional case. The resulting correction must be proportional to the square of the number of the adsorbed species, and it can therefore be expressed in terms of coverage as $a\theta^2$.

This derivation was first performed by Frumkin in 1926. He wrote the corrected equation as:

$$\Delta\gamma = -RT\Gamma_\infty ln(1-\theta) + a\theta^2, \tag{2.38}$$

the quadratic dependence resulting from taking into account all the interacting particle pairs.

The combination of this new equation of state with the Gibbs adsorption equation results in the *Frumkin adsorption isotherm*:

$$Bc = [\theta/(1-\theta)]\, exp(-2a\theta). \tag{2.39}$$

The quantity B, as in the Langmuir isotherm, depends on temperature and electric potential. As experiments have shown, this is true also for the value of a, which is called *attraction constant*. $a<0$ describes repulsive interactions, whereas $a>0$ corresponds to attractive interactions between the adsorbed species.

The Frumkin isotherm is most frequently used in the coverage range $0.2<\theta<0.8$. This is one of the most widely used adsorption isotherms in electrochemistry, particularly to describe the adsorption of surface-active organic molecules at electrodes. This isotherm takes into account the variation of the adsorption energy (enthalpy) at varying coverage, the reason for this dependence being the lateral interactions existing in the adsorbed layer.

2.4.1.3 The Stern Isotherm

The Stern isotherm generalizes the Langmuir isotherm to the case of electrically charged species. It does not take into account any lateral or dipolar interactions, but includes the work done on the charged species to transfer them from $\varphi=0$ to the potential φ. In this case the adsorption energy ΔG_{ads} can be written as

$$\Delta G_{\text{ads}} = \Delta G_0 + z_s F\varphi. \tag{2.40}$$

Thus the "adsorption constant" B depends in this case not only on temperature and on the specific chemical energy of adsorption ΔG_0 but also on the potential φ. The resulting isotherm takes the form

$$\mathrm{B_o} exp\left(-\Delta G_0/\mathrm{RT} + z_s F\varphi_i/\mathrm{RT}\right) \mathrm{c} = \theta/\left(1-\theta\right), \text{or} \tag{2.41}$$

$$\mathrm{Bc} = \theta/\left(1-\theta\right) exp(-z_s F\varphi/\mathrm{RT}) \tag{2.42}$$

This equation is a simplified form of a more complicated expression originally derived by Stern for the adsorption of two different species.

2.4.1.4 Adsorption, Double Layer Capacitance and Interfacial Tension

The Gibbs adsorption isotherm does not consider explicitly any effect linked to charges and electrostatic fields. These effects can be included however by substituting the chemical with the electrochemical potential, or, equivalently, by taking into account the work $z_s F\varphi_i$, in a similar way as it was done in the derivation of the Stern isotherm:

$$d\gamma = -\Gamma d\mu - q d\varphi \tag{2.43}$$

where $q = d\gamma/d\varphi$.

This relates the dependence of the interface energy on potential to the surface charge and can be rewritten in terms of the interface capacitance C_{DL}:

$$d^2\gamma/d\varphi^2 = -dq/d\varphi = -C_{\text{DL}} \tag{2.44}$$

Assume C_{DL} is constant (this is valid under the Helmholtz or the linear Gouy-Chapman approximation, or far away from the PZC). Integrating this relationship we obtain:

$$q = -C_{DL}\,(\varphi - \varphi_{PZC}) \tag{2.45}$$

$$\gamma = -C_{DL}(\varphi - \varphi_{PZC})^2/2 + \gamma_{PZC},\ \text{or} \tag{2.46}$$

$$\gamma_{PZC} - \gamma = C_{DL}(\varphi - \varphi_{PZC})^2/2. \tag{2.47}$$

This shows that γ is maximum at the PZC, and that under the approximation of constant C_{DL}, it changes quadratically with potential. Experimental results agree with this prediction, as shown for example in Fig. 2.6, depicting the capacitance and interfacial tension vs. applied potential for NaF solutions. In this figure, it should also be noted that the PZC remains approximately unchanged with electrolyte concentration.

These predictions however fail when adsorption of anions occurs at the surface. Figure 2.7 shows for example the measured capacitance and interface energy for KBr solutions. In this case, no clear minimum in the capacitance is observed, and at potentials positive with respect to the PZC the capacitance increases to very high values, of the order of 200 μF/cm^2. The interface energy still follows an approximately parabolic behavior, but the PZC shifts to negative values with increasing electrolyte concentration.

Finally, Fig. 2.8 illustrates an example of adsorption of neutral molecules. Neutral molecules can adsorb due to their polar nature or due to local, specific interactions. The capacitance is very small in the range of potentials corresponding to the adsorption of the neutral molecule, due to the fact that no change in surface charge occurs at potentials where the molecule is adsorbed. Peaks in capacitance are observed at the potentials where the molecules desorb. The interface energy correspondingly shows a deformed parabolic behavior.

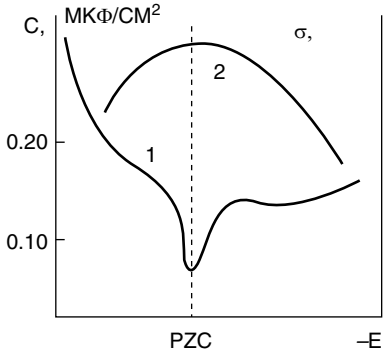

Fig. 2.6 Capacitance (a) and surface energy (interfacial tension) measured for NaF solutions

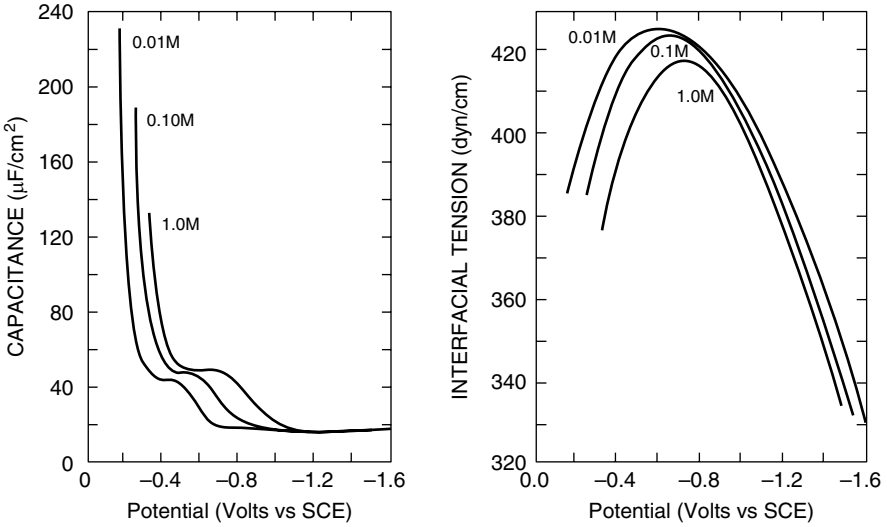

Fig. 2.7 Differential capacitance and interfacial tension for aqueous KBr solutions. (Adapted from E. Gileadi "Interfacial electrochemistry: an experimental approach" Addison-Wesley (1975))

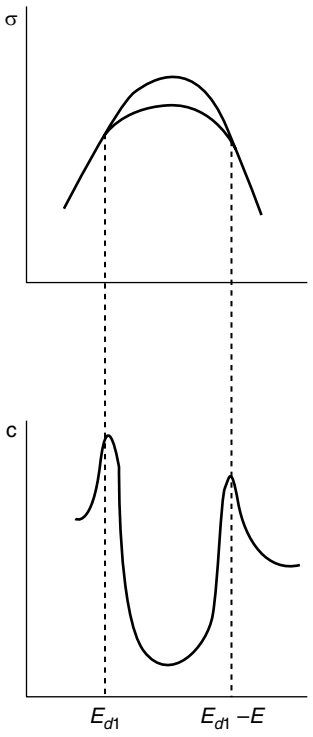

Fig. 2.8 Adsorption of neutral molecules: electrocapillary curve and capacity

2.5 Specific Adsorption

Now we return to the Gouy–Chapman model and consider ion adsorption in detail. Most ions upon adsorption can approach the electrode surface only up to the Outer Helmholtz Plane (OHP). Some of the ions in solution however actually approach the metal surface at a distance closer than the OHP; this may occur as a consequence of partial dehydration or when the ion interacts with the surface not only through electrostatic forces but also for example by forces of chemical origin. In such case these species form a *specifically adsorbed* layer*;* under the assumption of point-like species, this is located at a distance x_i from the electrode surface, where $x_i < x_o$. This distance determines the *Inner Helmholtz Plane* (IHP), hence the index *i*. Different species may in principle have different x_i, but usually only one inner plane is considered. This extended model of the double layer was introduced by Grahame.

In the following chapters we will discuss the process of charge transfer through the interface. During this process, the species that undergo charge transfer (the *electroactive* species) are located within the compact (Helmholtz) layer, either at the OHP, the IHP or somewhere in between. For this reason, a precise description of the potential distribution in this region is important in electrochemical kinetics.

Said system is schematically shown in Fig. 2.9. The charge at the metallic surface q_m is equal to the sum of charge q_1 at the IHP, and the remaining charge in the diffuse layer, q_2; this provides for the electroneutrality of the overall system:

$$q_m + q_1 + q_2 = 0 \tag{2.48}$$

The value of q_1 is determined by the quantity of specifically adsorbed species Γ: $q_1 = z_s F \Gamma$ where z_s is the charge of the specifically adsorbed ions and Γ their surface concentration (moles per area unit), as determined by the Stern adsorption isotherm, where the potential is that of the inner Helmholtz plane φ_i:

$$B_o exp\left(-\Delta G_0/RT + z_s F \varphi_i/RT\right) c = \Gamma/\left(\Gamma_\infty - \Gamma\right), \tag{2.49}$$

In this equation Γ_∞ is the limiting adsorption and the potential φ_i is equal to the sum of the potential at the OHP φ_0 which was found earlier and the potential drop between the two Helmholtz planes. This potential drop is determined by the charges

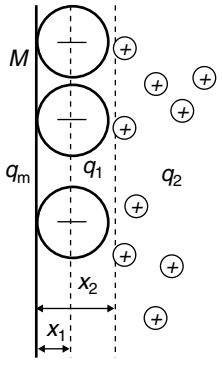

Fig. 2.9 Charge distribution at specific adsorption

(1) on the metal surface and (2) at the IHP. The former contributes the amount $q_m(x_o - x_i)/\varepsilon_0\varepsilon_1$ while the latter adds a term $q_1(x_o - x_i)/\varepsilon_0\varepsilon_1$. Consequently,

$$\varphi_i = \varphi_0 + [q_m(x_o - x_i) + q_1(x_o - x_i)]/\varepsilon_0\varepsilon_1. \tag{2.50}$$

One can see that the amount of specifically adsorbed species Γ depends on the potential at the IHP, but in addition this potential is also determined by the charge q_1 which is equal to $z_sF\Gamma$.

This result shows that the calculation of charge and potential distribution in the DL for a specific adsorption is not simple. Nevertheless, experimental data enable determination of the charge and potential distribution in this case. Several specific experimental and mathematical methods have been developed for their determination [9]. Here we only state that the simultaneous solution of Eqs. (2.49) and (2.50) can give in implicit form the dependence of q_1 (and consequently of φ_i) on the concentration of the specifically adsorbed species. The value of φ_0 was found in Sect. 2.3, in the discussion of the Gouy–Chapman model.

The overall potential difference between the solution bulk and the metal surface is

$$\varphi_m = \varphi_0 + [q_m x_o + q_1(x_o - x_i)]/\varepsilon_0\varepsilon_1. \tag{2.51}$$

The equations reported in Sects. 2.2–2.5 give the distribution of charge and potential at the Helmholtz planes and in the diffuse layer; a complete description of the system requires in addition knowledge of the parameters B_0, x_i, x_o etc., and allows a fit of most experimental data. These parameters may be estimated by using experimental data of DL capacitance over a wide range of potentials and of ionic concentrations (see Sect. 2.8).

It is necessary to note that the specific adsorption of ions can change significantly the potential distribution in the double layer. For example, at potentials more positive than PZC the value of φ_o is positive; however, if anions do adsorb specifically, their overall charge $|q_1|$ exceeds the metal charge $|\varphi_m|$. This leads consequently to a positive adsorption of the cations, as seen from Eq. (2.48). Then, the diffuse layer contains an excess of cations, leading to the potential distribution shown in Fig. 2.10. Phenomena of this sort explain the shift of PZC shown in Fig. 2.7, resulting from specific adsorption (in this case of Br^-).

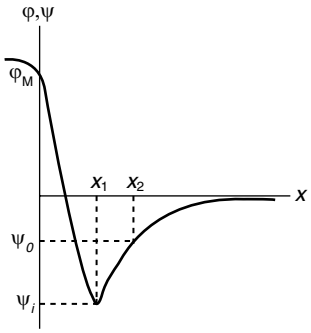

Fig. 2.10 One type of the potential distribution in the double at specific adsorption

A complete theory gives an explicit expression for this potential shift: $d\varphi_{ZCP}/d\ln c = RT/zF$ for the specific adsorption of z-charged ions (c is the concentration of the said ions); in reality the actual shift is often larger than this value. This is due to the discrete character of the charge distribution at the IHP.

2.6 Adsorption of Uncharged Organic Species

The structure of the DL is determined not only by the distribution of charged species but also by the presence of neutral surface-active, predominantly organic, substances. Such substances are usually employed in practical electrodeposition processes. Surface adsorption of these species does not change radically the electrical potential configuration, but influences the distribution of the charged species and also the permittivity in the dense layer. Adsorbed molecules may be modeled as electric dipoles oriented by the DL field; consequently, these do not contribute to the overall charge, but re-distribute it in the vicinity of the sites where they are adsorbed. The charge at free sites on the other hand does not change, leading to a *model of two parallel capacitors* for the interface [6]. In this model one capacitor is originated by the charge distributed over free sites (filled by the solvent molecules), and the other by the charge distribution at the sites covered by organic molecules. The overall charge is thus obtained as a sum over the two regions:

$$q = q_{\theta=0}\,(1-\theta) + q_{\theta=1}\theta \tag{2.52}$$

Here $q_{\theta=0}$ is the charge (per area unit) of the free sites and $q_{\theta=1}$ is that for covered sites; θ is the fractional coverage by organic molecules as it was introduced earlier. We will indicate these two contributions as C_0 and C'. The value of θ is governed by the adsorption isotherm which in this case depends on potential (or charge) of the electrode. As it was noted in Sect. 2.4, the Frumkin isotherm is best suited to describe the adsorption of organic species:

$$\mathrm{Bc} = \theta(1-\theta)^{-1}\, exp(-2a\theta)\,. \tag{2.53}$$

In most cases in fact it adequately describes experimental data. In this formula however the value of B is dependent on potential because the effects of replacing water in the DL with organics must be included into the treatment. When the DL capacitance changes from C_0 to C' the electrostatic work expended for this replacement (per mole of adsorbed species) is

$$\mathrm{W} = \left(C_0 - C'\right)(\varphi - \varphi_{\mathrm{PZC}})^2/2\Gamma_\infty \tag{2.54}$$

At the PZC this work is equal to zero, ant therefore B must have its maximum at this potential. In reality, the adsorbed species may have a non-zero dipole moment, thus shifting the potential of maximum adsorption to some point $\varphi_{\mathrm{PZC}}+\Delta\varphi$ just as a polarized dielectric volume produces a potential drop at an uncharged capacitor.

As a result,

$$\mathrm{B} = \mathrm{B}_0 exp\left[-\left(C_0 - C'\right)\left(\varphi - \varphi_{\mathrm{PZC}} - \Delta\varphi\right)^2 / \left(2RT\Gamma_\infty\right)\right]. \tag{2.55}$$

The PZCs for different metals are rather different, thus leading to the adsorption of the same organics within different potential ranges.

The shape of the adsorption isotherm slightly varies with a potential shift; this effect can be usually accounted for by including a linear dependence of the parameter a on potential.

Thus, by measurements of the DL capacitance as a function of electric potential and of the concentration of organic species it is possible to determine all the parameters describing the adsorption of organics. An interesting phenomenon is observed when performing these measurements: this consists in the presence of capacitance maxima at the edges of the adsorption region (Fig. 2.8), which is related to the sharp decay of adsorption in these regions.

Indeed, if the charge of the surface fraction partially covered by organics is $q(\varphi,\theta)$, then the differential capacitance is equal to

$$C = dq/d\varphi = (dq/d\varphi)_\theta + (dq/d\theta)_\varphi \, (d\theta/d\varphi) \tag{2.56}$$

The first contribution (the conventional capacitance) is equal, as seen from (2.52), to

$$(dq/d\varphi)_\theta = (dq_{\theta=0}/d\varphi)\,(1-\theta) + (dq_{\theta=1}/d\varphi)\,\theta = q = C_0\,(1-\theta) + C'\theta, \tag{2.57}$$

The second contribution is, as seen from (2.52)

$$(q_{\theta=1} - q_{\theta=0})\, d\theta/d\varphi, \tag{2.58}$$

which allows to rewrite (2.56) as

$$C = C_0\,(1-\theta) + C'\theta + (q_{\theta=1} - q_{\theta=0})\, d\theta/d\varphi. \tag{2.59}$$

This differs from the simple model of two capacitors in parallel by the third term, which is always positive (since both factors have the same sign). This term becomes important at the edges of the adsorption region due to the high value of $d\theta/d\varphi$; this explains the origin of the said maxima in Fig. 2.8.

Finally, it should be stressed that the discussion in this section concerns not only inert species simply blocking the surface but also neutral electroactive species, the surface concentration of which may govern the rate of the electrochemical process of interest.

2.7 Double Layer on Polycrystalline Solid Surfaces

Up to this point the surface was assumed to be macroscopically uniform. This is indeed the case for a liquid or monocrystalline electrode; in a polycrystalline electrode instead the various crystallographic facets have different properties, and at the

same potential the charges and capacitances of these facets may by different. These effects are particularly important for the compact layer. The diffuse layer on the contrary can be considered to be the same for the overall surface when the crystal grains are sufficiently small; with coarse grains having a size larger than the Debye length however each facet should also have its own diffuse layer.

There are attempts in the literature to describe a polycrystalline surface as uniform but having a finite roughness k_r (Sect. 1.4). In this case the roughness thus determined does not reflect an actual geometric roughness, but rather crystallographic features of the real surface, for example the existence of particular crystal facets, dislocations and other defects responsible for surface inhomogeneities.

Upon transition from the liquid to the solid state the double layer of the same electrode changes moderately; this was established by measuring the DL properties of a Ga electrode slightly below and above its melting point (about 30°C). Most studies of the double layer at solid surfaces require the use of well characterized structures such as dislocation-free monocrystalline surfaces, or surfaces with well-known step density. The opposite case however may also be of interest: very important information is found in fact through the use of a highly imperfect, liquid-type surface. This can be achieved by shearing or grinding. A freshly cut surface relaxes very quickly; therefore one should perform the measurements of interest very quickly. The cylindrical "cutting" electrode specifically designed for these investigations [10] is a very convenient electrochemical tool. The cutting of a thin metallic layer can be made immediately in the solution (with the potential applied), and measurements can be performed at any moment after surface renewal.

At sufficiently negative potentials C_{DL} depends weakly both on the surface state (solid or liquid) and on the chemical identity of the metal; under these conditions the roughness coefficient may be determined by correlating the results for a solid electrode with those measured on a mercury or amalgam electrode. For this process to be accurate however it is necessary that no adsorption of surface-active species occurs; this depends strongly on the metal identity.

In general, adsorption over dissimilar metal electrodes is significantly different; we have already noted that this is partly connected with the change of PZC; this can shift the region of adsorption up to 1 V. Additionally, the interaction of various metals with water may vary widely, resulting in a different width of the adsorption region. Finally, the adsorption energy as expressed by the parameter B_0 is determined by the electronic structure of both metal and adsorbate; in this respect, it has been established that maximum values of B_0 belong to species having definite ionization potentials I, which are specific for each metal ("*resonance potentials*" [11]). This statement is based mostly on the statistical treatment of the experimental data and has no deep theoretical foundation.

The most typical magnitude of I is 7.70–7.90 eV; this is characteristic for Cd, Sn, Bi, Pb and Cr. The approximate characteristic values experimentally found for copper, mercury, silver and zinc are correspondingly 7.2, 8.8, 9.0 and 9.4 eV; these values are close but not identical to the first ionization potentials of the metals. Oxidized areas of the surfaces have different "resonance potentials". Unfortunately, no data are available in the literature for other metals. The reported data provide a

guideline in choosing which substances may be strongly adsorbing at definite metal electrodes.

In comparing the *compact parts* of the double layer on different metals we recommend to divide the values of the corresponding capacitance into two contributions, one depending on the metal C_m and the other depending on the solvent C_s [12] as it is done for two capacitors in series (since the corresponding potential drops are additive):

$$C_1^{-1} = C_m^{-1} + C_s^{-1} \tag{2.60}$$

In this formula C_m does not depend on the electrical charge q_m nor on the solution properties, but, as the experiment shows, varies with the metal identity as

$$C_{m2}^{-1} = C_{m1}^{-1} + const, \tag{2.61}$$

the constant depending on the metal considered; m1 (e.g. mercury) can be taken as the standard.

C_s depends also on the charge, as follows

$$C_s^{-1}(\mathrm{m2}) = C_s^{-1}(\mathrm{m1}) + f(q) \tag{2.62}$$

As a first approximation, $f(q)=K(q-q_1)$; K depends on the metal identity, and the charge q_1 corresponds to $f(q)=0$, i.e. at the potential when all the solvent dipoles have the same orientation on all metals. Such analysis has no firm theoretical base but it provides a method to correlate available data on the behavior of surface-active compounds at different metal surfaces, a very important task in electrodeposition.

2.8 Some Calculations of Double Layer Parameters

Experimental data on C_{DL} as a function of potential allow determination of the charge q by integration:

$$q(\varphi) = \int C_{DL} d\varphi, \tag{2.63}$$

If the measurement is made in a given potential scale E (relatively to a definite reference electrode)

$$q(E) = \int C_{DL} dE \tag{2.64}$$

This is the analogue of the expression (2.45) for a variable C_{DL}. Integration is performed from the PZC to a generic potential value and gives the charge of the metal surface as a function of potential. Sometimes it is more convenient to integrate in the reverse direction from some negative potential (at which no adsorption takes place); in this case however one has to find the integration constant.

Table 2.2 Specific surface energies of metals (in J/m^2)

Ag	Al	Au	Bi	Co	Cu	Fe	Hg	Mg	Ni	Pb	Pt	W	Zn
1.0	0.95	1.3	0.42	2.0	1.5	2.0	0.51	0.60	2.0	0.51	2.0	2.8	0.97

The surface/interface energy γ is a significant quantity in the field of electrocrystallization because it determines the character of nucleation processes. As shown in Sect. (2.4), its value is related to the electrode potential as $q=d\gamma/d\varphi$; in a given potential scale E

$$d\gamma/dE = -q \tag{2.65}$$

at constant activities of the components. This is Lippman's *electrocapillarity equation*.

It is therefore possible to calculate the surface energy by double integration:

$$\gamma = \gamma_0 - \int\int C_{DL} dE^2. \tag{2.66}$$

The constant γ_0 corresponds to PZC. At this potential the surface energy has its maximum. Approximate values of γ for different metals at room temperature are given in Table 2.2. It should be noted that Eq. (2.65) is not completely general. First, it must be corrected by the contribution from the adsorption of the electrolyte components (Eq. 2.43):

$$d\gamma = -qdE - \Sigma\Gamma_i d\mu_i, \tag{2.67}$$

where Γ_i is the adsorption (surface excess) of component i, and μ_i its chemical potential. The effect of interface energy change is most pronounced in presence of specific adsorption, especially when covalent bonding of the adsorbed species with the metal occurs.

In the case of a solid electrode the reversible surface work σ does not coincide with the overall surface energy γ; instead:

$$\gamma = \sigma + d\sigma/dlnS, \tag{2.68}$$

the second term being the work done against the crystal bonds to change the electrode surface S; this term may be minimized by performing a very slow plastic deformation. As a consequence of this additional work term, Eq. (2.65) becomes:

$$(d\gamma/dE) = -q - dq/dlnS. \tag{2.69}$$

Based on Eq. (2.69), it is additionally possible to determine the characteristics of the compact layer. Equations (2.17–2.18) allow calculation of the capacitance of the diffuse layer C_2 at any concentration, charge or potential; the value of C is experimentally measured, and by use of Eq. (2.20) we can find the capacitance of the compact layer C_1, and therefore $\varepsilon_1/d=C_1/\varepsilon_0$.

The plot of $1/C$ vs. $1/C_2$ for solutions of different concentrations at constant charge is a straight line with slope equal to 1 (Fig. 2.11) intercepting the y-axis at the value of $1/C_2$ corresponding to the given charge. This value does not depend on

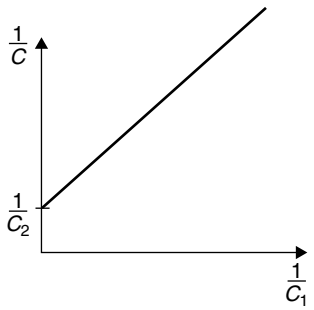

Fig. 2.11 Parsons–Zobel plot of $1/C$ on $1/C_2$

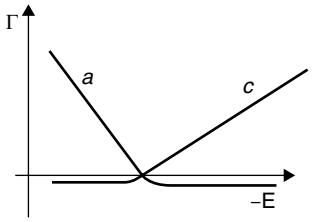

Fig. 2.12 Dependences of charges of cations and anions on the electrode potential

concentration, being only charge dependent. This plot (Parsons and Zobel [13]) is often used to determine the roughness coefficient k_f; for the case of a rough electrode the slope is k_f instead of 1.

Once the total charges are known, one may find the partial charges of the anions and cations in the diffuse layer. The dependence of such charges on electrode potential is shown in Fig. 2.12. Then, from the data for the electrolytes with and without surface-active species and specifically adsorbed species it is possible to calculate the variations in C, q and σ introduced by their presence.

For example, one can verify the validity of the DL model presented earlier for a given system by the following method [14]. The difference $C_{\mathrm{DL}}^{-1}(q, \mathrm{c}_1) - C_{\mathrm{DL}}^{-1}(q, \mathrm{c}_2)$ found from experimental data acquired at two different concentrations c (but at the same charge q) must be equal to the difference $C_2^{-1}(q, \mathrm{c}_1) - C_2^{-1}(q, \mathrm{c}_2)$ between the capacitances of the diffuse parts of the DL. This follows from Eq. (2.6) if we take into account that the capacitance of the compact layer depends only on q and not on the concentration. The latter difference can be easily calculated with Eq. (2.18) for any combination of c and q. Then if the two differences closely coincide one can conclude that the overall model is adequate.

There is one further important thermodynamic formula which is used to calculate the adsorption, derived from the expression for the chemical potential in an ideal solution $\mathrm{d}\mu = \mathrm{RTln}c$:

$$\Gamma = -(1/\mathrm{RT})\,(\partial\gamma/\partial ln\mathrm{c})_E \tag{2.70}$$

The methods of calculation of the various charge components and potential drops in the double layer have been extensively developed; these methods enable the deter-

mination of the set of parameters corresponding to the above models starting from experimental data. Details of these methods can be found elsewhere [15].

References

1. Delahay P. Double Layer and Electrode Kinetics. John Wiley & Sons, 1965
2. Impedance Spectroscopy: Theory, Experiment and Applications. Ed. By E. Barsoukov and J.R. Macdonald. J. Wiley & Sons, 2005
3. Vorotyntsev M.A., Kornyshev A.A., Electrostatics of Media with the Spatial Dispersion, Moscow, Nauka, 1993 (in Russian)
4. Kornyshev A.A., Vorotyntsev M.A., Canad. J. Chem., 1981, v. 59, No. 13, p. 2031
5. Grahame D.C., Chem. Revs., 41, 441 – 501, 1947
6. Frumkin A.N. in: Adv. In Electrochemistry and Electrochemical Engineering, New York, Interscience, 1961, v.1, p. 94
7. Stern O. Zeitschrift fur Elektrochemie, Bd. 30, s. 508 (1924)
8. Muller V.M. Soviet Journal of Colloids, v.9 No.5 (1976)
9. Adsorption of Molecules at Metal Electrodes, ed. A. Wieckowski, Marcel Dekker, New York, 1999
10. Beck R. Yu., Lavrova T.A. Transactions of the Siberian Branch of Acad. Sci. USSR, series Chemistry, 1971, No. 14, p. 1429 (in Russian)
11. Nechaev E.A. Chemisorption of organic substances on oxides and metals. Kharkov, 1989 (in Russian)
12. Badiali S., Amokrane J.P. Journ. Electroanalytical Chem., v. 266, p.21 (1989)
13. Parsons R. and Zobel F.G.R. Journ. Electroanalyt. Chem. 1965, v.9, No.5, p. 333.
14. Vorotyntsev M.A., Advances in Science and Technology (Itogi nauki i techniki), Electrochemistry, v. 21, 1984, 0.3 (in Russian)
15. Lyklema J. Fundamentals of Interface and Colloid Science, v.2, 1995, Academic Press

Chapter 3
Electrochemical Thermodynamics and Electrochemical Kinetics

3.1 Electrochemical Potential

The thermodynamic conditions of equilibrium for an isolated biphasic system include the equality of the *chemical potential* in the two phases. The conventional thermodynamic definition of chemical potential of a component *i* in a macroscopic system is

$$\mu_{\mathrm{i}} = \partial G / \partial N_{\mathrm{i}} \tag{3.1}$$

where N is the quantity of species i in moles, G the Gibbs free energy, and the derivative is taken under the conditions that T, p and the concentrations of the other components are kept constant. According to this definition, μ_{i} corresponds to the partial molal Gibbs free energy. In practice, μ_{i} is the change in Gibbs free energy when one mole of this component is added to a large amount of the mixture, so that the concentration of the other components is unchanged. It is usually assumed that μ_{i} depends on the thermodynamic activity a_i of the species i as

$$\mu_{\mathrm{i}} = \mu_{\mathrm{i}(0)} + RT \ln a_i. \tag{3.2}$$

μ_{i} maintains its physical meaning only in the absence of electric fields. When dealing with charged species, which always appear in electrochemistry, a more convenient quantity is introduced, namely the *electrochemical potential* $\underline{\mu}_i$ defined as

$$\underline{\mu}_{\mathrm{i}} = \mu_{\mathrm{i}} + zF\varphi \tag{3.3}$$

The second term on the right side represents the work done against a potential difference φ when transferring the charged species from infinity to inside the solution ("*Galvani potential*").

When the two phases (i.e. the metallic electrode and the solution) are in thermodynamic equilibrium their electrochemical potentials are equal:

$$\mu_1 + zF\varphi_1 = \mu_2 + zF\varphi_2 \tag{3.4}$$

Y. D. Gamburg, G. Zangari, *Theory and Practice of Metal Electrodeposition,*
DOI 10.1007/978-1-4419-9669-5_3, © Springer Science+Business Media, LLC 2011

Inversely, the electrochemical equilibrium is attained when the electrochemical potentials are equal. This implies that

$$zF\Delta\varphi_1^2 = \mu_2 - \mu_1, \tag{3.5}$$

where the μ_i are the chemical potentials in the two phases. The symbol $\Delta\varphi_1^2$ denotes the potential drop between the two phases, otherwise called *Galvani potential difference*. In general, the Galvani potential difference between two phases is determined by the difference of chemical potentials of the ions and/or electrons in the metal and in the electrolyte; the thermodynamic equilibrium in fact must be attained both for ions and electrons.

3.2 Equilibrium at Electrolyte-Solid Interfaces

Let us consider the equilibrium existing at an electrode/solution interface with respect to a specific electrochemical reaction, e.g.,

$$\mathrm{Ag}^0 \leftrightarrow \mathrm{Ag}^+(\mathrm{s}) + \mathrm{e}(\mathrm{M}). \tag{3.6}$$

The symbol e(M) denotes the electron in the metal, and the symbol s designates the solution. For this process we may write the following equilibrium condition:

$$\underline{\mu}(\mathrm{Ag},\mathrm{M}) = \underline{\mu}\left(\mathrm{Ag}^+,\mathrm{s}\right) + \underline{\mu}(\mathrm{e},\mathrm{M}). \tag{3.7}$$

Since metallic atoms in the crystal lattice are neutral we can write $\underline{\mu}(\mathrm{Ag},\mathrm{M}) = \mu(\mathrm{Ag},\mathrm{M})$; writing the chemical and electrochemical potentials explicitly Eq. (3.7) becomes

$$\begin{aligned}&\mu_{(0)}(\mathrm{Ag},\mathrm{M}) + RT\ \ln a(\mathrm{Ag},\mathrm{M}) = \mu_{(0)}\left(\mathrm{Ag}^+,\mathrm{s}\right) + RT\ \ln a\left(\mathrm{Ag}^+,\mathrm{s}\right)\\ &+F\varphi(\mathrm{s}) + \mu_{(0)}(\mathrm{e},\mathrm{M}) + RT\ \ln a(\mathrm{e},\mathrm{M}) - F\varphi(\mathrm{M}).\end{aligned} \tag{3.8}$$

Invoking the fact that the activities of the pure metallic phase and of the electrons in the metal are constant one can appropriately define their reference states and neglect the corresponding terms; after rearranging we obtain the following expression for the Galvani potential difference:

$$\begin{aligned}&\varphi(\mathrm{M}) - \varphi(\mathrm{s}) = \Delta\varphi_{\mathrm{M}}{}^{\mathrm{s}} = F^{-1}\left[\mu_{(0)}\left(\mathrm{Ag}^+,\mathrm{s}\right) + \mu_{(0)}(\mathrm{e},\mathrm{M}) - \mu_{(0)}(\mathrm{Ag},\mathrm{M})\right]\\ &+ (RT/F)\ln a\left(\mathrm{Ag}^+,\mathrm{s}\right) = \Delta\varphi_0 + (RT/F)\ln a\left(\mathrm{Ag}^+,\mathrm{s}\right)\end{aligned} \tag{3.9}$$

It should be pointed out that the above derivation is valid only for pure metal electrodes; in the case of an alloy electrode the activity of the metal atoms in the electrode is not constant. This situation will be explicitly considered in Chap. 10.

3.3 Electrode Potential. Nernst Equation

It is impossible to experimentally measure the Galvani potential between liquid and solid phases. In fact, if we were to perform this measurement, we would need to immerse another metallic electrode in the liquid, effectively introducing an additional interface. For this reason the potential of the solid electrode is conventionally measured with reference to some other electrode which has a strictly defined Galvani potential relative to the solution. Such a measurement gives the electromotive force EMF generated by the electrochemical cell consisting of this reference electrode and the electrode under study (Fig. 3.1). By using this method the solution drops out of the problem because the voltage measurement can now be performed between two metallic phases.

The second electrode is termed *reference electrode*. Many types of electrodes are feasible as reference electrodes; the most important property of a good reference electrode is the stability over time and reproducibility of its potential. As mentioned earlier, calomel and silver chloride electrodes are used most often in practice. Due to its unequaled stability and precision, the *Standard Hydrogen Electrode* (SHE) is chosen as the standard reference. This electrode consists of a platinized platinum surface immersed in an acidic solution having a hydrogen ion activity $a(H^+)=1$ in contact with hydrogen gas at atmospheric pressure. The Galvani potential difference of this electrode is set equal to zero at any temperature.

This electrode configuration allows formulation of the following definition for the electrode potential: ***Electrode potential E is the EMF of the electrochemical cell consisting of the SHE and the electrode of interest, at which the redox process takes place***.

In accordance with this definition, Eq. (3.9) can be rewritten as

$$E_{eq} = E_0 + (RT/F)\ln a(Ag^+, s); \tag{3.10}$$

E_{eq} is the equilibrium value of the potential when the silver ions have an activity equal to a, while E_0 is the equilibrium electrode potential when $a=1$, also called standard electrode potential.

In the case of metallic ions M^{z+} with charge +z, this equation takes the form

$$E_{eq} = E_0 + (RT/zF)\ln\left(a_M{}^{z+}\right) \tag{3.11}$$

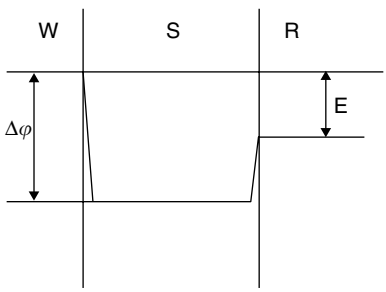

Fig. 3.1 The potential between the working electrode and the reference electrode. W – the working electrode, S – the solution, R – the reference electrode

This well-known dependence is referred to as *the Nernst equation* and plays a very important role in electrochemistry and electrodeposition. In the case of the electrochemical process $O + zE \leftrightarrow R$, where O is a generic oxidized species and R the corresponding reduced species, this equation takes the form

$$E_{eq} = E_0 + (RT/zF) \ln (a_O/a_R) \tag{3.12}$$

Its most general form is given for the reaction of Eq. (1.14) in Eq. (1.15). At room temperature the coefficient $RT/F = 0.0257$ V, and Eq. (3.12) can be written as

$$E_{eq} = E_0 + (0.059/z) \log (a_O/a_R) \tag{3.13}$$

where $0.059 = 0.0257 * \ln 10$.

3.4 Measurements of Electrode Potential

Control of the electrode potential is necessary not only at equilibrium but also under a variety of conditions when electrochemical reactions occur. It was noted in Chap. 1 (Sect. 1.6) that the deposition of a metal at a finite rate requires a negative shift of the electrode potential with respect to the equilibrium value; inversely, the dissolution of a metal requires a positive potential shift. Consequently, in order to control and monitor the process, measurements of the electrode potential may be necessary while current is passing through the electrolyte.

When no electric current is flowing, the electrode potential can easily be measured using a high-impedance voltmeter as the EMF of the cell consisting of the electrode of interest and a reference electrode; to obtain the correct result one must only add the potential of the latter with reference to the SHE. However, when current flows, this two-electrode cell is usually unsuitable. In these conditions, along with the working and reference electrodes, a third one is needed (the counter electrode) as a current carrying electrode; if the working electrode is a cathode, the counter electrode is an anode. The three-electrode arrangement is standard when performing electrochemical measurements.

While measurements are made the current flows only through the working and counter electrodes; ideally, no current flows through the reference electrode, and consequently its potential remains unchanged. This electrode is usually placed into a separate solution, connected to the main one with a salt bridge (Fig. 3.2). The bridge ends with a thin tip (*Luggin capillary*) ending very near the working electrode. This configuration helps to minimize the potential drop in solution between said tip and the working electrode; this potential drop in fact is included in the measured quantity, resulting in some error (Fig. 3.3). This is often referred to as an Ohmic error, but this term is not quite correct, as will be seen in the following; close to the electrode surface in fact Ohm's Law is not always fulfilled.

To avoid screening of the electrode surface by the Luggin capillary its tip is molded in a specific shape and placed not directly at the surface but at a distance

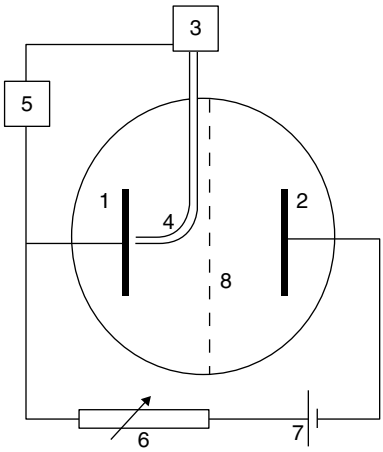

Fig. 3.2 Measurement of the electromotive force generated by the electrochemical cell consisting of the reference electrode and the electrode of interest. *1* is the working electrode; *2* is the counter electrode, *3* is the reference electrode, *4* the Luggin capillary, *5* a high impedance voltmeter, *6* the resistor for current monitoring, *7* the external battery, *8* an ion selective membrane

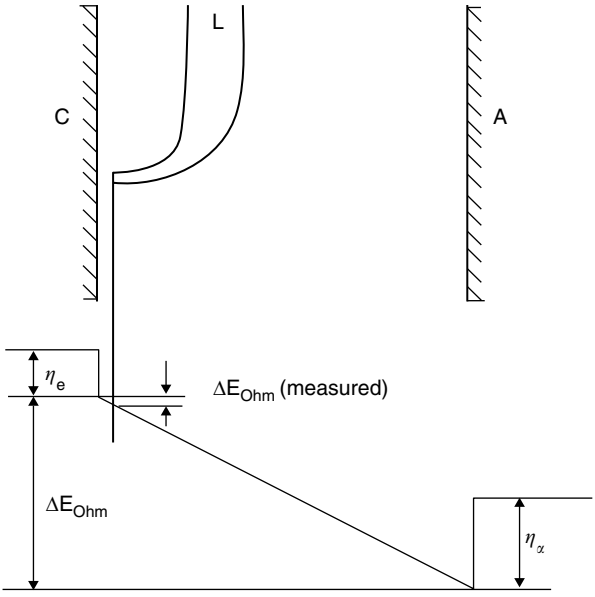

Fig. 3.3 The electrode potential measurement performed with a Luggin capillary minimized the ohmic potential drop included in the measured EMF

approximately equal to its diameter. In the absence of current flow obviously the capillary is not needed.

3.5 Theory of Charge Transfer

The rate and mechanism of electrode processes constitutes one of the most important topics in electrochemical kinetics. The corresponding theory is based on three fundamental concepts: (1) the theory of absolute reaction rates, (2) the double layer

structure, and (3) the relationship between the standard free energy and the activation energy of the reaction, sometimes referred to as Brønsted–Polanyi rule.

In chemical kinetics, the rate of the first order reaction $A \leftrightarrow B$ is given by:

$$v(mol/s) = k_f C_A - k_b C_B \tag{3.14}$$

In particular, far from equilibrium, when $[B] = 0, v = kC_A$. An expression for the rate constant $k(s^{-1})$ can be found by considering the transformation $A \rightarrow B$ to occur by the formation of an activated complex A*, from which it is equally probable for the system to transform to B or back to A. If $\Delta G^{\neq}$ is the free energy of the activated complex with respect to A, k depends on the *activation energy* $\Delta G^{\neq}$ as

$$k = (\kappa RT/N_A\hbar)\, exp\left(-\Delta G^{\neq}/RT\right) \tag{3.15}$$

The exponential term represents the probability of a generic reactant (atom or molecule) to overcome the energy barrier $\Delta G^{\neq}$ involved in the transformation from the reactant to the product, or equivalently the fraction of particles in the system that have energy at least equal to $\Delta G^{\neq}$. The pre-exponential term can be derived from the transition state theory, and represents the frequency of attempts to overcome the energy barrier; κ takes into account the possibility for the activated complex to transform back to A, while RT/N_A is the frequency factor for breakdown of the transition complex. At moderate temperatures the latter is of the order of 10^{-3} s^{-1}. $\hbar$ is Planck's constant, and N_A is the Avogadro number.

In the case of an electrochemical reaction $O + ne^- \rightarrow R$ (in particular, the electrodepostion reaction $M^{z+} + ze^- \rightarrow M_{met}$) our purpose is to write an expression that relates current density i to the concentration of the reactant $i = nFkC_O$. An additional feature of electrochemical reactions is that electrons are also involved; the quantity $\Delta G^{\neq}$ therefore necessitates a more thorough discussion. For this purpose it is convenient to present the energy landscape of the reacting system as a potential diagram (Fig. 3.4) showing the dependence of the standard free energy of the system vs. a generalized reaction coordinate.

Let us take for example the process of Zn electrodeposition: $Zn^{2+} + 2e \leftrightarrow Zn(M)$. Deposition and dissolution proceed at equal rates at the equilibrium potential. Under standard conditions the equilibrium requirement $\Delta G_0 = 0$ corresponds in this case to the electrode potential $E_{eq}\left(Zn/Zn^{2+}\right) = E_0 = -0.76$ V.

In the vertical axis of this diagram the Gibbs energy G is plotted as a function of a reaction coordinate. Curve 1 describes the variation in free energy of the system at equilibrium. The two minima on the left (G_A) and right (G_C) side correspond to the initial and final conditions, i.e. Zn^{2+} ions in the solution plus electrons in the metal (on the left) and Zn in the metallic phase (on the right), respectively. At equilibrium these energies are equal (curve 1). The maximum value $G^{\neq}$ (point B) is the energy of the activated complex. The potential barrier (the difference between $G^{\neq}$ and G_A) is the activation energy. In the case of electrochemical reactions $G^{\neq}$ corresponds to a specific configuration, with the solvent dipoles close to the electroactive species; this configuration is subject to fluctuations over time as a result of thermal motion, which result in solvent reorganization.

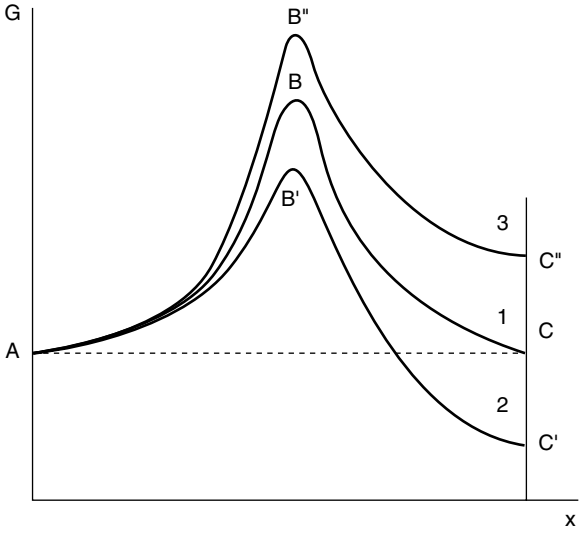

Fig. 3.4 Potential landscape diagram for a simple electrochemical one-electron transfer

Let us consider now how the energy landscape is changed when the electrode is polarized by some external power source. If the potential becomes somewhat more negative than −0.76 V then the equilibrium will be disturbed. The overall reaction will go forward, in the direction of the formation of metallic Zn. Curve 2, obtained by curve 1 by adding a linear energy term corresponding to the spatial variation of electron energy across the potential drop, explains the details of this process. The species Zn^{2+} following the path A–B′–C′ overcomes the barrier B′ and subsequently the system "descends" to the point C′ (i.e. metallic Zn is deposited). This time the energy corresponding to this point is lower than the energy of state A: consequently, this reaction proceeds at a finite rate. The maximum energy of the barrier also decreases, to the value B′; however its decrease is less than that of point C. It is readily seen therefore that the ratio $\Delta G^{\neq}/\Delta G_2$ is less than one; this ratio is called the *transfer coefficient* α. Another name for this quantity is *asymmetry parameter*, since it depends on the asymmetry of the free energy potential curve. For a symmetrical curve $\alpha = 0.5$.

At potentials more positive than E_{eq} the reaction proceeds in the backward direction; curve 3 illustrates this process. Since the sign of the potential drop is now opposite, the point C″ is higher than C, and correspondingly Zn electrochemically dissolves. The transfer coefficient of the reverse process, as it is easily seen, is equal to $(1-\alpha)$.

In the analysis of this type of diagrams it is important to define rigorously the quantity plotted along energy axis: this may be the Gibbs energy, the enthalpy or the internal energy. If, for instance, enthalpy is plotted, then the energy levels of A and C at equilibrium are not equal; indeed, they should differ by the entropic contribution of the electrode process: $Q = T\Delta S$. The activation energy also changes, by the quantity αQ.

The above analysis shows qualitatively that the change of activation energy is equal to only a fraction α of the overall change of the reaction energy $nF\Delta\varphi$. This is known as Brønsted–Polanyi rule; it was originally used for organic reactions and later (1932) extended to electrochemical processes.

Let us now restate these concepts more precisely and in a more general form.

The free energy per mole of the starting state A (O in the electrolyte and n electrons in the electrode) is equal to

$$G_A = \underline{\mu}_O + n\underline{\mu}_e = \mu_O - nF\varphi^* + n\mu_e, \tag{3.16}$$

where μ_O is the chemical potential of the species O, μ_e is the chemical potential of the electron in the electrode and φ^* is the potential drop between the (plane) electrode and the plane where the species O is located. This plane corresponds to the configuration of the initial system immediately preceding the electron transfer. Electron transfer results in the production of one mole of the metal; its free energy is $G_C=\mu_{met}$, and in electrochemical equilibrium (when $G_A=G_C$, or $\Delta G=0$)

$$\mu_0 - nF\varphi^* + n\mu_e = \mu_{met} \tag{3.17}$$

This equation shows that equilibrium can be perturbed by changing the potential φ^*; imposing a change in potential $\Delta\varphi^*$, the corresponding change in free energy is $\Delta G=nF\Delta\varphi^*$.

As a consequence, the activation energy $\Delta G^{\neq}$ changes by a fraction α of this value:

$$\Delta G^{\neq} = \Delta G_0{}^{\neq} + \alpha\Delta G = \Delta G_0{}^{\neq} + \alpha nF\Delta\varphi^*, \tag{3.18}$$

where $\Delta G_0{}^{\neq}$ is the activation energy for a standard Gibbs free energy of reaction $\Delta G_0=(G_C-G_A)_0$.

Substitution of this expression into Eq. (3.15) gives

$$k = K_0 exp\left(-\alpha nF\Delta\varphi^*/RT\right) \tag{3.19}$$

where K_0 contains all the factors independent of potential. The last equation describes the rate of an individual elementary process; in order to translate this quantity into a current density it is necessary to multiply this value by the concentration at the electrode interface of the electroactive species in the oxidized state c_O:

$$i_c = K_0 c_O\, exp\left(-\alpha nF\Delta\varphi^*/RT\right) \tag{3.20}$$

This approach ignores the atomic structure of the surface; it assumes in fact that the surface is uniform and the active centers for growth are uniformly distributed. Later in the book, when considering the crystallization problem, it will be necessary to take into account also the distribution and surface density of the active centers.

The potential $\Delta\varphi^*$ as used here also requires a specification; in general it is not the Galvani potential difference between the surface and the solution bulk. As it

was shown in the previous chapter, charge transfer takes place from a point located between the two Helmholtz planes, and its local potential differs from that of the bulk electrolyte by ψ'. In concentrated solutions $\psi' \to 0$, and it is possible to use immediately the potential scale E (because in this case $\Delta\varphi^* = E + \text{const}$),

$$i_c = K_0 c_O \exp(-\alpha n F E / RT). \tag{3.21}$$

If $\psi' \neq 0$ (most notably in dilute solutions, in the case of anion reduction or in presence of surface-active additives) two additional adjustments to the formula have to be taken into account (Frumkin, 1933). On the one hand, the concentration of charged species at the site of charge transfer c_O differs from that in the bulk c_B:

$$c_O = c_B \exp(-z f \psi') \tag{3.22}$$

In this formula $f = F/RT = k_B T/e$. This ratio (already used in Chap. 2) occurs frequently in electrochemical calculations; at 298 K it equals 0.025 V.

On the other hand, at the electrode potential E only a fraction $(E - \psi')$ influences the rate of charge transfer (Fig. 3.5). Taking both factors results in the following modification of (3.21):

$$i_c = K_0 c_B \exp(-z f \psi') \exp\left[-\alpha n F (E - \psi') / RT\right]. \tag{3.23}$$

This equation is more general. It is often written in the same form as (3.21):

$$i_c = k_c c_O \exp(-\alpha n f E), \tag{3.24}$$

but in this case the cathodic rate constant k_c is the effective quantity

$$k_c = K_0 \exp\left[(\alpha n - z) f \psi' / RT\right], \tag{3.25}$$

representing the influence of the double layer structure on electrode kinetics. The dependence of ψ' on potential leads to a functional dependence of k_c on potential.

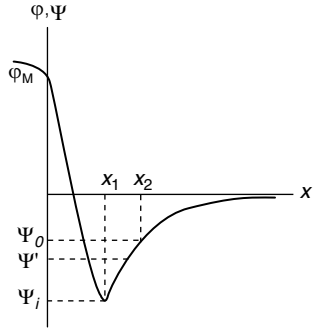

Fig. 3.5 The electrode potential relevant for charge transfer may differ from the actual electrode potential due to the position of the reducible species within the double layer

3.6 Exchange Current Density. Overpotential. Polarization Curves

Up to now we have discussed the rate of a simple one electron transfer reaction; however, there are at least two processes of this kind in every electrochemical reaction, i.e. the forward and backward reactions. Independent processes occurring in parallel are also possible. The backward process $R - ne \rightarrow O$ can be discussed in a similar way as the forward one; the corresponding current is described by the equation

$$i_a = k_a c_R \; exp(\alpha_1 f E) \tag{3.26}$$

The two processes proceed concurrently and independently at the same surface. The sum of (3.24) and (3.26) gives the total current at the electrode, which is characterized by the following features. First, with increasing potential one of these functions increases monotonically from zero, and the second decreases to zero; as a consequence a potential exists at which both currents are equal; at this potential the net current through the interface is zero. The corresponding potential coincides with the thermodynamic equilibrium potential E_{eq}. In fact, by equating (3.24) and (3.26) it follows that

$$E_{eq} = [(\alpha + \alpha_1)\, nf]^{-1} ln\, (k_a/k_c) + [(\alpha + \alpha_1)\, nf]^{-1} ln\, (c_R/c_O) \tag{3.27}$$

This is the Nernst equation with the constraint $\alpha + \alpha_1 = 1$, and with the activities substituted by concentrations. Consequently, it follows from the thermodynamic requirements that $\alpha_1 = 1 - \alpha$, and then there is no need to use both quantities.

The value of $i_c = i_a$ corresponding to the equilibrium potential is termed *exchange current density* and it is denoted as i_0. This current is a reminder that at E_{eq} a dynamic equilibrium is taking place between O and R, and the rate of their mutual transformations is determined by i_0.

The exchange current density corresponding to the standard potential is named standard exchange current:

$$i_0{}^0 = nFk_s, \tag{3.28}$$

k_s being the standard heterogeneous rate constant, i.e. the rate constant corresponding to the standard potential, when $c_R = c_O$ and then $k_a = k_c$, as can be derived from (3.27) if $E_{eq} = 0$.

The exchange current density for a one-electron transfer reaction can be expressed as

$$i_0 = i_0{}^0 c_O{}^{1-\alpha} c_R{}^{\alpha} \tag{3.29}$$

(the standard concentrations are equal to unity; in the case of metal electrodeposition c_R also equals 1). This dependence can be easily understood from Fig. 3.6: with decreasing M^{z+} concentration the curve for the cathodic process shifts in the negative direction, whereas the anodic one remains the same. Accordingly, the equilibrium potential shifts negatively with a smaller i_0.

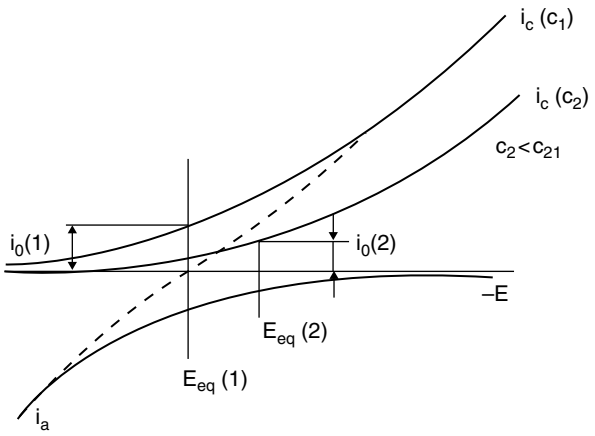

Fig. 3.6 The current–voltage characteristics for a one-electron transfer reaction: the partial currents and the total curve

The potential E at which a particular electrode process does actually proceed is often measured using its equilibrium potential E_{eq} as a reference. The value of $E-E_{eq}$ is the overpotential η of this process, as it was noted in Sect. 1.7.

The general form of the current–potential characteristics which takes into account both forward and reverse processes, when expressed in terms of overpotential assumes therefore the following form:

$$i = i_0 \{exp\,[-\alpha\ F\eta/RT] - exp\,[(1-\alpha)\,F\eta/RT]\} \tag{3.30}$$

This is the so-called *Butler–Volmer (B–V) equation*. The first term describes the partial current density of the cathodic process and the second that of the anodic one. The overall current density at a given potential may also be expressed in terms of the rate constant k.

Figure 3.6 shows the curves corresponding to the partial currents and to the total one; the latter goes through zero at the equilibrium potential. Close to this point the current increases linearly, while upon a greater shift from equilibrium exponential growth occurs.

It should be stressed that, unlike the value of k, which in general depends on potential (Eq. 3.25), the exchange current density i_0 is assumed to be strictly constant. The value of the transfer coefficient however depends on potential:

$$\alpha^* = \alpha + (\alpha n - z)\, d\psi'/d\eta \tag{3.31}$$

In some cases this effective transfer coefficient differs noticeably from the true value. This dependence is the result of a variable ψ'-potential; also, α is not rigorously constant unless the variation of free energy with the reaction coordinate is quadratic.

As seen in Fig. 3.6, at sufficiently cathodic overpotential (some tens of millivolts) the anodic process is slow and can be neglected; the cathodic partial curve consequently coincides with the overall one. The relation between the rates of the two processes is

$$i_c/i_a = exp\,(-f\eta) \tag{3.32}$$

For η_c=0.1 V this ratio is ≈50, and it increases with increasing η. Under these conditions the anodic term can be neglected and $i \approx i_c = i_0\, exp(-\alpha f\eta)$, or $ln\ i = ln\ i_0 - \alpha f\eta$, hence (using decimal logarithms, *lg*)

$$\eta_c = a + b lg i; \tag{3.33}$$

where $a = (2.3RT/\alpha F)\, lg\ i_0 = 2.3 lg\ i_0/\alpha f$, $b = 2.3RT/\alpha F = 2.3/\alpha f$.

This is the well-known *Tafel equation*. The portions of the curves $E - lgi$ where this law is obeyed are denoted Tafel regions, and their slope is called Tafel slope. This equation, originally found empirically by Tafel in the beginning of the 20th century, appears evident when starting from the B-V formula.

From Eq. (3.33) it is possible to derive the values of α (from the Tafel slope) and i_0 (by extrapolation of the Tafel region to the equilibrium potential, Fig. 3.7), as follows:

$$\alpha' = 2.3RT/bF, \quad lgi_0 = a\left(\alpha' F/RT\right). \tag{3.34}$$

The same procedures can be followed also for the anodic region; if the values of exchange CD and transfer coefficient are the same for the two branches, this signifies that in both regions the charge transfer process occurs through the same mechanism. The value of the Tafel slope at room temperature, assuming α=0.5, is ~0.118 V per decade.

It should be stressed that the described procedure gives immediately i_0 and α only for a one-electron transfer; for more complicated processes (see Sect. 3.7) various combinations of these quantities can be obtained, depending on the number of electrons exchanged, *n*.

The overall trend of the polarization curve is shown in Fig. 3.8. Using a fixed linear scale, close to E_{eq} the current density is very low, then it grows sharply, and both branches (cathodic and anodic) eventually go to infinity. In real systems however, as will be seen in the next chapter, the current density CD at high overpotentials is limited by ionic mass transfer to or from the electrode. With a higher value of i_0 a predetermined CD is attained at a lower overpotential; this means that the system is more reversible the higher i_0; the exchange current is therefore a measure of reversibility; conversely, it is also a measure of polarizability. An electrode is said

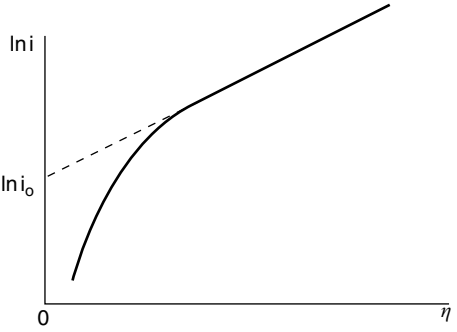

Fig. 3.7 Tafel curve, and extrapolation of the Tafel region to the equilibrium potential

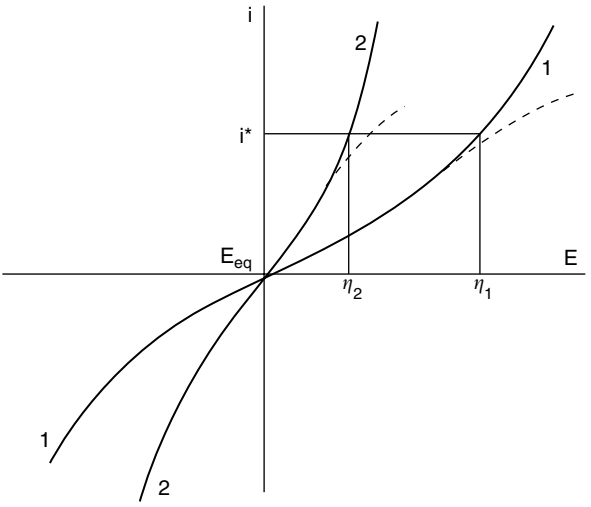

Fig. 3.8 The polarization curves corresponding for the two different exchange current densities. The curve 2 corresponds to higher i_0, then at the same current i* the overpotential is less. The dotted line corresponds to the diffusion limitations

unpolarizable when the potential drop across the interface is independent of CD (this occurs as $i_0 \to \infty$), and it is said *ideally polarizable* if the flow of faradaic current is forbidden ($i_0 \to 0$). In intermediate cases the electrode is referred to as being partially polarizable.

At overpotentials of about 0.1 V or more, one of the branches of the B–V characteristics can be neglected, and a semi-logarithmic Tafel characteristics describes the current–voltage relationship correctly. At low overpotentials instead, usually less than 0.01 V, it is possible to linearize the exponential terms in the B–V equation obtaining:

$$i \approx i_0 \left(1 + \alpha f \eta - 1 + \alpha_1 f \eta\right) = i_0 f \eta = i_0 F \eta / RT, \tag{3.35}$$

which is similar in form to the Ohm's law. The term RT/i_0F plays the role of resistance; it is called the *electron transfer (or Faradaic) resistance*. It is a purely resistive term, and it does not cause a shift in the phase angle between current and potential as AC flows through the electrode.

Formula (3.35) suggests a method of estimating the exchange CD alternative to performing the extrapolation of Tafel regions, by experimentally determining the slope of the i–η characteristics at low overpotentials. A further method of finding α is by using the concentration dependence of i_0 (3.29). In a logarithmic scale

$$lgi_0 = const + (1 - \alpha)\, lgc_{\mathrm{O}} + \alpha lgc_{\mathrm{R}} \tag{3.36}$$

Consequently, by determining i_0 at various c_{O} one can determine α. The dependence of i_0 on the equilibrium potential takes the form

$$dlgi_0/dE_{\mathrm{eq}} = 0.4343 z f \alpha \tag{3.37}$$

The characteristic features of the discharge–ionization step as described earlier are very common and do not change radically if the overall process is more complicat-

ed. Diffusive or chemical processes preceding or following the electron exchange cause only a variation of the actual concentrations of the electroactive species. The change of the ion nature (e.g. upon complex formation) on the other hand may affect the values of i_0 and α. In processes where the simultaneous transfer of n electrons occurs, F in (3.30) needs to be changed to nF; these processes however are relatively uncommon. Consecutive (multistep) processes are more general; they are explicitly considered in the following section.

It may be noted in advance that for divalent metal deposition the Eq. (3.30) to (3.37) are usually valid by changing F to $2F$ or f to $2f$, and making other minor modifications.

3.7 Multistep Electrochemical Processes

As already noted in Sect. 1.1, real electrochemical processes consist of several elementary steps, including electrochemical ones (similar to those discussed earlier), purely chemical ones (independent of the electric potential) and diffusion processes (which may be treated as reversible chemical steps of the first order).

Intermediate species produced in an elementary reaction in turn enter as reactants into the successive reaction; at steady state the concentration of the intermediates at each step is constant, and the rates of each elementary step are also constant. While the analytical treatment of the steady state is relatively simple, that of time-dependent systems, characterized by a time-dependence of the concentrations of the intermediates, is much more complicated. Time-dependent conditions often occur at the initial stages of a process, immediately after the current is switched on, or when a reacting species is consumed (e.g. when electroplating with non-soluble anodes). Theoretical calculations of reaction kinetics are usually performed for steady state conditions. It follows that experiments should be performed at the steady state if kinetic data are to be used in calculations. In particular, for multi-step processes the condition of constant concentration of the intermediates over time: $dc_i/dt = 0$, must be fulfilled for each intermediate species.

Let us consider a process consisting of two consecutive one-electron steps in which the intermediate product X is generated: (1) $O + e \leftrightarrow X$; (2) $X + e \leftrightarrow R$. The two steps have rate constants $k_{1,c}$ and $k_{1,a}$ for the cathodic and anodic components of the first process, and correspondingly $k_{2,c}$ and $k_{2,a}$ for the second one. The B–V equation applied to both steps gives

$$i_1 = k_{1c} c_O \, exp[-\alpha_1 f E] - k_{1a} c_X \, exp[(1-\alpha_1) f E] \tag{3.38}$$

and

$$i_2 = k_{2c} c_X \, exp[-\alpha_2 f E] - k_{2a} c_R \, exp[(1-\alpha_2) f E] \tag{3.38a}$$

At steady state the concentration of X, c_X is constant, and then both currents i_1 and i_2 are equal, because Eq. (3.38) represents the rate of formation of the intermediate, while the latter gives the rate of its consumption.

This condition allows calculation of c_X as a function of potential. At the equilibrium potential E_{eq} we obtain $i_1=i_2=0$. This gives the values of the exchange CD for both steps:

$$i_{01} = k_{1c}c_O \; exp\left[-\alpha_1 f E_{eq}\right] = k_{1a}{c_X}^0 \; exp\left[(1-\alpha_1)\, f E_{eq}\right] \tag{3.39}$$

$$i_{02} = k_{2c}{c_X}^0 \; exp\left[-\alpha_2 f E_{eq}\right] = k_{2a}c_R \; exp\left[(1-\alpha_2)\, f E_{eq}\right] \tag{3.39a}$$

The quantity ${c_X}^0$ is the equilibrium concentration of X (i.e. that corresponding to E_{eq}). These values should now be substituted into (3.38), and it should be taken into account that, since these two processes proceed in parallel, the observed rate of the overall process is the sum of the rates of the two steps (3.38) and (3.38a) or, equivalently, twice the rate of one step. Finally, using $\eta=E_{eq}-E$, the following equations are obtained

$$i = 2i_{01}\left\{exp\,(-\alpha_1 f\eta) - \left(c_X/{c_X}^0\right) exp\,[-(1-\alpha_1)f\eta]\right\} \tag{3.40}$$

and

$$i = 2i_{02}\left\{\left(c_X/{c_X}^0\right) exp\,(-\alpha_2 f\eta) - exp\,[-(1-\alpha_2)f\eta]\right\} \tag{3.40a}$$

After eliminating $c_X/{c_X}^0$ from these two expressions the *Vetter equation* [1] is obtained:

$$\begin{aligned} i =& 2\{exp[(\alpha_1+\alpha_2)f\eta] - exp[-(2-\alpha_1-\alpha_2)f\eta]\}/\{i_{01}^{-1}exp(\alpha_2 f\eta) \\ &+ {i_{02}}^{-1}exp[-(1-\alpha_1)f\eta]\}. \end{aligned} \tag{3.41}$$

Similar calculations for the case of three consecutive processes lead to a more complicated expression (which includes three exchange current densities), first derived by Losev [2].

Vetter's equation shows that the shape of the cathodic and anodic branches depends mostly on the ratio between the exchange currents of the two steps. In the vicinity of the equilibrium potential, the CD depends linearly on η, but the role of i_0 is played by the effective quantity

$$4i_{01}i_{02}/(i_{01}+i_{02}) \tag{3.42}$$

If $i_{01} >> i_{02}$ (fast first step) then this quantity is equal to $4i_{02}$, in the opposite case it is $4i_{01}$.

Far from E_{eq}, when one of the partial curves can be neglected, the cathodic Tafel region corresponds to the equation

$$|i| = 2i_{02} \; exp\,[(1+\alpha_2)f\eta]\,, \tag{3.43}$$

and the anodic one to

$$|i| = 2i_{02} \; exp\,[-(1-\alpha_2)f\eta], \tag{3.44}$$

These functions are indistinguishable from those obtained for the simultaneous transfer of two electrons, but with exchange CD equal to $2i_{02}$ and with a different, and obviously asymmetric, transfer coefficient. The shape of the curves therefore is the same as if two electrons were transferred ($n=2$), $\alpha_c=0.5(1+\alpha_2)$ and $\alpha_a=0.5(1+\alpha_2)$. However, farther in the cathodic region—and if diffusion limitations are neglected—the curve corresponds to the equation

$$|i| = 2i_{01}\ exp\ (\alpha_1 f \eta) \tag{3.45}$$

Extrapolation of this equation to E_{eq} gives twice the exchange CD equal to $2i_{01}$ (not i_{02} !); the Tafel slope in this region is also determined by the transfer coefficient of the first step α_1. This means that the cathodic branch in Tafel coordinates $E-lgi$ is curved between these regions, indicating a two-step process.

In the opposite case $i_{02}>>i_{01}$ (fast second step) a similar curvature is observed in the anodic branch of the characteristics.

Consequently, it can be stated that a large variation of the Tafel slope from its conventional value of 0.118 V, differences in exchange CD obtained by different methods and also a curvature of the curves $E-lgi$ may serve as diagnostic criteria of which electron is transferred more rapidly.

When the values of i_{01}, i_{02} and maybe i_{03} etc. differ significantly one can use a simpler method for calculation of the overall kinetics. The fast steps may be thought of as equilibrium ones, and the slowest step becomes rate limiting; then the concentrations of intermediates are governed by the Nernst equation. Commonly in the determination of kinetic rates it is assumed that the multistep reaction consists of m ($m\geq 0$) equilibrium steps, a successive slow step (which can be repeated ν times; this is the so-called stoichiometric number of the reaction), and ends with $n-m-\nu$ equilibrium electrochemical steps; the overall number of transferred electrons is n.

The corresponding calculations lead to the following limiting results: the Tafel slopes at sufficiently high cathodic and anodic overpotentials are respectively

$$b_c = -2.3[f(\mathrm{m}/\nu + \alpha_c)]^{-1}, \tag{3.46}$$

$$b_a = 2.3\{f[(\mathrm{n} - \mathrm{m} - \nu)/\nu + \alpha_a]\}^{-1} \tag{3.47}$$

In Table 3.1, tentative values of b_c and b_a (at $\alpha=0.5$ and $\nu=1$) are presented for different slow (rate limiting) steps.

3.8 Chemical Steps

Particular electrochemical kinetics features are observed when one or more chemical steps occur along with the electrochemical one. Evidently, only relatively slow chemical steps may influence the overall rate of the process. Slow chemical steps can

Table 3.1 Tafel coefficients b (in mV) for multielectron reactions ($\alpha = 0.5$, T = 25°C)

	Number of limiting step			
Total number of transferred electrons	1	2	3	4
1	$b_c = 118$			
	$b_a = 118$			
2	$b_c = 118$	$b_c = 40$		
	$b_a = 40$	$b_a = 118$		
3	$b_c = 118$	$b_c = 40$	$b_c = 24$	
	$b_a = 24$	$b_a = 40$	$b_a = 118$	
4	$b_c = 118$	$b_c = 40$	$b_c = 24$	$b_c = 17$
	$b_a = 17$	$b_a = 24$	$b_a = 40$	$b_a = 118$

either be preceding or following the electrochemical one. A chemical step preceding cathodic metal deposition can consist, for instance, in the separation of the ligand(s) from the electroactive species, its dehydration, protonation etc. Chemical steps can be homogeneous (occurring in the electrolyte region adjacent to the electrode) or heterogeneous (proceeding at the interface). We consider here the simplest cases.

Let the kinetics of the *preceding homogeneous step* be first order. Then at some distance x from the electrode

$$dc/dt = k[c_0 - c(x)] \tag{3.48}$$

In this equation c_0 is the bulk concentration of the reacting species, and $c(x) < c_0$ i.e. the substance is being consumed. The chemical process occurs within a region with thickness δ; neglecting any transport of this species due to the applied electric field (an assumption often valid, as will be seen in Chap. 4), the resulting concentration gradient causes a simultaneous diffusion of the species. From the second Fick's Law we have:

$$dc/dt = Dd^2c/dx^2, \quad \text{or} \quad Dd^2c/dx^2 = k(c_0 - c) \tag{3.49}$$

After integration

$$(dc/dx)_{x\to 0} = (c_0 - c)(k/D)^{1/2} \tag{3.50}$$

Since the current density, from the first Fick's law, is $i = nFD(dc/dx)_{x\to 0}$, it follows that

$$i = nFc_0(k/D)^{1/2}\,(1 - c_{x\to 0}/c_0) \tag{3.51}$$

This formula shows that in the case under consideration a limiting current density must be observed (at $c_{x\to 0} \to 0$)

$$i_{\lim} = nFc_0(k/D)^{1/2} \tag{3.52}$$

This is the *kinetic* limiting current, i.e. limited by the rate of formation of the electroactive species. In electrochemistry, limiting currents are more often of a diffusional nature; the latter can be easily identified because it depends strongly on hydrodynamic conditions and increases upon stirring of the solution. The kinetic limiting current on the other hand does not depend on stirring.

δ is termed the thickness of the reaction layer: $\delta=(D/k)^{1/2}$.

In the case of a *subsequent chemical step* of the first order the rate of the process is $v=k(c-c_0)$, c_0 being the equilibrium concentration of the product of the preceding electrochemical process; in this case $c>c_0$. Designating $kc_0=v_0$ we obtain

$$v = v_0\,(c/c_0 - 1), \text{ or for the CD} \tag{3.53}$$

$$i = i_0\,(c/c_0 - 1), \tag{3.54}$$

In this expression i_0 is the current density corresponding to the equilibrium rate of the two opposite branches of the chemical reaction.

The electrode potential is now determined by the chemical step and may be calculated according to the Nernst equation

$$E = E_0 + (RT/nF)\,ln\,(1 + i/i_0) \tag{3.55}$$

For $i>>i_0$ this leads to

$$\eta = E_{\text{eq}} - \text{E} \approx -(RT/nF)ln\,i_0 + (RT/nF)ln\,i \tag{3.56}$$

Equation (3.56) differs from the Tafel equation in the fact that the transfer coefficient α is missing. If the reaction has order p, then this equation takes the form

$$\eta \approx -(2RT/nF(p+1))ln\,i_0 + (RT/nF)ln\,i \tag{3.57}$$

allowing to find p from the experimental data.

In literature mixed cases are often discussed, and they are indicated as CE (chemical step followed by electrochemical step) or EC mechanism. More complicated mechanisms are sometimes considered such as ECE; these are more often encountered in relation to complicated reactions involving organic substances. The features of these mechanisms are studied in considerable detail elsewhere [3].

3.9 Ion Discharge Kinetics in Presence of Surface-Active Agents

The adsorption of surface-active substances (SAS) at the electrode surface may vary the rate of electrode reactions over a wide range; most often a rate decrease (inhibition) takes place. In other words, adsorption phenomena on the electrode tend to increase the overpotential for electrodeposition to occur (usually by about 0.1–0.2 V).

The adsorbed molecules or ions may be extraneous to the process of interest, but sometimes these are involved in the series of electrode reactions. For instance, in the discharge of complex ions the free ligands can play the role of SAS.

The influence of the adsorbed species on the electrode kinetics is expressed by some function f of the adsorption θ of the SAS, $f(\theta)$, the value of θ being determined by the adsorption isotherm.

The function $f(\theta)$ describes (1) partial blocking of the surface by the adsorbate, (2) transport of the discharging ion through the supplementary barrier $\Delta G(\theta)$ created by the adsorbed layer and (3) variations of the potential ψ' in presence of adsorbed species, particularly dipoles or ions.

Electrode blocking had been initially described simply by the factor $K_\theta=(1-\theta)$, because this expression determines the value of the surface free of adsorbate, but most experimental data showed that a more complicated dependence does exist: $K_\theta=(1-\theta)^r$ where r ($r\geq 1$) depends on the number density of adsorption sites occupied by the solvent, the adsorbed species and the activated state.

The additional barrier ΔG as usual adds a factor $exp(-\Delta G(\theta)/RT)$ to the reaction kinetics; as a first approximation ΔG is proportional to θ, and this dependence is usually written as $\Delta G/RT=S\theta$. The quantity S reflects various interactions in the adsorbed layer; it depends for example on the attraction parameter a of the adsorption isotherm. The role of the variation of the potential ψ' is also included in the value of S.

Both factors considered above lead us to the conclusion that in effect the overall rate constant in presence of a SAS k_θ can be described [4] as

$$k_\theta/k_0 = (1-\theta)^r exp\,(-S\theta) \tag{3.58}$$

or in logarithmic form

$$ln\,(k_\theta/k_0) = r ln\,(1-\theta) - S\theta \tag{3.59}$$

This expression permits to find the values of r and S from experimental measurements; the errors involved in this determination however can be relatively large. Thus at low θ, $ln(1-\theta)\approx-\theta$, and then $ln\,(k_\theta/k_0)=-(r+S)\theta$ which shows that one cannot find r and S separately.

Sometimes an additional term is included in (3.59) to describe a non-linear dependence of S on the coverage θ.

In turn, θ depends strongly on the electrode potential. This is the reason why the inhibition of metal deposition caused by adsorption is often observed only within definite potential ranges. As it was shown in Chap. 2, species of different nature are adsorbed at different regions of the electrocapillary curve. With increasing overpotential the coverage often falls (Fig. 3.9), not only due to desorption but also owing to the inclusion of adsorbed species into the growing deposit.

Incorporation in the deposit is one of the ways by which SAS are consumed at the electrode; other means may also be their electrochemical reduction or anodic oxidation. These processes may lead to contamination of the deposit and to degradation of its properties.

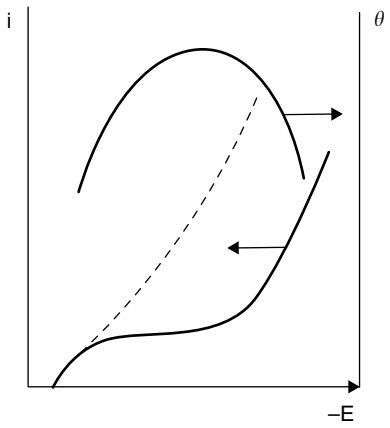

Fig. 3.9 The dependence of current density i and of the surface coverage θ on the potential E. The dotted line shows the current density in the absence of the adsorbed species

As for the transfer coefficient α, its value usually is not considerably varied at coverages up to 0.8–0.9. At high coverage however α often decreases and falls to zero. This is connected with a change in the limiting step of the process. At $\theta \rightarrow 1$ the surface is entirely covered by the adsorbate, and an increase in coverage is achieved only as result of the reorientation of adsorbed species. In these conditions the meaning of the quantity S changes: it is now the work of formation of a pore in the adsorbed layer in which the reducible species in the activated state is introduced. The corresponding shape of the curve E–i is shown in Fig. 3.10.

The step of the penetration of species through the adsorbed layer can become the limiting one; in these conditions the limiting current is described by the empirical equation [5]

$$i = kc\ exp\left(-a\theta^m\right)(m > 1). \tag{3.60}$$

The factor depending on the electrode potential drops out; formally, this corresponds to $\alpha \rightarrow 0$.

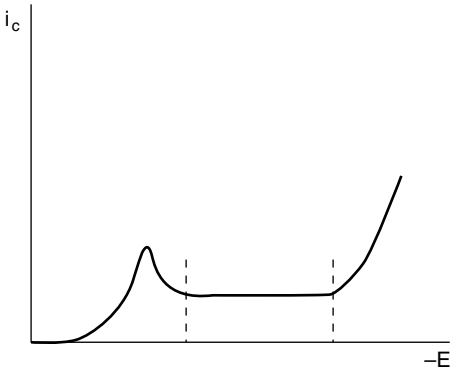

Fig. 3.10 Curve E–i with the region of high coverage

3.10 Peculiarities of the Discharge of Complexes

One of the methods for obtaining fine-grained metallic layers is using electrolytes containing complex compounds of the depositing metal ion. In this case the simple hydrated ions M^{z+} cannot discharge since their concentration is too small; they are mostly bound with ligands L. The cathodic discharge of complex species occurs at a more negative potential as compared with simple ions. This happens for two different reasons. The first one is that the equilibrium potential of the process is more negative, and the second is that the reaction occurs with a higher overpotential and polarizability. Both reasons result in a negative shift of the operating potential, but they are different and should not be confused.

(1) A more negative equilibrium potential shifts the overall operating region; it leads to suppression of contact deposition (displacement) of some metals (e.g., copper on steel) and provides for good adhesion of the deposit. In this respect, it is important to choose the most effective additives to achieve deposition of fine-grained coatings. (2) A higher polarizability provides for a better distribution of the metal throughout the surface along with an additional negative potential shift. Yet another result of both factors can be the acceleration of the side process of hydrogen evolution, resulting in a lower current efficiency.

The complex species discharging at the cathode are often anions, and this makes the discharge more difficult owing to their electrostatic repulsion from the negatively charged electrode. Adsorption of surface-active cations facilitates anion discharge, due to variations of the potential in the double layer.

Complex formation occurs step-wise, resulting in the simultaneous presence of several species $M^{z+}L_i$ $i=0, 1, 2, \ldots, n$; the most complexed species being $M^{z+}L_n$. The overall reaction of dissociation

$$M^{z+}L_{n.} \leftrightarrow M^{z+} + nL \tag{3.61}$$

has a stability constant (the square brackets indicate concentration)

$$K_n = \left[M^{z+}\right][L]^n / \left[M^{z+}L_n\right] \tag{3.62}$$

which determines the concentration of free ions M^{z+} and consequently the equilibrium potential.

The concentration of the different species $M^{z+}L_i$ $i=0, 1, 2,\ldots, n$ is determined by the values of all the intermediate stability constants K_i and by the total concentrations $[M^{z+}]$ and $[L]$. The specified values of K_i give a system of equations which, supplemented with equations for the material balance and neutrality, allows computation of the ionic composition of the solution.

It may be noted that as L is increased, the predominant species in the solution become those with increasing i (up to $i=n$ at high excess of L).

Usually two or three species are present simultaneously in the solution in comparable concentrations, only one of them being electroactive. If the predominant species is the highest one ($M^{z+}L_n$) then the equilibrium potential is

$$\begin{aligned} E_{\mathrm{eq}} &= E_0\left(M^{z+}/M^0\right) - RT/zF ln K_{\mathrm{n}} \\ &= RT/zF ln\left[M^{z+}\right] - nRT/zF ln\,[L]\,. \end{aligned} \tag{3.63}$$

It is noted that E_{eq} depends linearly on the logarithm of the metal ion concentration c, with slope RT/zF; this allows an experimental determination of z.

On the other hand, E_{eq} depends linearly on $ln\,[L]$:

$$\partial E_{\mathrm{eq}}/\partial ln[L] = -nRT/zF; \tag{3.64}$$

this allows to find the number of ligands n in the electroactive complex.

If measurements of E_{eq} are performed over a wide range of concentrations $[L]$, the linearity breaks down because at low $[L]$ the dominant species contains a lower number of ligands: $M^{z+}L_i i<n$. Actually, at each value of $[L]$ the dependence of E_{eq} on $[L]$ gives the correspondent value of I, resulting in a non-linear dependence.

Alternatively, decreasing $[M^{z+}]$ at constant $[L]$ also leads to variations in ionic composition of the solution. For this reason the kinetics of electrodeposition can vary when increasing the current density: as a result of consumption of the metal-containing species at the cathode the ratio $[M^{z+}]/[L]$ falls, resulting in bending of the E–i curve; this resembles the limiting current but its origin is of a different nature.

If the complex ions $M^{z+}L_k$ are the only ones taking place in the electrode process the exchange current density due to their discharge is, according to (3.29):

$$i_0 = i_0\,(0)\left[M^{z+}L_{\mathrm{k}}\right]^{1-\alpha}[L]^{\alpha k}. \tag{3.65}$$

At the same time the equilibrium potential, expressed by the concentration of reacting ions, is equal to

$$E_{\mathrm{eq}} = {E_{\mathrm{eq}}}^0 + (1/zF)\,ln\left\{\left[M^{z+}L_{\mathrm{k}}\right]/[L]^k\right\} \tag{3.66}$$

The last two expressions give the important formula

$$\partial\, ln\, i_0/\partial\, ln[L] = k + (1-\alpha)zf\;\partial E_{\mathrm{eq}}/\partial\, ln[L] \tag{3.67}$$

which can be used for the calculation of k and α from experimental measurements of i_0 and E_{eq} at different concentrations of L. When L is in excess, Eq. (3.64) is valid; this in combination with (3.67) gives

$$\partial\, ln\, i_0/\partial\, ln\,[L] = k - (1-\alpha)\,n. \tag{3.68}$$

In particular, at $k=n$

$$\partial\, ln\, i_0/\partial\, ln\,[L] = \alpha n. \tag{3.69}$$

All these equations are widely used in the study of electrochemical kinetics in solutions containing complex species.

Some additional features of complex discharge observed under diffusion limitations of the reaction rate are considered in Chap. 4.

References

1. Vetter K., Elektrochemische Kinetic. Springer-Verlag, 1961
2. Losev V., Molodov A., Encyclopedia of Electrochemisty of the Elements, Marcel Dekker, 1976, v. 6, p.1
3. Andrieux C.P., Saveant J.V. “Electrochemical Reactions” in: Investigations of rates and mechanisms of reactions, v. 6, 4/E part 2, J. Wiley and Sons, 1986
4. Afanasiev B., Damaskin B., Soviet J. of Electrochemistry, 1975, v. 11, No. 10. p. 1556
5. Loshkarev M., Kriukova A., Soviet J. of Physical Chemistry, 1948, v. 22.

Chapter 4
Influence of Diffusion on the Rate of Electrochemical Process

4.1 Ion Transport and Current

The concentration of electroactive ions c_i which determines the overall kinetics of the electrode process differs in general from the bulk ion concentration. This is a consequence of the location of ion discharge, which is at a potential ψ', different from the bulk solution potential, as it have been noted earlier. Additionally, at high overpotentials, the rate of discharge is very fast and ion reduction is limited by the rate of transport to the electrode surface. The steady state rate of the electrochemical process is in this case exactly equal to the rate of transport of the electroactive species from the bulk.

The rate of transport of charged species is the sum of three contributions: convection, migration and diffusion. The molar flux (i.e. the number of moles flowing through a unit area per unit time) of the generic species *i* is

$$\boldsymbol{M}_i = c_i \mathbf{v} + u_i c_i (-\nabla \Phi) - D_i \nabla c_i \tag{4.1}$$

where u_i is the mobility, and the other symbols have their conventional meaning.

The total current density due to the flux of the charged species is therefore

$$\mathbf{i} = F \sum\nolimits_i z_i \mathbf{M}_i \tag{4.2}$$

In this sum over all the ionic species in the electrolyte the convection term is zero due to the electroneutrality of any small volume larger than the Debye length, and two terms therefore remain: one due to the electric field, the other due to a gradient in concentration. An important consequence of this formula is that in general in an electrolyte the Ohm's law is not observed.

A more general expression for the current density due to the species i can be derived by considering that the overall driving force for mass transfer of a charged species i is the gradient of its electrochemical potential:

$$\mathbf{M}_i = c_i\{\mathbf{v} - D_i(\mathbf{grad}\underline{\mu}_i)/RT\},$$

Y. D. Gamburg, G. Zangari, *Theory and Practice of Metal Electrodeposition,*
DOI 10.1007/978-1-4419-9669-5_4, © Springer Science+Business Media, LLC 2011

where μ_i is:

$$\mu_i = \mu_i^0 + RT \ln a_i + zF\varphi.$$

The resulting current density of the species i (neglecting the convection term) is:

$$i_i = -D_i nF \, dc_i/dx + D_i c_i z_i nF f \, d\varphi/dx \tag{4.3}$$

where D_i takes into account the non ideality of the solution:

$$D_i = D_0[(1 + \partial\gamma/\partial c_i)] \tag{4.4}$$

Furthermore, by defining

$$D_i^* = D_i[1 + z_i f/(\partial \, ln \, c_i/\partial\varphi)] \tag{4.5}$$

Equation (4.3) reduces to

$$i_i = -D_i^* nF \, dc_i/dx$$

At a given cell potential, the electric field decreases with increasing concentration of the electrolyte. If a considerable excess of a supporting electrolyte (which does not participate in electrochemical reactions at the electrode) is present, the electric field is weak, is determined mainly by these ions and therefore does not change over time. It follows that the ions involved in electrochemical reactions only move through diffusion.

Thus, if we may neglect electric migration of species (a good approximation in presence of a considerable excess of the supporting electrolyte) the current density can be written simply as

$$i_i = -D_i nF \, dc/dx \tag{4.6}$$

In this equation, the factor nF transforms the diffusion mass flux into electric units, and x is the coordinate normal to the flat electrode surface. For $x \to 0$ this equation is universal and it holds true at any moment from the very beginning of the electrochemical process. The diffusion approximation for ionic motion may sometimes result in a counterintuitive behavior; for example negatively charged complexes (cyanides) may move towards the electrode even if it is polarized negatively.

It should be noticed that the same formula (4.6) for current density i can be also used if electric transport (migration) is taken into account, but in this case the effective diffusion coefficient D_i^* should be used. If the directions of migration and diffusion fluxes are the same, $D_i^* > D_i$, in the opposite case $D_i^* < D_i$. When the metal is reduced from the simple cation, both members have the same signs resulting in $D_i^* > D_i$; for the electroreduction of anions instead $D_i^* < D_i$. This approach however is not completely rigorous: D_i^* depends both on the coordinate and on current density, because upon increase of the potential gradient the contribution of migration increases. In any case, the form of Eq. (4.6) can be often useful and convenient.

The approach outlined above allows to use simple diffusion equations and simplifies the analysis of relatively complicated problems (e.g. in presence of different concentrations of the supporting electrolyte). A more rigorous treatment requires

the use of equations (4.3) written for all charged species in the solution; this will be described below in Sect. 4.6.

The electrode surface is here assumed to be uniform, in particular with respect to electrochemical processes; the concentration of active centers for example will be assumed to be very high. This assumption requires that no concentration gradient exists along the surface, and the ion concentration in the electrolyte depends only on the distance from the electrode, i.e. it is one-dimensional. Equation (4.6) corresponds to the concentration distribution at the electrode shown in Fig. 4.1; this concentration profile has been established experimentally by means of interferometric measurements. The concentration gradient of the electroactive species near the electrode is therefore constant in the layer with thickness δ. The ion concentration c changes linearly, if D^* is constant: this follows from the second Fick's Law

$$\partial c/\partial t = D\partial^2 c/\partial x^2. \tag{4.7}$$

At steady state the left side of this equation is equal to zero, then the right side should also be zero; It follows then that $\partial c/\partial x = const$. But at some distance $x > \delta$ from the electrode $c = const$; at $x = \delta$ the sharp change in slope of the function $c(x)$ is caused by convection.

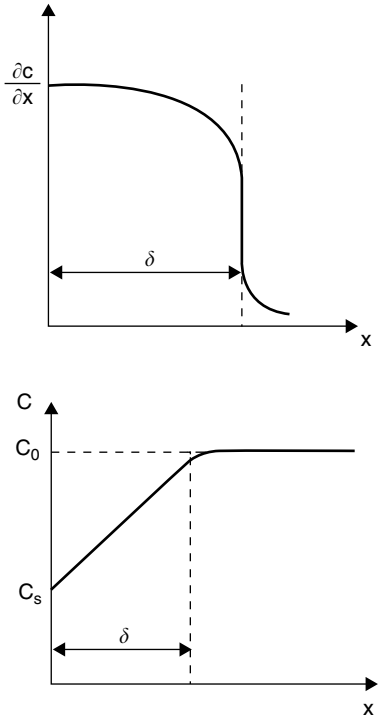

Fig. 4.1 Concentration profile near the electrode during electrodeposition

The layer $0<x<\delta$ in which the concentration varies is named *diffusion layer*. This concept was originally suggested by Nernst, so we shall indicate its steady state thickness as δ_N.

4.2 Diffusion

Under the diffusion approximation the second Fick's law is valid. This differential equation can be solved under the condition of constant electrode potential, finding a mass flux which decreases with the inverse square root of time. The thickness of the diffusion layer δ is also found by this solution to be time-dependent; in fact, immediately after switching the current on the concentration varies only in a very thin layer near the electrode, which expands initially as $t^{1/2}$, until natural convection starts to occur, due to density gradients. This is a complex process, whose description can be strongly simplified by using a rotating disc electrode (RDE). This electrode is considered in Sect. 4.8, and non-steady diffusion is discussed in Chap. 9.

Even in absence of solution agitation the process of natural convection results in the formation of a diffusion layer with a definite thickness. The ion concentration varies with position only in this narrow region near the electrode. This is the reason why mass transfer calculations for the region near the electrode are usually incorrect when they are made for a semi-infinite region; more precisely, they are correct only at small values of t. The correct boundary conditions should be set: (a) for the electrode surface and (b) for the border of the diffusion layer. The last condition is usually $c(\delta) = c_0$ or $\partial c/\partial x_{(x=\delta)} = 0$. The corresponding calculations require knowledge of the value of δ_N with a relative accuracy.

It is important to underline that in the majority of cases δ_N is equal for all the species present in the solution; this facilitates the corresponding mass transport and current calculations.

Under the approximation of natural convection in aqueous solutions the usual value of δ_N is approximately 0.03–0.05 cm, depending on viscosity and density of the solution, electrode geometry and electrochemical conditions. Upon stirring the diffusion layer becomes much thinner (down to 0.001 cm); in this case the force used for agitation maintains δ_N constant, better than natural convection does. At steady state δ_N on the electrode is constant in time at any position but varies spatially. The one exception is the rotating disc electrode (RDE, Fig. 4.2). For a correctly designed (and built) electrode of this type the thickness δ_N is the same over its entire surface; the current distribution can be easily calculated if the speed of rotation is given and also diffusion coefficient and viscosity are known. Calculations and measurements indicate that at RDE δ_N in cm is of the order of 0.01 $\omega^{-1/2}$ (ω being the rotation frequency, s^{-1}). A good approximation for δ_N is

$$\delta_N \approx 1.70 D^{1/3} \nu^{1/6} \omega^{-1/2}, \tag{4.8}$$

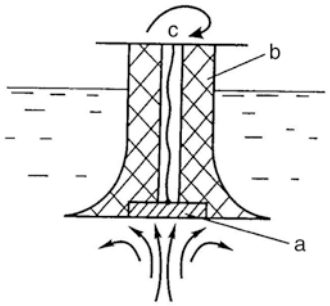

Fig. 4.2 Scheme of the rotating disc electrode

ν being the viscosity coefficient. The RDE is an instrument of great importance in experimental electrochemistry, and is regularly used for various experimental investigations. The theory of this electrode [1] is briefly presented in Sect. 4.8.

Values of δ_N at rotating electrodes of different shapes can be expressed by the general formula

$$\delta_N \approx K\omega^{-\alpha} \tag{4.9}$$

where α lies usually between 0.5 and 0.8 depending on the electrode type, K being established experimentally.

A set of formulas is available for calculation of δ_N at several conditions. Among others, at a single electrode swept by a laminar electrolyte flow

$$\delta_N(x) \approx 2.95 D^{1/3} \nu^{1/6} w^{-1/2} x^{1/2}, \tag{4.10}$$

where w is the flow velocity, and x is the distance from the electrode edge.

On the inner surface of a cylindrical tube of radius R

$$\delta_N(x) \approx 1.49 D^{1/3} R^{1/3} w^{-1/3} x^{1/3} \tag{4.11}$$

where w is the flow velocity at the tube axis, and x is the distance from the entrance.

For natural convection at a vertical plate and under laminar flow

$$\delta_N(x) \approx K(D\nu x/g)^{1/4}, \tag{4.12}$$

where g is the gravity factor, and x is the distance from the lower edge; K is close to 10 and depends on the derivative of solution density with respect to its concentration.

For the process of hydrogen evolution at an electrode δ_N varies inversely proportionally to the square root of the rate of gas evolution:

$$\delta_N(x) \approx (0.4 - 0.6) i(H_2)^{-1/2} \tag{4.13}$$

if δ_N is expressed in cm and $i(H_2)$ in A/cm^2.

Most of the expressions presented above are derived through the use of rather sophisticated hydrodynamic calculations; an example will be given in Sect. 4.8.

4.3 Limiting Current

The concentration gradient dc/dx in a diffusion layer of thickness δ_N can be expressed as

$$dc/dx = (c_0 - c_s)/\delta_N; \tag{4.14}$$

where c_0 and c_s are the ion concentration in the bulk and near the electrode surface, respectively; this follows from the constancy of dc/dx. No partial derivatives are used since a steady state condition is considered.

The current density provided by this concentration gradient is (4.6)

$$i = nFD^*(c_0 - c_s)/\delta_N. \tag{4.15}$$

In order to achieve a higher current i the surface concentration c_s has to fall, approaching eventually zero. Hence it follows that for given values of c_0 and δ_N a maximum value of CD, i_d, exists, which corresponds to $c_s \rightarrow 0$:

$$i_d = nFD^*c_0/\delta. \tag{4.16}$$

This value of current density is called limiting current density. Its existence was established by Brunner in 1903.

Evidently, the concentration c_s does not actually fall to zero. Its value can be found for any given value of i by imposing the equality of kinetic and diffusion currents at the steady state:

$$kc_s\, exp(\alpha nf\eta) = nFD^*(c_0 - c_s)/\delta_N. \tag{4.17}$$

When it is stated that the concentration falls to zero, this means only that c_s is small as compared with c_0.

A simpler way of finding c_s is by using the value of i_d: from the system of equations (4.15) and (4.16) follows

$$c_s = c_0(1 - i/i_d). \tag{4.18}$$

By applying the concept of limiting current any expression in which the value of diffusion layer thickness appears can be reformulated in terms of the limiting current. For this purpose, it is sufficient to insert δ from Eq. (4.16), and then the expressions for i_d under various conditions can be derived.

This procedure results in the following formulae:

For laminar liquid flow between two planes spaced by the distance h

$$i_d\,(x) \approx 0.98\, nFcD^{2/3}w^{1/3}h^{-1/3}\mathrm{x}^{-1/3} \tag{4.19}$$

where w is the mean velocity of the flow between the planes, and x is the coordinate along the electrode. This formula gives the limiting current density at the point x; then it is clear that $i_d(x)$ diminishes when moving farther away from the entrance into the channel. To obtain the average value for the overall length of the electrode this result should be multiplied by 1.5.

For an electrode swept by a solution moving with velocity w and with viscosity ν

$$i_d(x) \approx 0.34\, nFcD^{2/3} w^{1/2} \nu^{-1/6} x^{-1/2}. \tag{4.20}$$

In this case the averaged value is twice as much.

The limiting current at a RDE at any point of the surface is

$$i_d = 0.6\, nFcD^{2/3} \omega^{1/2} \nu^{-1/6}; \tag{4.21}$$

at a rotating cylindrical electrode it depends on its radius r:

$$i_d \approx K\, nFc(D\nu)^{0.65} \omega^{0.7} r^{0.4}. \tag{4.22}$$

The averaged limiting current to a vertical electrode with height h when natural convection occurs is close to

$$i_d \approx K\, nFcD^{0.75} (g/\nu h)^{0.25} \tag{4.22a}$$

The coefficient K in the two last cases lies usually between 0.1 and 1. For a better precision, an accurate value of K should be determined experimentally for the given electrode; g is again the gravity factor.

In the majority of monographs and reference books these formulae are often given in the form of relations between non-dimensional numbers; for example the Nusselt (Nu), Reynolds (Re) and Schmidt (Sc) numbers are widely used in mass transfer analysis.

The value of i_d often determines the operative current density in practical electrolysis. Usually, electrodeposition processes are performed at a current density less than one-half of the limiting one, more often $i < 0.4 i_d$. This limitation is dictated by the fact that at higher current the steady growth front of the deposit may become unstable, resulting in a rapid rise of the local protrusions and of the overall roughness. Dendrites also start to grow in these conditions. This issue is considered more thoroughly in Chap. 8; here we note only that the empiric coefficients (0.5 or 0.4 of i_d) are derived by the explicit evaluation of the current distribution at the electrode. In particular, due to a non-uniform current distribution the local value of CD can be significantly higher than the prescribed one and may come close to i_d.

The reasons for this local current excess may be due both to a non-uniform macroscopic distribution of current, generating peaks of current at isolated points of the electrode, or to the current microdistribution, resulting in very high current densities at microprotrusions.

4.4 Diffusion Overpotential

The presence of a diffusion layer near the cathode results, as we have seen, in a reduced concentration of the reacting species. Among other effects, this leads to a variation of the equilibrium value of the electrode potential, according to the Nernst equation. This shift of E_{eq} is named *concentration overpotential*. In the general case the value of the equilibrium potential (corresponding to new values of the surface concentrations $c_{O(s)}$ and $c_{R(s)}$) is

$$E_{eq} = E_0 + (RT/nF)\ln(c_{O(s)}/c_{R(s)}). \tag{4.23}$$

In this equation concentrations are used, and the activity coefficients are neglected. Equation (4.23) therefore substitutes the initial expression

$$E_{eq\,(0)} = E_0 + (RT/nF)\ln\,(c_O/c_R). \tag{4.24}$$

The difference between these values ΔE_{eq} is, as already noted, the concentration overpotential:

$$\eta_c = \Delta E_{eq} = (RT/nF)\ln(c_R c_{O(s)}/c_O c_{R(s)}); \tag{4.25}$$

in the case of metal deposition far from equilibrium this expression simplifies to

$$\eta_c = (RT/nF)\ln(c_{O(s)}/c_O), \tag{4.26}$$

or simply

$$\eta_c = (RT/nF)\ln(c_s/c_0). \tag{4.26a}$$

c_s and c_0 are the near-electrode and bulk concentrations of the discharging ions, respectively.

The origin of this overpotential is the slow diffusion of ions to the electrode, thus it is called *diffusion overpotential*, η_d. In general there may be other reasons for the onset of concentration variations; the term concentration overpotential encompasses all these cases.

Another form of (4.26) results from (4.18):

$$\eta_d = (RT/nF)\,\ln\,(1 - i/i_d). \tag{4.27}$$

Consequently, the value of the limiting current density would suffice to determine the diffusion overpotential at any given CD. The value of i_d is usually measured experimentally; if this last equation is written in the form

$$i = i_d\,[1 - exp\,(nF\eta_d/RT)]\,, \tag{4.28}$$

one can see that at high overpotential the current density approaches its limiting value i_d asymptotically, as shown in Fig. 4.3. In reality this expression is not rigorous due to possible heating of the solution at high CD along with contributions from migration and convection.

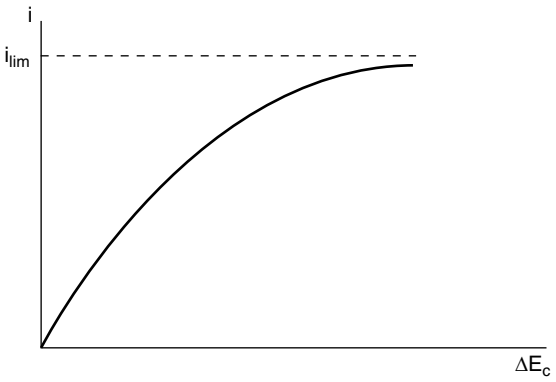

Fig. 4.3 Asymptotic approach to the limiting current

It is seen from this figure that when approaching the limiting current the potential tends to infinity; in practice this potential shift causes new electrochemical process, active in this potential region, to occur. In electrodeposition from aqueous solution for example hydrogen evolution always occurs.

Up to this point we have considered only the deposition process. The opposite process, i.e. the slow withdrawal of the electrode products (for example, the anodic dissolution of a metallic anode) can be discussed in a similar manner. In this case new species are formed near the anode ($c_s > c_0$), and the diffusion overpotential becomes

$$\eta_d = (RT/nF) \ln (1 + i/i_d). \tag{4.29}$$

When the rate of the anodic process is so high that the concentration of the species formed becomes higher than the solubility limit, a solid precipitate can be produced on the electrode surface which hinders the electrochemical process; this occurrence is usually referred to as salt-induced passivity.

In conclusion it should be stressed that *the concentration overpotential, contrary to the overpotential of charge transfer, is a thermodynamic quantity*: it consists in fact in a shift of the equilibrium potential. Its dependence on current density is secondary because its immediate reason is the drop in reactant concentration.

4.5 Mixed Kinetics

Very often the overall rate of the electrode process is governed simultaneously by the rate of electron transfer at the surface and of mass transfer in the solution. The charge transfer process determines the overall kinetics when the potential shift from equilibrium is small; under these conditions, ion depletion in the near-electrode layer is minor, and the overpotential is purely of an electrochemical nature. On the contrary, at high overpotentials, corresponding to CD values close to i_d, the overall process is dominated by the diffusion kinetics; in this region the approach to the

limiting current is accompanied by a sharp increase of the diffusion overpotential. At intermediate overpotentials both contributions are comparable. Next we discuss mixed kinetics in electrodeposition.

In the following it will be convenient to use the designations: $exp(-\alpha nF\eta/RT) = f_1(\eta)$; and $exp[(1-\alpha)nF\eta/RT] = f_2(\eta)$. Then the potential dependence of the cathodic partial current density in the BV equation can be written as $i = i_0(c_s f_1/c_0)$, and that of the anodic partial current density as $i = i_0 f_2$. The overall BV equation assumes then the form:

$$i = i_0\,(c_s f_1/c_0 - f_2). \tag{4.30}$$

On the other hand, it follows from (4.18) that $c_s/c_0 = 1 - i/i_d$; the combination of the two last expressions gives therefore $i = i_0[(1 - i/i_d)f_1 - f_2]$ or, after rearrangement

$$i = i_0(f_1 - f_2)/(1 + i_0 f_1/i_d). \tag{4.31}$$

This relationship is very useful when analyzing experimental data for the dependence of current density on electrode potential. This equation takes in fact into account both forward and backward processes as well as diffusion limitations.

After substitution of the values of f_1 and f_2 and taking the logarithm of both sides, we obtain

$$-ln\,[1 - i/i_d - exp\,(nF\eta/RT)] = ln\;i_0 - \alpha nF\eta/RT. \tag{4.32}$$

This formula allows finding the values of i_0 and α if i_d is known along with the dependence of i on the applied potential. To this end, it is sufficient to plot the left side of the equation against potential; the intercept on the i-axis will be i_0, and the slope $\alpha nF/RT$.

At high cathodic (negative) η the exponent $exp(nF\eta/RT)$ becomes negligibly small, and (4.32) simplifies to

$$-ln[i_d i/(i_d - i)] = ln\;i_0 - \alpha nF\eta/RT. \tag{4.33}$$

This form of the equation is equivalent to imposing that $f_2 = 0$; from (4.33) follows an instructive relationship between the limiting CD i_d, the kinetic value of CD, determined at the given potential by the BV equation, $i_k = i_0 f_1$ and the measured actual value i of the CD at the same potential:

$$1/i = 1/i_d + 1/i_k. \tag{4.34}$$

It must be stressed that in this equation i_k corresponds to the volume concentration of reacting ions c_0, not to the surface concentration c_s. This relationship can also be derived by considering the charge transfer reaction as occurring through a two-step process, when the two steps have similar rates; in this case the inverse of the total reaction rate will be the sum of the inverse of the rates of the various steps.

In the above calculations it is important to know the true value of c_s, but these measurements are not simple. Obviously, when ion discharge occurs very fast their surface concentration corresponds to the Nernst equation. This is true however

only at high exchange current density: $i_0 \gg i$. In general, for an electrodeposition process:

$$c_s = c_0 \left[exp\left(nF\eta/RT\right) + i/i_0 \; exp\left(\alpha nF\eta/RT\right)\right]. \tag{4.35}$$

This equation [2] involves only the measured values of overpotential and current density (along with i_0 and α), and it shows that actually for $i \ll i_0$ the Nernst equation is obeyed, i.e. the reaction is thermodynamically reversible. Otherwise, a non-zero overpotentia, η_e, is associated with the charge transfer process. In the case of mixed kinetics the overall overpotential η is the sum of two components:

$$\eta = \eta_e + \eta_d \tag{4.36}$$

but the electrochemical overpotential should be calculated taking into account the variation of reactant concentration near the electrode. In particular conditions η_d can be calculated by eq. (4.26a) where c_s is determined by Eq. (4.35).

The polarizability in the case of mixed kinetics depends on the current density; it falls from RT/i_0nF at low CD to $4RT/\alpha i_d nF$ at $i = 0.5i_d$ (it is assumed here that $i_0 \ll i_d$) and then increases when approaching the limiting current. The general formula for this dependence, excluding the region near the equilibrium potential, is

$$d\eta/di = (RT/\alpha nF)\, i_d/\left[i\left(i_d - i\right)\right]. \tag{4.37}$$

4.6 The Influence of the Electric Field on the Limiting Current

A more rigorous treatment of the mass and charge transport near the electrode requires the analysis of the motion of all species—charged and uncharged, electroactive or not.

For the electroactive species reacting at the electrode, as shown in Eq. (4.3)

$$-D_i dc_i/dx + D_i c_i z_i f d\varphi/dx = i/nf \tag{4.38}$$

For the species generated at the electrode instead:

$$-D_i dc_i/dx + D_i c_i z_i f d\varphi/dx = -i/nf \tag{4.39}$$

Finally, for the species taking no part in the electrode reaction

$$-D_i dc_i/dx + D_i c_i z_i f d\varphi/dx = 0. \tag{4.40}$$

This set of equations can be completed by imposing the condition of electroneutrality:

$$\sum c_i z_i = 0. \tag{4.41}$$

The solution to the above problem gives the concentration distribution near the electrode, the potential distribution and the value of the limiting current density. The solution for the particular case of an electrolyte where the electroactive ions

are present at low concentrations with an excess of indifferent ions (supporting electrolyte) shows that in such conditions electric migration can be neglected since the overall current through the solution is transferred by the supporting electrolyte.

In the case of a binary (z,$-z$) electrolyte without a supporting electrolyte Eq. (4.38) leads to $d\varphi/dx = zf(d\ ln\ c/dx)$, and then $d\ ln\ c/d\varphi = zf$. The substitution of this equality into (4.5) gives $D^* = 2D$. This shows that the migration process doubles the current density compared to pure diffusion. In the general case for z_c-charged cations and z_a-charged anions the coefficient by which the current increases is

$$\mathrm{k} = 1 + |z_c/z_a| \tag{4.42}$$

This result is valid only for one-component electrolytes, without any supporting additions. In presence of foreign electrolytes k diminishes. An analytical solution in this case can be found only in some particular cases; the corresponding calculation is not difficult. If both electrolytes, that providing the electroactive species and the supporting one, consist only of |z|-charged ions the analytical solution may be expressed as

$$\mathrm{k} = 2(1 + m)\{1 - [m/(m + 1)]^{1/2}\} \tag{4.43}$$

where m is the ratio of the supporting electrolyte concentration to that of the basic one. It is interesting that k in this equation does not depend on the diffusion coefficients: this phenomenon is of a purely electrostatic nature. Note that this approach ignores the incomplete electrolyte dissociation which may occur at high concentration and that may influence the results.

The processes by which the new ions are produced at the electrode as a consequence of the charge transfer reaction are also of interest as they may affect the reaction rate. Upon the cathodic discharge of the anion $[Ag(CN)_2]^-$ for example, metallic silver is deposited at the cathode whereas CN^- anions move from the electrode surface to the solution. The latter process will cause the limiting current to decrease down to 0.82 of the pure diffusion current.

On the contrary, the limiting current is enhanced when discharge of cations occurs. Nickel deposition from acetic solutions is an interesting example. The simplest electrolyte involves only two species: $NiAc^+$ (designated by the index 1) and Ac^- (index 2). The corresponding equations for this system are as follows:

$$D_1(-dc_i/dx + c_1 f\, d\varphi/dx) = i/(2F) \tag{4.44}$$

$$-(D_1 dc_i/dx + D_2\, dc_2/dx) + D_1 c_1 f\, d\varphi/dx - D_2 c_2 f\, d\varphi/dx = 0. \tag{4.45}$$

The first of these equations is written only for Ni-containing species whereas the second one for both kinds of species. Taking into account electroneutrality and setting $D_1 = D_2 = D$, one can derive

$$i = (2F^2/RT)D_1 c_1 f\ d\varphi/dx, \quad dc_i/dx = 0, \tag{4.46}$$

i.e. transfer of the electroactive ions occurs exclusively by electric migration, and the concentration gradient is equal to zero. Note that in this case $d\ ln\ c/d\varphi = 0$, and then $D^* \to \infty$.

In the more general case of discharge of z-charged complex $[M_pL_q]^z$ with z'-charged ligands

$$\left[M_pL_q\right]^z + ne \rightarrow pM + qL^{z'}, \tag{4.47}$$

where $n = z - qz'$ and the concentration of complex species is c, a similar set of equations (assuming $D_1 = D_2 = D$) leads to

$$i_d = nFDc(1 - z/z')/[\delta(1 - q)], \tag{4.48}$$

and this expression differs from the customary one (4.16) by the factor $(1 - z/z')/[(1 - q)]$, which shows the extent to which does the limiting current in this case differs from the usual situation. In the most general case, when the diffusion coefficient of the complex species D_1 differs from that of ligands D_2 (4.48) becomes [3]

$$i_d = nFD_1c(1 - z/z')/[\delta(1 - qD_1/D_2)]. \tag{4.49}$$

In presence of a supporting electrolyte the corresponding result will be intermediate between (4.49) and (4.16).

The enhancement of the limiting current due to electric fields is also known as *amplification of migration current*. This amplification is due to the increase of the migration flow of the species of interest due to the presence of some additionally introduced substance which is reduced concurrently. The qualitative explanation of this fact is simple: the migration is governed by the overall potential gradient, and this gradient depends in turn on all the discharging ions.

The maximum increase in the limiting current of a reducing z_c-charged cation as a consequence of the simultaneous reduction of a second cation in presence of a common anion can be expressed as

$$i_d = i_d^0\,(1 + |z_c/z_a|)\,; \tag{4.50}$$

this value is reached when the concurrent process also takes place at its limiting current. In presence of a supporting electrolyte this amplification is not as significant. It is clear that if the second cation does not discharge, for example when the corresponding reduction potential is not reached, then its salt can be treated as a supporting electrolyte, and the enhancement is absent; if the second cation is discharged at its limiting current then the situation is the same as in (4.42) for both currents, and maximum amplification occurs. In the intermediate cases the resulting current is also intermediate.

The system of equations (4.38–4.41) permits to calculate not only the currents but also the potential drop in the diffusion layer (the term Ohmic drop which is often

used in this context is incorrect because Ohm's Law is not valid here). The solution of the system shows that, e.g., as the limiting current is approached the potential drop increases sharply. The mathematical expressions describing these potential drops are very often quite similar to those for the diffusion overpotential. It is important to keep in mind that in fact we are dealing with two different quantities. The diffusion (or, in general, concentration) overpotential has a thermodynamic origin and depends directly on concentrations, whereas the "Ohmic" drop is associated with the electric field in the solution and depends directly on the current density.

4.7 Role of Diffusion in the Discharge of Complex Species

The discharge of complex species is often complicated by the fact that some intermediate steps of chemical nature are slow; these processes are discussed in Sect. 3.8. In the opposite case it is usually assumed that the chemical equilibrium

$$M^{z+}L_{\mathrm{n}} \leftrightarrow M^{z+}L_{\mathrm{k}} + (n-k)L \tag{4.51}$$

is maintained also when electric current flows; this means that the ratio

$$K_k = \left[M^{z+}L_{\mathrm{k}}\right][L]^{n-k} / \left[M^{z+}L_{\mathrm{n}}\right] \tag{4.52}$$

remains constant throughout the reduction process, both in the electrolyte and at the surface of the electrode, where the concentration of the reacting species $[M^{z+}L_{\mathrm{n}}]$ is reduced as result of diffusion limitations:

$$\left[M^{z+}L_{\mathrm{k}}\right]_{\mathrm{s}} = \left[M^{z+}L_{\mathrm{k}}\right]_0 (1 - i/i_{\mathrm{d}}), \tag{4.53}$$

or

$$\left[M^{z+}L_{\mathrm{k}}\right]_{\mathrm{s}} = K_k \left[M^{z+}L_{\mathrm{k}}\right][L]^{k-n} (1 - i/i_{\mathrm{d}}). \tag{4.54}$$

Substitution of this expression into (3.66) gives after simple rearrangement

$$i/(1 - i/i_{\mathrm{d}}) = \mathrm{i}_0 K_k \left[M^{z+}L_{\mathrm{k}}\right][L]^{k-n}\, exp\left[-\alpha z f\left(E - E_{\mathrm{eq}}\right)\right] \tag{4.55}$$

Hence it follows that if a set of measurements of current densities i is made at constant E, but at different $[L]$ then the value of $log[i/(1 - i/i_{\mathrm{d}})]$ varies linearly with $log\,[L]$, the slope of this dependence being equal to $(k-n)$.

Particularly, at $k=n$ the current density i does not depend on $[L]$. This independence indicates that the dominant complex is simultaneously the electroactive one. Just in this case (3.68) becomes (3.69), which we repeat here:

$$\partial\, ln\, i_0 / \partial\, ln\,[L] = \alpha n. \tag{4.56}$$

This equation permits to find the electrochemical parameters by measuring the exchange CD at various ligand concentrations.

If, however, the rate of a preceding or successive chemical step is slow, than the balance is disturbed, and the above relations become incorrect.

When the discharge of a complex species is accompanied by the generation of negatively charged ligands the limiting current of this process is enhanced with respect to the pure diffusion current. This increase can be significant; it depends on the relative concentration of the supporting electrolyte, on the diffusion coefficients of the various species and also on the dissociation characteristics of the complex. The analysis of the corresponding processes (such as dissociation, discharge, diffusion and migration) is complicated and it is based on the equations from Sect. 4.6.

4.8 Diffusion Layer on the Rotating Disc Electrode

It has been experimentally established that motion of a solid body in a liquid results in the formation of a *boundary layer*, that is a layer at the body/liquid interface where a gradient in the fluid velocity is set up because the liquid at surface moves together with the solid body. This phenomenon was first discovered by Prandtl in 1904. In the case of a rotating disc electrode (Fig. 4.2) the fluid near the solid surface rotates together with the electrode, but this motion is damped out with distance from the disc, owing to viscosity. The thickness of the boundary layer δ_{Pr} at a RDE is constant across the overall surface and is equal, as determined by hydrodynamic calculations, to

$$\delta_{Pr} \approx 3.6\nu^{1/2}\omega^{-1/2}. \tag{4.57}$$

It is apparent that the Prandtl's layer does not exhibit any sharp edge at the liquid side; (4.57) gives only the distance at which the velocity falls by about ten times.

The independence of δ_{Pr} on the coordinate, in particular, on the distance from the axis, is unique to the RDE. In other cases this thickness depends on the flow velocity w and on the distance x along the surface from the point where the flow runs on it:

$$\delta_{Pr} = const \cdot \nu^{1/2} w^{1/2} x^{1/2}. \tag{4.58}$$

In the case of the RDE the latter point may be identified with the center of the disc, and then $x=r$; besides, the flow velocity on the disc is $w=\omega r$. The substitution of these values into (4.58) immediately gives (4.57). One can say that the variation in x is counterbalanced by the corresponding variation in r.

It is necessary to stress that the boundary layer is not identical to the diffusion layer! Whereas the former is characterized by a velocity gradient, the latter is the layer in which the concentration of ionic species varies. In general the corresponding thicknesses are different, though the ratio of δ_N to δ_{Pr} is constant for a given solution and at a given temperature; normally δ_N is several times less than δ_{Pr}.

To find the value of δ_N at a RDE it is necessary to solve the equation of convective diffusion. In the simplest form and at the steady state $(\partial c/\partial t = 0)$ it can be written as

$$D\, d^2c/dz^2 = w(z)dc/dz \tag{4.59}$$

where we neglect the radial component of the velocity w; z is the distance along the axis. The function $w(z)$ is known from hydrodynamics; near the electrode it is

$$w(z) \approx -0.5\left(\omega^{3/2}\nu^{-1/2}\right) z^2; \tag{4.60}$$

here the sign "minus" is caused by the two axes being in opposite direction; the z axis is from the electrode while the velocity w is toward its surface.

The substitution of (4.60) into (4.59) gives after the first integration dc/dz as a function of z. This function is shown in Fig. 4.4; at small z

$$dc/dz \approx 0.61 D^{-1/3}\omega^{1/2}\nu^{-1/6}\,(c_0 - c_s)\,, \tag{4.61}$$

this value varying only a little at some distance from the surface of the RDE. This relationship allows to establish the thickness of the diffusion layer by extrapolation of the dependence $c(z)$ to the axis z. Then (4.61) gives the formula first derived by Levich [4] in 1942:

$$\delta_N \approx 1.62 D^{1/3}\nu^{1/6}\omega^{-1/2}. \tag{4.62}$$

At a later time more rigorous calculations [5] have found a slightly different coefficient near 1.7, as reported in Eq. (4.8). Experiments show that in real RDEs this coefficient lies between the indicated values. Obviously, the surface of the disc should be very smooth; in particular, the roughness should be much less than δ_N. Moreover, the coefficient depends slightly on the eccentricity. Further, the theory of the RDE is elaborated for a disc flush-mounted in an infinite plane; and hence the right design of the electrode should be as shown in Fig. 4.5.

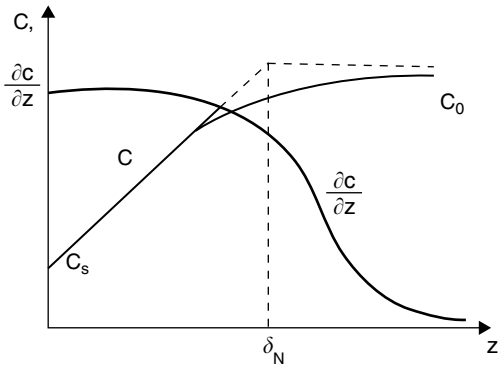

Fig. 4.4 dc/dz as function of z at RDE

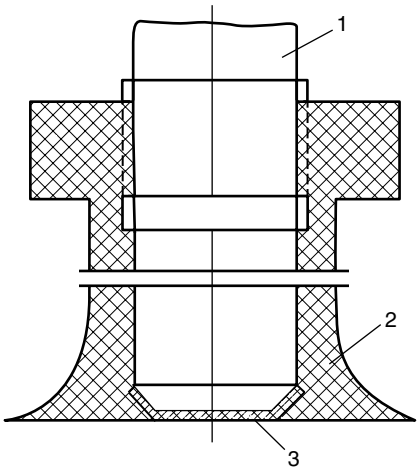

Fig. 4.5 RDE with the separable specimen

Division of (4.62) by (4.57) gives the very general formula

$$\delta_N/\delta_{Pr} \approx 0.5(D/\nu)^{1/3} \tag{4.63}$$

which is true not only for the RDE but also for many experimental configurations. In aqueous solutions this ratio corresponds approximately to $\delta_N \approx 0.1\delta_{Pr}$. Thus the diffusion layer for convective diffusion is much thinner than the boundary layer.

Levich formula shows that the diffusion layer at a RDE has a uniform thickness throughout its surface; in other words, the convective diffusion occurs uniformly over the entire surface. This unique property of the RDE is often characterized as equi-availability of all its points for the electrode process. However, it is necessary to underline that though the surface of a RDE has a truly uniform diffusion layer, this does not necessarily imply uniformity in terms of current distribution. An ideally uniform current distribution at a RDE can be achieved only at the limiting current density or in presence of a large excess of supporting electrolyte. Under other conditions the current density in the center can be much less than at the periphery (Chap. 7).

The RDE helps to establish whether the observed limiting current is of a diffusional nature; all one has to do is to plot the values of i versus $\omega^{1/2}$. If the current is truly the diffusion limiting current the dependence has to be linear, because i_d is proportional to $1/\delta_N$. The dependence $1/i - \omega^{-1/2}$ is linear not only for the limiting current (Fig. 4.6); its extrapolation at $\omega \to \infty$ (or $\omega^{-1/2} \to 0$) gives the reciprocal value of the kinetic current density (i_{kin}) determined by the BV or Tafel equation and corresponding to the given overpotential. It follows from the simple formula

$$i/i_{kin} = c_s/c_0 = 1 - ki\omega^{-1/2}. \tag{4.64}$$

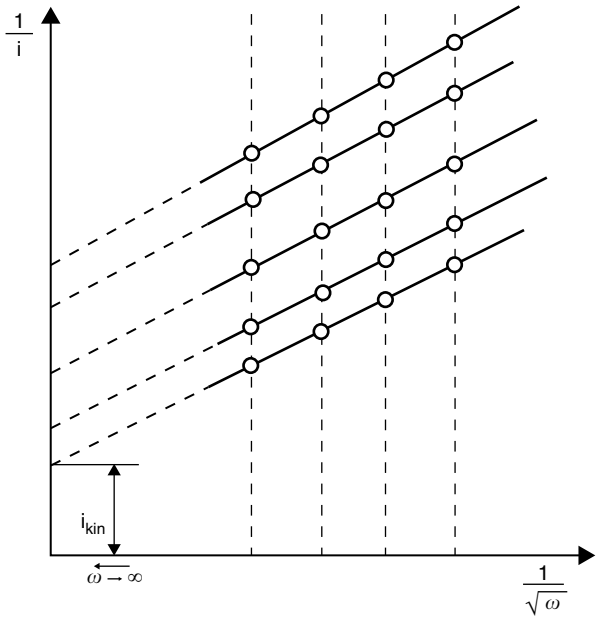

Fig. 4.6 Determination of the kinetic current density (i_{kin}) by extrapolation at $\omega^{-1/2} \rightarrow 0$

which also allows to calculate D, if ν is known. This method has been successfully employed since the 1950s when it was used for the first time by Frumkin and Tedoradse [6].

The rotating electrode is not only a very convenient tool for studies of mass transfer in electrode processes. By using a RDE at high rotation speed high current densities of electrodeposition or other electrode processes can be achieved, unattainable by other methods. Specific types of RDE are designed in order to perform studies of the structures and properties of the deposits formed at such extreme conditions; these include a separable specimen (Fig. 4.5). In several instances the rotating cylinders are more convenient (Fig. 4.7); the deposited foil can be cut along the axis and then unbent for further investigations.

The very useful construction of a RDE with a small working surface was invented by Beck in 1968 [7]. His construction comprises a metallic wire pressed into Teflon, the section of the wire being the working surface; the end section of the wire can be periodically cut (together with the Teflon isolation) by a hard ruby knife, immediately and in situ, without interrupting the measurement. This type of electrode is the solid-state analogue of the mercury drop used in polarography.

In studies of intermediate products generated during multistep processes the rotating disc electrode with a ring (*ring-disc electrode*) is successfully employed. This configuration consists in the conventional rotating disc electrode surrounded by the ring electrode, the latter being separated from the disc by a thin insulation layer (Fig. 4.8). The potentials at the disc and at the ring can be set independently. This configuration enables detection of the intermediate substance formed at the disc after it has been transported by radial convection to the ring.

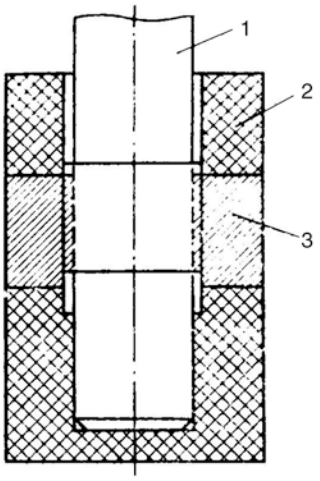

Fig. 4.7 Rotating cylindrical electrode

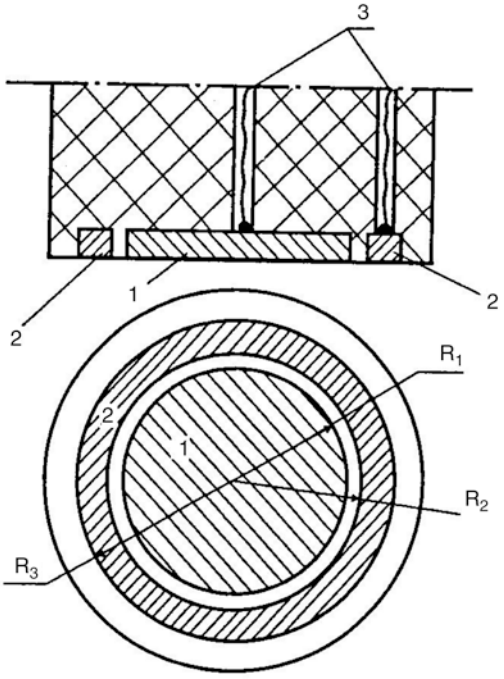

Fig. 4.8 Rotating ring-disc electrode

The key characteristic of ring-disc electrode is its *collection efficiency N*; it is the maximum fraction of the intermediate product which can be detected at the ring. This quantity depends only on electrode geometry, namely on disc radius R_1 and inner and outer ring radii R_2 and R_3. For different designs of the device the ratio

R_2/R_1 varies from 1.04 to 1.10, and the ratio R_3/R_2 varies from 1.2 to 1.4. In these conditions N is about 0.30–0.45; in general it can be computed by the following empirical formula:

$$N \approx 0.77 R_1/R_2 (R_3/R_2 - 1)^{1/2}. \tag{4.65}$$

When the intermediate is unstable its fraction determined at the ring is less than N and depends on kinetics of its conversion.

By way of example of this electrochemical tool application one can consider the two-step nature of copper electrochemical reduction from Cu^{2+} ions established through the use of the ring-disc electrode. The intermediate ions Cu^{+} were determined at the ring by the potential +0.65 V at which their reverse oxidation takes place. The measurements of the corresponding anodic current proved the existence of relatively stable Cu^{+} ions. More recently, the rate of the fast process $Cu^{+} + e \leftrightarrow Cu$ was measured by another method.

References

1. Levich V.G. Physico-chemical hydrodynamics. Moscow, 1952
2. Gamburg Yu. D. Russian J. Electrochemistry, 2002, v. 38, p. 1273
3. Engelgardt G.R., Davydov A.D., Soviet J. of Electrochemistry, 1988, v. 24, p.538.
4. Levich V.G. Acta Physicochim. URSS, 1942, v.17, p. 257
5. Gregory D.P., Riddiford A.C., J. Chem. Soc., 1956, p. 3756
6. Frumkin A.N., Tedoradse G.A. , Zeitschrift fuer Elektrochemie,1958, Bd. 62, s. 251
7. Beck R.Yu. , Lavrova T.A. Trans. Of the Siberian Branch Acad. Sci. USSR, chem.. series, 1971, v. 14, no. 7, p. 1429 (in Russian)

Chapter 5
Thermodynamics and Kinetics of Nucleation

5.1 Introduction

In the process of metal electrodeposition metal ions are reduced at the substrate, forming adsorbed atoms that diffuse on the substrate surface; these adatoms will eventually contact other adatoms, forming atomic clusters that may be stable or unstable. Unstable clusters will eventually disappear, while stable clusters will be able to grow, finally forming the film.

It is customary to assume that nucleation and crystal growth are consecutive steps of the phase transition; however, from the phenomenological standpoint these steps cannot strictly be separated: in fact, the two processes coincide. For example, if we consider the critical nucleus, the addition of the last atomic species to a subcritical cluster is assigned to a nucleation process, while the identical addition of the next adatom would constitute crystal growth.

The separate analysis of the two steps (subcritical and supercritical ones) however is convenient since this renders a thermodynamic analysis of the first step possible. The consequent growth obeys micro- or macroscopic kinetic laws, and at the critical point the two solutions have to be joined together. The conventional separation of the overall process into the two parts is based on a simple fact: up to the critical size the partition function for the nuclei size distribution is close to the equilibrium one: $Z(\mathrm{r}) = Z_0$. At larger sizes however the system departs from equilibrium and correspondingly its partition function departs from the equilibrium value: $Z/Z_0 \to 0$; the use of thermodynamics during film growth therefore is unsuitable.

In the following we will consider a metal cluster α_g containing a predetermined quantity $\boldsymbol{g}$ of atoms. In this context all these clusters are considered as nuclei (not only the critical ones). The growth of the clusters from the monoatomic ones α_1 to the supercritical ones will be described as a sequence of elementary processes:

$$\alpha_g + \alpha_1 \leftrightarrow \alpha_{g+1}.$$

The nucleus α_g can therefore be formed by only one way: as result of joining of one atom to the cluster α_{g-1}. If the nucleus is not critical another step is possible: the loss of one atom from α_{g+1}. Other mechanisms such as $\alpha_{g-m} + \alpha_m \leftrightarrow \alpha_g$ $(1 < m < g - 1)$ are assumed to be impossible.

Y. D. Gamburg, G. Zangari, *Theory and Practice of Metal Electrodeposition,*
DOI 10.1007/978-1-4419-9669-5_5, © Springer Science+Business Media, LLC 2011

5.2 Homogeneous Nucleation

The variation of the free energy ΔG upon formation of a three-dimensional cluster equals

$$\Delta G_3 = \sigma S - \Delta\mu V/V_\mathrm{m}, \tag{5.1}$$

where S and V are the surface area and the volume of the cluster, respectively, V_m is the molar volume, σ is the surface energy per unit area, $\Delta\mu$ is the variation of the chemical potential (the molar free energy) upon phase transition; σS represents a positive contribution to the cluster energy, $\Delta\mu V/V_\mathrm{m}$ a negative contribution under conditions where $\Delta\mu < 0$. For a spherical cluster of radius r, $S = 4\pi r^2$, $V = 4\pi r^3/3$, thus for a homogeneous surface (σ=*const*)

$$\Delta G_3 = 4\pi r^2\sigma - (4\pi/3)\, r^3\Delta\mu/V_\mathrm{m}. \tag{5.2}$$

In an electrochemical process $\Delta\mu$ is determined by the applied overpotential η : $\Delta\mu = zF\eta$.

Differentiating ΔG_3 with respect to r shows that the former has its maximum for a cluster radius equal to

$$r = r_\mathrm{c} = 2\sigma V_\mathrm{m}/\Delta\mu \tag{5.3}$$

A cluster of this size is called critical nucleus. For a prescribed critical radius this formula gives the corresponding $\Delta\mu$ and $\eta = \Delta\mu/zF$.

The volume of this cluster is therefore

$$V_\mathrm{c} = (32\pi/3)\,\sigma^3 {V_\mathrm{m}}^3/\Delta\mu^3, \tag{5.4}$$

and the corresponding ΔG_c equals (from 5.2)

$$\Delta G_\mathrm{c} = (16\pi/3)\,\sigma^3 {V_\mathrm{m}}^2/\Delta\mu^2, \tag{5.5}$$

The subscript "c" denotes "critical". A critical nucleus is in thermodynamic equilibrium with the surrounding phase; the subcritical ones dissolve with high probability, and the supercritical do grow.

A plot of the dependence of ΔG_3 on r is shown in Fig. 5.1. In the neighborhood of the point r_c this function can be approximated by the expression

$$\Delta G_3 = (4\pi/3)\, {r_\mathrm{c}}^2\sigma - 4\pi\sigma\,(r - r_\mathrm{c})^2. \tag{5.6}$$

Formula (5.3) is valid for clusters of any shape, but in general σ depends on the crystallographic indices of the corresponding facet. The knowledge of this dependence allows computation of the equilibrium shape of a crystal from the condition of minimal overall surface energy. The solution of this problem results in the well-known Wulff construction which is the generalization of (5.3):

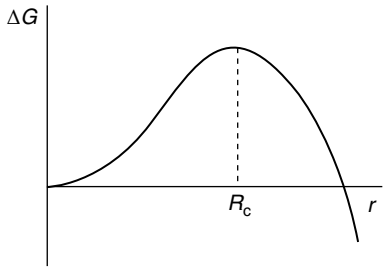

Fig. 5.1 The energy of nucleus formation ΔG_3 as function of its radius

$$h_i = const = 2\sigma_i V_m/\Delta\mu \tag{5.3a}$$

where σ_i is the surface energy of the *i*-th face and h_i is the distance of this face from a characteristic point in a crystal named its center. The equilibrium shape of a crystal consists a combination of flat facets, corresponding to low Miller indices. The areas of these facets decrease sharply for higher indices, thus the actual equilibrium crystal has several flat facets, joined by curved regions. It is important to understand that the equilibrium shape in general differs from that of the growing crystal: *the latter is determined not by surface energies, but by the growth rates of the various facets*. It is possible to derive an analogue of the Wulff construction valid for the shape of the growing crystal. Considerations of such kind may be useful in analyses at the microscopic level of the surface morphology of electrochemical deposits.

The Eqs. (5.4)–(5.6) remain valid for faceted clusters along with the spherical ones, but in the former case the numerical coefficients depend on the shape and can increase up to two times. E.g., for a cubic nucleus the coefficient in (5.4) is 64, in (5.5) it is 32.

Note that $V_m/\Delta\mu = v/(ze\eta)$ and that $\Delta G_c = V_c\Delta\mu/(2V_m) = 1/3\,(\sigma S_c)$; v is the volume of one atom in a cluster: $v = V_m/N_A$, while S_c is the overall surface area of a critical cluster. These expressions are quite general.

In the case of sufficiently small clusters it is more convenient to use the number of atoms in the cluster, $\boldsymbol{g}$, rather than their sizes. Obviously, the critical value $\boldsymbol{g}_c$ equals $g_c = V_c/v = V_c N_A/V_m$, and using (5.4) one obtains

$$\boldsymbol{g}_c = (32\pi/3)\,(\sigma/ze\eta)^3 v^2 \tag{5.7}$$

with the same considerations about the coefficient. The relationship between $\boldsymbol{g}_c$ and the energy of the critical nucleus is in general:

$$\Delta G_c = (1/2)\,ze\eta\ \boldsymbol{g}_c, \tag{5.8}$$

the coefficient ½ being independent of the shape of the nucleus and on other variables such as the nature of the metal, electrochemical conditions, the presence of a foreign substrate (heterogeneous nucleation) etc.

Numerical values of the quantities $(\sigma v^{2/3}/e)$ for different metals are given in the Table 5.1.

Table 5.1 The approximate values of $\gamma = v^{2/3}\sigma e^{-1}$ (Volts) for various metals at room temperature

Metal	γ	Metal	γ	Metal	γ
Ag	0.38	Fe	0.59	Pd	0.60
Au	0.50	Hg	0.27	Pt	0.70
Bi	0.27	In	0.28	Re	0.94
Cd	0.29	Mn	0.56	Rh	0.72
Co	0.57	Mo	0.82	Sn	0.34
Cr	0.49	Ni	0.58	W	0.98
Cu	0.45	Pb	0.30	Zn	0.32

5.3 Heterogeneous Nucleation

5.3.1 Three-Dimensional Nucleation

The nucleation on a foreign substrate is of specific interest for electrochemical crystallization. The spherical cluster becomes in this case a spherical segment having a common circular boundary with the foreign substrate; the radius of this base (Fig. 5.2) is equal to *r sin* α, where α is the edge angle.

From elementary geometry, it is found that the volume of a cluster of such a shape equals

$$V_{\text{het}} = \left(\pi r^3/3\right)(1 - cos\alpha)^2\,(2 + cos\alpha) = V_{\text{hom}}\left(1/2 - 3/4 cos\alpha + 1/4 cos^3\alpha\right), \quad (5.9)$$

where $V_{\text{hom}} = (4\pi/3)\,r^3$ is the volume of the corresponding homogeneous nucleus. The factor in brackets is always less than one. An expression identical to (5.9) can be written also for the free energy of the corresponding critical cluster with such a shape:

$$(\Delta G_c)_{\text{het}} = (\Delta G_c)_{\text{hom}}\left(1/2 - 3/4\ cos\alpha + 1/4\ cos^3\alpha\right). \quad (5.10)$$

Let us demonstrate this formula. The overall value of ΔG_c in this case consists of three components: the volume term, as in (5.2), equals

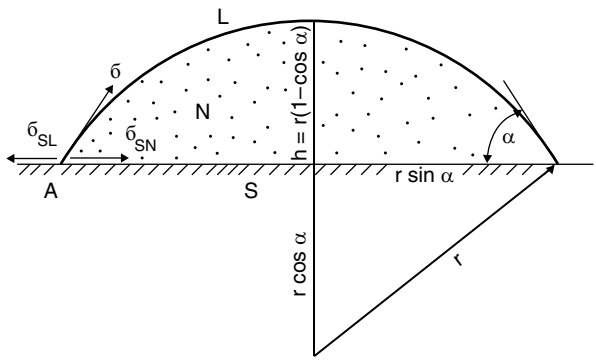

Fig. 5.2 Nucleation on a foreign substrate: S–substrate, N–nucleus, L–liquid (solution)

$\Delta G_c\,(1) = (4\pi/3)\,r^3\left(1/2 - 3/3cos\alpha + 1/4cos^3\alpha\right)\Delta\mu/V_m$. The surface energy term is the sum of two contributions: the first one is due to the formation of the boundary with the liquid phase, while the second one concerns the boundary with the substrate. The area of the first boundary is $2\pi r^2(1 - cos\alpha)$ and the corresponding specific surface energy between crystal and solution is σ_{cr-sol}, identical to σ in (5.2); thus the energy is $\Delta G_c\,(2) = 2\pi r^2\,(1 - cos\alpha)\,\sigma_{cr-sol}$. The same analysis for the second boundary leads to the term $\Delta G_c\,(3) = \pi r^2 sin^2\alpha\,(\sigma_{cr-sub} - \sigma_{sub-sol})$; the expression in brackets accounts for the replacement of the boundary substrate-solution by the novel boundary crystal-substrate.

Eventually for the overall energy we obtain $(\Delta G_c)_{het} = \Delta G_c\,(1) + \Delta G_c\,(2) + \Delta G_c\,(3)$, or

$$\begin{aligned}(\Delta G_c)_{het} = {} & (4\pi/3)\,r^3\left(1/2 - 3/4cos\alpha + 1/4cos^3\alpha\right)\Delta\mu/V_m \\ & + 2\pi r^2\,(1 - cos\alpha)\,\sigma_{cr-sol} + \pi r^2 sin^2\alpha\,(\sigma_{cr-sub} - \sigma_{sub-sol})\,;\end{aligned} \tag{5.11}$$

But, as it is seen from Fig. 5.2, the mechanical equilibrium for the point A requires

$$cos\alpha = (\sigma_{cr-sub} - \sigma_{sub-sol})\,/\sigma_{cr-sol} \tag{5.12}$$

The combination of (5.11) and (5.12) directly leads to (5.10).

In summary, the difference between the homogeneous and heterogeneous cases of nucleation can be taken into account by the only factor $\Phi < 1$

$$\Phi = V_{het}/V_{hom} = \mathbf{g}_{het}/\mathbf{g}_{hom} \tag{5.13}$$

For example, (5.7) may be rewritten as

$$\boldsymbol{g}_c = (32\pi/3)\,v^2(\sigma/ze\eta)^3\Phi \tag{5.14}$$

whereas (5.8) remains valid.

In many cases other notations may be useful instead of the boundary angle α, namely the adhesion energy σ_S

$$\sigma_S = \sigma - \sigma_{cr-sub+}\sigma_{sub-sol} \tag{5.15}$$

Also, a convenient quantity is Δσ, defined as

$$\Delta\sigma = 2\sigma - \sigma_{S.} \tag{5.16}$$

Using these definitions

$$\Phi = \Delta\sigma/2\sigma = 1 - \sigma_S/2\sigma, \tag{5.17}$$

and then

$$\Delta G_{het} = (\Delta\sigma/2\sigma)\,(16\pi/3)\,\sigma^3 {V_m}^2/\Delta\mu^2 = (8\pi/3)\,\sigma^2\Delta\sigma\,{V_m}^2/\Delta\mu^2 \tag{5.18}$$

$$\boldsymbol{g}_c = (16\pi/3)\,v^2\sigma^2\Delta\sigma/(ze\eta)^3 \tag{5.19}$$

As noticed earlier, the coefficient $16\pi/3$ is restricted to a spherical surface, while in the case of a faceted cluster it can be moderately different. For example, if the critical nucleus has the shape of a cuboid standing on its square base, its height is $2v\Delta\sigma/(ze\eta)$ and the base side $4v\sigma/(ze\eta)$; thus its volume equals $V_{\text{het}} = 32v^3\sigma^2\Delta\sigma/(ze\eta)^3$ and finally $g_c = V_{\text{het}}/v$, or

$$\boldsymbol{g}_c = 32v^2\sigma^2\Delta\sigma/(ze\eta)^3 \tag{5.20}$$

Equations of this kind are valid in all cases of three-dimensional nucleation.

The approximation (5.6) can be rewritten in the form

$$\Delta G_3 = \Delta G_c - \left(ze\eta/6\boldsymbol{g}_c\right)\left(\boldsymbol{g} - \boldsymbol{g}_c\right)^2 \tag{5.6a}$$

One more equation can be obtained by comparison of (5.4) and (5.5). The differentiation of (5.5) gives

$$d\left(\Delta G_c\right)/d\mu = -V_c, \tag{5.21}$$

and therefore

$$\boldsymbol{g}_c = -ze \cdot d\left(\Delta G_c\right)/d\eta. \tag{5.22}$$

This equation is of general validity, as it can be applied both for homogeneous and heterogeneous nucleation and is independent of the nucleus size [1].

5.3.2 Two-Dimensional Nucleation

At high overpotentials and/or for a high adhesion energy the height of the spherical segment in Fig. 5.2 may become equal or less than the atomic size $v^{1/3}$. This corresponds to the situation when the nucleus becomes two-dimensional. The variation of the volume energy in this case is $\Delta\mu V/V_m = \pi r^2 a\Delta\mu/V_m$, where a is the atomic size. At the same time the variation in the surface energy is $\pi r^2\Delta\sigma$ (resulting from the change of the substrate–solution with the cluster–solution interface). A third term must be added, due to the edge energy of the cluster perimeter: this equals $2\pi ra\sigma$. The net result for the two-dimensional nucleus energy ΔG_2 is therefore

$$\Delta G_2 = -\pi r^2 a\Delta\mu/V_m + \pi r^2\Delta\sigma + 2\pi ra\sigma. \tag{5.23}$$

It should be noticed that the last term could be taken into account also in the case of three-dimensional nucleation, but its contribution would be negligibly small.

The value of ΔG_2 is maximal at the nucleus radius

$$r_c = \sigma/\left(\Delta\mu/V_m - \Delta\sigma/a\right) \tag{5.24}$$

and equals

$$\Delta G_2 = \pi\sigma^2 a(\Delta\mu/V_{\mathrm{m}} - \Delta\sigma/a) \tag{5.25}$$

The same quantities can be expressed in another form by using the value of the area s occupied by one atom and the overpotential η:

$$r_{\mathrm{c}} = \sigma v/(ne\eta - \Delta\sigma s), \tag{5.26}$$

$$\Delta G_2 = \pi\sigma^2 s^2/(ne\eta - \Delta\sigma s). \tag{5.27}$$

For two-dimensional nucleation the "corrected" value of the chemical potentials difference between the species in the solution and in the cluster is often used: $\Delta\mu^* = N_{\mathrm{A}}(ne\eta - \Delta\sigma s)$ instead of the conventional $\Delta\mu{=}N_{\mathrm{A}}(ne\eta)$; this allows to write the above expressions more simply: $r_{\mathrm{c}} = \sigma V_{\mathrm{m}}/\Delta\mu^*$ and $\Delta G_2 = \pi\sigma^2 a V_{\mathrm{m}}/\Delta\mu^*$, or $\Delta G_2 = \mathrm{g}\Delta\mu^*/N_{\mathrm{A}}$.

Finally, it should be noticed that in heterogeneous nucleation the surface can be non-uniform: in particular it would include steps, kinks, angles, inclusions, etc.; all these imperfections can influence the nucleation by providing low energy sites where nucleation becomes more likely [2, 3].

5.4 Nucleation Mechanisms

The results outlined earlier show that *heterogeneous* nucleation is possible only under specific conditions. When $\Delta\sigma{\leq}0$ it can take place only if $\Delta\mu > -\Delta\sigma/a$ and would proceed through the two-dimensional mechanism. Thus the formation of a nucleus is possible at potentials more positive than the equilibrium one: $-\Delta\sigma/a < \Delta\mu < 0$; this phenomenon is termed underpotential deposition.

When $\Delta\sigma{>}0$ the nucleation is possible only if $\Delta\mu < 0$. At low overpotentials three-dimensional nuclei are formed, but for increasing η they become more and more flat until at $\Delta\mu = 2\Delta\sigma/a$ they become two-dimensional.

These findings lead to a classification of the possible morphologies of heterogeneous nucleation, which include the following three different growth mechanisms.

1. *Volmer–Weber mechanism*, for which the adhesion is weak $(\Delta\sigma > 0)$ and the following inequality holds: $0 < \Delta\mu < 2\Delta\sigma/a$. In this growth mode, three-dimensional nucleation takes place and then the discrete islands grow until they stick together. In this case the work of nucleation is relatively high, and the role of any factors decreasing it (surface defects, adsorption of impurities) is particularly important. When $\Delta\mu > 2\Delta\sigma/a$ two-dimensional nuclei are formed.
2. *Frank–Van-der-Merwe mechanism*; it is observed when adhesion is strong $(\Delta\sigma \leq 0, \Delta\mu > -\Delta\sigma/a)$. In this mechanism two-dimensional nuclei are

formed; they grow up to the monolayer, and the new nuclei are formed on top of the existing monolayer. This mode is characteristic of the growth of a metal on a substrate of the same metal.

3. *Stranski–Krastanov mechanism*. In this growth model two-dimensional nucleation occurs up to one or more atomic layers of the novel phase; thereafter a three-dimensional nucleation process starts. This takes place in the case when for thin layers $\Delta\sigma \leq 0$ whereas thicker layers show lower adhesion: $\Delta\sigma > 0$. This can be a consequence for example of internal stresses building up during the growth of several monolayers.

All three mechanisms have been observed experimentally.

The mechanism of nucleation determines not only the deposit structure but also the crystallographic correspondence (epitaxy) between the deposit and the substrate.

5.5 The Peculiarities of Electrocrystallization

At high overpotentials the number of atoms **g** in the critical nucleus becomes small, and this requires a different approach to the determination of the critical cluster size since quantities such as σ, Δσ and Δμ—based on thermodynamic concepts—lose their meaning at the near-atomic scale. This is one of the peculiarities of electrochemical crystallization, originated by the extreme non-equilibrium conditions achieved during electrochemical growth.

For this reason at high overpotentials it becomes more appropriate to express these values through the interatomic interactions and to calculate the overall energies by directly considering the atomic configurations of the clusters. It is additionally necessary to take into account the role of the next nearest neighbors along with the immediate ones. The surface, radius and volume of the clusters must be expressed through the number **g**; thus, the volume will be proportional to **g**, and the surface and radius will correspondingly be proportional to $\mathbf{g}^{2/3}$ and $\mathbf{g}^{1/3}$.

Calculations of such kind have been performed [4] and have shown that the above discussion and results are valid down to the smallest nuclei, with small corrections due to variations of the noted quantities and coefficients in the basic equations. The atomistic approach however is important when considering the nucleation kinetics; in this area it leads to important changes in the theory.

It should be noted that the above formulae do not account for some specific features of electrodeposition. For example, the values of σ and Δσ in reality depend on the electrode potential, electrode charge and electrolyte composition. As a consequence of specific adsorption of the electrolyte components to the electrodes for example both these quantities tend to decrease.

The dependence of σ on the electrode potential in the simplest case is

$$\sigma = \sigma_0 - {}^1\!/_2 C_{dl}(E - E_{zc})^2 \tag{5.28}$$

Due to the fact that the relative position of the *pzc* and the equilibrium potential vary for different metals, the dependence of surface energy on overpotential does not follow a general trend. Usually a variation of σ and Δσ by 1% results in a variation of the nucleation energy by 3% (this follows from Eq. (5.18)); the value of *cos* α also varies. The resulting dependence of ΔG_c on adsorption can become rather complicated.

The other quantity which governs nucleation is Δμ. In electrocrystallization this quantity depends on η; however the overpotential entering into the equations of this chapter is related to the equilibrium potential at the very point of the electrode where nucleation occurs. Thus the experimental values should be corrected by the concentration polarization in order for the equilibrium potential to be calculated correctly, and by the Ohmic potential difference for the given actual potential to be measured correctly. Under the condition of constant potential over the whole electrode the various components of the overpotential can differ at various points, therefore the crystallization overpotential (i.e. the value to be placed in the relevant equations) may vary from one point to another.

5.6 The Partition Function for the Nuclei Size Distribution

According to the thermodynamic theory of fluctuations [5] the equilibrium distribution of the clusters by their size has the form

$$Z_0(\boldsymbol{g}) = N \exp\left[-\Delta G_{\min}(\boldsymbol{g})/k_B T\right] \tag{5.29}$$

where $\Delta G_{\min}(\boldsymbol{g})$ is the minimum energy needed for the formation of the cluster of $\boldsymbol{g}$ atoms, N is the overall number of atoms in the system which can contribute to cluster formation, joining or splitting out of it. In electrodeposition N can be the number of ad-atoms per unit surface area. Thus, the equilibrium number of the clusters diminishes when increasing $\boldsymbol{g}$ up to $\boldsymbol{g}_c$, and then increases **(**Fig. 5.3**)**.

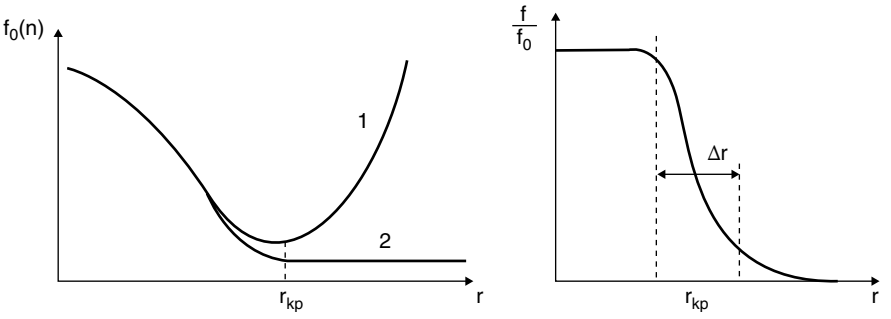

Fig. 5.3 Equilibrium f_0 *1* and non-equilibrium f *2* number of the clusters at increasing $\boldsymbol{g}$ up to $\boldsymbol{g}_c$ and further; f/f_0 falls sharply within Δr

This expression triggers a shift from a thermodynamic to a kinetic description of nucleation. Crystallization in fact requires to overcome the potential barrier ΔG_c determined by the characteristics of the critical nucleus. For this reason, from the most general point of view the rate of this process is equal to $K exp(-\Delta G_c/k_B T)$; the problem then reduces to the estimation of the pre-exponential factor.

The first attempt in this direction was made by Volmer (1926), who proposed that the flux $\boldsymbol{J}$ of clusters overcoming the critical size is

$$J = S_c\, \omega\, exp(-\Delta G_c/k_B T), \tag{5.30}$$

where S_c is the area of the critical nucleus and ω is the frequency of the collisions of atoms with its surface. This purely thermodynamic estimate however is very approximate. For a quantitative analysis of the crystallization kinetics it is necessary to consider the elementary processes of attachment and detachment of the atoms to and from the clusters in some size range close to the critical one. This is the subject of the following section.

5.7 The Steady State Nucleation Kinetics

5.7.1 Fokker–Planck Equation

We analyze here the problem of determining how many stable clusters are formed per unit time and per unit surface area from the bulk parent phase, if the values of ω and ΔG_c are known. This problem was considered theoretically [6] by Becker and Döring and independently by Zeldovich, using different methods. Both methods have their own advantages; a recent discussion can be found in [7]. In the following we shall obtain the same result with the simpler conceptual framework developed by Frenkel [5].

Let us denote the clusters made up of $\boldsymbol{g}$ atoms as $\boldsymbol{g}$-*cluster* or clusters of class $\boldsymbol{g}$; ω_is the notation for the frequency of the detachment of atoms *from its unit surface area* S_g. Thus the flux of $\boldsymbol{g}$-clusters transforming to class ($\boldsymbol{g}$–1) clusters can be expressed as $Z(\boldsymbol{g})\ S_g\omega\_$. The flux of ($\boldsymbol{g}$–1)-clusters transforming to class $\boldsymbol{g}$ clusters identically equals $Z(\boldsymbol{g}-1)S_{g-1}\omega_+$.

For a non-equilibrium distribution $Z(\boldsymbol{g})$ the net flux for the transition $(\boldsymbol{g}-1)\rightarrow \boldsymbol{g}$ is:

$$J_g = Z\,(\boldsymbol{g}-1)\ S_{g-1}\omega_+ - Z\,(\boldsymbol{g})\ S_g\omega\_. \tag{5.31}$$

Obviously, in equilibrium the quantities Z_0 are time independent, therefore the corresponding flux is equal to zero, and

$$Z_0(\boldsymbol{g}-1)S_{g-1}\omega_+ = Z_0\,(\boldsymbol{g})\ S_g\omega\_. \tag{5.32}$$

It is possible therefore to rewrite (5.31) as

$$J_g = Z(\boldsymbol{g}-1)S_{g-1}\omega_+\left[Z(\boldsymbol{g}-1)/Z_0(\boldsymbol{g}-1) - Z(\boldsymbol{g})/Z_0(\boldsymbol{g})\right] \tag{5.33}$$

This expression gives the general flux $\boldsymbol{J}_{\mathrm{g}}$ from ($\boldsymbol{g}$–1) to ($\boldsymbol{g}$). Identically, one may find the flux $\boldsymbol{J}_{\mathrm{g+1}}$ from ($\boldsymbol{g}$) to ($\boldsymbol{g}$+1). Then it is easy to understand that the difference between the two last fluxes is the rate of variation of the number of ($\boldsymbol{g}$)-clusters:

$$dZ\left(\boldsymbol{g}\right)/dt = J_{\mathrm{g}} - J_{\mathrm{g}_{+1}}. \tag{5.34}$$

For not too small values of $\boldsymbol{g}$ we may assume: (1) $S_{\mathrm{g}} \approx S_{\mathrm{g}-1}$, (2) $Z\left(g\right) \approx Z\left(g-1\right)$ and (3) the finite differences with unit step can be approximated by the derivatives:

$$J_{\mathrm{g}} - J_{\mathrm{g}_{+1}} = -dJ/d\boldsymbol{g}, \tag{5.35}$$

$$Z(\boldsymbol{g}-1)/Z_0(\boldsymbol{g}-1) - Z(\boldsymbol{g})/Z_0(\boldsymbol{g}) = d(Z/Z_0)/d\boldsymbol{g}. \tag{5.36}$$

Designating additionally $S_{\mathrm{g}-1}\omega_{+} = D\left(\boldsymbol{g}\right)$, we can rewrite Eq. (5.33) as:

$$J_{\mathrm{g}} = -D\left(\boldsymbol{g}\right) Z_0\left(\boldsymbol{g}\right) d/d\boldsymbol{g}\left[Z\left(\boldsymbol{g}\right)/Z_0\left(\boldsymbol{g}\right)\right] \tag{5.37}$$

This is the Zeldovich equation. After simple rearrangements and removal of the index ($\boldsymbol{g}$) the equation becomes $J_{\mathrm{g}} = -DdZ/dg + DZ\partial lnZ_0/\partial g$. But $lnZ_0 = lnN - \Delta G\left(g\right)/k_{\mathrm{B}}T$, as it follows from (5.29); then

$$J_{\mathrm{g}} = -DdZ/d\boldsymbol{g} + \left(D/k_{\mathrm{B}}T\right) Z\partial\Delta G/\partial\boldsymbol{g}. \tag{5.38}$$

Finally, (5.34) assumes the following form:

$$\partial Z/\partial t = -\partial J/\partial g = \partial/\partial\boldsymbol{g}\left(D\partial Z/\partial\boldsymbol{g}\right) + \left(1/k_{\mathrm{B}}T\right)\partial/\partial\boldsymbol{g}\left(DZ\partial\Delta G/\partial\boldsymbol{g}\right) \tag{5.39}$$

This is the Fokker–Planck equation; in this specific case it describes the "diffusion" of the cluster along the axis of its size $\boldsymbol{g}$, D($\boldsymbol{g}$) being the "diffusion coefficient" along the size axis. In more detail: the clusters transition from one class to another is described as a diffusion process which proceeds in the direction of increasing $\boldsymbol{g}$. The similarity of this process to linear diffusion is due to the fact that in both processes the separate objects can move along two opposite directions, but the overall system moves in one definite direction.

This equation is the basis for the analysis of the kinetics of numerous stochastic processes; in our case these are steady and non-steady nucleation.

5.7.2 The Non-Equilibrium Flux

It is important for the successive analysis that the number of small clusters with $\boldsymbol{g} \ll \boldsymbol{g}_{\mathrm{c}}$ be considerably larger than that of $\boldsymbol{g}_{\mathrm{c}}$, which are continuously removed from the system: the latter grow into supercritical nuclei and do not return into the set of nuclei with $\boldsymbol{g} < \boldsymbol{g}_{\mathrm{c}}$. At the same time the steady state flux $\boldsymbol{J}_{\mathrm{g}}$,sustained by the continuous removal of the supercritical clusters, does not depend on $\boldsymbol{g}$ (otherwise

the condition of steady state is invalid). But it is precisely this flux that causes the dissimilarity of the function $Z(\boldsymbol{g})$ from the equilibrium one $Z_0(\boldsymbol{g})$, for which $\boldsymbol{J}_g = 0$.

Therefore, for $\boldsymbol{g} << \boldsymbol{g}_c$ (where the flux is small relatively to the large number of clusters) the function $Z(\boldsymbol{g})$ is close to the equilibrium one $Z_0(g) : Z(g)/Z_0(g) \approx 1$. Quite the opposite, for $\boldsymbol{g} > \boldsymbol{g}_c$ $Z(\boldsymbol{g}) = const$ because each nucleus continues its growth, but $Z_0(\boldsymbol{g})$ in this range sharply increases (due to the decrease of ΔG, Fig. 5.1); thus $Z(g)/Z_0(g) \to 0$. The transition from the situation $Z(g)/Z_0(g) \approx 1$ occurs in a range of $\Delta\boldsymbol{g}$ near $\boldsymbol{g}_c$ (Fig. 5.3): if the cluster size is within this limits, the fluctuations can bring the cluster into a subcritical region. However, if $g > g_c + {}^1\!/_2 \Delta g$ it will grow with a probability close to 100%.

5.7.3 An Estimate of the Steady State Flux

The width of the region $\Delta\boldsymbol{g}$ is determined by the function $exp\,[\Delta G(\boldsymbol{g})]$ which is characterized by a very sharp maximum at $\boldsymbol{g}_c$. The width of this maximum can be estimated from Eq. (5.6a), giving for this function the Gaussian approximation

$$f(\boldsymbol{g}) = exp(-\Delta G/k_B T) \approx const \cdot exp\left[-\left(ze\eta/6\boldsymbol{g}_c\right)\left(\boldsymbol{g} - \boldsymbol{g}_c\right)^2/k_B T\right] \tag{5.40}$$

The half-width of this last function is close to $[(6\pi k_B T g_c)/(ze\eta)]^{1/2}$, thus this expression determines the range $\Delta\boldsymbol{g}$:

$$\Delta\boldsymbol{g} \approx \left[(6\pi k_B T \boldsymbol{g}_c)/(ze\eta)\right]^{1/2}. \tag{5.41}$$

Therefore, the decrease of the ratio $Z(g)/Z_0(g)$ from 1 to 0 takes place predominantly in this range of the cluster classes. It means that on average

$$d/d\boldsymbol{g}\left[Z(\boldsymbol{g})/Z_0(\boldsymbol{g})\right] \approx 1/\Delta\boldsymbol{g} = \left[(ze\eta)/\left(6\pi k_B T \boldsymbol{g}_c\right)\right]^{1/2} \tag{5.42}$$

Finally, by substitution of this quantity along with $Z_0(\boldsymbol{g})$, $D(\boldsymbol{g})$ and (5.8) into Eq. (5.37) one obtains

$$J = Nexp(-\Delta G_c/k_B T)(S_c\omega_+/\boldsymbol{g}_c)[\Delta G_c/(3\pi k_B T)]^{1/2}. \tag{5.43}$$

This equation differs from the thermodynamic one by the Zeldovich factor

$$Z = \boldsymbol{g}_c{}^{-1}[\Delta G_c/(3\pi k_B T)]^{1/2}, \tag{5.44}$$

which under usual conditions is of the order of 0.1.

The solution (5.43) coincides with the rigorous solution of the Fokker–Planck equation [6, 7]; it should be noted that in order to obtain this more precise solution

one should use the approximation (5.6a) and the fact that *exp* $[\Delta G(\boldsymbol{g})]$ exhibits a sharp maximum.

In logarithmic form Eq. (5.43) can be written as

$$\begin{aligned} ln\ J &= ln(NS_c\omega_+/\boldsymbol{g}_c) + {}^1\!/_2 ln[\Delta G_c/(3\pi k_B T)] - \Delta G_c/k_B T \\ &= ln(NS_c\omega_+/\boldsymbol{g}_c) + {}^1\!/_2 ln\,[\Delta G_c/(3\pi k_B T)] - (8\pi/3)v^2\sigma^2\Delta\sigma/\left[k_B T(ze\eta)^2\right] \\ &= K_1 - K_2/\eta^2 \end{aligned} \tag{5.45}$$

The substitution of the corresponding values in this formula gives the following two expressions:

$$K_1 \approx lnN + ln\,(v/ze) + lni_0 + {}^1\!/_2 ln\,(\mathrm{A}\sigma/kT) \tag{5.45a}$$

and

$$ln\ J = K'_1 + ln\ C - K_2/\eta^2; \tag{5.45b}$$

(the dependence on C is connected with that of i_0).

This means that in three-dimensional nucleation the logarithm of the steady state nucleation rate is inversely proportional to the square of the overpotential. An identical analysis for the two-dimensional nucleation leads to the expression

$$ln\ J = k_1 - k_2/\Delta\mu^*; \tag{5.46}$$

sometimes this is written in a simplified form

$$ln\ J = k_1 - k_2'/\eta. \tag{5.47}$$

The derivative of (5.45) with respect to η results in the extremely important equation:

$$\partial\, ln\ J/\partial\eta = \boldsymbol{g}_c ze/k_B T = \boldsymbol{g}_c zF/RT \tag{5.48}$$

This gives an expression useful for the calculation of $\boldsymbol{g}_c$ from experimental measurements of the rate of nucleation at steady state:

$$\boldsymbol{g}_c = (RT/zF)\partial\, ln\ J/\partial\eta \tag{5.49}$$

This finding is independent from the thermodynamic method. A rigorous atomistic analysis shows that (5.49) overvalues $\boldsymbol{g}_c$ by less than by one atom.

5.7.4 Peculiarities of the Steady State Flux Result

Let us analyze some parameters of the given solution. In the case of kinetic control of the process the frequencies ω+ and ω− coincide with the partial cathodic and anodic current densities at the given overpotential. For small clusters however these quantities differ from the ones corresponding to a flat surface due to the shift of the

exponential term for surfaces with high curvature. The cathodic component of the current for a cluster with radius r is

$$i_c(r) = i_0 exp(\alpha z F \eta / RT) exp(-2\alpha\sigma V_m / r RT), \tag{5.50}$$

whereas the anodic one equals to

$$i_a(r) = i_0 exp(-(1-\alpha) z F \eta / RT) exp(-(1-\alpha) 2\sigma V_m / r RT). \tag{5.51}$$

The equilibrium potential determined by the equality $i_c(r) = i_a(r)$ differs from that of the flat surface by the term

$$\Delta E_{eq}(r) = 2\sigma V_m / (zFr) = 2\sigma v / (zer), \tag{5.52}$$

which coincides with the usual thermodynamic equation (the Gibbs-Thomson term). Interestingly, the exchange current density i_0 at this new equilibrium potential remains the same. Thus, for subcritical clusters dissolution is faster than deposition; for critical ones the rates are equal, and the quantity ω coincides with the exchange current density, divided by ze:

$$\omega_c = i_0 / ze \tag{5.53}$$

independent of overpotential and of the critical nucleus size. This shows that the overall exchange current for the critical nucleus r equals $S_c\omega = D(g_c) = S_c i_0 / ze$. For the hemispherical nucleus $S_c = 2\pi r^2$, thus $D = 2\pi r^2 i_0 / ze = 8\pi v^2 \sigma^2 / \left[(ze)^3 \eta^2\right]$.

In the case when the attachment rate is controlled by diffusion the situation changes. Let us consider surface diffusion to a cluster with the shape of a spherical segment; if the surface diffusion coefficient is D_{sd},

$$\omega = D_{sd} \cdot 2\pi r_c sin\alpha; \tag{5.54}$$

and for a hemispherical nucleus $\omega = D_{sd} \cdot 2\pi r_c$. Thus the quantity $D(\boldsymbol{g}_c)$ depends now on the surface diffusion coefficient. Other quantities also can vary their meaning: N in this case is the quantity of adsorbed atoms at the surface, which depends on the overpotential:

$$N = N_0 \, exp\,(ze\eta / k_B T); \tag{5.55}$$

this dependence adds the additional term $ze\eta / k_B T$ to (5.45).

In the general case when both diffusion and kinetics play simultaneously a role, one can write

$$D^{-1} = D_{kin}{}^{-1} + D_{dif}{}^{-1}. \tag{5.56}$$

5.8 Non-Steady State Nucleation

When the electrode potential is instantaneously switched from an initial value to a different one, the steady state corresponding to a given nucleus flux $\boldsymbol{J}_{st}$ is established after a finite time, during which the cluster size distribution changes; most important is the case when the initial potential is the equilibrium value.

In this case the flux grows with time from zero to its steady value. This initial non-steady state period is known as induction time, τ. With the accuracy of 1%, $\boldsymbol{J}=0$ in the time interval $0<t<\tau$ and $\boldsymbol{J}=\boldsymbol{J}_{st}$ at $t>3\tau$. The values of induction time have been calculated for various situations. For the cluster redistribution by size, τ is close to

$$\tau \approx \mathrm{K}\sigma k_{\mathrm{B}}T/\left(zei_0\eta^2\right) \tag{5.57}$$

$(\mathrm{K} = 16/\pi^2)$: this expression can be derived by calculating the number of steps needed for the cluster to grow up to the critical size (approximately), or (exactly) by direct solution of the Fokker–Planck equation. In the case when diffusion limitations occur this equation takes the form (C is the concentration of the electroactive species)

$$\tau \approx K\sigma k_{\mathrm{B}}T/\left(ze\eta^2\right)\left[1/i_0 + 2\sigma v/\left(z^2e^2CD\eta\right)\right] \tag{5.57a}$$

The dependence $N(t)$ is shown in Fig. 5.4 approximately

$$N(t) \approx J(t - \pi^2\tau/6). \tag{5.58}$$

One more reason may originate the initial retardation of the nucleus growth. The curvature of the growing cluster surface, while the cluster is close to the critical one, leads to a decrease of the growth rate. Actually, as it was shown above, the critical nucleus at the corresponding overpotential is at equilibrium, and its average growth rate equals zero. Only after attachment of one additional atom the growth rate is finite, and further it increases up to the normal value when the cluster is several times larger that the critical nucleus. This transition occurs in a time interval close to that of the size redistribution of clusters, i.e. is given by Eq. (5.58).

There are other reasons for the induction time existence along with clusters redistribution and the buildup of a set of various sizes. Sometimes the buildup of ad-atoms must be proceed up to the value given by (5.55), in other cases it depends on the chemical or adsorption phenomena influencing the activity of the electrode

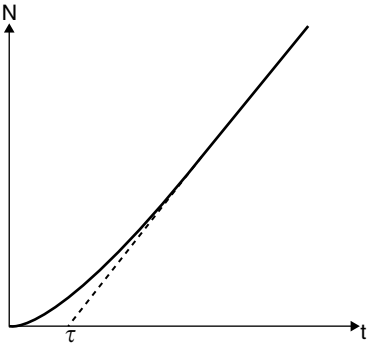

Fig. 5.4 Number of nuclei vs. time for a non-steady state process

(number of active sites), the actual value of τ being determined by the superior non-steady time.

5.9 Experimental Methods

The nucleation processes are of most interest during the initial stage of crystallization, especially at a foreign substrate; in the growth of thick deposits on the other hand the processes of steps propagation and the joining of new atoms to the lattice play a more important role. In reality the formation of new nuclei takes place during the overall deposition time simultaneously with the growth of the crystals. However, the true nucleation process, i.e. without extraneous factors, is observed only in specific conditions, and especially at the initial stage of growth. This is why the parameters determining these processes are derived from some specific experiments.

The earliest potentiostatic techniques consisted in measuring the time lag needed for the first nucleus to form: this is the time t_1 at which a current is observed to flow after a potential is applied at $t=0$. If the induction time is small: ($\tau << t_1$), a condition that can be satisfied by tailoring the applied overpotential, it can be easily shown that $J = 1/t_1$. The sets of values of $\boldsymbol{J}$ measured by this method at various overpotentials allow finding the quantities K_2 in (5.45) and the corresponding values of σ, ΔG_c and $\boldsymbol{g}_c$.

A modification of this method is a trial-and error method: the duration of the potentiostatic pulse is found at which the nucleus is formed in one half of the experiment time; obviously, this duration is identical to τ.

Another type of experiment is the double pulse technique [8]. The overpotential pulse is applied to the electrode initially conditioned at the equilibrium potential of the depositing metal. During the pulse a certain number of nuclei is formed, but they are invisible under the microscope; thus the second smaller pulse is applied at which no nucleation occurs, but the initially formed nuclei grow to a microscopically visible size; visibility of the nuclei is reached only by an appropriate duration of the second pulse. The number of nuclei N is established by visual counting, and then the dependence of N on the initial pulse duration, the overpotential and other conditions can be plotted. These data provide a wealth of information on nucleation processes.

One of the interesting facts established by these experiments is that N initially increases proportionally to the first power of time, as (5.58) predicts at $\boldsymbol{J}=\text{const}$, but then the curve $N(t)$ flattens out and reaches a limiting value N_0. There are two possible reasons for this observation. The first one is the limited number of active centers available at the surface; when these are exhausted N cannot further increase (at least at the given overpotential). The second reason consists in the decrease of the nucleation probability near the formed nuclei; that is, regions of excluded nucleation are developed around each nucleus because that nucleus captures most of the ad-atoms available around it, decreasing the probability of forming an additional

critical nucleus. The dependences $N(t)$ in the two cases are different, allowing to distinguish among them.

Instead of microscopic observations, the recording of the i–t dependence during the second pulse is also possible. This technique can be also applied to the determination of the number of nuclei, especially for large numbers; in general however the measured current depends on many factors, and any calculation requires some additional assumptions.

A very useful tool in nucleation and growth studies is the dislocation-free crystal surface. Specific electrochemical capillary techniques have been developed [9] for the preparation of such crystal facets. Experiments with dislocation-free silver surfaces have shown that during silver nucleation two-dimensional nuclei were formed at $\eta \approx 0.01$ V during the first 10^{-6} s. This set of experiments allowed also an estimation of the surface energy and exchange current density between ad-atoms and steps.

5.10 Kinetics of Mass Crystallization

We move on now to consider the processes involved in the growth of critical nuclei. Let an individual nucleus grow under potentiostatic conditions at a current density i determined by electron transfer kinetics and maintained constant in time and uniform over the whole surface. The rate of surface growth along the direction normal to the nucleus surface equals iV_m/zF, thus at time t the growing cluster will form a hemisphere with the radius $R = iV_m t/zF$ and the surface area $2\pi R^2$.

The overall current *I(t)* at this cluster is

$$I(t) = 2\pi R^2 i = 2\pi i^3 (V_m/zF)^2 t^2 \tag{5.59}$$

Upon lateral growth of a cylindrical cluster with a constant height h the growth is two-dimensional and the corresponding expression is

$$I(t) = 2\pi R h i = 2\pi h i^2 (V_m/zF)\, t \tag{5.60}$$

If the current density is time dependent, as it occurs under diffusion limitations, the cluster grows as $R = (2CV_m Dt)^{1/2}$ (where C is the concentration of the electroactive species), thus for hemispherical clusters

$$I(t) = 4zF\pi (DC)^{1/2} (V_m t)^{1/2} \tag{5.61}$$

If in the initial stage N_0 nuclei were formed instantaneously at the unit surface, the overall current *I(t)* will be larger by a factor N_0 under the condition that their growth is independent, i.e. when the clusters are very much apart from each other.

In reality the instantaneous formation of the entire set of nuclei is an idealized process; the term “instantaneous” here means that the time interval necessary for

their formation is much less than that of growth. Usually, assuming a linear kinetics for nucleus formation, the dependence *N(t)* can be expressed as

$$N(t) = N_0\left[1 - \exp(-\boldsymbol{A}t)\right]. \tag{5.62}$$

Upon exhaustion of the active centers this dependence is rigorous. Obviously, the induction time is presumed to be negligibly small. Thus, at $t >> \boldsymbol{A}^{-1}$ the nucleation is instantaneous, and the above expressions remain true. But in the opposite case of $t < \boldsymbol{A}^{-1}$ the nucleation can be assumed to proceed at a constant rate $\boldsymbol{A}\boldsymbol{N}_{0,}$ which is identical to $\boldsymbol{J}$. The expression (5.62) may be thus rewritten as

$$N(t) = N_0\left[1 - \exp(-\boldsymbol{J}t/N_0)\right]. \tag{5.63}$$

In the case $t < N_0/\boldsymbol{J}$ the nucleation law is called "progressive": $N(t)=\boldsymbol{J}t$.

It is easy to show that for progressive nucleation the Eqs. (5.59–5.61) assume different functional forms.

For example, in progressive nucleation with two-dimensional kinetically controlled growth

$$I(t) = \pi hi^2 \boldsymbol{J}(V_{\mathrm{m}}/zF)t^2. \tag{5.64}$$

For a three-dimensional hemispherical, kinetically controlled growth instead:

$$I(t) = (2\pi/3)i^3 \boldsymbol{J}(V_{\mathrm{m}}/zF)^2 t^3 \tag{5.65}$$

Comparison of the overall results for instantaneous or progressive; 2-dimensional or 3-dimensional nucleation, and growth under kinetic or diffusion limitations (altogether $2^3=8$ possibilities) show that the initial dependence *I–t* has the general form $I = const \cdot t^{\alpha}$, or

$$log I = const + \alpha log t \tag{5.66}$$

where α can have 6 different values: 0; 0.5; 1; 1.5; 2; 3 and therefore the experimentally obtained values for α can serve as the diagnostic criterion for the type of the process. The above possibilities are summarized in Table 5.1.

One can see that when $\alpha=1$ or $\alpha=2$ the relationship between exponent and nucleation mode is not unique; in these situations supplementary criteria should be used to determine with certainty the actual nucleation and growth mode.

It may be added that in the case of faceted and/or non-hemispherical clusters these coefficients vary, but Eq. (5.65) is still valuable. However, it should be taken into account that under mixed control α can take intermediate values.

The general model $N(t) = N_0\left[1 - \exp(-\boldsymbol{J}t/N_0)\right]$ leads to more complicated results. For instance, for a two-dimensional nucleus generated at the time τ, the current equals $I(t) = 2\pi hi^2 (V_{\mathrm{m}}/zF)(t - \tau)$; the number of nuclei formed in

this instant is $dN(\tau) = \boldsymbol{J}\exp(-\boldsymbol{J}\tau/N_0)d\tau$. The overall current at the time t is then found by integration over all the nuclei formed between $\tau=0$ and $\tau=t$, resulting in:

$$\begin{aligned} I &= 2\pi hi^2(V_\mathrm{m}/zF)J\int \exp(-J\tau/N_0)(t-\tau)d\tau \\ &= 2\pi hi^2(V_\mathrm{m}/zF)N_0\left[t - N_0/J + N_0/Jexp(-Jt/N_0)\right]. \end{aligned} \tag{5.67}$$

In the limiting cases $\boldsymbol{J} >> N_0/t$ or $\boldsymbol{J} < N_0/t$ this solution reduces to the simpler ones (5.60) and (5.64).

5.11 The Growth of an Individual Hemispheric Cluster Under Mixed Control

The models presented in the previous section are rather simplified, because it rarely occurs that during the whole growth process the kinetic or diffusion controlled regime remain predominant. Much more probable is an initial kinetically controlled growth followed by gradually arising diffusion limitations. In the following we describe the common case of the growth of an individual cluster for some given values of both the electrochemical and the diffusion parameters.

This growth mode has been analyzed in an extremely detailed manner by Fletcher [10]; here we obtain the same solution but in a simpler and more convenient form. We will consider the hemispherical diffusion of the electroactive ions to the cluster surface, followed by a subsequent charge transfer at its surface. The latter process is governed by the Butler–Volmer equation, and the concentration of the electroactive species is C_s, less that the bulk value C.

The non-steady state growth of a hemispherical cluster R is described by the well-known equation

$$\mathrm{d}R/\mathrm{d}t = D\,(C_0 - C_\mathrm{s})V_\mathrm{m}[(\pi Dt)^{0.5} + R^{-1}] \tag{5.68}$$

In the case of mixed kinetics (where both diffusion and charge transfer limitations are important) the surface concentration at the current density i is equal to

$$C_\mathrm{s} = C_0[\exp(zf\eta)] + (i/\mathrm{i}_0)\exp(\alpha zf\eta) \tag{5.69}$$

Under this condition (5.68) gives for the overall current

$$\begin{aligned} I = DzFC_0\left[1-\exp(zf\eta)\right]\left[(\pi Dt)^{-0.5} + R^{-1}\right]/ \\ \left[1 + (DzFC_0\exp(\alpha zf\eta)\left[(\pi D\mathrm{t})^{-0.5} + R^{-1}\right]/i_0\right] \end{aligned} \tag{5.70}$$

R is, as a rule, much less than $(\pi Dt)^{0.5}$, because the latter quantity is close to the radius of a diffusionally depleted region in the solution, from which the metallic hemisphere with radius R was formed.

Then the overall current to the cluster is approximately equal to

$$I = DzFC_0\left[1 - \exp(zf\eta)\right]/(R + \left[DzFC_0\exp(\alpha zf\eta)\right]/\, i_0) \tag{5.71}$$

Or

$$dR/dt = DV_mC_0\left[1 - \exp(zf\eta)\right]/(R + \left[DzFC_0\exp(\alpha zf\eta)\right]/i_0) \tag{5.72}$$

Setting $t=0$ at $R=0$ this differential equation leads to

$$t = R^2/(2DC_0V_\mathrm{m}) + RzF\exp(\alpha zf\eta)/\{V_\mathrm{m}i_0[1 - \exp(zf\eta)]\} \tag{5.73}$$

The right side of this expression is comprised of two terms, one of a diffusive and the second of a kinetic nature. Actually, at high exchange current density the latter term tends to zero, and then (under the additional condition that [exp($zf\eta$)<<1])

$$R \approx (2DC_0V_\mathrm{m}t)^{0.5} \tag{5.74}$$

which describes pure diffusion control.

On the contrary, under the same conditions but for small i_0

$$R \approx i_0\exp(-\alpha zf\eta)V_\mathrm{m}t/zF, \tag{5.75}$$

describing pure kinetic control.

Having designated the "effective diffusion coefficient"

$$D_\mathrm{eff} = 2DV_\mathrm{m}C_0[1 - \exp(zf\eta)] \tag{5.76}$$

and also the "kinetic rate"

$$V_\mathrm{kin} = i_0V_\mathrm{m}\left[1 - \exp(zf\eta)\right]/\left[zF\exp(\alpha zf\eta)\right] \tag{5.77}$$

(this quantity corresponds to linear growth rate under the kinetic regime), we obtain

$$t = R^2/D_\mathrm{eff} + R/V_\mathrm{kin}. \tag{5.78}$$

For $t >> D_\mathrm{eff}/4V^2_\mathrm{kin}$, $R \approx \left(D_{\mathrm{ef}\,f}t\right)^{0.5}$, and for $t << D_\mathrm{eff}/4V^2_\mathrm{kin}$ $R \approx V_{\mathrm{kin}}t$.

Substitution of R from (5.78) into (5.73) and simple rearrangements lead to the following expression for the overall current:

$$\begin{aligned} I &= I^*\varphi\left(t/t^*\right) \\ &= I^*\left[\left(1 + t/t^*\right)^{0.5} + \left(1 + t/t^*\right)^{-0.5} - 2\right] \end{aligned} \tag{5.79}$$

where

$$I^* = 2\pi (DC_0 zF)^2 i_0{}^{-1}[1 - \exp(zf\eta)]\exp(\alpha zf\eta) \tag{5.80}$$

and

$$t^* = D_{\text{eff}}/4V^2{}_{\text{kin}} \tag{5.81}$$

t^* here is a characteristic time depending on all the most important parameters of the process, t/t^* is the non-dimensional time, and I^* is the current at each cluster corresponding to $t/t^* \approx 5.854$.

The expression (5.79) contains both electrochemical and transport characteristics of the process. It contains t only as t/t^* and the shape of the dependence $I(t)$ is the same for different parameters.

When $t/t^* < 0.5, \varphi\,(t) \approx 0.25(t/t^*)^2$,

and
$$I \approx 2\pi\left[1 - \exp(zf\eta)\right]^3 V_{\text{m}}{}^2 i_0{}^3 z^{-2} F^{-2}\left[\exp(\alpha zf\eta)\right]^{-3} t^2 \tag{5.82}$$

During this period I is quadratic in t and depends strongly on i_0. The dependence on i_0 gradually becomes weaker but disappears only at $t/t^* > 25000$, when only diffusion plays a role:

$$I \approx 4\pi (DC_0)^{0.5} zF V_{\text{m}}{}^{0.5}[1 - \exp(zf\eta)]^{0.5} t^{0.5} \tag{5.83}$$

Obviously, at intermediate times the dependence on D and $i_0$is more complicated. The dependence I–t from Eq. (5.79) is shown in Fig. 5.5.

Over a wide time range (t/t^* from 25 to 25000) (15) can be approximated as

$$\begin{aligned} I \approx\ & c\text{onst} i_0{}^{0.1} (DC_0)^{1.45} V_{\text{m}}{}^{0.55} (nF)^{0.9} \\ & \left[1 - \exp(nf\eta)\right]^{1.55}\left[\exp(\alpha nf\eta)\right]^{-0.1} t^{0.55} \end{aligned} \tag{5.83a}$$

There is also an interesting time range $1 < t/t^* < 10$ when linear dependence exists:

$$I \approx 4i_0 DC_0 V_{\text{m}}\left[1 - \exp(nf\eta)\right]^2\left[\exp(\text{a}nf\eta)\right]^{-1}\left(t - t^*/4\right) \tag{5.83b}$$

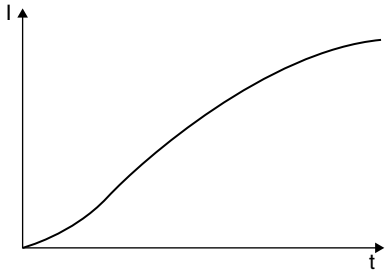

Fig. 5.5 *I–t* dependence for the growth of an isolated nucleus

In the case of the simultaneous growth of a number of clusters forming in a progressive fashion, the overall *I(t)* dependence may be found by integration. For the cluster which began to grow at the moment τ the current *I* at the moment *t* is equal to $I^*\varphi\left[(t-\tau)/t^*\right]$.

When considering the growth of a number of clusters in parallel the possibility of the overlap of such islands should be considered. The nucleation exclusion zones may start to overlap at very short times, thus the actual surface area occupied by these zones and by the clusters varies. This phenomenon is considered in the following section.

5.12 The Nucleation and Growth With Overlap

Let the new nuclei be generated stochastically at a rate $\boldsymbol{J}$ per unit surface area and let their growth proceed at a linear velocity iV_m/zF. Simultaneously the depleted zones start to propagate throughout the surface according to the diffusion laws. The radius of the zone R_z that formed at time *t* around a cluster generated at an earlier time τ is known to be

$$R_z = 2D^{1/2}(t-\tau)^{1/2}, \tag{5.84}$$

the area of this zone being $4\pi D(t-\tau)$. Under diffusion control of the growth the increment of this area during the infinitesimal time interval *dt* is equal to $4\pi Ddt$ independently of the time τ, thus for the overall $\boldsymbol{J}d\tau$ nuclei formed within $d\tau$ the area increment amounts to

$$dS = 4\pi \boldsymbol{J} Ddtd\tau, \tag{5.85}$$

and the same value represents the decrease of the area free of the diffusion zones.

At a given time these zones begin to overlap (Fig. 5.6), thus the linear decrease of the non-depleted surface area with time is not valid any more and the law describing the overlapping of these areas has to be determined.

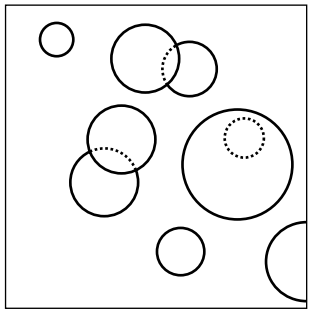

Fig. 5.6 Overlap of diffusion zones

Denote the fraction of the surface free of depleted zones at the time t by $q(t)$; by performing the integration over τ and over all the clusters initiated since $t=0$ to t we obtain:

$$dS = 4\pi \boldsymbol{J} Dq(t)tdt. \tag{5.86}$$

But on the other hand, the same increment of the surface area occupied by the depleted zones represents the decrease in the free surface area $-dq$. This leads to the differential equation for q:

$$dq/q = -4\pi \boldsymbol{J} Dq(t)tdt. \tag{5.87}$$

Since $q(\mathrm{t} = 0) = 1,$ one obtains

$$q = \exp(-2\pi \boldsymbol{J} Dt^2). \tag{5.88}$$

This is the fraction of the surface area over which nucleation can continue. The share of the surface area occupied by the diffusion zones around the growing clusters is equal to $1 - q = 1 - \exp(-2\pi \boldsymbol{J} Dt^2)$.

This result, which fully describes the overlap phenomenon, was originally obtained in a much more general form by Kolmogorov and independently by Avrami. This model can be used both under diffusion or kinetically controlled modes of growth, for two- and three-dimensional situations, etc. For the instantaneous nucleation mode $q = exp\,(-\pi N_0 Dt)$.

The overlap leads to a flattening of the transients I–t, which pass through a maximum I_{max} at a time t_{max} and subsequently show a decrease in I (Fig. 5.7). The experimental transient curves I–t obtained under various conditions correspond to these prediction. At instantaneous and progressive nucleation the shapes of the curves are somewhat different.

Combination of these results with the expressions (5.59–5.64) and others, governing the growth of non-overlapped clusters, leads [11] to well-accepted expressions for the overall I–t dependence under instantaneous or progressive nucleation. By fitting together the solutions corresponding to the different stages of the process the following expressions are obtained:

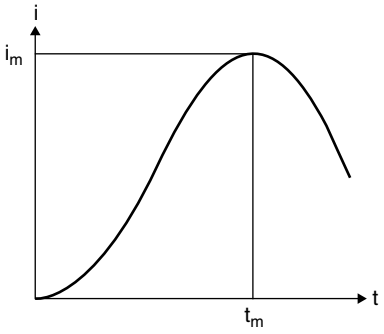

Fig. 5.7 The overall view of I–t dependence for mass crystallization

$$I(t) = zFC(D/\pi t)^{1/2}\{1 - exp[-N_0\pi kD(t - 1/A + exp(-At)/A]\} \tag{5.89}$$

where the dimensionless parameter $k = (8\pi CV_m)^{1/2}$. In the particular cases of instantaneous and progressive nucleation using the dimensionless coordinates $I^* - t^*$, where $I^* = I/I_{max}, t^* = t/t(I_{max})$, this expression becomes

$$\left(I^*\right)^2_{(inst)} = 1.9542t^*\left[1 - exp\left(-1.2564t^*\right)\right]^2 \tag{5.90}$$

$$\left(I^*\right)^2_{(progr)} = 1.2254t^*\left[1 - exp\left(-2.3367t^*\right)\right]^2 \tag{5.91}$$

The product $(I^2t)_{max}$ depends only on D and C and is equal in the first case to $0.1629D(zFC)^2$ and in the second one to $0.2598D(zFC)^2$.

The shape of these curves is very similar to that of experimental transients, thus permitting to establish experimentally the values of N, A etc. The actual conditions of overlap however are more complex than initially supposed during the development of the theory. For example, rarely the active centers are randomly distributed. For this reason it is unlikely that the extreme points I^* and t^* can be used for the calculations; the initial regions of the curves in general are more informative. Moreover, the theory does not take into account the overall shape of the I–t dependence for a single cluster (5.79).

In the same manner the overlap of growing three-dimensional clusters occurs when they start to form a continuous deposit. The problem of cluster overlap during deposit formation was analyzed in [6], where four possibilities were discussed: (1) instantaneous nucleation with diffusion-limited growth; (2) progressive nucleation with diffusion-limited growth; (3) instantaneous nucleation with kinetically controlled growth and (4) progressive nucleation with kinetically controlled growth.

In the three-dimensional case one should use the expressions for q at different heights of the clusters with respect to the substrate, then integrate over all the sections at various heights to obtain the overall volume (and therefore the overall electric charge used up for its formation). Finally, by differentiation of this charge with respect to time one obtains the dependence $I(t)$.

In this sophisticated case the dependences $I(t)$ are expressed through the Dawson's integrals, which are tabulated. The shapes of the curves (1)–(4) are plotted in Fig. 5.8 in the coordinates I^*–t^*. In all four cases the current goes through its maximum and then falls due to a decrease of the growing surface area: at this stage the surface is gradually smoothing.

One can see that the four cases differ from one another by the value of t^* at $I^* = ½$: its values are correspondingly 0.12, 0.40, 0.44 and 0.56. The cases (2) and (3) are close to each other, but in case (2) the initial portion of the curve corresponds to $i \sim t^2$, whereas in case (3) $i \sim t^{3/2}$. Moreover, case (2) is characterized by a specially pronounced decrease in I^* after the maximum is attained: I^* falls to 0.7 at $t^* = 2$. This allows identification of the actual mode of growth.

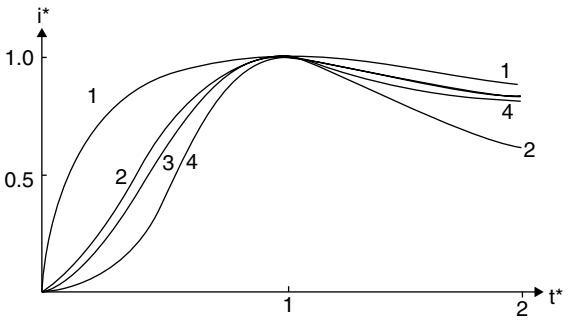

Fig. 5.8 Non-dimensional *I–t* dependences at different modes of the growth: *1*–instantaneous nucleation and diffusion growth, *2*–progressive nucleation and diffusion growth, *3*–instantaneous nucleation and kinetic growth, *4*–progressive nucleation and kinetic growth

In continuous two-dimensional nucleation, e.g., during growth of a thick metal layer, the nucleation on top of the first layer may start before completion of the first layer. Similarly the second, third etc. layers may start their growth on top of still incomplete previous layers. The resulting dependence *I(t)* is combined by adding a set of the transients considered above (Fig. 5.9). The corresponding curves for the subsequent layers have a time lag with respect to the previous ones along with some blurring which is due to their growth on top of incomplete layers.

Experiments indeed show oscillations of the total current, which tend to decay by the fifth or sixth layer. The corresponding calculations lead to the same result, the steady state current being close to that of the maximum value for the single layer.

In three-dimensional growth such oscillations do not exist, and only one maximum of the current is exhibited both theoretically and experimentally. This maximum as noted earlier is connected with the geometric leveling of the surface after separate hemispherical nuclei coalesce. The resulting decrease in current has a different nature compared to that exhibited under diffusion limitations. In the last case the Cottrell's decrease in current is much more pronounced, but the current does not fall to zero: the establishment of a diffusion layer thickness δ gives the minimum current $I = zFCD/\delta$.

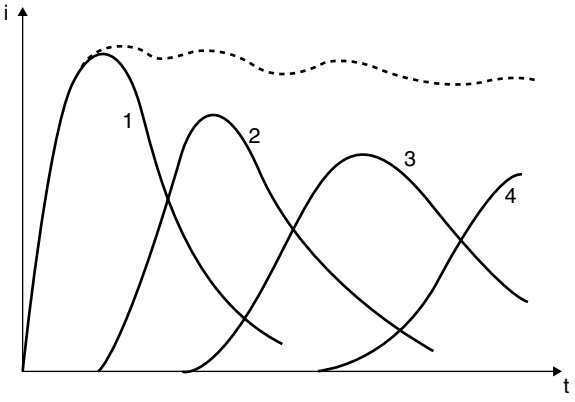

Fig. 5.9 The resulting dependence *I(t)* at polylayer growth

In conclusion we may list the important factors when analyzing nucleation and growth phenomena. These are the kinetics of the charge transfer and its dependence on potential and conditions at the surface; the volume diffusion and surface diffusion coefficients; the nucleation rate and its dependence on the surface activity and on the overlap between nuclei; the formation of new nuclei at the growing surface (secondary nucleation). All of these factors lead to a relatively complicated process which determines the morphology of the growing surface and to some extent the microstructure and properties of the deposit.

More detailed discussion on the topics of this chapter can be found in [12].

References

1. Kashchiev D. J. Chem. Phys. 1982, v.76 p. 5098
2. Chakraverty B.K., Pound G.M. Acta Metallurgica 1964, v.12, N0.8, p. 851
3. Hirth J. P., Pound G.M., Progr. Mater. Sci., 11. 1 (1963)
4. Stoyanov S. Thin Solid Films, 1973, v. 18, No 1, p. 91
5. Frenkel J. Kinetic Theory of Liquids, New York, Dover, 1955
6. Becker R., Döring W. Ann. Physik, 1935, Bd. 24, s. 719; Zeldovich J., Acta Physicochim. USSR, 18, 1943, p.1
7. Isaev V.A. Electrochemical phase formation. Ekaterinburg, 2007 (in Russian)
8. Kaischev R., Mutaftschiev B. Electrochimica Acta 10, p. 643 (1965)
9. Budevski E., Vitanov G., Bostanov V., Phys, Status Solidi 8, 369 (1965)
10. Fletcher S. J. Chem. Soc. Farad. Trans., 1, 79 (1983), 467
11. Scharifker B.R., Mostany J., J. Electroanal. Chem., 177, p. 13 (1984)
12. Milchev A. Electrocrystallization: fundamentals of nucleation and growth. Kluwer Academic Publishers, 2002, 265 pages

Chapter 6
Morphology of the Growing Metal Surface

6.1 Steps and Kinks

Electrocrystallization proceeds through the nucleation of stable clusters, followed by the attachment of adatoms to these clusters. The kinetics of attachment of incoming atoms to a flat macroscopic surface does not differ from that occurring during the growth of supercritical clusters about four times larger than the critical size; with smaller clusters on the other hand the attachment rate decreases, as discussed in Chap. 5. A rigorous description of the growth process however requires a more specific discussion, since the growing surface is characterized by various geometric and energetic peculiarities, which will be considered in this chapter.

While an ideal crystal surface can be obtained by cutting an ideal three-dimensional crystal along a definite crystallographic direction, a real crystal surface exhibit several defects. One of the characteristic features of a real crystalline surface is the step, i.e. the edge of a monoatomic or polyatomic plane, where the atoms are arranged to form a specific facet of a monocrystalline grain. Steps are usually aligned along a definite crystallographic direction with respect to the frame of reference determined by the noted grain.

Sometimes, steps exhibit an irregular shape. Facets with high Miller indices are intrinsically stepped (Fig. 6.1), and are referred to as *vicinal* surfaces; on the contrary, surfaces with low Miller indices are atomically smooth at zero temperature, and develop steps near room temperatures due to entropic effects.

The steps can be characterized by their height and by their average distance, the terrace width. A further characteristic is the distance between kinks along the step, l (Fig. 6.2). The kink, also called kink-site position, or half-crystal position, has a particular importance in the description of growth and dissolution processes. When attaching one atom at this location, or when removing one atom from it, a new but identical configuration is created; the overall crystal may therefore be formed or dissolved through the repeatable process of attachment or detachment to/from a kink site. For this reason the work required to remove one atom at a kink position equals the chemical potential change during the crystallization process and quantifies the characteristic energy of a large crystal (Kossel, Stranski). It should

Y. D. Gamburg, G. Zangari, *Theory and Practice of Metal Electrodeposition,*
DOI 10.1007/978-1-4419-9669-5_6, © Springer Science+Business Media, LLC 2011

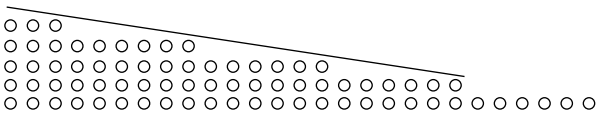

Fig. 6.1 Crystal facets with high Miller indices are described by steps on surfaces with low Miller indices

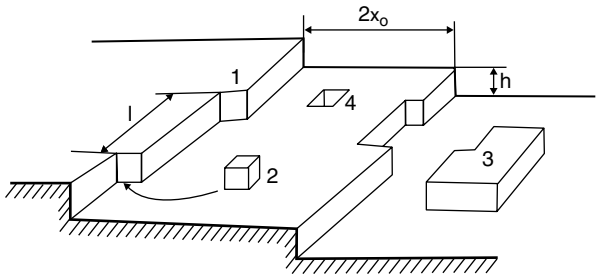

Fig. 6.2 Defects at real surfaces. *1* – a kink site at an atomic step, *2* – ad-atom, *3* – nucleus, *4* – a vacancy

be stressed that this statement is valid for an infinitely large crystal and relatively to the conversion of one mole.

The concept of average work of separation, developed on this basis by Stranski and Kaischev (1934) allowed the rigorous development of correlations between thermodynamics and kinetics in phase formation. This concept is used for example to determine the equilibrium crystal shapes, the textures of the forming crystals, or to calculate the surface energy of different crystal facets.

The surface density of kinks at a surface is one of the main factors determining the features of crystal growth. At each temperature the step has a definite equilibrium concentration of kinks, determined by the minimum of the free energy of the system $G = U - TS$. The presence of kinks increases entropy; therefore, for a sufficiently high temperature the increase in defect density stabilizes the surface, and a surface roughening transition is observed. This results in the smearing out of steps, as schematically shown in Fig. 6.3. In electrocrystallization this kind of surface can be observed even at low temperature since during growth the surface morphology

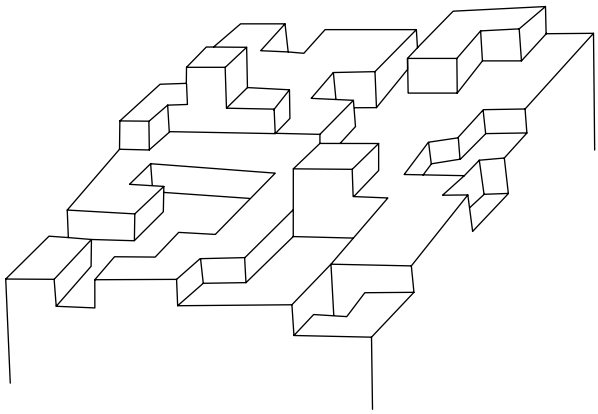

Fig. 6.3 An increase in temperature stabilizes defect formation, resulting in surface roughening and blurring of atomic steps

is not determined by thermodynamics; the growth form is determined instead by kinetic factors.

A rough surface consists of various incomplete monoatomic layers and is formed when the nucleation rate $\boldsymbol{J}$ is high whereas the growth rate I is low. The secondary nucleation over the previously formed clusters results in this type of surface independently of temperature; this is termed "kinetic roughness".

On a stepped surface the kink concentration can also differ considerably from the equilibrium value. The height of the steps, as will be shown below, is determined directly by kinetic processes. Upon adsorption of impurities a certain fraction of the kinks becomes poisoned, resulting in the formation of new clusters at the flat surface; an important role in this process is played by the screw dislocations, which provide for continuous crystal growth without the need for the formation of critical nuclei.

6.2 Adatoms and Adions

The separation work for an adatom on a flat surface (site 2 in Fig. 6.2) is much lower than the average value, therefore this atom can be considered as not fully belonging to the crystal lattice, especially in the case of a foreign surface. The term "adatom" or "adion" stresses not only the adsorbed state of the atom but also the possible fact that upon adsorption only partial charge transfer may have occurred; an adion retains part of its initial solvation species along with a partial charge.

The processes of adsorption (particularly in the underpotentional region) of metal ions (atoms) at foreign substrates is important both theoretically and from the standpoint of the various techniques for the formation of nanometric objects for quantum electronics, catalysis or other applications.

Upon adsorption on monocrystalline facets the adatoms at sufficiently high coverages can build structured islands with a well defined two-dimensional lattice; sometimes a definite lattice structure is formed in combination with electrolyte anions. A monolayer of adatoms can also be formed; the reconstruction of an adsorbed monolayer can take place at higher coverage, e.g. copper at a platinum (111) surface may reconstruct from a $(\sqrt{3}\times\sqrt{3})$R30º structure in presence with electrolyte anions to an epitaxial layer Cu(1×1) at full coverage [1].

The adions at a given potential are in equilibrium both with the solution and with the steps; under these conditions an equilibrium surface concentration of adions is achieved, with:

$$C_{\mathrm{ad}}(\eta) = C_{\mathrm{ad}(\eta=0)} exp(zF\eta/RT), \tag{6.1}$$

where $C_{\mathrm{ad}(\eta=0)}$ is the adion concentration at the equilibrium potential, in general different from zero.

If incorporation of adions into the lattice occurs preferentially at kinks, adion concentration is not uniform across the surface. There is therefore a difference be-

tween the mechanism of electrodeposition by the direct discharge of ions at the growth site and the surface diffusion mechanism. In the latter case the electron transfer can be considered as a two-step process even though it is a one-electron process. Upon transfer of the species from the solution to the surface a partial charge transfer takes place, and only upon final incorporation of the adion into the lattice the charge transfer is completed.

In principle both mechanisms are possible. In the literature one can find arguments in favor of both hypotheses. Energetic calculations show that the charge transfer to a flat surface with subsequent surface diffusion is preferred. Many experimental data however are usually adduced to support the mechanism of the direct ion discharge.

Characteristic features of the surface diffusion mechanism are considered below.

6.3 Normal Growth and Layer-by-Layer Growth

Independently of the actual mechanism, the growth at atomically rough surface and at a surface with relatively smooth steps proceeds by different processes. In the first case a high density of growth sites is stochastically distributed and at very close distance; thus the discharge and attachment of atoms to the lattice occurs across the whole surface and is not localized at a definite location. As a consequence only the overall displacement of the boundary metal—solution along its normal is observed; this process is called normal growth.

At a stepwise surface on the contrary the atoms do attach to kinks at the steps, resulting in the motion of steps along the terrace until the whole layer is covered. This is called the layer-by-layer growth mode. In this case the resulting growth rate in the normal direction is obtained by dividing the thickness of one layer h by the duration of its completion. The latter equals $2x_0/v_t$, where $2x_0$ is the distance between neighboring steps and v_t is the rate of the tangential step propagation. Thus the rate of normal growth in this case is $v_n = v_t\, h/2x_0$. Experiments show that macroscopic steps do simultaneously grow along both directions: normally and tangentially, the rates in both directions being approximately equal. Thus the overall rate of the normal displacement in layer-by-layer growth is

$$v_n = v_t(1 + h/2x_0). \tag{6.2}$$

There are no sharp boundaries between the two growth modes because the purely normal growth is the limiting case of the layer-by-layer growth for entirely blurred steps; if the step is not atomically smooth, it can exhibit normal growth along with the tangential one.

It is possible to determine the preferential growth mode ex situ by examining the morphology of the grown surface; sometimes this is the unique criterion. Usually in layer-by-layer growth distinct crystallographic features are seen during microscopic examination; definite crystallographic faces can in fact be distinguished along with the growth steps. On the contrary, in the case of normal growth the surface mor-

phology is mainly determined by the conditions of the growth front stability during motion of the phase boundary; that is by the electric field distribution along with the hydrodynamic conditions and adsorption of the additives.

Let us consider next the kinetics of normal and layer growth and then the morphology of the surfaces formed in the corresponding conditions.

6.4 The Rate of Normal Growth

Let us assume that the electrodeposit grows by atomic attachment to kinks at atomically rough surfaces by the mechanism of direct discharge at these kinks. Let the average distance between the kinks be l, and the surface density of the kinks $1/l^2$; the rate constants for the elementary processes of discharge and ionization are correspondingly k_c and k_a, and the concentration of electroactive species near the surface is C_s. The partial current densities for the attachment (cathodic) and detachment (anodic) processes are

$$i_c = (k_c C_s / l^2)\, exp(-\alpha nF\eta/RT) \tag{6.3}$$

and

$$i_a = (k_a / l^2)\, exp((1-\alpha) nF\eta/RT) \tag{6.4}$$

At low overpotentials the exponents can be linearized, thus leading to a linear dependence of the growth rate on overpotential:

$$i = (k_c C_s / l^2) nF\eta/RT; \tag{6.5}$$

at high overpotentials (6.3) is valid for the overall rate, because i_a is negligibly small.

The current density i corresponds to the rate of the normal growth (cm/s)

$$v_n = i V_m / nF. \tag{6.6}$$

One can see that these expressions determine the rate constants for electrodeposition used earlier. Namely, in this case the rate constants used for the uniform continuous surface are equal to the constants for the elementary events of charge transfer multiplied by the density of growth sites. This means that if the distance between the kinks varies with the overpotential, the usual electrochemical equations for discharge and ionization are not obeyed.

Besides, the value of C_s differs from the bulk value C due to diffusion limitations, as discussed in Chap. 4. As usual $l << \delta$ (the diffusion layer thickness), thus one can neglect the discrete character of the growth sites relative to the diffusion layer thickness; moreover, these sites move quickly along the surface. In other words, the overall surface moves along the normal at some constant rate v. However it is important that v is small relative to the diffusion rate, otherwise the diffusion problem

with a moving boundary must be solved. This occurs rarely in electrochemistry, but at high current densities it may be possible.

6.5 Rate of Step Propagation During Layer-by-Layer Growth

If adions are formed on the entire surface but incorporation of atoms into the crystal lattice takes place only at kinks, then the overall process becomes a three-step one. The two processes mentioned above are separated by a third: surface diffusion. Therefore the equation describing the dependence of current density on applied potential must include relevant parameters for all three processes, i.e. the surface diffusion coefficient D_s along with the rate constants and transfer coefficients of the charge transfer steps.

It is usually postulated that incorporation of the atoms into the kinks is very fast as compared to discharge on a flat surface or to surface diffusion. For this reason the concentration of adions near the steps is described by its equilibrium value. Moreover, adions are usually considered to be adatoms, thus their incorporation occurs without charge transfer. Under these conditions the dependence of i on η found for the line diffusion model is very close to the conventional Butler—Volmer equation

$$i = i_0\{exp(\alpha nF\eta/RT) - exp[-(1-\alpha)nF\eta/RT]\ (\lambda/x_o)\ tanh\ (x_o/\lambda)\} \quad (6.7)$$

and differs only by a factor $(\lambda/x_o)\ tanh\ (x_o/\lambda)$ where x_o is the half-distance between steps and λ is the so-called depth of surface-diffusion penetration defined as

$$\lambda = [(D_s nF/k_c)\exp(-\alpha nF\eta/RT)]^{1/2} \quad (6.8)$$

k_c and α being the rate constant and transfer coefficient for the cathodic process at the flat surface of a step. If $\lambda >> x_o$ the value of the hyperbolic tangent is close to x_o/λ, thus these quantities cancel from the equation, and one obtains its conventional form. In the opposite case the surface diffusion becomes the slowest step.

Much more general is the situation when incorporation is not as fast. In this case the kinetics of adion formation is described by

$$v_{loc} = C_v k_1 exp(-\alpha_1 zF\eta/RT) - C_{ad}k_2(\beta_1 zF\eta/RT) \quad (6.9)$$

where α_1 and β_1 are the transfer coefficients for the step of adion formation, and k_1, k_2 the rate constants of this step.

Under steady state conditions this rate is balanced by the surface diffusion flux

$$v_{loc} + \partial^2 C_{ad}/\partial x^2 = 0, \quad (6.10)$$

the boundary condition at the step being

$$(\partial C_{ad}/\partial x)\ (x = \pm x_0) = \pm v^* x_0/D_s \quad (6.11)$$

(v* is the average flux density).

The corresponding solution is

$$C_{\mathrm{ad}} = C_{\mathrm{v}} k_1/k_2 exp[-(\alpha_1 + \beta_1) zF\eta/RT] - \mathrm{v}^* x_0 \lambda D_{\mathrm{s}}{}^{-1} cosh(x/\lambda)/sinh(x_0/\lambda), \tag{6.12}$$

where λ was defined in Eq. (6.8). $\mathrm{v}_{\mathrm{loc}}$ is therefore

$$\mathrm{v}_{\mathrm{loc}} = (\mathrm{v}^* x_0/\lambda) cosh(x/\lambda)/sinh(x_0/\lambda) = (\mathrm{v}^* x_0/\lambda) coth(x/\lambda) \tag{6.13}$$

Let us now consider the limiting cases. At $x_{\mathrm{o}} << \lambda$ the value of *coth* (x_{o}/λ) is close to 1, implying that the current is uniformly distributed on the surface as in the previous case (6.7). On the contrary, for $x_{\mathrm{o}} >> \lambda$ this value is close to λ/x_{o}. In this situation the current is concentrated only at a narrow strip near a step; this process in fact is very close to the direct discharge at steps, but without taking into account diffusion in the solution.

The adions concentration at steps, i.e. at $x = x_{\mathrm{o}}$ is given by

$$C_{\mathrm{st}} = (C_{\mathrm{v}} k_1/k_2) exp[-(\alpha_1 + \beta_1) zF\eta/RT] - \mathrm{v}^* x_0 \lambda D_{\mathrm{s}}{}^{-1} coth(x_0/\lambda). \tag{6.14}$$

The concentration profile of adions between the steps is shown in Fig. 6.4.

The overall process might include an electrochemical stage at the steps, the final discharge of adions; in this case the value obtained for $C_{\mathrm{ad,st}}$ can be substituted in the conventional Butler—Volmer equation for this step (with its own parameters) to obtain the overall net equation. This derivation is discussed in [2].

Another possibility is the direct discharge at growth sites. Diffusion phenomena are usually neglected in the discussion of the corresponding problem, and the solution is a Butler—Volmer type equation involving the surface density of kinks. The case of diffusion limitations however differs significantly from the simple case of smeared-out active centers.

Ion diffusion from the electrolyte bulk to the surface steps can be considered as half-cylindrical diffusion (Fig. 6.5). For simplicity therefore, the step can be replaced when solving the problem with a half-cylinder with the same surface area, i.e. with diameter $2h/\pi$, and the distance between steps $2x_0$. The boundary condition at the step may be set as $i = k(\eta) C_{\mathrm{s}}$, whereas the bulk concentration at the diffusion layer boundary (at $y > \delta$) is C_0. A further simplifying condition can be $\delta > x_0$. However, the solution of this problem is not available at present. A careful calculation

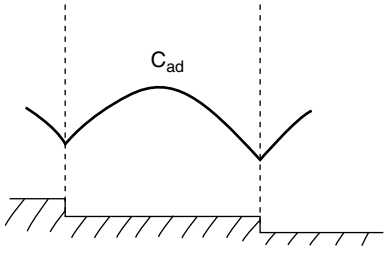

Fig. 6.4 The concentration profile of adions between atomic steps

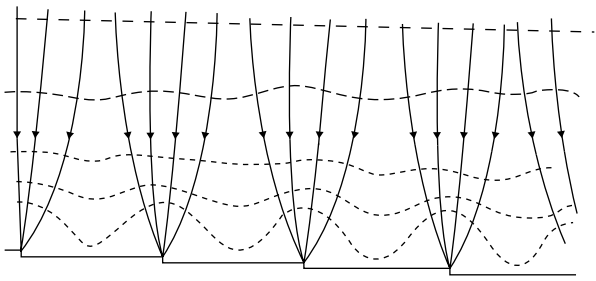

Fig. 6.5 Half-cylindrical diffusion to atomic steps

must provide an expression for the current density as a function of the thickness of the diffusion layer δ, the height of steps h and their relative distance $2x_0$, the diffusion coefficient D and the kinetic coefficient k.

$$i^* = kC_0 \cdot f(k,\ h,\ x_0,\ \delta,\ D). \tag{6.15}$$

k is the rate constant for the electrochemical process and depends on electrode potential. An approximate form of this dependence can be found in [3].

6.6 Nucleation Rate Distribution Between Growth Steps

During electrodeposition on a stepped surface, if growth occurs by step propagation, the components of the overall overpotential vary at different points of the surface. Immediately near the points of incorporation of new atoms into the crystal lattice the overpotential corresponds to that of charge transfer, but with increasing distance from the steps the concentration of adions grows, and the overpotential of surface diffusion increases too. The gradient of surface concentration is a driving force for surface diffusion which provides the transfer of adatoms to steps. If the adions concentration becomes higher than the equilibrium value the formation of new nuclei becomes possible; this concentration reaches its maximum value halfway between the steps

In the region farthest from steps the concentration is the highest and the rate of deposition is the lowest (here equilibrium can exist between dissolution of adions and deposition from the solution), but there is the highest probability of nucleation; in other words, the overpotentials of surface diffusion and of charge transfer are the lowest in this region, whereas the crystallization overpotential is the highest. In fact, in this region stripes can be found, characterized by a high nucleation rate.

In this situation it is difficult to find the average value for the nucleation rate throughout the overall surface because it depends on the distribution of adions (adatoms) concentrations. A possible approach to this problem is the following. Let the dependence of the nucleation rate on x be $\boldsymbol{J}(x)$; this dependence, as just noted, has a maximum at $x=0$.

The average value $\boldsymbol{J}_{\text{av}}$ equals

$$\boldsymbol{J}_{\text{av}} = 1/(2x_0) \int_{-x_0}^{x_0} \boldsymbol{J}(x)dx; \tag{6.16}$$

In the case of a sharp maximum this integral can be approximated by

$$\boldsymbol{J}_{\mathrm{av}} = \pi/(2x_0)[2\boldsymbol{J}(0)^3/|d^2\boldsymbol{J}(0)/dx^2|; \tag{6.16a}$$

therefore, the average value can be determined from the maximum value of $\boldsymbol{J}$ and the value of the curvature at the position of this maximum.

The rate of two-dimensional nucleation $\boldsymbol{J}$ in logarithmic form is

$$ln\ \boldsymbol{J} = ln\ K_1 - \pi\sigma^2 s/(k_{\mathrm{B}}Tze\eta) \tag{6.17}$$

where $\eta = k_{\mathrm{B}}T/ze\ ln(C/C_{\mathrm{o}})$; this is the analogue of (5.45) for two-dimensional nucleation. Using (6.1) (with simpler indices)

$$ln\ \boldsymbol{J} = ln\ K_1 - \pi(\sigma s/k_B T)^2/ln(C/C_{\mathrm{o}}). \tag{6.17a}$$

Here σ is the surface energy, s is the surface area occupied by one atom, C is the concentration of adatoms. The value of K_1 is determined by the frequency of attachment of new adatoms to the critical nucleus and by the Zeldovich factor which takes into account the deviation of the partition function of the nuclei sizes from the equilibrium one. When $C \to C_{\mathrm{o}}$ the rate of nucleation falls sharply; as a result, nucleation does not occur near growth sites (i.e. either near the new nuclei or near the kinks).

The average nucleation rate $\boldsymbol{J}_{\mathrm{av}}$ can be found in this case as

$$\boldsymbol{J}_{\mathrm{av}} = 0.5K_1 \int_{-\mathrm{x_o}}^{\mathrm{x_o}} exp(\pi(\sigma s/kT)^2/ln(C/C_{\mathrm{o}})dx \tag{6.18}$$

In order to calculate this integral one can substitute the actual concentration profile with a simple function $C(x)=C_{\max}-kx^2$. The corresponding calculations have been performed and have shown that the ratio between the averaged nucleation rate and its maximum value (occurring half-way through the steps) is close to

$$\boldsymbol{J}_{\mathrm{av}}/\boldsymbol{J}_{\max} \approx k_{\mathrm{B}}T(C_{\max}/C_{\mathrm{o}} - 1)^{1/2}/(2s\sigma) \tag{6.19}$$

Other methods of approximation for this calculation give very close values [4]

$$\boldsymbol{J}_{\mathrm{av}}/\boldsymbol{J}_{\max} \approx k_{\mathrm{B}}T\ ln(C_1/C_0)/[2s\sigma(1 - C_{\mathrm{o}}/C_1)^{1/2}]. \tag{6.20}$$

This ratio is approximately equal to the distance between the point with maximum nucleation rate and that with a rate half as much if the half-distance between steps is equated to unity. If said distance is of the order of atomic distances, this is tantamount to stating that nucleation is localized at the point $x=0$. In practice, a suggested value for the width of the stripe having the highest nucleation rate is about one tenth from the distance between steps.

6.7 Influence of Adsorption on the Rate of Crystallization

Most discussion of nucleation and growth processes assume that charge transfer takes place on a uniform surface. This approach however does not take into account the fact that electrocrystallization always occurs on a defected surface, with steps and kinks having a dominant role in those processes. In presence of an adsorbate a certain fraction of the kinks becomes blocked and as a result the concentration of growing nuclei diminishes.

In the Langmuir approximation for the adsorbate the fraction of blocked kinks is equal to

$$n_1 = C_{st}/[C_{st} + K\ exp(-Q/RT)] \tag{6.21}$$

where C_{st} is the concentration of adsorbate near the steps, and Q is the heat of adsorption. (6.21) follows immediately from the Langmuir isotherm

$$n_1/(1-n_1) = BC_{st},\ B = K^{-1}\ exp\ (Q/RT) \tag{6.22}$$

The distance L between free kinks increases as compared with the value L_0 observed in the absence of adsorbed species, which is determined only by the temperature (at equilibrium kinks lower the entropy of the surface):

$$L = L_o/(1-n_1) = L_o[1 + C_{st}/K\ exp(Q/RT)] = L_o(1 + \xi C_{st}) \tag{6.23}$$

Considering crystal growth by step propagation, the rate of this process v is inversely proportional to L, and for this reason

$$v = v_o(1-n_1) = v_o/(1 + \xi C_{st}) \tag{6.24}$$

If the adsorption isotherm at the kink sites is known one can estimate the growth kinetics; conversely, when the changes in kinetics upon adsorbate additions are known one can provide an estimate for the adsorption energy Q.

In normal growth, i.e. when growth occurs by addition of atoms not to steps but to kinks on an atomically rough surface, the rate of growth is inversely proportional to the square of distance between kinks. In this case however $L=L_o/(1-n_1)^{1/2}$, and in this connection (6.24) retains its validity.

It is necessary to emphasize that the fraction of blocked growth sites can be much higher than the averaged value of coverage θ measured by some independent method (for instance from the double layer capacitance), because adsorption at kinks is preferred. This can be the reason for the general non-linear dependence of i upon θ. In other words, the blocking effect is not described by the simple dependence

$$i_\theta = i_{\theta=0}(1-\theta), \tag{6.25}$$

where $i_{\theta=0}$ represent the current density at zero coverage, but by a more complicated formula. The equation

$$i_\theta = i_{\theta=0}(1-\theta)^r, \tag{6.26}$$

or other equations containing an exponential factor can reflect precisely the specific blocking of growth sites.

For the same reason total blocking can be achieved at $\theta << 1$. Under this condition the type of crystallization process changes, and new nuclei can develop independently of existing steps.

A further reason for inhibition of electrodeposition in presence of an adsorbate is a decrease in the coefficient of surface diffusion. Even if this stage is not limiting in absence of adsorbed species, it can become limiting at a certain coverage level.

6.8 Ohmic Drop Near a Growing Step

The problem of current distribution has been examined above for the case of a rough surface, where the active sites are present at high density across the whole surface. On the other hand, if the growing centers are localized (for example at steps) an ohmic voltage drop occurs only in the neighborhood of these points.

If the current is concentrated at steps of height h the voltage drop is approximately equal to

$$\Delta U \approx i\rho\delta \, ln(\pi\delta/h) \approx i\rho\delta(1 + ln(\delta/h)), \tag{6.27}$$

where δ is the diffusion layer thickness. In absence of such localization of the electric field to a step, $\Delta U = i\rho\delta$, consequently the term $i\rho\delta \, ln(\delta/h)$ quantifies the additional Ohmic drop.

When the distance between steps $2x_0$ is less than δ, the field distributions relative to nearby steps overlap, and the potential drop can approximately be written as the sum of voltage drops in a uniform field, each having thickness equal to $(\delta - x_0)$ and with a cylindrical symmetry ($r = x_0$):

$$\Delta U \approx i\rho(\delta - x_0) + i\rho x_0 \, ln(\pi x_0/h) \approx i\rho\delta + i\rho x_0 \, ln(x_0/h) \tag{6.28}$$

In this case the constriction of the field results in an additional contribution $i\rho x_0 \, ln(x_0/h)$. In general it may be concluded that the constriction of electric field near some lines results in the additional Ohmic drop

$$\Delta U \approx i\rho l \, ln(l/h) \tag{6.29}$$

where l is the lowest between the quantities δ and x_0. When the discharge takes place at stripes of width λ (see below) h needs to be substituted by λ.

This additional contribution is not large, since $ln(l/h)$ is generally less than 10 and l is small.

The other case is field constriction not at lines but at spots. Under these conditions

$$\Delta U \approx i_s\rho/\pi r, \tag{6.30}$$

r being the spot radius, and i_s the current to one spot. Let θ be the active fraction of the surface and N the number of spots per unit surface. Then $r=(\theta/\pi N)^{1/2}$, $i_s=i/N$, and finally

$$\Delta U \approx i\rho(\pi N\theta)^{-1/2} \tag{6.31}$$

When $\theta \ll 1$ the average distance between spots is approximately $l=N^{-1/2}$, and consequently

$$\Delta U \approx \pi^{1/2} i\rho l/\theta^{1/2} \tag{6.32}$$

Comparison of (6.32) and (6.29) shows that if the values of l in these expressions are of the same order of magnitude the value of ΔU in the case of spots does not exceed the value in the case of lines when $\theta < 0.01$.

Experiments show that for several systems the Ohmic drop due to field constriction can be comparable with the electrochemical overpotential, i.e. it may range up to 100 mV. This means that the fraction of active surface is less than 1%.

It is interesting that in the experimental measurements of *IR* by fast potential change at the moment of switching of current the additional contributions considered here are not included into the measured value of Ohmic drop [5].

6.9 Grain Size of Deposits as a Function of Overpotential

The relationship between the rate of nucleation and the growth of crystals is usually discussed when providing a theoretical treatment of the grain size in electrodeposits. It is generally agreed that at high rate of nucleation and slow growth fine-grained deposits are formed, and vice-versa. This rule is qualitatively obeyed in general, however it should be pointed out that, since said rates have different dimensionality, it is impossible to rigorously compare the two values. At the same time it can be easily derived that if each nucleus grows into one grain than its volume is

$$V = iV_m/(\boldsymbol{J}zF) = iv/(\boldsymbol{J}ze) \tag{6.33}$$

(here i is the current density, V_m is the molar volume of the metal and $\boldsymbol{J}$ is a nucleation rate expressed in $cm^{-2}s^{-1}$).

Both i and $\boldsymbol{J}$ depend upon the applied overpotential. If the measured value of overpotential is corrected for concentration factors, then the corrected value of η is related with i and $\boldsymbol{J}$, as shown earlier, as

$$ln\ i = ln\ i_0 + \alpha ze\eta/k_B T \tag{6.34}$$

and

$$ln\ \boldsymbol{J} = K_1 - K_2/\eta^2 \tag{6.35}$$

Substitution of these expressions into (6.33) leads to

$$lnV = ln(v/ze) + ln\ i_o - K_1 + \alpha ze\eta/k_BT + K_2/\eta^2 \tag{6.36}$$

On the right side of (6.36) the overpotential is present in two terms, one of which is proportional to η and the other inversely proportional to η^2. This combination always results in a minimum for the total sum. This means that the grain volume should be smallest in size when the deposit is obtained at the corresponding potential, which can be found by differentiation of (6.36):

$$d\ lnV/d\eta = \alpha ze\eta/k_BT - 2K_2/\eta^3 \tag{6.37}$$

Hence

$$\eta_c = (2K_2k_BT/\alpha ze)^{1/3} \tag{6.38}$$

For three-dimensional nucleation K_2 can be expressed as

$$K_2 = A\sigma^3 s^3/(k_BTz^2F^2) \tag{6.39}$$

(A is a factor of order 1 and depends on the nucleus shape, s is the surface occupied by one atom in a monolayer and σ is the specific surface energy of a metal), and therefore one obtains

$$\eta_c = (\sigma s/ze)(2A/\alpha)^{1/3} \tag{6.40}$$

(this value does not include a concentration overpotential).

Substituting actual values for σ and s it is seen that the overpotential corresponding to minimum sized grains can be as much as several hundreds millivolts and up to one Volt. Such values are rarely achieved in electrodeposition, and this is the reason why a decrease of the grain size with increasing overpotential is observed. Nevertheless, coarse grains have been obtained in some instances at very high current densities.

It is more difficult to give an estimate for the minimum grain size corresponding to the overpotential given by (6.40). For this purpose first of all it is necessary to find a value of K_1. The corresponding expression can be derived from (5.45) by substitution of the expressions for σ, ΔG, ω etc.:

$$K_1 \approx ln\ N + ln(v/ze) + lni_0 + \frac{1}{2}ln(A\sigma/kT) \tag{6.41}$$

Here N is the number of active sites per unit surface. Then, after substitution of K_1 and η_c one can obtain

$$ln\ V_{min} \approx 2/3(2A\alpha^2)^{1/3}\sigma S_m/RT - ln\ N - \frac{1}{2}ln(A\sigma/k_BT) \tag{6.42}$$

and, taking into account that the coefficient of the first term on the right is close to unity,

$$V_{\min} \approx N^{-1}(k_B T/A\sigma)^{1/2} exp(\sigma S_m/RT) \tag{6.43}$$

Therefore an average value for the grain diameter is

$$D_{\min} \approx (k_B T/A\sigma N^2)^{1/6} exp(\sigma S_m/3RT) \tag{6.44}$$

It is interesting that this minimum size depends mainly on N and σ and it does not depend on the exchange current density.

If we use realistic values for s and σ and also the maximum value for N we obtain $D_{\min} \approx 3$ nm, corresponding to amorphous deposits. This quantity may be lowered only by diminishing σ, e.g. by adding surface-active substances to the solution.

If deposition proceeds by two-dimensional nucleation then the expression for $\boldsymbol{J}$ changes to (6.19); combining this equation with (6.33) does not give a minimum value: in two dimensions, the larger is η, the smaller is D. This result is commonly observed. However, in a more general approach that takes into account the possibility of partial charge transfer during ad-ion formation, a factor β (coefficient of partial charge transfer) appears in the second term of (6.35), which can be close to the factor α in (6.36); this can result again in the appearance of a minimum in D as a function of electrode potential.

The picture shown here [6] is idealized and can be distorted if one grain is formed from more than one nucleus, and by other reasons as well. It seems however to closely describe actual observations for deposition processes on amorphous or polished substrates, especially in the case of thin layers.

6.10 Morphological Features of Compact Electrodeposits

6.10.1 The Morphological Types of the Deposit Surface

The morphological surface features of electrodeposits depend on the deposition rate, the degree of adsorption of impurities and to less extent on the overall set of the deposition conditions: temperature, concentration of the reducible species, mode of control of the electrical variables, the nature of the reacting ions as well as the presence of foreign cations and anions, pH and finally also on the character of the substrate, in particular its crystallographic orientation and the preliminary treatment. The substrate commonly retains its influence up to a certain deposit thickness; for thicker deposits the structure and morphology are determined only by the deposition conditions.

This means that for every set of electrodeposition conditions a specific surface morphology is observed which is relatively stable under these conditions. Each

monocrystalline facet, which is part of the overall surface, has its own characteristic growth rate and its own density of growth sites; while this facet is growing, new facets (with different Miller indices) may arise at the edges, and those facets grow according to their own properties.

By varying the electrode potential or the average current density the rate of the elementary growth processes changes, and the step density as well as other properties of the facets may also be modifed. The resulting stable shape of the surface corresponds to the new deposition conditions. One may suppose that this stable shape is determined by some extremum principle; it may for example correspond to the maximum growth rate at the given potential, or rather it may give an extremum value to some functional which may include both energetic and kinetic parameters. To our knowledge, this problem has never been tackled before. Unfortunately, discussions of the morphology of growth have been usually limited to qualitative descriptions.

Electrocrystallization under specific conditions results in a surface morphology that generally belongs to one of a set of typical growth morphologies, that may be observed both at monocrystalline and polycrystalline substrates. The use of monocrystals having a definite orientation allows a more detailed and precise understanding of the growth features, especially at the earlier stages, when the influence of the substrate is predominant. The strong effect of impurities on growth favors the use of extremely purified solutions, particularly in fundamental studies; nevertheless, most of the experimental data available in this field have been obtained using widely varying electrolyte purity conditions, therefore meaningful comparisons among different reports are usually impossible.

Most often the surface of electrodeposits exhibits a pyramidal, cuboidal or ribbed morphology; sometimes individual equiaxed polygons or elongated crystals are revealed by microscopic observation. The characteristic elements of these structures are the macroscopic steps. Specific cases are the spiral growth, spherical segments, dendrites and whiskers. Optical microscopy is sometimes sufficient to distinguish a definite type of surface, but the scanning electron microscope is the most appropriate tool to achieve a detailed morphological characterization. For high resolution of the separate microsteps and other fine details scanning tunneling microscopy has been often used in recent years.

6.10.2 Pyramids and Spirals

Pyramidal growth has been observed repeatedly by various authors with copper, silver, lead, cadmium and other metals. This kind of growth is commonly observed at low growth rates, corresponding to $i = 0.01 - 0.02$ A/cm^2 or less and to overvoltages less than 0.02 V, with weak or no adsorption of impurities. The current density in this case is in the same range as the exchange CD. Truncated pyramids occur sometimes, especially in presence of a low concentration of impurities; it is generally agreed that the truncation is due to the blocking of the top by adsorbed impurities.

Pyramids have not been observed during deposition onto high-index faces. This is probably the reason for the observed transition from a pyramidal to a block-shaped (or brick-shaped) morphology at higher current densities, when new facets with high Miller indices are formed at the edges of the of the monocrystalline faces, increasing the importance of the vicinal facets.

The experimentally observed pyramids are usually tri-, tetra- or hexahedral (very seldom pentahedral, resulting from twinning), depending on the orientation of the substrate surface. The lateral facets of the pyramids have a stepped structure, the step height h being of the order of tens to thousands of monolayers, depending on the adsorption of different species. The distance between the steps (terrace width) depends mainly on current density. The following equation is valid [7]:

$$tan\ \alpha = h/d = k\ ln\ i, \tag{6.45}$$

where α is the angle between a pyramidal facet and its base. This angle can vary continuously, thus the Miller indices of the pyramidal facets are high. The size of the pyramids usually increases proportionally with the deposit thickness.

The pyramidal growth can be considered a special case of spiral growth. The observation of clear spirals in electrocrystallization is more rare than that of pyramids; they are observed only at the low index facets of the substrate. With increasing CD the steps of the spirals decreases, whereas the rate of their propagation varies slowly. The spirals differ from the pyramids by their inclination with respect to the substrate, which is much lower: in the case of pyramids *tan* α is usually not less than 0.1, whereas the spirals are characterized by *tan* α≈0.01. The mechanisms of the formation of pyramids and spirals however can be similar: in both cases the role of screw dislocations is important. According to the theory of growth at screw dislocations, the step width of a spiral equals the radius of the critical nucleus; thus an increasing CD leads to a decreasing step width and therefore to increasing α, in accordance with (6.46).

The origin of the screw dislocations is not clear. The spirals have been obtained directly at defects on the substrate, but for sufficiently thick deposits the new dislocations generated during deposit growth play the main role. This issue will be discussed in Chap. 15.

6.10.3 Layered or Lamellar Morphology, and Other Morphological Types

The layered or lamellar morphological types of the deposits are relatively abundant, and the individual shapes may vary widely. The orientation and shape of the layers is determined by the substrate orientation: at smooth facets with low indices (100), (111) and (110) large, flat lamellas are observed, whereas at facets with high indices a rough lamellar surface is formed.

The macroscopic layers contain a number of microsteps, and in epitaxial growth these are oriented parallel to some crystallographic plane in the substrate. The lay-

ers can form terraces; they can have widely varying step width and height. The influence of the substrate can be distinguished in this case up to the thickness of tens microns.

The thickness of the step in macrolayers increases linearly with thickening of the deposit. The rates of the lateral and of the normal growth are the same, but the height (thickness) of the layer is much less than its step width. Thus a large fraction of the depositing metal is used up for growth along the normal direction; this follows from (6.2) at $x_0 >> h$.

At overpotentials larger than 0.1 V the layers often transform into polygonal (hexagonal, tetragonal etc.) blocks which constitute a specific type of lamellar growth. The transition region depends strongly on the concentration and type of impurities and its reproducibility is poor. It is possible that in this transition twinning processes, which begin at an overvoltage of 0.02 V or higher, may gain importance. It must be emphasized that repeated twinning is precisely the process leading to the formation of a polycrystalline deposit onto a monocrystalline substrate facet (along with non-coherent nucleation, which is important in the first stage).

Edge-like or crest-like surfaces, which sometimes are developed simultaneously with other growth forms, are also a particular case of layer growth; its distinctive feature is the formation of much more sloped layers; the crests are also aligned along definite crystallographic directions.

Another specific type of electrochemical deposit is characterized by a relatively smooth surface with irregularly positioned spherical segments of different sizes. At the early stage of deposition these segments are far apart, but upon thickening of the deposit their surface density increase, and at some stage the overall surface consists of overlapping segments. The basic components of such surface can be resolved only by electron microscopy, though the features can be relatively large. Sometimes at some locations a secondary feature can be initiated; more often the secondary features arise at the boundary of three features.

This morphological type is characteristically observed at high overpotentials (hundreds of mV). It is formed by normal growth in presence of surfactants, in parallel with hydrogen evolution and in presence of a colloidal or phase films at the surface. The internal structure of the deposits of this kind is fine-grained. Each spherical segment contains many, very small grains (less than 100 nm) which are randomly oriented, and a number of twin boundaries are also present. Very seldom the segments reveal some crystallographic features: at their surface small pyramids or crests in this case may be seen. Obviously, these are connected with twin boundaries which emerge at the surface.

6.10.4 On the Nature of Macrosteps

What is the reason for the bunching of the monoatomic steps into macroscopic assemblies? Probably, the energy gain of this configuration by itself is not a reason: the configuration is not an equilibrium one, but a growth form which is determined mainly by kinetic factors.

It is agreed that a main reason for macrosteps formation is the dependence of their propagation rate on the distance between them. This dependence is more pronounced in presence of adsorbing impurities: the succeeding step, moving in close proximity to the preceding one, moves along a fresh surface, whereas a distant succeeding step moves along a surface already covered by the adsorbed species, thus the velocity varies. Another reason of such dependence is an unequal diffusion flux to the moving steps in the two cases.

A quantitative analysis of step bunching was performed in [8]; the main relevant variable is shown to be the overall number of steps passing by a fixed point per unit time during crystal growth. This quantity q is named "the steps flux". It has been established that the condition for steady macrostep formation is a positive value of the second derivative

$$d^2q/dh^2 > 0 \tag{6.46}$$

where h is the steps spatial frequency. This follows from simple geometric considerations.

A further reason for step bunching is the fact that higher steps move more slowly than thinner ones. Thus the stochastic formation of a biatomic step is sufficient for the following monoatomic step to overtake it so that they can eventually coalesce to form the triple step, and so on. The resulting surface will depend on the initial fluctuations of the step widths; for the same reason the initial stochastic local deviations from the regular step distribution will result in the bunching under conditions fulfilling Chernov's condition (6.46).

This pattern is affected also by the concentration variations near the macrosteps, resulting from the consumption of the ions and adatoms during crystallization; the propagating step leaves behind it a decreased adatom concentration. The combination of this phenomenon with the adsorption slowing down the steps and with the secondary nucleation beyond the primary nuclei can result in the lamellar mode of growth.

One more cause of the bunching, clustering and other collective phenomena affecting surface morphology may be the non-linearity of the differential equations describing their rates of growth. Probably, the general problem can find an adequate description in the context of the equations of the form of the Korteweg—de Vries equation for soliton formation; to our knowledge, such treatment has not been attempted yet. Another possible phenomenon which may influence the formation of macrosteps is the Erlich-Schwöbel barrier, which hinders atoms from going down a step.

6.11 Crystalline, Irregular Roughness

The formation of macrosteps results in a definite roughness of the growing surface which under usual conditions is the order of 0.1 μm, but depends strongly on the metal under consideration and the deposition conditions. A much higher roughness

can be observed with polycrystalline surfaces. Surface sites with different crystallographic orientations exhibit different local current densities even if the overpotential is uniform throughout the overall electrode; this results in different growth rates.

Let us consider the roughness evolution for the simple model of a surface consisting of only two types of crystallographic facets. Let the current density difference be Δi at the average current density i. If the average deposit thickness is h and the average grain size is D ($h>>D$) the number of grains along the thickness is $N=D/h$. If at one surface site only one type of grain is formed, the height difference between the various sites would be $\Delta h=h\Delta i/i$. Due to the stochastic formation of the grains of both types this height difference is proportional not only to h, but also to $N^{1/2}=(D/h)^{1/2}$. The resulting dependence can be written as $\Delta h=K_r h^{1/2}$.

Thus one may expect the corresponding dependence between the root-mean-square roughness H and the thickness:

$$H = K_r h^{1/2}. \tag{6.47}$$

This relationship was confirmed experimentally, along with several other ones [9]. A proportionality between the roughness and thickness $H=K_r h$ is often observed, as well as a dependences such as $H = K_r h^{\xi},\ 0.5 < \xi < 1$. The transition from (6.47) to these functions can be associated with a grain size increase upon thickening of the deposit; actually, the grains which have higher growth rate gradually die out, thus the overall number of grains which grows simultaneously should diminish. This fact is known as the theory of geometric selection.

As will be shown in Chap. 8, the most characteristic dependence H–h is the logarithmic one. Therefore the various observed relationships may simply correspond to the observation of phenomena corresponding to various portions of the overall H vs. h curve. In the context of the crystalline structure of the deposits it is important to underline that the crystallographic irregularities, including grain boundaries, dislocations and other imperfections, have a definite impact in the evolution of roughness along with diffusion, hydrodynamics and electrochemical conditions.

References

1. Danilov A.I et al. Electrochimica Acta. 2005 v. 50, p. 5032
2. Gamburg Yu. D. Soviet J. of Electrochemistry, 1980, V.16, No.1, p.80
3. Chernov A. A. In: Modern Crystallography, Vol. 1. Moscow, Nauka, 1980 (in Russian)
4. Gamburg Yu. D. Soviet J. of Electrochemistry, 1999, т. 35, с. 658 – 660
5. Lezhava T.I. Diss. Theses, Moscow, Inst. of Electrochemistry, 1989
6. Gamburg Yu. D. Soviet J. of Electrochemistry, 1999, v. 36, p. 1157 – 1159
7. Seiter H., Fisher H., Albert L. Electrochimica Acta, 1960, V.2, p. 97
8. Chernov A.A. Progress in physical Sciences (Uspekhi fizicheskih Nauk), 1961, v. 73 No. 2, p. 277
9. Gnusin N.P., Kovarski N. Ya. The roughness of the electrodeposited surfaces. Novosibirsk, 1972 (in Russian)

Chapter 7
Potential Distribution in the Electrolyte and Current Distribution on the Electrode Surface

7.1 Statement of the Problem

The growth rate, composition, microstructure and properties of an electrodeposited metal or alloy are mainly determined by the potential and current distribution at the electrode. It is therefore essential to understand the phenomena that determine potential and current distribution in order to control the film characteristics. For example, an inhomogeneous current distribution may result in a non-uniform film thickness, with possible negative impact on the functional properties of the coating.

The current distribution depends on various characteristics of the electrochemical system, including (1) transport of the reactant species to the electrode, (2) the geometry of the electrochemical cell (the position and shape of the electrodes in the cell and the shape of the cell itself) and (3) the properties of the electrolyte and the electrolyte/electrode interface. In practice the electrolyte is usually chosen such that, with all the other factors being equal, it ensures the best (in most cases, the most uniform) current and metal distribution.

The problem of determining current and potential distribution within a generic electrochemical cell for a generic electrolyte is extremely complicated. In general, it should be taken into account that the flux density of charged species within the solvent is governed by diffusion (due to gradients in concentration), migration (due to the presence of electric fields) and convection (due to macroscopic motion of the electrolyte). Calculation of the convective velocity requires the solution of mass balance and momentum balance equations, combined with equations for the electric potential distribution. We simplify the problem by considering a dilute electrolytic solution where no convection occurs. This will enable the discussion of current distribution configurations in several examples relevant for practical applications.

Two problems can be formulated in this respect. The first one is the computation of the current and/or metal thickness distribution in a predetermined area and under specified boundary conditions. The second problem is the experimental and/or theoretical evaluation of the specific ability of the electrolyte to even out the current distribution, called its throwing power (TP), allowing to compare the ability of various electrolytes to give uniform deposits. A third associated problem is the

Y. D. Gamburg, G. Zangari, *Theory and Practice of Metal Electrodeposition,*
DOI 10.1007/978-1-4419-9669-5_7, © Springer Science+Business Media, LLC 2011

simulation and design of electrochemical reactors or similar devices that generate a predetermined current distribution.

A number of related problems can be formulated for processes such as electrochemical machining, modeling of electrolyzers, etc. Such problems will be considered in this chapter.

7.2 Primary, Secondary and Limiting Field Distributions. Polarization Fields

In an electrochemical cell the electrolyte occupies the volume V and is bound by the surface S, consisting of electrically conducting and insulating walls. When current flows, the electric potential varies throughout the volume V: $\Phi=\Phi(x, y, z)$ while the current density varies across the surface S: $\boldsymbol{j}=\boldsymbol{j}(x, y, z)$. The current at the nonconductive regions of the surface is zero; the sums of all the currents through the cathodic and anodic surface areas are equal in magnitude and opposite in sign to avoid charge build-up over time. The local current densities are determined by the corresponding potential gradients near S.

Electrostatics states that the potential distribution in the volume V can be determined by finding the function Φ which satisfies the equation

$$div\,[(1/\rho)grad\,\Phi] + F\sum\nolimits_i z_i div(\mathrm{D_i} grad \mathrm{c}_i) = 0 \tag{7.1}$$

$\rho=\rho(x, y, z)$ is the electrolyte resistivity; in general it depends on position due to the non-uniform concentration and temperature caused by current flow. Under the conditions of uniform resistivity and no concentration gradients (often this is acceptable) (7.1) transforms into the Laplace equation

$$\Delta\Phi = \partial^2\Phi/\partial x^2 + \partial^2\Phi/\partial y^2 + \partial^2\Phi/\partial z^2 = 0 \tag{7.2}$$

We consider here the solution at steady state and assume that the condition of electric neutrality is fulfilled in the overall volume V, i.e. the charge density in any infinitesimal volume is equal to zero.

The solution of the Laplace equation, i.e. the particular form of the function Φ is determined by the boundary conditions. These conditions depend on the type of boundary. At nonconductive walls its normal derivative must be equal to zero:

$$\partial\Phi/\partial n = 0 \tag{7.3}$$

At conductive surfaces, that is, the cathode and anode, in the simplest case the potentials imposed are constant, for example: $\Phi_a=0$, $\Phi_c=U$, U being the applied cell potential.

The above conditions correspond to the determination of the so-called *primary potential distribution* or primary field. Under this approximation, the potential drop

at any electrode/electrolyte interface can be neglected and therefore is independent on the local current density.

A complementary approximation could also be used, where the electrode current is imposed

$$\partial\Phi/\partial n = \text{const} = i\rho \tag{7.4}$$

This approximation is called *limiting potential distribution* or limiting field.

In either case, the solution of this problem gives the potential field $\Phi(x, y, z)$; simultaneously, within the former problem, the current distribution throughout the electrode surfaces is obtained from the relationship

$$i = \rho^{-1}\partial\Phi/\partial n. \tag{7.5}$$

The primary potential distribution corresponds to the *primary current distribution*; this will be shown to be the most inhomogeneous distribution possible for a given geometry. In this case the electrolyte surface adjacent to the electrode is equipotential, and the lines of current (corresponding to potential gradient) are orthogonal to the electrode surface, as shown in Fig. 7.1.

The limiting field case, on the other hand, corresponds to a uniform current distribution: $i = I/S$. In this case (as in the intermediate situations) the electrolyte region adjacent to the electrode is not an equipotential surface: the lines of current therefore form different angles with the electrode surface (Fig. 7.2).

In some cases the overall current I is provided instead of the cell voltage U. Then, for a non-uniform current distribution the conditions mentioned above have to be supplemented by the integral condition

$$I = \frac{1}{2}\int_{S} |i|\ \mathrm{dS} = (2\rho)^{-1}\int_{S} (\partial\Phi/\partial n)\mathrm{dS} = \rho^{-1}\int_{S_c} (\partial\Phi/\partial n)\mathrm{dS}; \tag{7.6}$$

where the integration is performed over the overall surface S of the electrolyte volume V, or over the cathode surface S_c only.

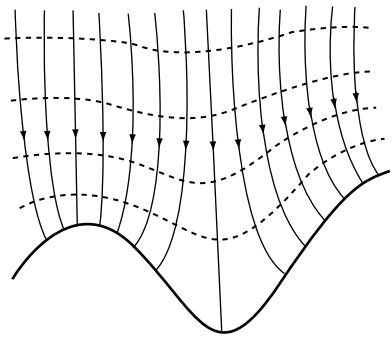

Fig. 7.1 Equipotential lines and current lines near the electrode under the primary field distribution approximation

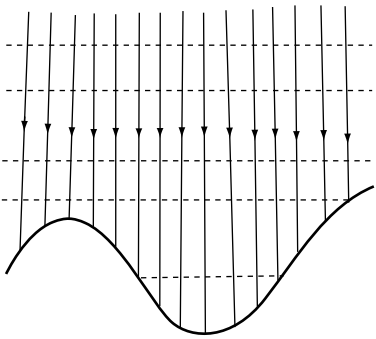

Fig. 7.2 Equipotential lines and current lines near the electrode under the limiting field distribution approximation

The primary field is governed entirely by the geometry of the system, including the shape of the electrochemical cell, the shapes and position of the electrodes. In geometrically similar cells with different overall dimensions the primary field distribution is identical. The field configuration therefore scales with the size of the cell, but remains otherwise identical; in other words, the mathematical solution remains the same.

A more general boundary condition at the cathode may be formulated as follows:

$$\Phi = U - \eta(i); \tag{7.7}$$

In this formula, the overpotential η is a predetermined function of current density, usually increasing monotonously with current density. This is the current-voltage characteristics of the electrode, as discussed in Chap. 1. Equation (7.7) shows that the applied potential difference U includes not only the ohmic potential drop in the solution but also the surface overpotential. In this case the main factor determining the current distribution is the electrode polarizability $\beta = \partial\eta/\partial i$. When $0 < \beta < \infty$ the potential field (called the *secondary potential distribution* Φ_2) is intermediate between the primary and limiting distributions that correspond to $\beta \to 0$ and $\beta \to \infty$, respectively. The corresponding current distribution (the *secondary current distribution*) is more uniform than the primary one, even if it is not entirely uniform as the limiting distribution. This is due to the monotonic character of the polarization curve: the surface overpotential is larger at higher current density.

A comparison between primary and secondary current distributions is usually done by keeping the integral currents through the electrode constant, more rarely by keeping the voltage across the cell constant.

The boundary condition (7.7) should use as $\eta(i)$ the actual current-voltage characteristic of the system under study. In practice however the calculations are performed using a Tafel characteristics: $\eta = a + b\ lg\ i$, which corresponds to

$$\beta = RT/\alpha nFi (\mathrm{i} < 0.7 i_{\mathrm{d}}). \tag{7.8}$$

or a linear dependence $\eta = \beta i$; in either case:

$$\Phi = U - (\beta/\rho)\, \partial\Phi/\partial \mathrm{n} \tag{7.9}$$

The linear case corresponds to (1) very low current densities (electrode potential near the equilibrium potential); in this case:

$$\beta = RT/nFi_0 \tag{7.10}$$

(i_0 is exchange current density) or to (2) high current densities under diffusion limiting conditions where $\beta \approx 0$; then for a current i of about $(0.3–0.7)i_d$

$$\beta = 4RT/\alpha nFi_d; \tag{7.11}$$

if i_d is about 8–10 times higher than i_0 then the polarization characteristics is linear in the overall interval $0 < i < 0.7i_d$.

When the current density is close to its diffusion limiting value the condition of limiting field is realized; in this case the current distribution becomes uniform. This condition is not usually suitable for metal deposition.

Let us consider the linear approximation $\eta = \eta_0 + \beta i$. The corresponding boundary condition is

$$\Phi = (U - \eta_0) + (\beta/\rho)\,\partial\Phi/\partial \mathrm{n}. \tag{7.12}$$

Actually this case is very common. As an example Fig. 7.3 shows the polarization curves for the metal deposition from a simple solution (a) and from the same solution with a surface active additive (b). Excluding the regions of very low CD, the boundary conditions in the two cases are the same: the only difference is that in presence of the additive the value of U should be changed to $U + \Delta\eta_0$, and then the current distribution will be the same (at the same integral current through the cell) though the cell voltage will be higher by an amount $\Delta\eta_0$.

It is important to notice that in this chapter we assume that the conductivity of the electrodes is much higher than that of the electrolyte. In the opposite case it is necessary to additionally solve the problem for the field in the electrode(s) and then fit the two solutions together. This problem is usually simplified because the electrode has only one dimension (wire or stripe); the current distribution in this case would depend on the point where the current is supplied.

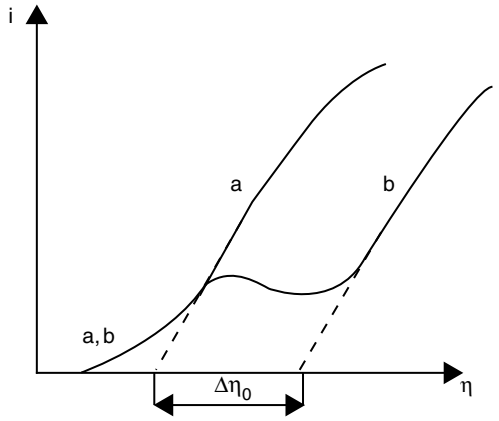

Fig. 7.3 Polarization curves for the metal deposition from a simple solution (*a*) and from the same solution with the surface active additive (*b*)

At variance with the primary distribution, the secondary electric fields in geometrically similar cells *are not similar*. This is due to the fact that the influence of the boundary conditions depends strongly on the scale of the cell.

Very often the overall distribution of potential in the volume V is not of interest; instead, only the potential in the immediate vicinity of a particular electrode is important – in fact, it is this region that determines primarily the current distribution at this electrode. In this case one of the boundary conditions may be set as $\Phi = 0$ at the surface well away from the electrode of interest. Any boundary condition can be set at this faraway surface, since this would not influence the field near the electrode of interest.

It should be stressed that the secondary field does differ from the primary one as a result of the different boundary conditions, and this difference is considerable only in the vicinity of the corresponding boundary. The secondary field may be considered as a superposition of the primary field (at the same integral current) and an additional field called *the polarization field*. This latter field does not contribute to the total current; it is concentrated only near the electrode, and its lines begin and end at this electrode, giving only some *redistribution* of the current density as compared with the primary one; this rearrangement always leads to a more uniform distribution. In other words, the polarization field results in the circulating currents as shown in Fig. 7.4. This field can be characterized by its local potential $\Phi_p(x, y, z) = \Phi_2 - \Phi_1$ and by its maximum potential $max(\Phi_p)$. As it is seen from Fig. 7.5, the local current density is equal to the vector sum of the primary CD and the CD given by the polarization field.

The concept of polarization field is convenient in the context of the overall problem of current distribution in electrochemical cells. Usually this field is equal to a fraction of the so-called limiting polarization field; the latter is defined as the vector difference between the primary and limiting fields (at constant integral currents). Obviously, this field can be determined by solution of the two corresponding

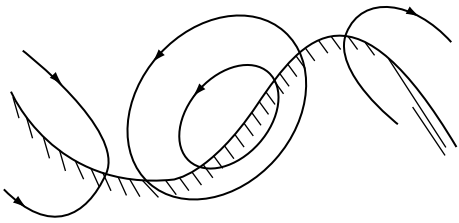

Fig. 7.4 Circulating currents resulting from the polarization field

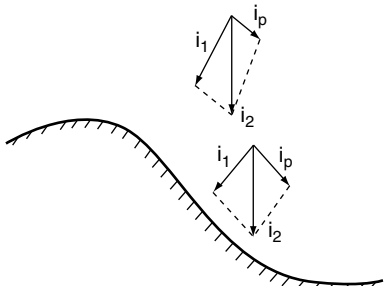

Fig. 7.5 Local current density (CD) as the vector sum of the primary and secondary CD

boundary problems. Then the secondary field is established as the sum of the primary field and a fraction of the computed limiting polarization field, this fraction being determined by the ratio β/ρ, as will be seen in the following. This method avoids the difficulties involved in the solution of more complicated boundary problems.

If the applied current causes a large variation in the local ion concentrations (especially near the electrodes), this leads to a concentration overpotential and to variations in the electrolyte conductance. The current distribution obtained under conditions when transport in the diffusion layer is significant is sometimes called *tertiary distribution*. The tertiary field and current distribution depend on the diffusion layer thickness δ (see Chap. 3); it differs from the secondary one in cases when δ is comparable to a characteristic dimension which governs the current distribution. The tertiary distribution approximation is especially important in determining current distribution at the microscale and also under non-stationary electrolysis conditions. The problem of determining the tertiary distribution is formally similar to that for the primary distribution, but it now concerns concentrations. The mathematical tools in the two cases are identical. The only difference is in the boundary condition which in the case of the tertiary field is imposed at the boundary of the diffusion layer.

In the most general form the tertiary distribution should be calculated as a function of position, since at different points of the electrode different polarization curves should be used due to local concentration variations.

7.3 Basic Principles of Calculation of Electric Fields in the Electrochemical Cells

In the general case, i.e. with arbitrary boundaries for the electrolyte volume and generic polarizabilities, the problem of the determination of the field in this volume and the current distribution at the electrodes require considerable calculational effort and various mathematical methods. Only specific cases have analytical solutions; the simplest ones are two-dimensional problems, which approximate well those configurations where the electrolyte volume extends mainly along one direction and the other two dimensions have a much smaller length. When an analytical solution exists, one can use it for testing the validity of approximate numerical solutions. Several examples of the determination of the primary and secondary fields are given in Sect. 7.4.

The most important mathematical methods are the following.

1. *The variational methods* are based upon the fact that the actual potential distribution in the volume corresponds to the minimum value of the overall Joule heat evolution. This principle can be applied to every problem of field distribution between conductors: for instance, according to this method, the currents in parallel conductors are inversely proportional to their conductances. In the general case the problem reduces to the minimization of a functional which gives the overall energy dissipated in the system:

$$Q_v = \int i E dV = \rho^{-1} \int (grad\Phi)^2 dV \tag{7.13}$$

The necessary condition for minimization of this functional is for the value of its variation to be zero; this is found by the common rules of variational calculus. The problem can thus be solved numerically.

This method can be easily extended to the case of the secondary distribution of the field by including the heat evolved at the electrodes q (which depends on the local overpotential η):

$$Q_s = \int q(\eta) dS. \tag{7.14}$$

2. *The method of finite differences* is widely used (often in combination with other methods) in numerical computations. It is based on the replacement of the partial derivatives by the corresponding finite differences.
   As $h \to 0$ the following equalities are exact:

$$\begin{aligned} \partial^2\Phi/\partial x^2 &= h^{-2}|\Phi[(x+h), y] - 2\Phi(x, y) + \Phi[(x-h), y]|, \\ \partial^2\Phi/\partial y^2 &= h^{-2}|\Phi[x, (y+h)] - 2\Phi(x, y) + \Phi[x, (y-h)]|. \end{aligned} \tag{7.15}$$

   By using the above equations, the two-dimensional Laplace equation for the function of interest (Φ) can be framed in a corresponding algebraic equation which includes the five points: (x, y), $(x+h, y)$, $(x-h, y)$, $(x, y+h)$, $(x, y-h)$, which for small h are very close together. Then one can cover the overall region of interest by a square netting with period h and then, while using the boundary conditions, write the system of the linear Eq. (7.15) for all the knots of the net including those at the boundary. The number of equations thus obtained is equal to the number of unknown values, so the system usually has only one solution, which can be solved by a computer. There are many varieties of such differential patterns which are appropriate for many types of problems.
3. *The method of conformal mappings* is a very powerful tool based on the theory of functions Z_1 of a complex variable Z. This method enables to solve all sorts of problems in field theory; it essentially consists in performing a one-to-one mapping of one domain onto the other, the latter having a much simpler shape. For instance, the domain between two curvilinear electrodes can be replaced by the stripe between parallel lines, and the half-plane by the unit circle. The transformation $Z_1 = \tan Z$ transforms a stripe into a circle, and the linear fractional mapping $Z_1 = (Z+1)/(1-Z)$ transforms the given semi-circle into a right angle, etc.
   It is established that the problem of conformal mapping (i.e. the mapping without changing the local extensions and angles) and the Laplace problem (7.1) for the same domain are equivalent and can be transformed into one another by simple integration or differentiation.
   Detailed tables of the conformal mappings convenient for practical applications are available.
4. *The method of boundary elements (matrix method).*
   This method is based upon the replacement of the real boundary by a multitude of straight segments: the overall length of a curvilinear electrode is divided into

n parts (of the same length, or shorter at regions characterized by a high current density). The solution is found in the middle of each segment by the finite difference method, and the current density is assumed to be constant on each segment.

The most general solution of the Laplace equation is obtained by the method of the integral transformations (using the Green's function method); this allows to find immediately the current distribution throughout the given electrode.

In two dimensions, the fundamental solution to the Laplace equation has the form

$$\omega = (1/2\pi)\ln(1/r);$$

then the basic equations have the form

$$\Phi(x, y) = \int \Phi(\partial\omega/\partial n)d\Gamma - \int \omega(\partial\Phi/\partial n)d\Gamma. \tag{7.16}$$

The above integrals are calculated over the boundary Γ. In the three-dimensional case the function ω is $\omega = 1/4\pi r$.

These rigorous equations are then replaced by the finite differences analogue for the system of *n* segments, resulting in a matrix operator with range *n*. The vector of interest Φ is obtained by the sum of *n* linearly independent contributions.

This method of calculation has one important advantage. The point is that the matrix construct for a given geometry can be used many times for different boundary conditions; the matrix is in fact determined only by the cell geometry. Therefore, when studying the current distribution in the same cell for different boundary conditions one can use the same matrix.

7.4 Typical Examples of Primary and Secondary Current Distribution

In this section various representative potential and current distributions will be derived explicitly. It should be stressed however that the final expressions presented here are valid only over distances much larger than the double layer thickness δ_{DL}. Over distances of the order of δ_{DL} the conditions of electroneutrality are invalid and the laws of microdistribution (to be discussed in Chap. 8) prevail.

7.4.1 The Strip-Shaped Cathode; Primary Current Distribution (PCD)

Let the cathode be an infinitely long strip of width $2L$ ($-L < x < L$). The problem (7.1) in this case can be simplified to

$$\partial^2\Phi/\partial x^2 + \partial^2\Phi/\partial y^2 = 0 \tag{7.17}$$

since along the z direction (the length of the strip) the field can be considered constant.

The boundary condition at the electrode plane ($y=0$) is

$$\Phi = \Phi_1 \text{ at } -L < x < L \text{ and } d\Phi/dy = 0 \text{ at } |x| > L. \tag{7.18}$$

To find the solution we need to use the non-dimensional coordinates $X=x/L$ and $Y=y/L$ and then carry out the conformal mapping which transforms the segment $(-L, L)$ into the entire x-axis:

$$X_1 + \mathrm{i}Y_1 = arcsin\,(X + \mathrm{i}Y)\,, \tag{7.19}$$

This gives

$$\Phi = U + const \cdot Re\,\{-i\ arcsin\,(X + \mathrm{i}Y)\}\,. \tag{7.20}$$

This leads to the following dependence of the current density under the primary distribution approximation, $\mathrm{i_p}$ (the subscript p signifies primary) on x:

$$i_\mathrm{p} = i_\mathrm{min} \cdot \left(1 - x^2/L^2\right)^{-1/2}. \tag{7.21}$$

Current density according to (7.21) increases at the periphery of the strip and tends to infinity at the edge; this is due to the concentration of all force lines of the field from the infinite region |x|>L. Nevertheless the average current density

$$i_\mathrm{av} = (1/2L) \int i(x)dx \tag{7.22}$$

is finite and equals

$$i_\mathrm{av} = i_\mathrm{min} \cdot \pi/2. \tag{7.23}$$

In the center of the strip (at $x=0$) $i=i_\mathrm{min}=i_\mathrm{av} \cdot 2/\pi \approx 0.64\ i_\mathrm{av}$. At $x/L \approx 0.77$ $i=i_\mathrm{av}$.

7.4.2 The Disc Electrode; PCD

The analytical solution for the disc-shaped electrode can be obtained using the same method. The solution is:

$$i_\mathrm{p}/i_\mathrm{av} = 0.5\left(1 - r^2/R^2\right)^{-1/2} \tag{7.24}$$

where r is the distance from the disc center, and R the disc radius. In this case, just as for the infinite strip, current density tends to infinity near the edge; in the center the CD is equal to one half of the average value. It is interesting that the average i is obtained at points farther from the center than what was found for the strip: in the case of a disc the regions having higher CD yield a larger contribution to the overall current. For the strip $i_\mathrm{av}=(2L)^{-1} \int i(x)dx$, whereas for the disc $i_\mathrm{av}=2R^{-1} \int ri(r)\,dx$. Rotation of the disc may result in a change of the current distribution, but this concerns only the secondary current distribution (SCD).

7.4.3 Gap Cells and Angular Cells with Linear Cathodes; PCD

These cells are often used as model systems; the first (Fig. 7.6) proposed by Mohler has a partition with a gap between the electrodes; the gap plays the role of a point-shaped electrode for the working electrode (cathode). This cell is very convenient for studies of current distribution in electrodeposition processes, but its disadvantage consists in a considerable current concentration near the gap, resulting in local heating. From this point of view the angular cells (Fig. 7.7) are more general and have wider applicability; among them the Hull cell in particular has found wide use.

Analytical calculations of current distribution have been performed for different types of cells; the results clearly depend on their geometrical shape. In all cases the resulting mathematical expressions are quite complicated; for this reason we present here only simplified formulas which may be invalid near the ends of the cathode (at the extreme points in fact the PCD can be zero or infinity).

In the gap cell the current distribution throughout the cathode depends on the ratio L/d (Fig. 7.6). The most widely used are the cells with $L/d > 2$; for these cells

$$ln[i_p(x_2)/i_p(x_1)] \approx (1.57L/d - 1.38)\Delta x/L. \tag{7.25}$$

In the angular cell the distribution depends first of all on the angle between the electrodes; with an angle of 45º and for a ratio between the maximum and minimum interelectrode spacing equal to 2

$$ln[i_p(x_2)/i_p(x_1)] \approx 3.7\Delta x/L, \tag{7.26}$$

where L is the length of the cathode.

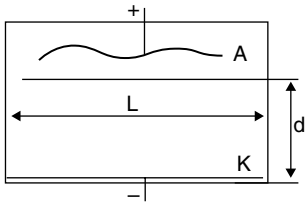

Fig. 7.6 Schematics of the Mohler cell. *A* is the anode and *K* the cathode

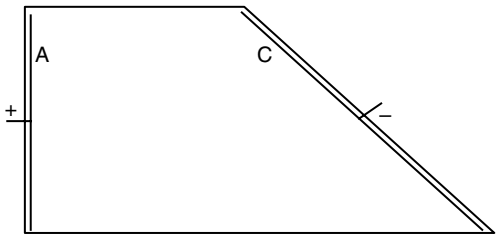

Fig. 7.7 Schematics of a Hull cell

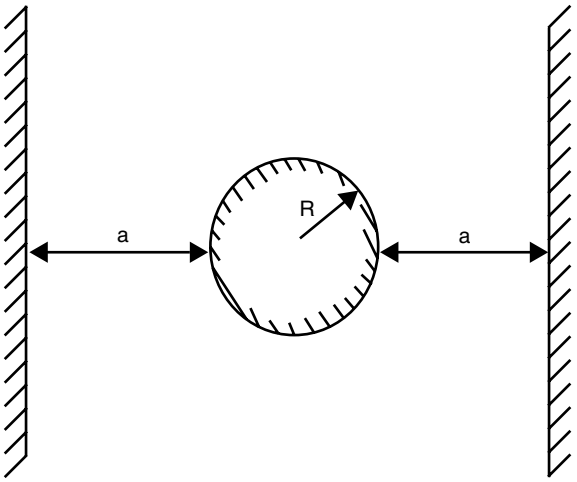

Fig. 7.8 Cylindrical cell

7.4.4 The Cylindrical Cathode

The PCD at a cylinder (of radius R) interposed between two planar anodes (Fig. 7.8), each one at a distance a from the former (a>R) may be characterized by the ratio of maximum and minimum CD which correspond the points a and b:

$$i_{\min}/i_{\max} \approx (1 - 3\mathrm{R}/a)^{1/2}. \tag{7.27}$$

7.4.5 The Sinusoidal Profile; PCD

This case is more general than the previous ones: the superposition of a series of sinusoidal profiles can generate a wide variety of electrode shapes; inversely, by application of a Fourier transform various profiles can be described as a series of sinusoids. Besides, the sinusoidal function has no angles and thus avoids infinities; at sharp angles in fact the primary current density may tend to infinity.

Let us consider the field in a two-dimensional region between two infinite one-dimensional surfaces, one of which is a planar anode and the second (the working electrode) has a sinusoidal profile. This profile is described by the function

$$y = p + H\ sin\,(kx)\,, \tag{7.28}$$

where p is the distance between the counter electrode and the mid-line of the cathode, H is the amplitude of the profile, and k its wave number: $k=2\pi/\lambda$; λ is the wavelength.

The two-dimensional Laplace Eq. (7.17) in this case has been solved [1] under the following boundary conditions: $\Phi=0$ at $y=0$, $\Phi=\Phi_s$ at $y=p+H\ sin(kx)$. The solution has the form

$$\Phi = \Phi_s\,[y/p - H\ sin\,(kx)\ \ sinh\,(ky)\,/p\ sinh(kp)] \tag{7.29}$$

This expression allows a determination of the derivative $d\Phi/dy$ at the extremum points of the profile:

$$d\Phi/dy = \Phi_s/p\,[1 + Hk\ coth\,(kp)] \tag{7.30}$$

Thus the current densities at the sites closest to the counter electrode ($sin\ (kx)=1$) and at the most distant ones ($sin\ (kx)=-1$) are respectively

$$i^{\wedge} = i_{av}\,[1 + Hk\ coth\ \ (kp)] \tag{7.31}$$

and

$$i^{\vee} = i_{av}\,[1 - Hk\ coth\ \ (kp)] \tag{7.32}$$

One can see that the difference Δi_p has its maximum value $\max(\Delta i_p) = 2i_{av}Hk\ coth(kp)$, or

$$\max(\Delta i_p)/i_{av} = 4\pi H\ coth(kp)/\lambda; \tag{7.33}$$

Two limiting cases are of particular interest: $kp >> 1$ and $kp << 1$, corresponding respectively to a very far and a very close counter electrode. In the first case $coth\ (kp) \approx 1$, and then

$$\max\left(\Delta i_p\right)/i_{av} = 4\pi H/\lambda. \tag{7.34}$$

Current distribution does not depend on p but only on the profile parameters H and λ. The steeper is the sinusoid, the larger is H/λ, and the less uniform the primary current distribution becomes.

In the latter case $coth(kp) \approx 1/kp$, and then

$$\max\left(\Delta i_p\right)/i_{av} = 2H/p \tag{7.35}$$

The variation of current density in this case is inversely proportional to the inter-electrode spacing p, as one should expect from Ohm's law.

7.4.6 Arbitrary Case; PCD

For an arbitrary placement of the electrodes the primary current distribution $i_p(x)$ (where x is the coordinate along the one-dimensional electrode) at a generic point of the electrode is inversely proportional to the local characteristic length l in the cell, i.e. the length of the current flow line corresponding to this point:

$$i_p\,(x) = U/\rho l\,(x) \tag{7.36}$$

Consequently the ratio of the current densities at the points x_1 and x_2 is

$$i_p\,(x_1)\,/i_p\,(x_2) = l_2/l_1. \tag{7.37}$$

If l_2 does not differ greatly from l_1, this can be written as

$$ln\left[i_p\,(x_1)\,/i_p\,(x_2)\right] = \Delta l_{12}/l. \tag{7.38}$$

If we consider the simplest case of an electrode the points of which are gradually farther apart from the counter electrode (as in a Hull cell), Eq. (7.38) may be rewritten as

$$ln\left[i_p\,(x_1)\,/i_p\,(x_2)\right] = k\Delta x_{12}, \tag{7.39}$$

or

$$i_p\,(x) = i_{p(x=0)}\;exp(kx), \tag{7.40}$$

where $k=dln\ l/dx$.

It should be noticed that the expressions (7.25), (7.26) etc. have the same form, each with a different explicit expression for k. The same operation can easily be performed with other expressions for $i(x)$, e.g. for (7.34) and (7.35), using the following approximation: $\max(\Delta i)/i_{av} \approx ln\,[i(\max)/i(\min)]$ if $\max(\Delta i) << i_{av}$.

7.4.7 Arbitrary Case; Secondary Current Distribution (SCD)

Under the assumptions of the SCD in order to calculate $i_s(x)$ it is necessary to take into account the potential drop at the boundary (surface overpotential) η, then (7.36) transforms into

$$I_s\,(x) = [U - \eta\,(x)\,]/\rho l\,(x)\,, \tag{7.41}$$

since in this case only a part of U represents the Ohmic potential drop. After differentiation and taking into account that both l and η depend on x this expression becomes:

$$di_s/dx = -\,(ki/l)\,/\,[1 + (\partial\eta/\partial i)\,/\rho l] = -\,(ki/l)\,/\,(1 + \beta/\rho l)\,, \tag{7.42}$$

where $\beta=\partial\eta/\partial i$.

This equation leads to the following expression for the current densities ratio at the points 1 and 2:

$$ln\ i_s\,(x_1) = ln\ i_s\,(x_2) + k\Delta x/\,(1 + \beta/\rho l)\,, \tag{7.43}$$

which differs from the corresponding expression for the primary distribution (7.39) by the factor $1/(1+\beta/\rho l)$.

This equation makes it clear that the non-dimensional parameter $\beta/\rho l$ is of great importance in the problems of actual current distribution at polarized electrodes. This quantity is known as the *Wagner number* $W=\beta/\rho l$. This number quantifies how much the secondary current distribution differs from the primary one. The polarizability β is here its average value within the operating range of current densities; ρ is the electrolyte conductivity at the operating temperature; l is some char-

acteristic length depending on the distance between the electrodes and on the cell configuration.

The Wagner number is important in the modeling and design of electrochemical cells as it determines the relationship between the primary and secondary current distributions. For example, the cells (1) and (2) with the same shape but differing in scale have the same current distribution only at the same W. More generally, in order to have the same current distribution the ratio of the cell sizes L_1/L_2 has to be equal to the ratio $(\beta/\rho)_2/(\beta/\rho)_1$.

The mathematical problem of SCD calculation is much more sophisticated in comparison with the primary one. Nevertheless, some electrode configurations admit analytical solutions in the cases of Tafel ($\beta=const/i$) or linear ($\beta=const$) polarization curves.

In the case of an infinite strip the SCD for a linear polarization characteristics has the form (this solution is exact)

$$I_s = \text{const}/\left[\pi - f\,(x)\,\rho L/\beta\right], \tag{7.44}$$

where $f(x)=[(1+x/L)ln(1+x/L) - (1-x/L)ln(1-x/L)-2]$. One can see that for $\beta\to\infty$ i_s becomes constant over the entire strip. The derivatives di_s/dx, as the calculation shows, at relatively high $\beta/(\rho L)$ are close to

$$di_s/dx \approx 1.5i/\left[L(1+2.5\beta/(\rho L))\right], \tag{7.45}$$

and consequently

$$ln\ i_s\,(x_1) = ln\ i_s\,(x_2) + 1.5\Delta x/\,(1+2.5\,(\beta/\rho L)) \tag{7.46}$$

Comparing this expression with (7.43) shows that the two coincide if $L=2.5l$, or $l=0.4L$.

An analytical solution is available also for a Tafel polarization characteristics; in the latter case the current distributes more uniformly at regions with lower CD and, inversely, non-uniformly at regions of higher current density; this occurs because for a Tafel polarization β falls with growing CD. The average i value, as for PCD, corresponds to $x\approx 0.77L$.

For disc electrodes, or for cells with angular and other shapes, analytical solutions for the secondary distribution are much more complicated; we can however present approximate expressions, useful at rather high β/ρ.

For the disc electrode:

$$ln\left[i_s\,(r)\,/i_s\,(r=0)\right] \approx 1.4r/[R(1+3.3\ \beta/(\rho R)]; \tag{7.47}$$

for the gap cell ($L/d>2$):

$$ln\left[i_s\,(x_2)\,/i_s\,(x_1)\right] \approx (1.57L/d - 1.38)\ \Delta x/\left[L(1+2.86\beta/(\rho L)\right]; \tag{7.48}$$

for the angular cell:

$$ln\left[i_s\,(x_2)\,/i_s\,(x_1)\right] \approx K\Delta x/\left[L(1+2.86\ \beta/(\rho L)\right], \tag{7.49}$$

where K depends on the angle and interelectrode spacing. In the last two formulae L is the cathode length.

7.4.8 The General Case

The former examples show that for different cell configurations the primary and secondary distributions of electric current throughout the electrode can be expressed in the general form:

$$ln\ i(x_2) \approx [ln\ i(x_1)] + \mathrm{K}\Delta x/[L(1+\mathrm{W})], \tag{7.50}$$

or

$$i(x) \approx i_{x=0} exp\,\{Kx/[L(1+W)]\}\,. \tag{7.51}$$

For the PCD W=0; for the SCD W=$\beta/(\rho l)$ can be calculated from the data for β and ρ and also the cell size: for example, for the angular cell it can be shown that W=2.86 $\beta/(\rho L)$, then l in the expression for W is equal to $L/2.86=0.35L$, etc.

Obviously, this concerns only relatively simple cell and electrode configurations. Besides, for the PCD (and at low values of W) the logarithmic dependence is disturbed near the electrode edges (the PCD of the local i may tend to infinity or to zero).

7.5 Throwing Power of Electrolytes and Polarizability of Electrodes. Standard Definition of Throwing Power

As stated in the beginning of this chapter, one of the problems associated with current distribution is the comparison of various electrolytes in terms of their ability to even out the primary current distribution in order to maximize deposit uniformity.

As it follows from the discussion in Sect. 7.4, the main parameter characterizing the ability of the electrolyte to give uniform current distribution, otherwise said throwing power TP, is the ratio β/ρ. This ratio integrates the properties of the electrolyte itself (ρ) with those of the electrode process of interest (β). The uniformity of current distribution in the given cell is determined by the Wagner number W; however, by standardizing the size l of the cell (this is equivalent to performing measurements in a cell of a given size and shape) then W becomes identical to the TP of the electrolyte.

Another interpretation of TP was proposed earlier; it is more convenient in practice to have the value of TP varying from 0 (when PCD and SCD coincide) to 100% (when the secondary distribution is uniform). This definition of TP was in use earlier than the Wagner number had been suggested, but their interdependence was understood only after a long time. The point is that W can vary from 0 to ∞, and consequently one can take as a measure of TP some function transforming the interval (0, ∞) into the interval (0, 1). The simplest function of such kind is

$$\mathrm{TP} = \mathrm{W}/(\mathrm{W}+1), \tag{7.52}$$

or, equivalently,

$$\mathrm{TP} = \beta/\,(\rho l * + \beta) \tag{7.53}$$

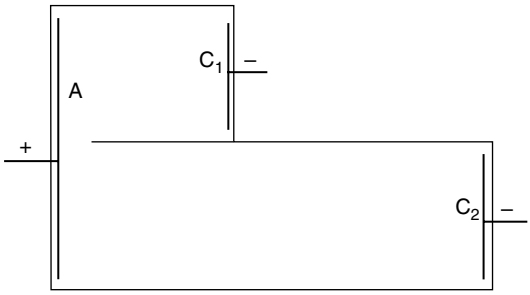

Fig. 7.9 Schematics of a stepwise (Field's) cell

where l^* is some length chosen as standard one. The advantage of this function lays in its simple physical meaning. It is not surprising, then, that TP is defined just in this manner in most of the proposed methods which are in wide use.

We may demonstrate this with several examples. The simplest case is that of two cathodes arranged at two different distances L_1 and L_2 from the anode (the stepwise cell or Field's cell, Fig. 7.9). It is evident that the ratio of secondary current densities at these two cathodes is

$$(i_1/i_2)_s \approx (L_2 + \beta/\rho)/(L_1 + \beta/\rho) = 1 + \Delta L/(L_1 + \beta/\rho); \qquad (7.54)$$

this follows immediately from the fact that the voltages between the anode and both cathodes are the same: $U(L_1)=i_1(\rho L_1+\beta)=U(L_2)=i_2(\rho L_2+\beta)$.

Naturally, consideration of the primary distribution leads to $(i_1/i_2)_p \approx L_2/L_1$.

Now we denote, as it is conventional, $i_1/i_2=m$, $L_2/L_1=K$; then (7.54) may be rewritten as

$$m = (K + \beta/\rho L_1) / (1 + \beta/\rho L_1) \qquad (7.55)$$

The substitution of this expression into the definition of the TP (7.52) gives

$$\mathrm{TP} = (K - m) / [K - m + (m - 1)\, l* / L_1] \cdot 100\%. \qquad (7.56)$$

Consequently, in order to determine the TP of the electrolyte it will be sufficient to measure the value of m at a certain K and additionally to know the ratio l^*/L_1, where l^* is the reference (standard) length and L_1 is the characteristic size of the cell.

For $l^*/L_1=1$ and $l^*/L_1=2$ correspondingly one obtains from (7.56) the widely known formulae

$$\mathrm{TP} = (K - m) / (K - 1) \cdot 100\% \qquad (7.57)$$

and

$$\mathrm{TP} = (K - m) / (K + m - 2) \cdot 100\%. \qquad (7.58)$$

We can conclude that these are not only simple expressions which conveniently give the TP values, but they also have a definite physical meaning. Moreover, one can derive various expressions for TP for different l^*/L_1 values. When $l^*/L_1=4$, for instance, (7.56) gives (this corresponds to the measurements in a small cell)

$$\begin{aligned} \mathrm{TP} &= (K - m) / [K - m + (m - 1) \cdot 4] \cdot 100\%, \quad \text{or} \\ \mathrm{TP} &= (K - m) / (K + 3m - 4) \cdot 100\%. \end{aligned} \qquad (7.59)$$

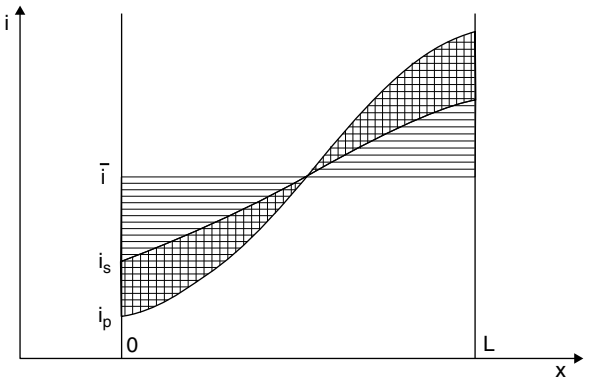

Fig. 7.10 Comparison between primary (i_p), secondary (i_s) and uniform (i_{av}) current distributions along the cathode 0–L

Obviously, the resulting value of TP must be the same obtained by using (7.58), but referred to measurements in a cell two times smaller. All these expressions satisfy the definition (7.52): TP = W/(1 + W). The standard length of the cathodes in angular or gap cells is 10 cm; this corresponds to l^* = 3.5 cm. It is exactly this value of l^* that corresponds to the present-day data on TP of different electrolytes. The ratio of maximum to minimum CD in the PCD approximation for these cells is about 10.

This method to determine TP has an important drawback: it is based on CD measurements only at two interelectrode distances. A more general method appears clear from Fig. 7.10, where curves for the primary, secondary and uniform current distribution are compared. The point at the cathode corresponding to x = 0 is the most distant from the anode; the CD i_p at PCD in this point is the smallest. The CD i_s at SCD here is higher but also less than the average one i_{av}. At the point x = L nearest to the anode the situation is opposite: $i_p > i_s > i_{av}$. The overall hatched region at the figure represents the non-uniformly distributed portion a of the overall cathodic current at PCD; the crosshatched portion b represents the improvement of uniformity at SCD. One can see from the figure that when the ratio $b/a = 0$ there is primary distribution (TP = 0), and at $b/a = 1$ there is absolutely uniform distribution (TP = 1). Then the throwing power can be defined as

$$\mathrm{TP} = 1 - b/a \tag{7.60}$$

In other words, if we define TP as $|i_p - i_s|/|i_p - i_{av}|$ in each point of the interval 0 < x < L, then (7.60) gives the integrally averaged value of TP [2].

In general the procedure of TP measurement is the following. For the model cell the PCD is known, so the value of a can be calculated; the unknown value of b can be measured by examination of the mass or thickness distribution at a sectioned cathode after electrodeposition.

For the gap cell shown in Fig. 7.6, this gives for an electrode for example divided in 5 sections

$$\mathrm{TP} = 1 - 3.14 \sum |m_i/M - 0.2| \tag{7.61}$$

($M = \Sigma m_i$). In the case of the uniform distribution ($m_i/M = 0.2$) this expression gives TP = 1; the PCD for this cell is $3.14\ \Sigma|m_i/M - 0.2| = 1$, and then TP = 0.

Besides, a simpler method for calculation of the integral TP was proposed [3]. It is based on an approximation of the expression (7.51) which leads to the following equation:

$$\mathrm{TP} = 1 - \mathrm{const}\,(m_{0.2}/M - 0.2); \tag{7.62}$$

$m_{0.2}/M$ is the part of the overall mass accounted for the most electrically loaded 1/5 part of the electrode. The constant in (7.62) depends on the cell size and shape and can be found by performing measurements in a given electrolyte with a known value of TP. The cells shown in Figs. 7.6, 7.7 have the value of this constant close to 5.0, and when performing measurements at these cells

$$\mathrm{TP} = 2 - 5 \cdot m_{0.2}/M. \tag{7.63}$$

This formula has a very simple meaning: with a uniform metal distribution $5 \cdot m_{0.2}/M = 1$, and then TP = 1. For the primary distribution at such a cell $m_{0.2}/M = 0.4$, and then TP = 0.

It is difficult to use all these methods of TP determination in agitated solutions; only weak agitation can be modeled by the electrolyte flow through the cell. Strong stirring can however be modeled by use of a cylindrical rotating cathode. It is convenient to locate the disc-shaped horizontal anode under the vertical cylindrical cathode and with an insulated bottom [4]. In this case the local current density at the cylinder decreases with the distance from the anode and depends on the rotation rate.

The TP found by one of the methods presented above represents not only a quantitative description of the electrochemical system but it also permits to make approximate calculations of the actual current distribution, notably if PCD is known. This is reasonable, since, as it has been noted, the PCD can be calculated for many different types of cells. If at some points A and B of the cathode surface the ratio of primary current densities is $(i_A/i_B)_p$ then the ratio of the secondary ones is $(i_A/i_B)_s = (i_A/i_B)_p^{(1-\mathrm{TP})}$. For example, for the standard cell in the PCD approximation $(i_A/i_B)_p = 10$; then, for TP = 25% $(i_A/i_B)_s = 10^{0.75} = 5.6$; SCD is thus more uniform.

We argue that this method for the estimation of SCD provides a rather fair picture of current distribution; it is much simpler than the direct mathematical solution of the correctly posed boundary problem.

7.6 Throwing Power and Cathodic Polarization. Methods for Improvement of Current Distribution

In any practical electrodeposition process from aqueous solutions, the actual working CD is always higher than the exchange CD i_0; consequently, the anodic partial CD at the cathode is negligibly small. In this case the general expression for the polarizability under mixed kinetics (diffusion and charge transfer) is:

$$\beta = RTi_d/[\alpha nFi\,(i_d - i)]\,. \tag{7.64}$$

This curve is symmetric with respect to the point $i=i_d/2$, and at this point the polarizability is at a minimum. Nevertheless, this very point is the optimum one from the point of view of TP. This paradox can be explained in the following way.

First, CDs above $i_d/2$ are not practical in electrodeposition since they often produce very coarse deposits; only in presence of various additives it is possible to obtain good coatings at such high CDs. As it is seen from (7.64) at $i=i_d/2$

$$\beta_{1/2} = 4RTi_d/(\alpha nFi_d)\,. \tag{7.65}$$

With $\alpha=1/2$ and $n=2$ this corresponds to $\beta\approx 0.1\text{V}/i_d$. Note that at $i=i_d/3$ and at $i=2i_d/3$ the polarizability varies only slightly: it grows to

$$\beta = 4.5RTi_d/(\alpha nFi_d)\,. \tag{7.66}$$

The value of β increases if we work in the same solution at lower CD, and therefore the TP increases, but if we simultaneously decrease the concentration while keeping conductivity the same (this requires a high concentration of the supporting electrolyte) β increases by a larger extent. For this reason if one uses a given solution it is better to work at CD less then $i_d/2$, but if the current density i is predetermined, then the concentration of metal ions in the solution should correspond to $i_d=2i$.

The use of surface-active additives to increase TP may be effective only when the polarizability increases at the optimum current density. If, for instance, the action of the additive consists only in reducing the exchange current density, this substance does not influence the TP.

It is important to underline that TP for metal deposition (TP_m) and TP for the current (TP_c) coincide only if current efficiency (CE) does not depend on current density. If CE increases at increasing CD, $TP_m<TP_c$, if CE falls, $TP_m>TP_c$. Consequently, from the point of view of providing good deposit uniformity it is better when CE decreases at high current density: if at some point of the electrode the CD is twice as much as its average value, the deposited metal thickness at this same point does not differ from the average one when CE is half as much. The dependence between these quantities is

$$\text{TP}_\text{m} = \text{TP}_\text{c} - (1 - \text{TP}_\text{c})\, d\ ln\,(\text{CE})\,/d\ ln\ i. \tag{7.67}$$

The dependence of CE on current density for various electrolytes is shown in Fig. 1.3; some values of the polarizabilities (within the working CD interval) are given in Table (1.3). Tentative values of TP_m are presented in Table 7.1.

In actual practice the best current distribution at the cathode(s) can be achieved by following certain additional practical rules. (i) When positioning the items to be coated in the bath, sufficient distances should be allowed between the items themselves, as well as between each one and the anode and between each one and the bottom of the cell or the surface of the solution. (ii) If possible, all the points of the cathode should be located at equal distances from the anode. (iii) It is better if opposite electrodes are well apart from each other. (iv) Solutions with higher conductivity and high polarizability are preferable. (v) It is appropriate to work at relatively low current density, in relatively diluted solutions and at high concentration of the supporting electrolyte; this condition is contradictory to the requirements

Table 7.1 Throwing power of various solutions for electrodeposition (averaged values for the operating current densities)

Metal	Type of electrolyte	Throwing power, %
Copper	Sulfate	8–12
	Sulfate with additives	12–16
	Cyanide	26–32
	Pyrophosphate	18–24
Nickel	Sulfamate	16–21
	Sulfate	10–15
Silver	Cyanide	38–44
	Thiocyanate	27–32
Tin	Stannate	23–27
	Sulfate	4–6
Cadmium	Sulfate	5–7
	Cyanide	22–25
Zinc	Sulfate	3–5
	Zincate	20–22
	Cyanide	28–33
Iron	Sulfate	4–8

of high electrodeposition yield and low cost, a compromise should then be sought. (vi) In some cases it is useful to utilize additional local anodes; for example, the interior corners tend to see a low CD. In the opposite cases (external angles) additional cathodes and screens can be used to decrease the local CD. In actual cases, sharp edges at the objects intended for electrodeposition have to be rounded off. (vii) Sometimes it is useful to isolate some parts of the anodes. (viii) When gas is evolved all the bubbles must have opportunity to reach the surface of the solution without any buildup in the electrolyte volume. (ix) Cylindrical items can be rotated around their axis during deposition.

In practice, we may use any combination of these and other methods; in each case the technologist has the opportunity to invent ingenious solutions for any specific problem.

Finally, in some cases the concept of *covering power* of the solution is used; this is not the same as the TP. This term is used when there is a lower limit of the current density below which no deposit can be obtained. In this situation deposition does not occur at sites corresponding to the lower CD values, e.g. at corners or at distant points of the cathode the deposit is absent. It is evident that in such a case it is necessary to provide the SCD at which this lower limit would not be reached at any point of the cathode.

7.7 Current Distribution on Microstructured and Nanostructured Electrodes: Through-Mask Electrodeposition

Electrodeposition is widely used in microelectronics and microsystems applications to deposit metal or alloy films through lithographic patterns with lateral sizes that may vary from 10 nm to 100 μm, and with aspect ratios (height of the feature/lateral

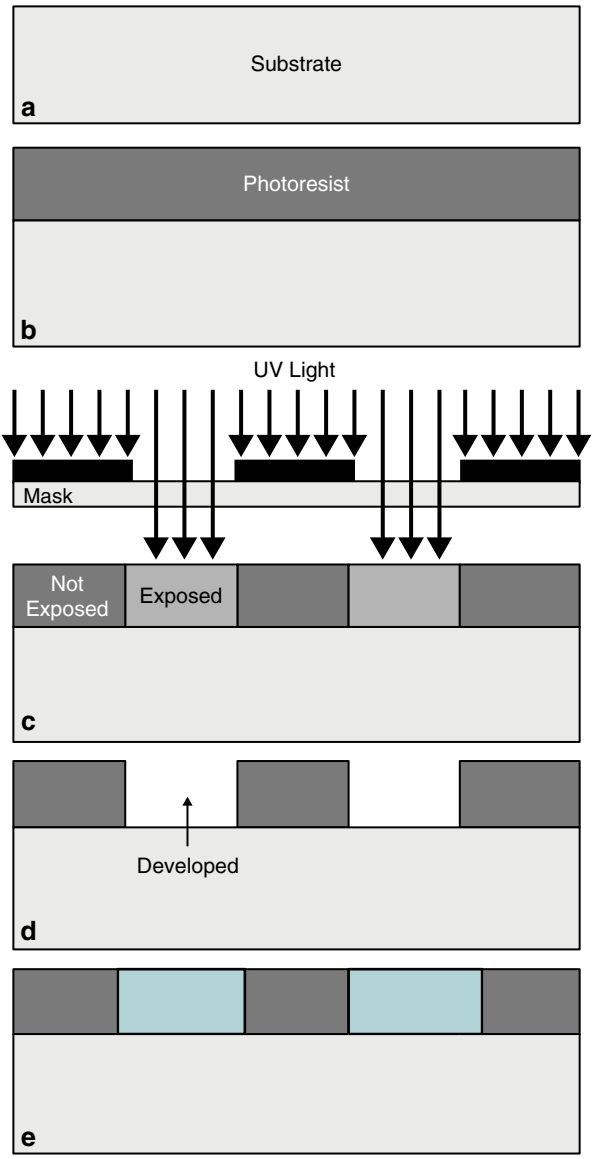

Fig. 7.11 The process of through-mask electrodeposition. **a** The substrate is coated by using a physical method with a conductive film; **b** the conductive substrate is spun with a photoresist; **c** A mask with the selected pattern is placed onto the substrate and UV light is shone through the transparent regions; **d** the photoresist is selectively dissolved at regions illuminated by the UV light, using a suitable organic compound; **e** the metal is selectively electrodeposited at conductive regions

size) that range from less than 1 to 100. This process is schematically shown in Fig. 7.11. First, a suitable photoresist is spun on a substrate that has been previously coated by a physical vapor deposition method with a metallic film. Successively, a mask containing a pattern of optically transparent regions is placed on the resist and ultraviolet (UV) light is shone through these regions to selectively illuminate corresponding areas of the resist. Regions of the resist exposed to UV light can be

dissolved by an organic solvent, exposing conductive regions of the substrate where electrodeposition could be made to occur selectively.

The rate of electrodeposition into these electrochemically active regions depends on the local value of current density *i* and on the process efficiency; in the case of alloys, also the composition depends on *i*. If the efficiency does not depend on *i* and *i* is uniform, growth rate will also be uniform. Film thickness and alloy composition uniformity are essential to the correct operation of the devices of interest; consequently, tools capable to predict the thickness distribution of films grown into patterned electrodes are essential.

A patterned electrode may contain thousands of devices and millions of different features. A comprehensive mathematical description of the geometry of the electrode therefore is practically impossible, and the corresponding current distribution problem is intractable. The quantitative description of current distribution in patterned electrodes has been simplified by considering the current distribution over different length scales separately. Typical patterned substrates contain thousands of devices, each with the same geometry; it has therefore become customary to consider the current distribution at three length scales: the *workpiece* scale, the *pattern* scale, and the *feature* scale [5, 6].

7.7.1 Current Distribution at the Workpiece Scale

The workpiece consists of the entire electrode, and current distribution over the entire electrode has been discussed in the previous sections. According to the previous discussion, the current distribution in this case is affected by the geometry of the cell, the location and size of the electrodes, the intrinsic kinetics of the system under study, and the electrodeposition conditions. At the workpiece scale, current distribution can be made more uniform in practice by varying the geometric features of the cell, and/or the deposition conditions; in particular, auxiliary electrodes (*current thieves*) may be used.

7.7.2 Current Distribution at the Pattern Scale

Within a single pattern or across few patterns the density of active regions may vary widely; in these cases it has been found that a non-uniform resist pattern causes the current density to be non-uniform. This phenomenon has been quantitatively analyzed and can be qualitatively understood by considering two nearby regions with the same superficial area, respectively with high (A) and low (B) resist coverage. The total voltage drop

$$V_{TOT} = V_{\Omega} + V_{kin}$$

between a region in the bulk of the electrolyte and the two electrode regions must be the same; since region A has a higher resist coverage the overall current through region A would be lower and the corresponding ohmic drop would also be lower: $V_{\Omega,A} < V_{\Omega,B}$. It follows that the voltage drop at the interface V_{kin} will be larger in region A, and the current density through the active area will also be higher, leading to a thicker film in regions with a higher resist density (lower active area). The actual enhancement in the deposition rate at regions with lower active area will depend on the relative importance of the ohmic drop and the voltage drop at the interface, or in other terms by the Wagner number W. When $W = 0$, the enhancement in current density in the region more densely covered by resist over the less dense is equal to the ratio of the fractional coverage by resist in the two areas. On the contrary, when W tends to infinity, the current distribution is completely uniform. It should be taken into account that for most applications a Wagner number between 1 and 10 would still give unacceptable variations in thickness across the pattern.

7.7.3 Current Distribution at the Feature Scale

Calculation of the current distribution within a single lithographic feature should take into account the dimensions of the feature with respect to the characteristic lengths involved in the electrodeposition process. Single lithographic features for example have dimensions such that ohmic drops across their length or thickness can usually be neglected. The feature dimensions may be smaller or of the same order of magnitude as the thickness of the diffusion boundary layer; in the latter case, the diffusion process may be enhanced with respect to one-dimensional linear diffusion. Finally, growth of the film within the feature changes the geometry of the problem, so that in any simulation of shape evolution this shape change should be taken into account, leading to a moving boundary problem.

Numerical simulations of film shape evolution in a lithographic feature of predetermined geometry should proceed by defining the geometry of the system (the active region and the region covered by resist on the cathode, the distance of the anode) and the flow field (in the simplest case of no fluid flow knowledge of the thickness of the diffusion layer is sufficient). The film shape evolution can be simulated by solving at any time step *t* the Laplace equation $\nabla^2\Phi = 0$ in the electrolyte volume and the mass conservation equations $\nabla^2 c_i = 0$ in the diffusion layer with the appropriate boundary conditions. Solution of these equations determinesthe current distribution at the cathode and therefore the instantaneous growth rate. Assuming that through a given time step Δt the growth rate is constant it is possible to determine the new film profile at $t + \Delta t$. By repeating this loop it is possible to determine shape evolution as a function of the geometry of the system and the deposition conditions, given the geometric features of the cell and the electrochemical characteristics of the electrodeposition system of interest.

References

1. Wagner C. J. Electrochem. Soc., 1951, v.98, p. 116, 1954, v. 101, p. 225
2. Nachinov G.N., Pomogaev V.M., Soviet J. Electrochemistry,1983, v. 19, No. 2, p. 230
3. Gamburg Yu. D. Russ. J. Electrochemistry, 2001, v. 37, No.7, p. 794
4. Dicusar A.I. et al., Russ. J. Electrochemistry, 2005, v. 41, No.1, p. 91
5. Dukovic J.O. "Computation of current distribution in electrodeposition, a review" IBM J. Res. Develop. 34 (5) (1990) pp. 693–705
6. Dukovic J. O. "Feature-scale simulation of resist-patterned electrodeposition" IBM J. Res. Develop. 37 (2) (1993) pp. 125–142

Chapter 8
Current Distribution at Rough Electrodes

8.1 Introduction

At a rough electrode surface, the local current densities at peaks and valleys are different even though the macroscopic current distribution over a given surface region is completely uniform. The conductivity of the electrode material is usually much larger than that of the electrolyte. In this case, the electric field in the vicinity of the interface is non-uniform: the equipotential surfaces reproduce the surface topography and the local current lines must be perpendicular to the surface (Fig. 8.1). The resulting local field pattern depends on the ratio of the conductivities of the electrolyte and the electrode, on the characteristics of the surface profile and also on the hydrodynamic conditions. In turn, any non-uniformity of the electric field results in a corresponding non-uniformity of the current density.

Electrochemical measurements at a rough surface determine only the average value of the CD, even if the roughness coefficient is taken into account. Consequently, different points of the surface simultaneously operate within different portions of the polarization curve; various surface patches may even exhibit different polarization behavior since electroactive species or inhibitors may be present at various locations with a different concentration, depending on the ability of these species to reach occluded regions of the electrode. This fact places some restrictions on the accuracy of any electrochemical measurements at rough electrodes; on the other hand, this is of basic importance to understand and predict the microprofile evolution during electrodeposition.

Any increase in surface roughness during metal deposition is usually undesirable, especially when thick layers are sought for, such as in electroforming. Dendrites formation in cathodic metal deposition should be avoided in order to obtain dense coating or, in the field of batteries, to increase electrode lifetime upon periodical charge and discharge. On the contrary, the electrochemical production of metallic powders or of high area electrodes requires deposition conditions leading to rapid roughness growth and dendrite formation. There are other situations when high roughness is desirable, for example when joining the deposited surface with nonmetallic materials. In any case, understanding and predicting the evolution of a surface profile during electrodeposition is of paramount importance.

Y. D. Gamburg, G. Zangari, *Theory and Practice of Metal Electrodeposition,*
DOI 10.1007/978-1-4419-9669-5_8, © Springer Science+Business Media, LLC 2011

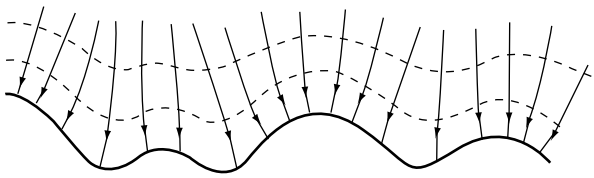

Fig. 8.1 The equipotential lines and the current lines in the primary field approximation near a rough surface

Such evolution depends directly on the current density distribution – and therefore the rate of metal deposition – at the microprofile. In the following we will always consider a one-dimensional surface, and the microprofile will be defined by the curve $y_s(x)$ characterizing a generic cross-section of a two-dimensional surface. The current distribution is determined by the electric field between the rough working electrode and an ideally smooth counter electrode. In this respect, two cases should be distinguished: kinetic control and diffusion control. In the former case the current distribution is obtained by solving the Laplace equation with the appropriate boundary conditions in the entire cell volume; in the latter case the current distribution is determined by solving Laplace equation in the electrolyte bulk and the diffusion equation in the diffusion boundary layer.

In the simplest case both electrodes are non-polarizable; the corresponding electric field or current density distribution gives the *primary* (field or current) distribution. When the role of the electrode polarization is taken into account, the *secondary* distribution is obtained; this involves a more complicated analysis. Finally, when the concentration field near the working electrode is considered, the corresponding solution to the problem gives the tertiary distribution. When considering realistic deposits with a definite crystallographic structure it will be necessary to take into account the dependence of electric field and current on the morphology and crystallographic orientation of the film.

The analysis given in the previous chapter, where the above concepts were discussed, concerns only an ideally smooth surface and does not take into account how the current is distributed over a surface rough at the micrometer scale. The microdistribution has its own characteristics, which require further analysis.

One of the most interesting cases of roughness evolution is *leveling*; this phenomenon is observed when adding to the electrolyte small concentrations of specific compounds known as levelers. Leveling is the ability of the electrolyte to produce deposits with a surface smoother than the substrate. This results from the fact that the deposition rate in presence of the leveling agent is larger at recesses and smaller at protrusions. A typical length scale for the roughness amplitude in microprofiles is less then 50 μm, i.e. less then the typical thickness of the diffusion layer. The terms “leveling power” and “microthrowing power” are used in this connection; their meaning will be explained later in this chapter.

In this chapter we discuss the fundamental concepts involved in the analysis of microscopic current distribution under various situations.

8.2 Coefficient of Current Distribution and the Basic Problem of Microdistribution

In order to quantitatively characterizate the current distribution at a rough surface we define the following quantities: x, $y_s(x)$, $i(y_s)$ and di/dy_s. x is the coordinate along the profile, $y_s(x)$ is the height of the surface at the position x, i is the local current density at the coordinate y. In general, i is not a function of y_s only; however, for simple periodic profiles other functional dependences are less important and will be neglected in the discussion of profile evolution. In the following it will be more convenient to use the logarithmic derivative $K = i^{-1} di/dy_s = d\,lni/dy_s$. In particular, when the maximum current density variation throughout the profile is much less than the average CD i_{av} ($\max(\Delta i) << i_{av}$) this formula can be substituted by

$$K = {i_{av}}^{-1} di/dy_s = d\,lni/dy_s. \tag{8.1}$$

The subscript s in (8.1) indicates that this coordinate relates only to points at the interface.

Additional parameters which characterize the profile and its roughness are as follows. If the amplitude of the roughness H, or the distance Δy of a generic point of the surface from its average line, or $max(\Delta y)$ are known, one can write the value of $max(\Delta i)$ as

$$max(\Delta i) = max(\Delta y)\, di/dy_s \tag{8.2}$$

Usually the value of the relative dispersion $max(\Delta i/i_{av})$ is small and one can neglect it when performing kinetic studies; however, in order to avoid systematic errors the use of smooth electrodes is recommended when carrying out experimental investigations.

The basic problem of microdistribution consists in the determination of the electrode profile at any time t if the profile is given at a time t_0 and the local current density $i(y_s)$ is known at every point.

The growth of the deposit at every surface point takes place in the direction of the radius of curvature of the surface; then the problem can be generally formulated as follows. If at the time $t=0$ the profile is described by $y_s(x, 0)$, then

$$dy_s/dt = const\; i(y_s)\left[1 - (dy_s/dx)^2\right]^{1/2}, \tag{8.3}$$

and the problem reduces to finding the corresponding solution which satisfies the condition

$$y_s(x, 0) = y_0(x). \tag{8.4}$$

Obviously, in spite of the difficulties involved in obtaining the general solution, numerical solutions can be found in numerous particular cases.

8.3 Geometric Leveling

In some instances a qualitative or approximate solution of the problem above can be found. Sometimes the influence of the two factors on the right side of (8.3) can be separated. The simplest situation is obtained when $i(y_s)$=const, i.e. the current is distributed uniformly. It is not difficult to demonstrate that in this case the profile varies with time, the amplitude of roughness often gradually reducing. This kind of smoothing of the surface is called geometrical leveling; it has been repeatedly observed, but not always adequately explained.

Geometrical leveling can be illustrated by Fig. 8.2, which shows the evolution of a single trench having sharp edges and rounded bottom; this specific shape is more convenient than the commonly used triangular trench profile for demonstration of some peculiarities of its evolution. With increasing deposition time the edges gradually become rounded, whereas the bottom, on the contrary, becomes sharp; this occurs at a deposit thickness h close to the initial radius of curvature of the bottom.

Until the bottom retains some roundness the depth of the trench remains approximately the same; its shape is altered, but leveling does not occur. After the bottom has become sharp however its depth H varies as

$$H = H_0 - h(1/sin\alpha - 1) \tag{8.5}$$

because the bottom moves more rapidly than the walls, by an amount $1/sin\alpha$. (α being the angle that the trench makes with the vertical). This formula is valid until the deposit thickness becomes equal to $1/2a\left[1 + (a/2H_0)^2\right]^{1/2}$, where a is the trench width (or the average step of the regular profile); after this the profile becomes "arc-shaped" (Fig. 8.3), and its evolution obeys a different law.

Generally, any profile evolves towards an arc-shaped one. The reason for this is that the curvature radius of convex regions is growing, whereas the curvature radius of the concave ones decreases; as a result the profiles (including irregular ones)

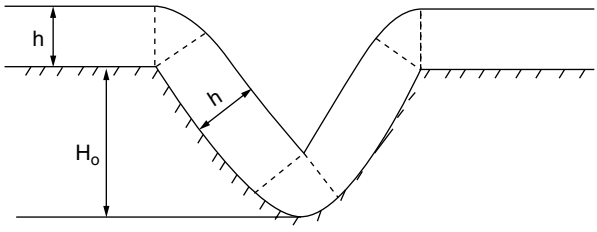

Fig. 8.2 Geometric leveling: the evolution of a single trench having sharp edges and rounded bottom

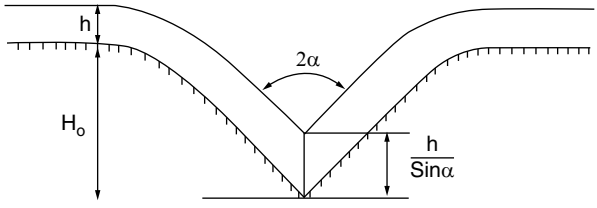

Fig. 8.3 The "arc-shaped" profile

sooner or later consist of convex segments; the corresponding two-dimensional surface always consists in convex spherical segments and never in concave regions.

The evolution of the arc-shaped profiles takes place in accordance with the following law:

$$H = H_0 - a^2 h/8R^2 = H_0(1 - h/R), \tag{8.6}$$

where R is the arc radius. This formula can be easily derived geometrically; it follows from the relationship $a^2 = 8RH_0$. After the film builds up to a thickness h we have $a^2 = 8(R + h)H \approx 8RH + 8hH_0$. By equating the right sides one has $R(H_0 - H) = hH_0$, and finally

$$H_0 - H = hH_0/R = a^2 h/8R^2. \tag{8.7}$$

This picture of the surface as consisting of numerous spherical segments is characteristic of electrochemically deposited metals, as noted in Chap. 6. Upon joining these segments together the profile becomes arc-shaped, and then the geometric leveling can decrease the overall roughness.

This decrease goes relatively slowly as compared with Eq. (8.5), because usually $H << a$. The geometric leveling can lower H only when H is of the same order of magnitude as a.

8.4 Microprofile Evolution as Result of a Non-Uniform Primary Current Distribution

The functional dependence of the local current density on y_s determines the evolution pattern of the surface profile; the sign of K (Eq. 8.1) is the most important factor in this respect. If $K > 0$, then the roughness increases during deposition; in the opposite case $K < 0$ a leveling process in addition to the geometric one occurs. This phenomenon is named "true leveling"; it is controlled by the factor $i(y_s)$ in the Eq. (8.3) and is discussed in Sect. 8.6.

For certain initial surface profiles, as we have seen, the geometrical leveling is not manifested, and the variation in the height H is completely determined by the value of K. A characteristic case for this behavior is the gently sloping sinusoidal profile:

$$y = H \sin(2\pi x/\lambda) \tag{8.8}$$

with the amplitude $H << \lambda$; this condition is justified later by Eq. (8.28). This profile is convenient as a standard in experimental studies of profile evolution. Another reason to study the evolution of a sinusoidal profile in detail is that any continuous function can be described as a Fourier series, i.e. an infinite sum of sinusoidal profiles of different wavelength. For usual profiles encountered in practical electro-

deposition, the amplitude of the sinusoid can be taken to be about 2–4 μm, and the period about 50–100 μm.

Let us find the rate of variation of H resulting from the dependence of i on y_s. In this case $max(\Delta i)=2H\, di/dy_s$. At the average deposit thickness h the variation of H is $h\, max(i)/i_{av}$, then $dH=[max(\Delta i)/i]\, dh$, or

$$dH/H = (d\, ln\, i/dy_s)\, dh. \tag{8.9}$$

Integration of (8.9) gives

$$ln\,(H/H_0) = (d\, ln\, i/dy_s)\, h \tag{8.10}$$

or, if the deposit thickness is written as $h=iV_m(CE)/nF)\tau$

$$ln\,(H/H_0) = (d\, lni/dy_s)\, iV_m(CE/nF)\tau \tag{8.11}$$

where H_0 is the initial amplitude, V_m is the molar volume of deposited metal, τ is the duration of the deposition, CE is current efficiency. It is interesting to note that

$$d\, ln\, H/dh = d\, ln\, i/d\, y_s = K, \tag{8.12}$$

in integral form

$$H = H_0\, exp\,(Kh). \tag{8.13}$$

Equation (8.12) shows that all the relations, in which the derivative $d\ ln\ i/dy_s$ is involved, are valid also for the derivative $d\ ln\ H/dh$.

The next problem is the determination of the very value of the quantity K. Under the primary distribution approximation the coefficient K_1 is determined by the Laplace equation for the field between the two equipotential surfaces, one of which is the surface of the rough electrode, the other being the plane boundary of the diffusion layer. The solution for the sinusoidal electrode was presented in Chap. 7 in reference to the discussion on the macroscopic field.

Current distribution throughout the cathode $y=\delta+H\, sin(kx)$ (δ is now the average thickness of the diffusion layer, H is the amplitude of the sinusoid, k is its wave number: $k=2\pi/\lambda$; λ is wave length) is given by Eq. (7.30)

$$i = i_{av}\left[1 + Hk\, sin(kx)\, coth\,(k\delta)\right]. \tag{8.14}$$

The current densities at the peaks and valleys are correspondingly

$$\hat{i} = i_{av}[1 + Hk\, coth(k\delta)] \tag{8.15}$$

and

$$\check{i} = i_{av}[1 - Hk\, coth(k\delta)]. \tag{8.16}$$

The derivative di/dy_s approximates to $\Delta i/\Delta y_s$, or $(\hat{i} - \check{i})/2H = i_{av}k\, coth\,(k\delta)$; then

$$K_1 = d\, ln\, i/dy_s = k\, coth\,(k\delta) \tag{8.17}$$

For the relative difference one obtains (8.15–8.16)

$$\Delta i/i_{av} = (\hat{i} - \check{i})/i_{av} = 2kH\ coth(k\delta). \tag{8.18}$$

Let us now examine the cases of short-wave and long-wave roughness. For $k\delta >> 1$ (or $\lambda << \delta$) the expression (8.17) becomes

$$K_1 = k = 2\pi/\lambda. \tag{8.19}$$

This means that for a significant change in roughness over a short length scale the distribution coefficient is equal to the wave number of the corresponding sinusoidal profile. For $k\delta << 1$

$$K_1 = 1/\delta. \tag{8.20}$$

Correspondingly, (8.18) in these situations gives, respectively

$$\Delta i/i_{av} = 2kH \quad \text{or} \quad \Delta i/i_{av} = 2H/\delta. \tag{8.21}$$

For the time dependence of the roughness amplitude one obtains

$$dH/dt = i_{av}(V_m M/nF)HK_1 \tag{8.22}$$

and then its dependence on the deposit thickness h is

$$dH/dh = HK_1 = kH\ coth\,(k\delta). \tag{8.23}$$

If we take into account that the diffuse layer thickness δ is constant:

$$ln\,(H/H_0) = [k\ coth\,(k\delta)]h. \tag{8.24}$$

This equation can be rewritten in a more general form which coincides with (8.10):

$$ln\,(H/H_0) = K_1 t = K_1^* h. \tag{8.25}$$

where K or K* depend on the deposition conditions.

Expressions of this kind have been obtained by various authors both theoretically and based on experimental data; they are valid in various contexts: for growing roughness and for leveling, at artificial profiles and for spontaneously rough films. This is due to the fact that (8.25) does not depend on the individual profile peculiarities and it is valid not only for sinusoidal profiles, but also for any continuous profile, because the latter can be described as a linear combination of sinusoidal functions (the harmonics in a Fourier series).

It is necessary to note, however, that as it has been just shown, the temporal evolution of the separate harmonics proceeds at different rates: the short-wave ones grow or decay more rapidly. For this reason not only the scale but also the shape of the profile varies with time. The microscopic irregularities of small wavelength when $K<0$ (in leveling solutions) die rapidly, but when $K>0$ they grow rapidly and may trigger dendritic growth. The actual profiles of the deposits do indeed show this regularity.

Formula (8.24) is strictly valid only for $0.01<k<0.6$, but within these limits is appropriate for any arbitrary current distribution; it is necessary only to determine

the actual value of $K = d \ln i / dy_s$ at the given polarization, concentration field and conductivity. The necessary information can be obtained by measurements of the characteristics of the sinusoidal profile at successive times.

Let us now discuss the simultaneous action of geometric factors and current distribution on roughness evolution.

In the general case, when both factors are acting: the geometrical one and the coefficient of current distribution, the amplitude of the profile varies along with its curvature. When $K<0$ the curvature of the valleys always increases (the radius of curvature becomes smaller), and the profile remains arc-shaped. On the contrary, when $K>0$, the curvature of the ridges always decreases. The curvature of the valleys at $K<0$ and of the ridges at $K>0$ can vary in any direction; this is shown in Fig. 8.4.

For example, when $K<0$ the radius of curvature at the bottom decreases due to geometrical reasons, but simultaneously it can increase as a result of true leveling; the bottom therefore grows more rapidly than other points. On the contrary, when $K>0$ the ridges grow more rapidly than other points, and this reduces the geometrical tendency to smooth the ridge; as a result the profile of ridges can become sharper and eventually may form whiskers or dendrites.

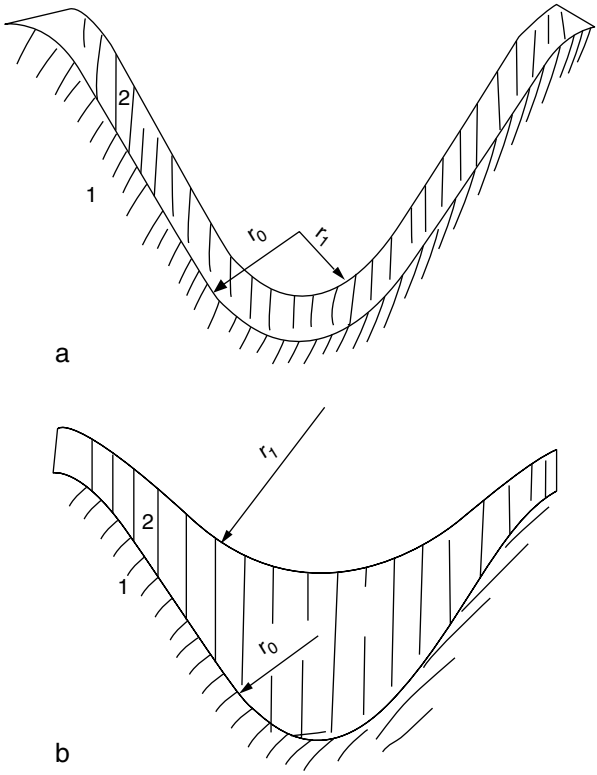

Fig. 8.4 The evolution of the trench profile at K = 0 and at K > 0; r_0 and r_1 – the initial and the final curvature radii, 1 – the substrate, 2 – the deposit

It is of interest to compare the relative importance of the field and geometrical factors. For example, for the evolution of an arc-shaped profile the value of *dH/dh* is determined mainly by the first harmonic, as it follows from (8.6)

$$dH/dh \approx -a^2/8R^2 = -H/R \approx kH^2/a. \tag{8.26}$$

On the other hand, Eq. (8.23) shows that

$$dH/dh \approx kH. \tag{8.27}$$

Consequently, considering the additivity of both factors

$$\sum dH/dh \approx kH(1 + H/a) \tag{8.28}$$

Thus, the roles of the geometric and field factors are related as *H/a*, i.e. as the ratio of the amplitude of the profile to its step; for sinusoidal profiles this corresponds to $H << \lambda$. We can see therefore that the geometry can influence the evolution of only relatively steep profiles.

8.5 Roughness Evolution Under Secondary and Tertiary Current Microdistribution

The secondary microdistribution approximation (SCD) differs from the primary one due to the influence of the conductivities of the solution ρ_s, that of the deposit ρ_d (usually it is assumed that $\rho_d = 0$) and the overpotential $\eta = \Delta E$.

The secondary current distribution was considered in Chap. 7 in the context of the macroscopic distribution problem; it is possible however to analyze the problem irrespective from the scale, whether it be a micro- or macroscopic current distribution.

The simultaneous solution of the Laplace equation for the electrolyte and the deposit for the profile $y_s = H\,sin(kx)$ under the condition $H < 1/k$ and at constant polarizability $\beta = d\Delta E/di$ has the form [1]

$$i = i_{av}\{1 + [k(\rho_s - \rho_d)\,H\,sin(kx)/(k\beta + \rho_s + \rho_d)]\} \tag{8.29}$$

For $\rho_d \to 0$ and $\beta \to 0$ (8.29) simplifies to $i = i_{av}[1 + (kH\,sin(kx))]$. The derivative of (8.29) is

$$di/dy_s = ki\Delta\rho/(k\beta + \rho_s + \rho_d) \tag{8.30}$$

where $\Delta\rho = \rho_s - \rho_d$. Assuming $\rho_s >> \rho_d$ Eq. (8.30) simplifies to:

$$K_2 = di/dy_s = d\,ln\,i/dy_s = k/(1 + k\beta/\rho_s) \tag{8.31}$$

Comparison of (8.30) and (8.19) shows that

$$K_2 = K_1\Delta\rho/(k\beta + \rho_s + \rho_d) \tag{8.32}$$

Thus, for $\Delta\rho=0$ the secondary current distribution coincides with the primary one; at high polarizability β and low ρ_s one can neglect the sum $\rho_s+\rho_d$ in the denominator, and then

$$d\,ln\,i/d\,y_s = K_2 = \Delta\rho/\beta \tag{8.33}$$

We see that when the solution resistance is low and the polarizability of the interface is high the SCD becomes practically uniform. For this reason the most usual methods for improvement of current distribution are the increase of (1) the conductivity (e.g. by the addition of the supporting electrolyte) or (2) the polarizability (e.g. by the addition of surface active substances or complexing agents).

In the general case, substituting into (8.32) the expression for K_1, we obtain

$$K_2 = k\ coth\,(k\delta)\ \Delta\rho/[k\beta\ coth\,(k\delta) + \rho_s + \rho_d] \tag{8.34}$$

When δ is small the value of $coth(k\delta)$ is close to $1/k\delta$; neglecting the resistivity of the metal $\rho_d \approx 0$, (8.34) becomes

$$K_2 \approx \rho_s/(\beta + \delta\rho_s) = 1/(\beta/\rho_s + \delta) \tag{8.35}$$

Then the difference between the current densities at the ridge and at the valley is

$$max(\Delta i/i_{av}) = H/(\beta/\rho_s + \delta) \tag{8.36}$$

This equation fully coincides with the corresponding formula for macrodistribution.

The equations for K_2 allow a description of the profile evolution during metal electrodeposition. For a constant CD the profile evolution is described by the same equations that are used to determine the primary distribution, only replacing K_1 by K_2:

$$d\,ln\,H/dh = d\,ln\,i/d\,y_s = K_2, \tag{8.37}$$

The polarizability has usually a positive value, and the resistivity of the metal is usually less then that of the electrolyte; then the derivative di/dy_s remains positive. Therefore under the secondary current microdistribution the profiles become coarser with time. The opposite situation $di/dy_s<0$ which is characteristic for the leveling electrolytes cannot be described in terms of secondary distribution but it requires further analysis of mass transfer and concentration fields near the electrodes, i.e. the tertiary current distribution.

The tertiary current distribution corresponds to the condition when the rate of deposition is completely determined by ion transport in the diffusion layer, close to the limiting current density. The problem of determining the current distribution is the same as for the primary distribution case, but the Laplace equation for the electric field must be replaced by the Fick equation for the concentration field in the diffusion layer. The corresponding calculations have been performed by Wagner [2], who showed that the evolution of the sinusoidal profile $y_s=H\ sin\ kx$ proceeds according to the equation

$$ln\,(H/H_0) = kh = (ki_{av}V_{at}/nF)\tau. \tag{8.38}$$

which is valid for the evolution of relatively smooth profiles in presence of a relatively thick diffusion layer.

This equation cannot be used, however, when considering the growth of, for example, a single protrusion resulting in dendrite formation, or for other profiles having sharp changes in the height H.

Electrodeposition under diffusion-limited conditions for a profile of this kind can be analyzed in the following way. The mass transfer coefficients to the valleys and ridges are $D/(\delta - \frac{1}{2}H)$ and $D/(\delta + \frac{1}{2}H)$, respectively; their difference when $\delta > H$ is

$$\Delta K_{\mathrm{m}} = D/\left(\delta - \frac{1}{2}H\right) - D/\left(\delta + \frac{1}{2}H\right) \approx DH/\delta^2. \tag{8.39}$$

This gives the rate of variation of H with time

$$dH/dt = DHcV_{\mathrm{at}}/\delta^2 \tag{8.40}$$

and then

$$ln\,(H/H_0) = (DcV_{\mathrm{at}}/\delta^2)t. \tag{8.41}$$

where c is the bulk concentration of the electroactive species.

The situation changes when the profile scale H is of the same order of the diffusion layer thickness δ. The local electric fields at the valleys and at the ridges become different; approximating the valleys and ridges by cylindrical surfaces of the same curvature $1/R$, we obtain for the corresponding limiting current densities

$$\hat{i} = nFDc/[R\,ln((R+\delta)/R)] \tag{8.42}$$

and

$$\check{i} = nFDc/[R\,ln(R/(R-\delta))]. \tag{8.43}$$

We obtain therefore

$$\begin{aligned} dH/dt &= (\hat{i} - \check{i})V_{\mathrm{at}}/2nF \\ &= (DcV_{\mathrm{at}}/2R)\,[\{[ln\,((R+\delta)/R)]^{-1} - ln\,(R/(R-\delta))]^{-1}\} \end{aligned} \tag{8.44}$$

The difference of the reciprocal logarithms when $\delta < R$ equals unity, thus

$$dH/dt = (\hat{i} - \check{i})V_{\mathrm{at}}/2nF = DcV_{\mathrm{at}}/2R \tag{8.45}$$

The radius of curvature R of the concave and convex parts of the sinusoid can be expressed in terms of k and H (H here is the amplitude of the sinusoid): $R = 1/(k^2H)$; then

$$dH/dt = \frac{1}{2}DcV_{\mathrm{at}}k^2H, \tag{8.46}$$

$$ln\,(H/H_0) = \frac{1}{2} DcV_{at}k^2 t. \tag{8.47}$$

This expression differs from (8.40) and (8.41) by the prefactor of t; however all these expressions have the same logarithmic form as (8.10). In all the cases considered the amplitude of the profiles does grow as deposition continues. Variations of the prefactor of t or H in the left side are connected with the different distributions of the concentration fields.

8.6 True Leveling

A number of commercial electrolytes can provide for smoother profiles during electrodeposition. This occurs when $K<0$ or when $di/dy_s<0$: the current density in these cases would be higher at valleys of the profile than at the ridges. Such current distribution is possible when a suitable inhibitor of the electrode processes is present in the solution, the inhibition being stronger when the surface concentration of the inhibitor is higher. The surface concentration of the inhibitor, in turn, depends on its mass transfer towards the interface: the ridges are more easily reachable by the diffusing species.

The latter statement indicates that an inhibitor with such properties must be an expendable substance; in fact it would be consumed at the electrode surface as the result of trapping/inclusion in the deposit or through electrochemical reduction into another product.

A detailed analysis of the corresponding processes can be effectively performed by using as the independent variables the mass transfer coefficients of the species influencing the current density.

If, for example, the local CD is controlled by mass transfer of the inhibitor, the difference between its values at ridges and valleys is

$$(\hat{i} - \check{i}) = (\partial i/\partial K_i) \cdot (K_{\hat{i}} - K_{\check{i}}), \tag{8.48}$$

K_i is the mass transfer coefficient of the inhibitor. For the inhibitor $\partial i/\partial K_i<0$, therefore $\hat{i}<\check{i}$.

After simple rearrangements,

$$(\hat{i} - \check{i})/i_{av} = (\partial i/\partial K_i) \cdot (K_{i(av)}/i_{av}) \cdot (K_{\hat{i}} - K_{\check{i}})/K_{i(av)}, \tag{8.49}$$

or

$$\Delta i/i_{av} = (\partial ln\, i/\partial K_i) \cdot \Delta K_i/K_{i(av)}, \tag{8.50}$$

where the symbol Δ refers to the difference of these values at ridges and valleys, and the $_{\text{symbol av}}$ indicates averaging of the corresponding values throughout the overall rough surface.

Actually, the local current density depends not only on the inhibitor mass transfer but also on that of the electroactive species; (8.50) then takes the more complicated form

$$\Delta i/i_{\mathrm{av}} = (\partial i/\partial K_{\mathrm{i}}) \cdot \Delta K_{\mathrm{i}}/K_{\mathrm{i(av)}} + (\partial i/\partial K_{\mathrm{m}}) \cdot \Delta K_{\mathrm{m}}/K_{\mathrm{m(av)}}, \tag{8.51}$$

where K_{i} is the mass transfer coefficient of the electroactive species.

The mass transfer coefficients depend here only on the concentration gradients, thus the problem of the current distribution reduces to the problem of the concentrations distribution.

When working at current densities much lower than the diffusion limiting one, the distribution of the electroactive species in the diffusion layer is approximately uniform. The mass transfer coefficients to the ridge and to the valley of the sinusoidal profile $y_{\mathrm{s}} = H \sin kx$ are correspondingly $D/(\delta - H)$ and $D/(\delta + H)$, and then

$$max(\Delta K_{\mathrm{m}}/K_{\mathrm{m(av)}}) \approx 2H/\delta. \tag{8.52}$$

Alternatively, the inhibitor is usually consumed at its limiting flux; then its concentration field is close to the primary electric field, and for a sinusoidal profile

$$max(\Delta K_{\mathrm{i}}/K_{\mathrm{i(av)}}) \approx 2kHcth\,(k\delta)\,. \tag{8.53}$$

We can see that the resulting value of $\Delta i/i_{\mathrm{av}}$ depends not only on the profile parameters H and k and on the thickness δ, but also on the factor $(\partial ln\ i/\partial K_{\mathrm{i}})$, which in turn is determined by the degree of inhibition in the system of interest. This factor (taken with the opposite sign) is therefore the measure of the leveling power of the electrolyte:

$$P = -\partial ln\, i/\partial ln\, K_{\mathrm{i}}. \tag{8.54}$$

Taking into account the general expression (8.51), the definition of P transforms into

$$P = -\Sigma\alpha_{\mathrm{j}}(\partial\, ln\, i/\partial\, ln\, K_{\mathrm{j}}). \tag{8.55}$$

The factor α_{j} accounts for the dissimilar concentration fields of the various species j.

Using this definition one can rewrite some of the equations derived earlier. Taking into account that $\mathrm{K} = d\ ln\ i/dy_{\mathrm{s}} = -kP$, (8.10) takes the form

$$ln\,(H_0/H) = kPh = (2\pi/\lambda)Ph. \tag{8.56}$$

This formula allows determination of P by measurements of the profile parameters at successive times during electrodeposition. This value can be compared with the data obtained by measurements of current or potential under controlled mass transfer. Actually, when the role of the inhibitor is important and if $\delta = const$

$$P = -\partial ln\, i/\partial ln\, K_{\mathrm{i}} = -\partial ln\, i/\partial ln\, c_{\mathrm{i;}} \tag{8.57}$$

in this expression c_i is the inhibitor concentration in the bulk. The last expression can be rewritten as

$$\partial ln\, i/\partial ln\, c_i|_\delta = (\partial \Delta E/\partial ln\, c_i)/(\partial \Delta E/\partial ln\, i) \tag{8.58}$$

Thus, through a series of potentiostatic measurements of CD, or by galvanostatic measurements of ΔE at various concentrations of the inhibitor one can find the value of P. This is precisely the ratio of the derivatives (8.58) that was initially called "leveling power" [3]. This theory has been found to be consistent with experimental measurements of the profile parameters [4, 5].

A very convenient experimental method for determining P can also be devised. At constant concentration of the inhibitor

$$-\partial ln\, i/\partial ln\, K_i = \partial ln\, i/\partial ln\, \delta; \tag{8.59}$$

using the rotating disc electrode (Chap. 4), $\delta = const/\omega^{1/2}$, thus

$$ln\delta = const - 0.5 ln\omega, \tag{8.60}$$

(ω is the angular rotation rate), and the net result is

$$P = \partial ln\, i/\partial ln\, \delta = -2\, \partial ln\, i/\partial ln\, \omega = -2(\partial \Delta E/\partial ln\, \omega)_i/(\partial \Delta E/\partial ln\, i)_\omega \tag{8.61}$$

This enables to find P by simple potentiostatic or galvanostatic measurements at the RDE; knowledge of P allows prediction of the microprofile leveling according to (8.56).

Most electrolytes not containing special additives do not exhibit particular leveling characteristics; they have $P \approx 0$ or $0 < P < -0.5$. For some specific leveling electrolytes $P \approx 1$; actually the value 1 corresponds to complete leveling ($H/H_0 = 0.01$) at the deposit thickness of $0.8\lambda \approx 5/k$, as it follows from (8.56).

The theoretical analysis of the inhibition (which brings to leveling) requires some data on the inhibition strength. As a first approximation one may assume the current decrease (at η = const) or the potential change (at i = const) as proportional to the surface concentration (coverage) of the inhibitor; sometimes however more detailed models are necessary. The simplest one is presented in the following.

The adsorption and desorption of the inhibitor are not balanced as a consequence of its consumption at the electrode due to incorporation into the deposit. It is postulated that the fluxes of the desorption and incorporation are both proportional to the coverage θ, correspondingly:

$$j_{des} = K_{des}\theta, \tag{8.62}$$

$$j_{inc} = K_{inc} i\theta \tag{8.63}$$

The flux of incorporation in accordance with the experimental data is also proportional to the current density. The flux towards the surface is equal to the rate of adsorption

$$j_{ads} = K_{ads}\, c_i(1 - \theta), \tag{8.64}$$

and then the solution of the resulting system of equations gives the value of the coverage:

$$\theta = K_{\text{ads}}\, c_{\text{i}} / \left(K_{\text{ads}}\, c_{\text{i}} + K_{\text{inc}}\, i + K_{\text{des}}\right). \tag{8.65}$$

As we can see θ decreases due to consumption of the inhibitor.

Further it is necessary to link the actual value of *i* at the given overpotential with the coverage. Different models are available in the literature, but at low θ they all reduce to

$$i_{\eta,\theta} \approx i_{\eta,\theta=0}\,(1 - B\theta) \tag{8.66}$$

By analysis of these expressions one can establish, on one hand, the dependence of the codeposition kinetics on the deposition parameters, and, on the other hand, the dependence of metal deposition kinetics on the inhibitor used, knowledge that is important both on its own and to facilitate an examination of profile evolution.

Nowadays the majority of the commercial electrolytes in the field of electrodeposition contain various organic inhibitors and brighteners, known by commercial names but involving well-known functional groups. Therefore information on the kinetics of metal deposition and organics consumption has an immediate practical importance: (1) when estimating the time intervals for electrolyte correction by the additives, (2) when considering the deposit purity and finally (3) when determining the optimum hydrodynamic conditions during deposition.

When $P<0$ another concept is sometimes used in addition to the leveling power; it is called *microthrowing power* (MTP). MTP is defined as $P+1$. If MTP is from zero to 1, then the rate of deposition at the microridges is higher than at microvalleys, but the current distribution is more uniform than the primary one. For $\text{MTP}=0$ the current distribution coincides with the primary one, and for $\text{MTP}<0$ the peaks grow very quickly. At high positive MTP the regions at the cathode which are more readily available for diffusion (not only microridges and peaks) grow more slowly than other sites; for instance, the current density is reduced at the edges of the cathode. At the same time the *macroscopic* distribution can act in the opposite direction: the current density at the edges has to increase. As a result the macroscopic and microscopic factors determining current distribution can act in concert; this is sometimes observed at millimeter-sized electrodes.

8.7 Stability of the Growth Front During Electrocrystallization

In the most general case the analysis of the actual electric field, concentration and current distribution requires complex computations for each shape of the interface; therefore numerical methods become very important. At the same time, an alternative and very different method to tackle this problem is available, which avoids the study of the particular field pattern near an irregular interface. This method

determines the conditions that provide the stability of the growing interface profile during electrodeposition [1]. The guiding principle of this method is discussed next.

The potential difference between a generic flat surface in the interior of the electrode ($y=0$) and some plane $y=d$ inside the electrolyte is

$$\Delta U = \rho_e i y_s + \rho_s i\,(d - y_s) + \Delta E(i, y_s); \tag{8.67}$$

the right side is comprised of the Ohmic drop in the electrode $\rho_e i y_s$ as well as in the solution $\rho_s i(d - y_s)$, and also the overpotential at the interface $\Delta E(i, y_s)$.

When the field is uniform ($d\Delta U/dy_s = 0$), then the variation of ΔE along the electrode is compensated by the variation of the Ohmic drop:

$$d\Delta E\,(i, y_s)/dy_s = i(\rho_s - \rho_d). \tag{8.68}$$

Let us introduce the parameter ε, equal to the difference between the two sides of this equation:

$$\varepsilon = i(\rho_s - \rho_d) - d\Delta E/dy_s = i\Delta\rho - d\Delta E/dy_s. \tag{8.69}$$

When $\varepsilon=0$ the field is non-distorted, and then $di/dy_s=0$; when $\varepsilon<0$ $di/dy_s<0$, and when $\varepsilon>0$ $di/dy_s>0$. In the last case the growth front becomes unstable: any accidental protrusion starts to grow at a higher rate than the other points at the surface and it cannot die out.

In this form, however, the criterion only gives the qualitative answer whether the growth front is stable or not; a quantitative treatment on the same grounds is also possible. It is natural to propose that di/dy_s is (as a first approximation) proportional to ε:

$$di/dy_s = k_1\varepsilon, \tag{8.70}$$

or

$$di/dy_s = k_1(i\Delta\rho - d\Delta E/dy_s)\,. \tag{8.71}$$

The last expression can be modified taking into account that the total derivative $d\Delta E/dy_s$ includes the partial one $\partial\Delta E/\partial y_s$ and also the term $(\partial\Delta E/\partial i)(\partial i/\partial y_s)$. The former term is determined by spatial variations of the diffusion paths towards different profile points, resulting in a shift of the polarization curves at such points. The latter term takes into account the polarizability. Thus, (8.71) is transformed into

$$di/dy_s = k_1(i\Delta\rho - \partial\Delta E/\partial y_s - \partial\Delta E/\partial i \times \partial i/\partial y_s) \tag{8.72}$$

and finally

$$di/dy_s = (i\Delta\rho - \partial\Delta E/\partial y_s)/(1/k_1 + \beta) \tag{8.73}$$

For $d\Delta E/dy_s=0$ this simplifies to

$$di/dy_s = (i\Delta\rho - \partial\Delta E/\partial y_s)/(1/k_1 + \beta) \tag{8.74}$$

Now it is interesting to compare this expression with that derived by direct calculation (8.30); this comparison shows that for the sinusoidal profile the coefficient k_1 equals $k/(\rho_s + \rho_d)$, where k is the wave number of the sinusoid. Thus

$$di/dy_s = (i\Delta\rho - \partial\Delta E/\partial y_s) / [(\rho_s + \rho_d) /k_1 + \beta] \tag{8.75}$$

and in the most common form

$$di/dy_s = (i\Delta\rho - \partial\Delta E/\partial y_s) / [(\rho_s + \rho_d) /K_1 + \beta] \tag{8.76}$$

where K_1 is the coefficient of the primary current distribution.

The last equation is especially valuable because it takes into account all the important factors, particularly the Ohmic potential drop, the polarization at the interface, the shape of the interface and the concentration variations in the diffusion layer. By substituting suitable values for these quantities one can find di/dy_s for different experimental conditions and therefore estimate the kinetics of the profile evolution.

The following are several examples of applications of the above method.

1. In the absence of concentration polarization and inhibition $d\Delta E/dy_s=0$, and in the usual case of $\rho_s >> \rho_d$ (8.76) simplifies to

$$di/dy_s = i\rho_s K_1/(\rho_s + K_1\beta), \quad \text{or} \quad dln\, i/dy_s = K_1/(1 + K_1\beta/\rho_s). \tag{8.77}$$

Assuming the polarizability $\beta = RT/\alpha nFi = 1/\alpha nfi$, we obtain

$$di/dy_s = iK_1/(1 + K_1/\alpha nfi\rho_s)\,. \tag{8.78}$$

2. In the presence of concentration polarization the dependence of ΔE on the concentration of electroactive ions is of importance. Under a uniform concentration field

$$c_s(y_s) = c_s(\text{av}) + i\left[y_s - y_s(\text{av})\right]/DnF \tag{8.79}$$

This corresponds to the following value of $d\Delta E/dy_s$:

$$d\Delta E/dy_s = -iRT/[Dn^2F^2c_0(1 - i/i_d)] \tag{8.80}$$

In this case the numerator in (8.76) takes the form

$$(i\Delta\rho + RT/[Dn^2F^2c_0(1 - i/i_d)]). \tag{8.81}$$

This shows that in this problem an additional resistance should be added to the Ohmic one; this term equals $RT/(Dn^2F^2c_s)$ and increases with increasing current density. This explains the progressive growth of the roughness at current densities close to the limiting one. Taking into account that the polarizability β in presence of a concentration polarization is $\beta = RTi_d/[\alpha nFi(i_d - i)]$, the final form of (8.76) at high CD is

$$di/dy_s = i[\Delta\rho + RT/(Dn^2F^2c_s)]/\{(\rho_s + \rho_d)/K_1 + RTi_d/[\alpha nFi(i_d - i)]\} \tag{8.82}$$

3. In presence of strong inhibition the leveling power P plays a dominant role:

$$\partial\Delta E/\partial y_s = \beta\partial i/\partial y_s = \beta kPi; \tag{8.83}$$

Then the expression for the full derivative di/dy_s (8.76) becomes $di/dy_s = (i\Delta\rho + \beta kP)/[(\rho_s + \rho_d)/K_1 + \beta]$. At high P it is close to the partial derivative, i.e.

$$\partial i/\partial y_s = kPi. \tag{8.84}$$

4. For a very high profile curvature an additional quantity must be added to the various terms considered so far: $\Delta E = 2\gamma V_{at}/nFR$ where γ is the surface energy. This addition is important, e.g., in the analysis of dendritic growth. For a sinusoidal roughness the curvatures at the bottom and at the top of the profile have the value $R = 1/(k^2H)$, and opposite signs; this leads to a potential difference between these two points $\Delta\hat{E} - \Delta\check{E} = 2\gamma V_{at}/nFR = 2\gamma V_{at}k^2H/nF$, and the corresponding potential gradient equals

$$\partial\Delta E/\partial y_s = (\Delta\hat{E} - \Delta\check{E})/2H = 2\gamma V_{at}k^2/nF \tag{8.85}$$

This value should be taken into account at very high k, that is for roughness at very small length scales.

5. The role of structural factors such as the crystallographic structure, structural defects, variation of the adsorption among grains with different orientation etc. can be described in a similar way as the influence of roughness; the equation for the profile evolution correspondingly has the form

$$dH/d\mathrm{h} = kH + k_{cryst} \tag{8.86}$$

The second term reflects structural non-uniformities; this term is usually between 0.01 and 0.1. After integration (8.86) gives

$$H = H_0\, exp\,(kh) + (k_{cryst}/k)\left[exp\,(kh) - 1\right]. \tag{8.87}$$

Due to the nonzero value of k_{cryst}/k the initially ideally smooth surface develops a roughness of about 1 μm at a deposit thickness of 10–1,000 μm.

8.8 Bright Deposits

Everything said in Sect. 8.6 on the leveling power is also true for the deposition of bright deposits. In this case the microscopic (less than 0.5 μm) surface irregularities are leveled. Sometimes the surface can be bright even for a much larger amplitude or irregularities, but this can be only be true for irregularities having very long length scale. The leveling of the smallest roughness occurs usually when thin adsorbed films on the surface hinder, but do not completely block, the inhibitor transport.

It is usually assumed that the mechanism of brightening is similar to that of leveling; it is not accidental that a number of leveling agents are simultaneously good

brighteners. On the other hand the scale of leveling is the same as the diffusion layer thickness, whereas the scale of brightening is much smaller and is close to the thickness of the surface films, which plays the same role for brightening as the diffusion layer does for leveling.

There are a number of brightening agents active in various solutions; among them are the acetylenic alcohols (such as butynediol), aromatic aldehyds, azo-, thioazo- and oxoazo-dyes, some ketones and sulfur-containing organic substances may be mentioned.

We can finally add that the mechanism of brightening during electropolishing is of a similar nature. The main difference lies in the nature of the surface film: during electropolishing a viscous film is formed which contains the dissolution products of the film that is being etched.

References

1. Baraboshkin N. A. Metal Electrocrystallization from the Melts. Moscow, Publishing House Nauka, 1976 (in Russian)
2. Wagner C. J. Electrochem. Soc., 1951, v. 98, p.116, 1954, v. 101, p. 225
3. Watson S.A., Edwards J. Trans. Inst. Metal Finishing, 1957, v. 34, p. 167
4. Muresan M., Varvara S. Leveling and Brightening Mechanisms in Metal Electrodeposition. Metal Electroseposition, Nova Science Publishers, New York, 2005, p. 1–45.
5. Kruglikov S. Itogi Nauki (Progress in Science), VINITI, Moscow, 1967, p. 117 (in Russian)

Chapter 9
Non-steady State Electrodeposition Processes and Electrochemical Methods

9.1 Non-steady State Diffusion

In the absence of faradaic processes the concentration of reacting species in the electrochemical cell is uniform, and no diffusion layer is formed at the electrode. After imposing an applied potential or a current to the electrode of interest, the concentration profile of the various electroactive species changes with time until it is stabilized by the balance of faradaic, diffusional and convective processes. A stationary diffusion layer with a definite thickness is eventually set up when the applied potential or current is constant in time; this situation was discussed in the previous chapter. Under non-steady state electrochemical conditions, which include in particular those cases where the current or potential vary with time, also the diffusion layer evolves with time. In this chapter, various time-dependent electrochemical phenomena will be considered, focusing particularly on their influence on metal electrodeposition. The concepts thus developed will also be applied to the study of electrode kinetics.

The interest for non-steady state processes in electrodeposition originates in the practical possibility to vary and control the structure and properties of electrodeposits (including their hardness, grain size etc.) in parallel with the possibility of accelerating film growth with respect to conventional continuous current methods. From the theoretical standpoint, the resulting knowledge on transient electrode processes can also be effectively applied to quantitative studies of electrode kinetics.

Electrode processes under conditions of time-varying current or potential can be steady state (quasi-static), or non-steady state, depending on the ratio between the system relaxation time and the characteristic time over which the control parameter (current or potential) varies. Often diffusion of electroactive species is the slowest process, with a characteristic time of 1–10 s; the typical response time of faradaic processes instead is of the order of 0.1–1 ms. The typical frequency range where transient effects in electrode processes will be significant is therefore 0.1–10^4 Hz. Electrochemical systems will be insensitive to current or potentials varying at much faster rates, while they will respond to much slower changes as if the control parameter were constant in time.

Y. D. Gamburg, G. Zangari, *Theory and Practice of Metal Electrodeposition,*
DOI 10.1007/978-1-4419-9669-5_9, © Springer Science+Business Media, LLC 2011

For especially short pulses or at high frequencies it is necessary to take into account the current used up to charge the double layer DL; not all the current in fact goes into the faradaic process during the initial application of a pulse. The duration of this charging process is about $\tau = RTC_{DL}/nFi$, C_{DL} being the DL capacity; τ is usually about 1 ms. Thus, at frequencies of about 1,000 Hz the faradaic current can be distorted by DL charging processes.

The most important effects of non-steady state diffusion include: (1) the gradual transition to a different value of the near-electrode concentration after switching the current on or off; (2) oscillations of the near-electrode concentration when passing an alternate current superposed to a constant value; (3) oscillations of the near-electrode concentration upon periodic reversal of the electrode polarity; (4) the variation of concentration when sweeping the current or the potential with time. The application of a sinusoidal current (with zero average) or of an on-off square current pulse are particularly important cases of the above phenomena.

The solution to any of the above problems is based on the differential equation for non-stationary diffusion, i.e. the second Fick's law:

$$\partial c/\partial t = D(\partial^2 c/\partial x^2 + \partial^2 c/\partial y^2 + \partial^2 c/\partial z^2) \tag{9.1}$$

together with the relevant initial and boundary conditions. In this equation x, y and z are the space coordinates in a Cartesian reference frame, t is the time and D the diffusion coefficient of the electroactive species; in the one-dimensional case this equation simplifies to

$$\partial c/\partial t = D\ \partial^2 c/\partial x^2 \tag{9.2}$$

where x is the distance from the electrode. The solution $c(x, y, z, t)$ or $c(x, t)$ allows determination of the concentration of electroactive ions at any point in the solution at any given moment in time; in particular, it provides the time dependence of the concentration of electroactive species near the electrode. If migration plays a role, then D is the effective diffusion coefficient introduced in Chap. 4.

The above-mentioned initial and boundary conditions depend on the actual electrochemical system being considered. For example, if the electrode is initially at its equilibrium potential and the current density i is switched on at time $t = 0$, then one boundary condition is:

$$\partial c/\partial x\ (0, t) = i/DnF. \tag{9.3}$$

This means that the concentration gradient near the electrode is determined by the imposed current density, which starts at $t = 0$ and is constant with time. Over time, the faradaic current causes a decrease in the concentration of the electroactive species which progressively progresses into the bulk of the solution, thus creating a diffusion layer of finite thickness. In some cases it may be mathematically convenient to consider this thickness as infinite. The second boundary condition is $c(x, \infty) = c_0$, and the initial condition is, naturally, $c(x, t = 0) = c_0$. In this case the solution is unique and gives the time dependence of the electrode potential through

a determination of the species concentration at the electrode, under the approximation of a stationary state: $E = E^0 + (RT/zF)\ lnc(0, t)$.

In the other case, when the electrode potential is sharply changed to a different value, the solution of this equation permits finding the dependence of current on time $i - t$ by determining the concentration vs. position, and the current as $i = zFD(dc(x, t)/dx)_{x=0}$. Similarly, other problems can be solved through the determination of the potentials, currents or concentrations by applying an arbitrary electric (current or potential) waveform.

In the following selected characteristic problems are discussed in detail.

9.2 On–Off Switching of the Current or Overpotential

The boundary condition to be added to Eq. (9.3) in this case should be imposed at the external boundary of the diffusion layer:

$$c(\delta,\ t) = c_0 \tag{9.4}$$

which means that at this position the concentration is unchanged. This condition is different from that usually used in diffusion problems, where the concentration at an infinite distance is specified. Our choice is due to the fact that in any real system under steady state condition a diffusion layer with definite characteristics is eventually set up.

The solution of Eq. (9.2) under these conditions is the following converging series

$$c_s = c(0,\ t) = c_0 - i\delta/DnF\left[1 - 8/\pi^2 \sum n^{-2} exp(-\pi^2 nDt/4\delta^2)\right]. \tag{9.5}$$

Taking only the first term as a first approximation we obtain

$$c_s \approx c_0 - i\delta/DnF[1 - exp(-\pi^2 Dt/4\delta^2)]. \tag{9.6}$$

This last expression permits to estimate the time necessary to attain the steady state under various deposition conditions. Thus, for $i = 0.35 i_d$ the steady state potential is attained within a 5 mV accuracy at ≈10 s, but for currents approaching i_d this time interval may increase to tens of seconds.

At small t and sufficiently high δ (more precisely, when $Dt/\delta^2 < 0.1$) this formula simplifies to

$$c_s \approx c_0 - 2i/nF(t/\pi D)^{1/2}. \tag{9.7}$$

This solution is exact in a semi-infinite space, i.e. when imposing the boundary condition $c(\infty, t) = c_0$ instead of (9.4).

Equation (9.7) allows to find the time at which the concentration at the interface (when $i > i_{lim}$) falls down to zero; this time is called the transition time t_t:

$$t_t = \pi D/4(nF c_0/i)^2 \tag{9.8}$$

When $i = i_{lim} = DnFc_0/\delta$ the transition time is

$$t_t = \pi\delta^2/4D \tag{9.9}$$

Combining (9.7) and (9.8) one obtains

$$c_s/c_0 = 1 - (t/t_t)^{1/2}. \tag{9.10}$$

The decrease in the concentration of the electroactive species at the interface introduces an additional term to the electrode overpotential, called the diffusion overpotential. This is given by the expression:

$$\eta_d = (RT/nF)\ ln\ (c_s/c_0) = (1/nf)\ ln\left[1 - (t/t_t)^{1/2}\right]. \tag{9.11}$$

This shows that when the transition time is approached the overpotential raises sharply, providing a method for an experimental determination of this quantity. It must be noted that (9.11) is valid only at relatively high current densities, when t_t is less than $\pi\delta^2/4D$. When switching on a current equal to the limiting value, the condition (9.6) would be met rather soon, corresponding to a linear increase of the diffusion overpotential with time.

Under pure diffusion control of the rate of the electrochemical process of interest, as (9.8) shows, the value of the product $it^{1/2}$ is independent of the current density. A decrease of this product at increasing CD indicates therefore that some other (non-diffusion) limiting step becomes important.

The possibility of using (9.7) instead of (9.5) is connected with the fact that the front of the concentration variations ("the concentration wave") propagates to a distance λ from the electrode into the bulk of the solution with the law

$$\lambda \approx (Dt)^{1/2} \tag{9.12}$$

While $\lambda < \delta$, i.e. when the concentration wave is close to the surface, the conditions (9.4) $c(\delta, t) = c_0$ and $c(\infty, t) = c_0$ coincide, and the simpler equation can be used. At small times however the use of Eq. (9.6) is more accurate.

When switching off the current the resulting mathematical problem is of the same nature as the switching on. When the initial surface concentration of the electroactive species is $c_s \neq c_0$, its time dependence after the current is switched off is approximately

$$c_s(t) - c_0 = (c_s(0) - c_0)\ exp(-\pi^2 Dt/4\delta^2). \tag{9.13}$$

A different situation arises when a constant overpotential is applied instead of a current. Consider in particular the case when the electrode is initially in the equilibrium state and then a potential is applied corresponding to the limiting current. The

resulting current depends on the hydrodynamic conditions in the solution, namely on the thickness of the diffusion layer. For a diffusion layer thickness δ the time dependence of the current density is

$$i \approx i_{\text{initial}}(1 - kt^{1/2}) = i_0 nF\eta/RT\left(1 - kt^{1/2}\right) \tag{9.14}$$

Obviously, under these conditions the current asymptotically decreases to the value $i_{\text{lim}} = DnFc_0/\delta$, corresponding to the limiting current density for the flat surface. When the diffusion layer can propagate indefinitely, i.e., when convection is completely absent, $\delta = kt^{1/2}$, and a different time dependence is observed:

$$i(t) = nFc_0(D/\pi t)^{1/2} \tag{9.15}$$

corresponding to the current decreasing from its initial value to zero. The time interval where $t \to 0$ in this case is not of interest: initially in fact the transient process involves double layer charging—thus avoiding infinities—and in practice is also dependent on the performance of the available instrumentation. In general the value c_0 represents the sum of the Ox and Red concentrations. Equation (9.15) was derived by Cottrell in 1902 and bears his name.

The current decrease according to a square root law is especially characteristic of the short initial transient of current passing through the electrode, immediately after switching on the potential. This phenomenon is widely used as a relaxation method for the study of fast electrode processes; it should however be pointed out that the Cottrell solution cannot be applied in the case of low currents, $i \ll i_{\text{lim}}$. For a stepwise potential change from the equilibrium value to an overpotential of several mV the corresponding current varies with time as

$$i = i_0 nf\eta\left(1 - kt^{1/2}\right) \tag{9.16}$$

($f = F/RT$). This allows finding i_0 by plotting i vs $t^{1/2}$ and extrapolating to zero time. This method is widely used for the study of relatively slow electrochemical processes, and allows a determination of i_0, α as well as other parameters of the electrode process under study. Fast processes cannot be studied by this method since the relevant transients are obscured by the capacitive charging of the double layer.

When the thickness δ is decreased the time needed to attain the steady state becomes shorter for any value of current density; this fact is used to facilitate data acquisition when plotting potential-time curves: the thinner is δ, the more quickly the readings corresponding to the steady state condition can be collected.

9.3 Superposition of a Sinusoidal Current

If an alternate current AC is superimposed to a constant (average) value then the current density at the electrode is described by

$$i = i_{\text{const}} + i_{\text{al}} \sin \omega t \tag{9.17}$$

ω being the frequency and i_{al} the amplitude of the alternate current. The concentration gradient near the electrode in this case periodically varies as

$$\partial c/\partial t\,(0,t) = (i_{\text{const}} + i_{\text{al}} \sin \omega t)/DnF \tag{9.18}$$

The surface concentration of electroactive species is varying also; the time dependence of this variation can be found from the solution of Eq. (9.2) with the boundary condition (9.18). The second boundary condition is imposed at the diffusion layer boundary, and it can be either in the form $c(\delta)=c_0$, or $\partial c/\partial x\,(\delta, t)=0$. Usually the solution is complicated [1] but if δ is known and the amplitude i_{al} is not very large, so that the limiting CD is not achieved, an approximate form of this solution is the following:

$$c(t) = c_1 + c_2\, sin\,(\omega t - \gamma) + c_0\, exp(-\pi^2 Dt/4\delta^2). \tag{9.19}$$

In the general case the rigorous solution consists of three terms. The first one is constant, the second one is periodic and the last one represents a relaxation. In the approximation of Eq. (9.19) the periodic term is is sinusoidal and the relaxing term is exponential.

The exponential term dies out relatively quickly; it is evident that at the time $t>2\delta^2/D$ it has decreased by 100 times and can therefore be neglected; this occurs by the cycle number n

$$n \approx \delta^2\omega/\pi D = 2\delta^2/(DT), \tag{9.20}$$

T being the period of the alternate current, and $\omega=2\pi/T$. The duration $t_0=4\delta/(\pi^2 D)$ is the relaxation time of the system; the exponential term falls 2.7 times from its initial value at this time. t_0 is about one half of the transition time.

The constant c_1 and the periodic c_2, γ parameters can be found by solving the diffusion equation without initial conditions; this gives approximately the following expression:

$$c_1 = c_0 - i_{\text{const}}\delta/DnF; \tag{9.21}$$

which corresponds to the electrolysis at a constant CD without alternating component;

$$c_2 = (i_{\text{al}}/nF)(2D\omega)^{-1/2} \tag{9.22}$$

and

$$\gamma = arcsin\left\{(sin\beta + sinh\beta)/\left(2\,sin^2\beta + 2\,sinh^2\beta\right)^{1/2}\right\}, \tag{9.23}$$

where $\beta=(2\delta^2\omega/D)^{1/2}$.

Approximately (Fig. 9.1): when $0<\beta\leq 1$ *sin* $\gamma\approx 1$; when $1<\beta\leq 3.2$ *sin* $\gamma\approx (1.14-0.15\beta)$; and when $\beta>3.2$ *sin* $\gamma\approx 0.71$.

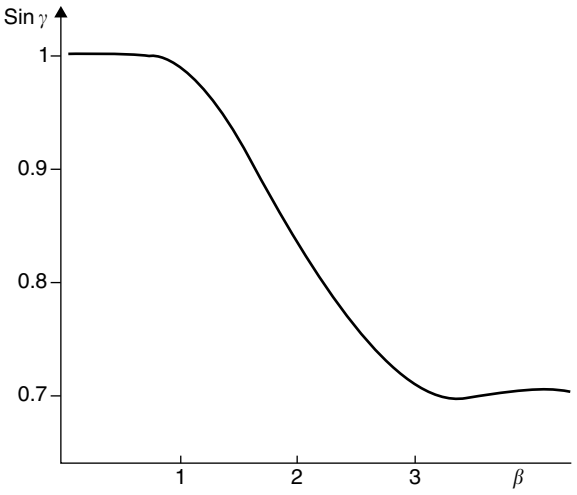

Fig. 9.1 The dependence of the phase shift angle on the parameter γ

In other words, the concentration near the electrode oscillates around the average value $c_1 = c_0 - i_{const}\,\delta/DnF$ corresponding to electrolysis at a constant current density; the oscillations take place with an amplitude depending on the frequency: $(i_{al}/nF)(2D\omega)^{-1/2}$ and with a frequency equal to that of the current but with the phase shift γ. This shift equals π/2 at small β and π/4 at large β. The non-dimensional parameter β is therefore an important quantity that defines the alternate current regime; it is related to the ratio of the penetration distance of the concentration wave to the diffusion layer thickness.

At high frequencies it is important to take into account the DL charging which can give an additional phase shift between current and concentration.

The concentration at the surface cannot fall to values lower than zero, thus giving a natural condition for finding the maximum amplitude of the AC:

$$i_{al} \le nFc_0(2D\omega)^{1/2} - i_{const}\beta. \tag{9.24}$$

If $i_{al}/i_{const} > 1$ then for some part of the overall period T the current through the electrode has the opposite sign; that is, it is anodic during the electrodeposition process (Fig. 9.2); this kind of processes are of the particular interest.

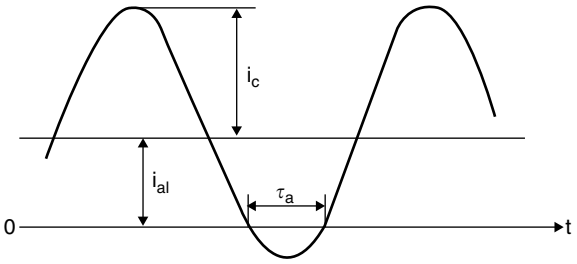

Fig. 9.2 The shape of $i - t$ dependence at $i_{al}/i_{const} > 1$

The experimental method based on the measurements of the complex electric impedance of the electrochemical system when imposing alternate currents (of low amplitude and with a wide frequency range) is named electrochemical impedance spectroscopy EIS and is one of the most powerful methods in electrochemistry [2]; this method is based on the measurement of the phase shift angle γ.

9.4 Steady State and Pulsating Diffusion Layers

By propagating into the solution bulk the amplitude of the concentration variation falls according to the law $exp[-(\omega/2D)^{1/2}\mathrm{x}]$ and the phase shift varies as $\gamma = \gamma(\mathrm{x}=0) + (\omega/2D)^{1/2}\mathrm{x}$. At the distance $\lambda \approx 5(2D/\omega)^{1/2}$ this amplitude decreases by more than 100 times and becomes negligibly small. Thus this distance λ is conventionally the boundary of the concentration wave propagation. It follows that the parameter β from the previous section can be approximated by

$$\beta \approx 10\delta/\lambda \tag{9.25}$$

Under usual conditions $\lambda << \delta$; this suggests a separation of the overall diffusion layer into two parts: the steady state and the pulsing ones (Fig. 9.3) [3]. This division is possible not only under alternate but also under pulsed (cyclic) currents with different shapes; in the latter case however the value of λ varies somewhat during the cycle.

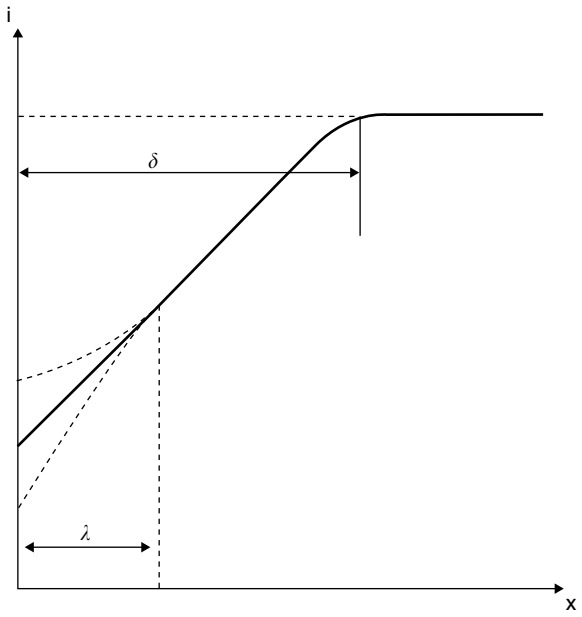

Fig. 9.3 The steady state and the pulsating diffusion layers

The separation of the diffusion layer into a constant and a pulsed part is not rigorously defined, but may be specified case by case in order to simplify the problem of non-steady state diffusion during electrodeposition. The resulting formulae are relatively simple and often sufficiently precise.

In the case of a periodically changing potential (instead of a current) the concentration varies in a similar way. Under a potentiostatic cathodic pulse the current density will fall resulting from the decreasing concentration; it is interesting that if, after the cathodic pulse the potential is returned to the value corresponding to the equilibrium one (at $c=c_0$), an anodic current will be observed due to the reduced concentration at the electrode ($c<c_0$), the corresponding equilibrium potential being more negative. Then an exponential recovery of the concentration will occur.

9.5 Rectangular Pulses

Application of a cathodic (i_c, t_c) followed by an anodic (i_a, t_a) rectangular pulse (including the case $i_a=0$, i.e. a pause) results in deposit growth only if the following condition is fulfilled

$$i_c t_c > i_a t_a \tag{9.26}$$

i.e. $q_c > q_a$; this expression is strictly true when the cathodic and anodic current efficiencies are both 100%; otherwise condition (9.26) becomes $q_c CE_c > q_a CE_a$. Under these conditions the average CD during the overall period is

$$i_{av} = (|i_c|t_c - |i_a|t_a)/(t_c + t_a) \tag{9.27}$$

Under this pulsed regime (pulsed reverse current, RC) the major parameters characterizing the electrodeposition process are the charges $q_c = i_c t_c$ and $q_a = i_a t_a$. The current density in a cathodic pulse can be very high, even 10–100 times the limiting one; the corresponding pulse duration however should be small, i.e. less then the transition time for the given current density. The temporal variation of c_s during the pulses is shown in Fig. 9.4.

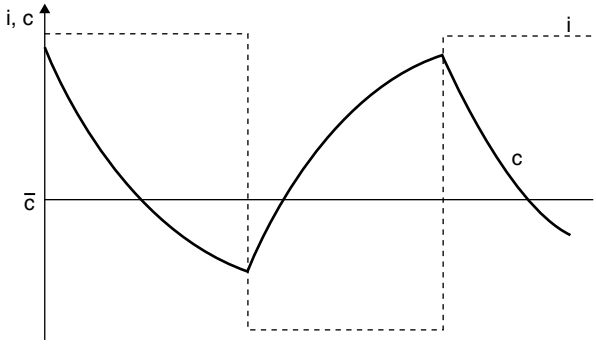

Fig. 9.4 Temporal variation of c_s during application of current pulses

For a quantitative determination of c_s vs. time the diffusion equation should be solved with the appropriate boundary and initial conditions, which in this case can be set as $i(t)=i_c$ for cathodic pulses, i.e. when $m(t_c+t_a)<(m+1)t_c+mt_a$ and $i(t)=i_a$ otherwise, i.e. when $(m+1)t_c+mt_a<(m+1)(t_c+t_a)$; ($m$ is an integer).

The solution of this problem [4] is an infinite series of the same type as (9.5). It can be expressed (as in the case of the superimposed alternate current) as the sum of a constant, a periodic and a decaying term; when the last one dies off to zero, at this steady state the two limiting surface concentrations are established:

$$\begin{aligned} c_1 = c_0 - 8\delta/(\pi^2 DnF) \sum_{k=0}^{\infty} {m_k}^{-1} \{ i_c [exp(-m_k t_a/t_0) \\ - exp(-m_k T/t_0)] \quad /[1 - exp(-m_k T/t_0)] \\ - i_a [1 - exp(-m_k t_a/t_0)]/[1 - exp(-m_k T/t_0)] \} \end{aligned} \tag{9.28}$$

where $m_k=(2k+1)^2$, $T=t_c+t_a$; at the end of the cathodic pulse (or, equivalently at the beginning of the anodic one or of the pause)

$$\begin{aligned} c_2 = c_0 - 8\delta/(\pi^2 DnF) \sum_{k=0} {m_k}^{-1} \{ i_c [1 - exp(-m_k t_c/t_0)]/[1 - exp(-m_k T/t_0)] \\ - i_a [exp(-m_k t_a/t_0) - exp(-m_k t_a/t_0)]/[1 - exp(-m_k T/t_0)] \} \end{aligned} \tag{9.29}$$

These equations are derived for example in [4]. The difference c_2-c_1 is the range of the concentration variations. In the particular case $i_a=0$ and infinite T (i.e. a unique pulse) (9.29) coincides with (9.5).

During each pulse, c varies exponentially following a law close to (9.6) and with time constant t_0. The expressions (9.28) and (9.29) can be used for any calculation connected with pulsed current electrodeposition. Thus, (9.29) allows finding the maximum cathodic current density at which c falls to zero at the end of the pulse. This value determines the maximum effective (average over one period) current density.

The general expression determining the ratio of the limiting diffusion current density to the maximum value of the average current density under pulsing current is obtained by applying the concept of the pulsating diffusion layer, and it has the form

$$i_{lim}/i_{av}(max) = 1 + (t_{pause})^{3/2} (T \cdot t_{pulse} \cdot t_0)^{-1/2} \tag{9.30}$$

This shows that the average current density is always less then the limiting one, therefore it is impossible to accelerate the deposition rate by applying pulsed currents. Nevertheless the pulsed current can be effective due to the fact that one cannot usually deposit thick compact metal films at the limiting current, whereas using a pulsed current of a suitable shape this can be possible. To find the corresponding maximum current density in the pulse one has to multiply the value of $i_{av}(max)$ from (9.30) by the factor T/t_{pulse}. At this high value of CD in the pulse nucleation

may occur much faster than under continuous current conditions: the number of nuclei is much higher for the same amount of deposited metal. The reason will be discussed in the next chapter, but here it can be stated for example that if CD increases two-fold, the nucleation rate increases ten times or more. This results in more fine-grained deposits.

9.6 Role of the Pause and of the Anodic Period

During the pause (or the anodic pulse) which follows the cathodic pulse, the concentration in the diffusion layer is restored towards its initial value due to diffusion processes and (for an anodic current) due to anodic dissolution of a deposit. Throughout the pause other processes can also be active at the electrode; e.g. the desorption of a surface-active additive can occur if the maximum of its adsorption corresponds to the pulse potential or, on the contrary, the adsorption may increase if the maximum corresponds to a more positive potential range. Passivation of the surface can occur as a result of dissolved oxygen adsorption; additionally, side electrochemical processes can proceed due to the energy stored in the DL (or, as it is usually stated, due to the DL capacitance discharge during the faradaic process).

The use of anodic pulses is often quite effective in achieving very smooth deposits with minimal structural defects. This is possibly due to the dissolution, during the anodic pulse, of the most active, i.e. defective regions or sites with a positive curvature (peaks) on the surface. If during a preceding cathodic pulse regions of this kind have formed, which may later grow into dendrites or sharp peaks, the subsequent anodic pulse does dissolve them primarily due to their higher free energy. Anodic periods which arise when superposing an alternate current with an amplitude larger than the direct current: $i_{al}/i_{const} > 1$ may cause the same effects.

In summary, three factors affect the structure and properties of coatings deposited with a pulsed current. These are: the surface concentration of the electroactive ions, current microdistribution at the electrode surface and adsorption of surface active additives. When analyzing adsorption not only thermodynamics but also kinetics is of importance: if the steady state is established slowly then actually some average coverage will be observed, whereas if adsorption occurs quickly the actual adsorption state can vary during the cathodic and anodic pulses.

9.7 Current Distribution, Current Efficiency and Inclusions of Impurities During Non-steady State Processes

The reverse current (RC) provides for a more uniform metal distribution (both at the macro- and microscales) relatively to DC.

Let us discuss this problem for the example of the current distribution at a rough profile. According to (**8.13**) if the initial roughness amplitude is ε_0 then after the cathodic pulse it becomes:

$$\varepsilon_1 = \varepsilon_0 \, exp(k_c h_c) \tag{9.31}$$

where h_c is the deposit thickness increase during this pulse, at 100% CE.

Then, after the subsequent anodic pulse,

$$\varepsilon_2 = \varepsilon_1 \, exp(-k_a h_a) \tag{9.32}$$

or

$$\varepsilon_2 = \varepsilon_0 \, exp(k_c h_c - k_a h_a) \tag{9.33}$$

Thus, the condition to achieve a more uniform distribution after the overall period, i.e. $\varepsilon_2 < \varepsilon_0$ is

$$(k_c h_c < k_a h_a) \tag{9.34}$$

or

$$k_c/k_a < h_c/h_a = i_c t_c / i_a t_a \tag{9.35}$$

Substituting the expressions for the secondary current distributions during the cathodic and anodic pulses, respectively, leads to

$$i_c t_c / i_a t_a > (1 + k\beta_c/\rho)/(1 + k\beta_c/\rho) \tag{9.36}$$

Thus a higher polarizability during the cathodic period than during the anodic one can provide a more uniform metal distribution in RC conditions [5]. Qualitatively, this is explained by a faster dissolution of the thicker regions of the deposit with respect to the thinner ones due to a high non-uniformity of the current distribution. More simply: if a region of the layer is two times as thick after the cathodic pulse, it is dissolving three times more quickly; then after partial dissolution the film uniformity becomes much better than under direct current.

This result is valid both for the micro- and macrothrowing power. Equation (9.36) says nothing about the absolute durations t_c and t_a, which should be chosen from practical considerations. Thus, for $t < 0.01$ s the share for the DL charging increases; on the other hand, for $t > 10$ s the dendrite formation during the cathodic pulse may become more important. The reverse or pulsed current can also be very efficient in suppressing dendrite formation. For a diffusion layer thickness δ and surface peaks having a height ε ($\varepsilon < \delta$), then, according to (8.41) the growth of this peak in the diffusion regime goes as

$$ln\,(\varepsilon/\varepsilon_0) = \left(ADc_0/d_m\delta^2\right)t, \tag{9.37}$$

where d_m is the density of the metal. If pulsed current is used, the actual duration of the deposition process is shortened (at the same average deposition rate) by the ratio t_c/T, since during the pause ε does not vary. Thus instead of (9.37) one obtains

$$ln\,(\varepsilon/\varepsilon_0) = \left(AD\mathrm{c}_0 t_\mathrm{c}/T d_\mathrm{m}\delta^2\right)t. \tag{9.38}$$

This expression shows that the ridges grow most quickly under constant current, i.e. for $t_c/T=1$. This is one reason for the pulsed current effectiveness in accelerating deposition. When DC electrodeposition is performed the process of dendrites formation accelerates sharply at $i>0.5i_{\mathrm{lim}}$ due to progressive growth of the occasionally formed peaks.

Under pulsed current the growth of dendrites is suppressed, thus allowing an increase of the average deposition rate. Another reason for dendrite growth inhibition is a higher crystallization overpotential, resulting in accelerated nucleation and the formation of fine-grained coatings.

The current efficiency of pulsed current processes varies in comparison with direct current; as a rule, it decreases due to the diffusion limitations during metal deposition. Nevertheless other phenomena may be active to vary CE in both cases. For example, other side processes may occur; in addition, the adsorption of surface-active additives may influence both metal deposition and side processes in various manners.

Often, purer and less defected deposits are formed using pulse electrolysis. This can be due to higher nucleation rates arising in presence of higher current pulses, which may also act to push adsorbed impurities aside by the growing front of the depositing metal, particularly in the lateral direction.

The degree of perfection of the crystal lattice can be a complicated function of the deposit purity and the electrolysis conditions. On one hand, a higher overpotential during the cathodic pulse may result in a decrease of grain size, and therefore in an increase of the fraction of defected material adjacent to the grain boundaries, an increasing dislocation density, the development of twins, stacking faults and also point defects. On the other hand, with a higher film purity, relaxation and ordering processes are not suppressed by the impurities, thus the defects that may form initially can disappear shortly after deposition, or already during deposition. Relaxation processes resulting in ordering of the crystal structure may also proceed during the pauses of the current. Thus the action of these oppositely directed factors hinders prediction of the influence of unsteady regimes on the structure and properties of the deposited metals.

9.8 Linear Current or Potential Scans; the Optimum Sweep Rate for the Acquisition of Polarization Curves

One of the most important methods to obtain information on electrodeposition processes is by plotting the dependence of *i vs. E*; these are called polarization curves. The equilibrium curve can be obtained plotting the characteristics point by point. Recording the same curve by applying a potential sweep on the other hand results in a non-equilibrium curve since the near-electrode concentration may not have

sufficient time to follow the electric signal; with a sufficiently slow sweep however the quasi-equilibrium curve can be obtained. From the point of view of the time required for data acquisition the sweep rate should not be too low. Thus determination of the optimum sweep rate is of interest.

A relatively simple case is the linear current sweep. The solution of the diffusion equation must be obtained under the following boundary conditions:

$$\begin{aligned} &c(x,0) = c_0, \\ &\partial c/\partial \mathrm{x}\,(0,t) = c_0 t/(\delta T) \\ &c(\delta,t) = c_0 \end{aligned} \tag{9.39}$$

The first and the third conditions are clear; the second one means that the current increases linearly resulting in a linear growth of the concentration gradient at the electrode. T is the overall time of sweep; this condition shows that after the time T the limiting diffusion current will be achieved.

The approximate solution of (9.2) under these conditions is

$$\mathfrak{c}(0,t) \approx \mathrm{c}_0[1 - t/T + K\delta^2/(3DT)], \tag{9.40}$$

where $K = 1 - \Sigma[\exp(-\pi^2(k+1/2)^2 Dt/\delta^2)/(2k+1)^4]$, a coefficient always less than one. At $t/T \ll 1$ this corresponds to a linear growth of the concentration gradient, i.e. to quasi-equilibrium conditions, but for a sufficiently fast sweep the third term in (9.40) becomes significant, and the equilibrium conditions are not attained.

In order to establish the maximum acceptable scan rate for plotting quasi-equilibrium data we may impose that the third term should be less than 0.01; thus one obtains

$$T > \delta^2/(0.03D). \tag{9.41}$$

For a sweep duration larger than this value one may consider the data collected as the equilibrium ones.

Putting $\delta \approx 10^{-2}$ cm (this corresponds to moderate agitation) and $D \approx 10^{-5}$ cm^2/s we obtain $T > 10$ s. The usual potential interval for such a plotting can be about 0.1 V: then the sweep rate is 10 mV/s; this is a value close to usual scan rates. For a thicker diffusion layer (i.e. 0.1 mm or more) however the sweep rate should be much slower.

The problem of determining the slowest admissible sweep rate is more complicated. The simplest condition for example may consist in the assumption that the deposit thickness obtained during one sweep must not exceed 1 μm, because deposits of this thickness rarely have high roughness, if the initial surface was smooth. Then the average current density for a linear current sweep from zero to the limiting current value is one half of the limiting current density:

$$i_{\mathrm{av}} = DnF\mathrm{c}_0/2\delta, \tag{9.42}$$

and this relationship, together with the Faraday law, immediately gives the duration T of the experiment corresponding to $h = 0.001$ cm:

$$T < 2h\delta/(Dc_0 V_m), \tag{9.43}$$

where V_m is the molar volume of the metal, about 10 cm^3/mol. Then

$$T < 2 \cdot 10^{-4}\delta/(Dc_0) \tag{9.44}$$

the linear size is here expressed in cm and the time in seconds.

Combining the two conditions one obtains

$$\delta^2/(0.03D) < T < 2 \cdot 10^{-4}\delta/(Dc_0). \tag{9.45}$$

If these measurements are performed with a RDE, the values of δ and therefore those of T can be found easily. The unique condition necessary for Eq. (9.45) to be not contradictory is that $\delta c_0 < 6 \cdot 10^{-6}$ mol/s cm. In the rare cases when this condition is not fulfilled, the curve can be recorded in successive segments at a new electrode each time or using the electrode with a renewed surface.

If a very thin electrolyte layer l is present between the two electrodes (typically thinner than 0.1 mm) the analysis of the behavior of this system is often simplified. The other advantage of such system is the very small quantity of the electrolyte used.

The transition time for these thin-layer cells is

$$t_t = nFlc/I \tag{9.46}$$

whereas the maximum current value for a linear sweep with the rate v (V/s) corresponds to the time

$$t_{peak} = n^2F^2lcv/4RT. \tag{9.47}$$

In order to simplify these measurements it is possible to lower the inter-electrode distance and/or also the size of the electrode itself; if this is of the same order as the diffusion layer thickness, the steady state convection is established quite soon after current switching: the value of $r^2/\pi D$ at $r = 0.01$ cm is about 1 s. These electrodes are named microelectrodes; beyond being useful due to the very short time necessary for concentration stabilization, they are also characterized by a uniform current distribution across its area, with a very slight edge effect. Moreover, when performing potential measurements at microelectrodes there is no need for close positioning of Luggin capillary: this can be located at any distance from the electrode because the Ohmic potential difference depends in this case only on the current I, electrode radius r and the solution conductivity σ. Thus, at high concentration of the supporting electrolyte and for a spherical electrode of radius r

$$\Delta U_{Ohm} = I/(4\pi r\sigma); \tag{9.48}$$

in the case of a disc electrode of radius r in a non-conductive plane

$$\Delta U_{\text{Ohm}} = I/(4r\sigma). \tag{9.49}$$

Finally, the limiting diffusion current density at this microelectrode is

$$i_{\text{d}} = nFcD/r. \tag{9.50}$$

References

1. Vetter K.J. Elektrochemische Kinetik. Springer – Verlag, 1961, s. 177
2. Impedance Spectroscopy: Theory, Experiment and Applications. Ed. By E. Barsoukov and J.R. Macdonald. J. Wiley & Sons, 2005
3. Ibl N. Surf. Technology, 1980, v. 10, No.2, p. 81
4. Popov K.T. et al. Surface Technology, 1982, v. 16, p. 209
5. Koshev A., Beck R., Lipatova T., Transactions of the Siberian Branch of the Soviet Academy of Sciences, chem. series, 1982, No.7, p. 126 (in Russian)

Chapter 10
Electrodeposition of Alloys

10.1 Introduction

The theory of codeposition of two or several metals is of particular interest, as the current trend in engineering and technology supports the replacement of individual metals by their alloys, which usually feature a wider spectrum of properties. This is particularly true in electroplating technology. In addition, the theory of codeposition is relevant even when individual metals are deposited, as the latter also contain codeposited metallic impurities; the problem of deposit purity is also partially an issue of alloy formation.

Alloy electrodeposition is technically a more complicated process as compared to the deposition of individual metals, as it requires a more stringent control of the composition of electrolyte and deposition conditions as well as closer monitoring of these parameters; it also poses additional problems owing to anode operation. As a consequence, development of a new process of alloy deposition is overall a more complicated research and development issue.

10.2 Applications of Electrodeposited Alloys

The scope for application of alloys electroplating is extremely diverse. At present, the following alloy types are most extensively used in engineering. These are classified according to their fields of application.

1. Protective-decorative. These include, in particular, Ni–Zn, Ni–Au, Ni–Cd, Ni–Sn, Au–Cu, Au–Ag, Cu–Sn.
2. Corrosion resistant: Zn–Cd, Zn–Sn, Cd–Sn, Cr–Ni, Cr–Re.
3. Soldered coatings: Sn–Pb, Sn–Bi, Sn–Sb, Sn–Ni, In- and Bi-based alloys.
4. Magnetic alloys: Ni–Co, Ni–Fe, Ni–Fe–Co, Co–W, Co–Pt, Fe–Pt.
5. Heat-resistant alloys: Cr–Mn, Cr–W, Cr–Mo, W–Fe.
6. Coatings replacing individual noble metals in electronics and jewelry: Pd–Ni, Au–Ni, Au–Co.

Y. D. Gamburg, G. Zangari, *Theory and Practice of Metal Electrodeposition,*
DOI 10.1007/978-1-4419-9669-5_10, © Springer Science+Business Media, LLC 2011

7. Antifriction alloys: Pb–Ag, In–Pb, Pb–Cu, Ag–Sn.
8. Adhesion coatings (supplying adhesion between metals and rubber): Cu–Zn.
9. Electric contact coatings: Ag–Sb, Ag–Pd, Au–Pd, Pd–Ni, Au–Ni, Au–Sb, Pd–In, Rh–In.

This list is far from complete and in the future will probably be extended both as a whole (new fields of application will appear) and within each field of application (new alloys).

Electrochemical alloys often feature properties and performance that are several times better than those of individual components even in comparison to metallurgical alloys. This is true in particular in regard to wear resistance, hardness, and corrosion stability.

At present, there are hundreds of alloys obtained using electrochemical methods. Most widespread are the alloys based on the metals of the iron group, the first group (Cu, Ag, Au), and noble metals.

10.3 Partial Polarization Curves for Alloy Components

10.3.1 Construction of Partial Curves

Alloy electrodeposition represents a particular case of the simultaneous occurrence of electrochemical processes within a definite potential range. In the case of alloy formation, these partial processes are rarely independent from each other. In many cases, a mutual influence of these processes is observed, though on the whole, their nature and kinetics in general remains unchanged as compared to individual deposition.

In studies of alloy electrodeposition, the most widespread experimental method is the extraction of partial polarization curves for each alloy component based on the analysis of deposits obtained at different potentials or current densities. The formation of binary (two-component) alloys is a relatively simple process, useful to understand the main features of such processes and the characteristics of the deposits obtained.

Figure 10.1 shows a typical $i_{ab}-E$ dependence, i_{ab} being the alloy deposition current density, and E the potential applied during electrochemical deposition of an alloy of two metals A and B; it is assumed that no parallel processes such as hydrogen evolution is occurring, or alternatively the current i_{ab} is already corrected for these processes, e.g. on the basis of the measurement of the evolved hydrogen volume or of electrochemical quartz crystal microbalance measurements.

The same figure shows the dependence of the deposit composition on the deposition potential (atomic fraction ω_a of component A). These data can be used to construct the i_j-E characteristics of the partial currents for each component, calculated on the basis of the Faraday's law. For this purpose, it is sufficient to find the following values for each potential E:

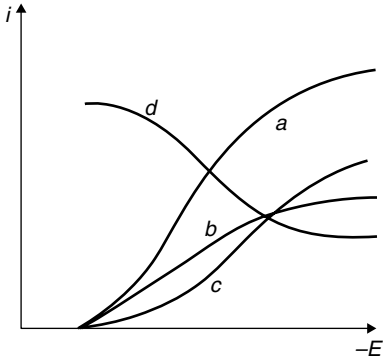

Fig. 10.1 (*a*) Overall polarization *curve* of alloy deposition; (*b*) partial *curve* for component A; (*c*) partial *curve* for component B; (*d*) dependence of the atomic fraction of component A on the potential

$$i_{\mathrm{a}} = i_{\mathrm{ab}} n_{\mathrm{a}} \omega_{\mathrm{a}} / (n_{\mathrm{a}} \omega_{\mathrm{a}} + n_{\mathrm{b}}(1 - \omega_{\mathrm{a}})), i_{\mathrm{b}} = i_{\mathrm{ab}} - i_{\mathrm{a}} \tag{10.1}$$

where n_j is the overall amount of transferred electrons per single atom of A or B.

In general, in the case a multicomponent alloy:

$$i_{\mathrm{j}} = i_{\mathrm{ab...n}} n_{\mathrm{j}} N_{\mathrm{j}} / \sum n_{\mathrm{j}} \omega_{\mathrm{j}} \tag{10.2}$$

The i_j/i_{ab} value is the partial current efficiency for component j.

The partial current plots thus constructed for A and B are also shown in Fig. 10.1.

The same calculations can be performed on the basis of composition data given as mass fractions N_m. In this case, it is expedient to first determine the **relative electrochemical equivalent of the alloy:** $\mathbf{K}_{ab} = \mathbf{K}_a \mathbf{K} q_b / (\mathbf{K}_a \omega_{mb} + \mathbf{K}_b \omega_{ma})$, where $\mathbf{M}_j$ are the electrochemical equivalents of the components. These equivalents, amounts of charge $Q = it$, and alloy deposit mass m_c can be used to find the current efficiency of alloy deposition:

$$CE_{ab} = m_{ab} F / Q \mathbf{K}_{ab} = i_{ab} / i, \tag{10.3}$$

where i is the overall current density.

The value of the partial current density of component A will then be found as:

$$i_a = \mathbf{K}_{ab} CE_{ab} i \omega_a / \mathbf{K}_a. \tag{10.4}$$

Of course, the end result remains the same.

The inverse problem of finding the overall current density on the basis of the partial values is trivial, as $i_{ab} = \Sigma_j i_j$ under the condition that all processes occur uniformly across the whole surface (i.e., none of them is localized at separate sites). The case of localization is considered for both the direct and inverse problems in Sect. 10.8.

10.3.2 Depolarization and Overpolarization

The presence of mutual interactions between the reduction processes of the single metals is demonstrated by the fact that the partial curves practically always differ

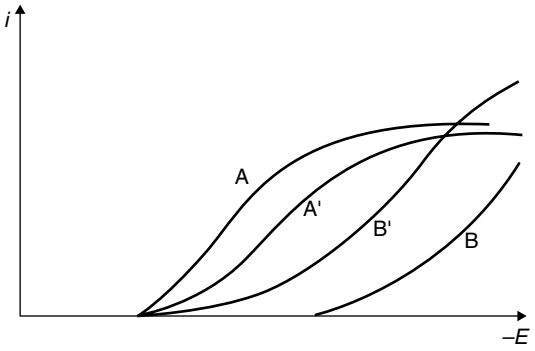

Fig. 10.2 Comparison between the partial current for alloy deposition and the total corrent in individual metal deposition for the alloy components *A* and *B*: element *A* exhibits overpolarization, while element *B* exhibits depolarization

from the corresponding curves obtained for the individual deposition of each of the components from a solution of the same composition, i.e. containing no ions of the other components; in these studies, the ionic strength of the solution is maintained constant by introducing additional non-discharging ions instead of the absent components. This adjustment is necessary to maintain the thermodynamic activity of the ions in the solution constant. If the partial curve is shifted in the negative direction as compared to the individual curve, then overpolarization of deposition of this alloy component is observed; in the opposite case, depolarization occurs.

For example, Fig. 10.2 shows the partial and individual curves for metals A and B. In the former case, overpolarization is observed, while in the latter case, depolarization occurs. The latter is a rather common case and it is observed, e.g., in the deposition of Zn–Ni, Cd–Cu, Tl–Pb alloys.

In this chapter, the letter A will always designate the more electropositive metal, while letter B corresponds to the more electronegative one.

The causes of depolarization and overpolarization are diverse. First, one must consider: (a) thermodynamic factors: variations in the activities of the components of the electrode material (the alloy) and of the interaction among ions in the solution; (b) surface-adsorption factors: variation in the surface charge value (or even its sign), formation of any films or layers on the surface, changes in the adsorption values (in particular, hydrogen) due to variation in the surface charge and composition; (c) kinetic factors: variation in the rate constants of electrochemical reactions due to variation in the properties of the substrate material.

10.4 Conditions for Alloy Formation

The potential window in which bulk deposit of any individual metal is formed at a sufficiently high rate, irrespective of the type of electrolyte and other conditions of deposition, usually does not exceed 0.2–0.3 V; for nobler metals such as Cu and Ag however this window may be much wider. For two metals to be deposited simultaneously with commensurable rates, it is necessary that the corresponding regions

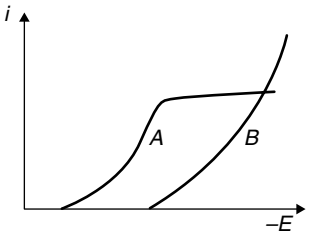

Fig. 10.3 Deposition of component *A* at the limiting diffusion current; the two *curves* represent the partial currents for components *A* and *B*

overlap. At the same time, the equilibrium potentials of different redox electrodes, corresponding to the potential window for deposition of the corresponding metals, may differ by 1 V and more. As a consequence, only few metal pairs feature sufficiently close redox potentials when deposited from solutions of their simple salts.

It follows thence that these regions must be brought closer when attempting to deposit an alloy consisting of components having widely different deposition potential regions. Usually the deposition region of the more positive of the two metals, i.e., A, is shifted in the negative direction. For this purpose, four main approaches are possible.

1. Deposition of component A at the limiting diffusion current (Fig. 10.3).

The potential required for the deposition of component B is reached by depleting the cathodic solution layer of ions of the component A, i.e., by generating a concentration polarization and simultaneously an dincrease in the charge transfer overpotential for A. Unfortunately, dendrites or powders are generally formed at the limiting current, and formation of bulk deposits is possible only under these conditions; in addition the fraction of element A incorporated in the alloy is limited by the concentration of A. In these conditions, dendritic growth may be avoided for example if the solution contains surface-active substances, able to inhibit such growth mode.

2. The simple addition of surface-active substances (SASs) may be sufficient to make alloy formation possible (Fig. 10.4).

In this case, it is required that SAS features selective inhibition with regard to A, affecting to a lesser degree the deposition kinetics of B. Effective inhibitors of the

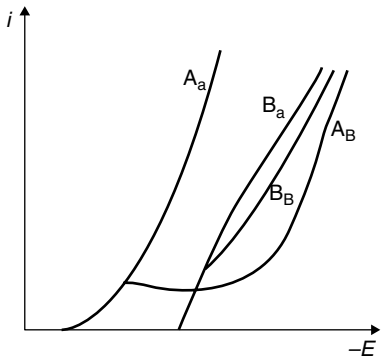

Fig. 10.4 Change in partial current *curves* for components *A* and *B* after introduction of SASs: the subscript (*a*) designates *curves* in the absence of SASs; subscript (*b*) *curves* in the presence of SASs

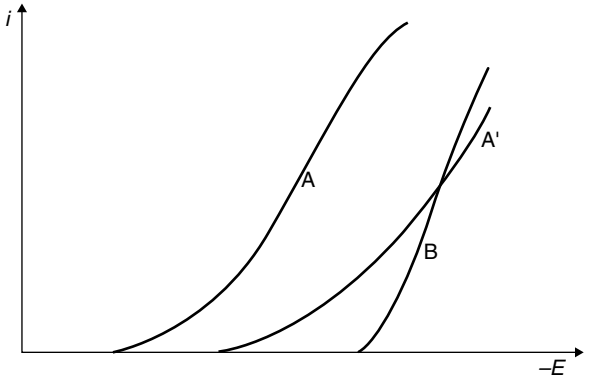

Fig. 10.5 Variation of the partial current *curve* of component *A* upon complex formation

cathodic process shift the region of potential of bulk deposit formation by hundreds of mV, which in many cases is sufficient for alloy deposition.

3. Complex formation between A (or both A and B) and ligands introduced into the solution (Fig. 10.5).

The most widely used ligands are cyanides, ammoniates, pyrophosphate, tripolyphosphates, aminoacetic and other organic acids, trilon B, gluconates, citrates etc. Complex compounds of the electropositive metals generally have high stability constants and feature higher polarizability, and consequently tend to draw the potentials of deposition of the two components closer. A comprehensive analysis of the codeposition process in presence of ligands forming the complexes with both metals [1] shows that alloys can be usually deposited if the ratio $z_B lg(\beta_A)/z_A lg(\beta_B)$ exceeds 1.5, where β_A and β_B are the stability constants of the corresponding complexes, z_B and z_A the electric charges of the aqueous ions.

4. Use of solutions concentrated in B but dilute in A.

The result achieved in this case is similar to the previous ones, but this approach is more limited as a shift in the potential by only 0.1–0.2 V requires dilution by approximately 2 orders of magnitude or more.

An increase in the temperature, mixing, nonsteady-state electric regimes, and other factors can also promote to a small extent alloy formation.

Finally, for some alloy systems a convergence of the deposition potentials of the two components can be the result of the alloy binding energy, i.e., purely thermodynamic factors. This important issue will be considered in detail in Sect. 10.9.

Thus, exploiting one of the above approaches or a combination of the same results in alloy formation at a certain potential E that can be expressed through the thermodynamic and kinetic parameters of both components:

$$E = E_0(\mathrm{A}) + (RT/n_\mathrm{a}F) ln\ a_\mathrm{a} + \eta_\mathrm{a} = E_0(\mathrm{B}) + (RT/n_\mathrm{b}F) ln\ a_\mathrm{b} + \eta_\mathrm{b} \tag{10.5}$$

where a_a and a_b are the actual activities of the electroactive ions in the electrode vicinity, E_0(A) and E_0(B) are the standard potentials of the corresponding redox electrodes, η_a and η_b are the total overpotentials of the two reduction processes.

It is in this form that the main condition for joint discharge of ions is usually written.

This relationship should be interpreted more in a symbolic form than as a guidance to actual calculations. In fact, the E_0 value in the case of alloy deposition is changed from the value for elemental deposition, since the activity of the given component in the alloy is not unity as in the case of a pure metal. The change in E_0 depends on the alloy composition, i.e., on the a priori unknown value of the partial currents at the potential E.

Furthermore, the a_j value may seem to affect the potential only to a small extent, as it enters only into the Nernst logarithmic term. In reality however, the overpotential η_j (both the concentration and charge transfer contributions) also depends directly on a_j.

Finally, without determining the η_j value, one cannot estimate the actual role of important factors such as complex formation, the inhibiting effect of SASs and the effect of the substrate.

Therefore, each alloy deposition system requires individual analysis of the kinetics of discharge of each component while accounting for all the characteristics of the cathode surface structure and composition, the double layer structure (including the sign of the surface charge), solution composition and concentration (including inhibitors), alloy formation energy and entropy.

10.5 Structure Types of Electrodeposited Alloys

In this section, with the generic term "structure" we designate both the surface morphology, which depends on the kinetics of deposition of each of the components, and the crystal structure, which in turn depends on the thermodynamic and kinetic conditions of the deposition process.

Alloys can be single-phase or multiphase, i.e., they may consist of one or several solid phases. In the following we disregard amalgams or liquid alloys. A phase is interpreted as a homogeneous fraction of the alloy volume; different phases correspond to materials with a different chemical composition and/or different crystal lattices; for example, cubic cobalt and hexagonal cobalt are two different phases with the same composition. It should be noted that a phase transition is possible between different phases, both during or after deposition.

Several main types of alloys are distinguished:

1. Alloys of the solid solution type (substitutional or interstitial).

In a substitutional solid solution, a fraction of the solvent metal atoms in the crystal lattice is substituted by the atoms of the dissolved component; in an interstitial solution, the dissolved atoms occupy the interstitial sites accessible between the lattice sites of the former. Thus, these alloys exhibit a crystal lattice close to the lattice of the main component, designated as the solvent; more precisely, the lattice type is the same, but the interplanar distances d may be changed.

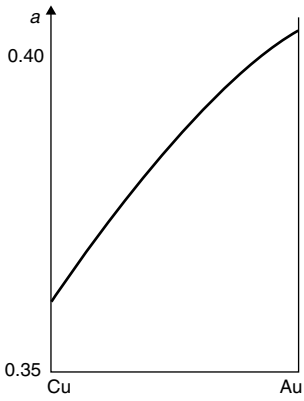

Fig. 10.6 Vegard's law for the gold–copper alloy

The change in d can be used to assess the fraction N of the dissolved component; a linear dependence between d and N is usually observed; this relationship is called Vegard's law.

The Vegard's law consists in the fact that $\Delta d = \omega(d_a - d_b)$, where d_a and d_b are the interplanar distances or lattice constants of the components, and Δd is the change in the interplanar distance (or lattice constant) as a result of solid solution formation; ω is the molar fraction of the dissolved component (Fig. 10.6). In this exact form, the law is observed quite rarely; more often, the effect of the dissolved component is stronger, leading to a faster variation of lattice constant with composition. However the linear dependence on ω, or on the percentage of the dissolved component

$$(\Delta d/d)_{\mathrm{a}} = kC_{\mathrm{b}} \tag{10.6}$$

is often valid in the alloy solubility region. In the case of a hexagonal lattice, the ratio of the two lattice constants a/c also changes as a result of solid solution formation and deviates from the ideal value of 1.633.

Solid solution formation is rather typical for electrochemically deposited alloys. Bulk alloys obtained through a metallurgical route also form solid solutions, but usually, the solubility of one of the components in the other at room temperature is rather low (about 1% or less) and becomes significant only under vigorous heating. High solubility is often observed in the cases when the two components have homotypic lattices with the lattice constants differing by not more than 15%. Some systems form a continuous series of solid solutions in a wide range of concentrations.

In electrodeposition from aqueous solutions, metastable supersaturated solid solutions with a concentration of the dissolved component above 10% and higher, are often formed. Supersaturated solid solutions often consist of very small crystals and may be decomposed under heating.

2. Alloys of the intermetallic compound type (intermetallics).

The crystal lattice of such alloys differs from the lattices of the individual components. This is easily determined with the help of X-ray analysis. A variety of intermetallic compounds, usually having a definite chemical formula of the A_xB_y type,

has been observed and studied. Their X-ray characteristics, including interplanar distances and relative reflection intensities, are tabulated and therefore identification of such compound presents no particular problem. These alloys are single-phase, i.e., they consist of homotypic crystals (grains). The properties of these structures can differ significantly from the properties of the individual components.

True intermetallic phases closely resemble chemical compounds as they feature an ordered structure with a very narrow compositional spread, i.e., they allow only small deviations from stoichiometry. Some intermetallic phases on the other hand may be observed within a limited compositional range, differing from the stoichiometric one. The range of stability of intermetallic phases depends on the variation of their free energy with composition, which is in turn a function of the solid state properties of the single components.

A more general case consists in "intermediate phases" ordered only in the low temperature region. These phases are also designated as electronic compounds, since they are formed when the ratio of the number of valence electrons to the number of atoms (e/a) is close to 1.5 (the Hume-Rothery's rule). To be more precise, at a value of $e/a = 3/2$, the β-phase with a body-centered cubic (BCC) lattice is formed; at $e/a = 21/13$, the γ-phase with a complex cubic lattice is formed; at $e/a = 7/4$, the ε-phase with a hexagonal close-packed (HCP) lattice is obtained. It is of interest to note that the ε-phases are characterized by an abnormally low overpotential of hydrogen evolution, so that the current efficiency of alloy formation decreases in the potential region corresponding to their formation.

All these compounds feature rather wide homogeneity regions, i.e., they are compounds of variable composition. These can be considered as solid solutions based on intermetallic structures, or rather, solutions of the component that is in excess compared to the stoichiometric composition. The homogeneity region in the case of metallurgical intermetallics corresponds to an e/a range varying from 1.3 to 1.9. Nonequilibrium (metastable) intermetallics can however be formed in electrocrystallization, widening the above range.

3. Alloys of the mechanical mixture type. These alloys resemble metallurgical alloys of the eutectic type and consist of small randomly mixed crystals of the two elemental phases. Such grains can generally be characterized by their form (equiaxial, oblong, lamellar) and size (average transverse size and dispersion or size distribution function). Crystals of each phase can have their distinct form and size distribution. Sometimes, e.g., the second phase can form small crystals localized at the interfaces of larger crystals of the first phase.

Alloys of the mechanical mixture type usually imply two-phase systems of the individual components, i.e., each small crystal represents metal A or B with its corresponding crystal lattice. Very often, one of the phases is in fact a solid solution of the second component, usually that of the more electronegative one in the more electropositive one. The grain boundary regions exhibit different features from either element and can be thought of as the third alloy component. Their structure and relative fraction of interfacial atoms determine to a considerable degree the properties of the deposit.

4. A limiting case of solid solution formation consists in the alloys of amorphous type; these are usually formed at high overpotentials and are characterized by the presence of short range ordering with an absence of long range ordering, i.e., their atomic configuration resembles that of a frozen liquid.

The structure of amorphous alloys, as opposed to alloys of types 1–3, cannot be characterized by grain shape and size, since—due to their lack of long range ordering—no grain boundaries can strictly be defined. The lack of long range order on the other hand determines to a large extent their properties; for example, amorphous alloys are often very hard due to the absence of dislocations, are highly corrosion-resistant due to the lack of grain boundaries, etc. Amorphous alloys are often formed upon codeposition of nonmetallic components, which, due to the difference in atomic size, act as amorphizing additives. Their role probably consists in inhibiting separate crystallization of the other alloy component and in causing a drastic decrease in the rate of diffusion processes which would result in ordering.

A transitional case between the crystalline and amorphous alloy type is the nanocrystalline alloy. In this case grains are formed, but their small size, typically in the sub-100 nm region, renders them difficult to distinguish from truly amorphous alloys. In these alloys a large fraction of the atoms is located at grain boundaries, and the characteristics of the latter determine to a large extent the properties of the entire alloy.

5. Alongside with these principal types, alloys of mixed character can be formed; these may simultaneously contain several different phases, e.g., a solid solution based on one of the components plus an intermetallic phase, different intermetallics, or solid solutions, etc. Such alloys are called multiphase and sometimes may be also classified as mechanical mixtures.

10.6 Phase Diagrams of Alloys

The various structures observed in binary alloys have been thoroughly studied and phase (equilibrium) diagrams have been constructed for thousands of systems; the availability of such phase diagrams strongly facilitates studies of alloy deposition. A phase diagram is constructed as follows. At each given temperature, “phase regions” are specified corresponding to the thermodynamic equilibrium states of the alloy of each composition, varying from the pure component A to pure B. Bulk phase diagrams are calculated or determined experimentally for equilibrium configurations; on the other hand electrodeposited alloys are obtained under non-equilibrium conditions. Equilibrium phase diagram therefore provide useful information to hypothesize the phases obtained in electroplated alloys, but do not predict exactly the phases observed. Fig. 10.7 for instance compares the equilibrium phase regions observed at room temperature in the bulk copper-tin system and those observed in the electroplated alloy; both include regions of solid solutions, intermetallic, and phase mixtures but the compositional phase boundaries are not the same.

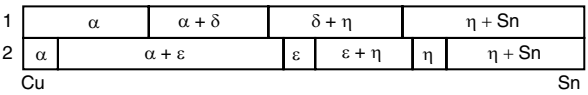

Fig. 10.7 Phase regions observed for the copper–tin alloy. (*1*) Electrolytic deposit; (*2*) equilibrium at 100°

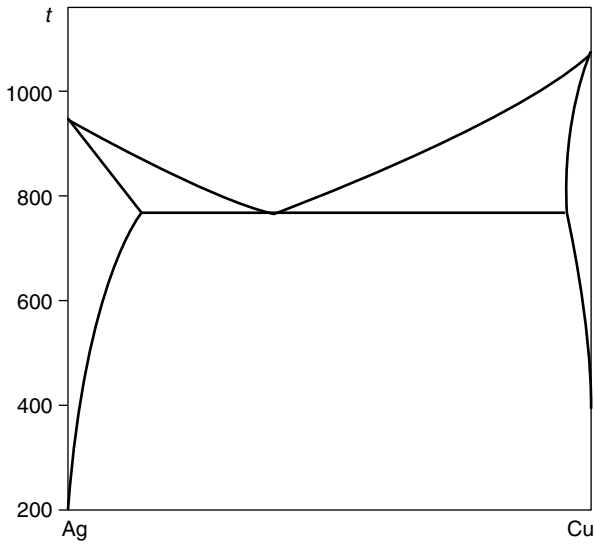

Fig. 10.8 Equilibrium phase diagram for the copper–silver alloy. The *upper* region represents the melt; at *intermediate* regions two solid solutions are present whose range of stability decreases with temperature; finally, at low temperature a mechanical mixture of the elements is stable

Upon an increase in temperature in the bulk diagram, the width of the equilibrium phase regions changes, some of them disappear, and also new ("high-temperature phases") ones may become stable. Starting from a certain temperature, a liquid phase regions appears, which under further heating extends to all alloy compositions. For example, Fig. 10.8 shows a phase diagram for the Ag–Cu alloy.

Equilibrium phase diagrams of binary alloys are widely used in metallurgy, where they are classified in detail; six principal types of diagrams are usually distinguished. A rigorous discussion of these diagrams however is beyond the scope of this book; in fact, in alloy electrodeposition it is usually sufficient to consider only the low-temperature part of the diagram, i.e., the set of phase regions of the type presented in Fig. 10.7. The high-temperature part of the diagrams is only of interest in cases when thermal treatment of the alloys is performed after electrodeposition.

The observed structure of some electrolytic alloys agrees well with equilibrium diagrams, either directly in the as-deposited form, and sometimes after aging but without thermal treatment. These alloys include, in particular, Cu–Zn, Fe–Ni, Ag–Au, Sn–Zn, Co–Ni.

In many cases however, alloys formed by electrocrystallization exhibit a structure that does not agree with the bulk phase diagrams; for example intermetallics, supersaturated solid solutions, high-temperature phases not described in the literature may be formed. Besides, phase regions may appear shifted as compared to

the equilibrium diagram (Fig. 10.7, 1 and 2). This is largely due to the film being formed under non-equilibrium conditions and from solutions and substrates which may show strong inhomogeneities; in addition, the formation of certain phases may be favored as a consequence of characteristic features of the nucleation and growth processes.

For this reason, electrolytic alloys of the same chemical composition obtained under different electrochemical conditions (overpotential, presence of SASs, temperature, mixing, etc) may feature different phase structure and therefore may differ drastically in physical, physico-chemical properties, corrosion stability in different media and performance characteristics such as wear resistance, microhardness, abrasiveness. An example of this is the Zn–Ni alloy system, known to form at least 5 different phases.

10.7 Alloys of the Mechanical Mixture Type

This type of alloys includes Sn–Pb, Cd–Zn, Zn–Sn, Ag–Pb, Cu–Pb, Au–Cu. They are formed in cases when the separate nucleation of both metals is favored, as each crystal grain is formed starting from a single or several nuclei.

Some of these alloys correspond to equilibrium phase diagrams, but sometimes mechanical mixtures may be obtained also in cases when the solid solution would be the equilibrium structure.

In the electrodeposition of such alloys, the substrate surface at each given time consists of two types of sites, whereby metal A is deposited on its own surface and the same happens for metal B. In reality, there is the possibility of the two processes of metal deposition to occur on the foreign surface, when the first layer of metal A can be formed after nucleation (of a monolayer or an array of single layers) on the surface of a grain of metal B or vice versa; this is in fact a necessary condition for the formation of a polycrystalline structure, as otherwise the deposit would consist of an assembly of intergrown columnar single crystals.

However, if the grain dimensions are not too small, then a large fraction of the material of each grain (i.e., the whole volume with the exclusion of a fraction of the grain boundaries) is formed by deposition on its own substrate. Therefore, with a good approximation each metal is deposited on its own substrate. In this case, the main factor that must be taken into account is that each reduction process occurs not across the whole surface but only on a surface region with an area corresponding to the bulk fraction of the given metal in the alloy:

$$S_{\mathrm{j}} = \omega_{\mathrm{j}} v_{\mathrm{j}} / \sum \omega_{\mathrm{j}} v_{\mathrm{j}} \tag{10.7}$$

where v_j is the volume of one mole of the component i.

Therefore, the fraction of the overall current density provided by the discharge of metal A is $i_a S_a$ and the overall current density i at the given potential E in the case of a binary alloy of the mechanical mixture type is:

$$i_{ab} = S_a i_a + S_{\mathrm{b}} i_b \tag{10.8}$$

Local current densities of deposition for each of the components i_a and i_b are, in general, different. The question arises whether these current densities differ from the corresponding current densities observed during the individual deposition of each component at the same potential E; in other words, whether the kinetics of each process is changed as compared to the deposition of an individual metal.

The answer to this question in each particular case is provided by comparison of the partial i_j–E curves with the individual curves. However, one must take into account that separation of the curve into partial ones as described in the procedure in Sect. 10.2 does not account for the surface fractions S_j; it was assumed in fact that each process would occur on the whole surface. Thence, in the case of a mechanical mixture, one must multiply the calculated i_j values by the volume (or, which is the same, surface) fraction of the corresponding component. This results in the following formulas instead of (10.4) and (10.2):

$$i_a = \mathbf{K}_{ab} C E_{ab} (\omega_a \rho_b + \omega_b \rho_a) / \mathbf{K}_a \rho_b. \tag{10.9}$$

$$i_a = i_{ab} n_a (\omega_a v_a + \omega_b v_b) / [v_a (\omega_a n_a + \omega_b n_b)] \tag{10.10}$$

where ρ_j are the densities of the components, v_j are their atomic volumes.

It is necessary to take into account that even if the kinetics of charge transfer are unchanged, the partial curve may differ from the individual one due to variation of the diffusion-migration mode of ion transport to the surface. In fact, for each individual process in the case of a mechanical mixture, the electrode functions as if it were partly blocked, which can result in a change in the concentration overpotential depending on the blocking degree, i.e., again, on the ratio of the areas of grains of A and B. To our knowledge, this problem has not been quantitatively solved yet.

Only after accounting for all the above factors, one can discuss other possible causes for discrepancy between the partial and individual curves, such as the role of the double layer structure, electrolyte composition, etc.

The dimensions of the crystallites of A and B are largely determined by the probability of formation of nuclei of metal A on the surface of metal B (and vice versa) at the working potential E. Therefore, if information on the nucleation of A and B under these conditions is available, one could predict the character of the deposit structure. One the other hand, based on grain size data, one can in principle derive data on nucleation. One of the possible methods for the solution of such problem is presented in Sect. 6.9.

10.8 Alloys of the Solid Solution Type

10.8.1 Underpotential Metal Deposition and Cathodic Metal Intercalation into a Foreign Substrate

Consider an electrolyte containing ions of components A and B. If the electrode potential is more negative than the equilibrium potential of component A, nucleation of this component and growth of nuclei of A becomes possible. Similar processes for component B are possible only for potentials negative to its equilibrium poten-

tial in the same solution. However, it is possible that the discharge of B may start in the absence of overpotential, i.e., at or above its equilibrium potential, right after the deposition of component A occurs. This results in atoms of B intercalating into the crystal lattice of A, without nucleation of B being necessary.

The equilibrium potential of B, E^0_B, is established upon the contact between ions of B and the metallic phase B, i.e., this potential corresponds to the presence of the bulk phase of B, or at least several monolayers of B. However, a monolayer, or a fraction of monolayer, of B on a foreign substrate may be in thermodynamic equilibrium with the same solution even at potentials more positive than E^0_B. This is indeed observed experimentally. Thus, atoms of B can be incorporated into the lattice of A forming a solid solution (possibly metastable) even under potential positive to the equilibrium potential of B.

Formation of adsorbed atoms (adatoms) of the metal on a foreign (inert) substrate of a more electropositive metal (i.e. adatoms of B on the surface of A) at potentials positive to those at which deposition of this phase, i.e., at least several monolayers of metal B, becomes possible is called *underpotential metal deposition*. Formation of the first monolayer may be possible at potentials 0.3–0.5 V positive of the equilibrium potential.

This phenomenon is usually studied by contacting metal A and a solution containing only ions of B, i.e., when no electrochemical reduction of A is possible.

So far, a large amount of experimental information on underpotential deposition has been accumulated. These data have been obtained mainly using the method of cyclic voltammetry, that consists in recording the current during direct and reverse potential sweep in the range where formation or dissolution of adatoms is the only or the main faradaic process. In Fig. 10.9 for example, at least two current peaks are observed in the anodic branch of the curve. The one pertinent to the equilibrium potential corresponds to metal phase dissolution, while those shifted in the positive direction stand for dissolution (more precisely, desorption) of adatoms.

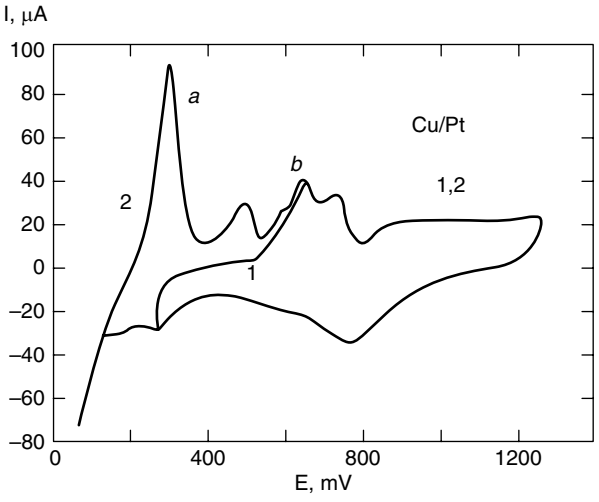

Fig. 10.9 Cyclic voltammetry *curves* for copper adsorption and desorption from a 0.01 M $CuSO_4$ + 0.5 M H_2SO_4 on polycrystalline platinum (A.I. Danilov, E.B. Molodkina, private communication). (*1*) Cycling limited to potential positive with respect to E_{eq} of copper; (*2*) cycling with copper phase formation. (*a*) copper dissolution peak; (*b*) desorption peaks of various types of adatoms. I in μA, E in mV vs. SHE

A positive shift in the maximum of the reduction peak as compared to the equilibrium potential quantifies the depolarization in the case of adatom formation, i.e., a change in the electrochemical potential of the reducing species under adsorption, while the area under the peak corresponds to the overall charge value. This area is proportional to the amount of adatoms and degree of charge transfer upon adsorption.

It has been found that the shift in potential approximately corresponds to half the difference in the electron work functions of metals A and B [2]. Qualitatively, but not quantitatively, this is explained by the effect of the electron work function on the energy of adsorption.

When the solution contains both components A and B, then the underpotential deposition of B occurs simultaneously with normal deposition of A, as a result of which an alloy is formed. In this case, a high solubility of B in A may be favored by a high overpotential for the deposition of A, providing a large driving force for the reduction of A atoms, or by kinetic factors, such as the non-equilibrium trapping of adatoms of B by the growing deposit of A, the presence of steps and kinks on the surface, and also an enhanced concentration of vacancies in the lattice of the solvent metal and a high fraction of grain boundaries in the overall volume. A correlation has also been found between the surface coverage by adatoms and content of B in the deposit [3].

Diffusion and intercalation of atoms of B into a defect lattice of A can occur simultaneously [4], especially at the stage of nucleation and growth of clusters of A, which contain more defects than a bulk metal. Under these conditions, a solid solution can be formed even for a very low equilibrium solubility; this is called a supersaturated solid solution. The process above does not always occur. For example, no diffusion processes were observed in the case of underpotential deposition of Cu with Pt or Pd.

The effect of cathodic intercalation of discharged metal ions into a foreign substrate with formation of a solid solution or an intermetallic [5] is by its nature similar to metal hydrogenation and also to the formation of amalgams during metal discharge on a mercury drop electrode. The first stage of the intercalation process is the formation of adatoms on the surface; the second one is diffusion into the cathode material according to the vacancy mechanism.

Studies of adatom layers performed in situ using the scanning tunneling microscopy method have shown that these layers may show an ordered structure. In addition, atom exchange with formation of a surface alloy is possible between the adsorbate atoms and substrate atoms.

10.8.2 Formation of Solid Solutions

Solid solutions based on the more electropositive component A are formed according to the mechanism discussed above.

Solid solutions are observed, e.g., in deposits of Fe–Ni, Fe–Co, Cu–Ni alloys, a number of copper and silver alloys with low melting point metals, and with certain alloys based on noble metals.

Formation of supersaturated solid solutions has been observed during deposition of copper alloys (component A) with tin, lead, thallium, bismuth, and cadmium, silver with lead, bismuth, and thallium, nickel with palladium and bismuth.

If formation of a solid solution is accompanied by strong lattice distortions requiring significant energy input, the probability of deposition of a separate phase of B increases, even if the solid solution is the thermodynamic equilibrium configuration. Copper with silver is deposited in the form of a mixture of crystals, instead of a solid solution; this behavior is in agreement with the equilibrium diagram.

Simultaneous deposition of two phases is also possible: often these two phases consist respectively in a solid solution and in a precipitate of the pure electronegative component. This case is observed at sufficiently high overpotentials, when component B exceeds the energy of distortion of the lattice of A (divided by nF), this providing the condition for formation of a separate phase B alongside with a supersaturated solid solution.

Formation of a separate phase of component B also enables the formation of a solid solution based on B, i.e. a more electronegative phase. Such a possibility can be realized if discharge of A on the surface of B is more probable than on its own substrate. Here, both the mixing energy and the zero-charge potentials can play an important role. For example, a solid solution of silver (component A) in copper has been obtained in the presence of alpha-naphthol and gelatine. It is not improbable that this is due to the opposite surface charge of the electrode fractions made of copper and silver, as a result of which adsorption of SASs on these surfaces may be different.

In general, SAS additives may affect the phase structure of alloys in different ways. This depends above all on the relative adsorption energies of this SAS on metals A and B, i.e., on the selectivity of its effect.

The grain size of deposits of the solid solution type depends on the alloy composition and usually decrease with an increase in the dissolved component concentration. Supersaturated solutions are especially highly dispersed.

Under thermal treatment of supersaturated solid solutions, these may be decomposed forming the dissolved component phase.

10.9 Intermetallic Compounds and Amorphous Alloys

Similarly to solid solutions, both equilibrium and metastable intermetallic compounds can be formed by electrodeposition.

Examples of electrodeposited intermetallics are: CuZn, Cu_5Sn, AgZn, AgCd, NiIn, PdIn (β-phases); Cu_5Zn_8, $Cu_{31}Sn_8$, Mn_5Zn_{21}, Co_5Zn_{21}, Ni_5Zn_{21}, Pd_5Zn_{21} (γ-phases); $CuZn_3$, Cu_3Sn, $AgCd_3$ (ε-phases). Intermetallics are also formed in the following systems: Cu–In, Ag–In, Cu–Cd, Mn–In, Au–Zn, Au–Cd, Au–Cu.

Formation of intermetallic compounds formed by iron group,metals such as Cu–Pd or Ni–Sn has also been observed. These compounds can be decomposed under heating, e.g., NiSn is decomposed at 250° to Ni_3Sn_2 and Ni_3Sn_4, which correspond to the equilibrium phase diagram.

The causes promoting formation of intermetallic compounds have so far been little studied. It is likely that their appearance, at least in certain cases, is due to diffusion processes resulting in the ordering of an initially formed highly supersaturated solution, since the "electron compound" thus formed is characterized by a lower free energy. Formation of intermetallics can possibly be interpreted also as a result of fast decomposition of a supersaturated solution.

In such cases, the main criterion for formation of an intermetallic phase is that the partial deposition rates of A and B, i.e., i_a and i_b roughly correspond to the stoichiometric formula of one of the above alloys. Besides, if an intermetallic compound is metastable, a sufficiently high overpotential is required to provide the necessary driving force. A special role can also be played by the specific surface energy value, which depends on the composition of the alloy surface layer and on the electrode potential applied during deposition; this affects directly the diffusion mobility of adatoms. Underpotential deposition and intercalation of component B into the lattice of A may also be an important process in the formation of intermetallic compounds.

Electrodeposited intermetallics are usually characterized by enhanced hardness at low ductility and also, when they contain iron group metals, special magnetic properties (e.g., enhanced coercive force).

In general, the formation of metastable phases by alloy electrodeposition is promoted by high overpotential, as a cause of deposition from complex electrolytes or adsorption of SASs.

Amorphous alloy deposits are usually formed when the atomic fraction of the codeposited component is sufficiently high (at least 15%), the atomic radii of the components differ significantly (by more than 15%) and besides, amorphizing additives (boron, phosphorus, sulfur, oxides, hydroxides, hydrides) are codeposited in parallel with the metal ions. Quite characteristic is the formation of amorphous alloys upon codeposition of refractory components (e.g., tungsten), that is also accompanied by inclusion of nonmetallic atoms.

At room temperature, amorphous alloys can be stable indefinitely, but an increase in the temperature results in their transformation into an equilibrium crystal form with precipitation of various borides, phosphides, sulfides, or oxides, depending on the alloy composition.

Usually the surface of a growing solid solution, intermetallic compound, or amorphous alloy is homogeneous, i.e., the sites where discharge of the components occurs are mixed randomly at the micro scale and are constantly change over time. It follows therefore that the calculation of the partial current densities in the above cases must be performed per total surface, without separating the fractions of the components.

10.10 Equilibrium and Steady-State Potentials of Alloys

The formation of a solid solution or of an intermetallic compound involves a change in the free energy of components A and B due to a gain in the heat of mixing and in the entropy of mixing; consequently, it results in a shift of the equilibrium potentials

of the components in the positive direction by $\Delta\Phi_j/zF$, where the partial free energy values $\Delta\Phi_j$ can be found from the following thermodynamic relation:

$$\Delta\Phi_j = RT\ ln\ \omega_j - (1-\omega_j)^2 E_{mix} \tag{10.11}$$

Here, E_{mix} is the integral heat of mixing, and ω_j is the molar fraction of the component j in the alloy. The E_{mix} values have been measured using different methods for a large number of systems. The term $RT \ln \omega_j$ accounts for an increase in configurational entropy due to the formation of a random alloy.

Another form of the relationship (10.11) is as follows:

$$\Delta\Phi_j = RT\ ln\ \omega_j - (1-\omega_j)^2 E^*_{mix} \tag{10.12}$$

where E^*_{mix} stays for $E_{mix}\omega_j(1-\omega_j)=E_{mix}\omega_A\omega_B$.

It is of interest to find out how the equilibrium potentials of the components change as a result of mixing. As follows from Eq. (10.11), the shift in the equilibrium potential of component A is:

$$\Delta E^A{}_{eq} = (RT/z_aF)\ \ln\omega_a - [(1-\omega_a)^2/z_aF]E_{mix}, \tag{10.13}$$

and in the case of component B, it is:

$$\Delta E^B{}_{eq} = (RT/z_bF)\ln\omega_b - [(1-\omega_b)^2/z_bF]\ E_{mix}, \tag{10.14}$$

The condition for the two equilibrium potentials to become closer is $\Delta E_a < \Delta E_b$, i.e., (assuming $z_A = z_B$):

$$RT\ ln\ (\omega_a/\omega_b) < (\omega_a - \omega_b)E_{mix}, \tag{10.15}$$

This condition is satisfied for a sufficiently low concentrations of the more electronegative component B. Thus, a significant convergence of the equilibrium potentials as a consequence of alloy formation occurs only under formation of dilute solutions of B in A.

The maximum convergence of potentials is reached for $\omega_b \to 0$. In the case of the content of B being 0.1%, it becomes 75 mV due to the entropy factor and 100 mV due to the energy factor, assuming a typical energy of mixing of 10 kJ/mol.

When the alloy is in contact with a solution of a definite composition, in general, no equilibrium is achieved. Only a particular choice of the solution composition can lead to equilibrium for both components. This statement is of course valid for both solid solutions, intermetallics and mechanical mixtures. Therefore, in the absence of an external current, a mixed potential is established, whereby one of the component dissolves selectively while the second one is deposited and can also intercalate into the foreign lattice. As a consequence, the alloy surface composition is changed, resulting eventually in the achievement of an equilibrium at a certain potential.

The dependence of the established potential on alloy composition is related to the actual phase diagram of the alloy, so that it is possible in general to infer the al-

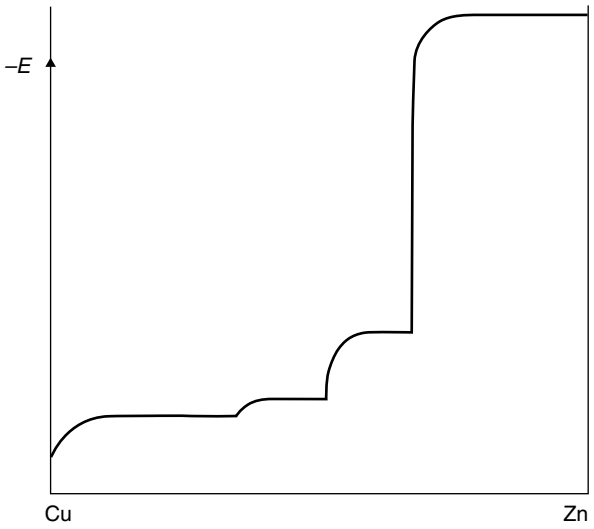

Fig. 10.10 Dependence of the steady-state potential on the alloy composition for the copper–zinc alloy system

loy phase configuration on the basis of measurements of the steady-state potentials. As a rule, the following regularities are observed:

1. In a range where mechanical mixtures of A and B, B and a solid solution, B and an intermetallic, or two intermetallics are observed, the potential is practically independent of the alloy composition and is determined by the potential of B.

2. In the region of stability of solid solutions, the steady-state potential changes gradually upon variation of the alloy composition. In the case of formation of an intermetallic on the other hand, a stepwise variation of potential occurs (usually, by tens of mV).

Figure 10.10 shows as an example of the dependence of the steady-state potential on alloy composition for the Cu–Zn system.

Thus, measurements of steady-state potentials can yield additional information to the results of direct microscopic and X-ray diffraction studies of the structure of deposits of alloys of different composition. At the same time, it is expedient to compare the data on the composition of alloys with the results of measurements of their structurally sensitive properties such as hardness, specific conductivity, etc.

10.11 Accounting for the Energy of Alloy Formation in Calculations of Potentials of Alloy Deposition

Equation (10.11) allows computation of the shift in equilibrium potentials only for a given alloy composition. If on the other hand the deposition potential is provided and characteristic i–E curves for the individual components are known, then one cannot state a priori the actual composition of the deposited alloy.

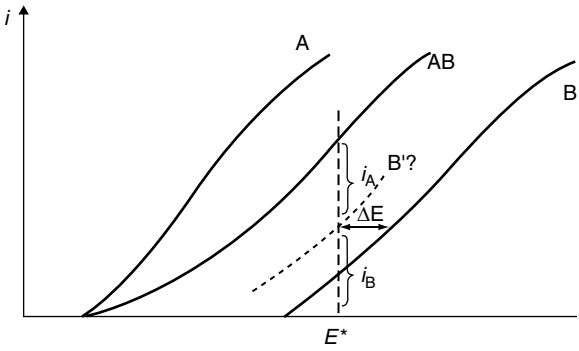

Fig. 10.11 Possible determination of alloy composition based on the current-potential *curves* for the individual components. *Solid lines* correspond to the *curves* of separate deposition of the components. *Dashed lines* correspond to the hypothetical partial *curve*

This situation is shown in Fig. 10.11. Let us determine the composition of the alloy deposited at the potential E^*. It is clear that for this purpose, one must construct the actual partial i_j–E curves for the components during alloy deposition. But the values of their shifts as compared to the known individual curves depend on the alloy composition, i.e., on the actual ratio of the deposition rates i_a and i_b at the potential E^*. Therefore, the problem turns out to be indeterminate.

Nevertheless, the solution can be found under the additional assumption that Eq. (10.11) determines not only the shift in the equilibrium potentials, but also the parallel translation of the whole partial curve [6]. Then if the partial current densities of codeposition of A and B at potential E^* are i_a and i_b, these values determine uniquely ω_a, the molar fraction of A, as

$$\omega_a = \mathbf{K}_a i_a/(\mathbf{K}_a i_a + \mathbf{K}_b i_b) \tag{10.16}$$

where k are the electrochemical equivalents of the components.

In turn, according to (10.11), the ω_a value determines the shifts in the potentials $\Delta E_a(\omega) = \Delta E_a(i_a, i_b)$ and $\Delta E_b(\omega) = \Delta E_b(i_a, i_b)$, which allows calculation of the potentials corresponding to the separate deposition of the components at the same current densities i_a and i_b: $E_a = E^* + \Delta E_a(i_a, i_b)$ and $E_b = E^* + \Delta E_b(i_a, i_b)$.

Denoting the known polarization curves for the separate deposition of the components as $E = f_a(i)$ and $E = f_b(i)$, we obtain:

$$E^* + \Delta E_a(i_a, i_b) = f_a(i_a) \tag{10.17}$$

$$E^* + \Delta E_b(i_a, i_b) = f_b(i_b) \tag{10.18}$$

The nature of the results just obtained is exemplified in Fig. 10.12. More detailed calculations allow additionally the identification of the following regularities:

1. Already at $E_{mix} = 0$, the composition of the deposited alloy differs significantly from that corresponding to the separate deposition of the components (dashed line in the figure) and depends more weakly on potential. This is due to the role of the entropic contribution in (10.11).

2. In all cases, deposition of both components starts simultaneously. Pure A is not deposited. Even at $E_{mix} = 0$, deposition of A and B starts simultaneously, i.e., at $E = E_a^0$, and at $E = E_b^0$, its content in the alloys is already rather high.

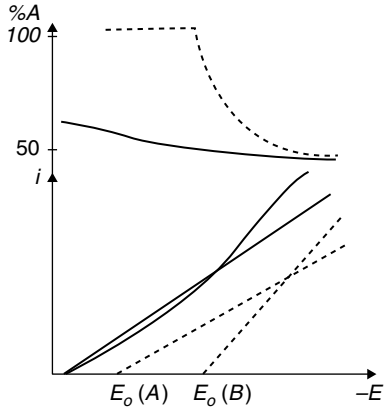

Fig. 10.12 Calculated partial *curves* (*A′*, *B′*) and dependence of the alloy composition (*I*) on the deposition potential. The *dashed line* corresponds to the individual deposition of *A* and *B*

3. In the case of $E_{mix}>0$, deposition of both components also starts simultaneously, but at a potential value positive to E_a^0. The shift in the new "equilibrium" potential as compared to E_a^0 is of the order of tens of mV.

4. For a sufficiently high enthalpy of mixing, one can achieve a situation (curve 1 in Fig. 10.12), when the alloy composition remains practically unchanged in a wide range of potentials.

It should be stressed that the assumption of a parallel translation of the partial polarization curves in the case of alloy formation is arbitrary. Indeed, the kinetics of elemental discharge on the alloy surface should change; e.g., the transfer coefficient may vary. However, conclusions 1–4 altogether retain their importance.

10.12 Nucleation and Growth of Metal Clusters on a Foreign Substrate upon Electrodeposition of an Alloy of the Mechanical Mixture Type

Let the frequencies of nucleation of A and B on the surfaces of B and A, respectively, be J_a and J_b. This means that J_bS_a nuclei of phase A are formed per unit time (s) on the surface of phase B with area S_a and J_aS_b nuclei of phase B are formed per unit time on the surface of phase A with area S_b. Consequently, the overall amount of crystallites of A per unit area (1 cm^2) in the time t is:

$$n_a = J_aS_bt \tag{10.19}$$

and the amount of crystals of B is

$$n_b = J_bS_at \tag{10.20}$$

The overall deposit mass over 1 cm^2 in this time is

$$m = QA/nf = ItA/nF \tag{10.21}$$

where A is the average atomic mass. The overall deposit volume in this time (per 1 cm^2) is

$$V = itA/nF = itV_{at}/nF, \tag{10.22}$$

where V_{at} is the average atomic volume of the alloy.

At the same time, the fraction of metal A in this volume is equal to surface fraction S_a, i.e., the volume of all crystallites of A is

$$V_a = itS_aV_{at}/nF, \tag{10.23}$$

Similarly, the volume of crystallites of B is

$$V_b = itS_bV_{at}/nF. \tag{10.24}$$

Consequently, the volume of a single crystallite of A is

$$v_{1a} = V_a/n_a = iV_{at}/J_anF \tag{10.25}$$

and the volume of a single crystallite of B is

$$v_{1b} = V_b/n_b = iV_{at}/J_bnF \tag{10.26}$$

Thence, it follows that the ratio of the diameters of the A and B grains is $(J_a/J_b)^{1/3}$. Besides, the data of the formula allow computation of the corresponding nucleation rates J_a and J_b:

$$J_a = IV_{at}/nFv_{1a}, \tag{10.27}$$

$$J_b = IV_{at}/nFv_{1b}, \tag{10.28}$$

For example, when I=0.1 A/cm^2, n=1 and V_{at}=10 cm^3/mol, v_{1a}=10^{-12} cm^3 (the particle size is about 1 μm), we obtain J_a=10^6 cm^{-2} s^{-1}.

This means that under certain conditions, on the average, a single nucleus of metal A is formed each millisecond on the electrode of metal B with the size of, e.g., 10^{-3} cm^2. This suggests the possibility to compare results of direct studies of heterogeneous nucleation with structural data. Similar studies can also be performed over a certain range of potentials after obtaining information on the nucleation kinetics.

Formula (10.25) can also be used when studying the deposition of individual metals. If one assumes that the growth of each grain occurs by layer-by-layer or normal growth and also by two-dimensional nucleation, while formation of a new crystal requires three-dimensional nucleation, then (10.28) provides the frequency of three-dimensional nucleation.

10.13 Effect of Various Factors on Alloy Composition

Let us discuss qualitatively the effect of deposition parameters on alloy composition.

It is obvious that if both metals are deposited in the Tafel region, then an increase in the current density, i.e., a potential shift in the negative direction leads to enrich-

ment of the alloy in the component with the higher αn value, as its discharge rate features a stronger dependence on potential. This generally concerns component B.

If one of the metals (more often, A) is deposited in the region of diffusion controlled or mixed kinetics, then its content in the alloy when increasing the overall current density decreases for the same cause. Stronger stirring, on the contrary, causes an enrichment in A.

The role of the temperature is often reduced to an overall decrease of the overpotential, as a result of which the alloy is enriched in component A, though the opposite trend is also possible if the discharge activation energy of component B is higher.

The effect of SASs is generally selective and depends in particular on the position of the zero charge potentials of the components. This also concerns the role of the concentration of ligands, solution acidity, and the presence of ions not participating directly in the electrode processes.

In some cases, a qualitative assessment of the dependence of alloy composition on the deposition conditions is possible. All such calculations are based on the analysis of polarization curves for components A and B in a certain range of potentials, where the discharge of each element is determined by electrochemical, mixed, or diffusion kinetics. Corresponding calculations are available in the literature for the dependence of alloy composition on the ratio of components in the solution [7] and on temperature [8]. Rotinyan and Kheifets [9] considered a number of regularities of codeposition of impurity metals, including the dependence on current density, component concentrations, and electrochemical parameters.

As an example, let us consider the dependence of alloy composition on the ratio of components in the solution and on the overall current density.

Let component A be deposited under diffusion control. This situation is characteristic of the deposition of impurity components contaminating the principal metal.

In this case the deposition rate (in mol/(cm^2 s)) of the main component B is

$$V_b = iCE/nF \tag{10.29}$$

and that of the impurity element is

$$V_a = K_{\mathrm{m}} C_a \tag{10.30}$$

where K_m is mass transfer coefficient from which the atomic fraction of the impurity can be determined

$$N_a = K_{\mathrm{m}} C_a \, nF/iCE \tag{10.31}$$

or

$$log \; N_a = \mathrm{const} - log \; i. \tag{10.32}$$

It follows thence that the impurity concentration in the deposit is proportional to its concentration in the solution and inversely proportional to the current density. The nature of the impurity, solution composition, its viscosity and temperature influence the degree of codeposition of the impurity into the deposit only indirectly, through the effect on K_m and CE. Therefore, contamination of the metal by impurities deposited at the limiting current depends weakly on its nature.

On the contrary, in absence of diffusion limitations, and by neglecting the anodic terms, for components A and B

$$i_a = k_a \, exp(-\alpha_a n_a FE/RT), i_b = k_b \, exp(-\alpha_b n_b FE/RT), \tag{10.33}$$

where k_j are the rate constants of the processes at a given reference potential.

Therefore, the value of $log(i_a/i_b)$ is

$$log(i_a/i_b) = log(k_a/k_b) - 0.43(\alpha_a n_a - \alpha_b n_b)FE/RT = \mathrm{m} + \mathrm{n}E, \tag{10.34}$$

and the value of $log(\omega_a/\omega_b)$

$$log(\omega_a/\omega_b) = \mathrm{m}' + \mathrm{n}'E, \tag{10.35}$$

where both cases $n > 0$ and $n \leq 0$ are possible.

Thus, the logarithms of the ratios of metal concentrations in the alloy and solution depend linearly on potential. Writing down equations for the discharge rates in the presence of SASs or from complex compounds with a common ligand, it is easy to obtain similar ratios.

In general, linear dependences of the following form are observed with a rather high accuracy:

$$log(\omega_a/\omega_b) = \mathrm{D} + \mathrm{G}x, \tag{10.36}$$

where x may be the logarithm of the overall current density $log\ i$, logarithm of the concentration of SAS $log\ c_{SAS}$ or ligand $log\ c_L$, logarithm of the ratio of concentrations of the ions of components in the solution $log\ ([A]/[B])$, pH of the solution, inverse absolute temperature $1/T$ etc. In this formula, the multiplicative coefficient G in each distinct case assumes a definite physico-chemical meaning; in particular, each time it represent a certain combination of parameters describing the discharge of A and B. The slope of these relationships changes (i.e., the corresponding curves feature a kink) under for example varying conditions of deposition of a given component, alloy structure, ionic equilibria in the solution etc. Therefore, presenting results of deposit composition in the form of a dependence of $log\ (\omega_a/\omega_b)$ on various process parameters represents a useful tool for studying alloy electrodeposition.

It will be noted that the above analysis is also applicable to studies of simultaneous metal deposition and hydrogen evolution, where it is convenient to present the results in the form of the dependence of $log\ [CE/(1-CE)]$ on the electrolysis conditions.

10.14 Electrodeposition of Multilayer and Surface Alloys

10.14.1 Multilayer Alloys

In recent years there has been increasing interest in the possibility of depositing multilayer coatings by alternating layers of two metals or alloys of different thick-

nesses, down to a few atomic monolayers. In particular, the ability to synthesize such materials by deposition from a single electrolyte, through the application of pulsed or more complex periodic deposition waveforms, has been clearly established and widely applied.

A more general possibility is the production of layers whose composition periodically varies via some predetermined law, sequentially becoming enriched in one component or another. These deposits are usually obtained by setting specific electrodeposition conditions to grow a multilayer precursor, followed by control of the mutual diffusion of the neighboring layers after deposition. It is also possible however to gradually vary the deposition conditions over time to produce a predetermined compositional gradient in the as-deposited condition.

These film materials may possess novel and unusual properties, making these systems very important from a practical standpoint. Applications of multilayer films vary from the possibility to combine different properties in the same coating (for example using multilayers made of alternate sublayers of Sn and Ni–P to combine the ductility of Sn to the hardness and wear resistance of Ni–P), to the emergence of novel phenomena (for example the observation of giant magnetoresistance in magnetic/non magnetic multilayers with thicknesses of the single layers below 10 nm).

In spite of the limitations of the electrodeposition method (for example, not all metals can be deposited, and some metal pairs are extremely difficult to codeposit) this method is promising in view of the simplicity of the apparatus and the facile yet precise control of the deposition conditions for the single layer. Numerous multilayered structures have been obtained in the course of deposition of Cu–Ni, Cu–Co, Cu–Pb, Ag–Pd, Ni–Mo, Sn–Ni etc., to name only a fraction of the abundant work available in the open literature.

A discussion of the mechanism of the formation of such structures should consider the electrochemical and diffusion conditions during the deposition process of the single layer and its dependence on the pulse mode and waveform, as well as the process of alloying and the nucleation on the foreign surface.

If the solution contains two different metal ions, each of which can be reduced under precisely determined conditions, there is in principle the possibility of obtaining alloys of these metals and also to achieve the successive deposition of layers of different composition. It is obvious that at a potential corresponding to deposition of A (the more electropositive metal) but more positive than E_{eq} of the metal B, only the relatively pure metal A can be deposited; the possibility of underpotential deposition of B should however be taken into account. In the region more negative than E_{eq} of the metal B, an alloy is deposited. This makes it possible to produce alloys of different compositions under various deposition modes, as follows: (1) by galvanostatic pulses intercalated with pauses; (2) by alternating galvanostatic pulses of different current densities (corresponding to regions A and AB); (4) by deposition modes (2) and (3) which however include pauses between all pulses or between pairs of pulses; (5) by deposition modes (1)–(4) while additionally including anodic pulses, for example to induce passivation; finally, (6) in all the modes mentioned above any pulse can have a more complicated structure (say, a train of very short pulses and pauses).

Each of these methods has its own characteristic features, some of which will be described in the following.

Using a pulsed on-off mode the features of the resulting multilayer depend on the magnitude and length of the pulses (i_p and t_p respectively) and on the difference ΔE_{eq} of the equilibrium potentials of A and B. If the CD does not exceed the diffusion limiting value for A and ΔE_{eq} is large enough, then only A is deposited (refer however to Sect. 10.11) and the layer thickness depends (at a given CD) only on the pulse length, which can be varied at will. With a small ΔE_{eq} however the potential for the deposition of B may be reached, as shown in Fig. 10.3, and an alloy will form. The situation becomes drastically different when $i_p >> i_{lim}$, and the actual result will depend on the transition time t_{tr} defined by the Eq. (10.37); for the metal A

$$t_{tr} = (\pi D_a/4)\, nFC_a/i_p)^2 \tag{10.37}$$

where the subscript "a" refers to metal A ions. If the pulse is longer than the transition time, the overpotential increases after the transition time is reached, and the potential for deposition of B is reached; as a result, an alloy is deposited, and the partial CD for A deposition drops. The time during which A is deposited is equal to t_{tr}, and the corresponding layer thickness is

$$h_a = (\pi D_a/4)(nFC_a{}^2 V_a/i_p) \tag{10.38}$$

where V_a is the molar volume of metal A. It follows that the smaller i_p and the higher C, the larger the thickness h_a. This thickness does not exceed the quantity $V_a C_a \delta$, δ being the thickness of the steady-state diffusion layer.

During the remainder of a pulse, an alloy of variable composition is deposited. In the subsequent off time a displacement process between ions of A and the component B can occur, as a result of which a fraction of the deposit dissolves preferentially component B. The kinetics of these processes can be analyzed using general electrochemical kinetics concepts, by determining the mixed potentials. Besides, if an off time is used, the deposit surface may be passivated; this can be achieved by introducing an additional, more positive pulse. In this case, the displacement process may be suppressed.

A different situation occurs if the first pulse is followed by another one with a higher CD, which as a rule exceeds the limiting current for A. In this second pulse, an alloy A–B is deposited, its composition depending on a combination of several factors and consequently potentially varying in the course of a pulse.

If A is deposited during a first pulse below the diffusion limiting CD, in a second pulse i_{p2} the surface concentration C_s of A ions starts to decrease in accordance with

$$(C_s/C_0) = 1 - (t/t_{tr})^{1/2} \tag{10.39}$$

where for a current density higher than the limiting one $t_{tr} < \pi\delta^2/4D$. During this time C_s decreases and the alloy composition changes. The thickness of a transi-

tion layer deposited while C_s is still below a steady-state value, does not exceed $i_{p2}\, t_{tr} = i_{p2}\delta^2 V_{av}/nFD$.

In principle, it could be possible to determine the current transient for each individual metal species at any time instant by solving together the equations for the mixed kinetics of either component and for any pulse or off time. However, in such calculations one should take into account a number of factors, and the considerations outlined above may have only tentative value. An additional reason for the formation of layers of various composition may be the formation of an alloy AB on a freshly deposited non-compact surface of A; in order to achieve this, the depositing atoms B may alloy with the previously deposited atoms A in a surface layer; the converse process is also possible. The thickness of such layers can reach tens of nanometers.

10.14.2 Surface Alloys

In a number of cases, electrochemical alloy formation occurs only at the electrode surface layer. Such electrochemical surface doping is often a convenient method of modifying the properties of the metal working surface.

Several methods of electrochemical synthesis of surface alloys are possible. For example, alloys may be formed through a spontaneous contact exchange process occurring in the case of immersion of metal (A or B) into the solution containing ions of another metal (B or A, accordingly). In these cases contact exchange is quite possible not only in the systems of metal B–cations of A, but also in the opposite case ("reverce cementing"). In the latter case, the B phase is deposited on the electrode simultaneously with formation of the alloy as a solid solution or as an intermetallic.

Surface alloys can also be obtained using the process of metal underpotential deposition combined with their cathodic intercalation into the substrate. If the substrate and deposited metal are capable to form a solid solution or an intermetallic, then, when setting the potential positive of the equilibrium potential of B, a cathodic current due to formation of adatoms and their intercalation into the surface metal layer is observed, which decreases with time. The observed current vs. time transient is determined by the rate of discharge of cations to adatoms (which is generally high) and diffusion coefficient in the metal (generally, low). Evidence of the diffusive character of the process is the linearity of the dependence of i on $t^{1/2}$ after a short transient where double layer charging and/or adsorption processes occur.

Changing the applied potential, one can control the composition of the alloy formed. Thus, surface alloys of Cu–Cd, Ag–Cd, Pb–Tl, Cu–Zn, Ni–Zn have been obtained, the first metal being the substrate material and the second one the intercalating component.

These processes are of interest both in practice, due to their ability to form unique alloys, and from the fundamental standpoint, as the solid solution of B in A is probably formed according to the intercalation mechanism under the condition of co-crystallization. Thus, the study of surface alloy formation is one of the methods

of elucidating the mechanism of alloy formation under codeposition of the various components.

References

1. Vinokurov E.G., Bondar V.V., The models for the description and prediction of alloys electrodeposition (in Russian), Moscow, VINITI, 2009.
2. Gerischer H., Kolb D., Przasnicky M., Surface Science, 1974, v. 43, p. 662
3. Podlovchenko B. I., Maksimov Yu. M.et al., Russ. J. Electrochemistry, 1994, v. 30, p.285
4. Karbasov B.G., Tikhonov K.I., Rotinian A.L., Internat. Soc. of Electrochemistry, 37th meeting, 1986, v.2, p. 142
5. Kabanov B.N., Astakhov I.I., Kiseleva I.G., Kinetics of the complicated electrochemical reactions, Moscow, Nauka, 1981, p. 200 (in Russian)
6. Gamburg Yu. D., Russ. J. Electrochemistry, 1994, v. 30, No. 2, p. 266
7. Akhumov E.I., Rosen B. Ya., Doklady Akademii Nauk SSSR, 1956, v. 109, p. 1149 (in Russian)
8. Kochergin S.M., Pobedimski G.R., Transactions of the Kazan Inst. Of chem.. Technology, 1964, v. 33. p. 134
9. Kheifets V.L., Rotinian A.L., Doklady Academii Nauk SSSR, 1952, v. 82, p. 423 (in Russian)

Chapter 11
Codeposition of Impurities

11.1 Sources of Impurities in Electrodeposits

Practically all the chemical species present in an electroplating solution can eventually be incorporated as impurities in electrochemically deposited metals. However, the mechanism and kinetics of their incorporation by the growing deposit can differ widely; similarly, the qualitative relationships between the concentration of impurity atoms in the solution and in the deposit and also their chemical state may vary significantly. For example, the relative content of the elements in the deposit can be higher than in the solution, or the same quantity can be lower by several orders of magnitude, depending on the mechanism of incorporation.

The inclusion of impurities is often a consequence of the presence of particular additives (usually organic) into the solution. Other impurities may be the result of the unintentional presence of various substances in solution, or may derive from cations or anions present in the solution itself.

Some impurities are generated on the growing surface as a result of chemical or electrochemical reactions, including dissociative adsorption, hydrate formation, or electroreduction. Other impurities may be simply adsorbed on the substrate without any chemical transformation. All the substances present on the surface where crystallization and growth of the metal deposit occurs can be eventually found in its bulk.

Direct inclusion of inorganic cations and anions into deposits occurs usually at extremely low levels. Their fraction in a deposit is usually of the order $10^{-5} - 10^{-4}$ by volume. Certain complex anions however may be incorporated at much higher fractions; for example, cyanides or halides can be included into deposits at concentration of approximately 10^{-3}, i.e., 0.1%.

Significantly higher amounts of impurities are frequently present in deposits grown from solutions containing organic compounds. Carbon is often found in such deposits, while sulfur is often present when plating from electrolytes comprising sulfur-containing compounds. Inclusion of hydroxide compounds is often observed, especially when the pH in the near-electrode region is sufficiently high to reach conditions of metal hydrolysis in the vicinity of the cathode.

Y. D. Gamburg, G. Zangari, *Theory and Practice of Metal Electrodeposition,*
DOI 10.1007/978-1-4419-9669-5_11, © Springer Science+Business Media, LLC 2011

Impurities within the metal or alloy are very important because they may cause a change in its properties. Therefore, the problem of codeposition or incorporation of impurities concerns not only the chemical purity of the deposit, but also their effect on its functional properties. For example the presence of only 0.01% of antimony causes a decrease in the conductivity of silver by 4%. The effect of non-metallic additions such as sulfur or phosphorus can be even more significant.

For this reason, it is necessary to utilize organic compounds with care, especially sulfur-containing brightening, leveling, and other agents that, while improving the deposit appearance, can result in a significant change in deposit properties, inducing for example brittleness or a decrease in conductivity. On the other hand, the opposite effect may also be observed, of an incorporated impurity causing certain deposit characteristics to improve.

11.2 Theoretical Analysis of the Codeposition Kinetics

In this section we derive an expression for the dependence of the impurity content in the deposit on its concentration in solution, current density, potential, temperature, pH of the solution, hydrodynamic conditions, and other deposition parameters.

In the simplest case, when the impurity is included into the deposit as a result of cathodic reduction in parallel with the main metal ion, the analysis of the codeposition kinetics does not differ from that considered in the previous chapter on alloy formation. However, inclusion of many impurities, especially non-metallic ones, is not directly related to electrochemical reactions but is instead the result of the adsorption of substances onto the electrode during growth of the deposit, which in turn causes an additional diffusional flux of these substances from the bulk of the solution. In this case, and assuming no chemical transformations of the impurity, one must consider four different stages the impurity species undergo during the incorporation process:

1. in the solution bulk, with a concentration C_v, mol/cm^3;
2. in the cathode layer, with a concentration C_s, mol/cm^2;
3. in the adsorbed state on the cathode surface, with an adsorption Γ, mol/cm^2 or coverage $\theta = \Gamma/\Gamma\infty$;
4. in the deposit bulk, with a concentration C_d, mol/g-atom of the metal.

In the following it is hypothesized that the impurity species in the adsorbed layer are in equilibrium with the adjoining solution layer, and that this equilibrium is described by a definite adsorption isotherm $\theta = \theta(C_s)$.

Moreover, it is usually assumed that the impurity concentration in the deposit is proportional to θ:

$$C_{\mathrm{d}} = k_{\mathrm{inc}}\theta. \tag{11.1}$$

This is tantamount to assuming proportionality between the codeposition (incorporation) rate v_{inc} (mol/g-atom·s) and the coverage and current density:

$$v_{\text{inc}} = k_{\text{inc}} i\theta / nF \tag{11.2}$$

Therefore, current flow results in a mass flux of the impurity towards the cathode. In the steady-state regime, this co-deposition flux is fully accounted for by the diffusion flux from the solution bulk:

$$v_{\text{inc}} = v_{\text{diff}} = K_m(C_v - C_s), \tag{11.3}$$

where K_m is the mass transport coefficient.

Thus, just as for the main electrochemical process, the codeposition of impurities occurs in various stages; in particular, we consider three steps: mass transport, adsorption, and capture. Experimental data for the incorporation of impurities in electrodeposits are generally in good agreement with the predictions calculated through the model outlined above.

Let us now consider the above stages in more detail.

11.2.1 Adsorption Equilibrium

The adsorption equilibrium in presence of a current, i.e., occurring simultaneously with the faradaic process, is generally shifted in comparison with adsorption in the absence of current. There are two causes for this. First, as shown in Chap. 2, the adsorption equilibrium constant B goes through a maximum near the potential of zero charge potential (pzc). Therefore, adsorption can either increase or decrease upon a shift in the electrode potential from an equilibrium or a steady-state value; this depends on the mutual positions of the pzc and the open circuit potential, as well as on the shift of the pzc in presence of the adsorbate layer. Second, the equilibrium is also shifted due to the fact that the rate at which the impurity is consumed as a result of its codeposition affects the rate at which the adsorbed species is exchanged with the solution.

Let us assume for simplicity a Langmuir adsorption isotherm,

$$\theta = k_{\text{ads}}/k_{\text{des}}/(1 + C_s k_{\text{ads}}/k_{\text{des}}) \tag{11.4}$$

or

$$\theta^{-1} = 1 + k_{\text{des}}/C_s k_{\text{ads}} \tag{11.4a}$$

where k_{ads} and k_{des} are the rate constants for adsorption and desorption, respectively. In the case under consideration, when adsorbate removal occurs not only through desorption, but also as a result of incorporation into the deposit or electroreduction to other compounds, the numerator in (11.4*a*), k_{des}, changes, assuming the form:

$$k_{\text{des}} + i(k_{\text{inc}} + k_{\text{red}})nF \tag{11.5}$$

since the rates of inclusion and reduction depend on the current density and, to a first approximation, are proportional to i. Thus, we have instead of (11.4a):

$$\theta^{-1} = 1 + [k_{\text{des}} + i(k_{\text{inc}} + k_{\text{red}})/nF]/C_{\text{s}} k_{\text{ads}} \tag{11.6}$$

From (11.6) it can be seen that if $i(k_{inc}+k_{red})/nF$ is comparable to k_{des}, then θ changes significantly, decreasing with an increase in i. A similar trend can also occur assuming any other type of adsorption isotherm. An experimental determination of this effect is possible in principle, but in practice it has not been performed so far; it follows that the constants in Eq. (11.6) are not known to a sufficient degree of accuracy. One can only qualitatively state that as the adsorption equilibrium on solid electrodes is often established rather slowly, the transient condition under consideration can be observed in practice and this is not only a hypothetical condition.

In many cases, the incorporation of impurities in the deposit occurs via irreversible adsorption with decomposition of precursor molecules, or alternatively as a result of the formation of insoluble compounds with the cathode material or with various intermediates of the electroreduction process, present on the growing surface or in the near-electrode region. Apparently, species of low solubility exhibit little tendency to desorb from the electrode and have long residence times on the surface, increasing the likelihood of incorporation into the crystal lattice. In some cases, both the unreacted impurity molecules and their fragments may be found in the deposit. In such cases, codeposition can be described via the scheme discussed in [1], where the process is hypothesized to occur through the following path:

$C_v \rightarrow$ diffusion $\rightarrow C_s \rightarrow$ adsorption $\rightarrow \theta \rightarrow$ inclusion into the deposit and/or decomposition with inclusion of fragments into the deposit.

The occurrence of decomposition reactions results in a strong irreversibility of the adsorption process and is responsible for example for the high capture rates of, e.g., sulfur during the electrodeposition of nickel, cobalt, or copper. In all cases characterized by high codeposition rates, the process is usually controlled by diffusion and therefore presents little dependence on the adsorption parameters.

11.2.2 Capture of Adsorbed Species

The often observed proportionality between the surface concentration and the amount of codeposited impurity follows from a mechanism usually referred to as "burying" or "disposal" [2] of the impurity in the growing film. This proportionality should be rigorously obeyed at low θ, but this requires co-deposition to be the only path of cathodic impurity consumption. If the impurity is partially reduced or participates in other reactions that do not result in codeposition but in diffusion of the products back into the solution, then the above hypothesis requires a constant ratio of the rates of codeposition and the rates of other processes. This is not always the case however; for example, the temperature can strongly affect the ratio between the capture and reduction rates.

It is easy to verify that the hypothesis $C_d = k_{inc}\theta$ is tantamount (in the case of 100% current efficiency) to the assumption that the codeposition rate is proportional to the current density and surface coverage:

$$v_{\text{inc}} = k_{\text{inc}} i\theta / nF. \tag{11.7}$$

The value of k_{inc} can be estimated from the ratio of $k_{\text{inc}} = v_{\text{at}}/v_{\text{imp}}$, where v_{at} is the atomic volume of the metal, cm^3/g-atom, and v_{imp} is the molar volume of the impurity, cm^3/mol (here we suppose for simplicity that all the adsorbed molecules are captured by the growing deposit, or that their residence time at the surface is sufficiently long).

But comparison of independent measurements of θ and C_{d} shows that the inclusion constant often appears to be much lower than the theoretical value, i.e., the system behaves as if only a fraction of adsorbed molecules is incorporated. There may be several reasons for this discrepancy. First, alongside with "disposal", the impurity molecules may be expelled from the growing deposit due to crystallization pressure. One can assume that only the molecules adsorbed on the growing surface fraction are incorporated into the deposit, while the molecules on the inactive surface are pushed away by the growing crystal front. Thus, instead of (11.7), we would have:

$$v_{\text{inc}} = \xi k_{\text{inc}} i\theta / nF, \tag{11.8}$$

where ξ corresponds to the active surface fraction. The role of crystallization pressure however is more appropriate for the inclusion of large particles rather than molecules.

The second cause of incomplete incorporation consists in the possibility of partial desorption of the molecules. The only molecules included in the deposit are therefore those with a residence lifetime on the surface exceeding a certain critical value corresponding to the growth of the deposited layer to a thickness sufficient to block them (Fig. 11.1). Obviously, even in the case of adsorption at a uniform surface, not all identical species have the same residence time and a certain lifetime distribution function should be considered [3].

This phenomenon is qualitatively due to the fact that all adsorbed species, nominally identical and adsorbed at a uniform surface, at any given time are equivalent in terms of their desorption probability, i.e., the desorption of both long adsorbed and newly adsorbed molecules is equally probable.

The probability distribution of the residence lifetime on the surface is:

$$f_t = (k_{\text{ads}})^2 C_{\text{S}} \tau \; exp(-k_{\text{ads}} \tau / C_s), \tag{11.9}$$

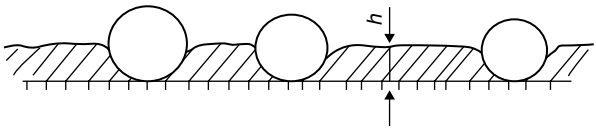

Fig. 11.1 The only molecules included in the deposit are those with a residence lifetime on the surface exceeding a certain critical value corresponding to the growth of the deposit of sufficient thickness

where k_{ads} is the adsorption constant, and C_s the surface concentration. From this expression, one can find the fraction of particles having a surface residence time above a certain given critical value, τ_c:

$$F(\tau_c) = (1 + 2\tau_c/\tau_{av})\ exp(-2\tau_c/\tau_{av}) \approx exp(-\tau_c/\tau_{av}). \tag{11.10}$$

Here, τ_{av} is the average lifetime on the surface, which is directly related to the adsorption energy:

$$\tau_{av} = \tau_0\ exp(Q/RT), \tag{11.11}$$

where $\tau_0 \approx 10^{-13}$ s. Thence, at room temperature $T = 300$ K,

$$Q(\text{kJ/mol}) \approx 75 + 5.9\ \log\tau_{av}. \tag{11.12}$$

Under usual electrodeposition conditions, the critical τ_c value corresponding to a shift of the deposit growth front by $h \approx 1$ nm, a typical molecular size (Fig. 11.1), is 0.01–10 s. Thus, for $Q < 60$ kJ/mol (0.6 eV/molecule), $\tau_{av} < \tau_c$ and incorporation should be weak, while for $Q > 80$ kJ/mol (0.8 eV/molecule), the impurity has a high probability to be captured by the growing deposit. Typical adsorption energies are of the order 0.4–1 eV/molecule, within the range discussed here.

Finally, the kinetics of impurity capture may depend on the surface distribution of the adsorbate: isolated molecules or small assemblies of the same are incorporated by the growing deposit faster than larger regions completely covered by the adsorbate. Therefore, one can assume that the mutual repulsion of adsorbed molecules assists incorporation, while their attraction hinders it. As a rule, in order to describe adsorption it is sufficient to use only the degree of coverage; however, for a given value of θ not only the residence time but also the distribution of adsorbed matter can be different, and can vary from the random distribution of adsorbed molecules to the formation of completely covered regions of large dimensions along with large regions free of adsorbate. The actual configuration depends on the interaction of the adsorbed species with the surface and among each other.

The average size d of regions covered by the adsorbate in absence of interaction between the adsorbate molecules can be estimated by the formula:

$$d \approx N^{-0.5}(1 - \theta)^{-1}, \tag{11.13}$$

where N is the number of adsorption sites per unit surface area. Computer simulations have provided more precise formulae for the size of the regions free from adsorbates: for $\theta < 0.07$ $d_{free} = N^{-0.5}\ \theta^{-1}$, for $0.07 < \theta < 0.8$ $d_{free} = 2\theta^{-0.83}\ N^{-0.5}$, and for $\theta > 0.8$ $d_{free} = 4N^{-0.5}\ \theta^{-1}$. The corresponding expressions for the areas covered with adsorbates are the same if θ is changed to $(1 - \theta)$. Notice that the size of the regions free from adsorbate can determine the size of the metal nuclei.

In the case of a sufficiently strong repulsion and not too high coverage, the adsorbed layer is dispersed across the surface and mainly consists of separate molecules. In this case, one can expect faster incorporation but hindered nucleation.

11.2.3 Mass Transport of Impurities to the Cathode

The rate of mass transport to the electrode may equal the rate of impurity incorporation in the deposit only in the absence of other paths for impurity consumption. Otherwise, one should consider the consumption rate for all the possible incorporation mechanisms. Including all possible paths is essential, since the incorporation rate for the various mechanisms is in many cases of the order of 1% or less of the overall consumption rate. Thus, instead of (11.3), we have:

$$v_{\text{inc}} = K_m(C_v - C_s)k_{\text{inc}}/k_{\text{cons}}. \tag{11.14}$$

where the constant k_{cons} characterizes overall mechanisms of the consumption—not only the incorporation unto the deposit but also electroreduction and chemical reactions. (11.14) shows that only some fraction of the impurity flux to the cathode is included into the deposit.

In the case of ionized impurities, mass transport includes both diffusion and migration. If the incorporated molecules are formed directly on the electrode or near the electrode as a result of chemical processes, then there is no effect of mass transport on the incorporation rate, since the molecules arriving at the electrode are all consumed there, creating a concentration gradient.

Often, alongside with the cathodic consumption, also an anodic consumption of impurities should be considered. Therefore, a direct comparison of impurity data obtained from the analysis of the deposit and the solution is sometimes inappropriate. The ratio of cathodic and anodic consumption depends on many factors, so that quantitative study of these processes requires physical separation of the cathodic and anodic compartments, for example using a membrane.

11.2.4 Derivation of the Main Equation

Taking into account the above exceptions, it is possible to move on to an analysis of the dependence of codeposition rate on the electrolysis conditions.

According to Eq. (11.14), taking into account the fact that the metal deposition rate is i/nF, we obtain:

$$C_{\text{d}} = K_m(C_v - C_s)nFk_{\text{inc}}/k_{\text{cons}}i. \tag{11.15}$$

On the other hand, according to Eqs. (11.1) and (11.4),

$$C_{\text{d}} = k_{inc}\theta\ (C_s, i). \tag{11.16}$$

(11.15) and (11.16) form a system of equations that can be solved by eliminating C_s if the functional dependence $\theta(C_s, i)$ is known. It is thus possible to obtain the general function $C_d(C_v, i, K_m, k_{\text{inc}}, k_{cons}, K_{ads})$, where the parameters in bracket determine completely the codeposition kinetics. Dependence of C_d on such factors as temperature, pH etc. is usually reduced to changes in one or several of the k, K constants.

In the case of a Langmuir adsorption isotherm, (11.16) becomes

$$C_{\mathrm{d}} = k_{inc}\theta\ K_{\mathrm{ads}}C_s/(1 + K_{\mathrm{ads}}C_s). \tag{11.17}$$

where $K_{ads}=k_{\mathrm{ads}}/k_{\mathrm{des}}$.

Considering the system of Eqs. (11.15) and (11.17) in the case of $k_{\mathrm{inc}}=k_{cons}$, and eliminating C_s:

$$\begin{aligned}&\left(K_{\mathrm{ads}}iC_{\mathrm{d}}{}^2/K_{\mathrm{m}}nF\right) - \left[1 + K_{\mathrm{ads}}C_{\mathrm{v}} + k_{\mathrm{inc}}K_{\mathrm{ads}}i/K_{\mathrm{m}}nF\right]C_{\mathrm{d}}\\ &+ k_{\mathrm{inc}}K_{\mathrm{ads}}C_{\mathrm{v}} = 0\end{aligned} \tag{11.18}$$

If the actual isotherm is close to a Langmuir type dependence, then one can use the experimental dependence of $C_d(i)$ and $C_d(C_v)$ obtained at a determined K_m value (i.e., under a controlled hydrodynamic regime, e.g., on a rotating disk electrode) to find all the parameters in the formulas (11.17) and (11.18).

In practice, the form of the function $\theta(C_s)$ is a priori unknown. However, Eq. (11.15) allows computation of this function on the basis of experimental data. Indeed, rewriting this equation in the form $C_{\mathrm{s}}=C_{\mathrm{v}}-C_{\mathrm{d}}i\,k_{cons}/(K_{\mathrm{m}}nF\,k_{inc})$, we obtain in the case of $k_{inc}=k_{cons}$:

$$C_{\mathrm{s}} = C_{\mathrm{v}} - C_{\mathrm{d}}i/(K_{\mathrm{m}}nF). \tag{11.19}$$

Thus, with the help of the following experimental data: (1) the dependence of $C_d(C_v)$ at $i=$const and $K_m=$const, (2) the dependence of $C_d(i)$ at $C_v=$const; (3) the value of k_{cons}/k_{inc}, one can find the dependence of $C_d(C_s)$. Finally, taking into account that $C_d=K_{inc}\Theta$, one can directly obtain the adsorption isotherm sought for. The value of k_{inc} can be determined, e.g., from the maximum of the C_d value thus obtained, assuming that $\Theta=1$. Below, we will describe yet another way for finding this constant.

This method has been used for example to determine the adsorption isotherm of paratoluenesulfamide (PTSA) on nickel (Fig. 11.2) [4].

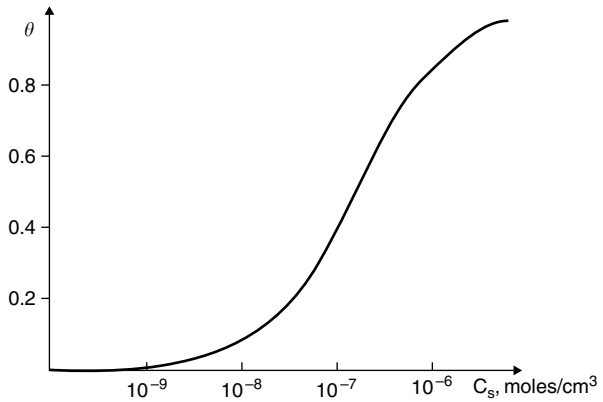

Fig. 11.2 Adsorption isotherm of PTSA on nickel. [4]

11.2.5 Limiting and Intermediate Cases

Analysis of (11.18) in general leads to rather cumbersome expressions. These formulas can be simplified by limiting the discussion to low bulk concentrations, when one can use the Henry isotherm. In this case, instead of (11.17) it is possible to use

$$C_d = k_{\mathrm{inc}} K_{\mathrm{ads}} C_{\mathrm{s}} \tag{11.20}$$

which together with (11.19) yields:

$$C_s/C_v = K_{\mathrm{m}}/(K_{\mathrm{m}} + (K_{\mathrm{ads}} k_{\mathrm{cons}} i/nF)) \tag{11.21}$$

Thus, in the case of a low impurity concentration in the bulk of the solution, there are two limiting cases: when $K_{\mathrm{ads}} k_{\mathrm{cons}} i/K_m nF >> 1$, then $C_s << C_v$; while if $K_{\mathrm{ads}} k_{\mathrm{cons}} i/K_m nF << 1$, then $C_s \approx C_v$. In intermediate cases, $C_s < C_v$.

It should be noted that the mass transport coefficients are rather similar for the majority of impurities usually incorporated into deposits; also, the k_{inc} values are often of the same order of magnitude. Consequently, considering standard deposition conditions, it is possible to divide all impurities into three classes, where the difference in behavior is largely due to a difference in K_{ads}. Following a change in the electrolysis conditions, a given species can shift from one class to another; in fact, K_{ads} depends on the electrode potential and besides, the value of $k = K_{ads} k_{cons} i/K_m nF$ increases with an increase in current density and/or diffusion layer thickness, as a result of which C_s decreases with i and increases with of stirring.

Assuming for typical deposition conditions: $k_{cons} = 0.001$, $K_m = 0.001$, $i = 0.01$, it is possible to calculate that $k << 1$ when $K_{ads} < 10^4$ and $k >> 1$ when $K_{ads} > 10^7$.

11.2.6 Adsorption Control of Codeposition

At low K_{ads}, the species of interest can form a sufficiently compact adsorption layer on the electrode surface only when $C_v > 10^{-4}$ mol/cm^3, i.e., 0.1 M. This concentration is too high to satisfy the requirement of being an impurity. Such substances under usual impurity concentrations yield therefore $\theta << 1$, which results in a very low inclusion rate. In the following, the case of $C_s = C_v$ is considered.

In this case, obviously the dependence of $C_s(C_v)$ follows closely the adsorption isotherm, under the assumption that $k_{inc}/k_{cons} = \mathrm{const}$; furthermore, mass transport does not affect codeposition, i.e., the process is controlled by adsorption. This situation is characterized by a weak dependence of C_d on i when $C_s = \mathrm{const}$. A decrease in C_d is typically observed when the temperature increases, as adsorption in this case decreases; also, in general a low impurity concentration in the deposit is obtained, as $K_{ads} k_{inc}$ is low (see Eq. (11.20)). However, a low impurity concentration in the deposit is not necessarily a consequence of diffusion control, as it can also be observed if the consumption does not occur by means of inclusion but mainly through other paths.

Adsorption control is characteristic of weakly adsorbed substances and quickly incorporated impurities. Indeed, at high K_{ads} instead of (11.21) we obtain:

$$C_s/C_v = 1 - k_{cons} i/(K_m C_v n F). \tag{11.22}$$

In this case, codeposition is controlled by adsorption, when the criterion $k_{cons} i/K_m C_v nF << 1$ is satisfied; in other terms, a high C_v value is necessary at a given current density, or a sufficiently low current density is required at a given C_v. Under such conditions, studies of codeposition kinetics do not require any control of the hydrodynamic regime, neither any investigation of the dependence of C_d on i.

11.2.7 Diffusion Control of Incorporation

When $C_s << C_v$, the impurity is consumed at the cathode at the limiting current. This condition is observed for example when leveling agents are used under conditions favoring their action. This circumstance is similar to the discharge of metallic impurities at their limiting current in parallel with reduction of the main metal, as considered in Chap. 10. All the trends discussed there can thus be extended to the case of the diffusion-controlled incorporation of non-metallic impurities. The most characteristic features in this process are the proportionality between the rate of inclusion of the impurity and its concentration in the solution bulk, as well as a drastic increase in the codeposition rate when stirring. Indeed, in this case, the equation for the rate of consumption v_{cons} (11.14) becomes

$$v_{\text{cons}} = K_m C_v. \tag{11.23}$$

This trend is particularly apparent when a rotating disk electrode is used. The codeposition rate in this case in fact increases proportionally to the square root of the rotation rate and is independent of the adsorption characteristics in a wide range of conditions. All other parameters being equal, C_d is inversely proportional to the current density, as v_{inc} is independent of the current density and the rate of metal deposition is proportional to i; it is also observed that C_d increases with temperature due to an increase in the diffusion coefficient. It should be noted that such direct relationship to mass transport underestimates significantly the available experimental data on codeposition obtained without control of the hydrodynamic regime.

Diffusion control of the codeposited impurities can also be observed when even weakly adsorbed impurities are consumed, i.e. in the case of low mass transport coefficient and high current density.

11.2.8 The Case of Mixed Control

If the C_s value is intermediate and is comparable to C_v, then the rate of incorporation depends both on adsorption and the diffusion parameters. In this case, it is most con-

venient to analyze the process using relationship (11.17), as suggested by Edwards [5]. However, deviations from this relationship are possible due, e.g., to coverage of a fraction of the electrode surface by the reaction products.

In the simplest case, if only the impurity is strongly adsorbed and a Langmuir adsorption isotherm is observed, then it follows from (11.17) that

$$C_s/C_d = 1/(K_{\text{ads}}k_{\text{inc}}) + C_s/k_{\text{inc}}. \tag{11.24}$$

Having calculated C_s, as described in Sect. 11.3, one can determine the dependence of C_s/C_d on C_s. A linear dependence is the criterion for the validity of a Langmuir isotherm; this expression allows a separate calculation of K_{ads} and k_{inc}.

As follows from (11.15) and (11.16),

$$C_d = k_{\text{inc}}k_{\text{ads}}C_v/(1 + K_{\text{ads}}k_{\text{inc}}i/K_m nF). \tag{11.25}$$

Thus, C_d is proportional to C_v and the dependence of C_d on i can be expressed as

$$C_v/C_d = i/(K_m nF) + 1/K_{ads}k_{\text{inc}}. \tag{11.26}$$

The slope of this dependence allows computation of K_m as required for calculations in (11.19); the initial ordinate yields the product $k_{\text{inc}}K_{\text{ads}}$. In the presence of other routes of consumption of the adsorbed species apart from incorporation, these relationships become somewhat more complicated.

11.3 Dependence of the Concentration of Impurities on Electrodeposition Conditions

The formulas discussed in the previous section allow a discussion of the dependence of C_d on the various electrodeposition parameters.

11.3.1 Dependence on the Current Density

At low i, as follows from (11.19), $C_s \approx C_v$, i.e., the coverage is determined only by the bulk concentration. On the other hand, it is easy to verify by comparing (11.23) and (11.2) that if impurities are consumed under diffusion control, i.e. at sufficiently high i,

$$\theta \approx K_m C_v\, nF/k_{inc}i. \tag{11.27}$$

The general dependence of θ on the current density in a wide range of current density is schematically shown in Fig. 11.3. This figure evidences that the often observed "cleaning" of the metal surface from adsorbates observed at high current density can be related not to a desorption process, but to a high consumption rate, in particular to the inclusion of impurities into the deposit.

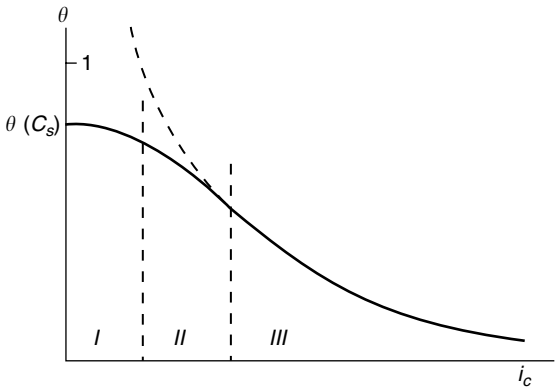

Fig. 11.3 Dependence of coverage on the current density. (*I*) adsorption region; (*II*) transition region; (*III*) diffusion region

However, the opposite is also possible if impurity adsorption occurs at negative potentials, i.e. in correspondence to high current densities.

Taking into account Eq. (11.22), one can assume that Fig. 11.3 shows also the functional dependence of C_d on current density. A similar dependence has been often observed experimentally. Based on the above dependence, it is generally convenient to present experimental data in the coordinates log C_d−log i.

11.3.2 Dependence on the Impurity Concentration in Solution

With a low impurity concentration in solution, C_d is proportional to C_v both under diffusion control and in the adsorption regime. The corresponding proportionality coefficient is $K_m nF/i$ in the first case and $k_{inc}K_{ads}$ in the second case.

With a high C_v, the codeposition rate is controlled by adsorption, as described by the relationship (11.22); such dependence is shown in Fig. 11.4, where the transition to adsorption control can be seen with an increase in the bulk concentration: C_d becomes in fact independent of C_v. Also in this case it is convenient to present the experimental data in the log C_v−log C_d form.

11.3.3 Dependence on Temperature

The effect of temperature can be rather complicated. If inclusion of an impurity occurs at the limiting diffusion current, then the codeposition rate is enhanced by an increase in temperature.

However, at a determined temperature, limitations in the adsorption rate may become apparent; these result in a decrease in the codeposition rate due to a decrease in K_{ads}. Thus, one can expect a maximum in the temperature dependence of the codeposition rate. This has been indeed repeatedly observed experimentally, partic-

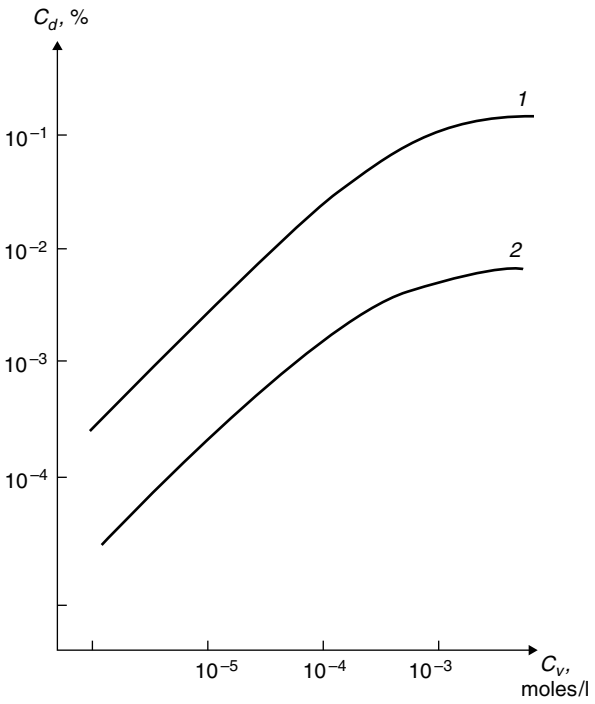

Fig. 11.4 Dependence of the impurity concentration in Ni deposited from sulfate solution on the concentration in the solution: *1*—Saccharine (i=40 mA/cm^2), *2*—Cumarine (i=80 mA/cm^2). [6]

ularly, in the case of sulfur inclusion into copper and nickel from sulfur-containing brightening agents. In some cases the observed temperature dependence could be more complicated; this can be due to (1) a change in the contribution of the codeposition process to the overall consumption rate, (2) a change in the surface density of the surface adsorption centers (dependent on the temperature), or (3) changes in chemical equilibria or chemical kinetics.

11.4 Factors Complicating the Codeposition Kinetics

The trends discussed in the previous section may be modified when the incorporation of impurities in the growing deposit leads to a change in the adsorption surface properties. Co-deposition of impurity species in fact may lead to changes in the deposit structure (decrease in grain size, increase in the fraction of grain boundaries in the material, increase in the density of crystal lattice defects), which will obviously affect the adsorption process. In this case, the impurity concentration in the deposit can increase faster than the concentration in the solution. One could also expect an increase in the density of active surface centers due to a decrease in the current density.

In such cases, a drastic change occurs sometimes in the surface structure in correspondence of a critical impurity concentration in the solution. Simultaneously,

one can also observe a drastic change in the codeposition rate. In this case, the observed change in surface structure may be related to the presence of other substances that are not necessarily incorporated in the deposit. Similar effects are due to a variation of the surface density of adsorption sites as a result of the presence of the second additive; more precisely, due to the structure changes induced by the same [6]. On the other hand, the codeposition process can be hindered due to competing adsorption, for example by replacement of a codeposited species by another one.

In general, two types of such effects are discussed: a gradual change in the adsorption properties of the surface in dependence of the electrodeposition conditions and a drastic change in these properties under conditions that induce structure changes.

Alongside with variations in the adsorption behavior, changes can also be observed with regard to diffusion processes. For example, the dependence of the codeposition rate on the presence of a certain compound can be due to changes in the viscosity of the solution or only of the near-electrode layer, which can simply be rationalized by a decreased concentration. A similar effect can result, e.g., from a change in the diffusion layer thickness induced by the impurity and caused, e.g., by a change in pH or current density.

On the whole, the effect of impurity incorporation can feature other anomalous properties, mainly of a chemical nature, that can hardly be described within a single scheme. For example, the codeposited compound can be the product of a specific interaction between the adsorbate and some intermediates of the electrochemical process [7]. Other causes for deviations from the systematic trends discussed above may include: formation of hydroxides in the near-electrode layer; competing adsorption of hydrogen ions; the presence of anodic process products in the catholyte; etc.

11.5 Chemical State of Codeposited Impurities

It is often very difficult to determine in which form a given impurity is present in the deposit, even by using state of the art physico-chemical methods. Chemical analysis of the deposit composition, for example by chemical or anodic dissolution, thermal annealing, or other methods of deposit treatment, may result in the destruction of the molecules initially present.

Physical methods usually yield information only on the elemental composition. X-ray diffraction analysis is valuable only in those few cases when the inclusions contribute a large fraction of the deposit mass, or if one manages to extract these inclusions from the deposit intact. Otherwise, one may be able to assess the composition of inclusions indirectly according to radiochemical analysis data, if differently labeled molecules are introduced into the solution. For example, in studies of sulfur codeposition with copper, nickel, or silver from thiosulfate-containing solutions [8], either “internal” or “external” sulfate in thiosulfate (S^{2-} or S^{6-}) has been labeled.

In the analysis of inclusions of organic molecules, one can, e.g., compare the observed ratio of element concentrations in the deposit with their ratio in the molecule. Most important is often the C/S ratio. If this ratio in the deposit is lower than in the molecule, then a part of the sulfur is probably not bonded to the carbon, suggesting decomposition of a part of the initial molecules with formation of the metal sulfide.

Oxygen in the deposits is usually in the form of oxides or hydroxides and may be also present within certain organic molecules. Hydrogen can be both in atomic and molecular form and within the hydroxide.

One must treat with special care the results of analysis of the deposit surface layers, as they can be affected by interaction with the atmosphere after the end of deposition. Information on buried layers is often more reliable.

The characteristics of the inclusions in deposits is largely determined by the form in which the substance is adsorbed on the cathode surface during electrolysis. For example, the presence of decomposition reactions of organic molecules resulting in high adsorption irreversibility leads to inclusion not of the initial molecules but, e.g., of sulfides. A significant role can also be played by complex formation. In this case, molecules released at the cathode during discharge of complex compounds can be included as a whole into the deposit.

11.6 The Incorporation of Inhibitors Into the Deposit and Inhibition of the Electrodeposition Process

Very often the species incorporated into electrodeposits are specific additives (brighteners, levelers) which strongly influence the electrode kinetics and in particular inhibit the electrochemical process at the cathode. This section discusses how it is possible to correlate data on cathodic polarization and impurity incorporation by making use of the concept of partial surface coverage and assuming a simple blocking action as the mechanism of inhibition.

Let us assume that a fraction θ of the cathode surface is covered with adsorbed species; deposition proceeds on the free surface only and the corresponding rate may be expressed by $i_1(E)$, where i_1 is the true current density on the free surface and E is the applied potential. Then $i=i_1(1-\theta)$, i being the apparent current density. By differentiating and expressing $\mathrm{d}\theta/\mathrm{dE}$ as $(\mathrm{d}\theta/\mathrm{di})^*(\mathrm{di}/\mathrm{dE})$ we obtain

$$di/dE = di_1/dE\,[(1-\theta)/(1+i_1 d\theta/di)] \tag{11.28}$$

It follows from this equation that the shape of the curve E–i is influenced both by the values of θ and $d\theta/di$. As θ and $d\theta/di$ drop at higher CD the curve approaches $i_1(E)$. This is well known and may be caused by desorption at more negative potentials, or by incorporation, reduction, decomposition etc, of the inhibitor; in this particular case the adsorption depends on the diffusion layer thickness and a leveling action takes place.

Let the adsorption behavior be described by the Langmuir isotherm $BC_s=\theta/(1-\theta)$; If the inhibitor is consumed at the cathode, its surface concentration C_s is

lower than the bulk concentration C_v. The consumption rate can be expressed as the diffusion flux of the inhibitor $K_m(C_v - C_s)$, which at steady state is equal to that of incorporation $k_{\text{inc}}\, i\theta$: $K_m(C_v - C_s) = k_{\text{inc}}\, i\theta$. Combining this relationship with the Langmuir isotherm one obtains after rearrangements

$$\theta^2 - \theta\,[1 + K_m/(Bk_{\text{inc}}i) + K_m C_v/(k_{\text{inc}}i)] + K_m C_v/k_{\text{inc}}i = 0 \qquad (11.29)$$

This equation gives the relationship among i (at a definite potential), k_{inc}, θ, B, C_v and K_m. Part of these quantities (i, C_v, K_m) are known in a given experiment; others can be calculated from measurements at several current densities. The coverage θ can be estimated independently by double layer capacitance measurements.

11.7 Hydrogenation of Deposits

Hydrogen reduction, which at sufficiently negative potentials occurs in parallel with metal deposition, may result in gas formation and release from the substrate or in hydrogen penetration through the growing deposit and into the substrate. This phenomenon is called hydrogenation; this process is in some respect similar to hydrogenation in absence of metal deposition, when hydrogen evolving at the electrode penetrates the crystal lattice. The properties of metals vary sharply upon hydrogenation, therefore this process is usually undesirable. The processes of hydrogen embrittlement, hydrogen cracking, hydrogen blistering for example are widely known phenomena that deteriorate the mechanical properties and surface quality of the material.

The ratio between the amount of hydrogen evolving as a gas into the atmosphere and that incorporated into the metal may vary in a wide range and depends both on the electrochemical conditions of deposition and the chemical characteristics of the metal. Usually the incorporated fraction is small, of the order of 1% or less. Obviously, the lower is the cathodic current efficiency, the higher is the intensity of gas evolution; no direct dependence between cathodic efficiency CE and hydrogenation is however observed: the latter represents a separate problem.

The concentration of hydrogen in different metal deposits may vary in a wide range: 1 g of palladium can incorporate up to the equivalent of 100 cm^3 of H_2 when converted to gaseous form under normal conditions; so high quantities correspond to the compounds Pd_2H or even PdH. The corresponding maximum amounts for chromium and iron are of about 5 and 2 atomic percent, respectively; Zn, Cd and Cu absorb much less hydrogen. This dependence on the chemical nature of the metal is partly governed by the hydrogen adsorption energy but depends also strongly on the presence of additives in the solution: thus, very small amounts of Hg or As in the solution increase hydrogenation sharply, whereas other elements and compounds inhibit it.

The diffusion coefficient of hydrogen in various metals at room temperature varies from 10^{-4}–10^{-5} cm^2/s (in Fe) to 10^{-10} cm^2/s in Ni, Zn etc. and depends on metal purity. Thus hydrogen transfers readily from various deposits into the steel substrate due to its high mobility in the latter.

If the substrate can dissolve only a small quantity of hydrogen, the problem of hydrogen incorporation in the deposit is relatively simple. At steady state a definite surface concentration or coverage by adsorbed hydrogen H_{ads} is achieved, and a fraction of this species is captured by the depositing metal while the remainder forms hydrogen gas by various mechanisms, including electrochemical desorption, recombination etc., depending on the electrochemical conditions [9]. The codeposited hydrogen may form a solid solution with the metal, metal hydrides or may nucleate small gas bubbles in the deposit bulk, along with hydrogen formed from organic molecules decomposed independently.

The problem of hydrogen incorporation differs from the capture of other impurities due to the fact that the hydrogen coverage is determined not only by diffusion and adsorption but also by the electrochemical conditions for the hydrogen evolution reaction (HER). Moreover, in the cases discussed above co-deposition was treated as a non-equilibrium process, whereas in the case of hydrogen an equilibrium is usually established between the hydrogen absorbed immediately under the surface (H_{abs}) and that adsorbed on the surface (H_{ads}), though this equilibrium is shifted as a result of codeposition.

Let θ be the coverage of atomic hydrogen at the surface of the depositing metal; in absence of deposition the equilibrium $H_{abs} \leftrightarrow H_{ads}$ occurs. The rate constants of the direct and reverse processes k^+ and k^- can be determined from membrane experiments, as discussed below; as noted, inhibitors and activators may vary these constants in a wide range.

During electrodeposition an additional non-equilibrium flux of hydrogen into the metal occurs; as discussed earlier, we take this flux to be equal to $k_{inc} i\theta$; then an analysis similar to that performed above shows that the concentration of hydrogen in the surface layer of the deposit is

$$C_d = \theta(k^+ + k_{inc} i)/[(1-\theta)k^- + i/nF] \tag{11.30}$$

This means that the concentration C_d differs from the equilibrium one existing at $i=0$. The electrode material, electrolyte composition and electrolysis conditions have a profound effect on this non-equilibrium value.

After deposition is over, some fraction of the incorporated hydrogen can diffuse back to the ambient. This process is accelerated at higher temperature, and therefore a heat treatment is often used to remove hydrogen from electrodeposits. Hydrogen however may diffuse not only into the atmosphere; an iron substrate for example with its high diffusivity for H may induce significant hydrogen incorporation. As a result, hydrogenation of the substrate takes place.

11.8 Mechanisms of Substrate Hydrogenation

Various mechanisms are active for substrate hydrogenation: hydrogen can penetrate for example through pores in the deposit, by solid state diffusion through the deposit or also directly from the initial layer of the deposit. These three mechanisms exhibit different hydrogen incorporation rates, therefore they can be distinguished from one another.

The first possibility corresponds to hydrogen evolution occurring directly at the substrate surface at locations corresponding to the bottoms of pores in the deposit, resulting in its immediate diffusion into the substrate. Hydrogen may evolve both on the substrate surface, at pore locations, and on the deposit surface. This process is active only until the pores exist, i.e. when the coating is discontinuous, usually up to a deposit thickness of about $h_{\text{lim}} \approx 0.01$ mm. Above this thickness hydrogenation of the substrate should stop.

The overall current density CD in this situation is a sum of three contributions: (1) CD of metal deposition, (2) CD of hydrogen evolution on the deposit and (3) CD of hydrogen evolution directly on the substrate; the available substrate surface exponentially decreases with increasing deposit thickness h, thus the third CD i_3 (the one of interest), diminishes as

$$i_3\,(h) = i_{3(0)}\,\exp(-\lambda h), \tag{11.31}$$

λ depending on the electrolysis conditions. It is impossible to separate the three current densities experimentally; it is possible however to use for this purpose available experimental data for the time dependence of the current efficiency CE during electrolysis: CE achieves its limiting value CE_{lim} when all the pores are covered; at this time i_3 goes to zero. Thus the overall hydrogen formed at the substrate is determined by the integral quantity $\int i_3\,(h)dh$, with h increasing from zero to h_{lim}, this latter condition corresponding to a non-porous deposit. Since this integral corresponds to the overall hydrogen evolved at the substrate, it is possible to assume that after this initial transient the incorporated hydrogen fraction remains constant.

The second possibile source of substrate hydrogenation is the hydrogen in the deposit; this contribution can be discussed by solving the diffusion equation for the hydrogen in the deposit with the boundary condition $C=0$ at the substrate surface; this corresponds to the hypothesis that the diffusion coefficient of H is much higher in the substrate than in the deposit. The corresponding analysis gives a logarithmic time dependence of the incorporated hydrogen; in other words, its volume increases continuously, contrary to the previous case. Besides, some additional hydrogen may transfer into the substrate even after electrolysis is over. The experimental values of this supplementary post-electrolysis hydrogen are sometimes very high; this contribution may result from the decomposition of organic inclusions in the deposit.

The third possibility is determined by hydrogen diffusion into the substrate from the initial layers of the deposit. Sometimes the initial thin layer formed near the substrate is very rich with hydrogen. This layer is characterized by an anomalously high solubility and diffusivity of hydrogen, atomic hydrogen being generated here at the very beginning of the electrolysis. A rigorous solution of the corresponding problem is difficult but an analysis of the simplified problem shows that for an initial hydrogen concentration in this layer C the volume transferred into the substrate at a time t is

$$V \approx C(0.5(Dt)^{1/2} - Dt/h) \tag{11.32}$$

where h is the deposit thickness at the same time. The second term represents the fraction transferred into the subsequent deposit.

Obviously, the amounts of hydrogen in the deposit and in the substrate should be measured in some way. A possible method requires heating the hydrogenated samples in vacuum (the substrate and deposit might be joined or separated) while the hydrogen pressure in the system is continuously measured. The resulting data show that there are several types of incorporated hydrogen, classified according to their bond strength with the metal. Correspondingly, the activation energies for diffusion and the temperature intervals at which these phenomena are activated are different. An alternative method of hydrogen estimation in the deposits is melting of the film and substrate; this method gives directly the overall hydrogen quantity.

11.9 Hydrogen Permeability of Membranes

Monitoring hydrogen permeation through a membrane is a particularly useful method to determine the kinetic constants of the surface processes involving hydrogen transport together with their diffusion coefficients.

The method [4] consists in the electrochemical generation of hydrogen at one side of the membrane and its electrochemical oxidation at the other side; in the steady state regime the oxidation current is equal to the hydrogen flux through the membrane; thus, a measurement of this current and the study of its dependence on the membrane thickness and the conditions of hydrogen generation gives the parameters of interest.

The flux of hydrogen into the membrane is $J_+ = k_+\theta$, where θ is the hydrogen coverage. The reverse flux is $J_- = k_- C_{\mathrm{d}(1)}(1-\theta)$, where $C_{\mathrm{d}(1)}$ is the hydrogen concentration at the membrane near its cathodic side. The actual flux is equal to

$$J_1 = J_+ - J_- = k_+\theta - k_- C_{\mathrm{d}(1)}(1-\theta). \tag{11.33}$$

The flux at the anodic side of the membrane is

$$J_2 = k_- C_{\mathrm{d}(2)}, \tag{11.34}$$

where $C_{\mathrm{d}(2)}$ is the hydrogen concentration at the membrane near its anodic side.

Inside the membrane a concentration gradient of the absorbed hydrogen is presentd, and the corresponding diffusion flux is equal to

$$J_3 = (C_{\mathrm{d}(1)} - C_{\mathrm{d}(2)})\mathrm{D}/\mathrm{L}, \tag{11.35}$$

where L is the membrane thickness. At steady state $J_1 = J_2 = J_3$, thus one obtains after simple rearrangements

$$J^{-1} = (2-\theta)/k_+\theta + (k_-/k_+)\mathrm{L}/\mathrm{D}. \tag{11.36}$$

This shows that by measurements of the current of the hydrogen oxidation current $i = J/F$ using membranes with various thickness L, one can find all the involved

quantities; moreover, only two thicknesses are needed in principle due to linearity of the dependence $J^{-1} - L$.

It would be very interesting to study by this method the simultaneous metal deposition and hydrogen evolution at the cathodic side of the membrane.

11.10 Conclusion

The adsorption-diffusion mechanism of impurity codeposition considered in this chapter has so far been proven for a number of compounds, mainly using radiochemical and analytical measurements combined with monitoring of the electrochemical process conditions. The experimental data thus obtained generally refer to the codeposition of impurities from specially introduced additives, including leveling, brightening, or wetting agents, that provide for rather high inclusion concentrations.

Much less data are available on the inclusion of impurities of inorganic electrolyte ions. It is known that sulfide sulfur in deposits of electronegative metals can sometimes be formed as a result of the reduction of sulfate present in the solution. On the other hand, a possible source of carbon is the dissolved carbon dioxide. Suspensions present in solution (e.g., anodic scale) result in contamination of the deposit by particles of insoluble chlorides, oxides, and other substances transported to the cathode by electrophoresis. However, in many cases, inclusion of inorganic ions is determined by their adsorption on the cathode, and the ratio of the concentrations of various incorporated impurities reflects the ratio of their adsorption values and concentrations in the electrolyte. In this case, the above theoretical analysis remains valid.

It often happens that the worst contaminated deposit layer is the one adjacent to the substrate. This is related to the conditions of formation of this layer. This initial layer has an island structure and is not continuous (this can be true up to a thickness of about 1 μm) and consequently may feature an increased specific surface area; moreover, the deposit can store in its pores adsorbed atoms and molecules and even small solution volumes.

References

1. Kruglikov S.S., Dolinin E.L., Metals Protection 1969, v. 5, p. 81, 183 (in Russian)
2. Webb M., Price P., Vermileya D., Acta Metallurgica,1968, v.6., p. 524
3. Gamburg Yu. D., Soviet J. Electrochemistry,1980, v. 16, No. 1, p. 83
4. Kruglikov S.S., Volkov V.A. Soviet J. Electrochemistry,1970, v. 6, p. 1033
5. Edwards J. Trans. Inst. Metal Finishing, 1964, v. 41, p. 168
6. Edwards J., Levett M.J. Trans. Inst. Metal Finishing, 1964, v. 41, p. 157
7. Prall J.K., Schreir L.L., Trans. Inst. Metal Finishing, 1964, v. 41, p. 29
8. Raub E., et al. Metalloberflache,1966, Bd. 20, p.62; 1968, Bd. 22, p. 75
9. Devanathan M.A.V., Stachurski Z., J. Electrochem. Soc., 1964, v. 111, p. 619

Chapter 12
Technologies for the Electrodeposition of Metals and Alloys: Materials and Electrolyte Selection, Substrate Preparation

Electrodeposition is a technology for the production of metals, alloys or composite films, characterized by a unique simplicity of implementation, low capital cost, and high versatility. This technique has been in use since the nineteenth century for the deposition of decorative films, as well as coatings that impart better corrosion resistance, or improved mechanical or wear properties. During the last 40 years however, electrodeposition has been applied to various aspects of manufacturing in electronics, leading to revolutionary advances; with an increased understanding of its fundamentals, it is being utilized today in an ever wider set of applications. In this chapter we discuss the set of materials that can be electroplated from aqueous solutions, their applications, and the methods involved in their manufacturing.

12.1 Materials Selection

The selection of the most appropriate material to be used in the electrodeposition of the coating of interest is based first of all on the functional requirements imposed on the coating; in some cases a unique material is suitable to perform the function sought for, while in other cases alternatives may exist.

In the following we discuss the most important functional properties of electrodeposited coatings and the various metals and alloys capable to perform these functions.

12.1.1 Decorative Properties: Au, Ag, Rh, Pt, Ni, Cr, Ni–Sn

The precious metals such as gold, silver, platinum, rhodium and their alloys are the most obvious choice for decorative applications since these materials are extensively used for jewelry and luxury items. In addition metals such as chromium, nickel

Y. D. Gamburg, G. Zangari, *Theory and Practice of Metal Electrodeposition,*
DOI 10.1007/978-1-4419-9669-5_12, © Springer Science+Business Media, LLC 2011

and several of their alloys have a pleasing appearance, appropriate for decorative applications. For these purposes, chromium is usually deposited on layered undercoats consisting of copper and then nickel on top. Such triple coatings are the most common decorative and protective deposits, commonly used on various steels and zinc alloys. Nickel–tin alloy deposition also appears to have considerable promise and is sometimes used instead of decorative chromium.

12.1.2 Enhancing Solderability and Welding: Sn Alloys, Ni, Cu, Au, Pd

Tin and its alloys are extensively employed to improve the solderability and corrosion protection of various surfaces. The materials used are often Sn alloys with various additions of lead, bismuth, and/or antimony. More recent alloy formulations tend to avoid lead and introduce silver; ternary or quaternary alloys are used to optimize both solderability and melting temperature. In the case of copper substrates, deposits of Sn–Ni are also of interest.

The alloy films used to increase solderability must provide for a reduced melting temperature and should be able to suppress the formation of whiskers, which may cause short circuits in the device. Soldering occurs via local heating, which may cause as a side effect interdiffusion among the various layers and/or the substrate. In this respect, nickel underlayers are of interest as barrier layers against the interdiffusion among the various device layers, for instance against the diffusion of zinc from the brass substrate into the finish coating. For the same purpose, sometimes tin or its alloys are deposited onto a previously formed copper layer, e.g. when coating various types of steel. Nickel coatings are employed as high-temperature solders; such films can provide both soldering and welding. For this purpose films of nickel or bilayers copper/nickel are deposited on top of tungsten or molybdenum surfaces.

12.1.3 Antifriction Properties: Pb or Sn Alloys, In, Au

Lead alloys containing tin (and in some cases also copper) are often used as antifriction materials. Sn–Ni alloy can also be utilized for this purpose; these alloys in particular are capable to retain lubricants at the surface. Coatings of lead alloys containing small quantities (about 2%) of other metals (copper, antimony, tin) have good antifriction properties and higher wear resistance than pure lead. Alloys containing indium are expensive, but they allow reliable operation under especially severe friction conditions. For particular applications, lead alloys with zinc or cadmium are resistant in oils, and gold deposits are good as lubricating layers in vacuum. Particularly interesting are composite coatings containing molybdenum disulfide as lubricant.

12.1.4 Corrosion Protection: Zn, Sn, Cd, Ni, Zn–Ni, Pd, Ag, Ag–Pd, Au

Electrodeposited coatings may provide corrosion protection by being sacrificial with respect to the substrate or by providing a dense, continuous coating that is not attacked by the external environment.

The most important electrodeposited material for corrosion protection is zinc. In the majority of cases a zinc deposit is anodic in reference to the substrate, i.e. corrodes preferentially with respect to the latter through galvanic protection. A relatively thin coating significantly increases the endurance of steel to corrosive conditions. Up to the temperature of 70°C Zn is able to protect different steels; white corrosion products inhibit further corrosion progress and increase the lifetime of the article. It should be noticed that anodic protection acts in such a way that, even if the sacrificial coating is discontinuous, the substrate does not corrode. In order to further improve their performance, zinc coatings can be additionally oxidized or painted. Better corrosion resistance is achieved by using Zn alloys such as Zn-Ni and Zn-Co, experimented with and in some instances even used for surface finishing in the automobile industry.

For application in marine environment and when coating high-strength steels, cadmium coatings are preferred; however, both the material and its production process are rather toxic, and as a consequence there is a tendency to decrease or eliminate the use of cadmium, and substitute it with more environmentally friendly materials.

Tin is widely used as a protective coating; in fact it has high corrosion resistance as a stand alone material in many environments, particularly in presence of organic compounds (e.g. foodstuffs).

Nickel coatings are cathodic with respect to steel, therefore they cannot protect steel anodically. However, Ni exhibits high corrosion resistance on its own and, in the form of a continuous coating, may protect the substrate as a barrier layer. The same can be said about silver, gold, palladium and other precious metals. These metals and alloys (for example, Ag–Pd) are used for the protection of copper.

12.1.5 Electrical Contacts and Conductivity: Cu, Ag and Its Alloys, Au and Its Alloys, Pd, Ni, Sn, Sn–Pb

Metals extensively used for electrical contacts include silver and its alloys as well as palladium or its alloys. Nickel is suitable in contact with hydrocarbons, and copper–tin alloys perform well in sulphur-containing environments. Hard gold, i.e. Au alloys containing a small percentage of Cd, Ni or Co are used for low-current contacts. Gold and palladium are often deposited on silver or nickel underlayers to minimize the use of precious metals. Silver may also be coated onto previously deposited nickel. More recently, silver alloys with antimony or with palladium are

utilized instead. These alloys are more stable and wear-resistant, but they have a larger contact resistance than the pure metal.

It should be noted that, besides the metals listed above, also tin (on nickel) or zinc layers can be used for electric contacts with moderate conductivity requirements.

Electrodeposited copper has been extensively used over the years to form conductive lines and vias for printed circuits; more recently, the use of copper has been extended to metal interconnects in the ultra large scale integration (ULSI) technology for chip manufacturing. The use of copper is justified by its high conductivity and by its relatively high melting temperature, sufficient to avoid electromigration effects. Higher stability with respect to operating temperature or corrosion resistance requirements may be achieved by using nickel, silver, palladium, rhodium, Sn–Pb alloy and also gold alloys containing 1–1.5% of cobalt or nickel. These coatings are deposited usually upon copper and nickel underlayers.

12.1.6 Hardness and Wear-Resistance: Cr, Ni, Ni–W, Ni–B, Rh, Sn Alloys

High hardness is characteristic of electrodeposited chromium, nickel, rhodium, palladium; these films are twice as hard (or more) than the corresponding bulk metals, due to the particular microstructure imparted by the deposition process. The alloys nickel–tungsten, nickel–molybdenum, and sometimes rhenium alloys or copper–tin may also be used as hard coatings. Chemically and electrochemically deposited nickel alloys containing boron or phosphorus also provide for considerable hardness and wear resistance, and they are used in some applications.

Chromium (including "milky" chromium) is best suited for use in conditions of severe friction. Some tin and nickel alloys may also provide reasonable performance in this respect.

12.1.7 Miscellaneous Properties

Nickel (no less than 6 μm thick) provides for a good barrier coating. Sometimes chromium is used for this purpose but it is difficult to deposit other metals upon its surface. Cobalt–phosphorus and its ternary alloys have been extensively used in recent microelectronic applications, in particular as barrier materials.

Magnetic coatings are mostly based on the iron group metals iron, cobalt and nickel, their mutual alloys or alloys with other elements. Suitable alloy compositions depend on the requirements of the application at hand. Properties of interest include the magnetization at saturation and at remanence, the coercive force, the magnetic susceptibility or the permeability. Soft magnetic materials, characterized

by a low coercivity and high magnetic susceptibility, are usually nickel and iron based alloys, whereas hard magnetic alloys, with a high coercivity and high remanence, are based on cobalt, cobalt-based hexagonal alloys, or on intermetallic alloys having non-cubic structures. Typical examples of the latter are the $L1_0$ tetragonal structures of Fe-Pt or Co-Pt.

Some of the best anti-friction and anti-galling coatings for threads are made of zinc; tin and Ni–Sn are also suitable. Cadmium and silver are used more seldom, since the former is toxic and the latter is expensive. Anti-friction coatings for specific purposes include copper for the protection of steel against carbon penetration during carburizing processes, or tin for the protection of copper wire against sulfide formation (by rubber isolation). Copper is sometimes deposited on steel before inducing plastic deformation to increase its ductility and also to achieve a better contact when grinding.

Specific optical properties are achieved when depositing silver, chromium, rhodium or nickel coatings from specially formulated solutions. These coatings can be reflecting (mirror-like) or, on the contrary, strongly light-absorbing (black). Silver has the highest reflectance whereas black chromium is the metal with the highest absorbance.

The applications and materials listed above are necessarily incomplete. Many others properties and requirements may be of interest; e.g. films of platinum or its alloys possess outstanding catalytic properties; lead protects various metals in sulfur-containing environments. Nickel and iron are used to repair worn machine parts which require precise corrections in their dimensions, while also supplying the required wear properties.

12.2 Deposit Thickness

Assessing the correct thickness of the overall deposit or the thicknesses of the various layers is an essential step in the design of the coating of interest.

In this respect, it is necessary to distinguish between average and minimum thickness: while thickness calculation using Faraday's laws gives the former one, pronounced inhomogeneities may be observed, with much thinner coatings often observed at recesses, valleys or at locations most distant from the anode or facing away from it. For this reason thickness control after deposition is necessary along with its previous calculation.

When dealing with coatings for corrosion protection for example the necessary thickness depends on the presumed operating conditions. In relatively mild environment a thickness of 10 μm is usually sufficient. At this thickness deposits become essentially non-porous. Thinner coatings may have through pores, where corrosion of the substrate can start. When using a barrier (anti-diffusion) base coating, the thickness of the top coating should exceed 6 μm. Decorative coatings of precious metals or chromium should have a thickness of about 3 μm, but sometimes due to cost limitation 1 or even 0.3 μm are applied.

Under more severe conditions (a corrosive environment, friction, high humidity and/or temperature) the thickness of useful deposits (including undercoats) should be raised up to 20–25 μm, and for particularly severe conditions to 30–40 μm or more. Under these circumstances it may be necessary to take into account the substantial change in size of the items that are being coated.

Electrodeposits on threads should usually have a thickness averaging about 1% of its step.

Finally, it should be mentioned that thick deposits are not necessarily better than thin ones because internal stresses are higher in thick layers and they may lead to embrittlement and cracking.

12.3 Selection of the Electrolyte

For any metal or alloy that can be deposited from aqueous solutions, there usually exist several types of electrolytes that permit to obtain a deposit with a suitable microstructure and properties. This raises the question of selection of the optimum solution. Common rules in this respect do not exist so we shall restrict our consideration to some typical examples.

In deciding on a particular process for zinc deposition for example we have to proceed from the distinction between acidic and alkaline electrolytes. Acidic solutions allow the use of very high current densities and consequently may produce thick coatings in a short time; however, they usually have low throwing power and therefore they are satisfactory only for articles having simple shapes. From this point of view alkaline cyanide or ammonia electrolytes tend to be much better. In most cases cyanide solutions give more uniform and protective deposits. On the other hand, cyanide solutions present several drawbacks which discourage their use. Most importantly, these solutions are highly toxic and their use is strongly discouraged and regulated by laws. Additionally, the rate of deposition and current efficiency are significantly lower than other electrolytes. Finally, both cyanide and cyanide-free alkaline solutions contain organic additives in presence of which hydrogenation of steel can occur.

Electrodeposition of nickel coatings as barrier layers (as an undercoat for silver, gold, palladium, tin alloys etc.) is usually carried out using sulfate solutions containing some chloride and boric acid. The deposits in this case are pure Ni; they have low internal stresses but no decorative appearance. Diluted chloride solutions are suitable for deposition of thin nickel base layers on corrosion-resistant steel. Sulfamate solutions give very good deposits with little internal stresses at high current density; these deposits are suited for soldering and mechanical machining but they tend to form passive film. The solutions specifically developed for decorative bright deposits contain additives such as saccharine or buthynediol; the resulting coatings are leveled, bright or semi-bright but they tend to have poor adhesion, poor solderability and are unsuitable for mechanical working.

In other situations electrolyte selection may be determined by environmental considerations, by the presence or absence of certain chemical compounds in the formulation, or by specific requirements imposed on coatings. The specific advantages and disadvantages of various processes are outlined in the following chapter(s). The properties of various deposits are described in Chap. 14.

12.4 Chemical and Electrochemical Degreasing

The process of preliminary cleaning includes the various operations intended for the removal of greasy compounds and oxide films from the surface to be plated, which can prevent adhesion and impair the appearance of the deposit. The metal in fact can be successfully deposited only upon a sufficiently clean surface, which in practice is contaminated by several types of greasy materials, namely, fatty compounds (oils and fats of plant or animal origin) and mineral oils. A metallic surface is also covered with oxide layers or scale which should be removed too. As a whole, the type and quantity of extraneous matter ordinarily present on the surface depends on the previous history of the article.

Surface cleaning begins with degreasing, which may be chemical or electrochemical.

Chemical degreasing. Firstly various organic solvents are used: chlorinated and/or fluorinated hydrocarbons, most commonly tetrafluoroethylene or perchloroethylene with addition of stabilizers; ethanol, paraffin and carbon tetrachloride can also be applied. Temperature may not exceed 60°C. Care must be exercised against inhalation as well as ignition since some of these liquids are flammable. Aluminum and magnesium alloys may by degreased in tetrachloroethylene, but not in trichloroethylene. At this stage removal of compounds that are not amenable to saponification occurs.

The next stage consists in alkali treatment. Fatty compounds can be separated by the action of hot solutions containing sodium carbonate, tri-sodium phosphate or pyrophosphate, liquid glass (sodium silicate), caustic soda (NaOH) and organic surface-active additives. When preparing these solutions sodium hydroxide is added at last and gradually. These solutions are alkaline, with pH that may vary in a wide range; a general-purpose solution contains for example NaOH 10 g/l, Na_2CO_3 $10H_2O$ 40 g/l and Na_3PO_4 40 g/l. When degreasing aluminum or zinc alloys however the NaOH concentration must be less than 1 g/l. A number of specific additives may be used in degreasing solutions (wetting agents, foam suppressors etc.); the best operating temperature for this solution is 70°C.

The duration of the process depends on the degree of contamination; in the case of steel it may average between 5 and 30 min; in the case of other metals from several seconds to 5 min. Best results are obtained when ultrasonic agitation is used (0.5–3 W/cm^2 at frequency of 20–30 KHz).

Electrochemical degreasing (both cathodic and anodic) is very effective and widely used along with chemical cleaning. The solutions are the same as with

chemical degreasing (with the exception of sodium silicate). These processes are characterized by the evolution of gas bubbles—hydrogen or oxygen, respectively—whereby the bubbles capture the impurities when they separate from the surface. These processes are carried out at 70°C, and using cathodic or anodic current densities of 3–6 A/dm^2. The duration of cathodic degreasing is about 1 min; that of the anodic process 5–20 s. (in the case of steel up to 5 min). Electrochemical degreasing however presents some drawbacks. During anodic degreasing partial oxidation of the surface may occur; in particular, in the case of tin, zinc or chromium their dissolution is also possible; this is why these metals should not be treated anodically. Cathodic degreasing may result in the deposition of thin films of foreign metals present in solution and/or in the hydrogenation of steel substrates. Consequently, it is preferred to degrease steel only anodically while other metals should be treated cathodically; practice recommends that in the last case an additional final anodic pulse of short duration be applied.

12.5 Pickling

Oxides and some other compounds present at the surface and capable to reduce adhesion of a deposit, or even to prevent deposition, cannot be removed with cleaning procedures. These substances can form either a thick scale or a thin tarnishing film, which are usually removed by pickling in a sufficiently acidic or sometimes alkaline solution. This is often done in combination with mechanical removal methods: grinding, brushing, etc.

The specific process to be used depends to a large extent on the substrate material but the majority of solutions consists of a mixture of acids (H_2SO_4, HCl, HNO_3, H_3PO_4, HF) or NaOH. The acidic solutions are usually preferred but the alkaline ones may be used for a previous treatment of heavily oxidized surfaces, in order to loosen the oxide layer. Furthermore, the addition of inhibitors, which do not affect the rate of oxide dissolution while simultaneously inhibiting chemical dissolution of the metal, is very useful.

Selection of a suitable pickling chemistry is a complex process which requires a detailed knowledge of the reactivity of metals and alloys and of their oxides. The following recommendations have been gained by practical experience.

Removal of scale from *ferrous metals*—standard steels and cast iron—is usually achieved by pickling in solutions of sulfuric or hydrochloric acids which should also contain inhibitors. Typically, the solution should contain 100–150 g/l of H_2SO_4; sometimes 50–70 g/l of nitric acid may be added; combination of the two acids is important since sulfuric acid decreases the rate of removal by nitric acid. A gentler pickling is achieved with the same concentration of sulfuric acid in presence of 150 g/l of NaCl or 1 g/l of KI; addition of some inhibitor is also necessary. Hydrochloric acid can also be used—the chloride is more soluble than the sulfate—but this solution is much more corrosive. A temperature of 60°C is suitable, and the duration of the process may be as much as some tens of minutes.

The sludge or the loosened scale and dirt formed during these processes are removed mechanically or chemically, in the last case by immersing the item in a mixture of sulfuric and nitric acids (80 + 80 g/l) at room temperature or with gentle heating.

In the case of corrosion-resistant steels, a previous loosening of the scale is often necessary. This is usually performed in a solution of 200 g/l of sulfuric acid for a duration of 30–40 min at 50–70°C. The subsequent process may be operated in a mixture of sulfuric, nitric and hydrofluoric acids (100 + 100 + 20 g/l) at room temperature or with gentle heating. Sulfuric acid may be substituted by H_3PO_4 for a milder pickling, and HF correspondingly by sodium fluoride. Hydrochloric acid is undesirable because it causes some unneeded corrosion problems.

The pickling of *copper and its alloys* (after heat treatment or after storage) is initially performed in a solution of 200 g/l H_2SO_4 at room temperature or, in the case of a thicker oxide layer, at 50–70°C. Dipping in this solution can give a bright or a matt surface. A bright surface can be achieved at room temperature in a solution of 1000–1100 g/l of sulfuric acid containing additionally 250–300 g/l of ammonium nitrate. Instead of the latter a mixture of nitric acid (50 g/l) and NaCl (10 g/l) may be used. A matt surface is obtained in 700 g/l of ammonium (or sodium) nitrate followed by treatment in sulfuric acid (700 g/l) or phosphoric acid (1300 g/l) for 15–20 min at room temperature.

Another good solution for pickling of copper alloys consists of sulfuric acid (100 g/l) and hydrogen peroxide (50 ml/l). The toughest pickling conditions occur in a mixture of equal volumes of concentrated sulfuric acid, nitric acid and water.

Articles made of *aluminum and its alloys* may be treated in a solution of sodium alkali (60 g/l) at 40–50°C with additions of agar (as inhibitor of metal pickling) and sodium gluconate (to enhance the solubility of the salts). Alloys containing high concentrations of Si should be pickled at 70°C in acidic fluorine-containing solutions, for instance 400–800 g/l of HNO_3 and 50–150 g/l of HF, the optimum concentrations depending on the alloy composition.

For *zinc castings*, treatment in diluted (20 g/l) sulfuric acid for 1–2 min is sufficient. *Magnesium-containing alloys* may be pickled at 20–30°C in diluted nitric acid (50–100 g/l), the sludge being then eliminated with a solution of chromic or hydrofluoric acid. For *lead alloys and solders* dilute solutions of HBF_4 (1:10) or HF (1:4) are suitable.

Molybdenum, tungsten and their alloys with other metals are effectively pickled in a heated solution of sulfuric and nitric acids (70 + 70 g/l) with the addition of 5–6 g/l of fluoride.

Titanium alloys are pickled usually in concentrated solutions (up to 1000 g/l) of H_2SO_4 either at room temperature or with heating. Sometimes sodium chloride or fluoride (30–40 g/l) is added. If the oxide film is previously treated in a hot alkaline solution (600 g/l of NaOH + 200 g/l $NaNO_3$) or even in molten alkali, then the process may be carried out in a more diluted acidic solution (120 g/l of sulfuric acid and 70–80 g/l of hydrofluoric acid). Another method for titanium treatment consists in its pickling for 1 min at 25°C in a mixture of nitric (200 g/l) and hydrofluoric (10 g/l) acids followed by cold water rinsing and then by treatment in a mixture

of sulfuric and hydrochloric acids (550 and 250 g/l correspondingly) at 50°C for 20 min.

In closing it may be noticed that after said operations all traces of the used substances are to be removed by repeated rinsing; for reactive metals thorough drying may also be necessary.

Nowadays many commercially available solutions exist for all listed processes. Besides, several reference books are published where the matter discussed here is presented much more comprehensively [1].

12.6 Additional Treatments

Sometimes other methods of surface treatment may be used, including electrochemical polishing, zincate treatment and activation (pickling) of the surface.

The basic ingredient of an electropolishing solution is phosphoric acid (900–1200 g/l) to which CrO_3 (50–70 g/l) and sulfuric acid (250–500 g/l) are often added. Water content in the solution may not exceed 20 wt%. Steel, copper and aluminum alloys for example may be anodically polished at 60–70°C in these solutions. Upon use of the correct polishing conditions (anodic current density and temperature) the surface becomes smooth and bright in up to ten minutes. The usual value of applied current density is 10–30 A/dm^2, but it is much more convenient to control electrode potential rather than current density. Its value may in each case be established experimentally. Lead, aluminum or stainless steel cathodes are used for electropolishing.

The mechanism of brightening action in electropolishing is somewhat similar to that occurring in cathodic electrodeposition in presence of specific additives (brighteners) which will be discussed later. The basic role is here played by the viscous film near the electrode inhibiting the products rejection into the bulk of the solution.

The process of contact deposition of a very thin zinc layer onto aluminum or magnesium alloys (the so-called zincate treatment) is used for providing good adhesion of the subsequent thick deposit of the needed metal. Alkaline zincate solutions are used for this purpose. The solution used for aluminum alloys contains 10 g/l of NaOH, 5 g/l ZnO and 10 g/l of Rochelle's salt; the duration of the process may be about 2 min at room temperature. Pure Al requires stronger alkaline solutions, to which a separately prepared solution of zinc sulfate is added. The finished solution contains 120 g/l of NaOH and 40 g/l of $ZnSO_4$. In this case the adhesion depends on the grain size of the resulting Zn film: small grains are desirable.

There also exist a number of specific methods used for providing electrodeposition on non-conductive surfaces, mainly plastics. These methods consist predominantly in oxidative etching in acidic solutions in order to obtain a surface with controlled roughness, followed by electroless deposition of copper or nickel-phosphorus alloy to provide for a conductive surface. After that, conventional electrode-

position may be performed. The details of all these methods are beyond the scope of the present book and can be found elsewhere [2].

References

1. Modern Electroplating, Schlesinger M., Paunovic M. (Ed.), 2000
2. Mohler J. B. Electroplating and Related Processes. Chemical Publishing Co., 1969

Chapter 13
Technologies for the Electrodeposition of Metals and Alloys: Electrolytes and Processes

A wide range of metals and alloys can be electrodeposited from aqueous solutions. These include most of the mid- and late transition metals, the precious metals, and some of the 4p, 5p and 6p elements. Some early transition metals (V, Mo, W) as well as the elements P and B can be co-deposited only simultaneously with the deposition of the iron group metals. Highly reactive elements cannot be electrodeposited due to their low redox potentials; the dissociation of the solvent is highly competitive with the reduction of these elements and the electrode cannot be made to assume the potential required for their reduction.

The choice of the optimum electrodeposition process for a given metal or alloy is highly dependent on the stability of the corresponding ionic species—or of their complexes—in solution. In the following the most common processes for the electrodeposition of engineering or decorative metallic coatings are described. Each section dedicated to a specific metal or alloy is structured as follows: first, the properties of the corresponding material are discussed, then the possible solution for electrodeposition are listed, the electrodeposition mechanism (if known) is presented, and finally some practical guidelines for process implementation are provided. This discussion is not meant to be comprehensive and the reader is encouraged to search the literature for up to date or specific information.

13.1 Deposition of Copper and Its Alloys

13.1.1 Properties and Fields of Application of Copper Deposits

Copper is widely utilized in electrodeposition technology; applications vary from an undercoat for successively plated layers, to conductor in printed circuit boards, to electroformed articles. Most recently, copper plating has displaced sputtering of aluminum in the manufacturing of semiconductor interconnects. The use of copper as an undercoat is favored by the fact that it is a relatively inexpensive metal and also has the very useful feature that it can be deposited on top of various substrates with little technological difficulties. Copper coatings easily correct pre-existing de-

Y. D. Gamburg, G. Zangari, *Theory and Practice of Metal Electrodeposition,*
DOI 10.1007/978-1-4419-9669-5_13, © Springer Science+Business Media, LLC 2011

fects on the substrates, such as holes, scratches, valleys. The various processes of copper deposition are characterized by a high current efficiency CE; several electrolytes also exhibit high throwing power TP.

13.1.1.1 Advantages

1. Copper has the highest electrical conductivity and thermal conductivity besides silver; this makes copper suitable for printed circuit boards and optical wave-guides.
2. As a metal, it is environmentally non hazardous; the waste treatment of copper electrolytes is in most cases simple, and the copper metal can be recycled.
3. It is an indispensable component of multilayer deposits.
4. Copper deposits usually have low internal stresses; very thick layers can be easily deposited.
5. Copper is ductile and can be easily polished; it is suitable for various mechanical working processes, since it withstands drawing and plastic deformation.
6. Copper can be soldered (immediately after deposition).
7. The deposits have good adhesion to most metals.
8. Copper is capable to protect steel against carburizing.

13.1.1.2 Disadvantages

1. Deposits have a limited chemical resistance, in particular under normal atmospheric conditions; as a consequence they cannot in general provide electrochemical protection of the substrate. As such, copper coatings can be used only after application of a varnish.
2. Diffusion into other metals is relatively easy, resulting in the need of barrier layers, especially at higher temperatures.
3. The deposits can alloy with solders resulting in formation of intermetallic compounds which can reduce solderability.
4. Copper is unstable in contact with many of organic substances.
5. Copper is not suited for hermetic connections, e.g. welded joints.

According to these properties, copper deposits are widely used as undercoatings for deposition of other metals as well as a metal for electroforming. Sometimes copper is deposited on steel articles before mechanical working with the aim to elevate plasticity. In the manufacture of printed circuit boards, electrodeposited copper plays the role of the current-carrying layer.

13.1.2 Solutions for Copper Deposition

Three types of solutions are in common use. These are acidic (sulfate), alkaline (cyanide and—more seldom—non-cyanide) and pyrophosphate (mildly alkaline)

Table 13.1 Solutions for copper deposition

No.	1	2	3	4	5	6
Components (g/l), conditions						
Copper sulfate ($5H_2O$)	180–240	50–80	90–130	100–120		
Copper cyanide					14–18	70–90
Sulfuric acid	50–60	160–220	190–250			
Potassium pyrophosphate				250–300		
Sodium cyanide					28–35	90–120
Sodium hydroxide						40–45
Sodium carbonate					15–20	
Potassium o-phosphate				40–60		
Chloride, ppm	30–80	30–80	40–80			
Nitrate				5–10		
Oxalate				20–25		
Ammonia				1,5–3		
Temperature	20–40	20–35	25–40	45–55	45–55	55–70
pH				8–9		
Current density, mA/cm^2	20–100	10–40	40–100	10–30	8–25	30–80

baths. The solutions based on fluoborate, ethylene diamine and some others are less common. Cyanide solutions have been widely used in the plating industry; however, due to the numerous environmental and occupational hazards involved, their use has seen a steady decrease since the 1970s.

The most common electrolyte compositions and operating conditions are shown in Table 13.1.

Table 13.1 shows that copper deposition can be performed either at a current density of 10–20 mA/cm^2, at room temperature and without solution stirring, or at CD as high as 100 mA/cm^2, when using agitation and elevated temperatures. The baths have high CE and some exhibit relatively good TP.

Acidic copper baths are not expensive; they are simple in composition, stable and easy to control. They have high CE and can tolerate high CD. At the same time acidic baths are characterized by poor TP (due to a low polarizability) and are unsuitable for the direct deposition onto electronegative metals, e.g. steel and zinc castings, due to the possible displacement deposition. Fluoborate solutions are more expensive than sulfate ones, and they are more corrosive and hazardous; the operating CD however may be higher due to the higher solubility of the corresponding salts.

Bath No. 1 is for general purposes; it can be used for example in decorative applications. Bath No. 2 is most suitable for printed circuit-boards (PCBs); bath No. 3 enables high-speed deposition on PCBs with strong agitation; it is particularly good for strip plating. A higher concentration of sulfuric acid improves solution conductivity and enhances TP, especially when the copper salt concentration is low. Throwing power can be improved by addition of 1 g/l potassium nitrate. At low H_2SO_4 concentration (less than 50 g/l) undesirable basic copper salts may precipitate as a result of hydrolysis. Chloride ions at a concentration of 60–80 ppm con-

tribute to decrease anode polarization and eliminate striations in the deposit; different concentrations however have harmful effects. Chlorides also contribute to keep internal stresses low and are essential for the adequate action of additive agents.

The TP of copper sulfate solutions is about 8–12%, and in the presence of additives can reach up to 16–18%.

Cyanide solutions have much better TP than acidic ones (26–32%) and, as an additional advantage, can be used for copper deposition on steel and other active metals. Solution control however is more difficult, and the operating CD is lower. The main drawback of these solutions is that they are toxic, necessitating special care during operation as well as an expensive and well documented waste treatment process. The baths contain excess of cyanide (also called "free" cyanide).

Non-cyanide alkaline baths use other complexes to replace cyanide; these operate at lower pH: about 8–9 instead of 11 for cyanide electrolytes.

Solution No. 5 is a strike bath, used for the deposition on steel or Zn alloys of an adherent, thin (up to 2.5 μm) Cu layer ready for subsequent metal deposition. This bath provides good TP and coverage. This bath is highly versatile, as it can be used both as a strike and for thicker deposits. Bath No. 6 has the highest CE among the cyanide solutions, and it allows relatively fast deposition.

Pyrophosphate copper solutions (bath No. 4) are used mainly for printed circuit boards and sometimes as a substitute of cyanide baths (for deposition upon steel) and also for electroforming applications. The deposits from these solutions exhibit particularly good ductility, the TP is high (18–24%), but the deposition rate is relatively low. These solutions are mildly alkaline and contain a considerable excess of pyrophosphate ("free" pyrophosphate) along with a certain quantity of orthophosphate (up to 60 g/l), ammonium nitrate and oxalate as buffer. Several baths of this type also contain sulfosalicilate (20 g/l).

13.1.3 Copper Plating for Semiconductor Interconnects

Since 1997 copper electrodeposition has been extensively used for the metallization of interconnects within semiconductor chips in the so-called Ultra Large Scale Integration (ULSI) technology, and for the manufacture of through-holes in multilevel integrated circuits and packaging. Electrodeposited copper has substituted sputtered aluminum, which below a certain interconnect size and above a certain density was reputed to be insufficiently resistant to electromigration. Electrodeposition at the time was found to be the optimum technology to fill high aspect ratio trenches having a lateral size of down to about 30 nm. The electrodeposition process used is called *damascene*, from an ancient technique to inlay various metals over one another. The damascene process differs from through-mask plating in that a thin seed layer is first deposited conformally onto a patterned surface in order to cover the whole surface, then copper electrodeposition is used to uniformly fill the trenches, and finally chemical-mechanical polishing is used to remove excess metal. The copper electroplating process must be able to fill extremely small, high aspect ratio

trenches without void formation. This is achieved by using a novel chemistry capable to deposit copper at the bottom of each trench faster than at the side walls, achieving the so-called superconformal growth. Many copper chemistries are currently employed to achieve superconformal growth in ever smaller trenches; a prototypical electrolyte is obtained by starting with a conventional acidic sulfate with additional sulfuric acid and essentially three additives. Polyethylene glycol (PEG) is typically used as a suppressor of Cu reduction, bis(3-sulfopropyl)disulfide (SPS) is used as an accelerator, and chloride Cl^- interacts with PEG to form a layer at the growing surface which inhibits growth. The inhibitor layer and the SPS compete for adsorption at the electrode, and the SPS preferentially adsorbs at regions of high curvature, where consequently copper growth is accelerated. This technology has more recently been extended to the plating of copper vias, characterized by wider trench size but by much higher aspect ratio, requiring the development of slightly different chemistries.

13.1.4 Solutions Make Up and Purification

Sulfate solutions can be prepared in the following way. The sulfuric acid is first dissolved in a water volume about 2/3 of the final solution volume, in a gradual manner and with continuous stirring. This exothermic process results in heating of the solution. Successively the necessary quantity of copper sulfate (pentahydrate) is added, and finally some more water is added up to the needed volume. The solution must then be purified with activated carbon, the latter being added at about 2–3 g/l, followed by stirring for 1–2 h. The solution can finally be pumped through a filter into a plating tank and operate for solution conditioning at a cathodic CD of 10 mA/cm^2.

In order to prepare a cyanide solution, potassium (or sodium) cyanide is first dissolved in water, followed by the dissolution of copper cyanide in this solution. Any different procedure is strongly discouraged since cyanides should always be present in alkaline solution to avoid the possible formation of hydrogen cyanide HCN, a highly poisonous compound. After allowing the solution to settle the remaining components may be added in the sequence corresponding to the listing provided in the recipe. After adding water up to the necessary volume the bath should be purified with activated carbon as described above; 30 min of agitation should usually suffice, followed by conditioning at 3 mA/cm^2. The same process should be performed repeatedly during operation of the bath.

More complicated is the process of preparing pyrophosphate solutions. Copper sulfate and potassium pyrophosphate should be dissolved separately in minimum water quantities, the mass of the latter salt being about 2/3 of the $CuSO_4 \cdot 5H_2O$ mass. The two solutions are then mixed together, and the resulting copper pyrophosphate precipitate is allowed to settle. This freshly prepared and rinsed copper pyrophosphate is readily soluble in a solution separately prepared containing the rest of the potassium pyrophosphate. The remaining components may be added to this solution after previous dissolution in water; finally, the volume should be

brought up to the desired level with water. The pH level can be corrected if necessary by addition of pyrophosphoric acid or 15–20% KOH. Sodium pyrophosphate may also be used to prepare this bath, but it is undesirable because of its much lower solubility.

13.1.5 Mechanism and Kinetics of Deposition

Deposition of copper from acidic baths occurs through two consecutive one electron transfer steps: $Cu^{2+} + e \rightarrow Cu^{+}$, and $Cu^{+} + e \leftrightarrow Cu$. The first step is slow and thus rate determining (its standard exchange current density is about $2 \cdot 10^{-3}$ A/cm^2), while the second one is a thousand times faster. The solutions always contain a small amount of Cu^{+} ions which are generated both by dissolution of the anode and by the reaction $Cu^{2+} + Cu \leftrightarrow 2Cu^{+}$, which may occur when the solution is in contact with metallic copper. At elevated temperature this equilibrium shifts to the right, so the concentration of Cu^{+} is higher in hot solutions. In solutions containing chlorides the Cu^{+} is stabilized at the electrode surface and copper reduction is accelerated by the occurrence in parallel of a second set of consecutive electron transfer processes: $Cu^{2+} + Cl^{-}_{ads} + e = CuCl_{ads}$ followed by $CuCl_{ads} + e = Cu + Cl^{-}$.

Copper discharge in cyanide solutions occurs from the complex ions CuCN or $Cu(CN)_2^{-}$ depending on current density. Copper is in the monovalent state, resulting in twice the electrochemical equivalent of Cu^{2+} and decreasing in half the charge required for its reduction. A similar effect could be achieved by copper complexing with thiourea. The standard exchange current density in cyanide solutions is relatively low (about 10^{-4} A/cm^2) and the Tafel slope is higher than in the case of acidic solutions, both effects resulting in a higher cathodic polarization, in addition to a much more negative equilibrium potential.

In the case of pyrophosphate the most probable cathodic process is the discharge of the complex anions of divalent copper $Cu(P_2O_7)^{2-}$ or $Cu(P_2O_7)_2^{6-}$.

13.1.6 Peculiarities, Anodes, and Additives. Removing Deposits of Poor Quality

Cyanide electrolytes contain carbonates due to the bath preparation method or generated during operation as a result either of anodic oxidation and hydrolysis of cyanide or by atmospheric carbonization. Carbonate acts as a buffer. Its maximum concentration is about 100 g/l; if it is higher it should be removed by the addition of $Ba(OH)_2$ or by cooling (only for sodium-containing solutions) in a separate tank.

Agitation (mechanical, by air flowing or ultrasonic) of acidic or pyrophosphate baths is quite desirable. In the case of cyanide baths agitation may be performed by mechanical stirring. A periodic treatment with carbon or peroxide is necessary to re-

move organic contaminants from both alkaline and acidic baths. In addition, all the above baths need filtration during operation, at the rate of 1–2 turnovers per hour.

Periodic conditioning at small current densities (0.3–1.0 mA/cm^2) is very useful for removing metallic ionic contaminants.

In some cases the use of non-stationary electric regimes (pulse current, i.e. current interruption, periodic reverse, AC superimposed etc.) provides for better deposit quality and electrolyte stability.

Anodic processes in copper electrolytes do not pose major problems when phosphorized copper anodes (up to 0.06% P) are used. Addition of phosphorus provides for improved mechanical properties and decreases detachment of Cu powder from the anode. The anode-to-cathode CD ratio should be in the range from 4:1 to 1.5:1. In the case of acidic electrolytes a black film of cupric oxide may be formed at the anode surface. The film does not influence anodic dissolution, and it is useful for additives function. The most dangerous impurities in the anodes are Sn and Bi: their concentrations should be less than 0.0001%. Zn, Pb, Ni and Sb are also undesirable. Bagged anodes are often recommended except for the pyrophosphate process, which needs naked OFHC (oxygen free high conductivity) copper anodes to avoid anode sludge.

The additives used in copper deposition depend upon the type of bath. Acidic baths usually contain several types of additives: polymeric (polyethylene glycol or other polyalkylene glycols) with molecular mass of about 1000–6000, acting as inhibitors, and leveling agents, which are consumed at the cathode at the diffusion limiting rate and raise the polarization as a result of their adsorption on the cathodic surface. Numerous leveling additives may be used; these are usually organic sulfonic acids or amines. Finally, the brighteners are usually compounds containing disulfide groups. Along with all these substances, thiourea and its derivatives are also used, as well as gelatin.

Cyanide solutions contain other types of additives due to the much more negative range of operating potentials. Particularly, inorganic compounds are used which upon dissociation generate metallic ions such thallium, tellurium, selenium, lead, sulfur-containing substances, or heterocyclic compounds.

The simplest way **to remove** copper deposits is dissolution at room temperature in a solution of chromium trioxide (250 g/l) with the addition of 100 g/l of ammonium sulfate.

13.1.7 Brass, Bronze and Copper–Nickel Alloys Plating

Brass, both yellow and white (depending on the actual zinc content) is used as a corrosion protective and decorative coating under mild corrosive conditions and also as a cheaper substitute of nickel undercoats for chrome.

The brass containing 30% Zn can be used for deposition on steel to facilitate the subsequent rubber coating; the adhesion of rubber to the brass in fact increases sharply.

Table 13.2 Solutions for brass deposition

No.	1	2	3
Components, conditions			
Copper cyanide	25–30	30–35	15–20
Zinc cyanide	8–12	8–12	80–85
Sodium cyanide	10–20	20–25	30–35
Sodium hydroxide		5–10	50–60
Ammonia (25%)	1–3	3–5	1–3
Sodium carbonate	10–20	6–8	
Temperature, °C	20–40	25–40	25–40
Current density, mA/sq. cm	15–25	3–5	10

Common bath compositions are presented in Table 13.2.

Bath No. 1 is used for decorative coatings on bright nickel undercoat; ammonia fluoride (2.5 g/l) may also be added to this bath. Bath No. 2 is the most versatile; addition of arsenic oxide (0.01 g/l) would form a bright coating. Bath No. 3 is intended for white brass deposition; 0.5 g/l of sodium sulfate is often added to the formulation provided.

The make-up of these solutions is the same as for similar copper baths. The presence of ammonia in solution is desirable because it favors a constant composition of the deposits over time. An alternative chemistry for brass deposition contains diphosphates; this electrolyte is obtained by first preparing a solution of potassium pyrophosphate (80 g/l), and then by separately dissolving and adding to the initial solution copper sulfate, zinc sulfate (1–2 and 1–1.5 g/l respectively) and sodium carbonate (20 g/l). Finally, a solution of boric acid (8 g/l) dissolved separately in warm water is added. The concentrations indicated refer to the final solution.

Deposition is performed using brass anodes, with an area twice that of the cathode, at a temperature slightly higher than room temperature, i.e. 25–30°C, in some cases up to 40°C.

The color of the deposited brass depends strongly on the deposition conditions, and mainly on the metallic ion concentrations in the bath. Color variations indicate the necessity of correcting the bath composition. Incorrect deposits may be non-uniform, grayish or pinkish in color. The cyanide and carbonate concentration must be maintained within relatively narrow limits, otherwise the quality of the coatings decreases and/or solubility of the anodes worsens.

Among the **bronzes**, the alloys containing 12–20% of tin have golden-yellow color and are corrosion-protective for steel in hot water. These coatings can be easily soldered; they also have good antifriction properties. At higher tin concentration the alloys become white in color, and exhibit low porosity and high hardness. These can be used as electrical contacts: even if they exhibit much higher contact resistance than silver, nevertheless they are more stable, harder and more resistant in sulfur-containing environments. The composition of possible solutions for brass electrodeposition is presented in Table 13.3.

Bronze is deposited at relatively high temperature, using bronze or bimetallic copper/tin anodes. When using tin anodes their surface is partly passivated; the extent of passivation may be controlled visually by the presence of an iridescent

Table 13.3 Solutions for bronze deposition

No.	1	2
Components, conditions		
Copper cyanide	35–40	15–20
Sodium stannate	30–35	100–120
Sodium cyanide	20–25	10–15
Sodium hydroxide	8–12	25–30
Temperature, °C	60–70	40–60
Current density, mA/cm^2	20–40	3–5

film; this film mediates anodic dissolution of tin as a four-valent (not divalent) ion. Anodic dissolution is aided by addition of Rochelle's salt (up to 50 g/l). In presence of divalent tin ions the deposits become dull, dark and porous. Insoluble (nickel) anodes are used for the deposition of bronzes with high tin contents.

Solutions are made by dissolving copper cyanide in a previously prepared NaCN solution. The solution must be settled, filtered or decanted into the bath. Finally, separately prepared solutions of sodium stannate and hydroxide are added to the bath, with further addition of hydroxide if needed.

Copper alloys with nickel are successfully deposited from a pyrophosphate solution. This can be prepared using a solution for copper deposition to which nickel sulfate (5–15 g/l of $NiSO_4 \cdot 7H_2O$) and Rochelle salt (20 g/l) are added. The alloy composition depends on the concentrations ratio of Cu and Ni ions in the electrolyte.

13.2 Silver and Its Alloys with Sb, Cu and Pd

13.2.1 Properties and Applications of Silver Deposits

Silver is used both in functional coatings and for jewelry. Silver films can exhibit beautiful white color and high reflection coefficient. Silver is the metal with the highest conductivity, favoring therefore the use of silver coatings as conductors and as electric contacts at the contact pressure 0.25–25 N and with currents up to 20 A. Since silver is more expensive than copper it can be substituted by the latter in some conductor applications.

13.2.1.1 Advantages

1. Silver has the highest reflectivity in the visible window of the electromagnetic spectrum, and it is therefore appropriate for mirrors and reflectors.
2. Silver deposits have low internal stresses; thick layers can therefore be deposited, suitable in particular for electroforming.
3. Silver has the highest electrical and thermal conductivity among all metals, and consequently the lowest contact resistance.

4. The metal is suitable for wave-guides, in printed circuits and electric devices both in applications at low and high current.
5. Silver is corrosion resistant in environments not containing sulfur, in presence of some organic compounds and also in organic acids, diluted inorganic acids, in alkaline solutions, and in peroxide melts.
6. It is ductile and withstands extreme mechanical deformation.
7. It is suitable as antifriction material in vacuum.

13.2.1.2 Disadvantages

1. Silver is unstable in environments containing H_2S or its derivatives, especially in presence of water. In these conditions Ag reacts to give dark and dull films consisting of Ag_2S. Ag tarnishes also in ozone; it is not resistant in ammonia and in strong acids.
2. Wear resistance of silver is low, but it may be increased by alloying with nickel, cobalt or antimony; as a metal it is eroded easily.
3. Silver has a very high surface diffusion coefficient and it tends to creep. Upon pressure contact and/or rubbing it has the tendency to weld, especially under high current and/or high mechanical contact pressure.

13.2.1.3 Applications

According to the above-listed properties silver coatings are used as electrically conductive and reflective layers, for the electroforming of wave-guide elements, as chemically resistant materials and sometimes for electrical contacts. Silver alloys (for instance, with Sb) are often deposited instead of the pure metal due to their increased hardness.

There are several methods to prevent tarnishing of silver, the best consisting in surface modification with self-assembled monolayers (e.g. of fatty acids); without water accessing the surface tarnishing diminishes sharply. Alloys of silver with palladium or nickel tarnish much more slowly.

The usual thickness of silver coatings varies between 3 and 30 μm.

13.2.2 Solutions for Silver Deposition

Silver has been plated since the beginning of the nineteenth century using electrolytes similar to most of the commercial solutions existing today, which are based on the silver cyanide complex in presence of excess cyanide. The most widespread electrolyte compositions for silver deposition are given in Table 13.4. Solution No. 1 is a strike solution for the deposition of very thin coatings, suitable to avoid displacement effects in presence of base metals and/or photoinduced Ag reduction. Such solutions operate at room temperature. Solution No. 4 is dedicated to deposi-

Table 13.4 Solutions for silver deposition

No.	1	2	3	4
Components (g/l), conditions				
Potassium dicyanoargentate	2–4	30–50	40–60	60–80
Potassium cyanide	70–90	20–40		45–50
Potassium carbonate	25–30	80–100	20–40	45–80
Potassium thiocyanate			200–250	
Temperature, °C	20–30	20–30	20–30	20–30
Current density, mA/sq cm	8–10	3–10	10–20	60–70

tion at high rate, under agitation; this electrolyte may additionally contain 20–30 g/l potassium nitrate and 10–15 g/l KOH. This solution, modified by the addition of 15 g/l Ni^{2+}, may also be used to obtain mechanically hard silver-nickel alloys. Solution No. 3 must have pH 9–10.

In all the above solutions the silver-containing salt is potassium dicyanoargentate [$KAg(CN)_2$]. As an alternative, it is possible to use silver nitrate as the metal source. The quality and properties of the deposits depend on the solution composition. At higher cyanide concentration overpotential increases, resulting in the deposition of fine-grained coatings, uniform metal distribution and better anodic dissolution. The optimum ratio of cyanide to silver ions is about 1–1.5. The throwing power is 38–44%. In order to deposit onto less noble metals and to avoid contact silver deposition, metal concentration must be 10 or more times lower than that of cyanide (usually less than 2 g/l of metallic ions).

Potassium salts are preferable to the sodium ones because they result in higher conductivity, higher solubility of the compounds that build-up during operation and a higher limiting current.

Due to the toxicity and waste treatment problems of the cyanide formulation several efforts have been made to substitute these electrolytes with more environmentally friendly ones. Attempts to use complexing agents such as thiourea, hydantoin (2,4-imidazolidinedione), uracil, succinimide, thiosulfate/sulfite or methanesulfonate have been reported in the literature. Most of these formulations suffer from contamination of the base metals following silver displacement, poor adhesion and inferior appearance, in many cases giving a yellowish tint. The thiosulfate formulation has been found to yield Ag films at low current density, but to form silver sulfide Ag_2S at current above the limiting value. Electrolyte formulations based on methanesulfonate are available, but they provide for limited stability and suffer from displacement deposition. Since most of the information on these electrolytes is proprietary, it is difficult to assess the potential of these electrolytes for commercial applications.

13.2.3 Solutions Make Up and Purification

The needed quantity of the potassium dicyanoargentate is dissolved in water, while potassium carbonate and cyanide are first dissolved in a separate container and then

mixed with a solution of the additives and added to the initial bath; water is finally added up to the needed volume. The cyanide often has low purity; in these cases it must be previously purified by addition of 2 ml/l of hydrogen peroxide; after 12 h 2 g/l of the active carbon is added. The final operation (after 2 h) is the filtration.

In absence of dicyanoargentate the bath can be prepared from silver nitrate by stoichiometric addition of the purified potassium cyanide. The most convenient way to do this is to add 3 parts of 5% KCN solution to 1 part of 40% $AgNO_3$ solution. After this operation the cyanide salt is precipitated, and after decantation it can be dissolved in excess KCN. Washing the precipitate of the nitrate ions is not necessary; at low concentration the nitrate does not hinder the electrodeposition process, and only slightly reduces the current efficiency. These operations should be carried out under red light to avoid photoinduced reactions and with caution.

The carbonate concentration under operation must not exceed 150 g/l; the excess (resulting from hydrolysis) has to be withdrawn by addition of calcium or barium nitrate (or cyanide) followed by filtration, otherwise anode dissolution is hindered. Another method to achieve the elimination of excess carbonate is to dilute the electrolyte and to partly replace it by the freshly prepared (carbonate-free) one. Sodium-containing solution can also be chilled (to 3 or 4°C) and filtered.

When silver additions become necessary, it is possible to dissolve the dicyanoargentate immediately in the bath. The cyanide (or thiocyanate) has to be previously dissolved in separate containers. In the case the bath were contaminated by impurities, it must be treated with H_2O_2 and activated carbon, as noted earlier.

There is one further method to prepare the solution with thiocyanate (No. 4). The silver nitrate is separately dissolved in minimum water; a solution of potassium carbonate and $K_4Fe(CN)_6$ is heated up to the boiling temperature then mixed with the former solution and finally boiled for 1.5 h. Red illumination during silver salt dissolution is needed to avoid its reduction. After boiling the solution becomes reddish-brown due to iron hydroxide precipitation.

After cooling down to 40 or 50°C the solution must be filtered through a filter with small pore size since high purity conditions should be achieved, especially with regard to the absence of sulfur compounds. The hydroxide group binds to a fraction of the silver ions; then it can be washed by hot deionized water (immediately into the bath) or separately treated by HCl addition and heating (in this case silver precipitates as AgCl).

The solution has yellow color and contains no free cyanide. As a rule, there is no need of conditioning at low current density. The throwing power of the thiocyanate solutions is about 27–32%.

13.2.4 The Mechanism of Silver Deposition

The metal deposition takes place mainly by the discharge of the $Ag(CN)^{2-}$ species, but sometimes other CN-containing species may be involved. The free cyanide ions are generated at the cathode as deposition occurs. The concentrations of the ions

that can discharge simultaneously are related by a set of equilibria, one of these being: $AgCN + CN^- \leftrightarrow Ag(CN)_2$. These equilibria are shifted as a result of various cathodic and anodic processes which generate additional species present in concentrations that cannot be predicted by equilibrium calculations. Besides, the cyanide is subject to hydrolysis and anodic oxidation, resulting in carbonate formation.

Current efficiency in silver deposition is very high (up to 99% or 100%). The cathodic polarization and polarizability during silver deposition are also high, resulting in very good throwing power and fine-grained structure. This is due to the low value of the exchange current density (10^{-4} A/cm^2); the transfer coefficient in purified solutions is about 0.25. These values vary in presence of organic additives or of some metallic ions; for example, in solutions containing small concentrations of Pb^{2+} the exchange current density and transfer coefficient both increase.

13.2.5 Peculiarities; Anodes; Additives

The solution for preliminary silver plating, which is necessary for good adhesion of the subsequent thick layer, contains about 1.5 g/l Ag^+, 6 g/l Cu^+ and 50 g/l KCN. This solution is operated at room temperature and current density 2 mA/cm^2 for 3 min; the article has to be immersed into the solution with the current on ("hot wire" process).

The silver coatings exhibit significant surface diffusion after deposition, giving rise to growth of small sized defects (scratches or pits).

Sometimes the deposits have a yellowish color; to eliminate this tint they can be washed in a solution of oxalic acid. The deposits incorporate C and N from the solution; this is probably due to cyanide adsorption and incorporation during deposition. At high cathodic potentials (more negative that—1 V) cyanide desorbs from the surface resulting in the deposition of high purity silver. Codeposition of CN^- with silver decreases at high concentrations of the free cyanide ions: this paradox is explained by the negative shift of the electrode potential with increasing CN^- concentration. An alternative explanation hypothesizes the formation of colloidal particles of AgCN at the electrode surface by the reaction $[Ag(CN)_2]^- = AgCN + CN^-$.

Undesirable impurities in the electrolytes include Fe^{3+} (the admissible concentration is no more than 2.5 g/l) and Cu^{2+} (no more than 8 g/l).

Anodes in silver plating are almost exclusively made of pure silver; the presence of copper in the anodes is quite undesirable. The anodic dissolution takes place uniformly and without any problems. Annealed silver can be used but Cu, Pb and other metals should be present at a low concentration, as they can somewhat inhibit the dissolution. Bagged anodes are preferable. During operation the surface can be dull or dark due to formation of cyanide and oxide. Anodic efficiency is less than 100%, so periodic correction of the silver concentration is necessary.

The inorganic **additives** used in silver plating are Sb, Se and also thiosulfate.

CS_2 is also used as a brightener. A number of organic substances (usually sulfur-containing) and surfactants have been tested; in their presence the deposit conductivity decreases, though the reflectance increases.

Table 13.5 Solutions for silver alloys deposition

No.	1	2	3
Components, conditions			
Potassium dicyanoargentate	60–90	25–30	50–55
Potassium dicyanocuprate	100–150		
Potassium cyanide	40–60	25–30	18–20
Potassium carbonate	15–25	20	25–30
Potassium hydroxide	10–15		
Palladium chloride		10–12	
Seignette salt			40–60
Potassium-antimony tartrate (tartar emetic)			10–15
Temperature, °C	18–25	18–25	18–20
Current density, mA/cm^2	5–10	8–10	3–5

Silver can be stripped from a steel surface by anodic dissolution in a solution of NaCN (or KCN), 75 g/l and NaOH (or KOH), 20 g/l, or by chemical dissolving in concentrated nitric acid. Silver deposited on brass may be removed by chemical dissolution at 80°C in sulfuric acid with a small addition (5% vol.) of nitric acid or sodium nitrate.

13.2.6 The Silver Alloys with Antimony, Copper or Palladium

Among the electrodeposited silver alloys the most important from the commercial standpoint are those with antimony, which increases the wear resistance of silver and also improves its behavior as electrical contact by decreasing its tendency to seizing.

The preparation of electrolytes for Ag–Sb deposition differs from that of pure silver electrolytes by the additional dissolution of the double salt potassium-antimony tartrate and of the Seignette salt; these components should be added after dicyanoargentate, cyanide and alkali are already dissolved.

The corresponding solutions compositions are presented in Table 13.5, No. 3. Data are also provided for the deposition of silver alloys with palladium (No. 2) and copper (No. 1).

13.3 Electrodeposition of Gold and Its Alloys

13.3.1 Properties and Applications for Gold Coatings

Gold deposits are very commonly used; this is due to their important technical characteristics, in particular the combination of corrosion resistance and the high con-

ductivity. Electrochemically deposited gold and its alloys are therefore widely used in jewelry and for electronic applications.

13.3.1.1 Advantages

1. Gold exhibits very high corrosion resistance in various media.
2. Gold-plated articles present a long lifetime. Low porosity in thin layers prevents the corrosion of the substrate.
3. Gold has a very high conductivity (only silver and copper are better in this respect) and low contact resistance together with good wear resistance.
4. Gold is characterized by very good ductility and low internal stresses. Gold is malleable and easily deformed without breaking.
5. Gold has usually a pleasant appearance.

13.3.1.2 Disadvantages

1. High cost
2. Soldering properties are poor: gold forms brittle intermetallic compounds with conventional soldering materials.
3. Pure gold (99.9%) tends to bond to other metals upon simple application of a pressure, upon rubbing, or when working as contact pairs.
4. Fine gold has low hardness and wear resistance. In this respect, gold alloys are preferred for electrical contacts, but their contact resistance is higher.
5. Gold has low corrosion resistance in molten salts such as soda, alkali and nitrates.

Gold coatings (including alloys) are used in accordance with these properties. The most widespread applications are the following: electrical contacts working at low current and voltage, electrical interconnects in printed circuits boards under extreme environmental conditions; anti-friction wear resistant coatings in vacuum conditions; for thermo-compression welding; as corrosion protective coatings in various media, and for decorative purposes and jewelry.

Thickness of gold deposits for these applications varies typically from 0.1 to 15 μm.

13.3.2 Solution Chemistries, Compositions and Operating Conditions

Numerous gold plating electrolytes are used commercially; the most common are alkaline, slightly acidic and neutral cyanide baths, which have been recently in part substituted by non-cyanide baths based on gold sulfites or thiosulfates.

The citrate-containing slightly acidic solutions of dicyanoaurate are the most wide-spread. Diluted solutions, also called strike solutions, are used for the previ-

ous deposition of thin layers on nickel undercoat to provide for a uniform base layer where the successive gold deposition would occur more uniformly. These solutions operate at pH about 4.0; more concentrated solutions are intended for heavy plating and operate at pH 3.8–5. These solutions are used for the deposition of gold alloys containing small amounts of alloying elements; the codeposition of Ni or Co for instance provides for harder coatings which may be soldered more easily.

Buffered phosphate and phosphonate solutions operate in the pH range of about 6.0–7.5 and allow the production of very pure, ductile and unstressed deposits suitable for electronic applications. Thallium, lead or some organic additives are used at very low concentrations in these solutions as brighteners.

The alkaline solutions usually contain a high concentration of free cyanide; they have no pronounced advantages but allow a longer service life. These solutions have progressively become less widespread. Alkaline solutions are sometimes used as strike solutions for the production of a thin finishing layer of the desired color.

Gold sulfite and thiosulfate baths are used in the alkaline or neutral range for electronic applications, in particular for the production of soft gold.

Table 13.6 summarizes various electrolyte chemistries for gilding.

The electrolytes No. 3 and 4 are used for the deposition of hard alloys; these alloys contain low concentrations of nickel or cobalt. At low cathodic current density (less than 0.5 A/dm^2) the efficiency of the process is quite low. Increasing the current density CE raises up to 70%, but upon further increase in CD the CE falls, thus favoring a higher throwing power.

The optimum current density for gold deposition is limited by the Au ion concentration in the electrolyte, which determines its cost; agitation of the same is therefore useful. A higher temperature and stronger agitation allow the use of a higher CD.

Cyanide-based electrolytes present several problems; the strong complexation by cyanides results in gold deposition occurring in parallel with hydrogen evolution, causing a decrease in plating efficiency. In microelectronics applications plating through polymeric resists is required, and cyanide is often incompatible with these resists, causing swelling and resist detachment, and resulting in underplating. Finally and most importantly, cyanide baths, particularly those at neutral and low

Table 13.6 Solutions for gold and its alloys deposition

No.	1	2	3	4
Components (g/l), conditions				
Potassium dicyanoaurate	7–12	8–12	8–12	6–8
Potassium citrate	70	150	60–70	
Citric acid	60–100	18–20	20–30	120
$K_2HPO_4 \cdot 12H_2O$		35–50		
Thallium sulfate		0.0007		
Cobalt citrate			0.5–2	
Nickel citrate				1–3
pH	3.8–5.0	6.5–7.5	3.9–4.2	4.2–4.6
Temperature, °C	45–55	60–80	35–40	20–40
Current density, mA/cm^2	6–8	8–12	10–15	5–8

pH, tend to release hydrogen cyanide, a highly toxic gas. This requires close control of the environment in the plating shop, adequate protection of the personnel, and strict requirements for waste treatment and disposal.

Gold sulfite $[Au(SO_3)_2]^{3-}$ and gold thiosulfate $[Au(S_2O_3)_2]^{3-}$ are two stable complexes of gold, having reported stability constants of 10^{10}–10^{27} and 10^{26}–10^{28}, respectively, which should be compared to that of cyanide $Au(CN)_2^-$, 10^{39}. Gold sulfite baths are non-toxic, are quite stable in alkaline conditions, but are subject to dissociation at pH < 7, leading to disproportionation of Au(I). Under acidic conditions, down to pH 4–5, organic amines or polyamines have been used to increase bath stability through the formation of mixed complexes. Gold thiosulfate complexes on the other hand are more stable, enabling in principle operation at lower pH, but they tend to dissociate. Mixed sulfite-thiosulfate baths have been developed, capable to operate under slightly acidic conditions.

Typical sulfite bath for soft gold electrodeposition are given in the following:

(a) Au sulfite [1]

Au(I) sulfite	0.15 M
Na_2SO_3 (total)	0.5 M
$Na_4P_2O_7$	0.3 M
pH 9.5–12.5	

(b) Au sulfite-thiosulfite [2]

$HAuCl_4$	0.05 M
Na_2SO_3	0.42 M
$Na_2S_2O_3$	0.42 M
Na_2HPO_4	0.3 M
pH 6	
T 60°C	
CD 5 mA/cm^2	

13.3.3 Solutions Make Up

Acidic cyanide solutions. Initially, citric acid and potassium citrate are dissolved in half of the final solution volume of warm (40°C) water. Successively, pH must be brought up to 4.0 or 4.5 with a concentrated KOH solution, after which the dicyanoaurate is added while continuously stirring; finally the volume is brought to the needed value. The neutralization process described above is necessary because in the opposite case a suspension of a poorly soluble Au compound would form in the acidic solution; the resulting bath will be unsuitable for use. The substitution of a fraction of the citric acid by potassium (not sodium) citrate is possible; sodium is an undesirable ion because of the low solubility of sodium dicyanoaurate which can precipitate in the solution volume and also at the anode, eventually leading to its passivation. The final solution is weakly acid (pH from 3.5 to 5.0); the phosphate solution is neutral (pH 7.0 ± 0.5).

Neutral, buffered cyanide solutions. In these solutions phosphate compounds are used as buffers. These baths are obtained by dissolving three components: citric acid, citrate and phosphate in 2/3 of the needed water volume, and then correcting the pH. After that the solution must be stirred for about half an hour with activated carbon (0.6–0.8 g/l) and filtered. The last operation is the addition of dicyanoaurate and thallium sulfate.

On a laboratory scale, the electrolyte can be prepared also by dissolving gold chloride in the cyanide solution. The chloride salt can also be made by dissolving fine gold in aqua regia (starting with HCl and then adding small amounts of nitric acid), the excess of acids being evaporated off after dissolution. These operations should be performed under good ventilation. The gold salt can decompose during heating, so these operations should be performed carefully. In order to prepare one liter of the electrolyte it is sufficient to take 3–4 g of pure gold and 20 g of potassium cyanide.

Gold sulfite baths are obtained most commonly from sodium, potassium or ammonium salts. Adjustment of the solution to the proper pH is recommended before adding the Au salt to the solution.

13.3.4 Peculiarities; Anodes; Impurities; Correction

Brass or copper substrates must be previously covered by a nickel undercoat not less than 1.5 μm in thickness; this layer prevents diffusion of zinc or/and copper into gold, which will deteriorate the properties of gold deposit.

The surface of this nickel film must be activated immediately before gilding; a cathodic activation lasting 1 min in a solution of 20 g/l KCN at 20 mA/cm^2 is best. Activation in HCl solutions is often recommended, but this may cause problems related to corrosion of the equipment. Another method of activation consists in the deposition of a very thin gold layer on top of the Ni film immediately after nickel deposition. This gold layer of 0.2–0.3 μm in thickness prevents the articles from passivation during storage, and should be deposited from a diluted electrolyte such that large overpotential may be applied and high nucleation densities may be achieved. The activation of this surface can be performed chemically in diluted sulfuric acid just before the deposition of a thick gold layer. This two-layer gold allows a decrease in the porosity.

To economize with the precious metal, selective deposition only at the locations of interest is used.

Deposits of different colors are obtained by addition of other metallic ions into the electrolytes. The codeposition of copper and zinc produces pinkish deposits, while silver provides for a greenish tint. Nickel cyanide reduces the yellow color thus giving the so called white gold. Color depends also on the grain size: fine-grained gold gives a pale yellow, whereas larger grains give a more reddish hue.

The best **anode** is platinized titanium; anodes of ruthenium or titanium oxide (dimensionally stable anodes, DSA®) can be used. On a laboratory scale platinum anodes may be more convenient.

Steel anodes, even corrosion-resistant stainless steel, are less desirable due to their slow anodic dissolution and consequent solution contamination; if steel anodes are used, the anodic current density should be relatively low (2 mA/cm^2); at lower CD however the citrate begins to oxidize. After operation the steel anodes must be withdrawn from the solution.

Anodes of pure gold or coated with gold dissolve well only in the presence of free cyanide in the solution at concentration between 1.5 and 2.5%, or at high current densities. Both lower and higher CN^- concentrations result in passivation of gold anodes, especially in presence of sodium. For this reason Au anodes are impractical.

Transition metal impurities in the solution, such as ions of Fe, Ni or Cu are particularly harmful; the maximum allowed concentration is 0.1 g/l; these ions can be eliminated by operating the bath at 0.5–1 mA/cm^2 for 2–3 h with a steel cathode. The excess cyanide may be as high as 0.3 g/l; boiling of the bath decreases easily their concentration to this value.

Stirring the freshly prepared solution with activated carbon, as discussed earlier, is useful for the elimination of organic compounds.

The periodic correction of solution composition during its operation is necessary to maintain its pH constant. In order to increase pH, KOH should be used as a 20% solution. On the contrary, if pH is too high, and this happens more often, a solution of citric acid partly neutralized by KOH may be used. If gold ion concentration is too small one can add dicyanoaurate solution; 1 g of deposited metal corresponds to 10 ml of the concentrated (145 g/l) solution.

The anodic dissolution of unneeded gold deposits is performed in pure sulfuric acid with a Pb cathode at 35–40°C.The anodic current density should vary from 1 to 10 mA/cm^2. **Gold extraction** from the spent electrolytes can be achieved as follows. Thin (up to 0.5 mm) aluminum plates are placed in a hot (70–80°C) solution, and gold is being deposited by displacement at their surface. The procedure is repeated until the new aluminum plates remain unchanged, i.e. white, upon immersion. Then the washed plates are dissolved in alkali, resulting in gold falling to the bottom of the container as a powder.

13.3.5 Electrolytes for Gold Alloys Deposition

The electrolytes No. 3 and 4 in Table 13.6 are intended for deposition of mechanically hard alloys containing small amounts (less than 1 at%) of cobalt or nickel; when preparing these electrolytes it is necessary to add the previously dissolved Co or Ni citrate (or sulfate) to the solution **before** the addition of dicyanoaurate.

An alloy containing up to 25% of silver can be deposited from the following solution (gram/liter, g/l): dicyanoaurate 12, silver cyanide 3, potassium cyanide 100 and potassium carbonate 20. The silver content in the depositing alloy increases upon agitation. Silver and gold form a solid solution; the additional introduction of copper cyanide (3 g/l) results in a ternary alloy, in which copper forms a separate phase with a very fine grained morphology.

The highly decorative pink ternary alloy containing 66% gold is deposited from the following electrolyte (g/l): dicyanoaurate 3, silver cyanide 0.05, potassium cyanide 16 and copper cyanide 25. Cadmium cyanide (0.2 g/l) or antimony tartrate (0.3–0.5 g/l) can be added to this solution in order to vary the appearance and properties of the alloy. The electrolysis is performed at 25–30°C; CD is 0.3 A/dm^2.

13.4 Electrodeposition of Zinc and Its Alloys

13.4.1 Properties and Applications

Zinc coatings are relatively inexpensive and present a multitude of advantages; as a consequence they occupy a very important place among the various types of galvanic coatings. A large fraction of the zinc electrodeposition processes is accounted for by the coating of steel sheets, strips, tubes, wires etc., and only about one fourth of the production is made for machine parts, fasteners, computer chassis and so on.

Zinc is chemically active; it easily dissolves both in acids and alkali and its electrochemical potential is rather negative (the standard redox potential is −0.7626 V_{SHE}). It is a relatively low-melting metal; it is also an essential element in a series of important alloys.

13.4.1.1 Advantages

1. Zn is resistant to corrosion in dry atmospheres containing CO, CO_2, Cl_2, NH_3, H_2S or other sulfur-containing compounds (such as those in petroleum and in liquid fuel), and in various organic liquids (alcohols, ethers, benzene etc.). In these conditions a thin and continuous film of oxide, sulfide or other non-soluble compound is formed at the surface, resulting in corrosion prevention. The rate of zinc corrosion in these cases varies from less than 1 to 6 mm per year, depending on humidity and pollution.
2. Zinc coatings can be used up to temperatures of about 250ºC.
3. Due to its low galvanic potential, Zn protects steel electrochemically.
4. Zinc is a low cost metal.
5. Pure Zn is appropriate for deposition on thread surfaces and for flanging; in addition, it is relatively ductile.
6. Coatings obtained without additives show low internal stresses.
7. Zn offers good adhesion to different substrates, including aluminum.

13.4.1.2 Disadvantages

1. It corrodes under high humidity conditions: in these cases the surface is being covered by a mixture of oxides, hydroxides and carbonates. The rate of corrosion rises sharply as the temperatures rises above 55ºC.

2. The decorative properties of Zn are usually poor; some solutions however give a aesthetically pleasing surface appearance.
3. Some widely used processes result in strong hydrogenation of the steel base.
4. As a consequence, Zn cannot be used for deposition on high-strength steels and springs.
5. Zn surfaces become dull upon environmental exposure; post-deposition surface treatments such as chromating are therefore needed.
6. Mechanical working of deposits of low purity is not recommended.
7. Zinc coatings cannot be used in contact with food-stuffs.

Zinc is used as a sacrificial corrosion protective coating; depending on the environmental exposure conditions their thickness should vary from 6 to 8 μm (for mild conditions) to 30–40 (for severe ones); for coating threads the thickness should approximately by 1/100 of the pitch.

Zinc alloys (Zn–Ni, Zn–Co, Zn–Fe, Zn–Sn) exhibit better anti-corrosive properties, higher hardness etc. than the pure metal; their cost however is higher and operating conditions to achieve alloy deposition are more difficult to achieve and control. Nevertheless several Zn alloys are used in the automotive and aerospace industry, as replacement of Cd coatings and when highly enhanced corrosion behavior is required. Finally, Zn alloyed with In provides good corrosion protection in oils along with anti-friction properties.

13.4.2 Electrolyte Formulations and Operating Conditions

Various types of solutions are used for Zn deposition, giving coatings with different appearance and properties. The most widely spread are the following ones: sulfate, alkaline cyanide, cyanide-free alkaline and acidic chloride.

The sulfate electrolytes have poor throwing power (3–5%), but the deposition rate can be very high; these solutions are therefore used for deposition on substrates with very simple geometry. Sulfate electrolytes for zinc plating may be additivated with for example dextrin or glue.

The cyanide solutions have relatively low efficiency, but TP is much better (28–35%). Moreover, the throwing power in terms of metal deposition rate is higher than that in terms of electric current due to the sharp decrease of cathode efficiency at increasing current density.

In the cyanide-free alkaline electrolytes cyanide is replaced by other complexing agents (e.g. polymeric amines with ternary or quaternary N atoms). Their throwing power is as high as 20–25%. However none of these solutions can operate without quite specific addition agents which can complicate the waste treatment.

Acidic chloride electrolytes are characterized by high exchange currents and deposition from such electrolytes usually results in dendrite formation. A high concentration of organic additives is necessary if bright deposits are sought for. These additives are classified in: carriers (polyalcohols and polyamines) and primary brighten-

Table 13.7 Solutions for zinc deposition

No.	1	2	3	4
Components (g/l), conditions				
Zinc sulfate	200–250	300–400		
Zinc chloride			30–60	150
Aluminum sulfate	20–40			
Aluminum chloride				25
Ammonium chloride	30–40		120–200	
Sodium chloride				250
Sodium sulfate		100		
Boric acid	15–20		5–20	
Sulfuric acid		8–10		
Ammonium thiocyanate			0–40	
Temperature, °C	15–30	20–70	15–40	25–35
pH	3.5–4.5		4.5–6.0	3.5–4.5
Current density, mA/cm^2	10–40	150–400	5–40	15–50

No.	5	6	7
Components (g/l), conditions			
Zinc oxide	12–15	38–45	40–60
Sodium cyanide		80–110	
Sodium hydroxide	80–120	70–90	
Sodium sulfide		0.1–1	
Ammonium chloride			240–260
Glycerol		5	
Temperature, °C	20–30	25–35	15–30
Current density, mA/cm^2	20–50	10–50	10–40

ers (aliphatic and aromatic compounds). The solutions used are mainly of two types, based respectively on ammonium chloride or potassium chloride.

The discharging ions are $Zn^{2+}(aq)$ in acidic solutions, $[Zn(OH)_4]^{2-}$ in alkaline ones, both $[Zn(CN)_4]^{2-}$ and $[Zn(OH)_4]^{2-}$ in cyanide electrolytes. The rate-determining step from cyanide and alkaline electrolytes is the same, as in both electrolytes the initial Zn complex transforms to $Zn(OH)_2$, whose two electron reduction to Zn is the slow step. The exchange current density in the case of complex ions is much lower, thus the polarizability and TP are much higher.

The most widely used electrolytes are listed in Table 13.7.

13.4.3 Electrolyte Preparation

For the preparation of acidic electrolytes the sulfates of zinc, sodium (for higher conductivity) and aluminum (as a buffer) are dissolved separately; the solutions are then filtered and mixed together. Dextrin and/or other additives are initially stirred in a small volume of cold water, heated up to achieve dissolution then added to the

main solution. In the case of strongly acidic solutions sulfuric acid is added (very slowly and carefully, under agitation) after the salts are dissolved.

The sulfate solutions must contain no more than 0.5 g/l of iron; the excess should be removed by hydrogen peroxide addition (0.5 g/l) to the warm solution; afterwards alkalis are added up to pH 6.0. Last, the precipitate of ferrous hydroxide is filtered. Solution No. 2 is used only for steel strips and wire deposition.

The electrolytes containing ammonium chloride are prepared by dissolution of ammonium chloride and then (after heating) of zinc chloride. The filtered solution is transferred into the electrolyte and the additives are dissolved by stirring. The electrolyte is than operated at 10 mA/cm^2 to eliminate impurities, mainly iron, copper, Cr(VI), Ni, Pb and Cd.

The all-chloride solution (No. 4) with aluminum chloride is also of interest; the aluminum salt in fact serves as an additive, giving whiter and smoother deposits; this electrolyte operates better with agitation.

Alkaline cyanide solutions are made of zinc oxide, sodium (or potassium) hydroxide and cyanide; some solutions include also a small amount of sulfide. The concentrations ratios of hydroxide and cyanide to the metal must be 3:1 and 2.5:1, respectively. For solution make up the cyanide and alkali are initially dissolved, and after that zinc oxide is gradually added, previously being mixed with cold water in the form of a paste. The solution thus obtained must be settled to remove insoluble impurities and decanted into the plating tank; at the end the remaining substances (glycerol etc.) are dissolved. The ionic impurities such as copper, tin and arsenic can be withdrawn with Zn powder (up to 0.5 g/l) with subsequent stirring and filtration. Pre-electrolysis at 2 mA/cm^2 is also useful.

The non-cyanide alkaline electrolytes are made up with sodium hydroxide and zinc oxide; the concentrations ratio NaOH to Zn is much higher than in cyanide solutions and exceeds 10:1. ZnO is dissolved adding small portions of the powder to a continuously stirred solution; the initially precipitated $Zn(OH)_2$ must be of white color. Anodic dissolution of Zn is also used. A distinction is made between the “low chemistry” and “high chemistry” baths; the latter ones are more concentrated, they have higher conductivity, higher CE and allow a wider range of operating conditions, but the operating cost in industrial applications is higher. The additives (brightener, grain refiner, wetting agent etc.) are added to both types of the solutions following the supplier instructions and recommendations.

Particular care should be devoted to carbonates formation. In both cyanide and cyanide-free caustic electrolytes carbonate builds up during operation, though it is not essential for the normal operation. At concentrations higher than 60–70 g/l the carbonate reduces the solubility of the constituents and the bath conductivity. In order to avoid this problem the excess carbonate can be frozen out by cooling to −5°C, or by addition of barium (or calcium) oxide; in the case of cyanide electrolytes also barium cyanide can be used for this purpose.

When required, a treatment with activated carbon (2–4 g/l) and/or permanganate (0.1 g/l) can be used to eliminate excess organics.

13.4.4 The Peculiarities; Anodes; Removal of Zinc Coatings

High strength steels are unsuitable for zinc plating from alkaline solutions; the reason is the hydrogen embrittlement caused by hydrogen reduction during plating and diffusion of the same in the substrate. Cadmium or alloy plating should instead be used in these instances. In other cases, hydrogenation may be effectively lowered by a prolonged (4 h minimum) heat treatment at about 200°C, the optimum regime depending on the properties of both substrate and coating. The addition of potassium titanate to the cyanide solutions reduces hydrogenation.

When using alkaline processes an alkaline cleaning is necessary; organic solvents are rarely used. Cathodic degreasing must also be excluded. Pickling of steel parts for their initial activation can be performed in all cases in 10% sulfuric acid at 50°C. Small additions of fluorides when cleaning and pickling are useful. In the case of cyanide-free alkali electrolytes an activation in 10% alkali is suitable.

Potassium salts are always better (in many respects) than sodium ones, but more expensive. Additives are used in most types of solutions; alkaline non-cyanide ones in particular can operate only in presence of additives.

The internal stresses in Zn deposits are compressive; they are not high and depend mainly on the types of additives used and their concentration.

Post-plating surface treatments are very often performed to avoid degradation of the surface appearance of the coating; conventionally conversion coatings from chromium-containing solutions or lacquers are used.

The preferred anodic material for zinc plating from acidic solutions is zinc metal of relatively high purity (99.9%); the main harmful impurities are Fe, Pb and Cd. Anodes of very high purity, however, are difficult to dissolve. The anode to cathode ratio is 1.5:1, and bagged anodes are used to avoid the separation of precipitates.

The anodes do chemically dissolve in the electrolytes, therefore it is preferable to extract them from the bath when not in use. In the case of alkaline solution, in addition to chemical dissolution the anodic efficiency is somewhat higher than the cathodic CE, thus the concentration of Zn ions or complexes increases with time, and the resulting concentration may be higher than tolerated. For this reason anodes made of low-carbon steel are preferable; these anodes are perforated and are about 1 cm thick; the anode to cathode ratio is 1:1. In alkaline solutions polypropylene anode bags must be used instead of the cotton ones.

Dissolution of unneeded zinc deposits can be performed in diluted hydrochloric acid, but the evolving hydrogen can adversely affect the steel substrate; therefore a 10% solution of aluminum nitrate or a 25% caustic solution at 60°C is a better medium for dissolution.

13.4.5 Electrolyte Corrections

In cyanide solutions the precipitation of foreign metallic impurities is necessary; this is achieved by addition of 0.2 g/l Na_2S. If the concentrations of Zn and alkali

must be increased, ZnO is added; if Zn and cyanide are both low then zinc cyanide may by added. If the Zn concentration is too high the bath can be diluted with water; after that caustic and KCN are added.

The acidic solutions sometimes need a pH correction; this is made by addition of acid or soda; the ammonium chloride solutions are corrected with a NH_3 solution to increase the pH or with HCl in the opposite case.

13.4.6 The Additives for Zinc Deposition

Numerous additives are used in zinc electrodeposition. They allow the production of smoother and brighter coatings, with higher hardness and compressive stresses. The cyanide-free alkaline solutions in particular cannot operate properly without additives.

Additives used in acidic solutions include aromatic and heterocyclic aldehydes, furfurals, imidazolic derivatives, thiourea etc. along with the more conventional dextrin, glue and naphthalene sulfonic acids. An effective combination of brighteners is acryl amine (1 g/l) together with acryl nitrile (0.3 g/l).

The cyanide solutions give smooth and bright deposits in presence of polyvinyl alcohol, as well as derivatives of quinone, aromatic aldehydes and amines.

Additives for the cyanide-free alkaline electrolytes include polyethylene glycol, aromatic aldehydes, gelatin as well as epichlorhydrine and 1,4-phenilediamine. These additives work synergistically, and this mutual enhancement is being used to develop better combinations of additives.

The optimum concentration of the additives ranges from 0.001 to 0.01 mol/l.

13.4.7 Zinc Alloys Plating

During the last twenty years, various zinc alloys deposition processes have transitioned from having a purely scientific interest to the stage of commercial use; earlier on, brass deposition was the only alloy plating process having industrial acceptance. Nowadays alloys of Zn with Ni, Co, Fe, Mn and Sn are used as well.

Zn-Ni alloys (15% Ni) are the best to provide sacrifical corrosion protection and wear resistance; they may be used as cadmium replacement and for the plating of fasteners. The ammonium chloride solutions for Zn-Ni deposition contain nickel chloride (hexa-aqueous) 80–110 g/l, zinc chloride 120–180 g/l, ammonium chloride 130–150 g/l. The solution contains also acetic acid (25–30 g/l) and 2 g/l of sulfosalicilic acid, pH 5–6. The acids and zinc chloride can be changed correspondingly for boric acid and zinc oxide. The bath operates at 30–40°C, CD 10–30 mA/cm^2; agitation and filtration are desirable.

The alkaline solutions for this alloy plating have low efficiency but a better throwing power. They are less concentrated and contain about 15 g/l Zn and 2 g/l Ni (as metals) along with 150 g/l of caustic and organic additives.

The electrolytes for Zn–Fe and Zn–Co deposition are similar; in particular, the alloy with iron can be deposited only from the alkaline electrolyte.

Zinc anodes (as for pure Zn plating) are recommended, while Ni, Co and Fe are periodically replenished during the operation by addition of the corresponding salts. Separate anodes of the other element are sometimes used, controlled by a separate power supply.

13.5 Electrodeposition of Nickel and Its Alloys

13.5.1 Properties, Applications and Peculiarities

Nickel electrodeposition is one of the most common metal plating processes; more than a half of the overall nickel produced worldwide is employed in the form of coatings. The reason for its widespread use lies in the combination of the numerous useful properties it exhibits together with a relatively low cost of the metal. One of its advantages is the tendency to passivation, providing corrosion resistance in a number of media, particularly in water, alkali, organic and mineral acids. Nickel deposits are cathodic with respect to steel and therefore cannot provide sacrifical protection to steel products.

13.5.1.1 Advantages

1. Nickel has relatively good wear resistance, which can be additionally increased by deposition as a composite material (i.e. with dispersed phase inclusions), by alloying or by deposition on top of a thin layer of a harder metal or alloy. The dispersed phase in composite coatings can also provide surface lubrication and increase wear resistance.
2. Relatively high hardness; electrochemically deposited Ni is harder than the corresponding bulk metallurgical metal.
3. Good ductility, especially when deposited from sulfamate solutions; such deposits can be easily polished and worked. Smooth Ni surfaces usually have a high reflectance.
4. Very good barrier anti-diffusion properties. Nickel is widely used as the barrier layer to prevent the diffusion of the substrate material to the deposit (e.g. gold) and vice-versa.
5. Relatively good electrical conductivity and contact resistance. Due to these properties nickel is used to enhance surface conductance. Nickel may be successfully used to coat electrical contacts operating under moderate electric loads and at temperatures up to 200°C.
6. Nickel shows a relatively high corrosion resistance in conventional media, in high humidity environments or in solutions of alkali or organic acids. Its pro-

tective properties with respect to various substrates or undercoats, e.g. copper, are often adequate.
7. Nickel deposits are easily soldered by using conventional solders; nickel practically does not diffuse in the solder and provides high strength and vacuum-tightness of soldered joints. Point welding can also be made.
8. Black nickel coatings show good light absorption properties and efficient heat removal.
9. Smooth, bright and leveled deposits can be obtained in the as-deposited condition, without need for polishing, in presence of specific commercially available additives. Highly decorative properties are provided also by semi-bright or satin finishes.
10. Nickel can be obtained in the form of very thick layers with low internal stresses; this enables the numerous applications of nickel in electroforming.

13.5.1.2 Disadvantages

1. After nickel deposition on steel the mechanical properties of the substrate can worsen, especially in the case of bright deposits; one of the reasons is hydrogenation.
2. As-deposited nickel from most solutions is not tolerant to mechanical work, such as elongation, beading or riveting.
3. Nickel is not stable in sulfur-containing media, in ammonia, in humid chlorine atmosphere.
4. Ni does not provide sacrificial corrosion protection of steel; discontinuous coatings may induce and accelerate corrosion of steel.
5. Nickel is a magnetic metal, therefore it cannot be used when non-magnetic materials are necessary.
6. Nickel deposits may often peel away from the basis metal. Achieving good adhesion with the substrate is a problem, and scrupulous care must be exercised to achieve the cleanest surface. Moreover, the adhesion of a subsequent deposit on top of a nickel surface is also problematic.
7. Nickel deposition is highly sensitive to impurities in the electrolyte.

The properties of nickel coatings outlined above determine the wide range of their practical application. They are used in fact for various purposes: as functional, protective and decorative coatings both in engineering industry, instrumental technology etc. Thick nickel deposits are used for electroforming applications. In chemical industry thick deposits are used for the protection of surfaces in contact with alkaline and other media. An additional important application is as barrier layers, preventing the diffusion of the substrate components into the overlying deposit and vice versa. Sometimes nickel is used as a wear resistant coating. Some of the shortcomings of nickel can be overcome by the use of nickel alloys.

A distinctive feature of nickel deposition is its high sensitivity to the solution pH. At higher acidity ($pH < 3.5$) the hydrogen evolution occurring in parallel with

nickel deposition becomes intense, resulting in a decrease in CE and hydrogenation of the deposit and even of the substrate. On the contrary, at pH > 5.6 the basic salts of nickel precipitate near the cathode and are incorporated into the growing deposit. Hydrogen evolution additionally causes an increase of pH near the cathode; the pH value in the layer adjacent to the cathode can be up to 2 pH units higher than in the bulk. For this reason nickel solutions must contain buffer agents, usually boric acid. Other buffering systems are sometimes used, such as acetic, malonic etc. Surfactants such as lauryl sulfate are added to the solution to facilitate the separation of hydrogen bubbles formed at the electrode during deposition.

13.5.2 Electrolyte Formulations

Nickel electrodeposition has a long history, starting with the ammonium sulfate solution developed by Adams in 1869 and continuing with Watts in 1916 who proposed the Watts' electrolyte still in use today. The most important types of solutions are listed in Table 13.8.

Table 13.8 Solutions for nickel deposition

No.	1	2	3	4	5
Components, conditions					
Nickel sulfate	250–300		250–300	120–400	140–200
Nickel chloride		300–400	40–60	3–4	30–40
Boric acid	30–35	25–30	30–35		25–40
Sodium chloride	10–20				
Sodium sulfate				50	60–80
Magnesium sulfate				30	
Saccharine			0.5–1.5		
pH	4.5–5.5	2.5–3	4.5–5.2	4.5–5.3	5.2–5.8
Temperature, °C	35–55	50–70	45–50	18–25	20–55
Current density, mA/cm^2	5–40	20–80	20–80	5–15	5–20

No.	6	7	8	9
Components, conditions				
Nickel sulfate				200–250
Nickel chloride	12–15	200–250	6–30	
Nickel sulfamate	300–360			
Nickel acetate			75–185	
Boric acid	30–35			30–35
Hydrochloric acid		60–80		
Saccharine	0.8–1.5			
Potassium fluoride				1.5–2.5
Sodium sulfate				40–60
pH	3.6–4.2		4.0–4.5	4.0–5.5
Temperature, °C	30–60	15–30	45–50	40–60
Current density, mA/cm^2	50–120	5–40	20–200	5–20

The concentrations are given, as in all tables of this chapter, in grams per liter (g/l) of solution (not water). The salts for electrolyte preparation are hydrated salts ($NiSO_4 \cdot 6H_2O$, $NiCl_2 \cdot 6H_2O$, $NiCH_3COO \cdot 4H_2O$ etc). All electrolytes may contain wetting agents and brighteners; the most popular ones are sodium lauryl sulfate (0.1–1 g/l), saccharine (0.5–2 g/l), phtalimide (0.1 g/l), butyne diole (0.1–0.4 g/l). Boric acid can be replaced by lower quantities of malonic acid. Nickel more often than other metals is used to grow composite coatings by the codeposition of foreign particles about 1 μm in size. These may be hard particles to increase wear resistance, lubricant particles etc.

The current density used in Ni deposition varies in a wide range. Its optimum value depends on the acidity: it is higher at lower pH; higher concentrations of boric acid (up to 40 g/l) can be used at high temperatures (60°C). Pulse plating processes have been shown to enhance coating properties and improve the process reliability.

Multilayer nickel coatings are often used (duplex or triplex nickel) to enhance corrosion resistance. The first layer is deposited from sulfur-free solution and can be mat or semi-bright; brighteners for semi-bright nickel give uniform deposits without the need of sulfur-containing compounds. This layer is electrochemically less active than the bright nickel. The second, thinner layer can be obtained from a solution with sulfur-containing additives, and the last one is deposited from a solution containing brighteners and levelers, where sulfur is used at a low concentration. The resulting coatings are bright and more corrosion-resistant than single-layered ones. The process is however complicated by the need to maintain the optimum concentration of additives in the various processes.

The organic additives for nickel deposition are numerous. The classification of additives is the following: (1) carriers: aromatic organic compounds to refine grain size and slightly increase brightness; (2) brighteners: formaldehyde, coumarin, thiourea, to increase brightness while promoting brittleness; (3) auxiliary brighteners: traces of metal ions (Zn, Co, Cd), butyne-diol, pyridinium, useful for leveling.

The throwing power of the various sulfate solutions is in the 10–15% range.

Sulfamate solutions are good for depositing thick nickel parts in electroforming applications, due to the low internal stresses and high ductility of the deposits. They can be operated at high CD, where the deposit properties remain good. TP is higher than in the case of sulfate solutions and approximates 16–21%.

Chloride is useful as an activator for anodic dissolution. All-chloride and high chloride electrolytes have high efficiency, but the mechanical properties of the resulting deposits are worse.

Deposits of black nickel are obtained from Zn-containing solution; the most popular composition (g/l) is as follows: $NiSO_4 \cdot 6H_2O$ 50, $ZnSO_4 \cdot 7H_2O$ 25, ammonium sulfate 45 and sodium thiocyanate 15. The deposition is carried out at 1–2 mA/cm^2, a deposit 1 μm in thickness is obtained in about 30–40 min.

13.5.3 Solutions Make Up and Purification

The preparation of nickel electrolytes should be performed with extreme care. Boric acid is dissolved while stirring in hot (60°C) water in a volume about 2/3 of the

final one. Successively nickel salts and other substances (except the additives) are dissolved. A separate dissolution procedure is used only for fluoride compounds, if they are part of the solution.

The additives should be dissolved in separate containers, using warm water. Saccharine, in particular, is dissolved to the concentration of 100 g/l, in a volume of water about one hundredth of the overall solution volume, then this solution is added to the final electrolyte, after a previous neutralization with NaOH. Phtalimide and sulfamides are mixed with hot water and added to the bath as suspensions. The organic sulfoacids are highly soluble, thus they can be dissolved in a small volume of water and neutralized. In some cases the sodium salts are used, and then neutralization is not needed. The wetting agents, butyne diol and sulfo salycilates should also be dissolved separately. The anti-pit agents, formalin and chloramines can be added immediately into the bath. All the operations for make-up of the electrolyte require strong agitation.

After the volume is brought to the necessary level, the solution must be purified. Recently developed solutions for bright nickel do not need frequent purification. The simplest purification process is carbon treatment, including the use of peroxide. The following procedure is generally sufficient for the initial period of electrolyte use. Freshly precipitated basic nickel carbonate, obtained by addition of Na_2CO_3 to nickel sulfate, is gradually added to the solution up to pH about 5.0; hydrogen peroxide is added to the concentration 1 g/l; stirring is necessary for about 30 min. Then activated carbon is added (2–3 g/l) and stirring continues for two hours. The solution is then settled and filtered.

The same treatment can be performed after a convenient production interval.

With subsequent operations an oxidation treatment with permanganate can be required. In this case the danger exists of an excess $KMnO_4$ resulting in the degradation of deposit properties (ductility etc.). Thus the needed quantity of permanganate must be determined by chemical analysis. Ion-exchange units can also be used as alternative.

After electrolyte purification as described above, a pre-electrolysis treatment at low current density should be performed after lowering pH down to 3.5. The undesired metallic impurities: copper, lead, zinc, cadmium, lead and also organics can be removed by this method. The most efficient current density varies to some degree; 2–3 mA/cm^2 is recommended. The best temperature is 60°C, duration up to 10 h. The cathode area should be large, agitation is necessary along with continuous filtration.

13.5.4 Anodes

Soluble nickel anodes are used as a rule. Any plates, sheets or rods of relatively pure nickel can be used. Such anodes however may easily passivate, especially at higher pH values, and may also form slurries. For this reason the most general recommendations consist in using a low anodic current density, adding activators to the solu-

tions (usually chlorides, perhaps fluorides) and placing the anodes into suitable bags (bagged anodes). Cast rolled anodes are often used. Several types of anodes contain up to 0.01% of sulfur and also silicon, nickel oxide, carbon. The film formed at their surface during dissolution impedes the precipitation of a slurry. Anodes of specific shapes (rhomboidal or oval) are convenient; during dissolution in fact their surface area decreases to a lower extent.

13.5.5 Correction and Elimination of Harmful Impurities

Copper, zinc, iron and some other metallic impurities are eliminated by standard purification procedures; it is more difficult to remove chromium ions. This can be achieved by reduction of Cr(VI) to Cr(III) by addition of potassium bisulfite: 3 g per each g of Cr(VI). Trivalent Cr ions can then be precipitated as hydroxides by bringing the pH to a value higher than 5.5. Organics are removed using a peroxide and/or permanganate treatment, as noted above.

Periodic modification of the electrolyte is necessary, first of all pH maintenance by addition of diluted acid. Concentration of the additives is regulated after passing a definite quantity of electricity; specifically, after 1000 Ah have passed through the electrolyte the consumption of buthyne diol is about 3 g, that of saccharine is 10 g, phtalimide 5 g. The brighteners can be simply added when coating luster deteriorates, the anti-pit additives instead after pitting of the coatings starts to be noticed.

Some additives need a periodic chemical (or spectrophotometric) analysis after passing 10–20 Ah/l of the solution.

13.5.6 Electrodeposition of Nickel Alloys

Nickel–cobalt alloys are of interest for their mechanical properties and for their potentially hard magnetic properties. Alloying improves the hardness of nickel and the corresponding materials are used in electroforming. With a suitable microstructure Ni-Co films are characterized by a relatively high coercive force. The alloys are deposited from solutions containing 150 g/l of Ni and Co sulfates (or 200 g/l each of sulfamates) along with boric acid (30 g/l) and chloride of potassium or magnesium (15 g/l). An anti-pit additive (0.1–1 g/l of sodium lauryl sulfate) is used. The sulfate solution operates at pH 4–5 and 40–60°C, whereas the optimum conditions for the sulfamate one are pH 2–4 and 20–25°C. Current density in both cases is 10–25 mA/cm^2. The composition of the alloy can be varied by variation of the Ni/Co concentration ratio in the solution.

Nickel–palladium alloys are used as an alternative to gold for electrical contact materials in electronics. The alloys are less expensive and harder than pure palladium. Electrolytes for Ni-Pd deposition are prepared by addition of sulfamine acid (aminobenzenesulfonamide) to a solution containing the chloride, amino-chloride

or amino-sulfate salts of nickel and palladium; ammonia is then added up to pH 8.3–8.5.

Nickel–rhenium alloys possess very high wear resistance and can be obtained from a solution of 50 g/l of nickel sulfate and 2 g/l of potassium perrhenate. The solution contains also 15 g/l of tartaric acid and 20 g/l of sodium tartrate; finally, a 25% ammonia solution is added (about 150 ml), until the pH is about 10.

Nickel–phosphorus alloys containing 10–15% of P are very hard in the as-deposited condition, where the system forms a nanocrystalline/amorphous solid solution. These alloys are metastable and tend to crystallize upon heat treatment at relatively low temperatures (200–400°C), precipitating the stable Ni phosphide phase Ni_3P. These alloys can be obtained from either acidic or alkaline electrolytes. In acidic electrolytes (pH 2–5) phosphorous acid H_3PO_3 or sodium hypophosphite NaH_2PO_2 (20–40 g/l) can be used as the phosphorous source. In alkaline conditions instead only the latter salt can be used. In both cases, the deposition must be carried out at a temperature of 90°C or higher.

Nickel–tin alloys have a very decorative appearance; they are solderable for a long time after deposition and are corrosion-resistant. The most convenient solution for Ni–Sn deposition contains (g/l) $NiCl_2 \cdot 6H_2O$ 250, $SnCl_2$ 50, ammonium fluoride 60. The organic additive 8-quinolin sulfonic acid (1.5 g/l) is also used. The solution operates at pH 4.5, temperature 50–55°C, CD 10–30 mA/cm^2, with nickel anodes.

The deposition of the very important nickel alloys with zinc is described in Sect. 13.4.

13.6 Chromium Electrodeposition

13.6.1 Properties and Applications

With reference to its electrochemical properties chromium is active; in fact it has a rather negative redox potential ($E^0(Cr^{2+}/Cr) = -0.90\ V_{SHE}$). However in most actual cases a very thin passive oxide film is formed at the surface, resulting in very good corrosion performance and reliable protection of the substrate. Its other properties such as hardness and pleasant appearance make chromium one of the most widely used metal coatings in industry. Cr is applied both for decorative and hard coatings. The decorative films are usually thin (less than 1.5 μm) and are deposited over nickel undercoating. The overall range of applications of functional chromium coatings is very wide.

13.6.1.1 Advantages

1. Cr films have high hardness (up to 11,000 MPa), much larger than the corresponding bulk metal, and provide a sharp increase in wear resistance of the

surface being coated. High hardness is retained up to about 350°C, but Cr can operate up to 480°C.
2. Cr retains its corrosion resistance at high temperature. It is stable at high air temperature, in cool sulfuric or nitric acids solutions, in oxidizing media, and it does not tarnish in sulfur (II)-containing atmospheres up to 400°C.
3. Chromium provides good adhesion with steel, nickel and copper; no peeling is observed. Additionally, it has good diffusion barrier properties.
4. The friction coefficient is relatively low, especially when using a lubricant. Micro-cracked chromium retains oil and its lubricating abilities are enhanced.
5. The deposition of both very thin and thick coatings (up to 0.5 mm) is possible.
6. Chromium has excellent brightness and pleasant appearance.
7. Black chromium has very high (97%) light absorption coefficient; the deposits are stable in vacuum.

13.6.1.2 Disadvantages

1. Low ductility and possibility of cracking; the fatigue limit of Cr-plated steel is consequently reduced.
2. It corrodes in HF and HCl.
3. Internal stresses are rather high; embrittlement, hydrogenation and cracking are observed.
4. Solderability and weldability are low; electrical conductivity is also poor.
5. Current efficiency of chromium deposition is very low; in combination with the necessity of 6-electron transfer it results in very high electricity consumption at low deposition rate.
6. Poor deposit distribution: Cr solutions have very low throwing power and covering power.
7. The deposition conditions should be very closely controlled.
8. The solutions and waste water are toxic and corrosive; local ventilation is necessary. Chromium acid “mist” is produced by gas evolution at the electrodes.

The most important applications of Cr coatings are the following.

- As decorative and protective coatings over nickel and copper. Such deposits protect steel against corrosion, simultaneously giving good appearance to the details of, for example, cars, motor cycles and bikes, medical instruments, domestic appliances etc. The thickness is usually in the range 0.5–1.5 μm, but deposits onto copper or its alloys may reach up to 10 μm.
- As wear- and corrosion-resistant coatings. For this purpose, Cr is used to plate for example the shaft necks, the piston rings, the cylinder walls, some tools for cold work, press tools and templates. In these applications the deposit thickness is about 10 μm, but sometimes it can be much thicker: for press tools 20–60 μm, for rings up to 0.2 mm.
- Sometimes mounting hardware is Cr plated. When plating threads the thickness of the deposit must be about 0.01 of its pitch.

- Cr coatings are used in the production of reflectors, searchlights etc., to enhance reflectance. The deposit does not tarnish in atmosphere at high temperature. The deposit thickness is 0.5 μm.
- Less commonly, Cr is used to repair worn-off parts of shafts, bushings, sleeves, spindles etc. made of quenched steel. The thickness can be up to 0.2 mm.

13.6.2 Bath Compositions

The most common hexavalent electrolytes use chromic anhydride CrO_3 as the metal source; in aqueous solutions this compound becomes chromic acid; more precisely it is the mixture of two acids: H_2CrO_4 and $H_2Cr_2O_7$. The chromium deposition in metallic form from this solution is possible only in presence of specific anions, which work as catalysts for chromium reduction up to Cr(0). Sulfuric acid is widely used at a concentration 100 times less (by mass) than CrO_3. Nowadays more common electrolytes use mixed sulfate-fluoride catalysts which work better than sulfate-only ones; the covering power and current efficiency in fact are higher, along with better adhesion. NH_4F (up to 6 g/l) is added; fluorosilicate can be used as well (N. B. fluorine-containing substances are highly corrosive! PVC-lined tanks are desirable). More recently, alkene–sulfonic acids have been used in order to enhance energy efficiency.

The concentration of CrO_3 varies in a wide range from 150 to 450 g/l; more diluted compositions are used to produce wear-resistant coatings, whereas the concentrated ones give decorative and protective coatings with lower hardness. The CE is the highest at 230–250 g/l (this is the most common concentration) and increases with higher current density.

The usual concentration of the catalysts is as follows. The single (sulfate-only) type contains sulfuric acid in the ratio 1:100 to chromium anhydride; an increase in its concentration produces porosity in the deposits. The combined catalysts may contain 2 g/l of sulfate and 4 g/l of sodium fluorosilicate. Methanesulfonate or methyl sulfochloride (1–3 g/l) can be also used; another possible additive is selenium dioxide. Recently, several types of organic additives (e.g. organic acid salts, alkyl sulfonic acids) are used which allow to raise current efficiency, TP, brightness and hardness of the coatings.

Sulfate can be added not only as H_2SO_4 but also as the strontium salt, which is dissolved in a separate container. The solubility of $SrSO_4$ is low, and it is added in a concentration slightly exceeding the solubility (about 6 g/l), so that the sulfate concentration is maintained automatically; such solutions are named self-regulating. For their preparation strontium carbonate is made to react with sulfuric acid in the solution; the resulting solution should be analyzed for sulfate.

The often recommended optimum operating temperature is 55°C, but the actual temperature depends on the type of the desired deposit and is related to the CD employed. Current efficiency is higher at lower temperature, thus 40°C is often recommended as optimum.

13.6.3 Preparation of the Electrolytes

Chromium anhydride is dissolved in 60% of the final water volume at 60–70°C; water must not contain ferrous or nickel ions. The commercial CrO_3 often contains sulfate, thus the solution must be analyzed, and excess sulfate, if present, should be eliminated by addition of barium carbonate or hydroxide, previously mixed with water. The mass of barium carbonate should be 2.2 times the excess sulfate. The solution is then stirred, settled and decanted. The final steps involve addition of the catalysts and finally adding water up to the final volume.

The solution ready for operation should contain about 2–3 g/l (maximum 8 g/l) of trivalent chromium ions; up to this concentration Cr(III) is necessary for correct operation. Other metallic contaminants (Fe, Ni, Cu etc.) along with nitrates and high concentrations of Cr(III) are harmful; distillated and deionized water must therefore be used.

If the solution contains organic additives, they should be dissolved after dissolution of the main components. Last, the solution is pre-electrolyzed at 50°C; the cathodic CD should be 0.1–0.15 mA/cm^2, and the anodic one 15–20 mA/cm^2, the total charge passed should be 6–8 A-h/l.

13.6.4 Peculiarities

Chromium is deposited from highly acidic solutions, resulting in intense hydrogen evolution and therefore low current efficiency. The process of metallic chromium reduction is complicated; the transitions Cr(VI) to Cr(III) occur very fast, whereas the following processes $Cr(III) \rightarrow Cr(II) \rightarrow Cr(0)$ are relatively slow; the Cr^{3+} ions have sufficient time to diffuse from the cathode into the solution. An equilibrium is finally established between the rate of Cr^{3+} formation and its anodic oxidation back to Cr(VI).

Current density in chromium plating is significantly higher than in other electrodeposition processes and can reach 1 A/cm^2. Current efficiency varies from 8% to 25%, the typical value being 15%. The reason of the low TP values is the low polarizability in the operating potential range, along with a higher cathode efficiency when CD is increased. The auxiliary anodes and shields are commonly used to improve metal distribution.

For example, in a typical solution CE increases from 10 to 20% for a CD increase from 0.15 to 0.65 A/cm^2; it is found that the deposition rate (in μm/min) can be expressed as $v \approx 1.7i - 0.14$. We assume that this linear interpolation method to estimate deposition rate is more convenient than the common procedure using data on CE, CD and the electrochemical equivalent. Needless to say, the coefficients depend on both the electrolyte and the temperature.

In chromium deposition it is important to control the consistency between the **temperature** and current density. The tool in the bath must be heated; thus the previous rinsing should be done in warm water.

Variations in deposition conditions result in essential variations in **deposits properties**. Thus, hard chrome plating solutions contain 240 g/l CrO_3 and fluoride-sulfate catalyst; they operate at 55–60°C and cathodic CD of 0.15–0.8 A/cm^2 (the anodic current is 1.3–1.5 times lower). At higher temperature and CD the wear resistance increases, and with higher CrO_3 concentration chromium films with a "milky" appearance can be obtained. This is a deposit of white color and with very low porosity, usually deposited on steel without undercoat and presenting good corrosion resistance at high temperature. The bright chromium is obtained only on a bright substrate. Decorative coatings are obtained at lower temperature.

During chromium deposition an important role is played by the **thin film** formed at the cathodic surface. This consists of intermediate chromium electrolysis products together with catalytic additives. The mechanical agitation can break the film, but ultrasound or forced electrolyte flow (about 1 m/s) for the same purpose are acceptable.

Internal stresses (IS) in deposits are very high, but in thick layers they are decreased due to cracking; stresses may by decreased by using pulsed current.

One of the reasons of high IS can be hydrogenation; hydrogen contents in Cr in fact can be very high. Heating to 200°C reduces the hydrogen content to an acceptable level.

The electric regime of deposition and the character of the pretreatment depend on the substrate. During deposition on steel after anodic activation (1 min at 0.3 A/cm^2 in a separate vessel to prevent Fe contamination) an initial high current pulse is used; in the deposition of hard Cr on previously plated Cr, anodic activation is employed, but after that the current is increased gradually (for 1–2 min) to the normal operating value. For deposition on copper or copper alloys the articles should be immersed into the solution with the potential applied ("hot wire"), whereas in the case of nickel undercoat a brief contact with the electrolyte without current application is not so harmful.

13.6.5 Anodes

Chromium anodes are not used because upon dissolution Cr(III) ions are formed, the excess of which is harmful. Lead or lead alloy (lead-tin or lead-antimony) anodes are commonly employed. In operation the anodes become covered by a dark-brown colored film of lead peroxide β-PbO_2; this film, on the one hand, plays a positive role by maintaining the Cr(III) balance. At this film trivalent chromium ions generated at the cathode are reoxidized to hexavalent form. For this purpose the anodic CD must be 1.3–1.5 times less than the cathodic one. On the other hand, however, the film has low electrical conductance thus causing inhomogeneities in the current distribution. From this point of view, the Pb − 7% Sn anodes are much better, since the film formed on these alloys have a higher conductance. Pure Pb anodes need a periodic chemical treatment and mechanical cleaning.

The second problem can arise in concentrated solutions where a yellow layer of lead chromate sludge is generated at the anode; this must be periodically removed.

At present there is a trend towards the use of platinum-coated titanium anodes; their surface is sludge-free but problems arise concerning the trivalent chromium balance.

13.6.6 Electrolyte Correction

The periodic adjustment of chromium electrolytes is necessary. First and foremost is the addition of CrO_3, which is dissolved in a separate vessel; the excess sulfate has to be removed by barium carbonate (or hydroxide) treatment. The decanted solution is moved into the working bath during a pause in its operation.

The chromium acid concentration C is often being determined by density (ρ) measurements: $C = 1450(\rho - 1)$, where C is in g/l and ρ is in g/ml. The density must be measured after cooling the solution to room temperature.

After contamination of excess Cr(III) the solution can be treated as in its initial preparation; the cation-exchange method is also very effective. Another method to reduce the trivalent ions concentration is to operate the cell for some time with agitation and with large anodes.

The correction by sulfate and other catalysts is performed every week based on chemical analysis data. Any deficiency in sulfate is restored by the addition of sulfuric acid. The ferrous ions excess can be reduced by addition of potassium hexacyano ferrate (yellow); the precipitate must be filtered.

A periodic decantation or filtration of the solution is quite desirable.

13.6.7 Trivalent Electrolytes

Trivalent chromium electrolytes have always aroused considerable interest due to the lower toxicity of the corresponding ion. Several promising processes are available but none of this is yet a full fledged commercial process. We can recommend the acidic solution [1] with the following formulation (g/l): $Cr_2(SO_4)_3 \cdot 6H_2O$ 100–150, potassium oxalate 20–30, aluminum sulfate (aqueous salt) 100, potassium sulfate 80. This electrolyte operates at pH about 2.0 or somewhat lower; the operating temperature is 35–40°C, CD 0.2–0.5 A/cm^2. The process is characterized by a relatively high current efficiency and higher throwing power.

13.7 Iron and Its Alloys

Electrochemically deposited iron is much harder then the metallurgical one; this is due to the very small grains formed in electrodeposited films and also to the carbon and hydrogen inclusions caused by the deposition process.

Iron is deposited usually to obtain thick coatings, for example for the repair of worn-off parts, or to produce magnetic alloys. In addition, specific fields in the

printing trades and engineering use iron deposition. Two types of electrolytes are recommended for applications: the sulfate and the chloride.

The typical sulfate solution contains 200–400 g/l of ferrous sulfate $FeSO_4 \cdot 7H_2O$ and also potassium, magnesium or aluminum sulfate (50–70 g/l); the solution must be acidified with oxalic, sulfuric or hydrochloric acid (1–2 g/l). This solution operates at 20–40°C and CD of 50–60 mA/cm^2; CE averages 85%, TP is 4–8%.

The components of the more common chloride solutions are ferrous chloride (200–500 g/l of the aqueous salt) and hydrochloric acid (up to 3 g/l; at higher concentrations CE decreases). Sometimes calcium, potassium or sodium chloride are added. Solutions of this type can be operated over a wide range of CD and the other working conditions do not need to be strictly specified; thus, temperature can be from 30 to 90°C; the acidity of hot solutions must be higher. Current density depends strongly on temperature and metal ion concentration, and can be as high as 300 mA/cm^2.

The current efficiency from chloride solutions is higher (up to 90%); internal stresses are lower than in the case of sulfate solutions. However chloride solutions form coatings more prone to corrosion. The solutions need long-term pre-electrolysis at 1–2 mA/cm^2.

The ferrous chloride concentration C in the simple electrolytes can be determined very simply by the density measurement: $C \approx 1740(\rho - 1)$, where C is the concentration of $FeCl_2$ in g/l, and ρ is density in g/ml.

High quality deposits can be obtained from methyl sulfate and sulfonate solutions, but these compounds are less available and the corresponding reduction processes are studied to a lesser extent.

Anodes for iron deposition are usually made from low-carbon steel and are bagged. Sometimes additional lead anodes may be used.

Iron deposition occurs always in parallel with hydrogen evolution; the occluded or absorbed hydrogen giving rise to embrittlement of the deposit can be partly removed by subsequent annealing processes, though a small fraction of hydrogen tends to remain in the crystal lattice until nearly the melting point.

One of the main problems in Fe deposition, particularly for magnetic applications, is the possibility of oxidation of Fe^{2+} to Fe^{3+}, due to oxidation at the anode and/or to reaction with oxygen dissolved in the electrolyte. In combination with the local increase in pH at the cathode due to hydrogen evolution, the presence of Fe^{3+} may lead to the precipitation of Fe(III) hydroxide, which is incorporated in the growing Fe films. The presence of Fe hydroxide results in embrittlement of the coating, decreases the saturation magnetization of the Fe films and affects their magnetic properties by generating defects that hinder domain wall motion.

13.7.1 Electrodeposition of Soft Magnetic Materials

Mutual alloys of the three iron group alloys, in particular iron-nickel alloys, are used to produce recording heads for magnetic recording systems and microfabricated magnetic components. The choice of these materials is due to the unique combination of a high magnetic moment, a high permeability and a low coercive force (< 1 Oe). Historically, the first material to be utilized in the fabrication of magnetic heads

was the Ni–Fe 19 at% alloy, called Permalloy, having a saturation magnetization of 1 T. Later, processes for the electrodeposition of materials with higher magnetic moment were developed, from Fe-rich Ni–Fe, to Fe–Co–Ni, to conclude with Fe–Co 35 at%, the ferromagnetic material with the highest available magnetization (2.4 T).

The solutions used for the deposition of these alloys are slightly acidic (pH ~ 2–3), and may contain either or both sulfates or chlorides of the various metals. Metal ion concentration is determined in part by the alloy composition sought for, and also by the fact that the Fe group metals exhibit the so-called anomalous codeposition, i.e. the less noble metal in the alloy is deposited preferentially. In order to deposit Permalloy for example the concentration of Ni salt (0.5 M) is kept 50 times larger than the Fe ion concentration (0.01 M). Buffering is needed in order to limit the pH increase at the interface resulting from the hydrogen evolution reaction; this is most often achieved by the use of boric acid (0.4 M).

Additives are used to better control the magnetic properties and to decrease the internal stresses; while many of these additives are proprietary, the most commonly used are saccharin (0.1–1 g/l), sodium lauryl sulfate or sodium dodecyl sulfate or sulfonate (SDS, 0.01–0.5 g/l).

Since Fe, Co and Ni present a similar dissociation behavior in aqueous solutions, electrolyte preparation follows the same steps described for the preparation of Ni solutions.

Typical electrolyte formulations and process conditions to obtain soft magnetic alloys with high magnetic moments are given in the following. The choice between metal sulfates or chlorides represents a compromise between deposition rate and stresses; the use of sulfates results in lower stresses but lower deposition rates. SDS and/or saccharin should be added in the concentrations suggested above.

Ni–Fe Permalloy

$FeSO_4$ or $FeCl_2$	0.01 mol/l
$NiSO_4$ or $NiCl_2$	0.50 mol/l
H_3BO_3	0.4 mol/l
pH 2.5–3	
CD 4–6 mA/cm^2	

Fe–Co–Ni

$FeSO_4$ or $FeCl_2$	0.01–0.02 mol/l
$NiSO_4$ or $NiCl_2$	0.12–0.15 mol/l
$CoSO_4$ or $CoCl_2$	0.1–0.15 mol/l
H_3BO_3	0.4 mol/l
NH_4SO_4 or NH_4Cl	0.3–0.45 mol/l
pH 2.5–3	
CD 3–4 mA/cm^2	

Fe–Co

$FeSO_4$ or $FeCl_2$	0.2–0.25 mol/l
$CoSO_4$ or $CoCl_2$	0.1–0.15 mol/l
H_3BO_3	0.4 mol/l
NH_4Cl	0.3–0.45 mol/l
pH 2–2.5	
CD 3–5 mA/cm^2	

13.8 Low-Melting Metals: Bi, Cd, In, Pb, Sb, Sn. The Alloy Sn–Pb

13.8.1 Bismuth

Bismuth electrodeposition is mainly utilized for the growth of bismuth-tin alloys, where Bi is added to inhibit the formation and growth of whiskers at the surface of the deposit. As a pure metal Bi is used sparingly; a typical application is as antifriction coating, not as good but less expensive than indium.

The simplest electrolyte for pure bismuth deposition is based on fluoborates. The solution consists of Bi fluoborate (350–380 g/l) and free fluoboric acid (up to 90 g/l). The deposition is performed at room temperature, the current density is 1–5 mA/cm^2.

13.8.2 Cadmium

Cadmium is a more expensive metal than zinc; besides, its chemical compounds are more toxic; therefore it is used infrequently. Cadmium however is much more resistant to corrosion in sea water and marine environments, in alkaline conditions and at high humidity; consequently, it is used as an alternative to Zn for corrosion protection in particularly demanding conditions. Cadmium is also less susceptible to hydrogenation, therefore it can be used for example for coating steel springs, where zinc would fail due to strong hydrogenation. Cadmium coatings are also effective barriers between steel and aluminum parts. They are easily formed with the substrate and easily soldered; additionally, they have a low coefficient of friction. Cadmium alloys with tin, nickel and zinc are used under conditions where the pure metal would be unsuitable.

There are several types of solutions for cadmium deposition (Table 13.9).

Table 13.9 Solutions for cadmium deposition

No.	1	2	3
Components, conditions			
Cadmium sulfate	40–60		
Cadmium chloride			40–50
Cadmium oxide		25–40	
Sodium cyanide		80–130	
Ammonium sulfate	240–250		
Ammonium chloride			200–280
Sodium chloride			30–40
Sodium sulfate		40–60	
Sodium hydroxide		20–30	
Urotropine	15–20		
Thiourea			7–10
pH	4–6		
Temperature, °C	18–30	18–30	
Current density, mA/cm^2	5–15	5–20	

Electrolyte No.1 is prepared by separate dissolution of cadmium and ammonium sulfates and hexamethylenetetramine. The solutions are mixed together in the working bath; successively the organic additives are added and pH is brought to 2.0 by addition of sulfuric acid. A pH correction to 4.0–5.5 is finally carried out. The TP of this solution is 5–7%.

The cyanide solution (No. 2) is prepared by dissolving a paste of cadmium oxide (mixed with water) or of freshly precipitated cadmium hydroxide in a previously made solution of sodium cyanide. Only after total dissolution the solutions of alkali and the other components are added as separate solutions. A frequently used additive is dextrin (8–12 g/l). This electrolyte has high throwing power (22–25%).

The chlorine–ammonia solution (No. 3) is prepared as follows. In 2/3 of the final solution volume the chlorides of ammonia, cadmium and sodium are dissolved sequentially, successively thiourea or polyethylene glycol is added together with organic glue, previously added to water.

The anodes for these electrolytes should be made of cadmium.

13.8.3 Indium

Indium can be used both in alloys with Pb or Cd, or as an individual coating. It is more resistant than lead in mineral lubricating oils, but its melting point is lower. Besides, indium has very low friction coefficient.

A suitable electrolyte may be most simply prepared by anodic dissolution of metallic indium in a solution of sulfamic acid at CD 100 mA/cm^2. When the concentration of indium sulfamate in the solution is about 100 g/l the other components are added, as follows: sodium sulfamate (150 g/l), NaCl (50 g/l) and also dextrose (6–8 g/l) and triethanolamine (2 g/l). The pH should be brought to 3. This electrolyte is characterized by relatively high values of CE and TP. The electrolysis takes place at room temperature, at 40–60 mA/cm^2. Anodes should be made of metallic indium.

An alternative solution is sulfate based. It contains indium sulfate (50 g/l), crystalline sulfates of sodium (10 g/l) and aluminum (10–12 g/l); gelatin is used as brightener; pH is 2.0–2.7. The deposition is performed at 20–25°C, CD 30 mA/cm^2, CE is about 70%.

13.8.4 Lead

13.8.4.1 Properties, Advantages and Disadvantages

Lead coatings are soft and lack decorative appearance, in most cases appearing dark grey and dull. Lead as a pure metal is rarely used as a galvanic protection coating. Pb electrodeposition is used essentially for the protection of steel, iron, copper, aluminum and their alloys against corrosion in sulfuric acid media and other sulfur-

containing environments. It should be noticed that Pb does not provide galvanic protection for most of the above elements.

Continuous lead coatings 50–150 μm thick are quite corrosion resistant in H_2S and SO_2 vapors and also in chromic acid. The coatings are stable in air, in chlorine atmosphere, and in organic liquids such as gasoline or other liquid fuels. This stability is due to the formation of thick, resistant Pb compound layers on the surface.

Lead however is not stable in environments that tend to form soluble chemical compounds with lead; examples are acetic and nitric acid, nitrates and alkali.

Lead has good antifriction properties, especially when alloyed with tin or copper. An additional field of application of lead electrodeposits is the galvanic technology itself: in some cases the fixtures that hold the plating articles in place must be coated with lead to avoid their dissolution in strongly reactive electrolytes, for example during electropolishing. Lead is also used as a material for insoluble anodes, for example in chromium deposition, and for lining of the walls and base of the electrochemical cell.

A relatively new field for electrodeposited lead is battery technology. While earlier only bulk lead was used for this purpose, more recently, with the need for miniaturization and weight decrease lead coatings have found some interesting applications.

Neither mechanical nor electrical properties of lead or of its alloys are of commercial interest. The only property of relevance is the easy formability of lead-coated steel parts; for this reason such parts are sometimes used in punching operations.

13.8.4.2 Electrolyte Formulations and Deposition Conditions

The solutions for lead deposition have simple formulations; they usually consist in 150–200 g/l of fluoboric or phenolsulfuric lead salts together with the corresponding acids. The first solution must additionally contain 50–100 g/l of fluoboric acid; the second one contains 25–40 g/l of para-phenolsulfuric acid. The concentrations of the free acids are the following: fluoboric acid 50–100 g/l, or para-phenolsulfuric acid 25–40 g/l.

In absence of lead fluoborate, this salt can be obtained by addition of lead oxide or carbonate to a solution of HBF_4. Other Pb salts can also be prepared by dissolution of lead carbonate or lead oxide PbO in the corresponding acids.

Glue is used as an organic additive. Gelatin, peptone and other substances forming colloidal particles can also be used; all these additives must be previously soaked in a separate tank in order for them to swell. After adding all the components together water is added up to the necessary volume.

The concentration of the additives is usually about 0.2–0.5 g/l. Without additives all the solutions described have a tendency to form dendrites. The additives are consumed during electrolysis and therefore a periodic adjustment of their concentration is required.

Alkaline solutions are also sometimes used; one of the most common can be prepared by dissolving PbO in a 4 M solution of sodium hydroxide; the final solution,

obtained after dilution contains about 5 g/l Pb (as metal) and 35–40 g/l of sodium hydroxide. Glycerol (0.1–1 g/l) can be added to this solution.

Deposition is performed at 10–20 mA/cm^2; working temperature is 25–30°C. Lead anodes are used; the electrolysis cell must be lead-lined. For the alkaline bath, the tank can be made of steel.

The anodic dissolution of indium (up to 30 g/l) in lead fluoborate electrolyte gives an electrolyte for the deposition of Pb–In alloy which has very good antifriction properties. The dissolution of In may be performed at 5 A/dm^2, using a steel cathode.

13.8.5 Antimony

Just like Bi, antimony is used almost exclusively in alloys (in particular with silver or tin) as an additive to enhance the properties of the pure metal deposits. Nevertheless, pure antimony can be of interest as a corrosion-protective coating.

Antimony as a pure metal deposit may be obtained from a solution of oxide Sb_2O_3 (50–100 g/l) and citric acid (300–350 g/l), which can be partly replaced by gluconic acid and potassium or sodium citrate (200 g/l). The deposition temperature must be 30–60°C, and the process is performed with antimony anodes. Cathodic current density ranges from 10 to 30 mA/cm^2; current efficiency exceeds 95%.

13.8.6 Tin

13.8.6.1 Properties and Peculiarities

Tin is anodic relatively to copper and its alloys and is cathodic with respect to steel; in presence of organic acids however tin is anodic to both metals. It is one of the best metal coatings to protect steel against corrosion. Tin protects copper conductors against sulfur that may be present when using rubber insulation; due to its non-toxicity tin is used for the internal lining of cans for foodstuff (tin-ware), for milk vessels and as a table cover. The adhesion of tin to various substrates is high; it is ductile and non-porous, especially after post-deposition melting. Finally, it has relatively low contact resistance.

The disadvantages of tin are its low hardness, low stability in marine atmosphere (it suffers from pitting corrosion) and easy oxidation at higher temperature. At low temperature it transforms to the grey powder form. Pure tin electrodeposits tend to grow whiskers after several weeks or months since deposition. When depositing tin on brass a nickel undercoat is necessary for the suppression of zinc diffusion from the substrate.

Tin may be deposited from both acidic and alkaline solutions; in the former, Sn deposition occurs from divalent ions, in the latter from four-valent ions. The acidic

electrolytes have very low TP (4–6%) and work only in presence of organic additives; these solutions are used only to coat articles of very simple shape. The alkaline stannate solutions have much higher throwing power (23–27%) and may work without additives. Due to the different oxidation state, the electricity consumption when using alkaline solutions is twice as large, and this ratio is actually nearer to three due to the lower current efficiency.

Tin is often melted after deposition (for 10–15 s in glycerol or castor oil at 250°C); in alternative, melting in a furnace at 500°C may be used while fluxing zinc and ammonium chlorides. After melting the solderability is retained for a long time.

13.8.6.2 Electrolytes and Deposition Conditions

The most common solutions for tin plating are presented in Table 13.10. Current density in acidic electrolytes is 10–20 mA/cm^2; using agitation up to 30 mA/cm^2 can be achieved. Alkaline solutions work at high temperature (70°C) and CD up to 50 mA/cm^2.

In order to prepare acidic solutions, the sulfuric acid is first added to the water dropwise, followed by phenol sulfonic acid and stannous sulfate. Gelatin is dissolved separately in a small volume of warm water, alpha (or beta)-naphtol is dissolved in ethanol, and both solutions are added to the main electrolyte while stirring. The solution needs filtration and pre-electrolysis at low current; several hours at 2–3 mA/cm^2 with a steel cathode are suitable. Periodic correction of the electrolyte acidity is also needed. If glue is used, it must be previously soaked in water.

Another type of acidic solution contains formalin. This is added to the solution at room temperature after dissolution of the acid. This solution works only in presence of brighteners such as butyne diol, which are separately dissolved in ethanol. Polymeric additives, usually derivatives of polyethylene glycol, are widely used for tinning.

Table 13.10 Solutions for tin deposition

No.	1	2	3	4
Components, conditins				
Tin sulfate	60–80			30–40
Tin chloride		100–110		
Potassium stannate			120–150	
Sulfuric acid	40–60			100–120
Phenol sulfonic acid	40–50			
Potassium hydroxide			20–25	
Potassium acetate			20–25	
Ammonium chloride		60–80		
Gelatin (glue)	1–2			
Naphtol	1			
Formalin (37%)				5–10
Buthyne diol				6–10
Potassium pyrophosphate		300–400		

For the preparation of alkaline electrolytes the sodium (or potassium) stannate is dissolved under strong agitation in the solution of the corresponding hydroxide. The solution must be left to settle for about one day and then poured in the electrolysis cell without any sediment. Upon operation at low CD the anodes should be covered by a thin golden colored film. It is important in fact for the anodes to dissolve properly, i.e. without the formation Sn(II). Divalent tin in a concentration higher than 2 g/l is harmful and must be oxidized by addition 1 g/l of 10% hydrogen peroxide. These solutions vary from bright grey to straw-colored. Stannous hydroxide may sometimes precipitate; in this case the solution settles as in the first preparation and should be filtered again. An excess of alkali results in a decrease in CE, thus this should be neutralized by acetic acid. Alkali solutions are sensitive to chloride, therefore thorough rinsing of the electrodes, cell and tools after any previous contact with Cl-containing solutions is necessary.

Fluoborate tinning electrolytes are also sometimes used. They are made up not only with fluoborate and fluoboric acid, but they contain also stannous hydroxide, which may be made by first precipitating tin with the addition of alkali to a chloride solution, then by dissolving—using strong agitation—in an excess of HBF_4.

The electrolytes need periodic adjustment of the composition. When the additives are exhausted in the acidic solution the voltage at a given current decreases; this is an indication that it is necessary to replenish the concentration. In alkaline electrolytes the addition of about 1 g/l of brighteners is necessary after passing 3–4 A-h/l of electricity. After 300–400 A-h/l a prolonged activated carbon treatment is necessary, consisting in the addition of 3–4 g/l active carbon, periodic stirring at high temperature for about one day, and final filtration. This should occur 4 or 5 times per year.

If needed, tin coatings may be dissolved anodically in 120 g/l NaCl solution at 30–40°C with a steel cathode; the cell voltage should be about 6 V.

13.8.7 Tin–Lead, Tin–Bismuth, and Tin–Zinc Alloys

Until recently the most widespread solutions for Sn–Pb alloy deposition have been the fluoborate ones. In the last few years however methane sulfonate formulations have been made available, which have the advantage to be less corrosive and provide for a better uniformity in alloy composition; as a whole, such solutions are very promising, in particular for plating processes in printed circuit boards (PCBs) manufacturing.

Various alloys of Sn–Pb are used for different applications, using compositions varying between 5 and 97% tin. Alloy composition is controlled by changing the concentration of Pb and Sn ions in solution. Deposits for PCBs containing 60–65% Sn are obtained from a solution of 40 g/l Sn(II), 20 g/l Pb (as fluoborates) and 100 g/l of free fluoboric acid. Boric acid (25–30 g/l) and organic additives are also necessary: commonly used additives are peptone or glue (0.8–1 g/l). In general, best solderability is achieved by minimizing the fraction of organics in the deposit.

Other commonly used additives are hydroquinone (as antioxidant) and beta-naphtol. Some poly-ethoxy compounds have been recently recommended. Cast lead anodes are commonly used; the lead in these electrodes must be of high purity, the most harmful contaminants being copper, antimony, bismuth, zinc and arsenic.

Carbon treatment, as in the case of tinning solutions, is necessary.

The methane sulfonic solutions are similar to the above, but the metals contents must be three times less, whereas the acid concentration should be twice as high.

Few at% of Bi added to tin can suppress whisker growth after deposition; such alloys are deposited from a solution of 35–45 g/l of stannous sulfate, 1 g/l of bismuth sulfate or nitrate, 120 g/l of sulfuric acid, and also formalin (5 ml/l), 5 g/l of glue and an organic brightener. Alkaline solutions may alternatively be used; these contain potassium stannate (200 g/l), potassium bismuthate (1 g/l) and potassium hydroxide (20 g/l). Steel anodes are used for Sn–Bi deposition.

Several types of tin–zinc electrolytes are available; recently, neutral cyanide-free baths are used along with the traditional cyanide-based ones. Tin is present as Sn(II); the deposits contain 70–90% tin. The pyrophosphate bath with methylene blue thyazine dye (that stabilizes stannous ions) is recommended.

13.9 Platinum Metals: Pd, Pt, Rh

These metals are all characterized by a high redox potential, a strong interaction with water, and exhibit similar water chemistry. The electrodeposition of these metals therefore is generally performed using similar electrolytes; optimum electrolytes however vary according to the stable ionic forms of the various metals.

13.9.1 Palladium

The distinctive property of palladium is its unique ability to absorb hydrogen along with its electrocatalytic properties. These reasons motivate the use of this metal as a seed material to start electroless metallization of non-conductive surfaces. The functional properties of palladium can be characterized as follows:

13.9.1.1 Advantages

1. High wear resistance, Pd works well under wear.
2. Contact resistance is low and stable up to 400°C.
3. High corrosion resistance in various media; does not tarnish in air.
4. Pd can be used as a barrier layer, especially as an undercoat for gold deposition; it provides films with low porosity.
5. The deposits are suitable for welding and soldering.

13.9.1.2 Disadvantages

1. Electrical conductivity is several times lower relatively to silver or gold.
2. Pd coatings usually exhibit strong hydrogenation, high internal stresses, and tendency to cracking in films thicker than 5 μm.
3. Upon contact with organic media Pd may tarnish.
4. Pd forms brittle intermetallic compounds upon soldering.

13.9.1.3 Solutions and Conditions of Deposition

Palladium has the highest tendency among the platinum group metals to absorb hydrogen, therefore suitable solutions should avoid to the maximum possible extent hydrogen evolution, which would lead to hydrogen absorption and consequent embrittlement. For this purpose, solutions stable in various pH ranges have been developed, based either on chloride or amine complexes, or both.

Solutions for palladium plating based on palladium chloride $PdCl_2 \cdot 4H_2O$ can give low-stressed deposits. These electrolytes are prepared by dissolving the Pd chloride in water and progressively adding this mixture to a 25% ammonia solution in the ratio 15–20 g of chloride per 100–150 ml of ammonia solution. Through this procedure palladium diamine chloride first precipitates and then dissolves in the ammonia excess. By adding 25–30 g/l of ammonium chloride, pH is finally brought to 9.0 and water is made up to volume. Deposition is performed at room temperature at 3–4 mA/cm^2.

In order to obtain non-porous bright deposits, the addition of 0.2–0.3 g/l of protalbic acid, or maleic anhydride (0.15 g/k), or chinoline (0.1 g/l) is recommended.

Palladium anodes do not dissolve in the electrolyte, thus platinum or platinized titanium can be equivalently used. Oxygen and chlorine evolve at the anode, resulting in a variation of the solution composition. In this connection it is recommended to separate the anodic half-cell with a ceramic diaphragm, while using ammonia (with added ammonium sulfate and carbonate) as the anolyte.

A simpler solution for palladium deposition (especially upon gold or silver) contains (g/l) 2–40 of $PdCl_2 \cdot 4H_2O$, 150–200 of a 25% ammonia solution, 20–50 of ammonium sulfate and 10–20 ml of hydrochloric acid (density 1.19). Saccharine is also added up to the concentration of 1 g/l. This solution has a pH of 8.5–9.5 and works at room temperature. Optimum CD is 5–15 mA/cm^2. The separation of catholyte and anolyte is necessary, the anolyte being a solution (100 g/l) of $(NH_4)_2SO_4$.

13.9.2 Platinum

Platinum is rarely utilized in conventional galvanic coatings; recently however this metal has found applications in turbine coatings as well as an electrocatalyst in fuel

cells and other energy conversion devices. Pt sometimes can be used as a corrosion-protective coating; besides, titanium is platinized to fabricate insoluble anodes. Platinized platinum is often used for electrochemical studies and in particular for the assembly of the standard hydrogen electrode.

Some properties of this metal are noted further.

13.9.2.1 Advantages

1. Very high chemical stability in almost any medium.
2. Platinum can be used as anodic material, for example in gold and chromium deposition.
3. The metal can be heated in air at and above 1000°C without suffering any permanent modification.
4. It is suitable as electrical contact material, especially at high temperatures and in corrosive atmospheres.
5. It has high resistance to abrasion.

13.9.2.2 Disadvantages

1. Pt deposits have high internal stresses.
2. The metal and its salts have a high cost.
3. It has the ability to diffuse easily into different metals.

13.9.2.3 The Solutions and Conditions of Electrodeposition

The most common salt used in platinum deposition is the chloride of the four-valent platinum ion $PtCl_4$ which is usually purchased in the form $H_2[PtCl_6]$. The simplest solution allowing deposition of relatively high-quality, though porous and non-bright, deposits contains 24 g/l of this acid and 120 g/l of sodium hydro phosphate. This solution can be used at a temperature from 20 to 50°C at CD 2–4 mA/cm^2.

Deposits with lower porosity may be obtained at a higher growth rate from the diamino dinitrite electrolyte. This is prepared by addition of ten-fold excess $NaNO_2$ into a hot (95°C) solution of $H_2[PtCl_6]$. After cooling 5% ammonium solution is slowly added until a neutral or weakly acidic pH is achieved. If this operation is conducted correctly a yellow precipitate is formed, the dinitro diamino platinum salt; this should be finally purified be recrystallization. The operating solution contains 20–30 g/l of this substance and 100 g/l of sulfamic acid; sulfuric acid may be used but it leads to inferior results. Deposition is performed at 60°C with platinum anodes; CD 10 mA/cm^2. The ammonia content of this solution should be adjusted, since it quickly evaporates at high temperature. Furthermore, the amino nitrite complex is unstable over long times. The solution is corrosive, and gold or silver undercoatings are often desirable.

13.9.3 Rhodium

This precious metal possesses a number of useful properties as listed below. The advantages of rhodium coatings make them quite a desirable metal for reflectors, electrical contacts etc., especially for operation in harsh conditions.

13.9.3.1 Advantages

1. Very high hardness (more than 8000 MPa), good wear resistance and strength, low wear.
2. Very high corrosion resistance in essentially all types of media, including sulfur containing and humid atmospheres.
3. Chemically stable in presence of fluorides, thus it can be used when processing devices that contain silicon transistors.
4. The reflectance of Rh is exceeded only by silver. It is good for reflectors, including thin films over silver surfaces. Optical and other characteristics are stable up to 350–450°C.
5. Pleasant appearance.
6. Relatively high electrical conductivity, low contact resistance.
7. The alloys with Co, In, W et al. have very useful specific properties, in particular wear resistance and hardness in combination with corrosion resistance.
8. They present good barrier properties, being able to prevent diffusion between layers of Cu and Au, Fe and Ag.

13.9.3.2 Disadvantages

1. High internal stresses (due to hydrogenation), cracking of thick layers.
2. Brightness of thick layers is lower.
3. The process of Rh deposition requires high purity of substances, including water. The reproducibility of the deposit properties is poor.
4. The solutions are toxic.

13.9.3.3 The Solutions Compositions and Deposition Conditions

Common are the sulfate solutions based on the aqueous salt $Rh_2(SO_4)_3 \cdot 14H_2O$. Its concentration may vary from 15 to 35 g/l. The solution contains also sulfuric acid (40–80 g/l) and magnesium sulfate (20–25 g/l). The addition of 10–20 g/l of sulfamic acid or 2–3 g/l of selenic acid results in the reduction of internal stresses in the deposits.

Deposition is performed at 20–40°C, at CD of 8–20 mA/cm^2, with rhodium anodes, anodic CD being 3 times less than the cathodic one. At higher anodic current density Rh ions can be oxidized to a higher valence; this occurrence can be

discerned by the solution color. Insoluble platinum anodes can be used. Current efficiency approaches 70%.

The solution can be prepared starting from chloride $RhCl_3$, which is the most abundant Rh salt. After its dissolution in hot water 30% alkali solution is added. The precipitate of Rh hydroxide has to be carefully rinsed (the presence of chloride is harmful, as also are Fe, Zn and Cu ions, at concentration more than 5 mg/l).

One further method of preparation is the anodic dissolution of rhodium in sulfate solution in presence of 2 g/l hydrogen peroxide using a superimposed alternate current (50 or 60 Hz, 0.15–0.5 A/cm^2). The excess peroxide is then removed by boiling, and the solution composition is adjusted by sulfuric acid and magnesium sulfate. The internal stresses in the deposits obtained from these solutions are lower than in the former cases.

The thickness of rhodium coating is 0.3–1 μm, rarely up to 3 μm; thicker deposits tend to crack. The alloys of Rh with Ni, In and Co are more ductile and less stressed; for alloys deposition it is sufficient to add 2–4 g/l of the corresponding sulfates to the sulfate-sulfamate rhodium electrolyte.

13.10 Troubleshooting Electroplating Operations: Some Possible Reasons for Poor Deposit Quality

While each of the processes described in this chapter has its own peculiar features, nevertheless there are several common reasons leading to deposits of inferior quality, which are characteristic to essentially all types of deposition processes and solutions. Here the most general cases are described.

1. Most frequently *poor adhesion of the deposit is accompanied by peeling off of the film and crack formation—this may occur spontaneously or during mechanical processing*. There are several reasons for these unwanted phenomena, the most common being an inadequate preliminary surface treatment or insufficient cleaning, in particular traces of grease or oxides remaining on the surface. Insufficient rinsing or unwanted impurities in the solution may also be at the origin of the poor surface quality. When high internal stresses are generated during growth, peeling may be observed in thick deposits. Additionally, it is possible that the operation conditions (temperature, current density) might not be correctly followed; sometimes discontinuities in the current supply may also result in poor adhesion.
2. *Dendrites, high roughness and "burning" at the edges and at protruding parts of the articles* often take place when the current density is too high—in these cases it is possible that the cathodic surface area is incorrect, or when agitation is insufficient. The same result is observed when the various articles to be plated are too close to one another, or too close to the anode; or when the current distribution is non-uniform. In this last case it is possible to reduce the current, to add supplementary anodes or screens and to rearrange the pieces to be coated.

3. *A coarse appearance of the surface, or its dark color* may suggest that particulates in suspension are present in the solution; most often these are originated by the anodic sludge. In this case the filtration of the overall bath is sufficient and—if necessary—the anodic bags may also be changed.
4. *Pitting, low ductility (i. e. brittleness) of the deposit, its non-uniform color with dark stripes and grayish tint* indicate that the solution may contain organic impurities or ions of some foreign metals; other possible reasons for this behavior are a weak agitation, too high a current density or a wrong pH value of the solution. To remove organics from the solution it is necessary to perform a treatment with active carbon, as described above. The removal of foreign metallic ions can be achieved by passing a low current through the solution for the necessary time; this method is referred to as pre-electrolysis (or dummying) and is also described earlier.
5. *Passivity of the anodes* (or filming of the anodes) causes the cell voltage to drastically increase, possibly resulting in the impossibility to provide the correct electric regime of deposition. Possible reasons for anode passivity are an incorrect anodic current density (either too high or too low) and also the lack of substances activating anodic dissolution, namely, chlorides, fluorides, free cyanide or other ions according to the type of the bath. Sometimes salt passivity develops at high electrolyte concentration or high organic concentration.
6. *The reduction of deposit brightness*, especially at hollow regions and at low current density indicates that the concentration of additive (brightener) has decreased to intolerably low levels. This usually occurs if the additive concentration is not adjusted on time (i.e. after the known quantity of ampere-hours of electricity has passed). In this case it will suffice to bring this concentration within the acceptable limits.
7. *Incomplete coverage of the surface by the deposit or non-uniform deposit* may occur when the various articles on a rack are screened by each other, when the anodes are improperly located and also when current density is too low. If there is little or no deposit (and/or the deposit is discolored) there is the possibility that the current is too low or contacts are poor, the connecting wires are too thin, the current had been interrupted etc.
8. Occasionally the deposits have poor quality even when *grown from a freshly prepared solution*. This is most often due to the presence in the solution of various impurities. Obviously, purification, cleaning and previous treatments of the solution have failed. This may be happening for instance when the supplier of the reagents has changed, or when using a new batch of materials. In these situations operating the solution for a certain time at low current density can help.
9. Oppositely, if the electrolyte is operated for a very long time without adjustments, especially when working with non-soluble anodes, *a sharp drop in current efficiency accompanied by deterioration of the deposit appearance* may be observed. This suggests that the concentration of the depositing metal in the solution has become too low and its adjustment is needed.
10. *Deposits of poor quality* are frequently observed when intermediate rinsing of the articles is insufficient or when harmful impurities are otherwise accumu-

lated in the rinsing bath. Usually one has to strike a compromise between the need for a good rinsing and the saving of water. In this respect, effective charts of the rinsing procedures have been developed, permitting to make these contrasting requirements compatible.

11. In addition to the maintenance errors listed above, each particular process has its individual peculiarities. Coating defects such as stripes, pits, poor adhesion, burnt, dull or dark deposits, etc., may be present. These imperfections are usually due to some deviations of the electrolyte composition and/or deposition conditions from their optimum. These deviations most frequently consist in having a wrong pH value in the bath, too low or too high a temperature or current density, accumulation of harmful impurities in the electrolyte, exhaustion of additives. For example in chromium deposition the most frequent reason for imperfections is an improper concentration of sulfate or fluoride. In copper deposition it may be an inconsistency between CD and copper ions concentration. In every instance, the experience of a skilled operator is necessary to pinpoint the reason for an anomalous process behavior.

References

1. J. Horkans, L.T. Romankiw, *Journal of the Electrochemical Society*, **124** (10), p. 1499–1505 (1977).
2. T. Osaka, et al., *Journal of the Electrochemical Society*, **144** (10), p. 3462–3469 (1997).

Chapter 14
Structure and Microstructure of Electrodeposited Metals and Alloys

14.1 Formation of the Polycrystalline Metal

The physical, chemical and mechanical properties, and consequently the performance of electrodeposited metals and alloys usually differ from the reference data reported for the pure metallurgical samples. These variations are due to two main factors: the peculiarities in the structure and microstructure of electrodeposited materials and the presence of impurities. In the case of alloys, the discrepancy between the actual phase structure of the electrodeposit and the equilibrium phase diagram plays an important role as well.

The morphological peculiarities of the surface structure formed during electrochemical crystallization were discussed in Chap. 6; obviously, such peculiarities reflect to some extent those observed in the internal structure. The effects related to the codeposition of impurities are also partly analyzed in Chap. 11. In this chapter we consider the formation of the internal structure and microstructure during electrodeposition.

The microstructure of electrodeposited coatings is determined first by the characteristics of the nucleation and growth processes. These phenomena in an electrochemical environment deviate strongly from the equilibrium conditions due to the large applied driving force for crystallization (the overpotential). Deposition rates are thus sufficiently high that the diffusing atoms at the surface do not have sufficient time to accommodate at equilibrium position but may be trapped in metastable configurations due to film overgrowth. The resulting structure is therefore highly defected and out of equilibrium. As a result, the properties of the deposits are often widely different from those of bulk materials due to the high concentrations of various structural defects; the microstructure of electrodeposits is thus closer to that of vacuum-deposited metallic films than to bulk materials. In particular, the mechanical properties of electrodeposited films are often superior to those of heavily deformed bulk metals, due to the high stresses and high concentration of defects.

No universally accepted classification of the structures in the field of galvanic coatings has been proposed up to now. The only appropriate attempt was made by Fischer in the 1950s [1], which was partially refined later by Winand. Fischer proposed a classification according to the three different types of microstructure:

Y. D. Gamburg, G. Zangari, *Theory and Practice of Metal Electrodeposition,*
DOI 10.1007/978-1-4419-9669-5_14, © Springer Science+Business Media, LLC 2011

(1) the basis-oriented reproducing type (layered structure), (2) the field-oriented textured type (columnar structure) and (3) the non-oriented dispersed type (randomly arranged fine grains). Additionally he considered the formation of field oriented isolated crystals; finally, the twinning type was later identified [2]. More recent investigations however have shown that the reality is much more complicated, and each structure type should be described individually in terms of its microstructural features. Thus, along with the absolute value of the grain size the degree of non-uniformity in size should be reported, as well as the grain shape, the preferential orientation (texture) of the grains, the presence and density of various defects, etc.

The surface morphology of the film is sometimes used to deduce its internal microstructure; however, the former is also affected by the interaction with the electrolyte; any information of this type should therefore be supplemented with characterization methods that directly probe the internal volume of the film.

The main structural features of polycrystalline films are the size and shape of the grains (or clusters of grains), together with the thickness and morphology of the grain boundaries. The *grains* are defined here as the largest sized microstructural features, those that can be revealed by optical microscopy, particularly after polishing and metallographic etching. Using this method, the grains are seen as regions with uniform contrast, different from the neighboring areas and characterized by well-defined edges. The size of these grains is usually in the range from 0.1 to several microns. More precise methods such as transmission electron microscopy and X-ray analysis show that these grains are further structured at a finer scale, and are separated from each other by twin or low-angle dislocation boundaries. The size of these so-called *sub-grains* is from 10 to 100 nm.

In electrochemically deposited metals the two-level structure outlined above is relatively uncommon: often in fact only the sub-grains are revealed. Sometimes light-wave optics is unable to show the grains, and the X-ray analysis of grain size gives an average coherence length of less than 100 nm; these features, unlike the usual sub-grains, can be highly disoriented relatively to each other. In addition, the grain size distribution can be very wide: along with grains with an approximate size much smaller ones may occur, especially in alloys. Sub-grains on the other hand vary in shape from thin plates, where the grains are divided by twin boundaries, to relatively conventional regions, divided by only one or two dislocations but revealed otherwise by X-ray methods.

One further structural characteristic of the deposits is their texture, which denotes the existence of some preferential crystallographic orientation of the grains. Film texture is important as it often influences the properties of galvanic coatings.

14.2 Grain Boundaries

The boundaries between grains or between sub-grains are characterized by their structure, the disorientation angle and by the presence of foreign inclusions. The fraction of this highly defected region near the grain boundaries is an important characteristic of the polycrystalline material.

The width of a grain boundary is estimated as 2–3 lattice constants a of the pure metal. Thus, for an average grain size D the overall surface area of the grain boundaries per unit volume amounts to approximately $3\ k/D$, where k is a form-factor close to 1. Consequently the overall volume of the defected material is $V = 6ka/D$ for a boundary width of $2a$.

Thus, the fraction of the boundary material is inversely proportional to the grain diameter; for $D = 20a$ it approximates 30%.

The reasons for the formation of polycrystals instead of monocrystals in electrodeposition are numerous; monocrystalline growth can take place only in very specific conditions. First, the growth initiates simultaneously at several points at the substrate, which is usually not a monocrystal. Thus the initially formed nuclei have a relative angular disorientation, resulting in the formation of defect regions when nuclei grow sufficiently to coalesce at the edges.

The instant at which coalescence occurs is of special interest. At this time in fact the two processes: (1) filling of the intergranular space by the metal grown from the solution and (2) withdrawal of this solution, occur simultaneously. During this time, bridges between the grains grow first, and successively the remaining gaps are filled with the metal; part of the solution as well as the adsorbed species may therefore remain trapped within these edge regions.

The average size of the grains depends on both the nucleation rate J and the growth rate v of the cluster; for a cluster radius r and with a molar volume V_m

$$dr/dt = v = iV_m/nF, \tag{14.1}$$

The simplest way to find the grain size D (average diameter) is the following.

On one hand, the radius of the cluster at the time τ after its formation is $r = v\tau$, thus the area occupied by this cluster equals $S = \pi r^2 = \pi(v\tau)^2$, and the corresponding time is

$$\tau = v^{-1}(S/\pi)^{1/2}. \tag{14.2}$$

On the other hand, the average duration of grain growth until its final area is S, assuming a nucleation rate J, equals

$$\tau = 1/(SJ). \tag{14.3}$$

Equating both expressions one obtains $S = v^{2/3}\pi^{1/3}J^{-2/3}$, thus $r = \sqrt{(S/\pi)}$, and

$$D = 2r = 2(v/\pi J)^{1/3} = 2(iV_m/\pi nFJ)^{1/3}. \tag{14.4}$$

The same result is obtained by equating the volume of N grains to the volume of the metal deposited during the formation of N nuclei.

In the initial stage, when nucleation at the foreign substrate occurs, the number of nuclei and the corresponding grain size are determined by the substrate conditions, which in general differ from those at the deposit's own surface formed during deposition. Besides, at this initial period a higher current density is often applied to accelerate nucleation, as this provides better adhesion of the deposit as well as fine-grained structure.

In the following stage nucleation occurs at the surface of the depositing metal, but the grain size D initially obtained varies quite slowly with the deposit thickness, thus the substrate influences film morphology up to a thickness of several microns and more. This influence is especially strong with solutions of high purity because the latter favor epitaxial growth of the subsequent layers, i.e. they reproduce the structure of the preceding ones. The adsorption of impurities disrupts this phenomenon, inducing three-dimensional nucleation and consequently a high probability of incoherent nuclei formation. The structure therefore varies rapidly with thickening of the deposit.

The following dependence of D on the thickness h is generally observed:

$$D(h) = D_0 + ah/(b + h) \tag{14.5}$$

Here, D_0 is the grain size in the layer adjacent to the substrate, a and b are empirical coefficients. This dependence can be found experimentally as well, e.g. by measurements of the hardness H at various thicknesses, since H depends on D (see the following chapter).

The size of grains and sub-grains is important as it determines to a certain extent the deposits properties. D is largely determined by the value of overpotential η during deposition (Chap. 1). Using Eq. (14.4) one can give an estimate of the dependence of D upon η: this is needed to introduce into (14.4) the dependences of J and I on overpotential.

This shows [3] that with increasing η the nucleation rate grows more rapidly than current density; in turn, this results in a reduction in size of the microstructural units. The minimum value is reached for a value of the electrochemical fraction of the overpotential close to

$$\eta \approx (2 \pm 1)\sigma S_m/(nF) \tag{14.6}$$

where σ is the surface tension of the metal and S_m is the area of a mole of the metal in a monolayer. The corresponding minimum size is estimated as

$$D \approx (k_B T/\sigma)^{1/6} N^{-1/3} exp[\sigma S_m/(3RT)], \tag{14.7}$$

N being the number of the active centers per unit area.

The overpotential given by (14.6) is relatively high and it can be actually reached only under uncommon conditions; for this reason, a monotonic trend towards smaller grain sizes is instead observed as a rule at higher cathodic potentials and/or current densities, in presence of surface-active substances, adsorbing brighteners etc., especially at low temperatures (Fig. 14.1). However, at very high current densities for copper or nickel deposition, achieved through a strong solution agitation, an increase in grain size was observed [4].

The presence of SAS usually changes the microstructure to a great extent. In particular, a higher concentration of twins and stacking faults as well as high dislocations densities were observed. These features are associated with an influence of adsorbed species on the rates of nucleation and growth, but also with more complicated phenomena. These include for example: (1) surface passivation of the growing cascade of bunched layers, resulting in the secondary nucleation of structurally

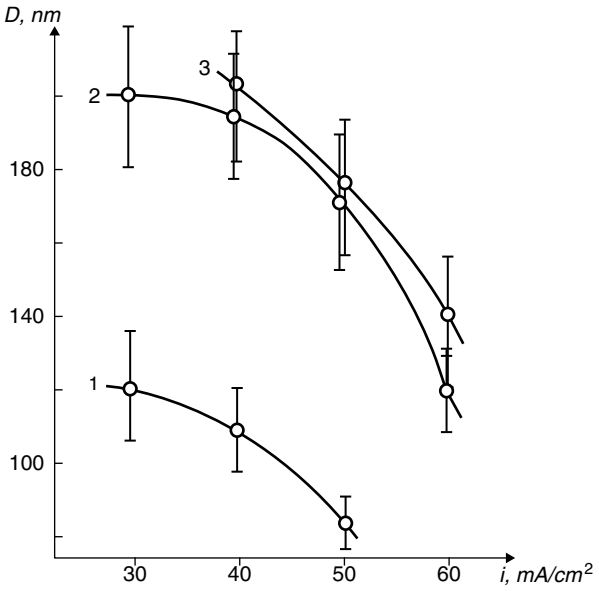

Fig. 14.1 The experimental dependence of the grain size D on current density i (copper from sulfate solution); the temperature at deposition: 1–20°C, 2–40°C, 3–50°C; at much higher CD (≈1 A/cm^2) D increases

independent nuclei, both at the passive surface as well as at the non-structured surface; (2) the blocking of the "right" points of nucleation (corresponding to the coherent nuclei), resulting in a higher probability of nucleation at the "wrong" points, giving rise for example to stacking faults; (3) the decrease in surface energy leading to a smaller nucleation energy; (4) the increase in interplanar distances. Besides, the thickness of a cluster of growing layers depends on the adsorption rate; since this cluster is monocrystalline, its thickness determines the sub-grain size.

The sub-grain boundaries often exhibit a dislocation structure when angular disorientation is low (about 10° or less); these boundaries therefore consist of dislocation nets.

The grain boundaries along with the twin boundaries and stacking faults are the possible two-dimensional structural defects. A complete description of these imperfections requires a combination of electron microscopy and X-ray diffraction; these methods in fact have shown that twinning and stacking faults are often formed in electrodeposited metals along with low- and high-angle boundaries.

The dislocations are one-dimensional defects; they influence the mechanical properties of the metals as well as the processes of crystal growth by providing preferred nucleation sites. In addition, low-angle (disorientation angle less than 10°) boundaries are made up of dislocations, and the stacking faults are the product of the splitting of full dislocations into partial ones. Finally, isolated dislocations may be present also in the bulk of the grains.

Point defects (vacancies, divacancies and interstitials) are also abundant in electrodeposits along with the two- and one-dimensional ones. These latter defects however can be in thermodynamic equilibrium due to the resulting increase of the crystal entropy; thus their equilibrium concentration increases with temperature.

Obviously, a discussion of the geometry and physics of lattice imperfections is beyond the scope of the present book; the reader is referred elsewhere [5]. Here we only attempt to emphasize the interrelations between the electrochemical conditions of growth and the characteristics of the resulting crystal lattice.

14.3 Stacking Faults and Twin Boundaries

Electrolytic deposits commonly exhibit a high concentration of two-dimensional defects, particularly when deposition is carried out in presence of SAS. These imperfections are mainly of two types: stacking faults and twin faults. Both types result from the disruption of the correct growth sequence of closely packed layers in the FCC structure. The FCC structure in fact can be visualized in terms of the superposition of three subsequent atomic layers shifted with respect to each other to fill the voids of the underlayer layer and to give the periodic stacking…ABCABCABC…; the stacking fault on the other hand is represented by defect in the above sequence, such as…ABCBCABCA…; a twin instead can be designated by the sequence…ABCABACBAC…

The stacking faults (SF) in electrodeposits have been revealed by X-ray diffraction methods; this is possible since such defects produce a regular shift of the diffraction peaks, in particular an anomalous approach of the (111) and (200) reflections. This shift is easily measured. More recently, the presence of stacking faults has been confirmed by direct transmission electron microscope observations of electrochemically thinned metal foils. Defects of this kind in the TEM give a characteristic striped pattern.

The probability for a new atomic layer to grow in an irregular position (and thus the resulting defect concentration) depends on the extent of coverage of the growing surface by adsorbed species: when shifting the potential from the region of maximum adsorption or upon a temperature increase the number of defects sharply falls.

An instability of the deposited structure over time has been sometimes observed in combination with relaxation processes in the crystal lattice; in some cases this phenomenon is due to the elimination of SF. The activation energy of this process is relatively low (less than 1 eV), thus the temperature interval where these processes are possible corresponds for Cu, Ni, Ag or Au to room temperature or slightly higher. It is important to note that when the concentration of impurities is higher these ordering processes slow down markedly. This is connected with the immobilization of the faults by the adsorbed species, resulting in an increase in the activation energy of self-diffusion processes in the lattice. Thus the temperature interval of these relaxation processes is shifted to higher temperatures.

For this reason the highest concentrations of two-dimensional lattice defects are observed not only under strong adsorption conditions, but rather when incorporation of the impurities into the deposits occurs [6]. Thus, in nickel deposits the maximum concentrations of SFs was observed at pH values close to hydroxide precipitation, corresponding to their inclusion into the deposits, as well as at high

concentrations of incorporated hydrogen. In copper deposits grown from ethylene diamine solutions an initially high concentration of SFs diminished very rapidly at room temperature due to the low impurity concentrations in these deposits. Upon mechanical activation of the growing surface by using fine hard particles maintained in suspension in the electrolyte, a maximum SF concentration was observed under conditions of moderate activation corresponding to intermediate SAS coverage and inclusion rate.

Obviously, the adsorbate as such does increase the probability of stacking fault formation as a result of a variation in interplanar distances, or by inhibiting occupation of the correct crystallographic sites by the adatoms, as it was noted earlier. For instance, in presence of the adsorbed species on part of the surface the growing atomic layer can be incomplete, and the faults can be generated by the subsequent growth. At the same time the incorporation of foreign species into the deposit stabilizes the SF due to pinning of the dislocations by impurities, or simply resulting from the reduced energy of the stacking fault, as observed for example in brass at high Zn concentrations.

A stacking fault can arise not only as a result of adsorption but also simply by joining two independently growing nuclei. In very pure deposits however this defect can die out in a short time due to self-diffusion processes in the lattice already during the deposition. It is interesting that the relaxation processes can occur faster not only at higher temperature but also at potentials far from the potential of zero charge pzc, if the deposit is left in the electrolyte [7].

The twin boundary is the common atomic plane between two regions in a crystal which are mirror images of each other perpendicularly to this plane. Twin boundaries, as well as stacking faults, are easily observed by TEM using the characteristic striped contrast observed in electron diffraction patterns (Fig. 14.2). The X-ray determination of twinning in fine polycrystals is more difficult than that of SF because it necessitates a precise measurement of the peak profiles followed by a precise calculation of their center positions. In the case of monocrystals on the other hand X-ray diffraction clearly detects the twins.

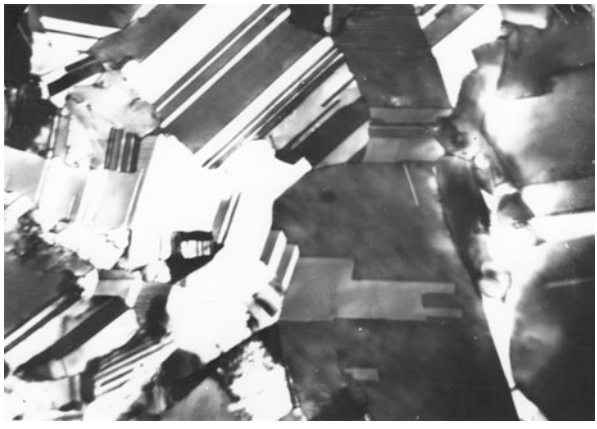

Fig. 14.2 Twin boundaries are easily observed by transmission electron microscopy due to the characteristic striped contrast. Copper deposit from pyrophosphate solution, the dimensions of the picture 4 × 6 μm

Twins have been observed in electrodeposits of nickel, copper and lead. They are characteristically observed at small current densities, but only when the overpotential is higher than some critical value. Actually, nucleation in twin positions needs additional energy with respect to single crystal growth. A correlation exists between the overpotential for the formation of twins arising in fcc structures and the twinning energy: the lower the energy, the lower is the overpotential at which these defects are formed [8]. In the case of spiral growth twinning does not proceed; however, as soon as two-dimensional nuclei are formed, twins are immediately produced.

Similarly to the stacking faults, twin boundaries also arise as a result of an irregular stacking sequence of atomic planes. The twins typically form numerous interlayers having thickness of the order of tens or hundreds of monolayers. This indicates that the average probability of twinning in actual conditions is 1%. Pangarov [9] predicted an increase in the probability of twinning with increasing overpotential. In fact, twinning is closely related with the occurrence of non-coherent nucleation processes and thus becomes more probable when the nucleation probability is higher. Thus, upon nucleation of gold or nickel on copper when deposition occurs from highly purified solutions, part of the surface has a twinned orientation [10]. Twinning was observed as well for silver deposition on silver and copper monocrystalline substrates.

If a new twin arises from the first one, and if this process is repeated, it is called multiple twinning; in this case the twin planes are not necessarily parallel to each other: twinning can in fact occur starting from any of the equivalent <111> atomic planes. This process is often responsible for the formation of polycrystalline structures, especially in the case of textured films. In presence of multiple twinning a specific crystallographic symmetry can arise, resulting in a pseudo pentagonal shape, which is frequently observed in scanning (or transmission) electron microscopy pictures. The semi-spheroid or cauliflower morphology, quite characteristic at high current densities, is also connected with multiple twinning; transmission microscopy of structures of such kind shows in fact the presence of many twinned layers.

Contrary to stacking faults, the twin boundaries cannot be annihilated at relatively low temperatures. Only during recrystallization, when self-diffusion is fast, a significant motion of the boundaries may start, which results in an overall change in the internal structure and in the formation of annealing twins.

The texture (preferential orientation) in electrolytic deposits is easily detected by X-ray diffraction; the textures are of interest due to their influence on the properties of the deposits. Two types of textures can be identified; the first is the emergent texture, generated at the nucleation stage and determined by the most probable nucleus orientation; this texture is characteristic of thin layers. The second type is the growth texture; this progresses during growth and is determined by the combination of several processes. The ratios of the growth rates along various crystallographic directions (geometric selection) along with multiple twinning and selective adsorption at different crystallographic faces can all be of importance.

In fcc metals the textures in the directions [111], [100], [110], [311], [210] and others can be observed; the reported sequence corresponds to an increase in surface energy of the corresponding plane and to an increase in overpotential. In hcp metals

the corresponding sequence is as follows [0001], [1011], [1120], [1010], [1122]. The transition from one texture to another is determined by the processes of multiple twinning along with energetic factors at the nucleation stage [9], and depends strongly on the adsorption of SAS.

The texture can be characterized by its quality, which can be interpreted as (1) the volume fraction of the coating having a certain orientation, or as (2) the average angular deflection from the ideal orientation.

14.4 Dislocations and Disclinations

The dislocation density in electrodeposits is frequently very high, of the order of $N \approx 10^{15}$–$10^{16}\ m^{-2}$. This value is higher than in heavily deformed or quenched metals and is close to the value at which the metal may collapse into powder.

The dislocation density can be calculated as the total length of the dislocation lines present per unit volume or, equivalently, the average number of intersections of dislocation lines with an arbitrary plane per unit area. The highest dislocation density is observed in deposits obtained at relatively high overpotentials.

The dislocations influence the mechanical properties of the metals such as strength, ductility and hardness. To a lesser extent, they influence also the electrical properties.

Depending on the nature of the metal and on overpotential, as well as on the stage of growth, various mechanisms exist for dislocations formation. At the lowest overpotentials (1 mV) crystal growth can occur on the dislocations present on the substrate surface or from the previously deposited layers. With increasing overpotential the number of active dislocations of this type may increase. The screw dislocations grow most easily. Later in the growth, at the boundaries of non-coherent regions new dislocations can arise. The “discrepancy” dislocations can result from a slight difference between the lattice constants of the substrate and the deposit. Any foreign species on the surface can also give rise to new dislocations. A complicated overall dislocation pattern can thus be observed, the primary (intergrown or initiated at the substrate) dislocations being the predominant ones.

At overpotentials of tens of millivolts nucleation may start, resulting in the formation of new grain boundaries, many of them being two-dimensional defects or having dislocation structure. The higher is the overpotential the more nuclei are formed, and the higher is the dislocation density.

The formation of dislocations depends on the incorporation of impurities. The deposit often grows through polyatomic layers forming thin platelets. When the crystal is of such kind, an irregular distribution of the incorporated species takes place: both adsorption and inclusion occur first at the film surface in contact with the solution. The concentration gradients result in local strains and consequently in the generation of novel dislocations. Generally, the inclusion of foreign metallic species or hydrogen atoms produces local variations of the lattice constant resulting in strains and dislocations generation.

A further contribution to dislocation formation comes from vacancies. The excess vacancies may coalesce in disc-shaped regions which at some critical size flatten, resulting in the formation of dislocation loops. These loops are often observed in metals of high purity, whereas in diluted alloys the excess vacancies prefer to bind with the atoms of the alloying component.

If a large share of the dislocations forms at the grain boundaries their density equals approximately

$$N \approx 3n/D^2 \tag{14.8}$$

where D is the grain size, and n is of the order of unity; this represents the number of dislocations present at one grain facet.

The specificity of the disclinations consists in the following. While the dislocation is characterized by its Burgers vector $\boldsymbol{b}$ (the lattice displacement obtained when circling the dislocation line), the disclination is described by an angular increment ω (Franck's vector). In short, this is equivalent to the elimination of a sector from the cylinder with the consequent joining of the facets thus produced. This results, for example, in the transition from 6-fold to 5-fold symmetry. Thus, the frequently observed pentagonal crystals in electrolytic deposits may be originated from disclinations [11].

14.5 Point Defects

The equilibrium concentration C of vacancies in metals increases exponentially with temperature, and the activation energy for their formation is about 1 eV. The activation energy for vacancies migration is of the same order of magnitude. The temperature dependence $C = C_0 \exp(-E/k_B T)$ is also true for divacancies and for interstitials; in the last case E is twice as large. At temperatures close to the melting point C may be as much as one vacancy (in thermodynamic equilibrium) per 10^4 or 10^3 atoms. A very quick cooling (quenching) of the metal from a high temperature can freeze-in any excess point defects because their annihilation requires relatively slow diffusion processes. A high concentrations of point defects has been observed also in metal foils condensed from the gaseous phase on solid substrates.

The electrodeposition process is in some respects similar to the condensation from vapor or from liquid to solid at the cooled substrate. The cooling process in evaporation is paralleled in electrodeposition by the charge transfer process; more precisely, the metal ion overcoming the energy barrier due to the charge transfer finds itself in a high energy configuration, which may be dissipated by the surface diffusion process. It is for this reason that the freshly deposited layers immediately after deposition contain an anomalous concentrations of vacancies and divacancies, as if they were quenched from the high temperatures. Only if deposition occurs very fast the defect concentration is high; when depositing slowly single crystals can be obtained.

Such analogy is not completely rigorous, however partial support to this can be found in the observation that high-temperature phases can be obtained in alloys deposited at high overpotentials, or in the formation of fcc cobalt (a high temperature Co phase) at high CD. In any case, various experimental methods (X-ray diffraction, dilatometry, positrons annihilation) evidence a high vacancy concentration in electrolytically deposited metals. In particular, the lattice constants measured in electrodeposited Pt, Pd, Cu, Ag, are very frequently smaller than the corresponding bulk values.

The observed concentration of point defects depends on their formation rate along with the kinetics of their migration towards the defect sinks: dislocations, grain boundaries etc., where the vacancy may annihilate. Actually what is moving are not the vacancies but the metal atoms; atomic diffusion however results in vacancies migration; in practice, this movement is similar to the diffusion along a concentration gradient. As it was noted earlier, this process has an activation energy close to 1 eV.

The highest initial vacancy concentration is observed at the initial surface layer; when this is overgrown by the successive layers there is insufficient time for equilibrium to be established. The rate at which the film orders depends on the surface energy, which in turn is a function of the electrode potential and is maximal at the pzc. For this reason the diffusion processes are enhanced when the potential shifts from the pzc. On the other hand, the rate at which vacancies form grows at increasing overpotential, as determined from the equilibrium potential. Therefore the resulting concentration of residual vacancies can be a complicated function of the electrode potential.

Contrary to vacancies, interstitial atoms have been detected in deposits of lead, bismuth and zinc, but only by indirect methods.

14.6 Post-Electrolysis Structure Relaxation

In the chapter on alloy deposition it was noted that the formation of non-equilibrium structures is a common phenomenon in the electrodeposition of alloys. A similar phenomenon is observed, although infrequently, in the deposition of pure metals. The post-electrolysis processes of partial relaxation of the internal stresses, the variations in electric conductivity, hardness and other structure-sensitive properties were known long ago. One may therefore conclude that non-equilibrium structures are formed very often during electrodeposition. The rate at which the as-deposited structure relaxes after electrolysis however can vary over a wide range of time scales. If these processes are rather fast and can be completed during deposition throughout the overall thickness of the deposited metal, the initially existing non-equilibrium structure cannot be detected. In other cases, on the contrary, rearrangement of the structure occurs so slowly that a steady, even if non-equilibrium, state is often realized. Most common is the situation when relaxation processes continue after deposition for some minutes, hours, days or weeks; these phenomena are usually designated post-electrolysis processes, ageing or recovery.

In practice, various relaxation processes may be active in parallel, such that some of the processes in the given specimen may be very fast, while others may occur at a moderate rate and some of them may even need a higher temperature to occur.

It must be noted that such temporal instability sometimes affects structural investigations. For example, the X-ray diffraction measurements or measurements of the deposit physical properties are time consuming, thus these studies should be performed at low temperatures to slow down any reorganization. Therefore the specimen must be kept cold, for example in solid carbon dioxide or in liquid nitrogen, during storage and during the measurements.

The relaxation processes consist first of all in the movement of point defects and their consequent annihilation, preferentially at dislocations or at grain boundaries, and also in a rearrangement of the dislocations as a result of strain. Finally, the movement of atoms in stacking faults and the growth of large grains at the expense of small ones (recrystallization) can also occur.

The motion of vacancies has a low activation energy and can consequently proceed at or below room temperature. Sometimes several stages of these processes can be distinguished. Thus, in silver deposits the fast process of surface diffusion and the relatively slow migration of divacancies could be distinguished by conductivity measurements.

At temperatures near 0.3 of the melting point in the absolute scale, defect rearrangement and the escape of codeposited hydrogen are observed. All these processes result in variations of the electric, magnetic and mechanical properties: in particular, the ductility increases, whereas tensile strength, hardness, stresses and conductivity decrease. These processes at the above mentioned temperature are usually completed in 1–3 h; the thermal annealing process should be performed in an inert atmosphere or in vacuum.

Recrystallization on the other hand occurs at higher temperatures—about 0.5 of the melting temperature, but in electrochemically deposited metals it may take place both at higher or at lower temperatures. This is connected with the degree of purity, the grain size, the density and type of defects and the stress state. In these conditions the diffusion processes accelerate, the incorporated organics decompose and sometimes the porosity increases along with grain growth. In the case of alloys the precipitation of supersaturated solid solutions or of other non-equilibrium phases is accompanied by pronounced changes of the properties. Obviously, these properties can be properly studied only in an inert atmosphere or under vacuum, except for inert metals such as Au or Pt.

It is possible to perform structural investigations in combination with the measurements of some property, say, electrical conductivity, while the coating is thermally annealed. This experiment would require passing through the specimen a weak current while the voltage drop through the sample along with its temperature are continuously recorded. In other cases the determination of structure and properties may require the periodic cooling and withdrawal of the sample from the heating chamber or furnace; this complicates the study and necessitates several lengthy measurements.

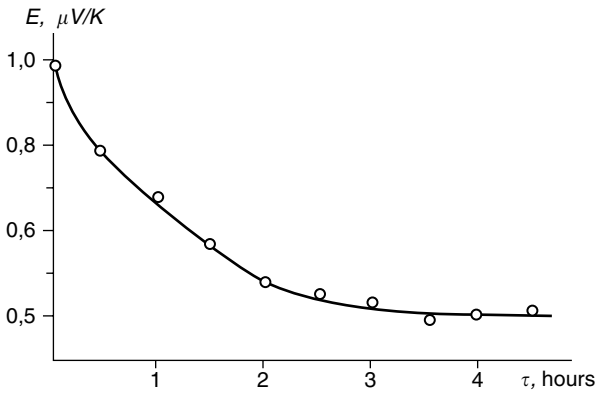

Fig. 14.3 The decay of the thermoelectromotive force between pure annealed copper and the electrodeposited sample (copper from the cyanide solution) during the heating at constant temperature 70°C

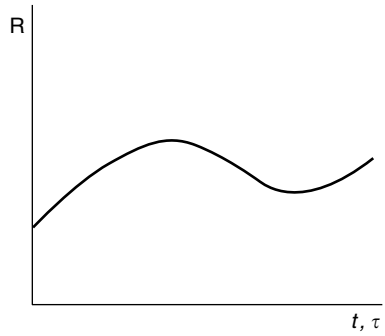

Fig. 14.4 Time dependence of the electrical resistance of a copper deposit (sulfate solution containing thiourea) during a linear increase of temperature t from 20 to 200°C. The falling part of the curve corresponds to the temperatures from 80 to 160°C. The rate of heating dt/dτ = 3°/min

The measurement of various properties over time while the sample is being thermally annealed leads to the determination of so-called "annealing curves". These curves can be obtained at various temperatures or while the temperature is rising at constant rate—Figs. 14.3, 14.4. In the analysis of these curves the time varying part is separated and it is assumed that the variation in this property is proportional to the concentration of some type of structural defects.

An important part of these studies consists in solving the diffusion problem corresponding to the actual experimental situation. This problem is facilitated by the fact that the solution—at constant temperature—very often has the form

$$c(t) = c_0 \exp(-KDt), \tag{14.9}$$

where c is the concentration of defects of a given type, and D is its diffusion coefficient.

In general the solution of the diffusion problems of this kind have the form of an exponential series. The first term however is the largest and plays the dominant role. The coefficient K in (14.9) is assumed to have the form $K = k/r^2$, r being the average diffusion path of the defect, while k depends on the problem geometry and is of the order of 10 (it can be, e.g., 4π), thus

$$c(t) = c_0 \exp(-10Dt/r^2), \tag{14.10}$$

By determining the annealing curves at several temperatures one can find the temperature dependence of D and then the corresponding activation energy E. The value of E may be compared with literature data in order to determine the nature of the corresponding process. For the independent calculation of D it is necessary to estimate r; this should be about one half of the subgrain size.

Various experimental methods have been developed for this purpose [12], including heating at a constant rate, a combination of isochronous and isothermal annealing etc. One of the simplest methods is based on (14.10). Differentiation of this equation gives in fact

$$dc(t)/dt = 10\, c_0 D/r^2 exp(-10Dt/r^2), \tag{14.11}$$

and then

$$c'(t)/c(t) = 10\, c_0 D/r^2 \tag{14.12}$$

Using the proportionality of c to the measured quantity, one can estimate D while r is known, or vice versa.

From the point of view of the deposit characteristics, the changes in properties occurring during heat treatment may be either advantageous or disadvantageous, each case requiring its own analysis. Thus, the solderability of tin coatings on a nickel substrate degrades at temperatures higher than 250°C due to the formation of the intermetallic $NiSn_3$. For the same reason the alloys Ni–Sn are not recommended when heating of the component is required. At temperatures higher than 350°C oxygen diffuses through silver; similarly, copper diffuses through gold coatings at 250°C up to 2.5 mm a month, and at 500°C up to 0.025 mm in three days, thus worsening the contact resistance.

Examples of the useful role of heat treatment are also numerous, however. Here we mention the formation of materials with high strength and ductility upon heating of the alloys Cu–Zn, Ni–Cd, Ni–Cr, as well as the increase in ductility of pure metallic deposits. Sometimes, very hard fine particles can be precipitated in the volume of the coating upon heating, resulting in a high alloy hardness. Finally, prolonged heating is necessary for the dehydrogenation of zinc-plated steels.

14.7 Techniques for Structural Investigations

The methods described in the previous section are indirect: structural features are in fact deduced from the measurement of some structure-sensitive property. Direct methods of structure investigations on the other hand are based on X-ray and electron diffraction; more recent advances in this field are based on probe methods such as scanning tunnel microscopy (STM).

Some of these methods are strictly surface sensitive, since the particles or radiation emitted during the experiment penetrate only to a limited depth; other meth-

ods are sensitive to the material bulk. Thus, electron diffraction is capable only to probe the surface or very thin (10–50 nm) layers whereas X-rays are capable to probe much thicker regions, providing approximately a bulk investigation method. A possible classification of these methods is based on the nature of the particles or radiation being detected. In Auger electron spectroscopy (AES) and in electron diffraction methods a beam of electrons impinges on the sample surface causing various electronic transitions and inducing excitations in the sample. After a short time the system relaxes and electrons are emitted and detected by suitable sensors to provide information on the material structure. In photoelectron spectroscopy, photons impinge on the surface and excite the system, which afterwards relaxes, again by emitting electrons. This class of methods includes XPS, SIMS, ESCA, EXAFS; these are increasingly used in the detailed analysis of surface layers; for more details, see for example [13].

The scanning tunneling microscopy method [14, 15] in schematically described in the following. When a very thin metallic (Pt–Ir or W) tip is placed in a vacuum near a conductive surface with a potential difference (approximately 1 V) relative to the tip, the tunneling current through the gap depends exponentially on the distance H between the tip and the surface. In general, a tenfold decrease of the current i is observed when the distance increases by 0.1 nm. Upon scanning the surface with the tip, i is recorded at constant H, or vice versa. This provides a picture of the electronic distribution of the surface down to the atomic level; such distribution can in most cases be approximated to the topography of the surface. One variation over this method is scanning electrochemical microscopy; in this case the tip is a microelectrode and the measurements are performed directly in an electrochemical cell. One of the difficulties in the application of these methods is the possible ambiguity in the interpretation of the data; nevertheless, unique information may be achieved on the structure of monocrystalline facets, the presence of steps and kinks, the presence of adsorbed molecules etc.

X-ray diffractometry is one of the most useful methods in structural studies. Its main advantage is the high statistical significance of the data acquired: the volume involved in each measurement is rather large thus providing high reproducibility of the results. Moreover, the measurements have high precision and can be performed under various conditions, including low and high temperatures, inert atmosphere and even directly (*in situ*) in an electrochemical cell.

There are two types of questions in metal plating that can be answered with X-rays methods. First, one can determine the structure types of the phases present in the deposit, their lattice constants, the presence or absence of a texture as well as its orientation, and the type of alloy: solid solution, intermetallic compound or mechanical mixture. The second problem is the measurement of grain size; in the case of X-ray diffraction this corresponds to the size of coherently diffracting regions along the direction perpendicular to the film surface; in addition, X-ray diffraction may probe the dislocation density, microstrains, twins and stacking faults in the film.

The first problem is solved by recording the overall diffraction pattern in a wide range of diffraction angles, and then the list of the angles θ_i at which peaks in the

diffracted intensity are observed are analyzed. These values of θ_i are determined by the set of interplanar distances existing in the lattice. Thus, by knowledge of the diffraction angles one calculates said distances d_i using Bragg's formula

$$d_i = \lambda/(2sin\ \theta_i) \tag{14.13}$$

where λ is the wavelength of the given X-ray radiation. The most common is copper radiation, where $\lambda = 0.15405$ nm for the most intense line $K\alpha_1$.

Finally, it remains only to correlate the obtained set of d_i with standard tables in which the data for all known substances are tabulated. Sometimes two or more metals, alloys or crystal structures are present in the specimen, thus one should separate the data from each other. In case that the actual data differ somewhat from the tabulated ones, it may signify either that the exactness of the system was low (for this reason a standard sample must be used in parallel with those of interest), or that structural defects are present in the lattice. For example, the presence of vacancies results in the decrease in d in the range of 0.01%. This degree of accuracy can usually be achieved in X-ray measurements.

The second type of problems needs a precise analysis of both the positions and profiles of the specific peaks along with those of the standard sample. In this analysis, standard computer programs are used based on a Fourier analysis of the profile shapes. These programs allow computation of the subgrain size, the microstrains, dislocations density and sometimes reveal the presence of stacking faults and twin boundaries. Simpler formulae for rough approximations exist along with the said programs.

Several methods based on electron microscopy are widely used in the study of electrolytic deposits. Transmission electron microscopy needs very thin samples which are made from metal foils, first separated from the substrate, by electrochemical polishing. A common method consists in electropolishing until a small hole is formed in the film; then in proximity of the hole the film is sufficiently thin to be electron transparent. The thickness at these regions is about 10–50 nm, and the electron energy can be of the order of 10^5 eV or higher. The contrast in the corresponding patterns (Fig. 14.2) contains a large amount of information on the internal structure of the deposit; in particular, it is of interest to correlate this data with X-ray data. The theory of electron contrast has been thoroughly developed, and the interpretation of both images and diffraction patterns is best tackled by a specialist.

Contrary to electron transmission, scanning electron microscopy is a surface sensitive method. This is a quite informative and convenient method for the study of surface morphology, roughness, the shape of grains, the presence of pores, inclusions etc.; many instruments are also capable to combine the imaging process with the local analysis of elementary chemical composition, and other can generate diffraction images using backscattered electrons.

Physical methods of investigation are increasingly used in the field of galvanic coatings; we hope indeed that a more thorough and well informed use of such methods would contribute to solve ever more theoretical and practical problems in this field.

References

1. Fischer H. Elektrolytische Abscheidung und Elektrokristallisation von Metallen. Springer, 1954
2. Povetkin V.V., Kovenski I.M., Structure of Electrodeposits. Moscow, Metallurgy Ed., 1989
3. Gamburg Yu. D., Russ J. Electrochemistry, 1999, v. 35, p. 1157
4. Bueren, H., Imperfections in Crystals (1960).
5. Gamburg Yu. D., Soviet J. Electrochemistry, 1978, v. 14, No. 12, p. 1965
6. Polukarov Yu. M., Soviet J. Electrochemistry, 1968, v.2, p. 937 (in Russian)
7. Kozlov V.M. Transactions of the Siberian Branch of the Acad. Sci. USSR, chem.. series, 1986, No. 6, p. 22
8. Pangarov N.A., Velinov V. Electrochimica Acta, 1968, v. 13, p. 1641
9. Thomson E.R., Lowless R.R., Electrochim. Acta, 1969, v. 14, p. 269
10. Atanassov N., Vitkova S., Rashkov S., Izvestia Bulgarian Acad. Sci, 1977, v. 10, No. 2, p. 247 (in Bulgarian)
11. Vikarchuk A.A., Volenko A.P. et al., Russian J. Electrochemistry, 2004, v. 40, p. 207
12. Damask A.C., Dienes G.J., Point defects in metals. Gordon & Breach Science publishers, 1963
13. Woodruff D.P., Delchar T.A., Modern techniques of surface science, Cambridge Univ. press,
14. C. Julian Chen “Introduction to Scanning Tunneling Microscopy” Oxford University Press, USA, 2nd Ed. (2007)
15. K. Itaya, Progress in Surface Science 58 (3), 121–247 (1998)

Chapter 15
Physical Properties of Electrodeposited Metals and Alloys. Quality Control and Testing Methods

15.1 Introduction

The properties of electrodeposited metals deviate to a greater or lesser extent from the standard values reported for pure bulk materials obtained by metallurgical methods (for example, crystallized from the melt), which usually exhibit a structure close to the equilibrium one. These deviations are mainly due to a higher density of structural imperfections and the presence of impurities (among these hydroxides, sulfides or organic substances) uncharacteristic of the corresponding bulk metals. In particular, the observed variation of deposit properties appear to be related to the grain boundaries, more precisely to the volume of defected region localized near the boundaries, the presence of precipitates or impurities—in particular oxides and hydroxides—and finally to the structural features of these regions, for example, the angular disorientation of neighboring crystals.

In electrodeposited alloys the phase structure may furthermore be different from that predicted by the equilibrium phase diagram, in particular, as a result of the formation of supersaturated solid solutions.

Formation of non-equilibrium structures in electrolytic deposits is related to the peculiarities of the processes of electrochemical nucleation and growth of metallic crystals, and above all with the high overpotential at which the films are grown and the adsorption of impurities. In turn, the properties of electrodeposits depend on the conditions of electrocrystallization through their structure and purity. A decrease in grain size, as well as the inclusion of foreign particles, for example, lead to an increase in hardness. Tensile strength, ductility and other properties of the deposits can change by orders of magnitude when current density, deposition temperature or pH of the solution are varied. The electrical resistance usually differs from the standard values by 1 to 15% but deposits containing impurities can show a resistance several times higher.

Y. D. Gamburg, G. Zangari, *Theory and Practice of Metal Electrodeposition,*
DOI 10.1007/978-1-4419-9669-5_15, © Springer Science+Business Media, LLC 2011

15.2 Specific Electrical Resistance

The importance of the electrical properties of galvanic coatings in application has increased lately due to the extensive applications in microelectronic devices. Most important is the deposition of layers with high electrical conductivity σ; this can be attained by high purity and high structural quality of the deposits.

The value of specific resistance or resistivity $\rho = \sigma^{-1}$ depends primarily on two factors: (1) the thermal vibrations of the crystal lattice (which increase with temperature, causing the value of ρ to increase), and (2) the presence of crystal imperfections (grain boundaries, dislocations, point defects, stacking faults etc.) along with impurities. These factors are accounted for in the Matthiessen's rule (1864):

$$\rho\,(\mathrm{T}) = \rho_{\mathrm{T}} + \rho_{\mathrm{D}} = \mathrm{bT} + \rho_{\mathrm{D}}, \tag{15.1}$$

which reflects the additivity of the two contributions, the proportionality of the thermal contribution to the temperature and the relative independence of the structural part on temperature.

It follows from this rule that with rising temperature the relative role of imperfections and impurities decreases. For this reason one of the methods to estimate metal purity and lattice perfection consists in performing conductivity measurements at two temperatures, namely that of liquid helium (4.2 K) and at room temperature (293 K). With an ideal lattice and high metal purity the ratio of the two conductivity terms is of the order of several hundreds, whereas a distorted structure and the presence of impurities reduce this value to several tens or even less.

Structural defects in the pure metal lead to an additional resistivity originated by two contributions. The first is the non-uniformity of the electrical charge density distribution and the second is connected with the lattice deformations near the defect. The total influence of dislocations on resistivity is of the order of 10^{-9} Ω m at their highest concentration; point defects, stacking faults and twin boundaries along with the grain boundaries can elevate the resistivity to about 10^{-8} Ω m at their highest concentration [1].

The contribution to resistivity from impurities can be much higher. The dependence on grain size D has the view $\rho = \rho_0 + k/\mathrm{D}$, k depending on the properties of the grain boundaries. This depends on the distribution of the incorporated species; in the case of molecular/atomic level dispersion in the matrix this influence is strong; however, if the impurity forms isolated dispersed inclusions or concentrates at grain boundaries its influence is weaker. An exception to the above arises when grain boundaries are completely surrounded by an insulating impurity layer; in this case the resistivity may rise tenfold or more.

Electrolytic deposits with the highest conductivity are obtained by depositing from a simple—i.e. without complex compounds or organic additives—purified solution at elevated temperature (40–60°C), at moderate current density and without stirring. In presence of small quantities of uncontrolled impurities in the solution the conductivity may decrease by 1–2%; the same result is obtained by cooling down the solution to room temperature, or by moderate agitation.

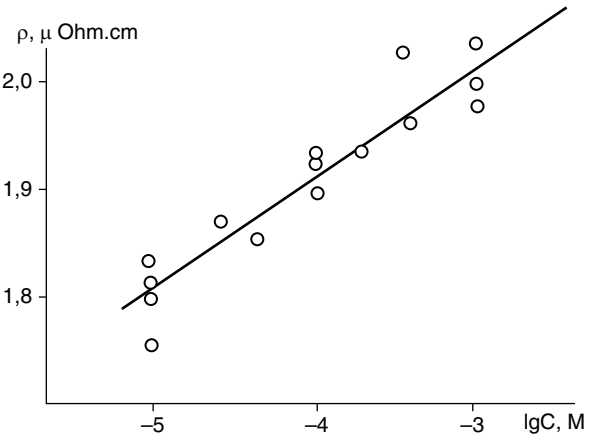

Fig. 15.1 Dependence of ρ on the logarithm of the concentration of the additive in the solution

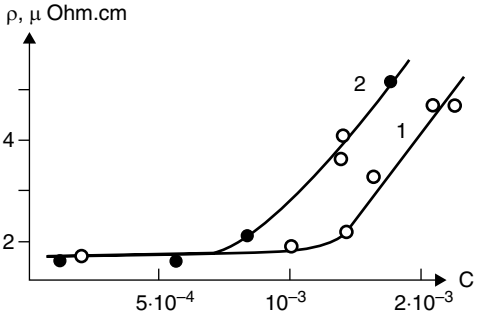

Fig. 15.2 Dependence of the resistivity of copper deposits on the concentration of o-phenantroline in the solution; 1 – E = +0.1 V, 2 – E = – 0,1 V (SHE)

The addition of surface-active substances, ligands, or extraneous metallic ions, can raise the value of the resistivity to a larger extent, usually by 10–20%, but sometimes by 2–3 times. In presence of polyethyleneimine the resistivity of copper has been observed to increase up to 10 times. A characteristic linear dependence of ρ on the logarithm of additive concentration is usually observed (Fig. 15.1), though other functional dependences have also been seen (Fig. 15.2). If adsorption and inclusion of the additive is limited to a certain potential window, its influence on electrical properties is limited to this region. The degree of such influence (especially for the brighteners and leveling agents) depends on whether the additive is codeposited with the metal or if it only induces changes in the deposit structure or substructure. The fraction of the change in resistance Δρ caused by structure variations can be eliminated by low-temperature (up to 150°C) annealing, while elimination of the remaining part requires a higher temperature. The annealing curves ρ–T obtained during heating in vacuum or in an inert atmosphere sometimes do reflect the stepwise changes in ρ corresponding to the various atomic processes involved, including annealing of point defects, diffusion and segregation of impurities, etc. (Fig. 15.3).

An influence of pH may be observed in the case when hydroxide precipitation occurs at the cathode surface, accompanied by its incorporation within the metal.

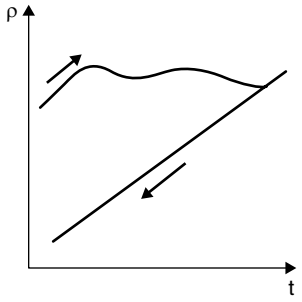

Fig. 15.3 Electrical conductivity as a function of temperature in a thermal annealing experiment during heating and the subsequent cooling stage

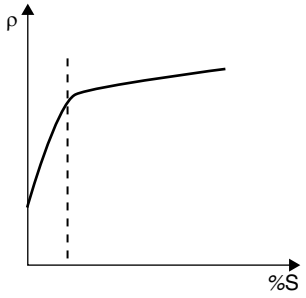

Fig. 15.4 Resistivity of copper deposit vs. sulfur inclusions, showing a kink in correspondence of the solubility limit of S in the lattice

The hydrogenation of the deposit on the other hand exerts only a moderate effect. More pronounced effects are seen if a superimposed alternate current or a pulse reverse current is applied, because these electric regimes tend to give deposits of higher purity and therefore better conductivity.

The inclusion of impurities into a depositing metal is possible only up to the solubility limit in the growing structure; these limitations are seen for example in the inclusion of sulfur or phosphorus from additives containing these elements into copper and nickel deposits. The plot of resistivity vs. sulfur concentration in copper deposit for instance exhibits a deviation at the limiting solubility of S (Fig. 15.4).

The resistivity of alloys is always higher than in pure metals. This is due to the fact that additional electron scattering may occur at lattice distortions near the solute atoms; an additional contribution derives from the smaller grains formed in alloys, which generate a higher grain boundary density. The general dependence of ρ on alloy composition is that of an inverted parabola with the maximum at the equiatomic composition. However, in the case of intermetallic structure formation, the corresponding values of ρ may deviate from this trend.

Measurements of electrical conductance are useful when performing studies of structural evolution in the deposit after or also during ageing or annealing. For example, phase precipitation from a supersaturated solid solution is accompanied by a decrease in resistivity. In these measurements it is important to take into proper account also the porosity of the electrodeposited layers, which causes an increase of the overall resistance; thus one has to distinguish the resistivity of the material from the resistance of the actual sample.

15.3 Measurements of the Specific Electrical Resistance

Several methods are used in practice to measure the conductivity of a film. The first one is based on monitoring the potential drop across the sample while an alternate current is passed through it. The sample is usually deposited on top of a thin foil or fine wire. This method does not need separation of the deposit from the substrate; moreover, the measurement can in principle be performed in situ, during deposition. Its disadvantage is, however, its low precision. Nowadays this method is rarely in use.

The second method necessitates separation of the deposit from the substrate; these measurements are made with precise and sensitive bridges or with high-impedance ohm-meters using a four-contact device to prevent the contribution of the contacts to the measured voltage difference. This technique is the most versatile, but it is convenient only for foils above a certain thickness. Thin foils are very inconvenient to use, since they curl into a coil due to surface forces; thick foils on the other hand have a very low resistance, which is difficult to measure precisely.

The samples used in these techniques are usually deposited onto polished stainless steel, titanium or other metal with low adhesion to the deposit. Samples with the desired configuration can be obtained by photolithographic techniques or by etching, or simply by mechanical cutting off the separated foil. The sample must by highly uniform in thickness and structure. Its length is usually 50 mm or longer. For this purpose, it is convenient to use a well polished vertical cylinder cathode (maybe rotating); after deposition in fact the deposit can be cut along the height and separated from the substrate.

The device used for this measurement is shown in Fig. 15.5. The distance $\boldsymbol{l}$ between the contacts for the measurements of potential drop $\boldsymbol{U}$ is about 30 or 40 mm, the distance between the current contacts varies between 40 and 50 mm. The cross

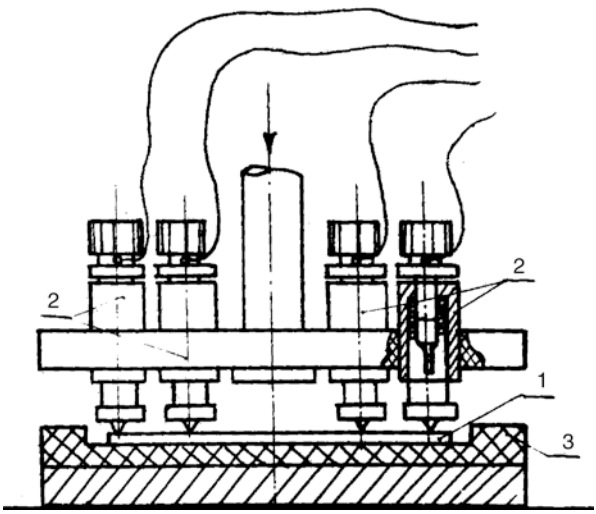

Fig. 15.5 Device for the measurement of the deposit conductivity; *1*—the sample, *2*—the contacts, *3*—the insulator

sectional area S can most simply be found by weighing the sample: if the overall length of the sample is L, its mass is m and density D, then $S=m/(LD)$. The value of resistivity is then equal to

$$\rho \approx \mathbf{U}S/Il = \boldsymbol{U}m/(I\,L\boldsymbol{l}D). \tag{15.2}$$

The current I must not be too high and is usually about 0.01 A.

This measurement can also be performed using a device with the contacts in a square arrangement. In this case the current is made to flow across one diagonal and the voltage is measured with the other pair of contacts. The resistivity is determined as

$$\rho \approx 9.06\,\boldsymbol{U}h/I, \tag{15.3}$$

h being the sample thickness. The overall size of the sample must in this case be much larger than the distances between the contacts.

The instrumental error in these measurements is about 1% or more. It is difficult to attain better results, mainly because of the difficulties in achieving a good thickness uniformity. In four-contact measurements it is also necessary to have good contacts at all points; then each contact must have its own retaining device. It is also desirable to coat the contacts with gold to minimize contact resistance.

The third method is used mainly to monitor resistance during heat treatment or post-electrolysis processes; it consists in the measurement of potential drop along a sample deposited on a highly resistive substrate. A thin conductive layer (platinum, nickel or other material) with a known resistance (about 1 Ω) is deposited by any method upon ceramics, plastics, glass etc. Then the layer of interest is deposited, and its resistance is measured; the resistance of the substrate in this case can usually be neglected.

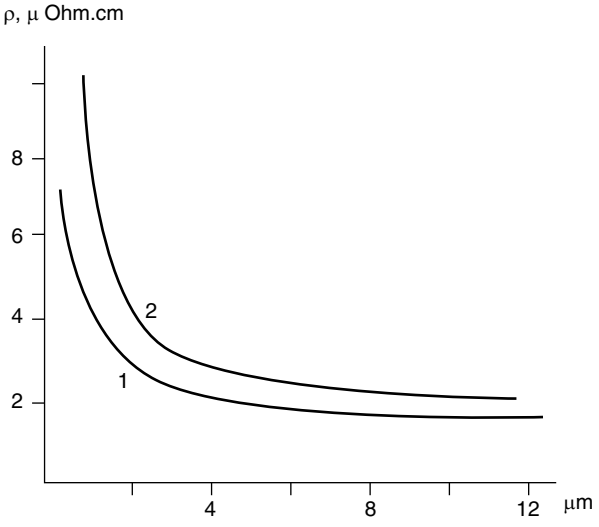

Fig. 15.6 Dependence of the measured resistivity on the thickness of copper deposits *1*—sulfate solution, *2*—pyrophosphate solution

Table 15.1 The resistivity of copper electrodeposits at 25°C

Electrolyte type	pH	Current density, kA/m^2	Resistivity, μΩ cm
Sulfate		0.1–0.5	1.72–1.73
Sulfate with additives		0.1–0.5	1.75–1.92
Pyrophosphate	8.2	0.07–0.1	1.74–1.82
Pyrophosphate	6.0	0.07–0.1	2.16–2.18
Ethylenediamine	6.0	0.2–0.3	1.82–1.96
Ethylenediamine	8–9	0.2–0.3	1.78–1.94
Cyanide		0.1–0.3	1.73–1.74
Cyanide with additives		0.1–0.3	1.80–1.84
Fluorosilicate		0.3–0.5	1.73–1.74
Fluoruborate		0.2–0.5	1.72–1.73

Table 15.2 The resistivity of silver electrodeposits at 25°C

Electrolyte type	pH	Current density, A/m^2	Resistivity, μΩ cm
Cyanide		10–20	1.70–1.72
Ferrocyanide	10.0	20–30	1.72–1.78
Ferrocyanide with thiocyanate	9.4	30–40	1.66–1.69
Pyrophosphate–ammonia	8.1	20–40	1.75–1.78
Trilonic	10.1	40–60	4.18–4.45
Sulfite	8.8	20–30	1.80–1.85
Iodide	7.1	15–20	2.00–2.07
Sulfosalycilate	9.0	80–200	1.90

Very thin deposits show increased resistance due to their porosity: deposits thinner than 10 μm usually contain through pores which can be seen at low magnification in thin deposits detached from the substrate. This porosity depends strongly on the material used as a substrate, its preliminary treatment and on the deposition conditions. Figure 15.6 shows the dependence of the measured resistivity on the thickness of copper deposits, demonstrating that comparisons between different metals should be performed only using films above a certain thickness. At large thickness for example the resistivity values of the same metal deposited from different solutions can be compared. Data on the resistivities of electrodeposited copper, silver and nickel are given in Tables (15.1, 15.2, 15.3 and 15.4).

These data also provide an estimate for the variation in resistivity of other metals electrodeposited under different conditions.

15.4 Thermoelectric Force and Contact Resistance

Measurements of thermoelectric force are convenient in some cases as an additional method to monitor the electrical properties of the deposit. A sample containing impurities or defects in crystal structure exhibits a well defined thermoelectric force E_T

Table 15.3 The resistivity of nickel electrodeposits at 25°C

Electrolyte type	Resistivity, μΩ cm
Sulfate	6.84–7.92
Sulfate with additives	8.20–11.90
Sulfamate	7.88–8.24
Fluoroborate	8.18–8.62
Chloride	8.20–8.45
Acetate	7.30–7.70

Table 15.4 The influence of organic additives on the resistivity of copper electrodeposits at 25°C

Electrolyte type	Additive	Concentration	Current density, A/dm^2	Resistivity, μΩ cm
Sulfate	Acrylamide	0.1 g/l	2–4	1.90–1.93
Sulfate	Benzotriazole	0.1 g/l	2–4	3.15–3.26
Sulfate	Thiourea	0.1 g/l	2–4	1.95–2.00
Sulfate	o-phenantroline	0.001 M	1–2	1.92–1.94
Sulfate	Organic dyes	0.1–1 g/l	2–4	1.82–2.18
Sulfate	LTI (commercial)	1 ml/l	2	2.14
Sulfate	Novostar (commercial)	5 ml/l	2	2.47
Pyrophosphate (pH = 9.0)	Citric acid	20 g/l	1.2	2.40
Pyrophosphate (pH = 9.0)	Trioxyglutaric acid	7 g/l	1.2	9.2
Pyrophosphate (pH = 9.0)	Sodium gluconate	20 g/l	1.2	2.44

when paired with the same metal, but only if the latter is pure and well crystallized. This value E_T is small ($\sim 10^{-6}$ V/K) but it can be easily measured [2].

The corresponding measurement is relatively uncommon, but it has definite advantages among which the independence from sample configuration, porosity, surface roughness etc. At each temperature the electromotive force is determined only by the nature of the two metals and by the temperature difference between the contacts. The measured value is proportional to the resistance contribution from the defects and impurities but it is much more sensitive than a resistivity measurement at ordinary temperatures.

The resistivity, measured at very low temperature (4.2 K, liquid helium temperature) presents a much larger relative contribution from defects and impurities, according to Matthiessen's rule; the value of the ratio $R_T = \rho(293\ K)/\rho(4.2\ K)$ gives the same information as E_T, but the measurement of E_T is much simpler. R_T is inversely proportional to this contribution and therefore $E_T = \text{const}/R_T$; for copper E_T (in microvolts per degree Kelvin) is close to $2/R_T$.

In order to perform thermoelectric force measurements it is advisable to cool one of the contacts (if one of the contacts is heated, defect annealing may occur); additionally, good temperature control of the contacts is needed (Fig. 15.7). Maintaining a temperature difference of about 10 K between the contacts should be sufficient.

The value of E_T is particularly sensitive to bulk impurities; the impurities concentrated at the grain boundaries influence E_T to a much smaller extent. From the results of the measurements it is possible to assess the presence and nature of the

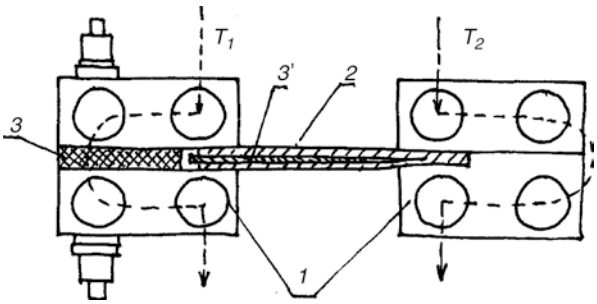

Fig. 15.7 Measurement of the thermoelectric power: *1*—the electric contacts, *2*—the substrate, *3*—the insulator, *3′*—the deposit

impurities or defects, and in the case of diluted alloys it is possible to draw conclusions on the distribution of the alloying component.

The contact resistance R_c is a property difficult to properly define because of its dependence both on the electrical and mechanical characteristics of the sample, as well as on the conditions of the measurements. Nevertheless, its practical importance along with the theoretical simplicity of its measurements has led to an increased interest in contact resistance. The control of R_c is used, for instance, in the study of alloy phase structure and for monitoring phase transitions during aging. R_c is measured as the ratio $\boldsymbol{U}/I$, where $\boldsymbol{U}$ is the potential drop at the contact, and I is the current at which the measurement is made.

The theory of contact resistance is based on the hypothesis that the actual contact between two rough surfaces takes place at separate "contact spots", the number and size of which depend strongly on the roughness characteristics (the average height and the average distance between the protrusions) and on the mechanical load at the contact. When modeling the problem, the contribution of the contacting ridges is taken into account along with the electric resistance caused by the crowding of the current lines near the contact spot **(**Fig. 15.8**)** Obviously, the result depends both on the resistivity of the material and on its mechanical properties, which determine the area of the contact spots.

The mechanical aspect of the theory of contact resistance is based on a development of the Hertz theory of mechanical contact between solid bodies. The relative area of contact between two surfaces can be expressed approximately as

$$S_r = dq/HE \tag{15.4}$$

where d is the average distance between the contacting spots, q is the net value of the pressure on the contact ($q = P/S$, S being the overall area of the contact zone,

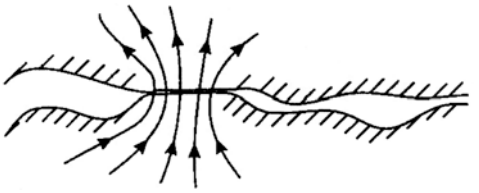

Fig. 15.8 Electric current lines near the contact spot

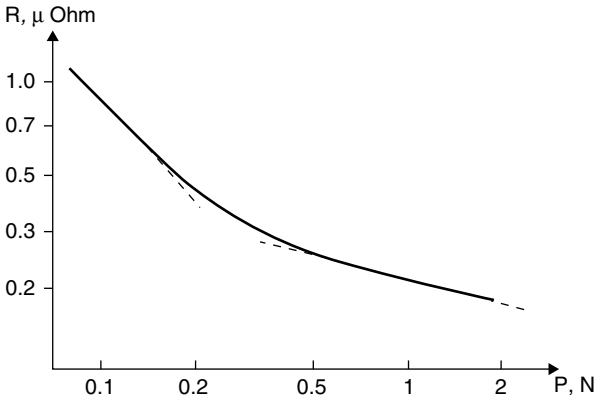

Fig. 15.9 Logarithm of the contact resistance R_c vs the logarithm of the mechanic loading P; the kink marks the transition between elastic and plastic deformation at the contact

not only of the spots), H is the average height of the roughness and E is Young's modulus.

The absolute value of the displacement of the contacting surfaces (towards each other) resulting from the compression of the peaks is

$$\Delta H \approx H(dq/HE)^{1/3}. \tag{15.5}$$

These equations are usually sufficient for finding the dependence of R_c on the mechanical pressure. The value of (dq/HE) is a non-dimensional coefficient, determining the value of R_c of a rough surface.

Contact resistance always decreases when increasing mechanical load. At relatively low contact pressures, corresponding to elastic deformation, R_c is approximately inversely proportional to the load q, whereas at high loading, corresponding to plastic deformation, R_c is proportional to $q^{-1/3}$. This result allows to distinguish the two types of deformation by plotting log R_c vs log q (Fig. 15.9). One further interesting observation consists in the possibility of decreasing R_c by alloying (contrary to ρ, which can only increase); the reason is the variation of the alloy mechanical properties or of some properties of the surface film.

The best experimental method to measure contact resistance uses crossed cylinders (Fig. 15.10); the most common implementation utilizes metallic wires of about 1 mm in diameter. The load varies from 0.01 to 10 N. A smooth loading transient is very important for the quality of the measurement, along with the absence of electrical current during mechanical loading: spark ignition in these conditions would invalidate the successive measurement. After repeated measurements it is necessary to change the point of contact between the samples. The resistance of the samples themselves together with that of the current connecting wires can be taken into account by performing a reference measurement with contacting wires welded together.

The contact resistance is highly sensitive to the formation of corrosion products and especially to the presence of surface films, formed by corrosion, organic or polymeric residues. Very thin tarnishing films formed in an ordinary atmosphere can increase R_c twice or more. At high mechanical pressure the films can be de-

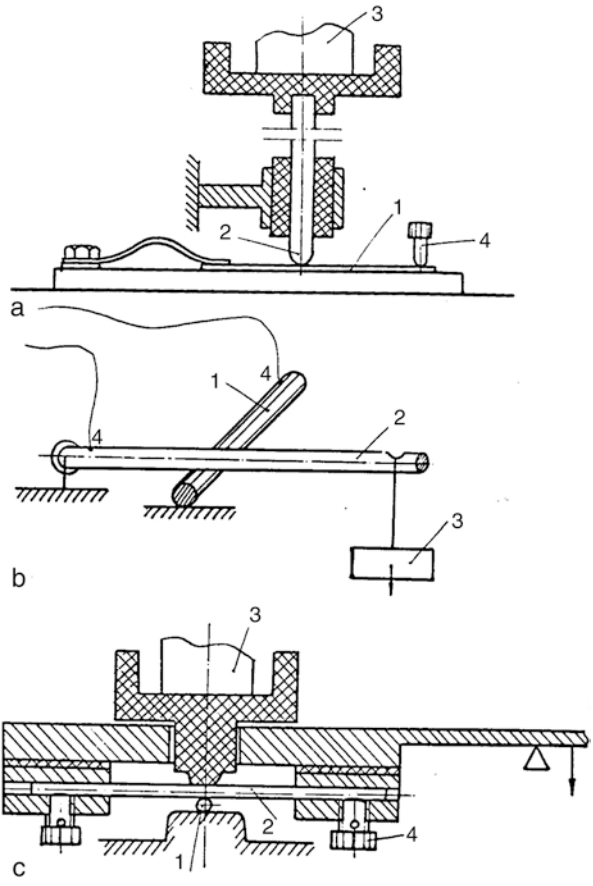

Fig. 15.10 Devices for the measurement of contact resistance: *1*—the sample, *2*—the counter sample, *3*—the load, *4*—the contacts

Table 15.5 Contact resistance (in milliohms) between homologous contacts in a crossed wire configuration (both wire diameters 1 mm, loading per contact 20 g)

Deposit	Au	Ag	Cu	Ni	Ag–Sb	Zn	Pd	Ni–Pd
R_c	1.2–1.6	0.9–2.5	1.1–2.3	3.5–4.0	1.9–2.2	4.0–5.5	5.8–6.5	6.5–7.0

stroyed, and the value of R_c falls. In the case of thin deposits, diffusion of the metal from the substrate can also influence the result of the R_c measurement.

Some data on contact resistance are given in Table 15.5.

15.5 Magnetic Properties

Thin ferromagnetic films produced by electrodeposition are of interest because the magnetic properties of thin films (less than 10 μm) can be widely different from those of bulk materials. In particular, the magnetic properties of a given material

can be tuned in a wide range by changing the deposition conditions. Electrodeposition permits to coat large surfaces and parts of complicated shape and allows facile control of coating thickness.

The most important magnetic properties of a ferromagnetic metal are exhibited in its magnetization curve, which relates the magnetization (i.e. the magnetic moment per unit volume) to the applied magnetic field. These properties are the saturation magnetization (the value of magnetization at high fields), the magnetic permeability (the ratio at which magnetization changes with field), the magnetization at remanence (i.e. in absence of an external field) and the coercive force or coercivity (the magnetic field at which the magnetization is zero). Additional information on these quantities can be found elsewhere [3].

Both hard (i.e. with high coercive force) and soft (low coercive force) magnetic coatings can be obtained by electrodeposition. The latter can be magnetized in relatively low fields (less than 1000 A/m) and are characterized by high permeability, and can therefore be used in transformers, inductors or in electromagnets. These materials are mainly based on nickel–iron alloys and can contain also molybdenum, cobalt and phosphorus. Hard magnetic materials include mainly heterogeneous (two-phase) cobalt alloys containing nickel, tungsten, molybdenum, platinum or phosphorus. The codeposition of phosphorus allows tuning of the magnetic properties in a wide range; above a critical fraction in fact phosphorous may form non-magnetic phosphides that tend to precipitate at grain boundaries and therefore isolate magnetically the crystal grains, inhibiting magnetization switching at low fields. Fe-based hard alloys such as Fe–Pt have been also recently obtained by electrodeposition. Hard magnetic coatings possess a high residual magnetization and need high external magnetic fields (up to 10^5 A/m) for saturation, and can be used accordingly as permanent magnets.

The magnetic properties of these films are determined mainly by their structure and by inclusion of hydrogen or other impurities. The coercive force depends strongly on internal mechanical stress, as this generates inhomogeneous regions where magnetization can be switched only with difficulty. In the case of cobalt deposits there is a wide difference in magnetic properties between the deposits with cubic and hexagonal lattices: cubic Co (which is usually deposited at $pH < 2$) has a low coercive force, whereas hexagonal Co can be highly coercive. The alloy composition, size and shape of the grains are also of importance along with the thickness of the film. In some cases the film texture has an important role in determining the directional dependence of the magnetic properties: in this case the direction of easiest magnetization can be made coincident with that of the external field, facilitating magnetic saturation at low fields. The variation of the magnetic properties under different deposition conditions, or after heat treatment or aging can usually be explained in terms of the corresponding variations in the structure and composition of the deposits.

15.6 Ductility

The most important mechanical characteristics of metals are the tensile strength σ and the relative elongation ε. Other important properties of electrolytic metal deposits are the internal stresses, hardness and adhesion to a substrate. For practical

purposes wear resistance is also important. In some cases one may be interested in measuring also friction coefficients under various conditions, and the elasticity modulus E.

Failure of a metallic sample under mechanical loading is a result of the occurrence of cracks which are formed and propagate under loading. Usually in these conditions a reduction of the cross-section (necking) of the sample takes place in a certain region, leading to an increase of the local stress, causing plastic flow and finally leading to failure.

Measurements of local deformations show that usually the failure of film samples 10–100 μm of thickness occurs when most of the elongation is located near the crack region; necking on such samples is not observed. The length Δl of this elongation zone, where more than half of the total deformation is concentrated, is usually 10–20 h, where h is the thickness of a sample. Ductility is characterized by the overall relative elongation at failure, but this value depends strongly on the thickness of the sample and on the test specifications. Therefore the data available in the literature are frequently non-comparable and should be used only as a guideline. As an example we can specify that a relative elongation of 4–5% is high for samples of about 20 μ in thickness but it is low for 100-micron thick samples.

A logarithmic dependence between sample thickness and its elongation under load is frequently observed. In electrolytic deposits however this dependence can be more complex, reflecting the influence of several factors. First, in thicker deposits the density of mobile dislocations under load can grow and their activation is observed. The surface is a region where dislocation bands are formed, and with thicker films the relative importance of surfaces decreases. Besides, plastic flow depends strongly on the grain size and shape, in particular the grain size along the film thickness. If only several grains are present a relative displacement of these grains may occur during sample deformation. Foils with a columnar structure may have only one grain across the thickness and the above deformation mode would be inactive, resulting in a less ductile material. It is therefore necessary to take into account that the size of grains varies with thickness. Deposition upon foreign substrates results in a fine-grained microstructure in a thin film, while with the deposition proceeding the grains in successive layers become coarser until their size stabilizes, reaching a value characteristic of the given conditions of deposition.

The dependence of ductility on thickness can therefore be to some extent indirect, reflecting the dependence of grain size on thickness. Finally, it should be taken into account that most of the measured deformation is located in a short region near the failure location, and other parts of the tested sample are much less deformed. Therefore the actual result of ductility tests depends on the relative length, width and thickness of the sample. Thus, comparison of test results should be made only for samples of identical length and thickness; in addition, the availability of data within a certain interval of thickness may provide a better picture of the actual ductility.

In order to achieve reproducible results on the ductility of an electroplated material, experience shows that on average the samples should be about 40–80 mm long with a width of 8–12 mm. The measurements should neglect the evaluation of stress concentrators, and the speed of deformation should be sufficiently low (for example

1 mm/min), otherwise the tests will not be quasi-static, and failure will be observed at smaller deformation.

Electroplated films in the as-deposited state usually have rather low ductility, but this can grow sharply after heat treatment. In general, deposits composed of fine grains with stacking faults or twins are most ductile. Ductility is due to the presence of mobile partial dislocations, therefore these should not be blocked by impurities. A decrease in ductility resulting in brittle films can be caused by the formation of dislocation bands, or by the precipitation of impurities at grain boundaries; for example, as a result of pushing off the impurity particles from the growing front of a deposit at low growth rates.

Alongside with deformation tests, ductility can frequently be estimated indirectly and qualitatively, for example, by occurrence of cracks in a deposit in the course of deformation (elongation or bending) of the supported sample.

A further method for increasing ductility besides heat treatment is important in practice; this consists in the introduction in the electroplating solution of some organic additives. For example, the ductility of copper may increase by addition of dimercaptobenzo-thiazole or acrylamide to the electrolyte. The additive acts by changing the growth mechanism and therefore its microstructure.

15.7 Tensile Strength

Deposit strength depends on film thickness, sample geometry and on the type of deformation; however, it is less sensitive to these parameters than the relative elongation. Strength tends to change with respect to the value measured in thick films only in films thinner than 10 μ. The strength of thin layers is usually higher, but the opposite trend may also be observed, particularly in cases when thin coatings have a different microstructure from thick ones. For example, porosity of a thin layer, a possible increase in hydrogen content and the substrate influence on the structure may all play a role in a possible decrease in strength. Practice shows that when studying tensile strength it is sufficient to consider deposits with thickness in the 10–60 μm range.

Strength (the breaking stress σ_B as well as yield point) is determined not only by the material but also by its microstructure, in particular by the density of dislocations N. The general dependence has the form

$$\sigma_B \approx \sigma_B{}^o + kN^{1/2} \tag{15.6}$$

where $k \approx 0.1$ N/m.

The $N^{1/2}$ dependence is related to the fact that the theoretical strain for dislocation motion is proportional to Young's modulus (more correctly—to the modulus of rigidity G) and to the square root of N. Dislocations in metals are immobilized by surfaces and by impurity atoms, therefore thin deposits with a high density of impurities or precipitates can be stronger and less ductile in comparison with thick deposits of high purity.

A high strength can be achieved in deposits with a small grain size. In fine-grained metals (grain size of 0.1 μ or less) the yield point as well as the hardness and resistance to fatigue improve; with regard to the breaking stress, the dependence on grain size D is of the form

$$\sigma_B \approx \sigma_B{}^o + kD^{-1/2} \tag{15.7}$$

(Hall [5], Petch [6]), k being a constant. For yield strength in particular this formula has a rigorous theoretical basis. Neighboring grains hinder sliding processes inside a given grain and therefore limit mobility of its boundaries; therefore in fine grained films mechanical properties strongly depend on grain size. The Hall—Petch law (15.7) is quite general, but when it is applied to hardness and strength it should be considered simply as an empirical relationship. The coefficients in this equation depend on the microstructure of the grain boundaries, their angular disorientation and the density of impurities.

As a result of all the effects discussed above the breaking stress of electrolytic deposits can exceed 2–3 times the usual values characteristic of metallurgical samples, including cold-rolled metals.

As a rule, the strongest deposits are also the least ductile. However, in some cases a positive correlation between strength and plasticity has also been observed. Most likely, deposits with low ductility can suffer brittle fracture due to stress concentration at cracks before their true strength is reached.

Upon heat treatment the deposit strength usually decreases monotonically with a rise in temperature; an increase in both strength and hardness however may sometimes be observed as a result of redistribution of impurities. The relative elongation is almost always enhanced upon heating, and in a case of annealed samples pronounced plasticity (after the yield point is passed) is observed in the stress-strain diagram.

It is of interest to elucidate possible correlations between the deposition potential of a metal and its mechanical strength. A linear correlation between strength and the root square of the overpotential has been discussed [4]. This is probably related to the fact that a fraction of the energy involved in electrochemical film formation goes into the crystal lattice in the form of dislocation energy. The density of dislocations should therefore be proportional to the overpotential, and then the specified dependence is simply a consequence of the Hall–Petch law.

The dependence of strength on the applied current density instead can be more complex. With current density the overpotential and, hence, the dislocation density increase, but as a rule the codeposition of impurities decreases at higher current density. Quite often an observable increase in hardness is related mainly to an enhanced rate of impurity capture by the growing deposit. The effect of impurities is quite often stronger of all other factors; strength however depends not only on impurity concentration, but also on the details of its distribution in a deposit. A uniform distribution of fine inclusions leads to increasing strength, whereas segregation of impurities at grain boundaries reduces it. The role of impurities is well illustrated by the sharp change in the properties of nickel deposits at pH above 5.5, when precipitation of hydroxides at the interface and their incorporation by the

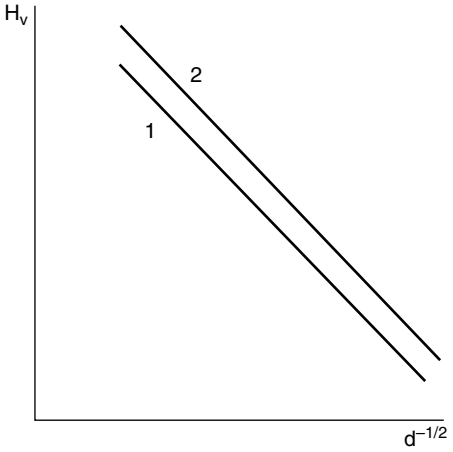

Fig. 15.11 Hall—Petch relationship for Ni deposits: *1* high purity nickel; *2* nickel with impurities

growing deposit becomes possible. The relative role of impurities and of grain size is illustrated by Fig. 15.11, where a Hall—Petch dependence for Ni deposits with a different degree of purity is shown.

A rise in electrolyte temperature leads almost always to more ductile samples with smaller strength—both due to a decrease in overvoltage, and to the higher purity of the deposits thus obtained; by increasing temperature in fact adsorption of impurities and hence their inclusion is reduced.

15.8 Methods of Measurements of Strength and Ductility

In some applications there are stringent requirements imposed on the hardness, strength and ductility of electrochemical metal deposits. The deposit should not crack while in service (either as a result of external loadings or due to its own internal stresses) and should not fail before the substrate material. For this purpose it should simultaneously possess sufficient strength and a certain ability to deform before failure; in other words, it should not be brittle.

The basic characteristics of strength and ductility of a metal are reflected by its stress—elongation diagram, which is constructed by applying a variable force to a properly designed sample and measuring the corresponding elongation. The tangent to the slope of this diagram is equal to the modulus of elasticity of the material, and its characteristic points give limiting values of ductility and strength, as well as absolute and relative elongation (at failure), the main parameters needed to quantify ductility. Other characteristics of a metal, such as its hardness and wear resistance are related to these major properties.

These stress-strain diagrams are usually obtained by using thick cylindrical samples while the electrodeposits are usually thin films or foils; therefore the determination of the mechanical properties of the latter has some specific features.

First of all, as it was noted earlier, the foil samples (separated from the substrate) break in such a way that a significant part of the elongation is located near the failure region. This occurs also in the case of wire deformation; thin foil samples however do not practically exhibit any neck formation. It follows then that about half of the overall deformation is located in a region of length approximately 10–20 times the sample thickness, i.e. for a foil thickness of 50–70 μm that region is less than a millimeter. Practically this means that the absolute elongation of a sample is independent of its length, and, hence, the result of measurement of relative elongation depends on the length of a sample. Therefore, testing of a series of samples should be carried out using an identical geometry and the same device.

Correct preparation of a sample for mechanical tests (separated from the substrate) is essential. It is necessary first of all to provide a low film adhesion to the substrate. For this purpose titanium, glassy carbon, stainless steel or other materials with low interfacial energy should be used as substrates. It is also possible to reduce adhesion to the substrate by various methods, such as graphitizing of the surface, or to selectively dissolve the substrate in a suitable etching solution.

In the case of thin foils, the results of a mechanical test depend on their thickness because the initial structure of the deposit is different from its internal region. For a thickness larger than 8–10 μm the strength should remain constant.

A sample with a suitable shape can be cut or etched off from the foil separated from the substrate. Usually the width of the sample is smoothly increased near the ends to facilitate grip by the clips of the mechanical testing machine; in alternative, larger plates may be joined to the ends of the sample by soldering. One of the difficulties involved in the measurements is the occurrence of stress concentrators due to the cutting. In this case, it is recommended etching the samples away by a template. In addition, the deposit should have a uniform thickness, otherwise failure will occur at the thinnest region, the one corresponding to the lowest current density. The best measure of elongation is the distance between marks drawn on a sample, not scratches. In recent years, deformation sensors have been extensively used to measure deformation at different location of the same sample.

A convenient way to measure sample strength is by using a sample in the form of a ring tape, which can be stretched by two cores inserted into a ring (Fig. 15.12).

During the tests it is necessary to avoid a skew of samples at their grips because this leads to a non-uniformity of the stress and then to distortion of results. Similar distortions are observed also when deformation speed is too large. Optimum speed does not exceed 2 mm/min.

Other methods, unrelated to strain tests, are also available for quality monitoring of the mechanical properties. So, it is possible to bend a sample around of a conic

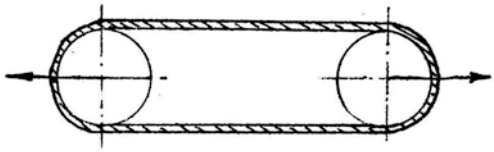

Fig. 15.12 Stretching by the two cores inserted into a ring

Table 15.6 Breaking stress σ_B of the electrodeposited metals, MPa

Deposited metal	Cu	Ag	Au	Ni	Zn	Cd	Cr	Fe	Pb
Strength	150–400	170–200	60–120	300–600	80–110	60–90	130–380	400–900	15–20

pattern, registering the radius of curvature at which the cracks begin to form. In the case of rather brittle deposits it is possible to bend them forming a U-shaped sample together with the substrate directly in a micrometer, pulling together the ends of the sample by turning the screw. Alternative methods may involve indenting of a ball or a punch with a spherical head into the sample. As a rule, this kind of methods give overestimated values of the relative elongation.

Some characteristic data on the tensile strength for various galvanic coatings are presented in Table 15.6.

15.9 Microhardness

Microhardness, as well as ductility, is a material characteristic that cannot be defined rigorously; however, it can be measured simply enough and is important for technical applications; that makes it one of the most important parameters describing the mechanical properties of metal deposits. The literature data on microhardness of some electrodeposited metals are rather numerous, though they are not always comparable, as microhardness is sensitive to purity of the solutions and depends on the thickness and purity of the deposits as well as on other factors. The hardness is a complex function of the deposit composition, microstructure and geometry and varies in a wide range. For instance, the microhardness of silver electrodeposits can vary from 400 to 1900 MPa. Unfortunately, the results of various authors are often widely scattered.

Hardness measurements are performed with microindenters using low loads (1 N or less), so the measured value is called microhardness.

The dependences of microhardness on CD, temperature, overpotential etc. can be explained first of all in terms of the variation of sample purity and grain size, similar to the measurement of other mechanical properties.

The deposits obtained from solutions of high purity are usually less hard than those obtained from common electrolytes, but they also have appreciably higher hardness relative to metals produced by metallurgical methods. An exception is observed only for low-melting metals, which recrystallize at room temperature and consequently lose the hardness observed in the as-deposited state.

In general, deposits obtained at higher cathodic potentials exhibit higher hardness. In part this is explained by the reduction of grain size; however it is difficult to directly relate hardness and grain size. The reason is that both smaller grains and increase in hardness can be caused by a common reason, i.e. the inclusion of foreign particles. In most cases, consideration of the various aspects of the growth process

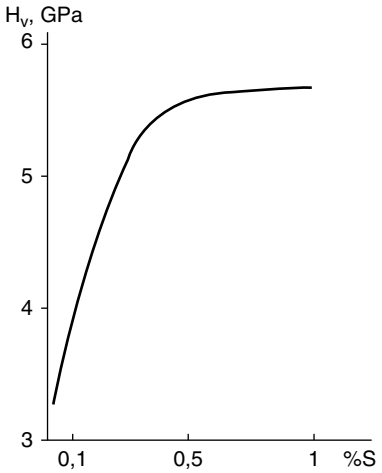

Fig. 15.13 Dependence of microhardness on Ni deposits on sulfur concentration in the deposits

allows a thorough explanation of the experimental data. For example, the influence of impurities on hardness is complex: impurities incorporated in deposits in fact can cause distortions of the crystal lattice, raise density of dislocations and reduce their mobility.

Most often, hardness is higher than usual in presence of sulfur (which comes from additive molecules and in the case of nickel deposits also from sulfamate), or carbon (e.g. from citrate or other organics and from carbon dioxide). Other impurities are phosphorus (from the anodes, from pyrophosphate or other phosphorous-containing species) and hydrogen. The fraction of these impurities can be up to and above 1%. Some Ni deposits contain up to 0.1% of hydroxide codeposited at a high interfacial pH value; the microhardness of Ni deposits obtained at pH higher than 5.5 is especially high. Figure 15.13 shows the dependence of hardness H on sulfur concentration in the deposits; one can see that at low concentrations H raises sharply, but when the limit of solubility is reached, hardness remains constant due to NiS precipitation. A similar behavior is observed in hard gold deposits due to cobalt codeposition.

It has been established by cross-sectional hardness measurements that the hardness depends on the distance from the substrate. This is mainly due to the dependence of grain size on this distance.

Microhardness is usually measured with specially adapted optical devices combining the possibility to engrave a diamond pyramid at fixed loading with a subsequent optical measurement of a diagonal of this footprint. In a rather wide range the area of a print is proportional to loading and inversely proportional to hardness. Therefore hardness is determined as the ratio of the applied load to the specified area of a lateral surface of a pyramid (which is proportional to the square of the measured diagonal). In the case of the standard 136° pyramid the formula defining the microhardness is

$$\mathrm{H} = 1.854\ P/d^2 \tag{15.8}$$

Table 15.7 Microhardness H_v of galvanic coatings, MPa

Metal (alloy)	Microhardness H_v	H_v after annealing
Ag	800 ± 200	270 ± 30
Ag (bright)	2300 ± 400	300 ± 50
Ag–Sb	1600 ± 200	
Au	800 ± 200	220 ± 40
Au–Sb	2500 ± 500	
Au–Co	2900 ± 500	
Cd	400 ± 100	250 ± 50
Co	4000 ± 700	
Cr (hard)	9000 ± 1000	3000 ± 400
Cr (milky)	5000 ± 800	
Cu	800 ± 300	530 ± 100
Cu–Sn	4500 ± 800	
Fe (hot soln.)	1800 ± 200	1600 ± 200
Fe (cold soln.)	5400 ± 800	1800 ± 200
Fe–W	11000 ± 1000	
Ir	8800 ± 800	
Ni (mat)	2500 ± 500	1700 ± 200
Ni (bright)	4200 ± 800	1900 ± 200
Ni (el.-less)	5600 ± 1000	7800 ± 1000
Ni–Sn	6500 ± 500	
Ni–Pd	3000 ± 500	
Os	8600 ± 800	
Pb	100 ± 20	
Pb–Sn	140 ± 20	
Pd	2600 ± 500	480 ± 40
Pt	3100 ± 500	450 ± 6t0
Rh	7800 ± 1200	1200 ± 100
Ru	9200 ± 1000	2600 ± 300
Sn	160 ± 30	140 ± 20
Zn	500 ± 100	420 ± 50
Zn–Co	3200 ± 300	
Zn–Ni	1000 ± 200	

P is the load in Newtons, *d* is the diagonal length of the imprinted square in microns. The conditions of the measurements are the following: the roughness of the surface must be lower than 0.5 μm, otherwise the prints may not be sufficiently sharp and clear; the usual loads are 0.1–1.0 N; the thickness of the deposit must not be less than a half of a measured diagonal, otherwise the hardness of the substrate influences the results.

Typical values of H, characteristic for electrochemically deposited metals, are shown in Table 15.7. The values in this Table are averaged, and actual values may differ by as much as 20%; during aging the hardness can fall as result of lattice rearrangements and/or redistribution of impurities. The microhardness of copper deposits falls by about 20–40% in about 6 months, depending on the additive used. These relaxation processes are accelerated at higher temperature, especially near

Table 15.8 The recrystallization temperatures of galvanic coatings in degrees Celsius: t_b—temperature of the beginning, t_e—temperature of the end of recrystallization

Metal	Ag	Cr	Cu	Ni	Zn	Co	Fe	Pd	Rh
t_b	100	600	200	450	120	500	500	500	700
t_e	300	800	400	600	130	650	700	700	900

Table 15.9 The microhardness of copper deposits from simple sulfate solutions

Deposition Temperature	Current density			
	1	2	4	6
20	920	980	1060	1270
40	810	850	920	1020
60	750	790	880	950
80	700	740	810	860

the recrystallisation temperature of the metal (Table 15.8). In presence of impurities this temperature shifts towards higher values.

The values of microhardness correlate not only with strength of the metal but also with the internal stress, wear resistance and brittleness. For example, Cr–V deposits have the highest H (about 13,000 MPa) only when the internal stresses are higher than 1000 MPa.

The overall character of H dependence on the deposition conditions is illustrated by Table 15.9, from which it is seen that as a rule the hardness is lower at higher deposition temperature and at lower current density.

A correlation can be established between microhardness H and strength of a given sample; this dependence is often expressed as $\sigma \approx 0.3$ H, though in real cases the relationship can differ from this average formula. A more general formula has the form

$$\sigma \approx k_1 H + k_2, \tag{15.9}$$

where k_1 and k_2 are empirical coefficients appropriate only within a given series of measurements.

Microindentation allows also an estimate of the resistance to fracture development. At loads more than 5 N some cracks near the pyramid are formed; they then propagate from the footprint along its diagonals.

15.10 Internal Stresses (IS)

One of the most important characteristics of electrodeposits is their internal stress. After deposition the metal of the deposit is in a compressive or in a tensile state, as if it was first compressed or extended, respectively, and then glued in this state to the substrate (Fig. 15.14). The extended deposit compresses the substrate, and, on the contrary, the compressed deposit stretches it. The tensile stresses (usually con-

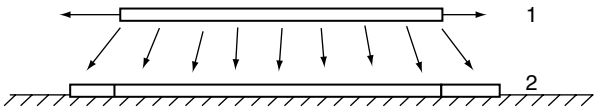

Fig. 15.14 Schematics of a deposit under a tensile stress state: *1*—the unstressed deposit, *2*—the stressed deposit at the substrate

sidered positive) are typical of nickel, iron, cobalt, chromium, rhodium, palladium, manganese, gold alloys. High tensile stresses in thick deposits can result in cracking of the latter. Compressive (negative) stresses are more characteristic of low-melting metals such as zinc, lead, tin, bismuth, cadmium and indium. These deposit do not crack but cleavage can occur with peeling or flaking from the substrate.

The internal stresses depend strongly on the electrolysis conditions. As a rule, IS increase at lower current density and temperature or at higher pH. Under non-stationary electrodeposition conditions IS are usually lower. Impurities can change IS in both directions.

Relatively thin deposits have higher stresses than thicker ones. During film growth however the stresses in the region closer to the substrate vary as a result of two effects. The first one is the influence of the material deposited successively, the second is the post-deposition stress relaxation. The stresses in copper, silver and some other metals decline in a time frame of several days or weeks after the end of electrolysis.

There are several hypotheses concerning the origin of IS, related to various mechanisms for IS generation. Compressive stresses are initially generated during the growth of isolated nuclei, while tensile stresses are generated later by the coalescence of these initially separated nuclei. Studies of crystallization both from the vapor and from electrolytic solutions have shown that tensile stresses arise when several islands join together; coalescence occurs by islands snapping together when there is a small gap between them, and this leads to tensile stresses, even if the separate islands initially had a compressive stress.

Invoking these stress-generation mechanisms for electrodeposition allows the interpretation of a number of experimental data. For example, the tendency of IS to increase at high current density can be caused by an increase in the number of nuclei and increased defects at contact regions. An increase in temperature leads to the acceleration of diffusion processes, which contributes to close such gaps, etc. This mechanism, however, operates only in rather thin layers. In thicker layers the tensile stresses may increase due to the continued formation and coalescence of new islands; in low melting point metals however compressive stresses may be generated, seemingly due to injection of diffusing adatoms within the grain boundaries.

The internal stresses also depend on the energy stored in the crystal lattice. This energy is caused by the overpotential applied during metal deposition, and may be stored in the form of elastic deformations of the crystal lattice. Actually, metals obtained at high overpotential are usually more stressed.

Codeposited impurities can induce stresses of either sign. On the other hand, the inclusion of foreign species by itself does not cause any macroscopic stresses. Only post-electrolysis changes in the state or distribution of such foreign species may lead to stress evolution. Even in absence of special additives the stresses can arise as a result of inclusion of hydroxides during their subsequent decomposition or dehydration. A change in volume of adsorbed molecules after their incorporation can also contribute to the internal stresses.

Hydrogen occupies a special place among the substances that may be incorporated in a deposit. Incorporated hydrogen can partly leave the deposit by diffusion resulting in a reduction of its overall volume and development of tensile stress. If hydrogen however accumulates in the voids inside a deposit in the gaseous form a compressive stress is observed; extraction of this hydrogen results in tensile stresses. In addition to the direct action of included hydrogen, its evolution in parallel with metal deposition leads to alkalinization of the near-electrode layer, favoring the inclusion of hydroxides into the deposit.

Hydroxide inclusions can in some cases decrease the stress; this happens when their influence is opposite to that of other factors. A well-known example of this effect is the decrease of tensile stresses in nickel deposits in presence of saccharine, which can be so high that the overall stress changes sign. By raising its concentration in the electrolyte the stresses diminish, and at about 1 g/l they cross zero. Compressive stresses often increase in presence of additives.

The role of point defects is similar to that of inclusions. Vacancies or microscopic voids lead to tensile stress, whereas interstitial atoms cause compressive ones. The mechanisms of the corresponding processes have been studied rather extensively.

Finally, stresses may arise due to a variation in the distribution of dislocations with thickness. In very thin layers misfit dislocations arise at the substrate interface due to differences between the two crystal lattices. Though most of the experiments in this area concern deposition from the gaseous phase, such mechanism are assumed to be valid also in electrocrystallization. This concerns only epitaxial crystallization, i.e. the case when the structure and lattice of a deposit continues that of a substrate. If on the other hand three-dimensional nucleation leads to the formation of a different deposit structure the stress in thin layers is considerably lower. In this case the stresses arise, as stated earlier, at the moment of joining of the islands, during the first stage of crystallization.

Table 15.10 presents data on IS in several metal deposits. The data are tentative because of the very strong influence of the deposition conditions. As a rule, the stresses in Zn, Cu, Sn, Pb, Ag, brass and bronze do not exceed 50 MPa; the stresses in Ni, Fe, Au and their alloys can be up to 300 MPa. Most stressed are Co, Pd, Rh and especially chromium.

Table 15.10 Characteristic values of internal stresses in galvanic coatings obtained from electrolytes without additives, at room temperature, thickness 10 μm. The sign "minus" corresponds to compressive stresses

Cu	Ag	Au	Ni	Zn	Cd	Bi	Cr	Fe	Sn	Pb	Co	Pd	Rh	Sb
20	−60	160	270	−20	−5	−20	800	240	−15	−5	400	500	700	−10

15.11 Methods of IS Measurement

The simplest and most common to measure IS in-situ, during growth is the so-called method of the bending cathode. The metal of interest is deposited on one side of a flexible narrow and thin plate, the opposite side being insulated by a varnish, and the curvature of the sample is measured during deposition. The easiest way is to monitor such curvature is to register the displacement of the free end of a cantilever sample (Fig. 15.15), for example by bouncing a laser from the bottom region of the sample. In the presence of compressive stress this end is displaced away from the anode, in the opposite case it shifts towards the anode. The relationship between the force causing the displacement of the cantilever and its bending is provided by the Stoney's equation [1].

The solution of the relative mechanical problem shows that when the Poisson coefficients of the materials of the deposit and the substrate are the same (this requirement is almost always satisfied with sufficient accuracy) the stress σ in thin deposits is expressed by the equation

$$\sigma = \mathrm{E_s}\, df/dh\ \mathrm{d}^2(1 + 4\gamma\theta - 2\theta)/[3l^2(1-\mu)], \qquad (15.10)$$

where f is the shift of the free end, $\gamma = \mathrm{E_d}/\mathrm{E_s}$ is the ratio of the Young's modulus of the deposit to that of the substrate, $\theta = \mathrm{h/d}$ is the ratio of the deposit thickness to that of he substrate, l the length of the sample, μ is Poisson's coefficient ($\mu \approx 0.3$).

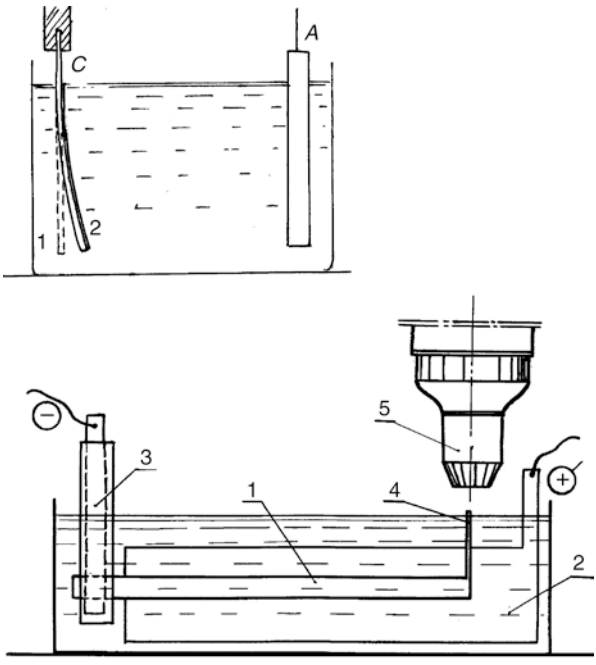

Fig. 15.15 Measurement of the internal stress by control of the displacement of the free end (*4*) of a bending cathode (*1*). *2* the solution, *3* the, *5* the microscope. *A*—anode, *C*—cathode

A different method to monitor stresses involves the automatic measurement of the elongation or compression of the strip cathode by sensing the inductive or capacitive components of the electrical response of the sensor gauge. In this case the deposit is applied to both sides of a thin and long strip, the length of which varies due to internal stresses in the deposit. The variation of the sample length depends on the stresses:

$$\sigma = dl/ldh[0.5\mathrm{E_s}\mathrm{d}/(1-\mu_\mathrm{s}) + \mathrm{E_d}h/(1-\mu_\mathrm{d})]. \tag{15.11}$$

Here it is taken into account that metal is deposited onto both sides of the substrate. The value of σ is the stress in a layer corresponding to the thickness h.

Instead of a plate sometimes a wire is used. In this case however the wire should not be too thin, and deposition should be performed under potentiostatic control or at a constant controllable increase of current, because the surface area increases during deposition.

In addition, the method using a spiral contractometer is in use; this is a variation of the bending cathode method, but instead of a strip a long spiral strip is used, which is more sensitive to the stress.

As a result of such measurements the dependence of stress on the thickness of the deposit is obtained. The calculated stresses are, first, averaged over the entire area of the deposit, and, second, they correspond to the instantaneous deposition of this layer. Upon deposition of new material the stress in the layers deposited earlier varies corresponding to the requirement of force balance for the entire sample, just as in an initially unstressed substrate a compressive stress develops when depositing a metal having tensile stress. In this sense the underlying layers plays the role of the substrate for the later ones. Therefore it is always important to specify what stress is meant in each particular case: initial local, initial average (for the overall thickness), residual local (that is post-electrolysis) or residual average. Finally, quite often some post-electrolysis stress relaxation occurs. It is necessary to note that until recently in most publications on this topic such distinction has not been explicitly discussed.

Besides the mechanical methods, a convenient X-ray method may also measure internal stresses; this is however much less sensitive and demands a rather complicated equipment. When performing X-ray based measurements of stress it is necessary to distinguish between macroscopic stresses (our focus here) and microstresses (more exactly, microdistortions). Macrostresses can be determined from the shift of the maxima at different angles between the sample and the beam; the corresponding lattice parameters are different (this method is known as $\sin^2\psi$-method).

Microstresses instead can be derived from X-ray data by the analysis of the peaks shape. Microdistortions are directly connected with the dislocation structure of the deposits. They have no sign (since both compressed and elongated microregions are present near the dislocations) and usually are of the order of 10^{-3}.

15.12 Adhesion of the Deposit to a Substrate

Adhesion of a deposit to the substrate is one of its basic characteristics. Depending on the application, in electrodeposition either very strong or very weak adhesion may be required. Weak adhesion is necessary when the coating should be separated from the substrate and be used independently (for example, in electroforming); strong adhesion is needed in all other cases. Strong adhesion can be achieved by favoring a direct atomic interaction between the deposit and the substrate (for example, in epitaxial growth when the structure of a deposit reproduces that of the substrate), or may result from the mutual diffusion of these materials, resulting in the formation of an intermediate layer. Sometimes, such intermediate layer may be created on purpose by depositing a third material. Finally, adhesion can be strong simply as a result of mechanical mutual interlocking due to the roughness of the deposit and substrate surfaces.

The above implies that good adhesion depends on:

1. Preliminary processing of the substrate surface, including for example cleaning, polishing, etching and exposure of the structure at the atomic level,
2. Conditions of the formation of the first layers of a deposit, whether they promote nucleation, if any displacement process occurs, etc.,
3. Processing the system substrate—deposit after deposition, for example, by annealing at a sufficient temperature to provide mutual diffusion of the elements.

For each particular pair substrate—deposit the optimum conditions to achieve good adhesion may vary and depend on both the chemical and physical properties of the metals or alloys involved. Often the best adhesion is achieved by carrying out procedures developed in published research work or as described either in the standards, specifications, or in other literature.

Issues of adhesion concern also any deposition method of metallic layers on nonmetallic substrates, including electroless deposition, vacuum condensation, etc.

In the next sections we will discuss the most common methods to achieve strong adhesion along with the methods of adhesion testing.

15.13 Methods to Provide Strong Adhesion

Among the metals and alloys used as substrates for electrodeposition only few of them easily allow good adhesion: copper, brass and low carbon steel. It is on the other hand challenging to deposit on light metals such as aluminum, magnesium and berillium, as well as on nickel or stainless steels. It is especially difficult to achieve good adhesion onto tungsten, molybdenum, titanium, tantalum, niobium; these metals are convenient to use, on the contrary, as substrates that allow easy separation of the deposits from them. Precious metals are applied as substrates only for specific scientific research. Particular problems may arise when depositing on

non-conducting substrates such as glass, ceramics and plastics: in all these cases the preliminary formation of adherent conducting layers is necessary.

Low adhesion is observed first of all at surfaces contaminated with organic, fatty compounds. It follows that degreasing of a surface must be the first stage of any technological process in electrodeposition. The second reason for low adhesion is the formation of thin oxide films (of nanometer thickness), which spontaneously form in very short times at most pure metal surfaces exposed to air. Hence, an important stage of substrate preparation is the removal of these films, for example, by pickling or etching in acidic solutions; it should be noticed that etching differs from pickling, since the former refers to the process of removing some metal together with the oxide. As a result of such activation not only an oxide-free surface is obtained, but also its roughness and therefore the area of contact of a deposit with the substrate increases. The same effect is sometimes achieved by simply using mechanical grinding; for example, by sandblasting. Some methods combining degreasing and etching, including electrochemical ones, have been developed as well.

When depositing more noble metals on electronegative metals such as aluminum, magnesium, berillium or their alloys, the substrate surface is covered at the initial growth stage by a thin film of these metals resulting from contact displacement, often leading to weak adhesion of the coating. For such systems the so-called zincate method has been developed, which consists in the preliminary formation of a thin and adherent zinc layer by immersion into an alkaline zincate solution. The stannate treatment is similar. Alkaline species provide dissolution of the superficial oxide and allow good adhesion of the displaced metallic layer. Directly after this step, a very thin nickel layer, grown for example from a Wood's solution, consisting in diluted nickel chloride and hydrochloric acid or a copper layer from a cyanide solution is often deposited; such procedure promotes the formation of a high density of fine grains in the subsequent deposit, which improves its adhesion.

Immersion of the cathode in the electrolyte when the current is already on, or while an initial current pulse is applied, is sometimes sufficient to achieve good adhesion: this method in fact suppresses the process of contact exchange by shifting the electrode potential in the negative direction.

In the case of aluminum or its alloys a preliminary anodization, consisting in the formation of an oxide film by applying a positive potential to the sample immersed in a solution of a phosphoric acid is performed. In such a way, a porous film adherent to the substrate and having rather high adhesion to the depositing metal is formed. An additional method consists in the introduction in the electrodeposition solution of special activators (for example fluorides) and/or of substances suppressing the contact displacement at the initial stage of deposition.

The above mentioned diluted Wood's solution is widely used for deposition on corrosion resistant steel, especially in combination with a preliminary treatment in a solution of sulfuric or hydrochloric acid.

An additional method of improving adhesion is heat treatment of a coated article; the optimum temperature for such process depends on the particular substrate–coating combination; the duration of the process is usually 1–2 h. Though the diffusion

processes proceed at a significant rate only at 700–800°C, nevertheless in many cases for the given purpose it is sufficient to heat in vacuum at 150–200°C.

Very good adhesion is obtained in epitaxial deposition, that is when the deposit structure reproduces that of the substrate at the atomic scale. This can be achieved only if the difference between the lattice parameters of the two metals does not exceed 15% and also only if preliminary pickling is performed. Surface alloying between the substrate and deposit can in some cases improve the adhesion.

Methods of preparation for nonmetallic surfaces have been developed as well. In these cases the choice of a suitable method depends mainly on the nature of the nonmetallic material of choice. It is obvious that preparation of a surface of silicon or germanium differs essentially from that of glass, ceramics or plastic. The general rule in this case is the need to increase the area of the contact surface between deposit and substrate, i.e. the roughness factor; additionally, the formation of a conductive interlayer is necessary.

15.14 Methods of Adhesion Measurement

Various qualitative and quantitative methods to study adhesion have been developed. Qualitative methods allow only to distinguish between strong and weak adhesion, while semi-quantitative methods may provide, for example, a ranking on a 3 or 4-mark scale. With the help of quantitative methods the adhesion is precisely measured in definite units, for example, using the SI system.

Let's first consider the relatively simple qualitative methods.

The simplest methods are hammering, squeezing or bending of the sample; they need no comments. The next are grinding, polishing or scratching/brushing. This testing method is used for deposits no more than 30 μ thick and is carried out for short times (15 s), by vigorously polishing a surface on a polishing rotating table with application of a polishing paste, or by scratch-brushing it with wire brushes. The absence of swellings, local peeling or flakes indicates good adhesion. Sometimes for this purpose it is sufficient to rub a coated surface with a cylindrical metal core. The most suitable method is chosen by taking into account the configuration of the article and its operational conditions. It is necessary to consider however, that in most cases the articles are used in conditions that are considerably more forgiving than during testing; therefore, the peeling at a break, for example is not necessarily a negative indicator.

For thinner coatings (up to 10 μ) the method of drawing a grid of perpendicular scratches using a sharp tool so that the coating has been cut through can be used. Afterwards, the absence of peeling in the rectangles just mentioned is checked. Coatings on a wire are checked by controlling whether any peeling is present after the wire has been wound on a core (up to 10 turns). The diameter of the core must be 3 times more than that of the wire. Suitable adhesion tests for coatings on springs consist in etching the peeling formed after stretching a spring. The cracking of the coatings when winding or stretching is usually permissible. These methods, as well as the grid method discussed above, can also be used as semi-quantitative ones.

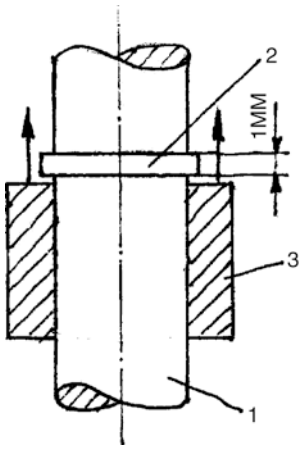

Fig. 15.16 Measurement of adhesion using a ring-shaped film; *1*—the rod, *2*—the deposit, *3*—the cylinder

Similar information on adhesion is obtained by methods requiring a heat treatment. The coated articles are heated up 150 or 200°C (in the case of steel articles the temperature can be raised up to 300°) for one hour, then they are cooled in water or in air and the presence of swellings or bubbles is checked.

We now discuss the quantitative methods.

The methods of detaching a deposit from the substrate are numerous. For this purpose many devices exist, some of which are represented in Figs. 15.16–15.19; the corresponding procedures are clear from each figure. In most devices the force F necessary for detaching a certain area S of the deposit from the substrate in the perpendicular direction is measured. In some cases (Fig. 15.16) the adhesion strength is measured by longitudinal shift of a ring-shaped deposit along the surface of the cylinder. As this force appears to be proportional to the specified area, the adhesion is defined as the ratio P = F/S. In this example adhesion has the dimensionality of the usual strength of a material (N/m^2, i.e. Pa). If the P value becomes larger than the tensile strength of both materials—substrate and deposit—failure takes place not at the interfaces, but at the region with lowest strength; this can be determined visually. In this case the method gives the strength of the metal that breaks; with regard to adhesion one can only say that it exceeds this limit, i.e. is very high.

In another group of methods, adhesion is measured by cleavage of a deposit from the substrate. The force at which the coating comes off a substrate should now be normalized with respect to the cleavage line (Fig. 15.17). In this case the adhesion is quantitatively determined as the force per unit length of such line, or as energy per unit area (i.e. as the work spent in the formation of a unit area per unit surface of separation), and is measured in N/m or J/m^2.

The methods using conical (sometimes cylindrical) cores are rather convenient. In these cases the coating is deposited at a surface with through holes, into which a pin is inserted, the end of which is level with the substrate surface (Fig. 15.18). After deposition the pins are torn off from the coating or, on the contrary, are pressed through the substrate causing the peeling of the deposit. It is assumed that the peel-

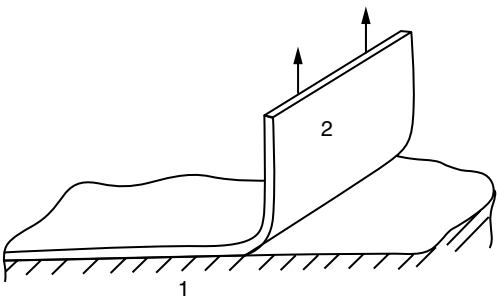

Fig. 15.17 Adhesion measurement by cleavage; *1*—the substrate, *2*—the deposit

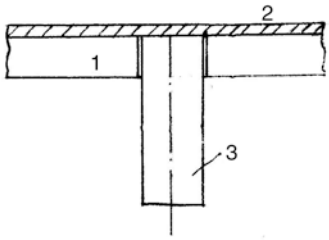

Fig. 15.18 Adhesion measurement using pins; *1*—the substrate, *2*—the deposit, *3*—the pin

ing or cleavage methods give in most cases more accurate and realistic estimates of the adhesion strength than methods of tearing away the deposit.

The process of film cleavage, even when it is measured per unit area, actually occurs at a definite line: the growing bubbles for example arise between the cleaved area of a deposit and the substrate, and further separation proceeds along the edges of these bubbles. The maximal force registered during cleavage is simply proportional to the maximum length of all the existing edges; this length initially grows, but at some stage starts to decrease, reaching zero at the moment of full separation. As the actual length of this line may vary, the results obtained by the two methods are not always comparable.

When using the peeling method the strength of the deposit should be sufficiently high for it not to be torn instead of being peeled. Therefore if the deposit is thin enough, it needs to be thickened up to the necessary thickness; in cases of strong adhesion this requires no less than 100 μm.

If a method involving pins is used, it is necessary to determine first their diameter so that no cutting of the deposit may occur. As a rule, their diameter is close to 2 mm.

The disadvantage of the peeling method is that part of energy is spent for plastic deformation of the separated coating and consequently the result of these measurements depends on thickness and properties of a deposit. Avoiding this error is possible by applying the cylindrical core technique (Fig. 15.19). Then it is possible to preliminary measure the work involved in this deformation by measuring a sample with zero adhesion, and successively subtracting this work from the actual results.

It is important to note that the actual work of adhesion considerably exceeds the work for the formation of two surfaces formed during cleavage, that is σS, where σ is the specific surface energy. This is connected with the fact that upon destruction

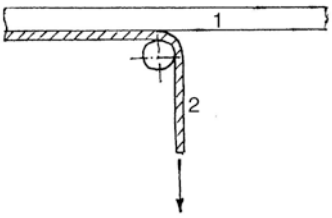

Fig. 15.19 Adhesion measurement using a cylindrical core; *1*—the substrate, *2*—the deposit

of an adhesive bond rather thick layers of materials of the substrate and the coating are being deformed, reaching about tens of atomic layers or more.

15.15 Porosity

Film porosity strongly influences several functional properties of galvanic coatings, especially the corrosion resistance; therefore it is among the most important properties that need to be closely controlled.

Below a certain thickness a deposit does not form a continuous layer due to the presence of numerous small pores. These are generated during the growth process, whereby in the initial stage separate nuclei are formed, which grow into separate islands and only successively coalesce into continuous coating. Pores also result from the attachment of hydrogen bubbles to the surface. In this case the pores form microscopic channels running through the deposit down to the base metal, affecting the corrosion resistance properties of the coating. This problem concerns first of all materials that can be electrodeposited only with simultaneous hydrogen evolution, such as nickel, cobalt or iron, but not only them.

The average thickness at which the deposit becomes continuous depends on the initial density of the nuclei, on the morphological growth features, on the process of secondary nucleation (i.e. the formation of new nuclei upon those formed earlier), and also on hydrogen evolution. In other words, porosity is closely related to the deposition conditions, especially at the initial stage, similarly to what happens with adhesion.

Sometimes non-porous deposit can be obtained at a thickness of 1 μm, but in the opposite limit even 20 μm thickness may be insufficient to eliminate pores. A typical thickness to obtain a coating with limited porosity is about 10 μm.

There are several methods to measure the porosity of corrosion resistant coatings deposited on corrodible substrates. The most popular ones are the following: (1) immersion in a liquid corrosive medium; (2) immersion in a corrosive vapor; (3) place the sample in contact with a filter paper soaked with an electrolyte corrosive solution, perhaps while simultaneously applying an electric current; (4) finally, the corrosive medium may be in paste form.

All these are direct methods, which are reduced to the immediate counting of the pores per unit area. In addition, some indirect methods are available, based for exam-

ple on the quantity of substrate metal transferred into the corrosive medium during a definite period, or on the current density related to the substrate dissolution in an acidic electrolyte at a definite potential. Let us consider said methods more thoroughly.

Immersion of a sample in a liquid or vapor corrosive medium is mostly a qualitative method; the results depend on the medium composition. The corrosive medium interacts with the substrate metal, and the number of pores is registered by visual inspection at low optical magnification. In the case of gaseous atmosphere it is possible to model a typical industrial environment by using sulfuric and nitric acids and also hydrogen halides and hydrogen sulfide. In liquid solutions the same compounds are used along with sodium chloride.

The reproducibility of the results from the above tests is relatively low; groups of closely located pores can be seen as one spot, whereas some small pores may not be seen. In order to overcome this problem, coated steel samples can be immersed in electrolytes containing hexacyanoferrate and connected as the anode. The hexacyanoferrate can determine the concentration of ferrous ions in solution, enabling a quantitative determination of the corrosion rate. In addition, the pores in this case are exhibited as colored spots.

The method of contacting with filter paper results in the formation of colored spots resulting from the reaction of the base metal with substances in the electrolyte. The impregnated filter paper is laid on the deposit surface for a half hour and then the flushed and dried paper is examined under a microscope to count the number of colored points per unit area.

The electrographic method is a development of the previous one; an aluminum plate is laid over the paper and is polarized as a cathode, while the sample is the anode; the elements of this cell are pressed together and a current of 0.01 A/cm^2 is passed for 1 min. In both methods the corrosive substance is NaCl and the indicator is $K_3Fe(CN)_6$. Various solutions compositions and the corresponding color of the porosity are given in Table 15.11.

The pastes in which the corrosive agents along with indicators are added are based on titanium oxide (15 g for 10 ml of the solution). Typical compositions of the pastes are presented in Table 15.12.

Table 15.11 Typical solutions for porosity tests

Deposit	Substrate	Solution, g/l	Duration, min.	Spots color
Ni	Steel	$K_3Fe(CN)_6$ 10, NaCl 20	5	Blue
Ni	Cu, Cu alloys	The same	10	Red to brown
Cu–Ni	Cu, Ni, steel	The same	10	Red-brown: pores to Cu Blue: pores to steel. Yellow: pores to Ni
Cr, Ni–Cr, Cu–Ni–Cr	Steel, Cu and alloys, Ni	$K_3Fe(CN)_6$ 10, NaCl 60, NH_4Cl 30	10	The same
Sn	Steel	$K_3Fe(CN)_6$ 10, NaCl 5	60	Blue
Cu	Steel	$K_3Fe(CN)_6$ 10, NaCl 5	20	Blue

Table 15.12 Typical solutions for paste porosity tests

Substrate	Solution	Spots color
Steel (all deposits except Zn and Cd)	1 g of o-phenantroline in 100 ml of 0,1 m HCl	Red
Aluminum and Its alloys	Aluminon 2% soln (2 parts), H_2O_2 20% soln (1 part)	Pink
Zn and its alloys	0.5 g of diphenylthiocarbazide in 100 ml of ethanol (1 part), 0,5 m NaOH (2 parts)	Pink-lilac

All the methods presented above provide only for a relative determination of porosity; they are convenient for the comparison of different samples and for selection of the best one.

In scientific research work, electrochemical methods are also applied for determination of the relative area of the substrate metal exposed to the electrolyte. This fraction is equal to the ratio of the dissolution currents of the substrate pre- and post-deposition. As an alternative, any electrochemical process that can occur at the substrate but not at the deposit may be used.

15.16 Corrosion Resistance

Both full-scale and accelerated corrosion tests are performed usually not on the deposit itself but on the system substrate—deposit. The most used is an atmosphere of salt spray or fog, prepared by using 3 or 5% (sometimes up to 20%) salt solution at 25–35°C; acetic acid can be also added to the solution up to pH of 3.2 ± 0.1. This atmosphere simulates marine or industrial conditions.

The corrosion resistance is measured by weighing the sample, or by measuring its physical properties, or in terms of its outward appearance, or finally by the time at which the corrosion sites can be seen under determined conditions.

Specific corrosion resistance tests have been developed for oxide and phosphate coatings; for example, the oxide layer on steel can be tested in a copper sulfate solution to assure its continuity. The appearance of red dots of the deposited copper indicates the presence of porosity. This method can be applied also for Zn deposits.

Most of these methods have been developed not for galvanic coatings but for the corrosion of individual metals or alloys; for this reason, they do not often work adequately with metallic coatings, especially taking into account the differences between anodic and cathodic coatings, the multilayer coatings having properties different from those of single layers, etc. Besides, it should be taken into account that the electrode potentials presented in the tables correspond to ideal conditions; the potentials measured in the actual environment may differ considerably from these values. Table 15.13 lists the stationary potentials of several materials in aerated water (pH 6.0) along with their potentials in sea water (pH 7.5) and their standard potentials.

Table 15.13 The stationary potentials (vs. SHE) of selected metals: a) in aerated water; b) in see water; c) standard potentials. Temperature 298 K

Metal	Zn	Cd	Pb	Sn	Fe	Ni	Ag	Au
a	−0.80	−0.57	−0.28	−0.18	−0.10	+0.12	+0.19	+0.30
b	−0.81	−0.52	−0.26	−0.19	−0.39	+0.05	+0.15	+0.24
c	−0.762	−0.402	−0.126	−0.136	−0.036	−0.238	+0.799	+1.500

15.17 Solderability

There are several testing methods to assess the solderability of galvanic coatings. The simplest one consists in measuring the surface covered by a solder drop with a definite mass after it has spread on a surface: the larger the surface the better the solderability. Solderability of course will also be a function of the solder used.

Obviously, said area of spreading is connected with the edge wetting angle and therefore with the surface energy of the solder and the surface. The higher the surface energy of the sample, the larger is the area. If the radius of a small drop is r, then the area of spreading is about

$$S \approx 4r^2\sigma_w\,(2\sigma - \sigma_w) \approx 4r^2\sin^2\alpha(1-\cos\alpha)^{-2} \qquad (15.12)$$

where σ_w is the wetting energy, σ is the surface tension of the molten solder (about 0.5 J/m^2), α the edge angle at wetting.

The second method is based on the immediate measurement of the variation in surface energy upon wetting. Suitable devices control the force applied when dipping the tested surface into the molten solder. The advantage of this method is the simultaneous monitoring of the time at which the overall wetting is reached; the force in fact changes with time compared to the initial one when the surface contacts with the solder. This duration is usually about several seconds.

The variation in the energy during wetting can be 0.1–0.6 J/m^2. If the measured value exceeds 0.4 J/m^2 the solderability is high, at less then 0.2 J/cm^2 it is inadequate.

The best solderability is offered by tin (or its alloys) deposited from solutions without organic additives, then zinc deposits (without additives), gold and its alloys (excluding silver rich alloys), palladium, and also alloys of nickel-iron or nickel-phosphorus. Rhodium deposits and also many metals deposited in presence of organic additives often present bad solderability.

15.18 Control of the Deposit Thickness

Deposit thickness and its homogeneity are among the most important parameters of engineering coatings. The approximate value of the thickness is usually known from the current density, the duration of the process and current efficiency; however, the actual local thickness may differ markedly from the calculated value due to inhomogeneous current distribution.

A simple method of thickness control is the jet method based on the dissolution of the deposit using a jet or drops of the etching solution. Sometimes a modification of this method is used: instead of a continuous jet or dropping the etching drops are periodically put on the surface. The precision of this method is about 20%; it depends on a variety of factors, including the operator experience.

The solution composition is chosen individually for each deposited metal, such that the etching rate is kept within 0.1–1.0 μm/s. The jet is made to fall from a pipette (the orifice of 1–2 mm) on the deposit surface, inclined with respect to the horizontal, from a height of 3–5 mm. The end of the process is determined by visual inspection. At first the duration τ_0 of the dissolution of some known thickness h_0 is measured, and then the thickness of interest is determined as

$$h = h_0 \tau / \tau_0. \tag{15.13}$$

It is important to check the temperature constantly, because the dissolution rate approximately increases by 1.5 times for each 10°C increase in temperature. Several versions of this method have been developed: for example, the volume of the spent solution can be measured instead of the duration of the dissolution.

The compositions of the solutions corresponding to different types of deposits are presented in Table 15.14.

More accurate results are obtained by the total stripping of the deposit with a suitable etchant from a predefined area; then the mass difference Δm of the sample may be determined pre- and post- stripping, or the analytical determination of the metal in the stripping solution may be performed. The only requirement in this case is precise information on the area S and the deposit density γ. The thickness is determined as

$$h = \Delta m / (S\gamma) \tag{15.14}$$

Table 15.14 The composition of solutions for the measurements of deposits thickness by stripping method

Deposit	Solution	Substrate	The sign for termination of stripping
Copper	$FeCl_3$ 300 g/l	Steel	Pink spot
	$CuSO_4$ 100 g/l	Nickel	White spot
		Zinc	Black spot
Nickel	$FeCl_3$ 300 g/l	Steel	Pink spot
	$CuSO_4$ 100 g/l	Copper or its alloys	Pink or yellow spot
Zinc	NH_4NO_3 70 g/l $CuSO_4$ 7 g/l HCl 1 m 70 ml/l	Steel	Pink spot
Chrome	HCl (concentrated) 200 ml/l	Nickel	White spot
	H_2SO_4 (concentrated) 100 ml/l	Steel	Pink spot
	$FeCl_3$ 60 g/l, $CuSO_4$ 30 g/l, Ethanol 100 ml/l		
Silver	KI 250 g/l, I_2 7.5 g/l	Nickel, copper, alloys	The substrate appears

Coulometric measurements during anodic dissolution of the deposit are also possible; in this case it is difficult to check the end of the process: either the current should stop, or the potential should change sharply; moreover, the anodic current efficiency must be constant (100% efficiency is best).

The metallographic method is rather laborious; the corresponding techniques are described in metallography manuals and consist in preparing a cross-section of a sample with the attendant polishing and chemical etching of the section for its microscopic study. This method is convenient for research work: it permits not only to measure the film thickness but also to study the structure of the deposit and its interface with the substrate along with the microstructure including grain shape and size, pores, inclusions etc. In addition, metallographic sections may be used to perform microhardness measurements at various distances from the substrate, as well as to study current microdistribution at rough surfaces. In thin deposits this method is less useful since it is necessarily less precise.

In research work the film thickness may also be measured as the height of the step formed when removing a small area of deposit. This measurement can be made optically, with a micrometer or using a profilometer; the latter instrument may use a mechanical or an interferometric method. A similarly destructive method of thickness measurements consists in the partial removal of a deposit with a grinding wheel of sufficient radius (Fig. 15.20). In this case the thickness is determined as

$$h = \left(R^2 - l^2/4\right)^{1/2} - \left(r^2 - l^2/4\right)^{1/2} \tag{15.15}$$

The various symbols are indicated in the figure.

There is also a number of convenient non-destructive instruments for thickness testing available commercially. Most of these are electromagnetic thickness gauges or use methods generally based on eddy current.

The magnetic methods of thickness determination are limited to non-magnetic deposits on a ferromagnetic substrates; this is based on strongly joining the film to a magnet and applying a force to cleave the film from the substrate, measuring the force at pull-off. With increasing deposit thickness the separating force would decrease. In magnetic indicating testers permanent magnets are used, whereas in electromagnetic induction systems an alternate magnetic field is applied. The corresponding electronics measures the magnetic flux at the surface thus determining the thickness. Some of these testers need periodic calibration and verification. Their readings depend on the surface roughness and curvature. In magnetic deposits the

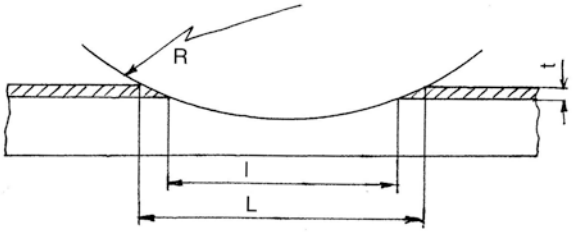

Fig. 15.20 Thickness measurement by partial removal of a deposit

dependence of their properties on the deposition conditions should be taken into account. The tolerance is about 5–10%, but in some cases in can be much better (down to 1%).

The testers based on eddy currents (Foucault currents), which are caused when a conductor is exposed to a changing magnetic field, are convenient when the electrical properties of the deposit and of the substrate differ significantly, for example for metallic coatings on non-metals or for non-conductive coatings on non-ferrous metals.

Ultrasonic gauges may also be used, mostly on non-conductive substrates.

The X-ray or radiation control of the thickness is well suited for the non-destructive determination of thickness in a suitable thickness range. The method depends on the determination of the penetration length of the X-ray radiation, which is different for different metals. For thin deposits, devices based on the back scattering of beta-radiation are also convenient.

15.19 The Peculiarities of the Properties of the Electrodeposited Alloys

The properties of electrodeposited alloys may differ widely both from the properties of similar metallurgical alloys and from the properties of the constituent metals. Alloying is very useful as it enables fine tuning of the properties of interest; such properties however do not always vary in the direction that may be predicted from the properties of the metal being added; for example, the presence of chromium in the anodes used for Fe-Ni deposition can sharply decrease the deposit hardness as result of chromium inclusion.

The hardness of an alloy usually increases upon addition of an alloying metal in the lattice of the elemental material; upon solid solution this increase is proportional to the concentration of the dissolved metal and to the difference in the atomic volumes. Thus high hardness is observed in solid solutions of cobalt in Rh and Rh in Co, W in Fe, Nb in Ni, In in Pt etc. The supersaturated alloy of Cd in Cu is relatively hard despite the fact that cadmium is softer than copper.

The hardening can result from the immediate interaction of the dislocations in the matrix structure with the dissolved solute atoms and especially with particles 10–20 nm in size.

It is important to note that alloys of the same composition can have very different properties, resulting from the different phase structure and microstructure.

In general, the role of the alloying components is always compounded with the variation of the grain size along with the inclusions of foreign atoms and clusters into the grains of the solvent metal.

The electrical resistivity of alloys is always higher than that of the pure individual components. For example, brass has a resistivity 2–5 times higher than copper; the addition of 5% boron into nickel results in a two-fold increase in ρ. The contact resistance can however decrease upon alloying, as it has been noted earlier.

Table 15.15 The properties of gold and its alloys coatings

Alloying metal	% of alloying metal in the deposit	Microhardness, MPa	Wear resistance (in relation to gold)	Electric resistivity, μΩ cm
No	no	1050	1	3.40
Nickel	3	1900	5–7	
	10	2200	7	22.0
	15	2500	10	40.0
Cobalt	1	2850		4.0
	5	2920	10	14.0
	10	3000	15	115
	17	2990		
Silver	5	1400	4	9.0
	10	1650		8.0
	16	1840		12.0
	31	1850	9	12.5
Antimon	2	2030	15	8.8
	5	2100		
	10	2350		38
	15	2600		52
Copper	10	1950	1.4	8.5
	20	2100	2.6	16

It is interesting that in some cases the effect of impurities in electrochemically deposited samples is weaker than in metallurgical ones: the codeposition of Co with gold, which highly increases Au hardness, only weakly influences the conductivity. In another example, the influence of codeposited phosphorus and other impurities in nickel and copper is relatively weak.

Some examples of the alloying influence on deposits properties are given in Tables 15.15, 15.16 and 15.17.

Table 15.16 The properties of silver and its alloys coatings

Alloying Metal	% of alloying component in the deposit	Microhardness, MPa	Wear resistance (in relation to silver)	Electric resistivity, μΩ cm
No	no	900	1	1.60
Organic brightener	?	2400	4	2.00
Antimony	0.5	1200	4	2.50
Palladium	1.0	1250	2	
	4.0	1570	4	4.70
Nickel	1.5	1200	5	1.90
	3.5	1300	20	2.00
Cobalt	1.0	1050	3	2.50
	7.3	1250	23	3.50
Bismuth	1.5	1900	4	1.65
Lead	4.0	1900		
Tin	10	1860		
Copper	20	2400		
Thallium	12	1800		

Table 15.17 The properties of palladium and its alloys coatings

Alloying Metal	% of alloying component in the deposit	Microhardness, MPa	Wear resistance (in relation to palladium)
No	no	2200	1
Tin	25	3000	0.6
Bismuth	20	2200	0.6
Nickel	25	3200	14
Cobalt	25	3200	25

References

1. Seeger A. Canadian J. of Phys., 1956, v. 34, p. 1219
2. Abeles F., Compt. Rendus, 1953, v. 237, p. 796
3. Magnetic Properties of Metals. H.P.J. Wijn (Editor), Springer, 1991
4. Tikhonov K.I. Soviet J. Electrochemistry, 1971, v.7, p. 1349
5. Hall E., Proc. Phys. Soc., 1951, B64, p. 747
6. Petch N., J. Iron Steel Inst., 1953, 173, p. 25

Index

A
adatoms, 14, 97, 123, 125, 128, 130, 131, 140, 218, 219, 221, 231, 323, 356
additives, 16, 20, 61, 73, 127, 162, 182, 183, 199, 201, 214, 220, 221, 258, 259, 262, 268–271, 276, 277, 280, 284–289, 291, 293–295, 298–300, 303, 305, 306, 308–310, 316, 336, 338, 341, 342, 348, 357, 368
adhesion, 73, 101–104, 266, 271, 275, 277, 284, 291, 297, 298, 307, 314, 316
adions, 14, 125, 128–130
adsorption, 9, 17, 18, 70, 71, 103–105, 111, 125, 127, 132, 136–138, 140, 182, 186, 199, 201, 208, 219–221, 231, 233–235, 269, 271, 277, 320–325, 335, 337, 350
adsorption equilibrium, 235, 236
alternate current, 19, 190, 193–196, 198, 199, 314, 338, 339
aluminum, 259, 261, 262, 265, 268, 283, 284, 286–288, 301, 302, 304, 305, 360, 361, 366
amorphous alloys, 214, 220, 221
amplification of migration current, 89
antifriction materials, 254
antimony, 254, 255, 274, 278, 284, 300, 307, 310
asymmetry parameter, 59

B
barrier coating, 256
bismuth, 220, 254, 304, 309, 310, 327, 356
boundary layer, 91, 93, 166, 170
brass, 254, 271, 272, 278, 289, 307, 323, 357, 360, 371
breaking stress, 348, 349
brightening, 187, 234, 245, 252, 262
bronzes, 272, 273
burning, 314
Butler–Volmer equation, 115, 128, 129

C
cadmium, 19, 137, 220, 254, 255, 289, 294, 304, 305, 356, 371
chemical potential, 53, 60, 98, 123, 284
chromium, 19, 22, 24, 253, 254, 256, 257, 260, 271, 288, 295–301, 306, 312, 316, 356, 357, 371
cobalt, 211, 256, 257, 274, 280, 283, 295, 327, 346, 353, 356, 365, 371
codeposition, 20, 183, 205, 210, 214, 221, 224, 227, 232, 234–236, 239, 241, 242, 244–246, 249, 252, 280, 282, 293, 303, 317, 346, 349, 353, 372
collection efficiency, 96
compressive stress, 289, 356–359
concentration overpotential, 84, 85, 135, 149, 217, 275
conductivity, 15, 17–19, 21, 24, 147, 156, 162, 169, 176, 178, 203, 223, 234, 255, 256, 266, 267, 271, 273, 275, 277, 279, 286, 287, 290, 297, 311, 313, 327, 328, 336, 338, 339, 372
consecutive steps, 97
contact resistance, 21, 256, 272, 273, 279, 290, 307, 313, 330, 340, 341, 343–345, 371
contact spots, 343
contractometer, 359
copper, 2, 7, 15, 19, 24, 73, 96, 125, 137, 219, 220, 254–257, 261, 262, 265–273, 278, 279, 282–284, 287, 291, 294, 297, 300, 305–307, 310, 316, 320, 323, 324, 330, 332, 337, 338, 341, 342, 348, 354–356, 360, 361, 367, 369, 371, 372
covering power, 163, 297, 298
cracking, 258, 297, 300, 311, 313, 356, 362

Y. D. Gamburg, G. Zangari, Theory and Practice of Metal Electrodeposition,
DOI 10.1007/978-1-4419-9669-5, © Springer Science+Business Media, LLC 2011

current density, 4–13, 15, 17, 20, 21, 23, 24, 58, 60, 62–64, 69, 70, 74, 77, 78, 82–88, 90, 93, 94, 110, 113, 115, 116, 127, 128, 130, 132, 134, 136–138, 141, 144–148, 151, 152, 154, 155, 157, 161–163, 165, 166, 169–171, 173, 178, 180–183, 185, 190, 192, 193, 195, 197, 198, 202, 204, 206, 207, 216, 226–228, 230, 234–236, 241–247, 250, 258, 262, 267, 270, 275–277, 280, 283, 285, 286, 293, 294, 298, 299, 304, 307, 313–316, 319, 320, 335, 336, 349, 351, 355, 356, 366, 368
current efficiency, 12, 16, 18, 24, 73, 162, 174, 199, 201, 207, 213, 236, 248, 250, 258, 266, 276, 298, 299, 301, 302, 307, 308, 315, 368, 370
current thieves, 165

D
damascene, 268
Dawson's integrals, 120
Debye length, 77
decorative properties, 285, 291
degreasing, 17, 259, 260, 288, 361
dendrites, 83, 137, 176, 199, 201, 209, 306
depolarization, 12, 208, 219
diffractometry, 331
diffusion, 14, 15, 17, 18, 65, 77, 78, 80, 82, 84–86, 88–93, 107, 110, 111, 113–122, 126–130, 133, 140, 141, 143, 147, 161, 166, 170, 179, 181, 183, 184, 189–192, 194, 197–202, 204, 209, 214, 219, 221, 227–231, 254, 257, 271, 274, 277, 282, 288, 290, 291, 297, 307, 313, 326–329, 337, 345, 356, 357, 360, 361
diffusion layer, 18, 80, 93, 121, 127, 129, 130, 133, 149, 166, 170, 174, 178, 179, 181, 185, 187, 189–191, 193–200, 202, 203, 230, 241, 246, 247
diffusion overpotential, 84, 192
Discharge of Complexes, 73
double layer, 57, 61, 73
ductility, 21, 221, 229, 257, 268, 279, 290, 293, 294, 297, 315, 325, 328, 330, 335, 347–350, 352

E
electrical contacts, 2, 255, 272, 274, 279, 290, 313
electrical resistance, 21, 335, 336, 339
electroactive species, 3, 8, 14, 18, 58, 60, 66, 69, 70, 77, 79, 87, 88, 111, 113, 115, 127, 169, 179, 181, 189, 190, 192, 194
electrochemical equivalent, 4, 207, 224, 270, 299
electrochemical potential, 53, 219
electrode, 1, 2, 4–11, 14, 16–18, 20, 23, 24, 53–65, 69–74, 77–88, 90–96, 104, 105, 110–112, 141, 143, 145–158, 160–162, 165, 166, 169–171, 174, 180, 182, 184, 189–195, 197, 199, 201–204, 208, 210, 217, 219, 220, 226, 231, 262, 265, 269, 270, 277, 292, 312, 357, 367
electrode potential, 6–9, 11, 17, 55, 57, 61, 130, 136, 137, 147, 190, 191, 217, 221, 235, 241, 262, 277, 327, 361, 367
electrode processes, 10, 16, 94, 180, 189, 193, 227
electropolishing, 187, 262, 306, 332
elongation, 291, 346–352, 359
epitaxial growth, 21, 138, 320, 360
equilibrium potential, 58, 62–65, 67, 73, 74, 84, 85, 87, 105, 110, 112
exchange current density, 110

F
Faraday law, 203
ferromagnetic films, 345
Fokker–Planck equation, 107, 108, 111
Frank–Van-der-Merwe mechanism, 103

G
Galvani potential, 53–55, 60
grain, 123, 134–136, 141, 213, 214, 216, 226, 262, 282, 287, 293, 318, 319, 326, 328, 338, 346, 347, 349, 356, 370
grain boundaries, 21, 141, 201, 214, 216, 219, 245, 318, 319, 321, 325–328, 335, 336, 342, 346, 348, 349, 356
grain size, 20, 21, 134, 135, 141, 189, 201, 217, 220, 245, 262, 282, 293, 318–321, 326, 328, 331, 335, 336, 347, 349, 350, 352, 353, 371

H
Hall–Petch law, 349
hardness, 21, 189, 206, 221, 223, 229, 256, 272, 274, 279, 285, 289, 290, 295–298, 307, 313, 320, 325, 327, 328, 330, 335, 346, 349, 350, 352–355, 371, 372
heterogeneous nucleation, 99, 102, 103, 226
Homogeneous Nucleation, 98
Hume-Rothery's rule, 213
hydrogen evolution, 10–12, 16–18, 73, 81, 85, 139, 206, 213, 228, 249, 250, 252, 280, 291, 299, 302, 303, 311, 365
hydrogenation, 18, 219, 248–250, 258, 260, 285, 288, 291, 292, 297, 300, 304, 311, 313, 338

I
impedance, 56
impurities, 20, 21, 103, 125, 136, 137, 139, 140, 199, 201, 205, 227, 260, 271, 276, 277, 282, 283, 287, 288, 291, 294, 295, 314–317, 320, 322, 323, 325, 335–338, 341–343, 346, 348–350, 353–355, 357, 372
incorporation, 17, 20, 71, 125, 126, 128, 130, 182, 233–239, 242, 243, 245–249, 277, 322, 323, 325, 337, 349, 357
indium, 254, 304, 305, 307, 356
inhibition, 70, 71
instantaneous nucleation, 119–121
intercalation, 217, 219, 221, 231
intermetallics, 212–215, 220–223
internal stress, 16, 21, 258, 266, 268, 273, 279, 284, 288, 291, 293, 302, 303, 311–314, 327, 346, 355–357, 359
interstitials, 321, 326
iron, 21, 206, 220, 221, 256, 257, 260, 265, 276, 287, 290, 295, 301, 302, 305, 346, 356, 365

L
lead, 2, 67, 68, 71, 103, 116, 121, 122, 137, 220, 222, 254, 257, 258, 261, 271, 280, 294, 300, 302, 305–307, 309–311, 324, 327, 335, 336, 356, 357
leveling, 24, 121, 170, 172, 173, 175, 178, 182, 186, 187, 271, 293, 337
leveling power, 170, 181–183, 185, 186
Levich formula, 93
lifetime, 169, 255, 279
limiting potential distribution, 145
Luggin Capillary, 57

M
macrodistribution, 23, 178
magnetic coatings, 346
magnetoresistance, 229
mass transport, 80, 235, 239, 241, 242
mechanical mixture, 21, 213, 216, 217, 331
metastable phases, 221
microthrowing power, 170, 183
migration, 14, 77, 78, 84, 88, 89, 91, 143, 190, 326–328
mixed kinetics, 86, 87, 115, 161, 227, 231
morphology, 6, 9, 21, 99, 122, 124, 126, 127, 136–138, 140, 170, 211, 283, 318, 320, 324, 332
multilayers, 229

N
Nernst equation, 56, 62, 68, 70, 84, 86, 87
nickel, 2, 16, 19, 22, 24, 88, 220, 253–258, 262, 271–275, 280, 282, 283, 289–297, 299, 300, 302, 304, 307, 320, 322, 324, 330, 338, 340–342, 346, 349, 353, 356, 357, 360, 361, 365, 368, 371, 372
nucleation, 17, 97, 100–107, 109, 112–114, 118–123, 125, 130–132, 134–136, 139, 140, 198, 199, 201, 216–219, 225, 226, 229, 238, 282, 317, 319–321, 324, 325, 335, 357, 360, 365

O
overlap, 118–120, 122, 133, 209
overpolarization, 207, 208
overpotential, 63, 64, 70, 71, 73, 84, 85, 87, 90, 93, 98, 103, 105, 109–112

P
palladium, 24, 220, 255, 256, 258, 274, 278, 295, 296, 310, 311, 356, 368, 373
peeling, 297, 314, 356, 362–364
phase diagrams, 214–216
pickling, 260–262, 288, 361, 362
pitting, 16, 295, 307
platinum, 19, 55, 125, 253, 257, 282, 301, 311, 312, 314, 340, 346
polarizability., 11, 64, 73, 184
Polarization Curves, 62, 65
polarization field, 148, 149
porosity, 21, 272, 279, 282, 298, 300, 310, 312, 328, 338, 341, 342, 348, 365–367
preceding homogeneous step, 69
primary potential distribution, 144, 145
progressive nucleation, 120, 121
pulse, 112, 113, 190, 197–201, 229–231, 260, 271, 300, 338, 361

R
recrystallization, 312, 324, 328, 355
reference electrode, 55, 56
reflectance, 257, 277, 290, 298, 313
residence time, 20, 236–238
resistivity, 144, 178, 336–338, 340–343, 371, 372
rhodium, 253, 256, 257, 313, 314, 356
ring-disc electrode, 94
rotating disc electrode, 80, 94, 182
roughness, 4, 6, 10, 23, 24, 83, 92, 125, 140, 141, 169–173, 175, 176, 185, 186, 200, 202, 262, 314, 332, 342–344, 354, 360–362, 370
roughness coefficient, 4, 169

S
secondary microdistribution, 177
secondary potential distribution, 146

silver, 6, 15, 24, 55, 88, 113, 137, 219, 220, 253–258, 266, 272–279, 282–284, 307, 311–313, 324, 328, 330, 341, 352, 356, 368, 372
sinusoidal current, 190, 193
soft magnetic materials, 302
solderability, 254, 258, 266, 308, 309, 330, 368
solid solution, 21, 211–214, 216–223, 231, 249, 283, 296, 328, 331, 338, 371
stacking faults, 20, 201, 320–324, 328, 331, 332, 336, 348
Standard Hydrogen Electrode, 55
stannate, 273, 308–310, 361
stirring, 11, 18, 70, 80, 161, 259, 267, 269, 270, 281, 287, 293, 294, 308, 309, 336
Stranski–Krastanov mechanism, 104
sub-grains, 318, 320
sublayers, 229
subsequent chemical step, 70
substrate, 9, 11, 17, 18, 21, 22, 97, 99–102, 104, 112, 120, 136–139, 164, 165, 170, 176, 208, 211, 216–220, 231, 253–255, 257, 260, 266, 279, 288, 290–292, 296, 300, 304, 307, 319, 320, 325, 326, 330, 332, 339–341, 345, 346, 348, 350–367, 369–371

T
Tafel equation, 18, 93
Tafel Region, 64
Tafel slopes, 68
tarnishing, 260, 274, 344
tensile strength, 328, 346, 348, 352, 363
tensile stress, 22, 355–357, 359
texture, 318, 324, 325, 331, 346
throwing power, 24, 143, 158, 160, 200, 258, 266, 275–277, 280, 285, 289, 293, 297, 301, 305, 308
tin, 2, 220, 254–258, 260, 272, 273, 287, 296, 300, 304, 306–310, 330, 356, 368
true leveling, 173, 176
tunneling microscopy, 137, 219, 331
twin boundary, 323
twinning, 138, 139, 318, 321, 323–325

U
underlayers, 254–256
underpotential deposition, 9, 103, 218, 219, 229, 231

V
vacancies, 219, 321, 326–328, 332
Vegard's law, 212
Vetter equation, 67
Volmer–Weber mechanism, 103

W
Wagner number, 156–158, 166
wear resistance, 23, 206, 216, 229, 254, 256, 278, 279, 289, 290, 293, 296, 300, 310, 313, 347, 350, 355

X
X-ray, 20, 21, 212, 213, 223, 318, 321–324, 327, 328, 330–332, 359, 371

Z
Zeldovich equation, 107
Zeldovich factor, 108, 131
zinc, 2, 18, 19, 24, 254–262, 267, 271, 272, 282, 284–289, 294–296, 304, 307–310, 327, 330, 356, 361, 368
zincate, 262, 361
zincate treatment, 262